Development of fluorescent biosensors and inhibitors to probe and target CDK4/cyclin D in melanoma

Camille Prevel

Collège Doctoral du Languedoc-Roussillon

THÈSE

Pour obtenir le grade de

Docteur

Délivré par l'UNIVERSITÉ DE MONTPELLIER

Préparée au sein de l'école doctorale SCIENCES CHIMIQUES ET BIOLOGIQUES POUR LA SANTÉ

Et de l'unité de recherche INSTITUT DES BIOMOLÉCULES MAX MOUSSERON

Spécialité : Biochimie et Biologie Moléculaire

Présentée par CAMILLE PRÉVEL

DÉVELOPPEMENT DE BIOSENSEURS FLUORESCENTS ET D'INHIBITEURS POUR SUIVRE ET CIBLER CDK4/CYCLINE D DANS LE MÉLANOME

Soutenue le 11 Décembre 2015 devant le jury composé de

Madame May MORRIS, DR2, IBMM	Directrice de thèse
Madame Florence MAHUTEAU-BETZER, CR1, Institut Curie	Rapporteur
Monsieur Lluis FAJAS COLL, Professeur, UNIL	Rapporteur
Madame Céline GONGORA, DR2, IRCM	Examinateur
Monsieur Frédéric BIHEL, CR1, UMR7200 CNRS/UdS	Examinateur

CDK/cyclins play a central role in coordinating cell cycle progression, and in sustaining proliferation of cancer cells, thereby constituting established cancer biomarkers and attractive pharmacological targets. In particular, CDK4/cyclin D, which is responsible for coordinating cell cycle progression through G1 into S phase, is a relevant target in several cancers including melanoma, associated with mutation of CDK4, cyclin D, $p16^{INK4a}$ and pRb.

As there are no sensitive and direct approaches to probe CDK4/cyclin D activity in physiological and pathological conditions, the first goal of my thesis has consisted in engineering a fluorescent biosensor to probe this kinase *in vitro* and *in cellulo.* Once characterized and validated *in vitro,* the biosensor was applied to detect CDK4/cyclin D alterations in biopsies from human skin and melanoma xenografts in fluorescence-based activity assays, and in living cancer cells by fluorescence microscopy and timelapse imaging.

Moreover, only few inhibitors are currently available to target CDK4/cyclin D and most of them bind the ATP pocket. As such, the second major goal of my thesis project has consisted in identifying non-ATP competitive inhibitors, either through rational design of peptides or by screening small molecule libraries. To this aim, two fluorescent biosensors were engineered which discriminate compounds that target the interface between CDK4 and cyclin D, or that perturb the conformational dynamics of CDK4, respectively, from ATP-pocket binding compounds. Fluorescence-based screening assays performed with these biosensors lead to identification of hits, which were validated and characterized *in vitro* and in cell proliferation assays, and which constitute promising candidates for selective chemotherapy in melanoma.

Key words : CDK4/cyclin D, melanoma, fluorescent biosensor, diagnostic assay, inhibitors, HTS

Les CDK/cyclines jouent un rôle majeur dans la progression du cycle cellulaire et dans le maintien de la prolifération des cellules cancéreuses, constituant ainsi des biomarqueurs clés et des cibles pharmacologiques attractives. Plus particulièrement, l'activité de CDK4/cycline D, kinase responsable de la progression de la phase G1 et de la transition G1/S, est dérégulée dans de nombreux cancers dont le mélanome. Cette hyperactivation est associée à des mutations, à l'amplification ou à la surexpression de CDK4, cycline D, $p16^{INK4a}$ ou encore pRb.

Comme aucune approche sensible et directe n'existe pour évaluer l'activité de CDK4/cycline D dans des conditions physiologiques et pathologiques, le premier objectif de ma thèse a consisté à développer un biosenseur fluorescent permettant d'étudier cette kinase *in vitro* et *in cellulo.* Une fois caractérisé et validé *in vitro,* le biosenseur a été appliqué à la détection d'altérations de CDK4/cycline D dans des biopsies de peau humaine et de xénogreffes de mélanome dans des essais fluorescents d'activité kinase, ainsi que dans des cellules cancéreuses vivantes par microscopie de fluorescence et vidéo microscopie.

Par ailleurs, peu d'inhibiteurs sont actuellement disponibles pour inhiber CDK4/cycline D et la plupart d'entre eux ciblent la poche de fixation de l'ATP. C'est pourquoi le second objectif de ma thèse a consisté à identifier des inhibiteurs non compétitifs de l'ATP, soit par élaboration rationnelle de peptides, soit par criblage de petites molécules. A cette fin, deux biosenseurs fluorescents ont été développés qui permettent d'identifier soit des composés ciblant l'interface entre CDK4 et cycline D, soit des inhibiteurs allostériques capables de perturber la dynamique conformationnelle de CDK4. Des essais de criblage par fluorescence réalisés avec ces biosenseurs ont conduit à l'identification de touches qui ont été validées et caractérisées *in vitro* et dans des essais de prolifération cellulaire, et qui constituent des candidats prometteurs pour une chimiothérapie sélective du mélanome.

Mots clés : CDK4/cycline D, mélanome, biosenseur fluorescent, diagnostic, inhibiteurs, HTS

A mes parents

Remerciements

J'aimerais remercier le Professeur Jean Martinez de m'avoir accueilli au sein de l'IBMM et d'avoir accepté de co-diriger ma thèse.

Je remercie le Dr Florence Mahuteau et le Pr Lluis Fajas de m'avoir fait l'honneur d'accepter d'évaluer mon travail de thèse.

Je remercie également les Drs Céline Gongora et Frédéric Bihel d'avoir accepté d'examiner ce travail.

Je remercie chaleureusement ma directrice de thèse, le Dr May Morris. Merci de m'avoir donné la possibilité d'apprendre la biologie et merci de m'avoir fait confiance pendant trois ans. Merci de m'avoir fait profiter de ton expertise scientifique, merci pour tous tes conseils, ton soutien et ton écoute.

J'aimerais ensuite remercier tous mes collègues du CRBM/CPBS/IGMM où j'ai commencé ma thèse et de l'IBMM où je l'ai terminée. J'ai passé trois ans entourée de gens formidables et grâce à vous, l'aventure a été belle et inoubliable! Merci aux thésards et post-docs pour toutes ces soirées et ces sorties. Mention spéciale à François, Nabila, Marion, Ngoc, Sarah, Ilaria, Davide, Mattias, Karidia, Sophie, Eric, Mathy, Daouda, Monia, Naïma, Baptiste, Clément B., Clément S., Lubo, Jérémy C., Laurent, Dominique, Saïd, Loïc, Thibault, Jérémie N., Joseph, Carmen, Morgane, Coline, Cindy, Salomé et Léa. Merci aux filles de la culture cell : Marion, Audrey, Salomé, Coline, Cécile et Carmen !

J'aimerais remercier tout particulièrement mes partenaires de course à pied: Ngoc, Sarah, Daouda, Eric, Marion, Clément et Baptiste.

Un grand merci à mon équipe, Marion, Morgan, Carmen, Juan Antonio, Ngoc, Inès, Jacques, Axelle, Elvira et Céline. J'ai eu beaucoup de chance d'être entourée de collègues comme vous. Un remerciement particulier à Ngoc, pour tout ce que tu m'as appris au labo et pour tout ce qu'on a partagé en dehors. Merci Morgan, pour ton aide et ta gentillesse, et bravo : tu as réussi à me supporter du début à la fin de ma thèse ! Marion, merci pour tout, pour ton énergie, ta bonne

humeur et ton soutien sans faille, heureusement que tu étais là !! Merci Carmen de m'avoir fait partager ton expérience post-doc et merci surtout pour toutes tes ondes positives ! Juan Antonio, merci de nous avoir apporté un peu d'Espagne au labo !

François, mon frère, tu fais partie des plus belles rencontres que j'ai eu la chance de faire pendant ma thèse. Merci pour tous ces bons moments : la Jacqueline, les soirées, les restos et les trucs bizarres et insolites que tu aimes tant !

Nabila, ma complice de début de thèse, ma voisine de Vert-Bois, j'ai été ravie de vivre cette aventure avec toi.

J'aimerais remercier Julie Bayle pour sa gentillesse, sa disponibilité et tous ses précieux conseils concernant l'après-thèse.

Je tiens à remercier Véronique Josserand et Julien Vollaire pour les manips *in vivo*. Je remercie également Nicolas Floquet pour les expériences de docking. Je remercie aussi Pauline Henri et Laurent Meunier de nous avoir fourni les biopsies de peau, pour leur expertise, leur aide et leur gentillesse.

Merci à la plateforme MRI et plus particulièrement à Virginie, Sylvain et Simon pour la microscopie. Je n'oublie pas Julien, pour ce magnifique screen et pour tous les bons moments passés devant le robot !

Je souhaite remercier Bruno Maurel, le roi du bricolage, d'avoir toujours été là pour nous sauver de situations parfois un peu catastrophiques.

Je remercie les équipes de Muriel Amblard, de Marcel Garcia et de Jean-Louis Banères pour leur gentillesse et pour nous avoir si souvent dépannés en matériels ou produits.

J'aimerais remercier Jocelyne Gauthier, Muriel Fitoussi et Sylvie Corneille pour leur aide administrative et leur réactivité.

Je remercie mes parents, parce que vous êtes parfaits et parce que sans vous tout cela n'aurait pas été possible. Merci à mes deux sœurs adorées, Pauline et Gaëlle, d'être toujours à mes côtés.

Merci à toute ma famille, de Villers, de Villedieu, de Vire, d'Anisy, du Mans, de Nantes et de Chandigon. Merci à ma deuxième famille : Christian, Martine, Marion et Nico. J'ai de la chance d'être si bien entourée.

Je souhaite remercier mes copines d'école d'ingé, parce que chaque WE passé avec vous est magique ! Mention spéciale à Caro qui m'a supportée et soutenue pendant ces trois années !

Merci à mes amis de longue date : Mathilde, Guillaume et Charles. C'est toujours un plaisir de vous revoir en Normandie et de passer des vacances avec vous !

Et enfin, j'aimerais te remercier Baptiste. Sans toi, je n'y serais jamais arrivée. Merci de m'avoir fait décrocher du travail le WE, merci de m'avoir soutenue, de m'avoir aidée à relativiser et à déstresser et merci d'être toujours là pour moi.

Abbreviations

Abl : Abelson murine leukemia viral oncogene homolog

AFP : Autofluorescent protein

APC : Anaphase Promoting Complex

BiFC : Bimolecular Fluorescence Complementation

CAK : CDK-Activating Kinase

CAMK : Calmodulin/Calcium regulated kinases

CDK : Cyclin-Dependent Kinase

CHEF : CHelation-Enhanced Fluorescence

CKI : CDK inhibitor

CLK : Cdc-Like Kinase

CML : Chronic Myeloid Leukemia

CPP : Cell-Penetrating Peptide

CRM1 : Chromosome Region Maintenance 1

δEF1 : δ-crystallin enhancer factor 1

EDTA : EthyleneDiamineTetraAcetic acid

EGFR : Epidermal Growth Factor Receptor

ERK : Extracellular signal-Regulated Kinase

ELISA : Enzyme-Linked ImmunoSorbent Assay

FDA : Food and Drug Administration

FLiK : Fluorescent Labels in Kinases

FLIM : Fluorescence Life Time Imaging

FRET : Förster Resonance Energy Transfer

GFP : Green Fluorescent Protein

GSK3β : Glycogen Synthase Kinase 3β

HBV : Hepatitis B Virus

HCS : High Content Screening

HCV : Hepatitis C Virus

HIV : Human Immunodeficiency Virus

HTS : High Throughput Screening

IR : InfraRed

JNK : c-Jun N-terminal Kinase

MAPK : Mitogen-Activated Protein Kinase

MCL : Mantle Cell Lymphoma

NES : Nuclear Exclusion Sequence

NF1 : Neurofibromin 1

NIR : Near InfraRed

NLS : Nuclear Localization Sequence

NP40 : Nonidet P-40

NSCLC : Non Small Cell Lung Cancer

PAABD : Phospho Amino Acid Binding Domain

PBD : Polo Box Domain

PKA : Protein Kinase A

PKC : Protein Kinase C

PKG : Protein Kinase G

Plk1 : Polo-Like Kinase 1

PTB : PhosphoTyrosine-Binding

Rb : Retinoblastoma

RDF : Recognition-Domain-Focused

SDS-PAGE : SDS-PolyAcrylamide Gel Electrophoresis

SH2 : Src-Homology 2

SPF : Surface Plasmon Resonance

TK : Tyrosine Kinase

TKL : Tyrosine Kinase-Like

TSC2 : Tuberous Sclerosis Complex 2

UBF : Upstream Binding Factor

Introduction

1. CDK/cyclins and cell cycle regulation

1.1. The cell cycle

The cell cycle enables all living organisms to grow and divide by generating two daughter cells from one mother cell. The rhythm at which cells are renewed varies from one organism to another and even from a cell to another. In eukaryotic cells, the cell cycle is controlled by a complex system of regulatory enzymes involved in different signaling pathways. The cell cycle is divided into four key phases: three interphase phases (G1, S and G2) where the cell grows, accumulates all necessary nutrients and synthesizes DNA for cell division, and the mitotic (M) phase where the cell divides into two daughter cells (Figure 1) (Harper and Brooks, 2005; Morgan, 1995, 1997; Nurse, 1975).

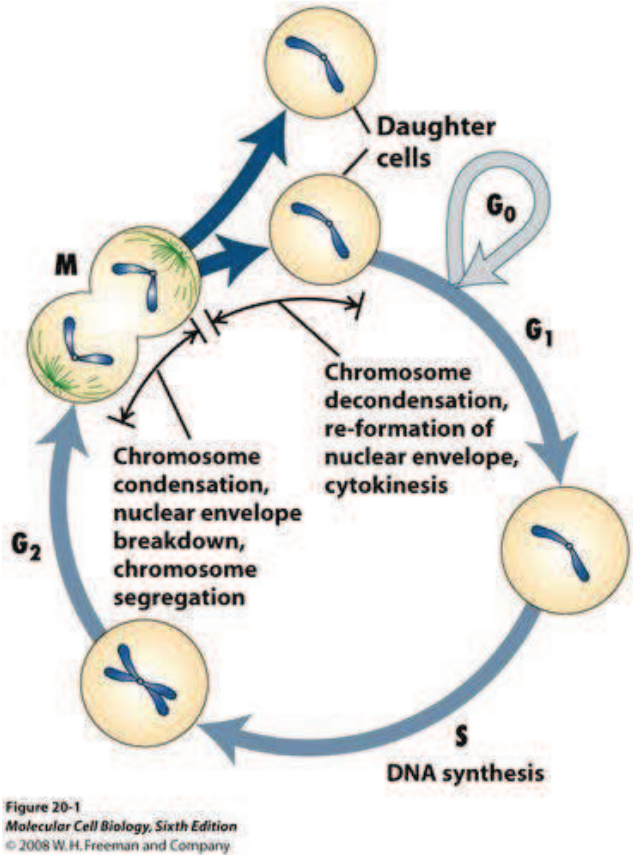

Figure 1: Eukaryotic cell cycle phases. The cell cycle is divided into four phases : M, G1, S and G2 (from (Lodish, 2008)).

The cell cycle starts with **G1 phase** during which cells grow in size and synthesize proteins and RNA that are required for DNA replication.

Then, during the synthesis phase, commonly called **S phase**, chromosomes are replicated, leading to the production of two identical chromatids.

Between DNA replication and mitosis, in **G2 phase**, cells continue to grow and prepare for mitosis.

The fourth step of the cell cycle is defined by the mitotic phase (**M phase**). This phase corresponds to the division of one mother cell into two identical daughter cells. It is a four-stage process.

- During prophase, chromosomes condense and the separation of the two centrosomes induces formation of the mitotic spindle.
- Metaphase is the stage where the condensed chromosomes align in the middle of the cell, the nuclear envelope is disassembled and chromosomes are attached to microtubules.
- During anaphase, the chromatids split, segregate and move toward opposite poles of the cell.
- Telophase corresponds to the stage where chromosomes reach the centrosomes which lead to the formation of the daughter cells' nuclei.
- The final stage of mitosis is cytokinesis which is defined by the formation of two daughter cells containing the same genetic material (Sagona and Stenmark, 2010).

Following these 4 stages, if cells lack growth factors and nutrients, they exit the cell cycle and stay in a quiescent state which is called the G0 phase. However, this process is reversible and cells can, upon growth factor stimulation, reenter the cell cycle.

Cell cycle checkpoints are essential to ensure that each phase is accurately completed before entering the next phase. They are crucial to avoid abnormal events such as mutations which can further be implied in tumorigenesis (Lazzaro et al., 2009). Upon detection of DNA damage or incomplete processes, checkpoints such as the DNA damage checkpoint and the DNA replication checkpoint refrain cell cycle progression to enable repair and correction of these abnormal events or induce cell cycle arrest. In 1974, Pardee demonstrated the existence of a G1 checkpoint, also named restriction (R) point or point of no return, which occurs 2-3 hours prior to the onset of DNA synthesis and from where cells no longer require growth factors to complete the cell cycle and irreversibly commit to the cell division process (Pardee, 1974).

1.2. The discovery of CDK/cyclins

In addition to cell cycle checkpoints, network of enzymes that control cell cycle progression were discovered through studies in starfish, yeast and Xenopus (Hartwell et al., 1974; Labbe et al., 1988; Nurse, 1975). Cyclin-dependent kinases (CDKs) were first identified, described and cloned in the 1970s–1980s as gene products involved in regulation of the cell division cycle (Hartwell et al., 1974; Labbe et al., 1988, 1989; Lee and Nurse, 1987; Lohka et al., 1988; Nurse, 1975). CDK/cyclins form a family of serine/threonine proline-directed protein kinases that, by definition, catalyze the transfer of a phosphate group from ATP onto a serine or a threonine residue (Figure 2) (Cohen, 2002; Rubin and Rosen, 1975).

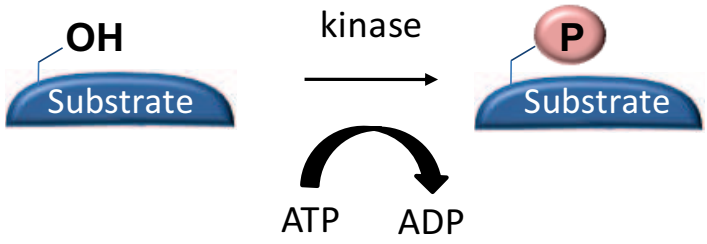

Figure 2: The phosphorylation process. This reaction is catalyzed by kinases and consists in the removal of a phosphate group from ATP, followed by its covalent attachment to amino acids with a free hydroxyl group, namely, serine, threonine, and tyrosine.

CDK/cyclins are heterodimeric complexes which contain a catalytic CDK subunit and a regulatory cyclin subunit. These kinases are part of the CMGC sub-family which also contains MAPK (Mitogen-Activated Protein Kinases), GSK3 (Glycogen Synthase Kinase 3) and CLK (Cdc-like kinases) (Figure 3).

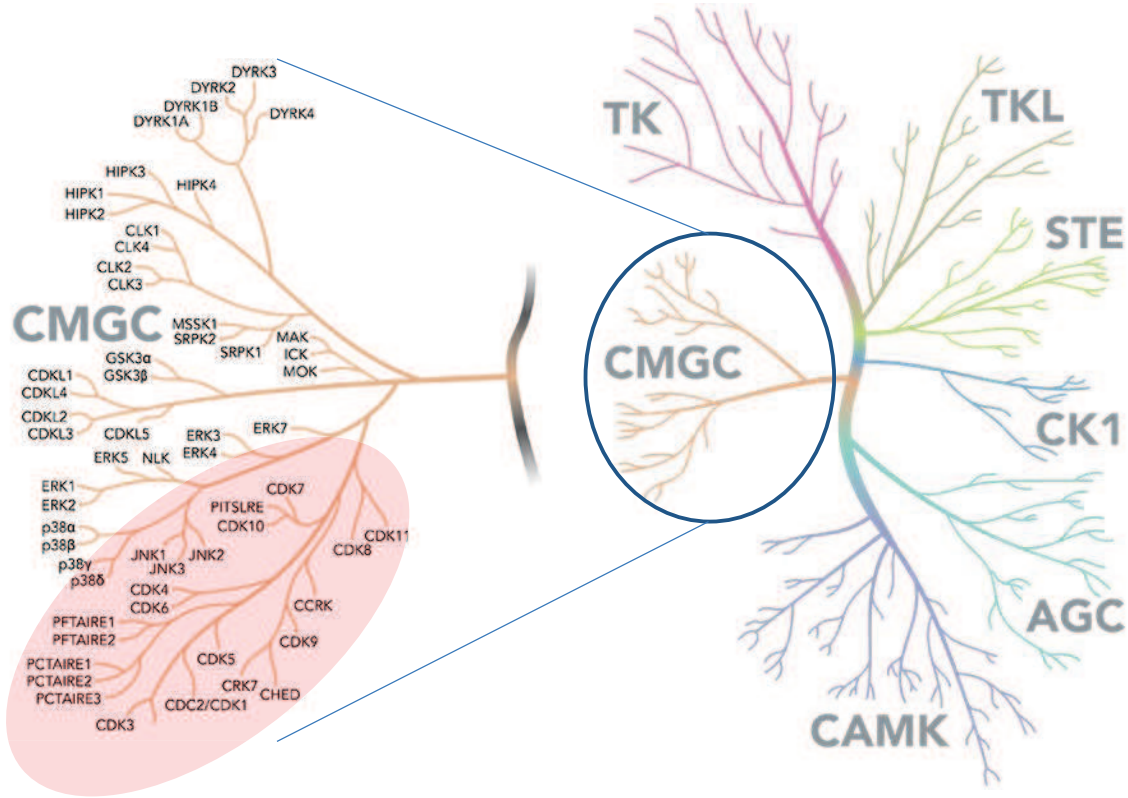

Figure 3: The kinome tree (adapted from https://www.horizon-genomics.com/available/kinome). The human genome harbors 518 genes encoding a kinase domain. 7 kinase sub-families have been defined : AGC named after the Protein Kinase A, G, and C families (PKA, PKG, PKC)**; CMGC** for CDK, MAPK, GSK3 and CLK**; CAMK** best known for Calmodulin/Calcium regulated kinases (CAMK) in CAMK1 and CAMK2 families**; CK1** for Cell Kinase 1**; STE** for Homologs of the yeast STE7, STE11 and STE20 genes**; TK** for Tyrosine Kinases**; TKL** for Tyrosine Kinase-Like proteins.

After several decades of studies, twenty CDKs and about the same number of cyclins have been identified (Malumbres and Barbacid, 2005) (Table 1). Besides a well-known role in cell cycle regulation, a wealth of non-cell cycle functions has been reported for CDK/cyclin complexes including transcriptional regulation, epigenetics, DNA damage response and repair, neuronal differentiation, synaptic trafficking and remodelling, glycogen synthesis and lipogenesis, angiogenesis, haematopoiesis, ciliogenesis and spermatogenesis (Figure 4) (Lim and Kaldis, 2013; Prével et al., 2014a).

Symbol	Synonym	Identity to CDK1 (%)	Cyclin-binding domain	Main activating cyclin
CDK1	Cdc2, Cdc28	100	PSTAIRE	A1, A2, B1, B2

CDK2		65	PSTAIRE	A1, A2, E1, E2
CDK3		63	PSTAIRE	E1, E2, A1, A2, C
CDK4	PSK-J3	42	PISTVRE	D1, D2, D3
CDK5		56	PSSALRE	p35, p39
CDK6		43	PLSTIRE	D1, D2, D3
CDK7	MO15, CAK, STK1	38	NRTALRE	H
CDK8	K35	28	SMSACRE	C
CDK9		34	PITALRE	T1, T2, K
CDK10		37	PISSLRE	Unknown
CDK11	Cdc2L1, Cdc2L2	26	SMSACRE	L1, L2
PITSLRE		35	PITSLRE	Unknown
PFTAIRE1	Pftk1	44	PFTAIRE	Unknown
PFTAIRE2		41	PFTAIRE	Unknown
PCTAIRE1	Pctk1, Crk5	45	PCTAIRE	Unknown
PCTAIRE2	Pctk2	48	PCTAIRE	(Cables1)
PCTAIRE3	Pctk3	45	PCTAIRE	Unknown
CRK7	CrkRS, CD2L7	17	PITAIRE	Unknown
CHED	Cdc2L5	16	PITAIRE	Unknown
CCRK		37	PNQALRE	Unknown

Table 1: The mammalian CDKs and their activating cyclins (adapted from (Malumbres and Barbacid, 2005))

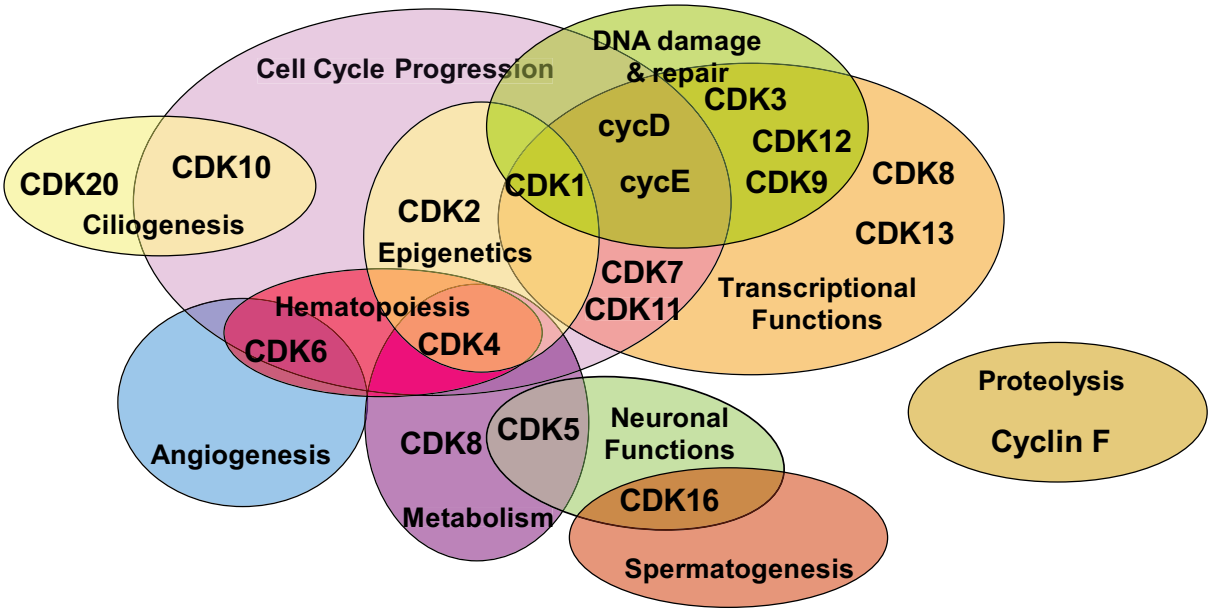

Figure 4: Functions of cyclin-dependent kinases. Schematic representation of the functional diversity of CDKs and their converging contributions to subsets of biological processes (from (Prével et al., 2014a))

1.3. The CDK/cyclins involved in cell cycle regulation

1.3.1. Roles throughout the cell cycle

Only four CDKs play a role in the cell cycle. CDK1/cyclin A-B, CDK2/cyclin A-E, CDK4/cyclin D and CDK6/cyclin D are in charge of regulating the different cell cycle transitions (Malumbres, 2011; Morgan, 1997). The sequential activation of these different CDK/cyclin complexes drives the transitions through the different phases of the cell cycle (Figure 5). CDK4-6/cyclin D ensure the progression through G1 phase and CDK2/cyclin E is responsible for G1/S transition. CDK2/cyclin A is involved in regulation of S phase, CDK1/cyclin A is responsible for progression through G2 phase whereas CDK1/cyclin B is activated during mitosis. Finally, besides an essential role in transcription, CDK7, in association with cyclin H, forms a complex termed CAK, the CDK-Activating Kinase, which is involved in activation of several CDK/cyclins through phosphorylation of the CDK activation loop (or T-loop) (Fisher, 2005).

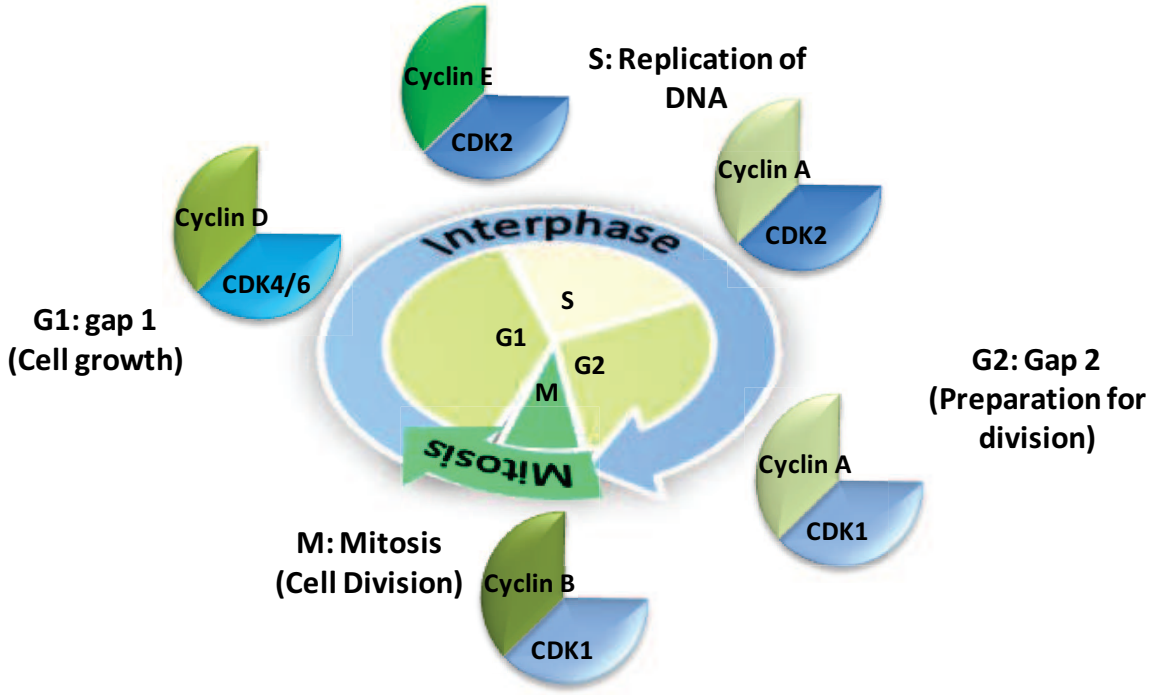

Figure 5: Cell cycle regulation by CDK/cyclins (from (Peyressatre et al., 2015)).

Studies on mice have demonstrated that inactivation of genes coding for cell cycle CDKs was not lethal, except for CDK1/cyclin B, because of compensatory mechanisms between the different complexes (Santamaría et al., 2007; Satyanarayana and Kaldis, 2009; Sherr and Roberts, 2004). Surprisingly, these losses of function only affect the development of specialized cell types. The examples of *CDK4* and *CCND1* gene knockouts are detailed in paragraph 2.2. Only the absence of CDK1 leads to a cell cycle arrest, meaning that the other CDKs cannot compensate the loss of CDK1 (Santamaría et al., 2007).

1.3.2. Regulation of CDK/cyclins

Monomeric CDKs are catalytically inactive and acquire basal kinase activity through binding of a cyclin partner. Following their assembly into heterodimeric complexes, CDKs are subject to reversible activating and inhibitory phosphorylations which complete activation of the kinase (Boutros et al., 2006; Kaldis, 1999; Morgan, 1995, 1997). They are subject to inhibitory phosphorylation which prevents ATP binding, on Thr14 and Tyr15 residues, for CDK1 and CDK2, by Wee1 and Myt1 kinases (Coleman and Dunphy, 1994; Morgan, 1997). They are then activated through activating phosphorylation of threonine 161 (Thr161 in CDK1) by the CDK-activating kinase CDK7/cyclin H and

dephosphorylation of Thr14 and Tyr15 residues by members of the Cdc25 phosphatase family (Boutros et al., 2006; Kaldis, 1999).

Besides these phosphorylation/dephosphorylation events, CDK/cyclins are also regulated through interactions with structural inhibitors called CDK inhibitors (CKIs). The INK4 family of CKIs comprises proteins composed of multiple ankyrin repeats ($p16^{INK4a}$, $p15^{INK4b}$, $p18^{INK4c}$ and $p19^{INK4d}$) which specifically bind CDK4 and CDK6 and either prevent or compete with cyclin binding (Jeffrey et al., 2000). CDK/cyclin activity is also regulated by association with the Cip/Kip family of CKIs ($p21^{Cip1}$, $p27^{Kip1}$, $p57^{Kip2}$) which bind and maintain CDK/cyclin heterodimers in an inactive form (Sherr and Roberts, 1999).

Figure 6 provides a schematic representation of the general molecular mechanism of assembly and regulation of CDK/cyclins, although some variations occur depending on the CDK.

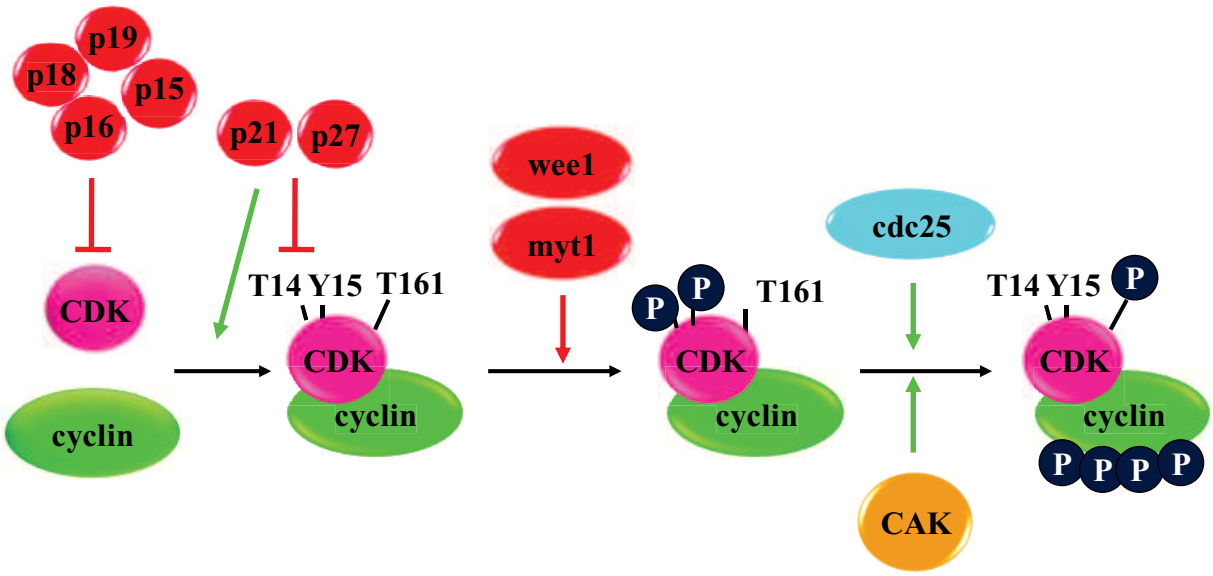

Figure 6: Schematic representation of the general molecular mechanism of assembly and regulation of CDK/cyclins (from (Prével et al., 2014a)).

The mechanism of CDK/cyclin assembly has been described for CDK2/cyclin A and provides key information to gain insight into the molecular basis of CDK/cyclin complex activation (Brown et al., 1999; Hagopian et al., 2001; Jeffrey et al., 1995; Morris et al., 2002; Russo et al., 1996). These studies reveal that cyclin binding is a two-step process which consists first in the rapid association between the PSTAIRE helix in the N-terminal lobe of CDK2 and the α5 helix of cyclin A (Figure 7). This step

leads to reorientation of the CDK ATP-binding pocket, aligning it with the catalytic cleft in a position which is appropriate for transfer of phosphate onto the substrate. The second step corresponds to a slower isomerization of the CDK C-terminal lobe which promotes a conformational switch of an activating segment termed the T-loop, partially stabilizing it in a position which favours subsequent phosphorylation by CAK. Phosphorylation further displaces the T-loop into a position stabilized through interactions between the phosphate group and several residues within the C-lobe of the CDK, thereby generating a fully accessible substrate-binding site.

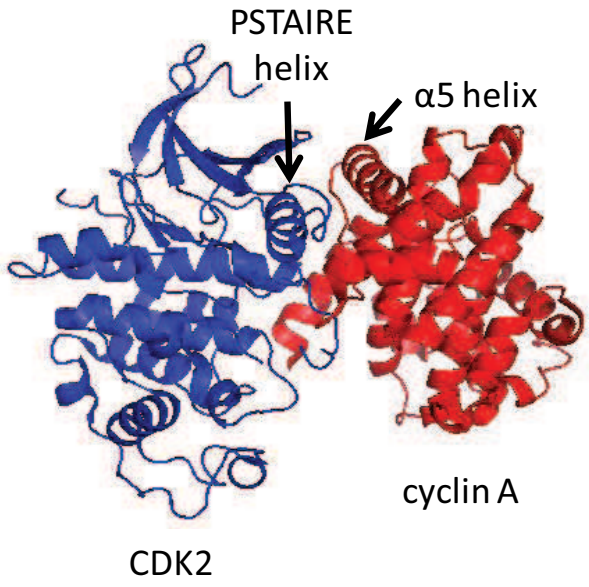

Figure 7: Crystal structure of CDK2/cyclin A (PDB 1QMZ)

1.4. CDK/cyclins and cancers

1.4.1. Definition and hallmarks of cancers

Cancer is a generic term for a large group of diseases that involve abnormal cell growth with the potential to invade or spread to other parts of the body (Hanahan and Weinberg, 2000) (http://www.who.int/mediacentre/factsheets/fs297/en/). Other terms used are malignant tumours and neoplasms. Cancer can be defined as the rapid generation of abnormal cells that grow beyond their usual boundaries, and which can then invade other parts of the body and spread to other organs, the latter process is referred to as metastasizing.

Hanahan and Weinberg have proposed 6 characteristic features of all cancer cells associated with tumor progression (Hanahan and Weinberg, 2000) (Figure 8):

- self-sufficiency in growth signaling
- insensitivity to anti-growth signals
- evasion of apoptosis
- enabling of a limitless replicative potential
- induction and sustainment of angiogenesis
- activation of metastasis and invasion of tissue

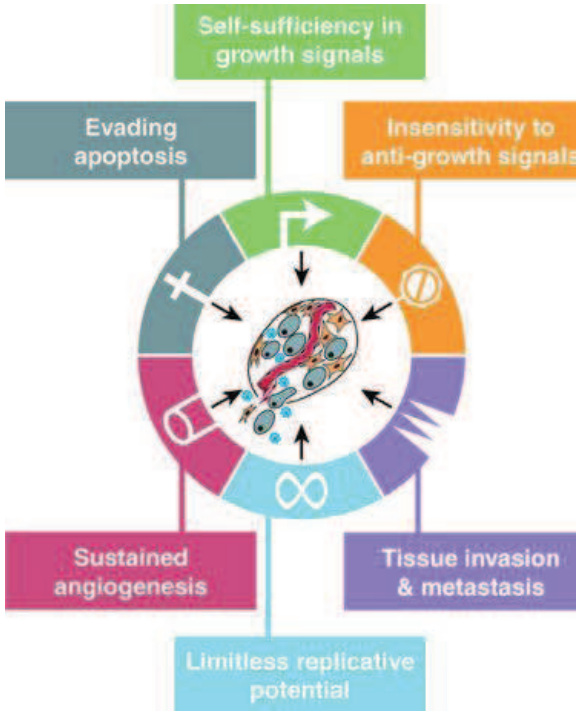

Figure 8: Schematic representation of the characteristic features of all cancer cells associated with tumor progression (from (Hanahan and Weinberg, 2000)).

Cancer develops through accumulation of several genomic alterations including mutations, amplification and overexpression. Most of these deregulations affect two types of genes, the tumor suppressor genes and the proto-oncogenes, which, once altered, act as drivers of cancers (Vogelstein et al., 2013; Zhu et al., 2015). A tumor suppressor is a protective gene that normally limits the growth of tumors. If a mutation appears in this gene and causes a loss or reduction in its function, the cell can progress to cancer, usually in combination with other genetic changes (Sun and Yang, 2010). pRb

and p53 are two well-known examples of tumor suppressor proteins which are frequently mutated or deleted in cancers. In contrast, a proto-oncogene is a normal gene which, when altered by mutation, becomes an oncogene that can contribute to cancer (Croce, 2008). Most normal cells undergo apoptosis when critical functions are altered. Activated oncogenes can cause those cells designated for apoptosis to survive and proliferate instead. CDK/cyclins are not formally considered as oncogenes but highly contribute to sustain proliferation of cancer cells. In the literature, CDK/cyclin hyperactivity associated with mutations or aberrant expression has been widely described (Figure 8) (Malumbres and Barbacid, 2001, 2007) (COSMIC database http://www.sanger.ac.uk/genetics/CGP/cosmic/).

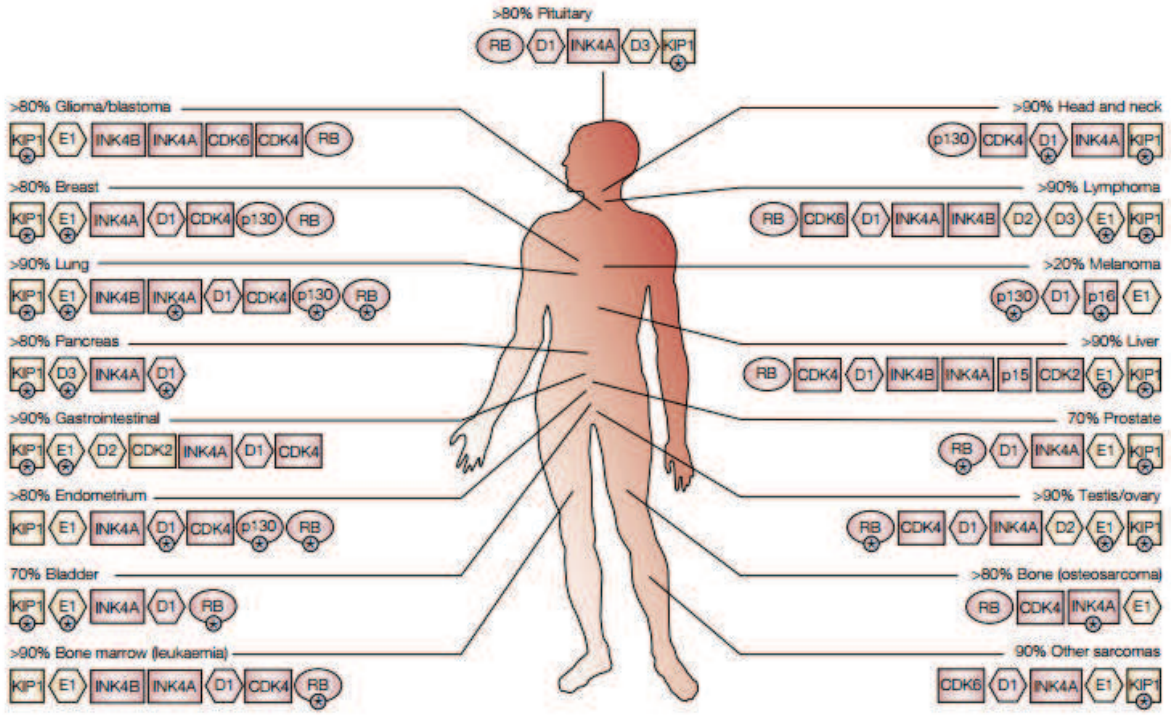

Figure 9: Genetic alterations of G1/S regulators in human cancers. Only alterations that occur in more than 10% of primary tumours have been considered. The loci in which specific genetic or epigenetic alteration have been defined are in pink. The alterations for which no mechanistic explanation has been provided are in yellow. Alterations relevant for tumour prognosis are indicated by asterisks (from (Malumbres and Barbacid, 2001)).

1.4.2. Causes of cancers

Both internal factors (including inherited mutations (5-10%), hormone deregulations, and immune disorders) and environmental factors promote genetic alterations and constitute the onset of

tumorigenesis (Anand et al., 2008; Shang, 2007). The vast majority of cancers, some 90–95% of cases, are due to environmental factors (Anand et al., 2008). Common environmental factors that contribute to cancer death include tobacco (25–30%), diet and obesity (30–35%), and infections (mostly due to viruses such as Human papillomavirus, Epstein Barr virus, Kaposi's sarcoma-associated herpes virus, human T-lymphotropic virus 1, HIV, HBV, and HCV) (15–20%) (Anand et al., 2008). Up to 10% of total cancer cases may be induced by radiation, both ionizing and nonionizing, typically from radioactive substances and ultraviolet (UV), pulsed electromagnetic fields (Belpomme et al., 2007). Cancers induced by radiation include some types of leukemia, lymphoma, thyroid cancers, skin cancers, sarcomas, lung and breast carcinomas. The remaining percentage (15-20%) is due to other factors like stress, physical activity, environmental pollutants or carcinogens such as asbestos (Anand et al., 2008; Hodgson and Darnton, 2000).

1.4.3. CDK/cyclins as therapeutic targets for cancer therapy

CDKs, as cancer biomarkers, constitute attractive targets for the development of anti-cancer drugs. Over the last two decades, many efforts have been invested to develop potent inhibitors of CDK/cyclins (Asghar et al., 2015; Fischer et al., 2003; Garrett and Fattaey, 1999; Lapenna and Giordano, 2009).

Targeting the ATP binding site, essential protein/protein interfaces, hydrophobic pockets or allosteric sites which are exposed only in inactive intermediates are part of the strategies developed to inhibit CDK/cyclin activity (Cohen and Alessi, 2013; Fang et al., 2013; Liu and Gray, 2006; Pommier and Cherfils, 2005). These approaches are detailed below in paragraph 3.

It has to be mentioned that, despite the large number of CDK inhibitors which are currently undergoing clinical trials, only one inhibitor has been approved for clinical use so far. Indeed, on February 2015, FDA (Food and Drug Administration) granted approval to Palbociclib, a CDK4/6 inhibitor for use in combination with letrozole for the treatment of post-menopausal women with estrogen receptor (ER)-positive, human epidermal growth factor receptor 2 (HER2)-negative advanced breast cancer (http://www.fda.gov/Drugs/InformationOnDrugs/ApprovedDrugs/ucm43288

6.htm).

2. CDK4/cyclin D

2.1. Primary sequences of CDK4 and D-cyclins

2.1.1. CDK4

CDK4, formerly called PSK-J3, is a 34-kDa serine/threonine kinase. CDK4 was first cloned from HeLa cells and then from mice cells, based on its homology to mixed oligonucleotide probes representing highly conserved regions of other mammalian kinases (Hanks, 1987; Matsushime et al., 1992).

Figure 10 displays the primary sequence of human CDK4 with its main functional elements such as the ATP-binding domain and the T-loop.

```
> CDK4_HUMAN

MATSRYEPVA EIGVGAYGTV YKARDPHSGH FVALKSVRVP NGGGGGGGLP ISTVREVALL
RRLEAFEHPN VVRLMDVCAT SRTDREIKVT LVFEHVDQDL RTYLDKAPPP GLPAETIKDL
MRQFLRGLDF LHANCIVHRD LKPENILVTS GGTVKLADFG LARIYSYQMA LTPVVVTLWY
RAPEVLLQST YATPVDMWSV GCIFAEMFRR KPLFCGNSEA DQLGKIFDLI GLPPEDDWPR
DVSLPRGAFP PRGPRPVQSV VPEMEESGAQ LLLEMLTFNP HKRISAFRAL QHSYLHKDEG
NPE
```

Figure 10: Primary sequence of human CDK4 (source: www.uniprot.org/). Functional elements, which will be further described, are highlighted as follows : ATP-binding domain ; Inhibitory phosphorylation site: Y17 ; Cyclin-binding domain: PISTVRE ; Start and end of the T-loop ; Activating phosphorylation site: T172 (adapted from (Lim and Kaldis, 2013)).

2.1.2. Human D-type cyclins

Although only one cyclin D has been identified in mice, drosophila and many other organisms, three D-type cyclins, cyclin D1, cyclin D2 and cyclin D3, have been found expressed in most human proliferating cells (Sherr and Roberts, 2004). All three can bind CDK4 and CDK6 proteins. They are closely related as shown in Figure 11 which displays the sequence alignments of these proteins. The human cyclin D1 and cyclin D2 proteins are 51% and 62% respectively, identical to human cyclin D3, and 62% identical to each other (source: www.uniprot.org/).

```
CCND1 MEHQLLCCEVE-TIRRAYPDANLLN-DRVLRAMLKAEETCAPSVSYFKCVQKEVLPSMRK 58
CCND2 --MELLCHEVD-PVRRAVRDRNLLRDDRVLQNLLTIEERYLPQCSYFKCVQKDIQPYMRR 57
CCND3 --MELLCCEGTRHAPRAGPDPRLLGDQRVLQSLLRLEERYVPRASYFQCVQREIKPHMRK 58
         :*** *      **  * .**  :***: :*  **   *  ***:***::: * **:

CCND1 IVATWMLEVCEEQKCEEEVFPLAMNYLDRFLSLEPVKKSRLQLLGATCMFVASKMKETIP 118
CCND2 MVATWMLEVCEEQKCEEEVFPLAMNYLDRFLAGVPTPKSHLQLLGAVCMFLASKLKETSP 117
CCND3 MLAYWMLEVCEEQRCEEEVFPLAMNYLDRYLSCVPTRKAQLQLLGAVCMLLASKLRETTP 118
      ::* *********:****************:*:  *. *::******.**::***::** *

CCND1 LTAEKLCIYTDNSIRPEELLQMELLLVNKLKWNLAAMTPHDFIEHFLSKMPEAEENKQII 178
CCND2 LTAEKLCIYTDNSIKPQELLEWELVVLGKLKWNLAAVTPHDFIEHILRKLPQQREKLSLI 177
CCND3 LTIEKLCIYTDHAVSPRQLRDWEVLVLGKLKWDLAAVIAHDFLAFILHRLSLPRDRQALV 178
      ** ********.:: *.:* : *:::: ****:***:  ***: .:* ::   .:.  ::

CCND1 RKHAQTFVALCATDVKFISNPPSMVAAGSVVAAVQGLNLRSPNNFLSYYRLTRFLSRVIK 238
CCND2 RKHAQTFIALCATDFKFAMYPPSMIATGSVGAAICGLQQDEEVSSLTCDALTELLAKITN 237
CCND3 KKHAQTFLALCATDYTFAMYPPSMIATGSIGAAVQGLGAC----SMSGDELTELLAGITG 234
      :******:****** .*   ****:*:**: **: **        ::   **.:*: :

CCND1 CDPDCLRACQEQIEALLESSLRQAQQNMDPKAAE-EEEEEEEEVDLACTPTDVRDVDI 295
CCND2 TDVDCLKACQEQIEAVLLNSLQQYRQDQRD------GSKSEDELDQASTPTDVRDIDL 289
CCND3 TEVDCLRACQEQIEAALRESLREASQTSSSPAPKAPRGSSSQGPSQTSTPTDVTAIHL 292
       : ***:******** * .**::  *           ...:  . :.*****  :.:
```

Figure 11: Sequence alignements between cyclin D1, cyclin D2 and cyclin D3 (source: www.uniprot.org/)

2.1.3. Cyclin D1

Compared with cyclin D2 and cyclin D3, the functional characterization of cyclin D1 and its role in human cancer have been much more studied and reported in the literature (Musgrove et al., 2011). In 1991, human cyclin D1 was first cloned by introducing a cDNA library prepared from a human glioblastoma cell line into a budding yeast strain that lacked *CLN1* and *CLN2* and was conditionally deficient for *CLN3* function (Xiong et al., 1991).

Figure 12 displays the primary sequence of human cyclin D1 with its main functional elements including the Rb binding domain and the cyclin box.

```
> CCND1_HUMAN

MEHQLLCCEV ETIRRAYPDA NLLNDRVLRA MLKAEETCAP SVSYFKCVQK EVLPSMRKIV
ATWMLEVCEE QKCEEEVFPL AMNYLDRFLS LEPVKKSRLQ LLGATCMFVA SKMKETIPLT
AEKLCIYTDN SIRPEELLQM ELLLVNKLKW NLAAMTPHDF IEHFLSKMPE AEENKQIIRK
HAQTFVALCA TDVKFISNPP SMVAAGSVVA AVQGLNLRSP NNFLSYYRLT RFLSRVIKCD
PDCLRACQEQ IEALLESSLR QAQQNMDPKA AEEEEEEEEE VDLACTPTDV RDVDI
```

Figure 12: Primary sequence of human cyclin D1 (source: www.uniprot.org/). Functional elements are highlighted as follows (adapted from (Alao, 2007; Musgrove et al., 2011)):

LXCXE motif: required for RB binding

RXXL motif: required for APC (Anaphase Promoting Complex) mediated following genotoxic insult degradation (Agami and Bernards, 2000)

Cyclin box: mediates CDK4 binding and is necessary for interaction with p21, p27 and p57

LLXXXL motif: C-terminal leucine-rich motif which binds an LXXLL motif in the steroid receptor co-activators SRC1 and AIB1 (McMahon et al., 1999; Zwijsen et al., 1998)

T286: residue that, when phosphorylated, triggers ubiquitin-mediated degradation (see paragraph 2.8)

2.2. Phenotypes of mice lacking CDK4 or D-cyclins

As previously described in paragraph 1.3, studies on mice have demonstrated that inactivation of genes coding for any interphase CDK was not lethal because of compensatory mechanisms between the different complexes (Santamaría et al., 2007; Satyanarayana and Kaldis, 2009; Sherr and Roberts, 2004). CDK4 knockout in mice only induces abnormal development of β-pancreatic cells and leads to insulin-dependent diabetes (Rane et al., 1999). Triple knockout of cyclin D1, D2 and D3 leads to death due to anemia and defects in heart development (Kozar et al., 2004). Table 2 reports in details the phenotypes of mice with disrupted cyclin D and CDK4 genes.

Cyclin D1	Viable	Small body size, hypoplastic retinopathy, defective beast lobuloalveolar development during pregnancy, and uncharacterized neuropathy with altered clasping reflexes	(Fantl et al., 1995; Sicinski et al., 1995)
Cyclin D2	Viable	Defective ovarian granulosa cell development and female sterility. Males have hypoplastic testes but are fertile. Abnormal postnatal cerebellar development due to a reduced number of granule neurons and loss of stellate interneurons. Impaired proliferation of peripheral B-lymphocytes	(Huard et al., 1999; Lam et al., 2000; Sicinski et al., 1996; Solvason et al., 2000)

Cyclin D3	Viable	Hypoplastic thymus with loss of T-cell maturation from double-negative (CD4−, CD8−) to double-positive (CD4+, CD8+) cells due to cytokine-independent defects in pre-TCR signaling	(Sicinska et al., 2003)
Cyclin D2 and D3 (D1 only)	Embryonic lethality before E18.5	Death likely is due to severe megaloblastic anemia. Other hematopoietic lineages were not evaluated.	(Ciemerych et al., 2002)
Cyclin D1 and D3 (D2 only)	Death at P1, but a few survive to 2 months	Neuropathy leading to meconium aspiration is cause of early death. Survivors fail to thrive and exhibit hypoplastic retinas.	
Cyclin D1 and D2 (D3 only)	Viable but die within first three postnatal weeks	Retarded growth and impaired coordination. Inhibited postnatal cerebellar development, and hypoplastic retinas	
Cyclins D1, D2, and D3 (no D-type cyclin)	Dead by E16.5	Severe hematopoietic deficits affecting number and proliferative capacity of stem cells and multipotential progenitors. Fetal liver lacks progenitors and cannot reconstitute lymphoid or myeloid function after transplantation. Death due to anemia and	(Kozar et al., 2004)

		defects in heart development. MEFs can be propagated in culture but exhibit greatly reduced susceptibility to transformation by oncogenic Ras + Myc, E1A, or DN-p53	
Cdk4	Viable	Small body size. Most males are sterile due to hypoplastic testes and low sperm counts. Female sterility is due to defects in the hypothalmic–pituitary axis, abnormal estrus, and failure of corpus luteum. Abnormal development of pancreatic-islet cells leads to insulin-dependent diabetes within the first 2 mo of life. MEFs can be propagated in culture with decreased ability to enter the cell cycle from quiescence; they express aberrantly high levels of $p21^{Cip1}$ and resist transformation by oncogenic Ras + DN-p53.	(Moons et al., 2002; Rane et al., 1999; Tsutsui et al., 1999; Zou et al., 2002)

Table 2: Phenotypes of mice with disrupted cyclin D and CDK4 genes (from (Sherr and Roberts, 2004))

2.3. Role in the cell cycle

Under normal conditions, most cells in multicellular organisms remain in a quiescent state (G0 phase) and do not divide. Upon stimulation by extracellular signals such as growth factors, cells can reenter the G1 phase of the cell cycle. CDK/cyclin complexes involved in the regulation of G1 phase and G1/S transition are CDK4-6/cyclin D and CDK2/cyclin E. They have been demonstrated to be involved in the G1 checkpoint (or restriction point; see paragraph 1.1) from where cells no longer require growth factors to complete the cell cycle and irreversibly commit to the cell division process (Blagosklonny and Pardee, 2002). Indeed, the phosphorylation of the members of the retinoblastoma protein family

(pRb, p107 and p130) by CDK4-6/cyclin D leads to E2F transcription factor derepression inducing transcription of cyclin E which is required for G1/S transition (Ho and Dowdy, 2002) (Figure 13).

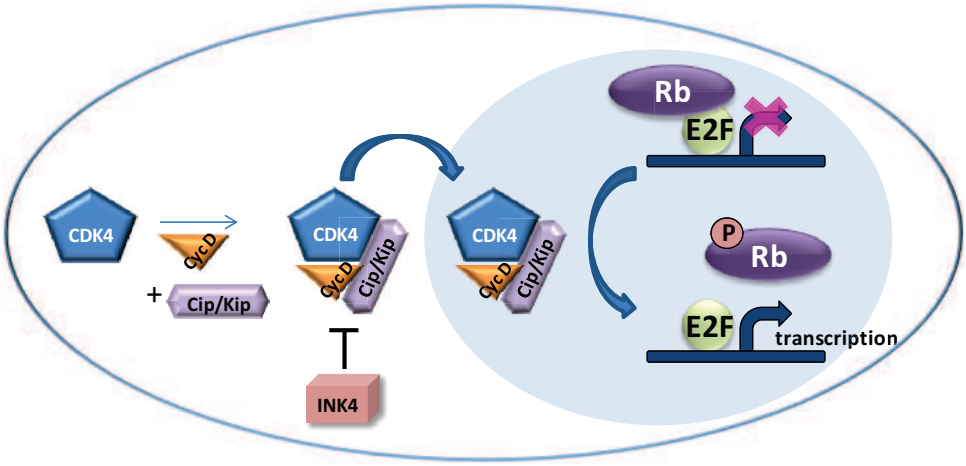

Figure 13: Function and regulation of CDK4/cyclin D (from (Peyressatre et al., 2015)). The expression of cyclin D (orange) via mitogenic signals leads to its association with CDK4 (blue) and formation of the complex. The binding with Cip/Kip proteins (light purple) is required for assembly of the complex and its nuclear localization. The activity of CDK4/cyclin D activity is negatively regulated by interaction with the INK4 protein family (pink). Once activated, CDK4/cyclin D regulates the progression through G1 phase and the transition into S phase. CDK4/cyclin D phosphorylates the retinoblastoma protein (Rb) (dark purple) inducing the derepression of E2F transcription factors (green) which allows the transcription of genes which are required for G1/S transition.

More recently, it has been shown that CDK4/cyclin D activates pRb by mono-phosphorylation and that CDK2/cyclin E executes all the remaining inactivating phosphorylations (Narasimha et al., 2014). The complete phosphorylation of pRb then allows for complete release of E2F factors, which may act as transcriptional activators (Boonstra, 2003).

Besides a function in G1 phase progression and G1/S transition, Gabrielli and co-workers have reported a role of CDK4, in complex with cyclin D3, in G2/M transition (Gabrielli et al., 1999). They have provided evidence for a CDK4/cyclin D3 activity in late S/G_2 phase that appears to be required for normal cell cycle progression through G_2 phase into mitosis. Indeed $p16^{INK4a}$ accumulation, in response to UV radiation, leads to inhibition of CDK4 activity which appears to be involved in the G_2 phase delay observed.

2.4. Differences between CDK4 and CDK6

The human CDK4 and CDK6 proteins are 64% identical to each other (source: www.uniprot.org/). Because of this high sequence identity and their similar expression profiles, they have been widely thought to act redundantly to regulate the cell cycle through the phosphorylation of pRB. However, novel functions of CDK6 have been recently uncovered and several studies highlight differences between CDK4 and CDK6. For example CDK6, when proliferation is inappropriate, plays a role in halting cellular growth through a mechanism involving the accumulation of the p53 and p130 growth-suppressing proteins (Nagasawa et al., 2001). Moreover, CDK6 has been found to be involved in angiogenesis (Kollmann et al., 2013). Indeed, Kollmann and collaborators have demonstrated that CDK6 was part of a transcription complex that induces the expression of the tumor suppressor $p16^{INK4a}$ and the pro-angiogenic factor VEGF-A. Differences in subcellular localization and in the timing of nuclear localization of CDK4 and CDK6 have also been described (Mahony et al., 1998; Nagasawa et al., 1997). Moreover, CDK4 and CDK6 are differently deregulated in cancer cells (Bellail et al., 2014; Chilosi et al., 1998; Corcoran et al., 1999; Costello et al., 1997; Dobashi et al., 2004; Peyressatre et al., 2015; Puyol et al., 2010; Sotillo et al., 2001a; Wölfel et al., 1995).

2.5. Other roles of CDK4/cyclin D

Beyond its role in cell cycle progression, CDK4/cyclin D is also essential for control of metabolic processes such as lipid synthesis, glycolysis, and mitochondrial function (Fajas, 2013). For instance, Fajas and collaborators have demonstrated an adipogenic role of CDK4 and cyclin D3 through positive regulation of PPARγ activity, a ligand-activated transcription factor belonging to the nuclear receptor superfamily activity (Abella et al., 2005; Sarruf et al., 2005).

Moreover, CDK4 is involved in controlling proliferation of specific cell types such as pancreatic β cells (Martín et al., 2003). The lack of CDK4 expression in mice leads to insulin-deficient diabetes due to a reduced number of pancreatic cells. It has been shown that the CDK4-pRB-E2F1 pathway was involved in glucose homeostasis through regulation of the expression of Kir6.2, a key component of the KATP channel involved in the regulation of glucose-induced insulin secretion in pancreatic β-cells (Fajas et al., 2010).

Aggarwal and co-workers have also demonstrated a role of CDK4/cyclin D in epigenetic regulation through Mep50 phosphorylation (Aggarwal et al., 2010). Indeed, accumulation of nuclear CDK4/cyclin D1 during S-phase triggers increased PRMT5/MEP50 activity, thereby specifically reducing *CUL4* expression.

Other functions of cyclin D1 have also been described such as a role in HR-mediated DNA damage repair (Jirawatnotai et al., 2011; Li et al., 2010). Indeed, analyses of cyclin D1 interactors have revealed a network of DNA repair proteins, including RAD51, a recombinase that drives the homologous recombination process (Jirawatnotai et al., 2011).

Finally, a nuclear role of cyclin D1 in NF-Y, Stat, Creb2, Elk1, Znf423 and Cux1 transcription, independent of CDK4, has been discovered by performing a genetic-proteomic screen (Bienvenu et al., 2010).

2.6. Other substrates of CDK4/cyclin D

CDK4-6/cyclin D complexes are mostly known for their role in G1 phase. Thus, the pRb family members ($p105^{Rb}$, p107, $p130^{Rb2}$) are the best known substrates for CDK4. However, CDK4/cyclin D also phosphorylates other substrates including Smad3, a protein which has a key function in mediating the TGF-beta growth-inhibitory response; the DNA replication factor Cdt1; the nucleolar transcription factor upstream binding factor (UBF); the bone-specific transcription factor Runx2; and possibly the tumour suppressor tuberous sclerosis complex 2 (TSC2) (Bockstaele et al., 2006; Liu et al., 2004; Matsuura et al., 2004; Shen et al., 2006; Voit et al., 1999; Zacharek et al., 2005).

2.7. Regulation of CDK4/cyclin D activity

The activity of CDK4/cyclin D is regulated by phosphorylation/dephosphorylation events. Phosphorylation of residue Tyr17, close to the ATP binding site, maintains CDK4 in an inactive conformation (Figure 14). This site of phosphorylation is equivalent to Tyr15 of the well-described CDK1 kinase which undergoes inhibitory phosphorylation by WEE1 and MYT1 (Mueller et al., 1995; Parker and Piwnica-Worms, 1992). However, these two kinases do not phosphorylate CDK4. Instead, phosphorylation of CDK4 on Tyr17 is performed by Src kinases (Martin et al., 2008). Cdc25A

phosphatase performs the dephosphorylation of this residue, leading to the partial activation of CDK4 (Boutros et al., 2006; Iavarone and Massagué, 1997; Terada et al., 1995). Activating phosphorylation on Thr172 residue by the CAK CDK7/cyclin H allows a full activation of CDK4 and this is essential to promote G1 progression (Schachter et al., 2013) (Figure 14).

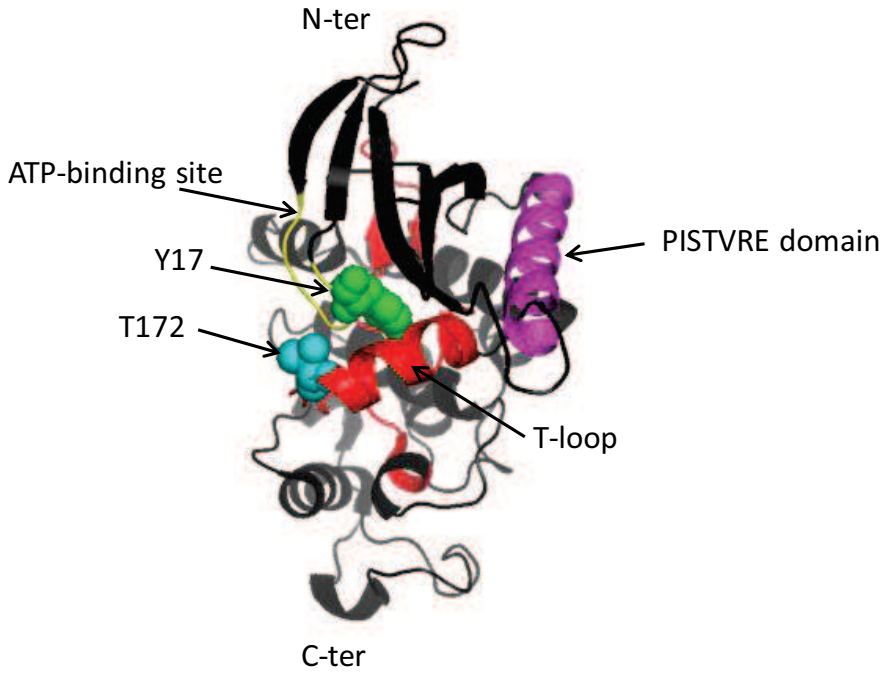

Figure 14: Crystal structure of CDK4, in complex with cyclin D3 (not shown here) (PDB 3G33). The functional elements are highlighted as follows: ATP-binding domain; Inhibitory phosphorylation site: Y17; Cyclin-binding domain: PISTVRE; Start and end of the T-loop; Activating phosphorylation site: T172

Besides these phosphorylation/dephosphorylation events, CDK4/cyclin D activity is also regulated by CKIs (Figure 13). Its activity is inhibited by interaction with the INK4 proteins which can bind both monomeric CDK4, preventing its association with cyclin D, and the CDK4/cyclin D complex, forming an inactive ternary entity (Jeffrey et al., 2000). CDK4/cyclin D activity is also regulated by association with Cip/Kip proteins (Sherr and Roberts, 1999). At low concentration, they act as positive regulators by enhancing the binding between CDK4 and cyclin D and the translocation of the dimeric complex into the nucleus (LaBaer et al., 1997). Indeed, p21 and p27 contain a NLS sequence (Nuclear Localization Sequence) but not cyclin D and CDK4 (Bockstaele et al., 2006; Sherr and Roberts, 1999). At higher concentrations, Cip/Kip proteins inhibit CDK4/cyclin D activity. It has to be noted that,

through the sequestration of p21 and p27, CDK4/cyclin D plays a second non-catalytic role in G1 phase progression by facilitating CDK2 activation (Figure 15). Indeed, sequestration by CDK4/cyclin D of Cip/Kip proteins, which also bind CDK2/cyclin E, lowers the inhibitory threshold and facilitates activation of this complex (Sherr and Roberts, 1999).

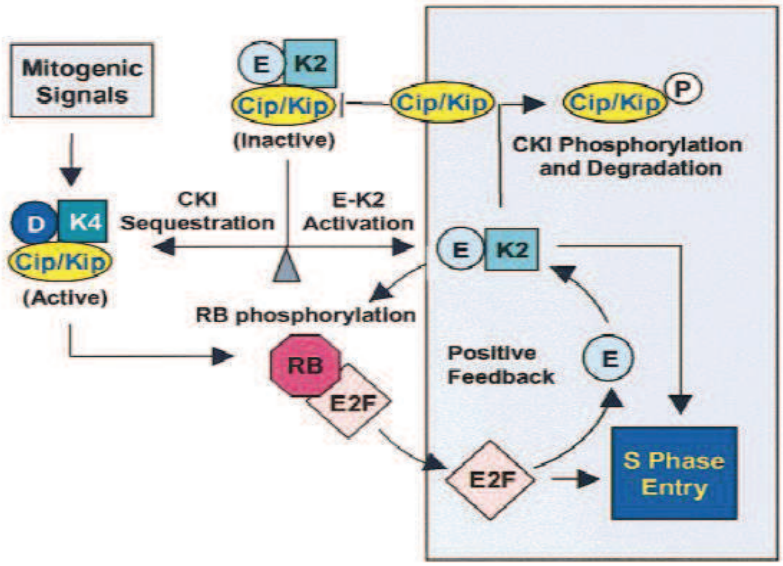

Figure 15: Regulation of CDK4/cyclin D and CDK2/cyclin E by Cip/Kip proteins (from (Sherr and Roberts, 1999)). Mitogenic signals promote the assembly of active CDK4-6/cyclin D complexes with a Cip or Kip protein. Sequestration of Cip/Kip proteins lowers the inhibitory threshold and facilitates activation of the CDK2/cyclin E complex. The cyclin D- and E-dependent kinases contribute sequentially to Rb phosphorylation, canceling its ability to repress E2F family members and activating genes required for entry into S phase.

Recently, it has been demonstrated that Cip/Kip proteins also play a role in transcriptional regulation of genes repressed by p130/E2F4 complexes by recruiting and regulating the activity of specific CDK/cyclin complexes on the promoters (Orlando et al., 2015). It is well-known that, during the G1 phase of the cell cycle, sequential phosphorylation of p130 by CDKs disrupts p130/E2F4 complexes allowing gene expression. Orlando and collaborators have demonstrated that, in early and mid G1, p27 recruits CDK4/cyclin D2-D3 complexes on the promoters by its amino terminal domain; and in late G1, these complexes are substituted by p21/cyclin D1/CDK2. In cells lacking p27, CDK4/cyclin D2-D3 do not associate to the promoters and phosphorylation of p130 and transcription of target genes is increased. In p21 null cells, CDK2/cyclin D1 are not found on the promoters and transcription is elevated.

2.8. Expression, degradation and subcellular localization

Regarding D-type cyclin expression, it has been demonstrated that, in Swiss 3T3 cells, different mitogenic stimuli could induce disparate responses in cyclin D1 and cyclin D3 expression (Anderson et al., 2010). Indeed, activation of the PI3K/AKT/mTOR pathway results in generation of active cyclin D3 whereas activation of the Ras/Raf/MEK/ERK pathway leads to cyclin D1 transcription.

Upon activation of these pathways, D-cyclins are synthesized in the cytoplasm by ribosomes and then associate with CDK4 which is, like other CDKs, believed to be continuously expressed. Two transcription factors are involved in CDK4 expression. The first one is the zinc finger-homeodomain transcription factor, δ-crystallin enhancer factor 1 (δEF1), which has been shown to upregulate CDK4 transcription via the E2-box element on the CDK4 promoter (Hu et al., 2014). The second one is the proto-oncogene c-MYC which has been found to induce a rapid increase in CDK4 mRNA levels through four highly conserved c-MYC binding sites within the *CDK4* promoter (Hermeking et al., 2000). In *c-Myc*-deficient cells, serum-stimulated induction of *CDK4* mRNA is attenuated and delayed. These cells exhibit an extension of their G1 and G2 phases, leading to an increase in cell-doubling time from 18 h to 50 h.

Once assembled, the CDK4/cyclin D complex shuttles from the cytoplasm into the nucleus, thanks to Cip/Kip proteins, to phosphorylate its nuclear substrate Rb (Bockstaele et al., 2006; LaBaer et al., 1997).

Cyclin D1 is an unstable protein with a short half-life of 24 min (Alao, 2007; Diehl et al., 1998). Cyclin D1 is mainly degraded in the cytoplasm via the 26S proteasome in an ubiquitin-dependent manner (Alao, 2007). This mechanism involves cyclin D1 phosphorylation on Thr286 residue by GSK3β (glycogen synthase kinase 3β), which promotes relocation of cyclin D1 in the cytoplasm through association with the nuclear exportin CRM1 (Chromosome Region Maintenance 1) (Diehl et al., 1998). Indeed, this phosphorylation induces a conformational change in cyclin D1 that exposes a nuclear export sequence (NES) (residues 290 – 295) that is recognized by CRM1 (Alt et al., 2000; Benzeno and Diehl, 2004; Moore, 2013).

2.9. Structural and mechanistic features of CDK4/cyclin D

2.9.1. Assembly and activation of CDK4/cyclin D

In its monomeric conformation, CDK4, like other mammalian CDKs, is inactive. CDK4 activation requires first the binding with its regulatory subunit cyclin D.

The mechanism of assembly is believed to be similar for the different CDK/cyclin complexes. However, some elements of specificity induce differences in substrate recognition and in biological and physiological functions. The comparison of CDK2/cyclin A and CDK4/cyclin D crystal structures indicate that the interaction between the PISTVRE helix of CDK4 and the α5 helix of cyclin D is conserved whereas interactions between the C-terminal lobe of CDK4 and cyclin D are not (Figure 16) (Day et al., 2009; Lolli, 2010; Takaki et al., 2009). CDK2/cyclin A displays a "closed" conformation in contrast to the "open" conformation of CDK4/cyclin D. Moreover, it has been demonstrated that CDK4, although bound to cyclin D1 and phosphorylated on Thr172, is in an inactive conformation (Day et al., 2009). It was therefore suggested that substrate binding and association with Cip/Kip proteins might induce a closed conformation and favor complete activation (Day et al., 2009; Takaki et al., 2009). However, a recent study based on molecular dynamics with excited normal modes suggests that a closed conformation may exist in CDK4/cyclin D1, resembling that of CDK2/cyclin A (Floquet et al., 2015).

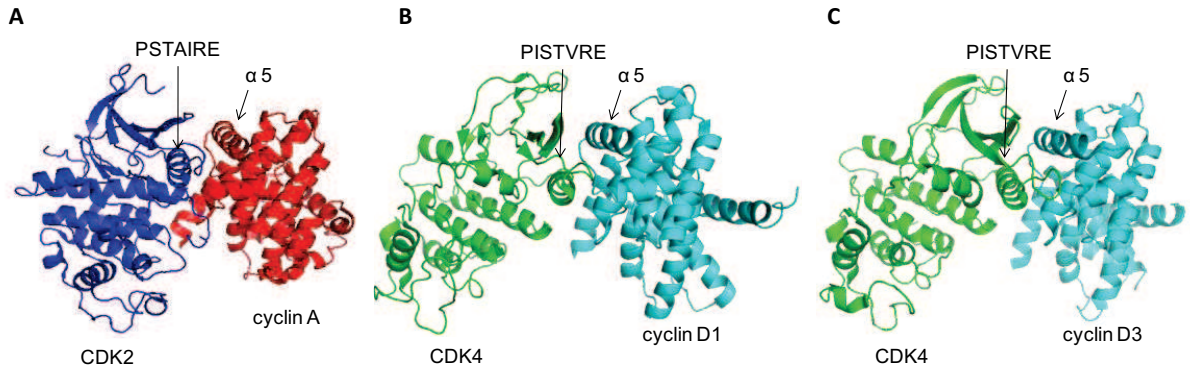

Figure 16: Representation of CDK2/cyclin A (PDB 1QMZ), CDK4/cyclin D1 (PDB 2W99) and CDK4/cyclin D3 (PDB 3G33) crystal structures.

2.9.2. Rb binding

The sequence of Rb can be divided in four domains, the N- and C-termini and the pocket A and B domains. Numerous studies have demonstrated that the Rb protein interacts with the LXCXE motif present in transcription factors and in some cyclins through its B domain (Lee et al., 1998). More recently, a site within the C-terminal domain of Rb (amino acids 893 to 910) was found to be required for cyclin D1-CDK4-dependent phosphorylation of Rb both *in vitro* and in cells (Wallace and Ball, 2004).

2.10. CDK4/cyclin D deregulation in cancers

Deregulation of the $p16^{INK4a}$ / CDK4/6-cyclin D / pRb pathway is one of the most frequent events in cancers, suggesting that inhibition of CDK4 activity constitutes a relevant therapeutic target for cancer therapy (Musgrove et al., 2011; Sherr, 1996). Figure 17 illustrates the genetic alterations found for the different components of this pathway.

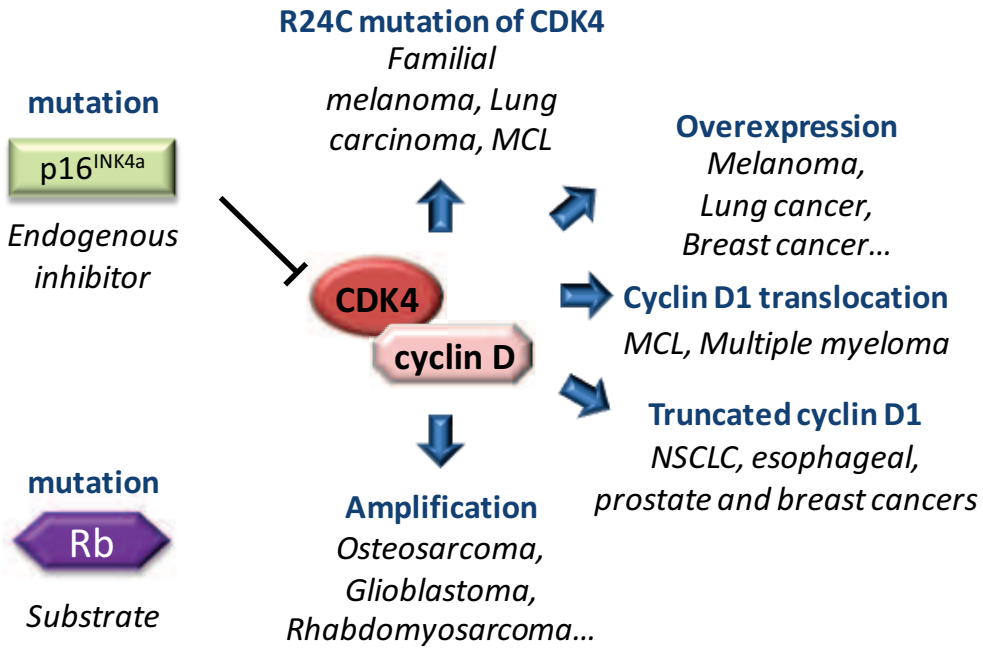

Figure 17: Deregulation of CDK4/cyclin D activity in human cancers associated with R24C mutation of CDK4, mutation of $p16^{INK4a}$ or Rb, overexpression or amplification of CDK4 or cyclin D

Genetic inactivation of $p16^{INK4a}$, inhibitor of CDK4/cyclin D, constitutes one of the most frequent mutations in human cancers (Rocco and Sidransky, 2001). Inactivation of $p16^{INK4a}$ gene by deletion, mutation or hypermethylation, results in a defective inhibition of CDK4 which leads to a deregulated activity (Brown et al., 2004; Kawaguchi et al., 2003; Pinyol et al., 1998; Xing et al., 1999).

The loss of Rb protein function by phosphorylation, mutation or viral oncoprotein binding leads to a malignant phenotype (Giacinti and Giordano, 2006). Indeed, as a direct consequence of this loss of function, E2F transcription factors are released, thus inducing a cell cycle deregulation. This genetic alteration is observed in a variety of human tumors, including retinoblastoma, osteosarcoma and small-cell lung carcinoma (Horowitz et al., 1990).

The CDK4 R24C point mutation causes loss of CDK4 binding to $p16^{INK4a}$, and consequently leads to constitutive activation of CDK4 (Wölfel et al., 1995). This mutation has been identified in several cancers including familial melanoma and lung cancers (Chawla et al., 2010; Puyol et al., 2010; Sotillo et al., 2001a). It has been also described that mice harboring c-*myc*-3'RR/$CDK4^{R24C}$ and c-*myc*-3'RR/$p53^{+/-}$ phenotypes spontaneously develop B lymphomas, demonstrating a role of CDK4 in the development of lymphomas (Fiancette et al., 2011; Vincent-Fabert et al., 2012). In a high percentage of liposarcomas and neuroblastic tumours, CDK4 gene is also found to be amplified (Easton et al., 1998; Tos et al., 2000).

Cyclin D1 amplification is observed in 5-30% of NSCLC (Non Small Cell Lung Cancer). In 18-76% of these cancers, high expression of cyclin D1 has been reported and correlates with a poor prognostic for patients (Gautschi et al., 2007; Musgrove et al., 2011). In lung cancer, CDK4 or cyclin D overexpression induces apoptosis in cultured cells with normal Rb protein (Dobashi et al., 2004). Moreover, NSCLC mediated by KRAS are particularly dependent on CDK4, and targeting this kinase has been proposed as therapeutic strategy for this type of cancer which resists to conventional therapies because of the lethal interaction between ablation/inhibition of CDK4 and KRAS (Puyol et al., 2010).

High levels of cyclin D1 are also frequently encountered in breast cancers either through genetic amplification or overexpression (Gillett et al., 1994). In neuroblastoma, genetic aberrations of cyclin D1, including overexpression, have also been reported (Molenaar et al., 2012). In mantle cell lymphoma, cyclin D1 is translocated to the IgH promoter (hallmark aberration). These translocations are also found in multiple myelomas (Chesi et al., 1996).

Table 3 summarizes the deregulations of CDK4 and cyclin D identified in human cancers.

CDK4	Amplification	refractory rhabdomyosarcoma, osteosarcoma, glioblastoma	(Park et al., 2014; Schmidt et al., 1994; Wei et al., 1999)
	Overexpression	melanoma	(Smalley et al., 2008)
		lung cancer	(Dobashi et al., 2004)
	Amplification /Overexpression	osteosarcoma, sporadic breast carcinoma, uterine cervix cancer	(An et al., 1999; Cheung et al., 2001; Wunder et al., 1999)
	R24C mutation	familial melanoma	(Chawla et al., 2010; Sheppard and McArthur, 2013; Sotillo et al., 2001a, 2001b, 2005; Tsao et al., 2012; Vidwans et al., 2011; Wölfel et al., 1995; Zuo et al., 1996)
		lung carcinoma	(Puyol et al., 2010)
		mantle cell lymphoma	(Vincent-Fabert et al., 2012)
	38 simple coding mutation / 25 missense mutations / 12 synonymous mutations	wide variety of cancer tissues	COSMIC database http://www.sanger.ac.uk/genetics/CGP/cosmic/
Cyclin D	Overexpression	follicular mantle cell lymphoma, lung cancer, breast cancer, head and neck, esophageal cancer	(Kim and Diehl, 2009)
		colorectal adenocarcinomas	(Seong et al., 1999)
		lung cancer	(Dobashi et al., 2004)

		pancreatic cancer	(Gansauge et al., 1997)
		endometrial carcinoma	(Moreno-Bueno et al., 2004)
	Amplification /overexpression	head and neck carcinoma	(Akervall et al., 1997; Meredith et al., 1995; Michalides et al., 1997)
	IGH translocation and overexpression	multiple myeloma	(Bergsagel and Kuehl, 2005; Chesi et al., 1996)
		mantle cell lymphoma	(Bertoni et al., 2006; Li et al., 1999)
	Mutation that disrupts phosphorylation-dependent nuclear export	esophageal cancer	(Benzeno et al., 2006)
	Truncated form (cyclin D1b) (A870G polymorphism) / Nuclear Accumulation	NSCLC	(Betticher et al., 1995; Gautschi et al., 2007; Li et al., 2008)
		esophageal and prostate cancer	(Burd et al., 2006; Knudsen et al., 2006)
		prostate cancer	(Comstock et al., 2009)
		breast cancer	(Millar et al., 2009)
	Truncated form (cyclin D1b) and its co-expression with cyclin D1a	breast cancer	(Abramson et al., 2010)
	cyclin D1a isoforms with truncated 3' UTRs, not alternatively spliced cyclin D1b mRNA	mantle cell lymphoma	(Wiestner et al., 2007)

	isoforms / alterations of *CCND1* 3' UTR structure		

Table 3 : CDK4 and cyclin D aberrations associated with cancer (from (Peyressatre et al., 2015))

2.11. CDK4/cyclin D in melanoma

Malignant melanoma, which arises from deregulated proliferation of melanocytes, is one of the most aggressive malignancies in humans and is responsible for 60–80% of deaths from skin cancers (Bandarchi et al., 2010). In the European Union, among all cancers, melanoma is placed seventh in terms of incidence (Figure 18).

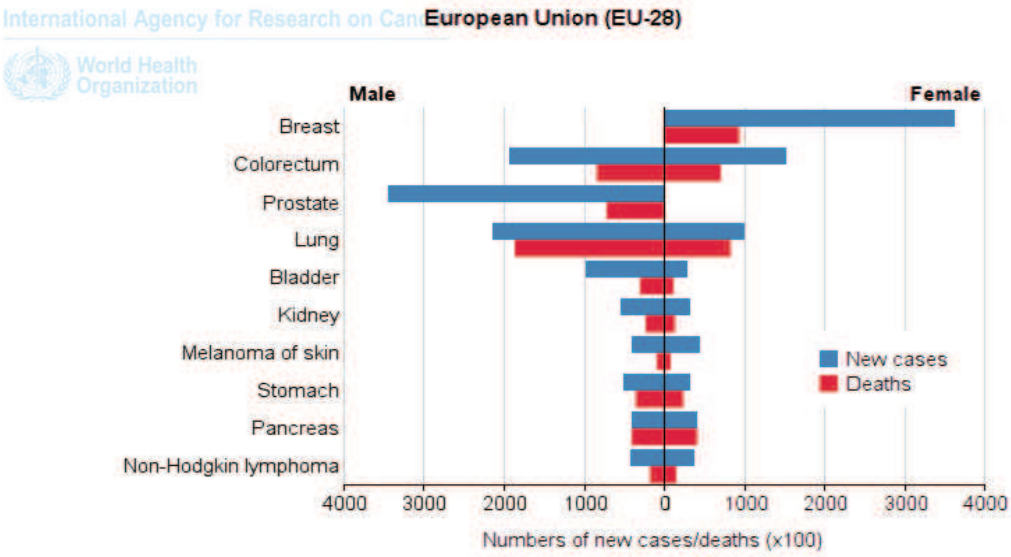

Figure 18: Incidence and mortality of cancers in the European Union (from http://globocan.iarc.fr/)

One of the most significant risk factors for melanoma is a family history of the disease. It is estimated that approximately 10% of melanoma cases report a first- or second-degree relative with melanoma (Hayward, 2003). Moreover, sun exposure has been shown to be a leading risk factor for melanoma (Garibyan and Fisher, 2010).

Melanomas are classified in 4 subtypes, according to their whole-exome sequencing and their significant mutated genes (Cancer Genome Atlas Network, 2015):

- the BRAF subtype which is the largest genomic subtype (52% of samples), defined by the presence of *BRAF* hot-spot mutations

- the RAS subtype which represents the second major subtype (28% of samples), defined by the presence of *RAS* hot-spot mutations

- the NF1 subtype which presents mutations of *NF1* (Neurofibromin 1) (14% of samples)

- the triple Wild-Type Subtype which is characterized by a lack of hot-spot *BRAF*, *N/H/KRAS*, or *NF1* mutations.

Recently, analysis of a whole-exome sequencing data from 121 melanoma tumor/normal pairs enabled the discovery of six novel genes (*PPP6C*, *RAC1*, *SNX31*, *TACC1*, *STK19* and *ARID2*) as potential drivers in melanoma (Hodis et al., 2012).

2.11.1. Detection of melanomas

To detect this aggressive cancer, a wide panel of suitable serologic and immunohistochemical biomarkers has been described (Utikal et al., 2007). The most widely used serological biomarker molecules are the melanocyte lineage/differentiation antigens S100-beta and melanoma inhibitory activity (MIA). They serve for early detection of metastasis or tumor relapse since their serum concentrations strongly correlate with patients' tumour load. Some pro-angiogenic factors such as VEGF (Vascular Endothelial Growth Factor), cytokines like interleukin-6 (IL-6), HLA molecules or other molecules like LDH (Lactate Deshydrogenase) are also used as biomarkers of malignant melanoma (Utikal et al., 2007). Besides these serum markers, several immunohistochemical markers have also been reported for the detection of malignant melanoma including tumour suppressors, such as $p16^{INK4a}$ or pRb, or cell cycle associated proteins such as cyclin D.

2.11.2. Most common treatment options for melanoma

To treat this cancer, several factors have to be considered including the thickness of the primary melanoma, the rate of melanoma growth, the presence of specific genetic changes in melanoma cells, and also the stage of the melanoma. Earlier stages are often rather easy to treat by surgery. However, stage IV which corresponds to metastatic melanoma is incurable. Immunotherapy such as Ipilimumab which targets the immune system and targeted drugs like Vemurafenib which targets BRAF mutants have shown to be efficient for this stage (Banaszynski and Kolesar, 2013). Indeed,

selective BRAF inhibitors including Vemurafenib and Dabrafenib achieved significant response rates (~50%) in clinical trials and were recently granted by the FDA for the treatment of malignant BRAF V600E/K melanomas (Hertzman Johansson and Egyhazi Brage, 2014). However, a significant number of these patients demonstrate intrinsic resistance and do not respond to BRAF inhibitors, and the majority of patients who initially respond acquire drug resistance and relapse within 6–12 months (Chapman et al., 2011; Long et al., 2012). Hence, new therapeutics targeting different pathways are still actively sought for the development of more targeted and more efficient treatments.

2.11.3. CDK4/cyclin D : an established biomarker for melanoma

The $p16^{INK4a}$ / CDK4/6-cyclin D / pRb pathway is deregulated in 90% of melanomas. In human and mouse melanoma models, activation of this pathway is tightly related to BRAF and NRAS mutant in melanocyte transformation. RAS/RAF/MEK/ERK pathway is deregulated in 65-90% of metastatic melanomas, increasing more the $p16^{INK4a}$ / CDK4/6-cyclin D / pRb pathway and therefore cyclin D1 expression (Chawla et al., 2010; Chin et al., 2006).

The importance of CDK4 protein in cancers has especially been described following the identification of the R24C mutation in the CDK4 locus which predisposes to melanoma (Wölfel et al., 1995; Zuo et al., 1996). However, a weak incidence of spontaneous melanomas has been demonstrated in $CDK4^{R24C/R24C}$ mice. An increased incidence of spontaneous melanomas occurs in mice expressing the HRAS (G12V) oncogene in melanocytes, in a R24C context (Chawla et al., 2010).

The risk of developing melanomas is also enhanced by CDK4/cyclin D hyperactivation due to cyclin D amplification (18% of melanomas) or loss of $p16^{INK4a}$ (deletion of *CDKN2A* in 50-60% of metastatic tumors) (Tsao et al., 2012).

Thus, this kinase constitutes a key biomarker for the diagnostic of melanomas and a relevant therapeutic target (Sheppard and McArthur, 2013).

3. Inhibitors of CDK/cyclins

3.1. ATP-competitive compounds

For a long time, plant extracts have been used to treat cancer (Mann, 2002). Indeed, the American Indians used, for example, extracts from the roots of may apple, *Podophyllum peltatum*, as an effective treatment for skin cancers. This medicine led to identification of a group of anticancer agents known as the podophyllins, which include etoposide and teniposide, two topoisomerase inhibitors. Other anti-cancer products have been extracted from natural sources including bacteria, fungi, marine sponges and plants, such as olomoucine, staurosporine, butyrolactone, flavopiridol, meridianin, variolin, hymenialdisine and indirubin (Mann, 2002; Peyressatre et al., 2015). The determination of their molecular nature as purine and pyrimidine analogues enabled a better understanding of their inhibitory potential (Gray et al., 1998; Noble et al., 2005). These molecules were classified as ATP-competitive compounds meaning they could bind the ATP binding site thereby inhibiting kinase activity through competition with ATP (Figure 19A). Because toxic side-effects and limited selectivity arise with this first generation of compounds, a second generation of synthetic ATP-competitive drugs harboring less toxicity and greater efficacy were developed such as RO3306, Dinaciclib, PD-0332991 and AT7519 (Table 4) (Malumbres et al., 2008; Sausville, 2002).

3.2. Non ATP-competitive inhibitors

Although some of these ATP-competitive compounds are undergoing clinical trials and offer promising results for cancer therapy, issues such as lack of efficacy, limited selectivity and emergence of acquired drug resistance are frequently associated with these inhibitors (Fang et al., 2013). Indeed, the 518 members of the human kinome bear a conserved ATP pocket and it is therefore quite difficult to be specific for one kinase in particular by targeting this binding site. Hence, alternative approaches that do not target the ATP pocket have been investigated to inhibit CDK/cyclin activity. These strategies involve targeting protein/protein interfaces, hydrophobic pockets distinct from the ATP-binding pocket, which are exposed only in inactive intermediates, or allosteric sites (Cohen and Alessi, 2013; Fang et al., 2013; Liu and Gray, 2006; Pommier and Cherfils, 2005).

Peptides targeting protein-protein interfaces (Figure 19B) (Table 4)

To inhibit CDK/cyclin activity, an alternative approach consists in interfering with substrate recognition or by targeting crucial protein-protein interfaces (PPI). PPI are essential for the assembly of the complex. Indeed, the dynamic interactions between the two sub-units enable stabilization or modulation of both the conformation and the catalytic function of the complex. Identification of such compounds is often led by high throughput screening of small molecule libraries or by rational design of peptides mimicking the interfaces (Arkin and Wells, 2004). This approach has been successfully used to target different multimeric and multiprotein complexes, such as p53/MDM2 complex (Chène, 2004). Several peptide inhibitors have been designed to target PPIs between CDKs and substrates, between CDKs and cyclins and between CDK/cyclins and p21/p27/p107 proteins that target the cyclin-binding groove (Abate et al., 2013; Cirillo et al., 2011; Esposito et al., 2013; Gondeau et al., 2005; Orzáez et al., 2009).

Small Molecule non-ATP competitive Inhibitors—Allosteric Inhibitors (Figure 19C) (Table 4)

Recent efforts to target CDK/cyclins have been invested in the development of compounds which do not compete with ATP, and allosteric inhibitors that bind sites which are not conserved across the kinome (Eglen and Reisine, 2010). Allosteric sites are only accessible in specific conformations. Thus, inhibitors bind and stabilize kinases in an inactive conformation and prevent transition through an active state. They are therefore expected to exhibit superior selectivity profiles (Cohen and Alessi, 2013; Eglen and Reisine, 2010; Fang et al., 2013; Liu and Gray, 2006; Zhang et al., 2009). This class of compounds is not simple to design rationally and requires identification of hydrophobic pockets distinct from the ATP-binding pocket, which are only exposed in inactive intermediates; or identification of allosteric sites. Identification of such compounds is therefore often performed by high throughput screening following identification of an allosteric site (Jahnke et al., 2005; Lebakken et al., 2012; Liu and Gray, 2006; Prével et al., 2014b).

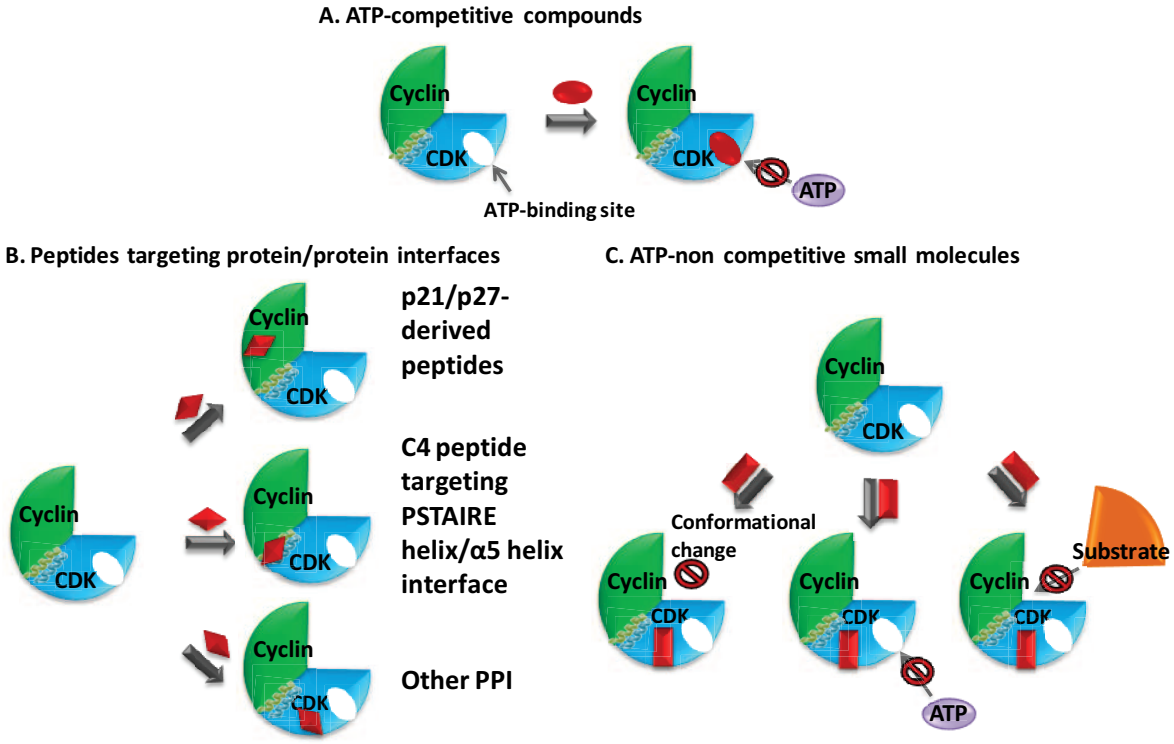

Figure 19: Strategies for targeting cyclin-dependent kinases (from (Peyressatre et al., 2015)).

(A) ATP-competitive inhibitors. They bind the ATP pocket and compete with ATP binding.

(B) Protein-protein interface inhibitors. They target essential and specific protein/protein interactions either between CDKs and cyclins, or between CDK/cyclins and p21/p27/p107 proteins-targeting the cyclin-binding groove. The second example represents an inhibitor, C4 peptide, which targets the primary interface between CDK2 and cyclin A (more precisely between the "PSTAIRE" helix of CDK2 and alpha 5 helix of cyclin A) (Gondeau et al., 2005).

(C) Non ATP-competitive small molecules. They prevent ATP binding by targeting sites which are remote from the ATP pocket, so as to stabilize enzymatically inactive conformations or interfere with conformational transitions associated with kinase activation, compete with substrate or ATP binding.

Inhibitor	Target	References
ATP-competitive inhibitors		
Roscovitine (purine)	CDK5, CDK2, CDK1, CDK7, CDK9	(De Azevedo et al., 1997; Bach et al., 2005; Bettayeb et al., 2008; Chang et al., 1999; Demange et al., 2013)
Staurosporine (alkaloid)	CDK1, CDK2, CDK4	(Gadbois et al., 1992; Tamaoki

		et al., 1986)
Olomoucine (purine)	CDK1, CDK2, CDK5	(Glab et al., 1994)
Butyrolactone I	CDK1 > CDK2	(Kitagawa et al., 1993)
Flavopiridol	CDK2, CDK4, CDK6, CDK9	(Christian et al., 2007; König et al., 1997; Lin et al., 2009b; Losiewicz et al., 1994; Patel et al., 1998)
Indirubin-5 (purine)	CDK1 > CDK2 > CDK5	(Hoessel et al., 1999)
PD-0322991 (Palbociclib)	CDK4, CDK6	(Cen et al., 2012; Fry et al., 2004; Guha, 2013; Toogood et al., 2005)
Dinaciclib	CDK1, CDK2, CDK5, CDK9	(Feldmann et al., 2011; Parry et al., 2010; Paruch et al., 2010)
AT7519	CDK2, CDK4, CDK5, CDK7, CDK9	(Mahadevan et al., 2011; Santo et al., 2010; Squires et al., 2009, 2010; Wyatt et al., 2008)
Peptide inhibitors targeting protein/protein interfaces		
Interface peptide	CDK2/cyclin A	(Mendoza et al., 2003)
C4 peptide derived from cyclin A	CDK2/cyclin A	(Gondeau et al., 2005)
Hexapeptide - targets cyclin A surface pocket	CDK2/cyclin A	(Canela et al., 2006)
Spa310 and derivative from p130/pRb spacer domain	CDK2/cyclin A	(Bagella et al., 2007; Giordano et al., 2007)

CDK4 derived C-terminal hexapeptide	CDK4/cyclin D	(Warenius et al., 2011)
Interface peptides derived from p35	CDK5/p35	(Chin et al., 1999; Shukla et al., 2013; Sundaram et al., 2013; Zheng et al., 2002, 2005, 2010)
Small molecule non-ATP competitive/allosteric inhibitors		
CPD1 3alpha-amino-5alpha androstane	CDK5/p25	(Corbel et al., 2011; Zhang et al., 2011)
Allosteric pocket in CDK2/Cyclin A/p27	CDK2/cyclin A/p27	(Corsino et al., 2009)
Chrysin-derivative - allosteric site	CDK2 and CDK4/CDK6	(Liu et al., 2013)

Table 4: CDK inhibitors

3.3. CDK4/cyclin D inhibitors

As CDK4/cyclin D is a relevant target for anticancer therapy, many efforts have been made to identify new and specific inhibitors of this kinase.

3.3.1. ATP-competitive inhibitors

In 2000, Barvian and co-workers found that pyrido[2,3-d]pyrimidin-7-one compounds were potent inhibitors of CDK/cyclins (Barvian et al., 2000) (Figure 20A). Through screening of a chemical compound library, they identified some hits which display modest selectivity for CDK4 versus other kinases. Chemical modifications of the original template led to identification of PD 0183812, as a potent and highly selective ATP competitive inhibitor of CDK4 and CDK6 kinase activity. Rb positive cell lines demonstrated a G1 arrest when treated with PD 0183812 and a reversible block in proliferation (Fry et al., 2001) (Figure 20B).

Based on the recent demonstration that modification of the C2-side chain to a 2-aminopyridine provided inhibitors with exquisite selectivity for CDK4/6 *in vitro* and *in cellulo*, compound 43 (PD-0332991) was identified as a drug candidate for the treatment of cancer (Toogood et al., 2005).

PD-0332991 (now called Palbociclib) is an orally active, highly selective inhibitor of CDK4-6/cyclin D that blocks retinoblastoma (Rb) phosphorylation in the low nanomolar range (IC_{50} = 11 nM) and CDK6

(IC_{50} = 16 nM) (Figure 21). It has no activity against a panel of 36 additional tyrosine and serine/threonine kinases. It is a potent antiproliferative agent against retinoblastoma (Rb)-positive tumor cells *in vitro*, inducing an exclusive G1 arrest, with a concomitant reduction of phospho-Ser780/Ser795 on the Rb protein (Fry et al., 2004). PD-0332991 inhibits MDA-MB-435 breast carcinoma cell proliferation with an IC_{50} of 0.16 µM. A similar value was found for Colo-205 colon carcinoma cell line (0.13 µM). *In vivo*, the therapeutically active doses of PD-0332991 administrated *per os* in mice were 12.5, 37.5, 75 and 150 mg/kg.

Another inhibitor called 8-cyclopentyl-2-[4-(4-methyl-piperazin-1-yl)-phenylamino]-7-oxo-7,8-dihydro-pyrido[2,3-d]pyrimidine-6-carbonitrile (7x) was found to be a potent multikinase inhibitor with potent inhibitory activity against the CDK4/cyclin D1 and ARK5 kinases, inducing apoptosis of tumor cells at a concentration of approximately 30-100 nM (Reddy et al., 2014).

Highly selective CDK4 inhibitors have also been identified by modifying a 2-aminoquinazoline scaffold (Bathini et al., 2005) (Figure 20C).

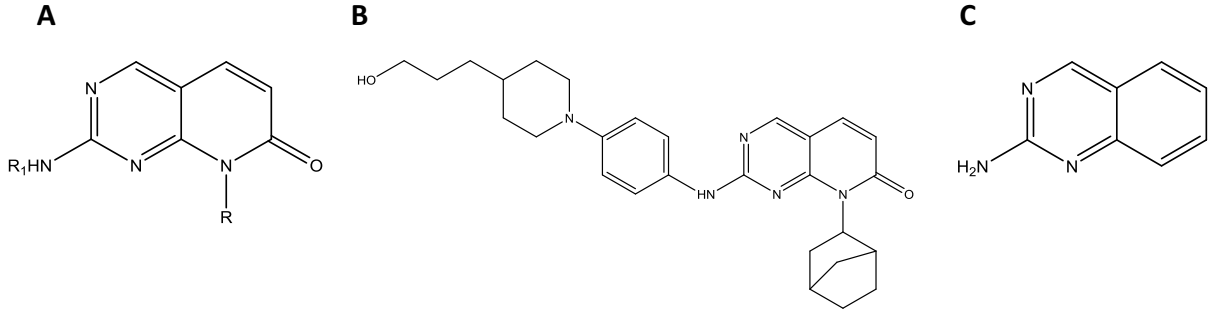

Figure 20: Chemical structure scaffolds which led to the development of CDK4/cyclin D inhibitors

(A) pyrido[2,3-d]pyrimidin-7-one scaffold (Barvian et al., 2000)

(B) Chemical structure of PD 0183812 (Fry et al., 2001)

(C) 2-aminoquinazoline scaffold (Bathini et al., 2005)

Currently, three inhibitors which compete with ATP are currently in clinical trials (Asghar et al., 2015; Dickson, 2014; VanArsdale et al., 2015) (Figure 21). Palbociclib has recently been approved by the FDA to treat ER^+ (HER2-negative) metastatic breast cancer in combination with letrozole, an

aromatase inhibitor (VanArsdale et al., 2015). It is also currently tested for liposarcoma and mantle cell lymphoma in phase II or III.

In vitro studies have demonstrated that another CDK4 inhibitor, Ribociclib (also called LEE011 (Novartis)), caused G1 arrest and had antitumor activity in several models, including melanoma with BRAF or NRAS mutation, breast cancer and neuroblastoma (Infante et al., 2013; Kim et al., 2013; Rader et al., 2013). Ribociclib inhibits CDK4 and CDK6 with an IC_{50} of 10 nM and 39 nM, respectively. *In cellulo* studies have demonstrated that the growth of 12 of 17 neuroblastoma cell lines was significantly impaired in response to CDK4/6 inhibition with LEE011 (mean IC_{50}= 30 +/- 68 nM, sensitive lines only) (Rader et al., 2013).

A third CDK4 inhibitor, Abemaciclib (LY2835219 developed by Ely Lilly) is also currently tested in phase I for NSCLC and hormone receptor-positive metastatic breast cancer (Asghar et al., 2015). Abemaciclib inhibits CDK4 and CDK6 with IC_{50} values of 2 nM and 10 nM, respectively. The proliferation of MDA-MB-361, a breast cancer cell line, was reduced by 50% when treated with LY2835219 at 90 +/- 31 nM (Gelbert et al., 2014). Interestingly, this compound has been shown to cross the blood-brain barrier and could therefore be potently used for treating brain cancers (Sanchez-Martinez et al., 2011). Indeed, the $p16^{INK4a}$ / CDK4/6-cyclin D / pRb pathway is commonly altered in glioblastoma multiforme (GBM), mostly by homozygous deletion of *CDKN2A/B*, genes which code for $p16^{INK4a}$ and $p15^{INK4b}$ respectively (He et al., 1995; Jen et al., 1994; Ueki et al., 1996).

The principle adverse event of these three inhibitors is neutropenia which is probably a result of transient growth arrest in hematopoietic precursor cells (Roberts et al., 2012).

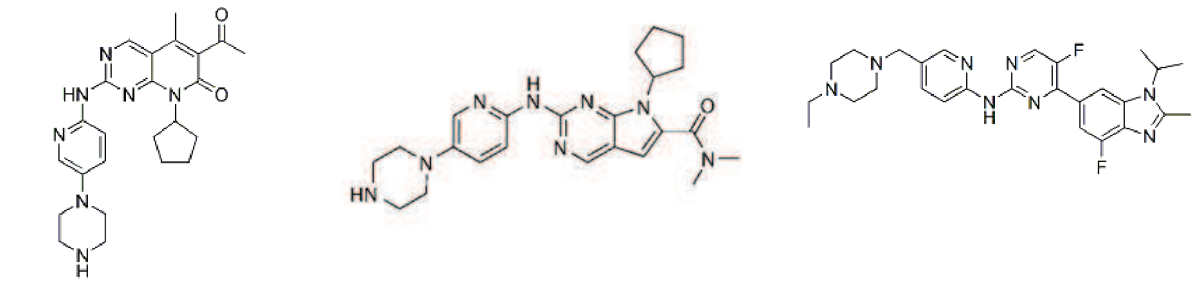

Palbociclib (PD-0332991) Ribociclib (LEE011) Abemaciclib (LY2835219)

Figure 21: Structures of ATP-competitive CDK4/6 inhibitors

3.3.2. Non ATP-competitive inhibitors

Regarding non-ATP competitive strategies, Warenius and coworkers have targeted a non-kinase domain of CDK4. A hexapeptide deriving from a C-terminal loop outside the kinase domain of CDK4 and its cyclic derivatives, used at 200 µM, proved to be efficient in killing several cancer cell lines whilst sparing keratinocytes and fibroblasts (Figure 22) (Warenius et al., 2011).

Chemopreventive properties of Chrysin (5,7-dihydroxyflavone), a natural flavonoid widely distributed in plants, have been reported against various cancers. A chrysin derivative, referred to as compound 69407, was found to be an efficient ATP-non competitive inhibitor of CDK2 and CDK4 that binds an allosteric pocket in these kinases (Figure 22) (Liu et al., 2013). Results of *in vitro* kinase assays indicated that it inhibited CDK2 and CDK4 kinase activities with IC_{50} values of 8.3 and 8.4 µM, respectively. This compound attenuated cell cycle progression of EGF-stimulated cells at the G1 phase and inhibited the G1/S transition, causing loss of retinoblastoma phosphorylation by CDK4/6 and CDK2. It also reduced tumor growth in a mouse xenograft model of human epidermoid carcinoma (A431 cells).

Besides targeting CDK4, some efforts have been invested to target cyclin D. For instance, Tiemann and collaborators have downregulated *CCND1* and *CCND2* expression in two mantle cell lymphoma (MCL) cell lines with siRNAs to investigate the cytotoxic effect of combining siRNAs with conventional chemotherapeutic agents (Tiemann et al., 2011). They have demonstrated that siRNAs targeting cyclin D1 and cyclin D2 enhance the cytotoxicity of chemotherapeutic agents (etoposide and doxorubicin) in MCL cell lines. The reduction in cyclin D expression by siRNAs resulted in decreased IC_{50} values for both doxorubicin and etoposide. This study highlights the fact that, combination of siRNA-mediated inhibition of the D-cyclins, along with chemotherapeutic agents, could potentially be used to lower the effective doses of the chemotherapeutic agents and reduce drug-related toxicities.

Figure 22 summarizes the different strategies developed to inhibit CDK4/cyclin D activity.

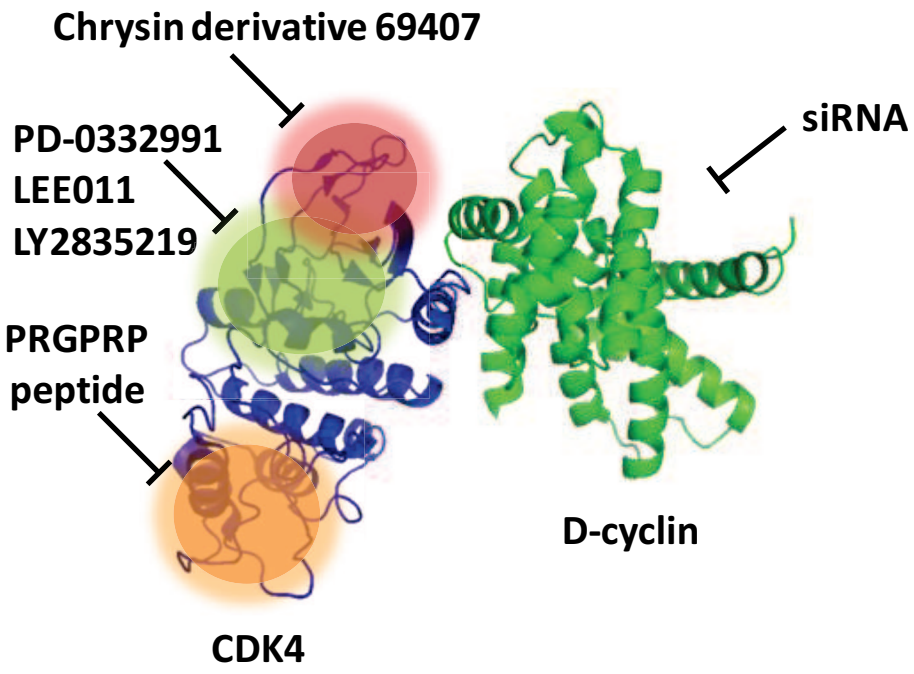

Figure 22: Inhibitors of CDK4/cyclin D.

CDK4 targeting: three ATP-competitive inhibitors targeting the ATP binding site, PD-0332991 (Palbociclib), LEE011 (Ribociclib) and LY2835219 (Abemaciclib) (Asghar et al., 2015; Dickson, 2014; VanArsdale et al., 2015); a hexapeptide PRGPRP (Warenius et al., 2011); and a chrysin derivative 69407 (Liu et al., 2013)

D-cyclin targeting: downregulation of *CCND1* and *CCND2* expression by siRNAs (Tiemann et al., 2011)

4. Fluorescent biosensors for probing protein kinase activity

4.1. Concepts around fluorescent biosensors

4.1.1. Definition of a biosensor

Biosensors can be defined as tools which combine a biological or biomimetic element that can probe a specific target, with a physicochemical transducer which converts the recognition event into a detectable and measurable analytical signal (Lee, 2008) (Figure 23). They allow to monitor target proteins in a sensitive, robust, quantitative and reproducible fashion, and respond to target changes in a dynamic and reversible fashion.

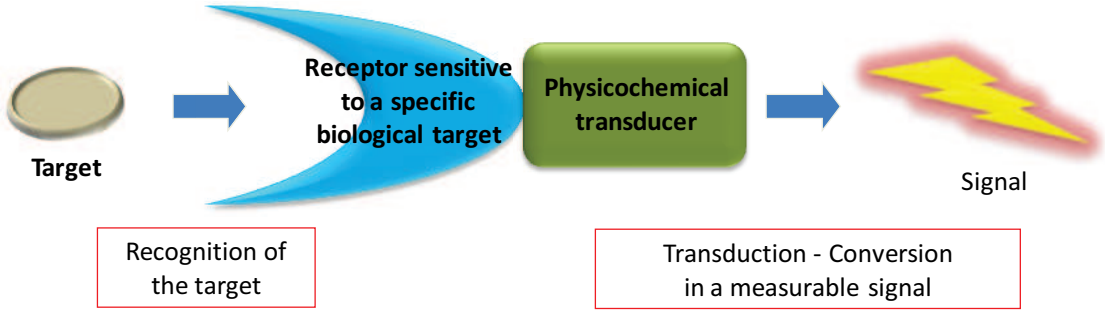

Figure 23: Schematic representation of a biosensor. It combines a receptor, sensitive to a specific biological target, and a physicochemical transducer.

In 1962, Clark and Lyons were the first to describe the concept of biosensors with their work on electrodes for monitoring glucose concentrations in the blood of patients (Clark and Lyons, 1962).

Since then, the development of eletrochemical, electronic and microbial biosensors has enabled the detection of ions, small molecules, proteins or DNA (Sokolov et al., 2009; Su et al., 2011; Turner, 2013). A wide variety of optical biosensors have also been developed. In optical biosensor technology, the main used biological materials are the optocouple enzyme/substrate, antibody/antigen, and nucleic acids/complementary sequences (Dey and Goswami, 2011). The mechanism of detection of many optical biosensors is based on the phenomenon of Surface Plasmon Resonance (SPR). Binding of a target analyte to a receptor on the surface of thin layer of gold (or other materials) leads to changes in the local index of refraction, inducing a change in the resonance conditions of the surface. Indeed, a thin layer of gold on a high refractive index glass surface can absorb laser light, producing electron waves (surface plasmons) on the gold surface. This phenomenon occurs only at a specific incident angle and wavelength and highly depends on the surface of the gold. Hence, binding of a target to a receptor on the gold surface produces a detectable and measurable signal. Several model membrane systems have been developed for use with optical biosensors (Cooper, 2002).

More recent developments of optical biosensors have been based on fluorescence technologies, and have occupied a central role in modern fundamental and biomedical research (Ibraheem and Campbell, 2010; Lemke and Schultz, 2011; Morris, 2010; Nhu Ngoc Van and Morris, 2013; Wang et al., 2009).

4.1.2. What is fluorescence?

4.1.2.1. History

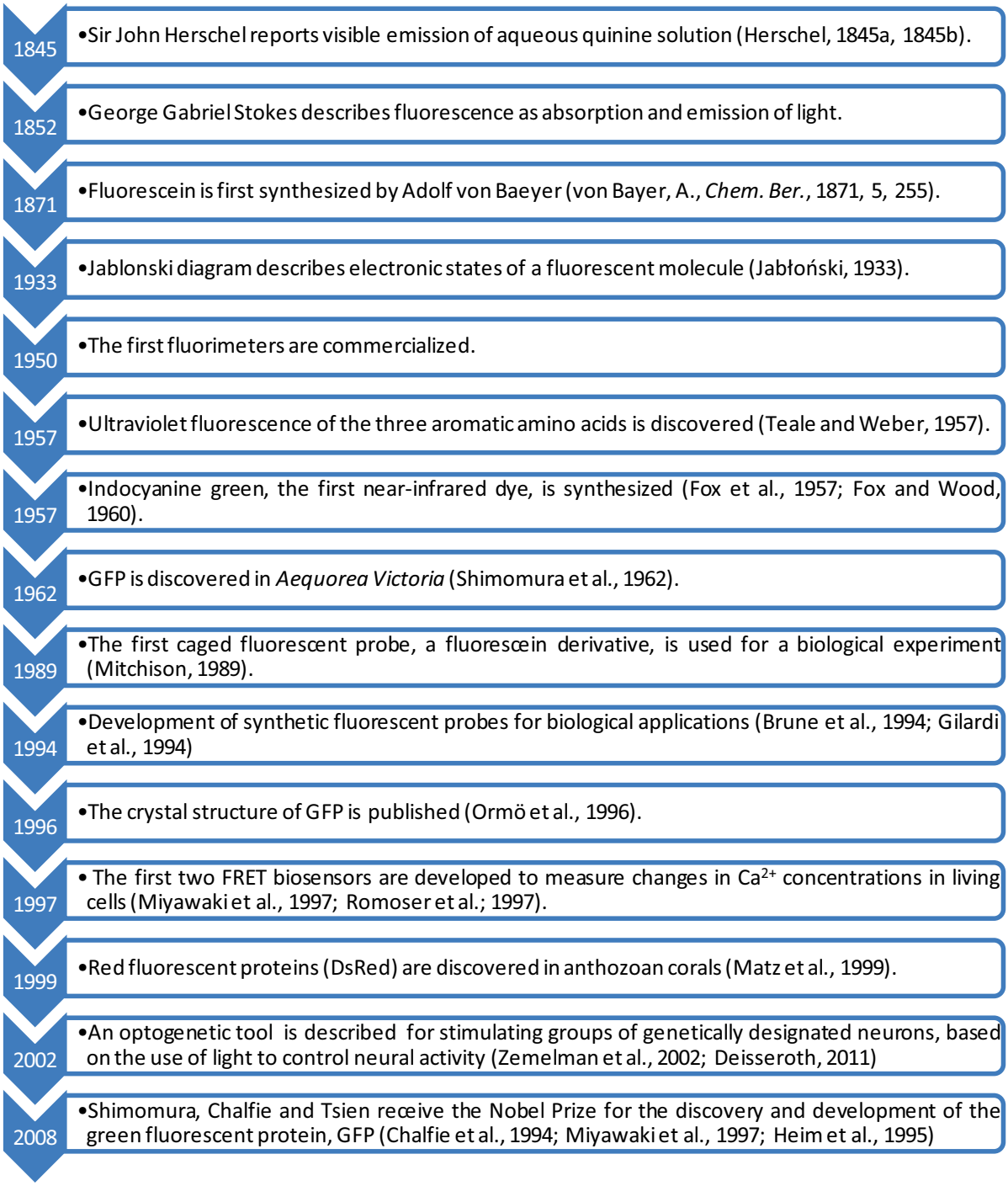

Figure 24: History of fluorescence: timeline (Brune et al., 1994; Chalfie et al., 1994; Deisseroth, 2011; Fox and Wood, 1960; Fox et al., 1957; Gilardi et al., 1994; Heim et al., 1995; Herschel, 1845a, 1845b; Jabłoński, 1933; Matz et al., 1999; Mitchison, 1989; Miyawaki et al., 1997; Ormö et al., 1996; Romoser et al., 1997; Shimomura et al., 1962; Teale and Weber, 1957; Zemelman et al., 2002)

4.1.2.2. Principle of fluorescence

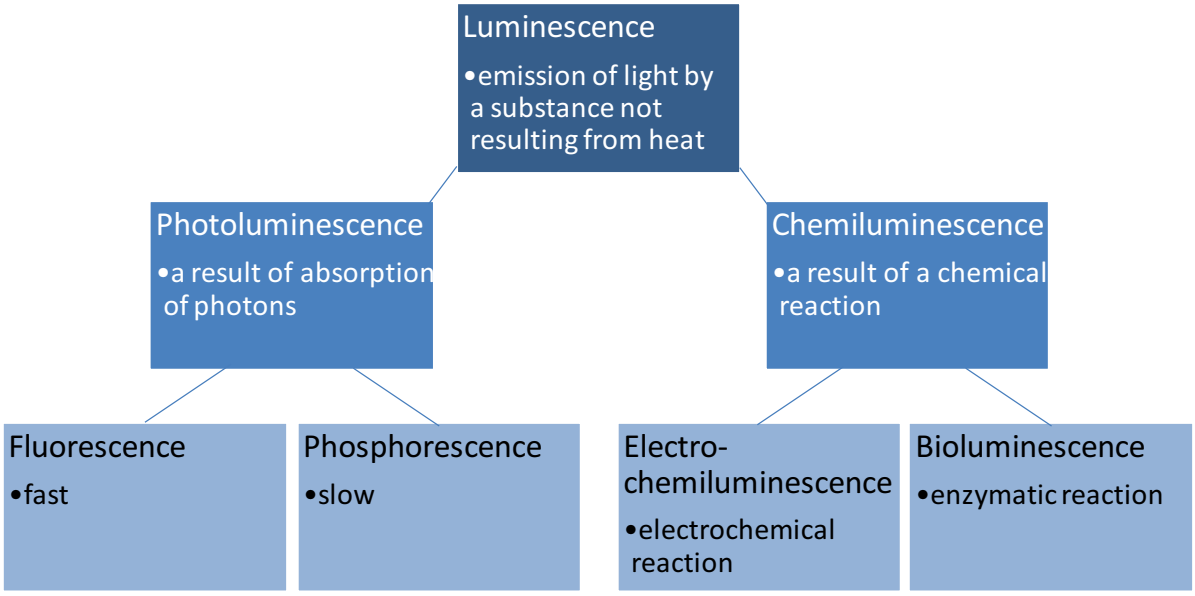

Figure 25: Different types of luminescence

Photoluminescence is formally divided into two categories - fluorescence and phosphorescence - depending on the nature of the excited state (Figure 25 and Figure 26A) (Lakowicz, 1999). It is defined as the emission of light from any substance, and occurs from electronically excited states.

More precisely, this process involves (1) photon absorption by a fluorophore giving an excited state and (2) relaxation of the excited state by emission of another photon (Figure 26). When absorbing a photon, a molecule gains energy and enters an excited state. One way for this molecule to relax is to emit a photon, thus losing its energy.

Fluorescence is distinct from phosphorescence since the kinetics of emission are much faster in the first process. Indeed, fluorescence results of singlet–singlet electronic relaxation (typical lifetime: nanoseconds) whereas phosphorescence results of triplet–singlet electronic relaxation (typical lifetime: milliseconds to hours). The Jablonski diagram describes these different electronic states and transitions upon excitation and relaxation (Figure 26A).

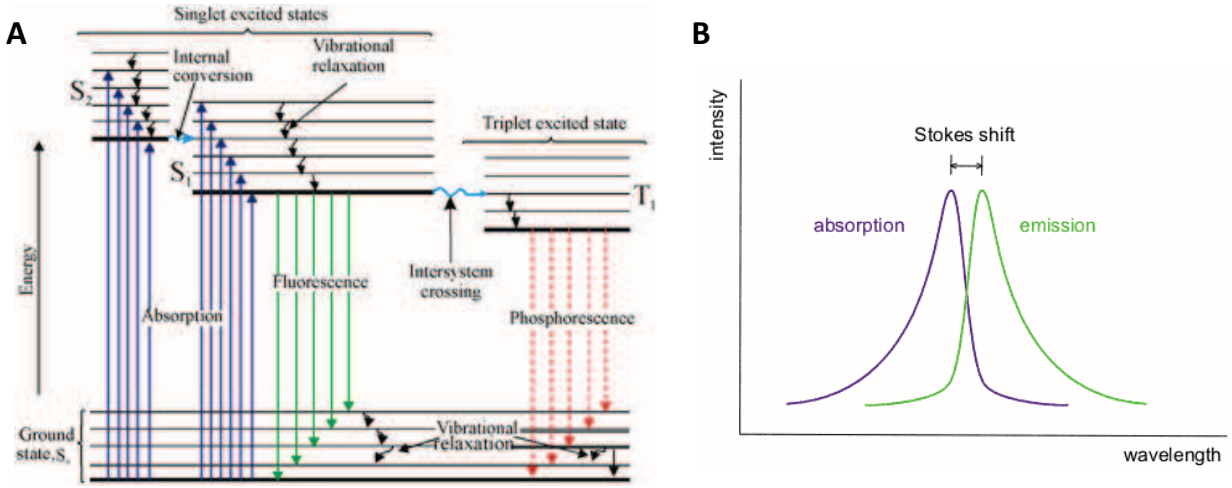

Figure 26: Principles of fluorescence

(A) Jablonski energy diagram of fluorescence

(B) General excitation and emission spectrum of a fluorophore

Molecules that can absorb light and emit fluorescence are called fluorophores and are characterized by a spectrum of light absorption and emission. Fluorophores typically contain several combined aromatic groups, or plane or cyclic molecules with several π bonds (Lakowicz, 1999).

Their electronic state transitions are correlated with a particular wavelength (λ) and energy (E) required for their excitation. The wavelength of light is inversely proportional to its energy and can be illustrated by a simple equation $E=hc/\lambda$ where h is Planck's constant with a value of $6.626.10^{-34}$ J.s and c is the speed of light with a constant value of 3.10^{8} m/s. Each fluorophore is defined by its maximum absorbance wavelength λabs and its emission wavelength λem. Because of a partial loss of energy, an emitted photon carries less energy and is characterized by a longer wavelength than that of the excitation photon. The difference between emitted photon energy and excited photon energy is named “Stokes shift” and varies according to the solvent polarity (Figure 26B) (Lakowicz, 1999; Stokes, 1852). This cycle of excitation-emission events can be repeated until the fluorophore is damaged. This phenomenon, due to extended illumination, is called photobleaching. Other photophysical properties allow to characterize a fluorophore. The **molar extinction coefficient** (**ε**) is related to the capacity of a fluorescent molecule to absorb photon energy at a given wavelength. The **quantum yield** (**Φ**) corresponds to the capacity of a fluorophore to re-emit absorbed energy and is

equal to the number of emitted photons divided by the number of absorbed photons. **Fluorescence lifetime** (**τ**) is defined as the average time the fluorophore stays in its excited state before emitting a photon, tipically between 0.1 and 100 ns.

4.1.2.3. Principle of FRET

Förster Resonance Energy Transfer (FRET) is a mechanism which involves energy transfer between two fluorophores (Förster, 1948). A donor fluorophore, in its electronic excited state, can transfer energy to an acceptor fluorophore through non-radiative dipole-dipole coupling. Three conditions are required for efficient FRET between donor and acceptor: overlap between donor emission spectrum and acceptor absorption spectrum; alignment of the transition dipole moments of the donor and acceptor fluorophores; and distance between fluorophores (Förster, 1948; Lakowicz, 1999; Stryer and Haugland, 1967). The latter is crucial for FRET and generally comprised around 1 to 10 nm. FRET between a donor and an acceptor promotes increase in fluorescence intensity of acceptor and decrease in intensity of donor fluorescence associated with decrease in lifetime of the donor. This technology is frequently used to measure protein-protein interactions, conformational changes or protein activation (Ibraheem and Campbell, 2010; Lakowicz, 1999; Lavis and Raines, 2008; Lemke and Schultz, 2011; Stryer and Haugland, 1967; Wang et al., 2009).

4.1.2.4. Principle of solvatochromism

Some fluorophores are sensitive to changes in their local environment such as pH, viscosity and solvent polarity. This sensitivity to changes of solvent polarity is called solvatochromism. It is defined as the ability of a chemical substance to change color due to a change in solvent polarity, which leads to stabilization of either ground or excited state of the fluorophore, which consequently affects the energetic gap between these states (Reichardt, 1994). The Imperiali group has provided a detailed description of this phenomenon (Figure 27) (Loving et al., 2010).

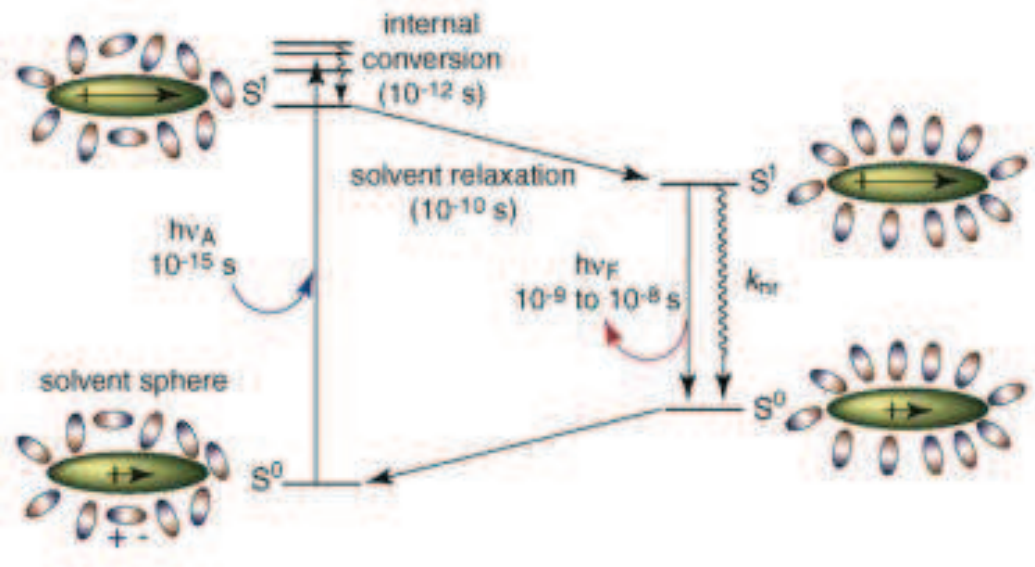

Figure 27: Origin of solvatochromism effects on fluorescence (from (Loving et al., 2010))

Upon absorption of a photon of appropriate energy, the fluorophore is promoted to an excited singlet state and adopts a dipole moment that differs significantly from that of the ground state. To accommodate this larger dipole, the molecules of the solvent sphere reorient dipoles, resulting in a more ordered arrangement. This step is named solvent relaxation and leads to a decrease in energy of the excited singlet state, which reduces the energetic gap between these states. Finally, when the fluorophore returns to the ground state by emission of a photon, the latter is of a much longer wavelength, i.e. a much lower energy, than that which was originally absorbed during excitation.

Incorporation of this type of fluorophores into biological systems can therefore provide information on local changes in environment of probes such as conformational changes, switches between active/inactive conformations, activity or protein-protein interactions. Hence, they have been widely used for the development of fluorescent biosensors (Loving et al., 2010).

A large number of solvatochromic fluorescent probes have been developed including PRODAN, Coumarin derivatives, Dansyl derivatives and Merocyanines such as Brooker's Merocyanine (Brooker et al., 1951; Loving et al., 2010; Reichardt, 1994).

4.2. Fluorescence imaging for monitoring protein kinase activity

Due to the importance of CDK/cyclins as cancer biomarkers, efficient approaches for probing kinase activity are required.

Currently, the most developed approaches to study kinase activity are based on radioactivity or antigenic approaches which require specific antibodies that recognize phosphorylated residues (Jia et al., 2008).

In *in vitro* radioactive-based assays, kinase activity is correlated with incorporation of radiolabelled phosphate into kinase substrates and therefore requires the use of enzymatically active kinases. Radioactive product analysis is performed by scintillation proximity assay, autoradiography or gel-permeation (Ma et al., 2008; Sittampalam et al., 1997). Although these radioactive methods have been widely used in laboratories, they are laborious and time-consuming. Moreover, they do not allow to follow the reaction kinetics and further lack the physiological cellular environment. Cell-based methods have been developed to incorporate ^{32}P directly into cells. Nevertheless, these approaches are end-point, poorly sensitive, require cell lysis and substrate protein isolation and purification (Nhu Ngoc Van and Morris, 2013).

Non radioactive cell-based assays have been implemented to probe kinase activity, using an ELISA (enzyme-linked immunosorbent assay) approach that employs phosphorylation-specific antibodies (Ma et al., 2008; Versteeg et al., 2000).

Another *in cellulo* method, based on the use of a fluorogenic peptide substrate (rhodamine 110, bis peptide amide) has been developed (Kupcho et al., 2003). In its unphosphorylated form, the peptide is cleaved, thereby releasing free rhodamine 110. In its phosphorylated form, it is prevented from cleavage and the compound remains as a non fluorescent peptide conjugate.

Unfortunately, none of these methods allow for real-time studies and provide real insights into the dynamics and enzymatic kinetics of the targeted kinase in its native environment.

Fluorescence imaging is particularly well suited to address this challenge. It allows visualization of dynamic processes in living cells overtime, thereby providing precious information on subcellular localization, behavior of intracellular targets or protein/protein interactions (Chudakov et al., 2010;

Morris, 2010; Weissleder and Ntziachristos, 2003). Fluorescence imaging technology displays many advantages such as high intrinsic sensitivity and selectivity, high spatial and temporal resolution, non destructive imaging, broad spectrum wavelengths and real-time kinetic analysis.

Fluorescent biosensors of protein kinases offer precious means of probing enzymatic activities in a continuous fashion *in vitro*, and in real time in living cells, and to study the kinetics of kinase activation, as well as the response to protein kinase inhibition (Bastiaens and Pepperkok, 2000; Lippincott-Schwartz and Patterson, 2003; Lippincott-Schwartz et al., 2001; Nhu Ngoc Van and Morris, 2013). They also allow to monitor conformational changes of protein kinases (Tarrant and Cole, 2009). Additionally, they provide a sensitive means of visualizing shuttling between different subcellular compartments with high spatial and temporal resolution (Giepmans et al., 2006).

With the aim of monitoring protein kinase activity, two types of fluorescent biosensors have been developed: genetically-encoded biosensors and non genetic protein/peptide biosensors.

4.3. Genetically-encoded fluorescent biosensors

4.3.1. Discovery of AFPs - Development of genetic fluorescent biosensors

Green Fluorescent Protein (GFP) (λexc = 395 nm; λem = 508 nm) has been the first auto-fluorescent protein (AFP) to be discovered. It has been isolated from bioluminescent jellyfish *Aequorea Victoria* in 1962 (Shimomura et al., 1962). Crystal structure of GFP, published in 1996 by Örmo and co-workers, showed that a fluorescent group imidazolinone was trapped inside a “barrel” formed by eleven beta-sheets (Ormö et al., 1996).

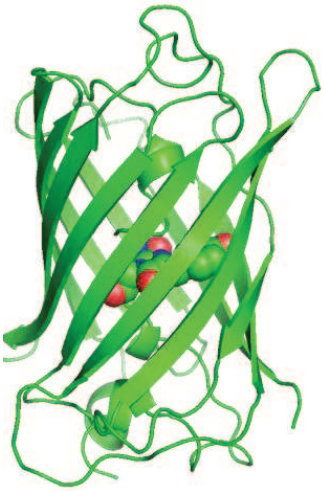

Figure 28: Crystal structure of Green Fluorescent Protein. A fluorescent group imidazolinone is trapped inside a "barrel" formed by eleven beta-sheets (PDB 1EMA) (Ormö et al., 1996)

A panel of GFP derivatives including Cyan Fluorescent Protein (CFP) and Yellow Fluorescent Protein (YFP) has been generated by mutations leading to modifications of colors and spectral properties (Pakhomov and Martynov, 2008). These fluorescent reporters have been widely used to obtain many physiological information such as protein localization in living cells (Bastiaens and Pepperkok, 2000; Lippincott-Schwartz and Patterson, 2003; Lippincott-Schwartz et al., 2001; Wouters et al., 2001). As AFPs are very robust with respect to genetic fusions to their N- and C-termini, they can be genetically fused to any protein targets (Frommer et al., 2009). Hence, they have led to the development of a wide panel of genetically-encoded fluorescent biosensors, allowing the monitoring of numerous biological processes *in cellulo* such as kinase activity (Nhu Ngoc Van and Morris, 2013).

Three sub-families of genetic fluorescent biosensors, FRET-based fluorescent biosensors, biosensors based on BiFC (Bimolecular Fluorescence Complementation) and pH-sensitive biosensors, will be further described in the following paragraphs.

4.3.2. FRET-based fluorescent biosensors for probing protein kinase activity

To monitor protein kinase activity, FRET-based fluorescent biosensors incorporate a pair of genetically-encoded AFPs together with a kinase-specific substrate sequence and a Phospho Amino Acid Binding Domain (PAABD) which recognizes phosphorylated residues in the substrate domain (Aye-Han et al., 2009; Ibraheem and Campbell, 2010; VanEngelenburg and Palmer, 2008). So that,

when the substrate sequence is phosphorylated upon addition of active kinase, the PAABD recognizes this phosphorylation site and undergoes a conformational change, thereby altering the distance between AFPs and the orientation relative to one another. Phospho-tyrosine residues are recognized by proteins with modular Src-homology 2 (SH2) and phosphotyrosine-binding (PTB) domains while pSer/Thr-binding proteins and domains currently include 14-3-3, WW domains and forkhead-associated domains (Lu et al., 1999; Yaffe, 2002; Yaffe and Elia, 2001; Yaffe and Smerdon, 2001).

Two different types of FRET biosensors have been implemented for probing kinase activity: single-chain and two-chain biosensors (Figure 29).

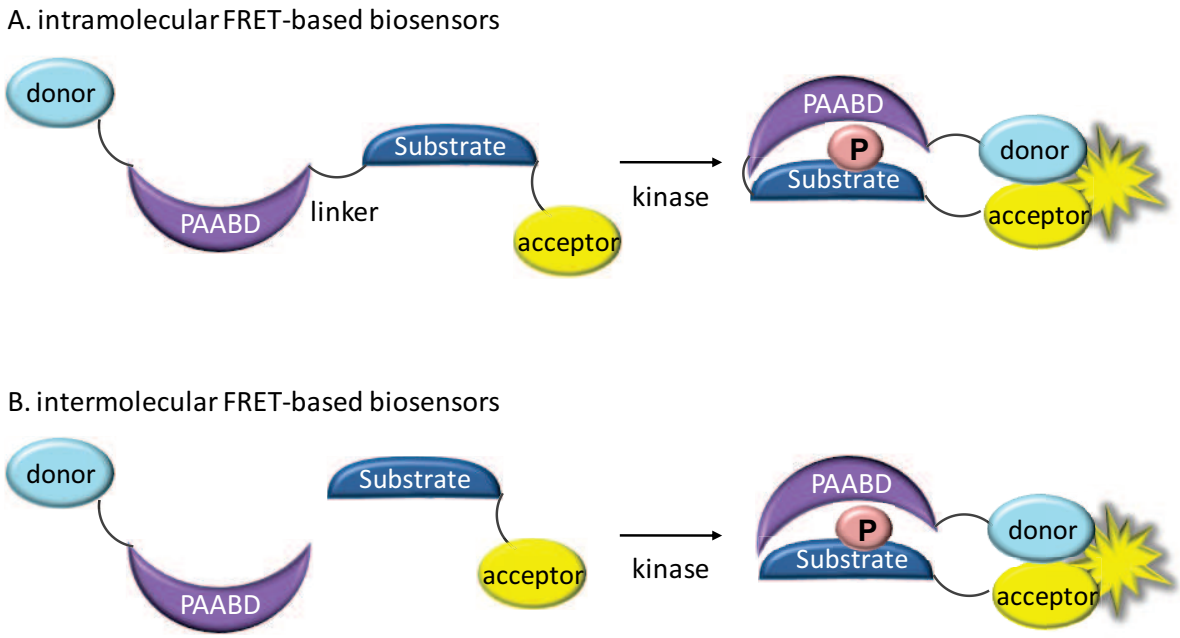

Figure 29: FRET-based biosensors of kinase activity

(A) Intramolecular FRET: a single-chain biosensor bears a pair of AFPs

(B) Intermolecular FRET: two-chain biosensors in which the two AFPs are genetically fused with two different proteins

These approaches have been used *in cellulo* to probe activity of both tyrosine and serine/threonine kinases such as Protein Kinase A (PKA); Protein Kinase C (PKC); Src, Epidermal Growth Factor Receptor (EGFR) and Abl tyrosine kinases; and ERK and JNK MAP kinases (Fosbrink et al., 2010; Ting et al., 2001; Violin et al., 2003; Zhang et al., 2001); for review (Nhu Ngoc Van and Morris, 2013)).

Regarding CDK/cyclin kinases, only one FRET-based genetic biosensor has been described to probe CDK1/cyclin B activity so far, which is further detailed in paragraph 5.1 (Gavet and Pines, 2010).

4.3.3. Biosensors based on BiFC (Bimolecular Fluorescence Complementation)

The strategy of Bimolecular Fluorescence Complementation is based on the intrinsic ability of some fluorescent protein variants, when expressed in a split form tagged to a pair of interacting proteins, to refold properly into the β-barrel structure and thus reconstitute the fluorescent form of the protein (Ibraheem and Campbell, 2010). Based on this technology, two-chain biosensors have been engineered in which the molecular recognition element is fused to one fragment of the fluorescent protein and the analyte protein to the other (Figure 30).

To date, no BiFC-based biosensors have been reported to probe protein kinase activity.

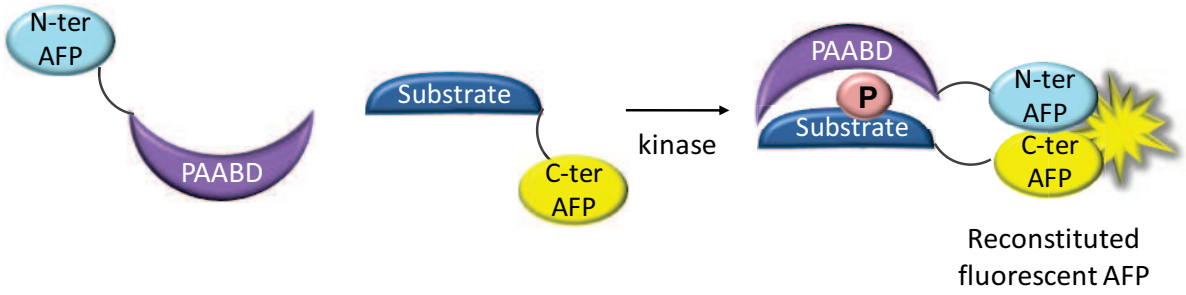

Figure 30: Biosensors based on BiFC, in which two fragments of a split AFP are brought together as a consequence of target recognition, or in this case phosphorylation, thereby reconstituting the intact and fully fluorescent protein.

4.3.4. pH-sensitive biosensors

This class of biosensors is based on the use of auto-fluorescent proteins whose spectral properties vary according to the pH (Ibraheem and Campbell, 2010). Figure 31 provides an example of a pair of AFPs whose the acceptor is sensitive to pH. At low pH, spectral properties of the acceptor fluorophore make the FRET impossible. A FRET signal is only obtained at high pH.

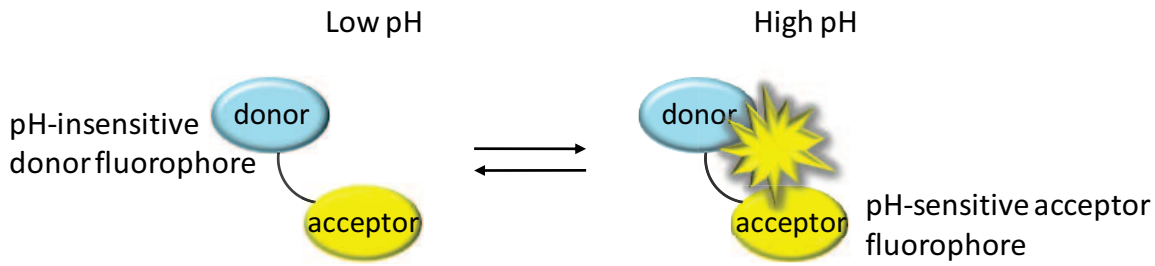

Figure 31: pH-sensitive biosensors. In this example, the acceptor fluorophore is sensitive to pH

4.3.5. Pros and cons of genetically-encoded fluorescent biosensors

Genetic biosensors are regarded as easy to engineer and transfect. However, they display some drawbacks such as limitation to *in cellulo* applications, heterogeneous expression in a population of cells, lack of control over expression, large size and sometimes mislocalization (Ciruela, 2008; Giepmans et al., 2006; Morris, 2010; Waters, 2007, 2009). Moreover, FRET fluorescence intensity is often not easy to be analyzed with a microscope because it depends on excitation intensity, photobleaching of fluorescent chromophores, and absorption by the sample. To circumvent these barriers, fluorescence lifetime imaging (FLIM) is commonly used, although this technique remains technically challenging (Wallrabe and Periasamy, 2005). In contrast to intensity-based FRET measurements, the FLIM-based FRET measurements are insensitive to photobleaching, concentration of fluorophores and biosensors, excitation power, and can thus filter out artifacts introduced by variations in the concentration and emission intensity across the sample (Berezin and Achilefu, 2010).

4.4. Non genetic peptide/protein fluorescent biosensors

4.4.1. Principle

This second strategy is based on the coupling of small synthetic probes onto peptides or proteins. In the case of protein kinases, protein/peptide sequences are often derived from domains that recognize specific targets such as substrate sequences surrounding a phosphorylation site. Upon phosphorylation of the substrate sequence by target kinase, the spectral properties of the synthetic

probe are altered directly or indirectly through intramolecular conformational changes or recognition of a PAABD.

Three different approaches have been developed to monitor protein kinase activity.

4.4.2. Biosensors based on environmentally-sensitive probes

This first class of biosensors is based on probes that are sensitive to changes in their local environment such as pH, viscosity and solvent polarity (solvatochromism; defined above in paragraph 4.1.2.4).

Different approaches have been employed to reach this goal: phosphorylation itself or recognition and binding of the phosphorylation site by a PAABD (Figure 32) (Lu et al., 1999; Yaffe, 2002; Yaffe and Elia, 2001; Yaffe and Smerdon, 2001). Several examples are given in the following reviews : (Chen et al., 2004; Lawrence and Wang, 2007; Nhu Ngoc Van and Morris, 2013; Sharma et al., 2008).

The position of the fluorescent probe is essential and varies between biosensors: on the phosphorylatable residue itself, immediately adjacent to the residue or proximal to it (i.e., 2–5 residues away).

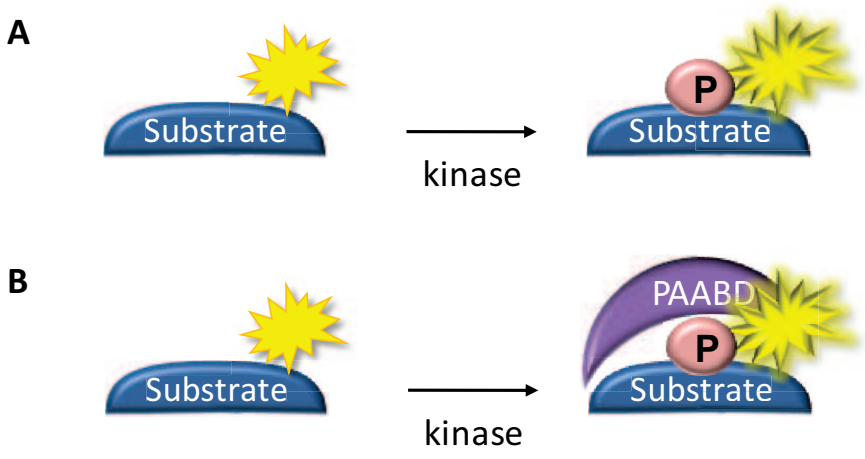

Figure 32: Environmentally sensitive peptide-based kinase biosensors

(A) by phosphorylation itself (Yeh et al., 2002)

(B) upon binding of a phosphopeptide recognition domain, such as SH2 for phosphotyrosine (Wang and Lawrence, 2005)

4.4.3. Biosensors based on chelation-enhanced fluorescence (CHEF)

Some fluorophores have the ability to coordinate metal ions such as Ca^{2+}, Mg^{2+} and Zn^{2+}. Proximal phosphorylation of the peptide substrate increases the number of negative charges thereby improving the chelation of these cations. Metal-ion-induced, chelation-enhanced fluorescence (CHEF) technology relies on fluorophores whose electronic structure and consequently spectral properties are modified upon chelation (Haas and Franz, 2009). Lawrence and collaborators have implemented a family of PKC substrates through incorporation of a Ca^{2+}-sensitive fluorophore containing a tetracarboxylate chelating site which had been previously developed by the group of Tsien (Figure 33A) (Chen et al., 2002; Minta et al., 1989). Imperiali and coworkers have designed a peptide biosensor, based on CHEF technology, to selectively report on kinase phosphorylation. The originality of the approach is the use of the Sox (sulfonamide-oxine) dye as a solvatochromic probe which derives from 8-hydroxyquinoline (Shults et al., 2003). Upon phosphorylation of the Sox-containing peptide, the chromophore binds Mg^{2+} and undergoes CHEF. A Recognition-Domain-Focused (RDF) has been engineered with extended binding sequences and added to the sensor to increase the specificity of recognition. This biosensor has shown to be efficient for probing a panel of kinases such a PKC, Pim2, Akt1, MK2, PKA, Abl, Src, and IRK in cell extracts (Figure 33B) (Luković et al., 2008).

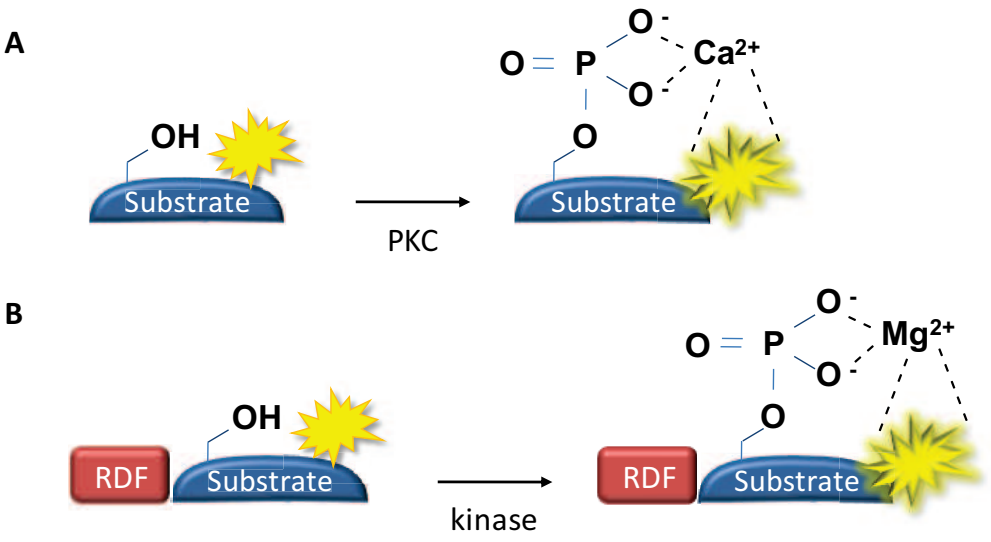

Figure 33: Chelation-enhanced fluorescence

(A) PKC biosensor based on a Ca^{2+}-chelation sensitive fluorescent probe incorporated close to the phosphorylation site (Chen et al., 2002)

(B) Recognition-domain-focused (RDF) Sox biosensor (Luković et al., 2008)

4.4.4. Biosensors based on quenching/unquenching strategies

The first strategy for quenching/unquenching fluorescent probes is based on the photophysical properties of aromatic amino acids including tyrosine and tryptophan. Indeed, due to the presence of π/π stacking interactions between aromatic groups, they constitute potent tools for quenching organic dyes. In particular, tryptophan has been used in a numerous assays for inter- and intramolecular fluorescence quenching of organic dyes (Marmé et al., 2003).

A similar approach has been developed by Lawrence and collaborators that uses the phosphorylatable tyrosine residue as a quencher that silences the fluorescence of a proximal fluorophore. Upon phosphorylation, the π/π stacking interactions are disrupted, thereby inducing a complete enhancement of fluorescence (Figure 34A) (Wang et al., 2006a).

As this strategy is only applicable to residues containing tyrosine groups, the group of Lawrence has developed the "deep quench" strategy for serine and threonine residues. It is based on the addition of a quencher in solution to prevent the fluorophore from emission. Upon phosphorylation, the quencher is displaced because of binding of a phosphorecognition domain to the phosphorylated serine or threonine residue. This binding then promotes significant fluorescence enhancement of the environmentally sensitive probe (Figure 34B) (Sharma et al., 2007). This approach has been successfully implemented for monitoring PKA activity in mitochondria using Coumarin as fluorescent probe, Acid Green 27 as quencher and 14-3-3 domain as PAABD (Agnes et al., 2010).

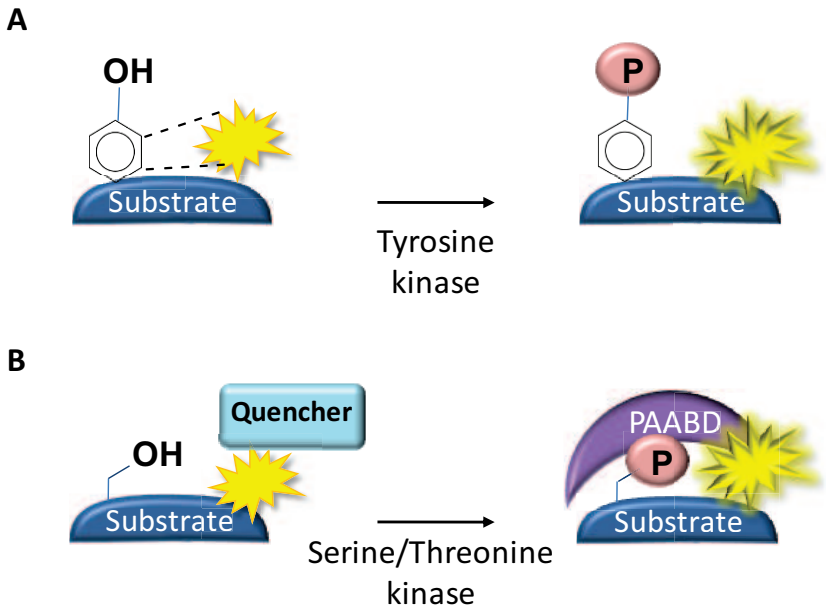

Figure 34: Quenching/unquenching strategies:

(A) applied for monitoring tyrosine kinase activity

(B) applied for monitoring serine/threonine kinase activity

4.4.5. Photoactivation strategies

With the aim of optimizing the signal-to-noise (S/N) ratio, controlling the timing observation of the reaction and increasing the intensity of the response, photoactivation strategies have been implemented by "caging" the phosphorylatable residue with a photo-labile group which can be released upon UV irradiation. Phosphorylation by the kinase is only possible after photoactivation (Figure 35). This strategy allows a reduction of non-specific basal fluorescence and offers a better spatio-temporal resolution. Moreover, it allows control of activation of the biosensor over time (Lee et al., 2009).

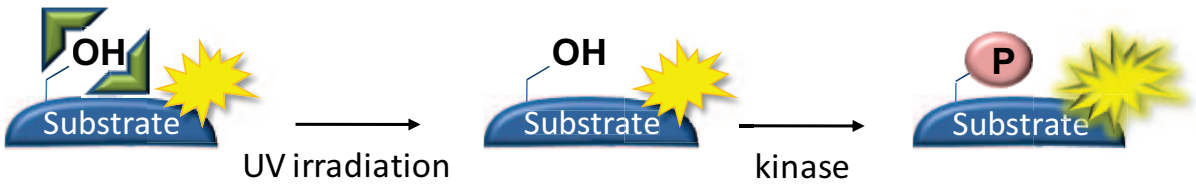

Figure 35: Light-activation strategies

4.4.6. Pros and cons of non genetic protein/peptide fluorescent biosensors

This type of biosensors displays many advantages including versatility in design and engineering and large choice of the nature and position of incorporation of the fluorescent probe. Moreover, peptides and proteins can be easily obtained by chemical synthesis or recombinant protein expression and purification. Finally, handling and storage of peptides are simple and up-scaling is quite straightforward.

However, the main issue is their inability to cross cell membranes, which is why they require means for efficient internalization in living cells and *in vivo* (Kurzawa et al., 2010). This may be addressed through microinjection or administration thanks to cell-penetrating peptides (CPPs) such as PEP and CADY2 (Kurzawa et al., 2010; McNeil, 2001). For instance, microinjection has been used to internalize a biosensor capable of visualizing the changing activation of endogenous, unlabeled Cdc42 in living cells (Nalbant et al., 2004). In addition, the cell-penetrating peptide TAT has been used to internalize in living cells a non genetic fluorescent biosensor for dynamic monitoring of phosphorylation by Abl kinase based on fluorescence lifetime imaging microscopy (FLIM) (Damayanti et al., 2013). Non-covalent strategies that form CPP/protein or CPP/peptide complexes have also been developed to deliver biosensors in living cells for probing CDK/cyclins (Kurzawa et al., 2011; Van et al., 2014).

4.5. Fluorescent biosensors for HTS of protein kinase inhibitors

Several strategies have been developed for high throughput screening (HTS) of chemical compound libraries in view of identifying novel inhibitors of protein kinases (Ahsen and Bömer, 2005; Allen et al., 2006; Hanson and Hanson, 2008; Taylor, 2010; Wolff et al., 2006; Zaman et al., 2003). The first of these were essentially based on conventional activity-based assays described above in paragraph 4.1. To replace these time consuming and invasive techniques and perform HTS assays, several fluorescence-based approaches have been developed such as scintillation proximity, FRET, fluorescence polarization, luminescence and AlphaScreen assays (Ahsen and Bömer, 2005; Zaman et al., 2003). More specifically, fluorescent biosensors have been implemented to monitor protein kinase activity in high content and high throughput screening formats (Chen et al., 2004; González-Vera, 2012; Lawrence and Wang, 2007; Morris, 2013; Nhu Ngoc Van and Morris, 2013; Sharma et al.,

2008; Tarrant and Cole, 2009; Zhang and Allen, 2007). They offer precious tools for screening in living cells thereby assessing inhibitor potential in a physiological environment (Carpenter, 2007; Hanson and Hanson, 2008; Lang et al., 2006; Taylor, 2010; Wolff et al., 2006; Zanella et al., 2010).

Four classes of fluorescent biosensors, illustrated in Figure 36, have been developed for HTS/HCS applications: genetically-encoded FRET biosensors, environmentally-sensitive biosensors, positional biosensors and FLiK (Fluorescent Labels in Kinases). The first two biosensors have been described in detail in paragraphs 4.3 and 4.4. Positional biosensors are genetic fusions of an AFP that bear a subcellular localization sequence (generally NLS (Nuclear Localization Sequence) or NES (Nuclear Exclusion Sequence)). Exposure of this sequence is modulated in response to target activation/inhibition. Thus, they give information on the target activation/inhibition through changes in their subcellular localization and constitute potent tools for HCS (Figure 36-2A).

Most of the strategies described above contain a PAABD and led to identification of ATP-competitive compounds. Therefore, with the aim of screening allosteric inhibitors which bind and stabilize only the inactive conformation of kinases, FLiK (Fluorescent Labels in Kinases) biosensors have been developed (Figure 36-2C). They contain a kinase scaffold in which fluorescent probes are introduced into specific positions and serve as sensors of ligands that bind a specific conformational state. FLiK assays have been successfully applied to identify inhibitors of p38αMAPK, Src and Abl through HTS assays (Getlik et al., 2012; Schneider et al., 2012; Simard et al., 2009a, 2009b, 2009c, 2010; Zhang et al., 2010).

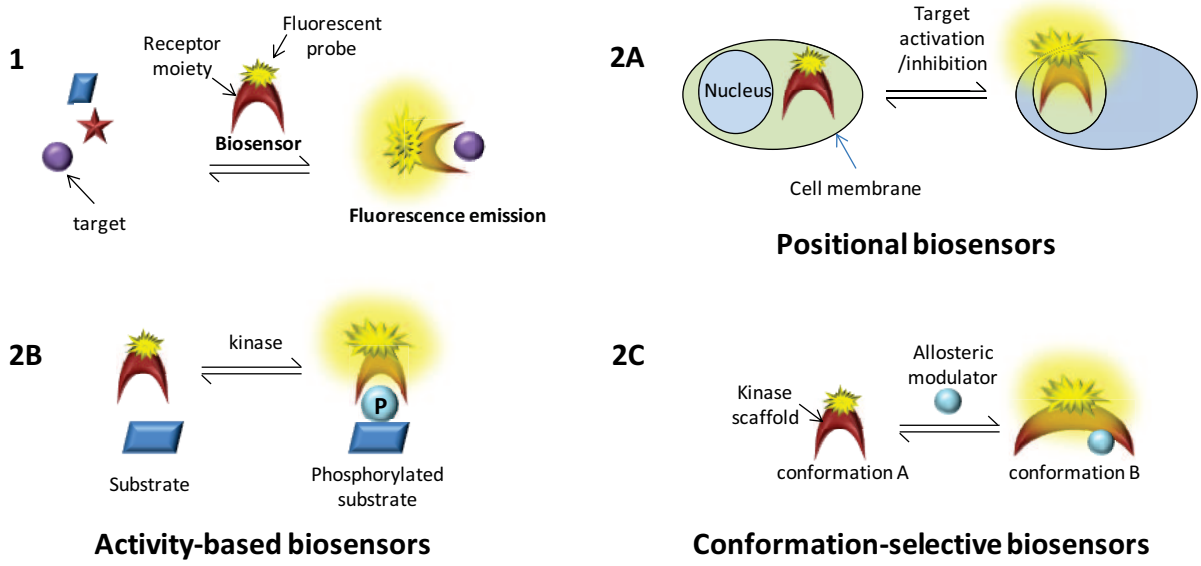

Figure 36: Fluorescent Biosensors used for HTS (from (Prével et al., 2014a))

1. Schematic representation of a fluorescent biosensor

2. Different examples of fluorescent biosensors – A: Positional biosensors convey information on the activity of the target through changes in their subcellular localization. B: Activity-based biosensors. C: Conformation-sensitive FLIK (fluorescent labels in kinases)-based approach

Specific criteria are required for successful application of fluorescent biosensors to HTS. Biosensors should be highly specific and sensitive, they should respond in a dynamic and reversible fashion leading to robust and reproducible signals. Calculation of the Z-factor enables to assess a HTS assay. Indeed, it takes into account the difference between positive and negative controls, the signal-to-noise (S/N) ratio and the variability of the assay (Ahsen and Bömer, 2005; Allen et al., 2006; Inglese et al., 2007; Sui and Wu, 2007; Zaman et al., 2003; Zhang et al., 1999). Z-factor is equal to $1 - \frac{3(A^+ + A^-)}{B^+ - B^-}$, where A^+ and A^- correspond to the standard deviations of positive and negative controls, whilst B^+ and B^- are the average responses for positive and negative controls. An assay is considered suitable for a screen if the Z factor is greater than 0.5 (Inglese et al., 2007; Prével et al., 2014b; Zhang et al., 1999).

Table 5 provides a panel of examples of fluorescent biosensors validated or implemented in HTS assays.

Biosensor Name	Biosensor Type	Target	Z factor	Dye / Probe	Comments	References
PKA	Genetic, positional	PKA		GFP-NLS-NES	cellular assay	
GPCR	Genetic, positional	GPCR		GFP	cellular assay	(O'Dowd et al., 2007)
PPIB	Genetic, positional	P53/hDM2	0,64	GFP-NLS-p53 / mRFP-NLS-NES-hDM2	high content screen for protein/protein interaction inhibitors	(Dudgeon et al., 2010)
EGFRB	Genetic, positional	EGFR	0,56	GFP-EGFR	high content screen for modulators of EGFR function	(Antczak et al., 2012)
AKAR 2	Genetic, FRET	PKA	< 0.5	FRET couple of AFPs	HTS	(Allen et al., 2006)
AKAR 3	Genetic, FRET	PKA	0,84	FRET couple of AFPs	HTS	(Allen et al., 2006)
Pickles	Genetic, FRET	Bcr-Abl		FRET couple of AFPs	Proposed for HTS / HCS	(Lu and Wang, 2010; Mizutani et al., 2010)
C3	Genetic, FRET	Caspase 3	0,87	FRET couple of AFPs	HTS performed to identify anticancer compounds from Chinese medicine	(Tian et al., 2007)
Kinase Chemosensors	Environmentally-sensitive	Akt, MK2, PKA		SOX (sulfonamide oxine)	Validation for multiplex screening using cell extracts	(Shults et al., 2005)
Sox Chemosensor	Environmentally-sensitive	Serine/threonine Protein kinases		SOX (sulfonamide oxine)	Proposed for HTS	(Shults et al., 2006)
ERK1/2 chemosensor	Environmentally-sensitive	ERK1/2		SOX (sulfonamide oxine)	Proposed for HTS using cell extracts	(Luković et al., 2009)
p38α chemosensor	Environmentally-sensitive	p38 alpha		SOX (sulfonamide oxine)	Proposed for HTS	(Stains et al., 2011)
Bcr-Abl & Lyn Biosensors	Environmentally-sensitive	Bcr-Abl & Lyn			Proposed for HTS	(Wang et al., 2010)
DFG Biosensor	FLIK	P38α		Acrylodan	validation with focused library of pyrazolourea derivatives	(Simard et al., 2009b)
DFG Biosensor	FLIK	P38α		Acrylodan	HTS performed on 35000 compounds	(Simard et al., 2009a)
P-loop Biosensor	FLIK	P38α		Acrylodan	validation with library of DFG-in or -	(Simard et al., 2010)

					out conformation ligands	
MAPK Insert Biosensor	FLIK	P38α	>0.7	Acrylodan	validation with library of 2-arylquinalozines	(Getlik et al., 2012)
DFG Biosensor	FLIK	cSrc		Acrylodan		(Simard et al., 2009c)
Myristate Pocket	FLIK	Abl	>0.84	Acrylodan	amenable to HTS	(Schneider et al., 2012)

Table 5: Fluorescent biosensors validated and/or implemented in HTS assays (from (Prével et al., 2014b))

4.6. *In vivo* applications – Development of near-infrared probes

Two issues in fluorescence imaging have to be taken into account for the development of fluorescent biosensors *in vivo*. The first one is photobleaching and phototoxicity induced by the excitation light (Hoebe et al., 2007). The second drawback is absorption/autofluorescence of tissues in visible spectrum (especially from 400 nm to 600 nm) which results from absorbers like water, hemoglobins and lipids (Weissleder and Ntziachristos, 2003). The use of InfraRed (IR) and Near InfraRed (NIR) probes has been considered as one of the key strategies to circumvent this issue (Frangioni, 2003, 2008; Koide et al., 2012; Lin et al., 2009a; Lukinavičius et al., 2013; McCann et al., 2011; Shcherbakova et al., 2012; Shcherbo et al., 2010; Subach et al., 2011).

NIR light displays many advantages compared to visible light including minimal photodamage to biological samples, deep tissue penetration, and low background autofluorescence of biomolecules in the NIR range, so that high contrast can be obtained between the imaging probe and background tissue. While a wide panel of NIR fluorescent probes has been developed, most of them display limitations for bioimaging. Indeed, they suffer from photobleaching, or do not emit adequate fluorescence in aqueous media due to molecular stacking or poor water-solubility (Ho et al., 2006; Marx, 2015). So far, only cyanine dyes (Cy5 and Cy7) have been widely used for the development of NIR fluorescent biosensors (Mishra et al., 2000; Peng et al., 2011). In the past few years, silica-containing rhodamine (SiR) fluorophores have been developed and constitute a novel class of NIR fluorophores which present superior characteristics for *in vivo* fluorescence imaging and live-cell super-resolution microscopy (Koide et al., 2012; Lukinavičius et al., 2013; McCann et al., 2011).

4.7. Fluorescent biosensors as diagnostic tools – biomedical applications

Through all the examples mentioned in the previous sections, fluorescent biosensors, be they genetic or non genetic, have proven their utility and their efficiency *in vitro* and *in cellulo*.

In recent years, they have also been a source of inspiration for biomedical applications, including diagnostic assays, in the development of complementary assays or as alternatives to the more traditional antigenic and/or genomic approaches (MayC Morris, 2012).

For example, a genetically-encoded FRET biosensor that reports on Bcr-Abl kinase activity has been applied to identify cancer cells from CML (Chronic Myeloid Leukemia) patients and to monitor drug response and resistance (Lu and Wang, 2010; Mizutani et al., 2010; Tunceroglu et al., 2010). Two peptide fluorescent biosensors have also been implemented to simultaneously visualize the tyrosine kinase activities of both Abl and Lyn in cells from CML patients (Wang et al., 2010). This last example demonstrates that fluorescent biosensors can be applied for multiplex screening. In the same assay, it becomes possible to use several biosensors coupled to different fluorescent probes. In drug discovery programmes, it therefore allows to monitor several targets simultaneously and gain information on the specificity of drugs (Carlson and Campbell, 2009; Piljic and Schultz, 2008; Welch et al., 2011).

For a completely different biomedical application, a fluorescently-labeled peptide biosensor that binds preferentially to nerves has been injected in mice and allows the visualization of peripheral nerves during surgery. It offers a promising means for developing image-guided surgery by facilitating surgical repair of injured nerves and by helping prevent accidental transection (Whitney et al., 2011).

In 2014, Griss and collaborators have developed semisynthetic bioluminescent biosensors that enable to measure precisely drug concentrations (Methotrexate and Cyclosporin A) in human blood samples, directly by spotting minimal volumes on paper and recording the signal using a simple point-and-shoot camera (Griss et al., 2014). In 2015, Courbet and co-workers have developed bacterial biosensors to detect pathological biomarkers (nitrogen oxides and glucose) in human urine

and serum via amplifying genetic switches and logic gates (Courbet et al., 2015). These last two examples constitute a major breakthrough in drug and biomarker monitoring and, more generally, in diagnostic assays.

5. Biosensors to probe CDK/cyclins

5.1. A FRET-based biosensor for probing CDK1/cyclin B1 activity

Only one genetic FRET biosensor has been described to probe the activity of CDK1/cyclin B1 so far (Gavet and Pines, 2010). This biosensor was engineered through incorporation of a pair of genetically-encoded AFPs together with a PAABD derived from the Polo Box Domain (PBD) of Polo-Like Kinase 1 (Plk1) and a CDK1-specific substrate sequence which derives from the autophosphorylation site of cyclin B1. The biosensor was introduced into HeLa cells through electroporation. When the substrate sequence was phosphorylated by active CDK1/cyclin B1, the PAABD recognized this phosphorylation site and underwent a conformational change, thereby inducing a 15% FRET increase between mCerulean (λexc = 433 nm; λem = 475 nm) and YPet56 (λexc = 517 nm; λem = 530 nm). It has proved to be a potent tool for probing CDK1/cyclin B1 and allowed to demonstrate that this complex was activated just before the disassembly of nuclear envelope, thereby initiating the events of prophase (Figure 37).

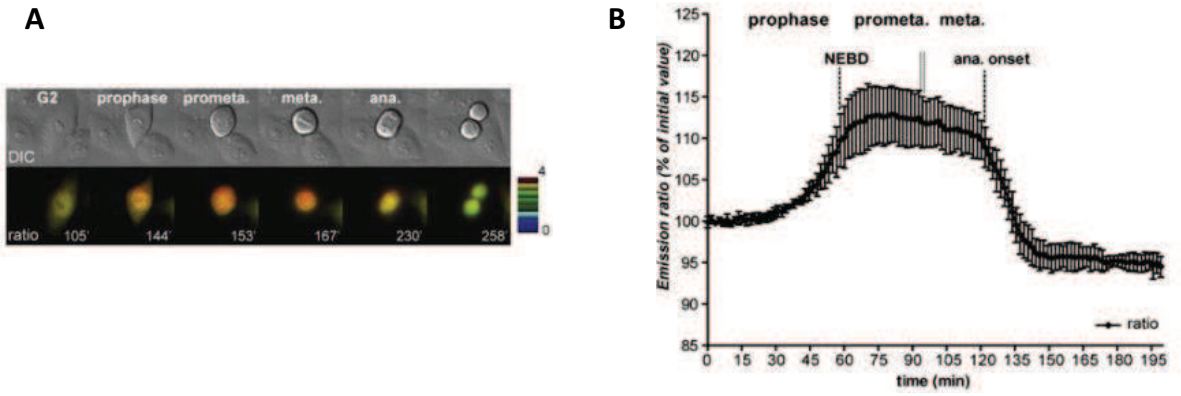

Figure 37: HeLa cells expressing the CDK1/cyclin B1 activity biosensor (from (Gavet and Pines, 2010)). (A) Intensity-modulated display representation of the FRET dynamics during mitotic progression. (B) Average curve of the quantification of the emission ratio over time in 6 different cells. Quantification curves demonstrate that CDK1/cyclin B1 is activated just before the

disassembly of nuclear envelope (NEBD). At this stage, the greatest FRET signal enhancement is obtained (15%).

5.2. CDKSENS, CDKACT and CDKCONF to probe CDK/cyclins

Three classes of non genetic biosensors, CDKSENS, CDKACT and CDKCONF, have been designed in our team (Figure 38).

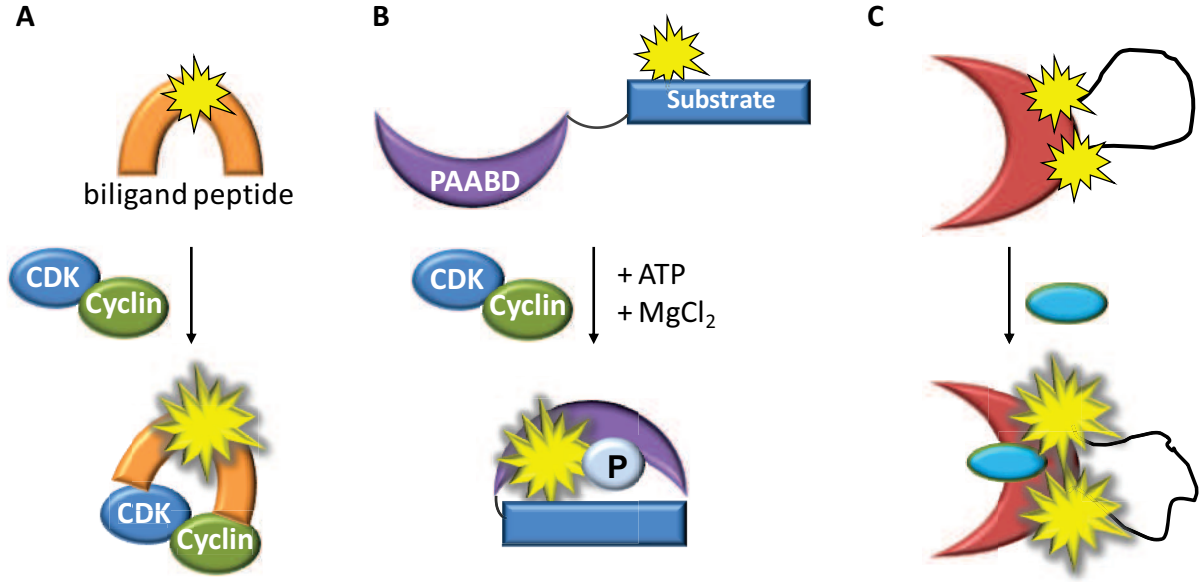

Figure 38: The three families of non genetic fluorescent biosensors developed in the team: (A) CDKSENS; (B) CDKACT; and (C) CDKCONF.

5.2.1. CDKSENS

The team has developed a family of fluorescent peptide biosensors, CDKSENS, that reports on the relative abundance of CDK/cyclins (Kurzawa et al., 2011). CDKSENS is a family of biligand peptides composed of a CDK-binding sequence and a cyclin-binding sequence, and bearing a unique cysteine which is coupled with an environmentally-sensitive probe whose fluorescence increases in a sensitive fashion upon recognition of its targets (Figure 38A).

CDKSENS displays a biligand affinity for recombinant CDKs and cyclins *in vitro* and retains endogenous CDK/cyclin complexes from cell extracts. Cy3-labelled CDKSENS, when introduced into living cells through complexation with the cell-penetrating carrier CADY2, reports on the relative abundance of CDK/cyclins through fluorescence imaging and ratiometric quantification. The biosensor further allows for detection of differences between different healthy and cancer cell lines,

thereby enabling to distinguish cells that express high levels of these heterodimeric kinases, from cells that present decreased or defective assemblies.

5.2.2. CDKACT

Few years later, the team has designed a family of fluorescent peptide/peptide biosensors, CDKACT, that reports on CDK/cyclin activity through changes in fluorescence of an environmentally-sensitive probe (Van et al., 2014). CDKACT biosensors contain a substrate sequence and a Phospho Amino Acid Binding Domain (PAABD) that recognizes the phosphorylated substrate sequence. The substrate sequence contains a unique cysteine, proximal to the phosphorylation site, onto which an environmentally-sensitive cyanine fluorescent probe is coupled. The PAABD derives from the Polo Box Domain (PBD) of Plk1 in which all cysteine residues were mutated to serines. Upon phosphorylation by CDK/cyclins, the biosensor undergoes a conformational change, thereby altering the spectral properties of the fluorescent dye (Figure 38B).

CDKACT allows a comparison of enzymatic activity of recombinant kinases (25-40% fluorescence enhancement), probing endogenous activities in lysates from healthy and cancer cell lines in a sensitive and quantitative fashion (60% fluorescence enhancement in HeLa cell extracts) and monitoring inhibition by small molecules.

Cy5-labelled CDKACT, when fused with a red fluorescent protein and introduced into living cells through complexation with the cell-penetrating carrier PEP1, allows to monitor the oscillatory activity of CDK/cyclins throughout the cell cycle by time-lapse imaging and ratiometric fluorescence quantification (Cy5/RFP ratio).

5.2.3. CDKCONF

With the aim of identifying allosteric inhibitors of CDK2, the team has developed a protein biosensor, CDKCONF, based on FLiK (Fluorescent Labels in Kinases) technology (see paragraph 4.5). The biosensor contains a CDK2 kinase scaffold in which fluorescent probes are introduced into specific positions and serve as sensors of ligands that bind a specific conformational state of CDK2 (Figure 38C). CDKCONF has been implemented for screening the French National Chemical Compound

Library (18480 compounds) (Tcherniuk et al., in revision). The screening led to identification of compounds that interfere with the T-loop of CDK2 and selectively inhibit CDK2 activity and cancer cell proliferation.

Objectives

My thesis comprises two parts, the first concerning the development of a fluorescent biosensor for probing CDK4/cyclin D activity; the second devoted to the identification of CDK4/cyclin D inhibitors, either by screening small molecule libraries or through rational design of peptides.

1. Development of a fluorescent biosensor for probing CDK4/cyclin D activity

Currently, kinase activity is largely detected by radioactivity or antibody-based approaches. However, these approaches do not provide real insights into the dynamics and enzymatic kinetics of the target kinase in its native environment. As such, my first goal was to develop a non genetic fluorescent biosensor that could monitor CDK4/cyclin D activity. Different protein and peptide variants of the biosensor were characterized *in vitro* using recombinant CDK4/cyclin D and cell extracts derived from melanoma cell lines in which CDK4/cyclin D is deregulated. The biosensor was then applied to detect CDK4/cyclin D alterations in biopsies from human skin and melanoma xenografts in fluorescence-based activity assays and in living cancer cells through fluorescence microscopy and timelapse imaging.

2. Identification of CDK4/cyclin D inhibitors

A. Identification of non-ATP competitive compounds targeting CDK4/cyclin D

To this aim, two fluorescent biosensors were engineered to identify competitors of essential protein/protein interfaces between CDK4 and cyclin D, and allosteric inhibitors that perturb the conformational dynamics of CDK4, respectively. Once validated, the biosensors were implemented to screen two small molecule libraries. Hits were characterized in fluorescence titration and activity assays so as to determine their mechanism of action and their ability to inhibit CDK4/cyclin D, as well as in proliferation assays in melanoma cell lines.

B. Development of peptide inhibitors that target the CDK4/cyclin D interface

The second objective of this section was to develop peptide inhibitors that interfere with essential protein/protein interactions between CDK4 and cyclin D. The mechanism of action of these peptides was determined *in vitro* in binding/dissociation assays, using recombinant CDK4 and cyclin D. Their

inhibitory potential towards CDK4 activity was characterized in fluorescence-based activity assays, as well as in proliferation assays in melanoma cell lines following cell-penetrating peptide-mediated delivery.

Results

1. Development of a fluorescent biosensor for probing CDK4/cyclin D activity

1.1. Concept

A generic fluorescent protein/peptide biosensor family, CDKACT, was previously developed by the team for probing CDK/cyclin activity *in vitro* and in living cells (Van et al., 2014). In order to generate a fluorescent biosensor which would respond specifically to CDK4/cyclin D, we designed a new family of CDKACT derivatives with a substrate specific to CDK4.

This novel family of biosensors consists of three domains:

- a **Phospho Amino Acid Binding Domain** (PAABD) which recognizes pSer ou pThr

- a **CDK4-specific substrate sequence** derived from the retinoblastoma protein (Rb), from residue 790 to 801, which is specifically phosphorylated by CDK4/cyclin D (S795 residue) (Grafstrom et al., 1999). A unique cysteine was introduced at position -2 relative to the phosphoserine for labelling with a synthetic environmentally-sensitive fluorescent probe (YKFCSSPLRIPG).

- a short glycine-rich **linker** to ensure flexibility between the two domains.

So that, phosphorylation of the substrate sequence by active CDK4/cyclin D induces an intramolecular conformational change due to recognition of the phosphorylated sequence by the PAABD which alters the local environment of the probe and consequently its spectral properties (Figure 39).

Three variants of CDK4 biosensors were designed: a recombinant protein and two synthetic peptides, which bear the same substrate sequence combined with different PAABDs via a short/long linker.

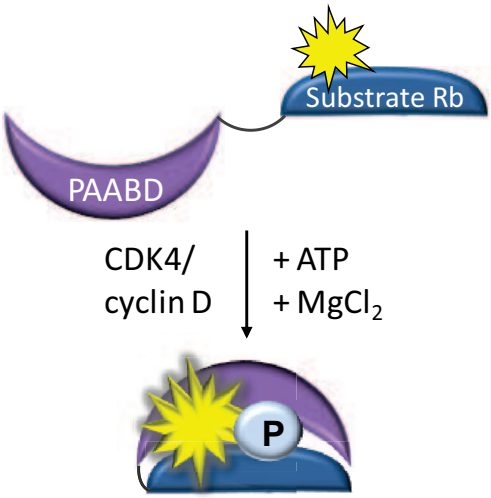

Figure 39: The biosensor consists of a CDK4-specific substrate sequence derived from pRb in which a cysteine residue was introduced at position -2 relative to the SP phosphorylation site (795), and a phospho amino acid-binding domain (PAABD) which recognizes the substrate sequence phosphorylated by CDK4/cyclin D kinase.

1.2. CDKACTRb

1.2.1. Design

First, a 57 kDa **GST-CDKACTRb** protein biosensor was developed, containing a PAABD derived from the Polo Box Domain of Plk1 (García-Alvarez et al., 2007), from residue 367 to 603 (237 amino acids) in which all cysteine residues were mutated to serines (materials and methods) (Figure 40A). CDKACTRb therefore contained a single cysteine, close to the phosphorylation site, for labeling with fluorescent probes such as Cy3 (Figure 40B).

A **B**

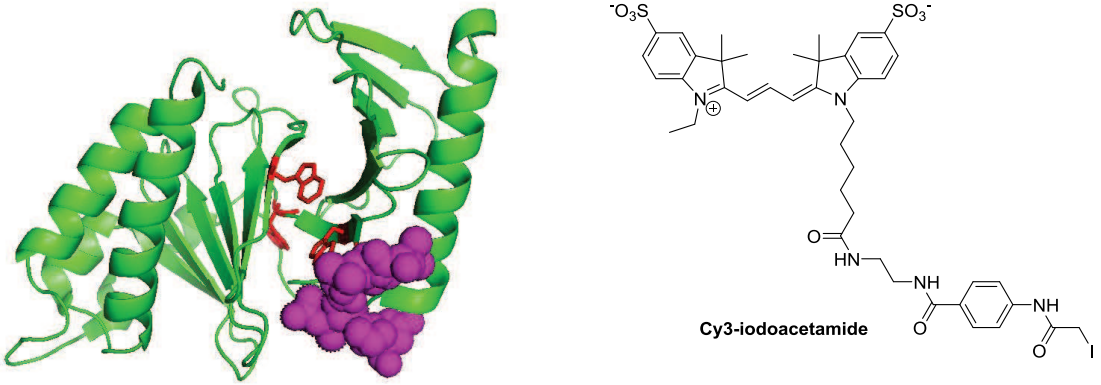

Figure 40: (A) Crystal structure of the Polo Box Domain of Plk1 in complex with a Cdc25 phosphopeptide (PDB 20JS). (B) Chemical structure of Cy3-iodoacetamide.

1.2.2. Biosensor engineering

CDKACTRb protein biosensor was engineered by recombinant protein technology in fusion with a GST tag (materials and methods). It was expressed in *E.coli* and expression was verified by SDS-PAGE (57 kDa). It was purified by affinity on glutathione sepharose and gel filtration chromatography (Figure 41) (materials and methods).

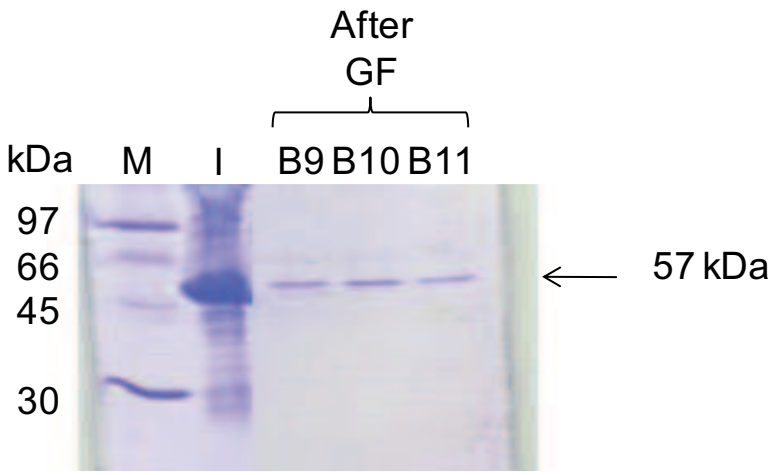

Figure 41: Expression and purification of GST-CDKACTRb. M: marker protein; I: protein induction; After Gel Filtration (GF) B9-B11: Protein fractions from gel filtration FPLC purification.

1.2.3. CDK4, cyclin D1 and CIV engineering

In order to characterize the biosensor *in vitro*, recombinant CDK4 and cyclin D1 proteins were produced. Activation of the complex was achieved using the CDK-activating kinase CIV of *Saccharomyces cerevisiae*. CDK4, cyclin D1 and CIV were constructed by recombinant protein technology in fusion with a GST tag (materials and methods). They were expressed in *E.coli* and expression was verified by SDS-PAGE (GST-CDK4 and GST-cyclin D1: 59 kDa; GST-CIV: 67 kDa) (Figure 42). They were purified by affinity and gel filtration chromatography (Figure 42) (materials and methods). GST-CDK4 / GST-cyclin D complex was formed following individual purification of each subunit and incubation of stoechiometric concentrations, then further incubated with 50 nM CIV to ensure its activation.

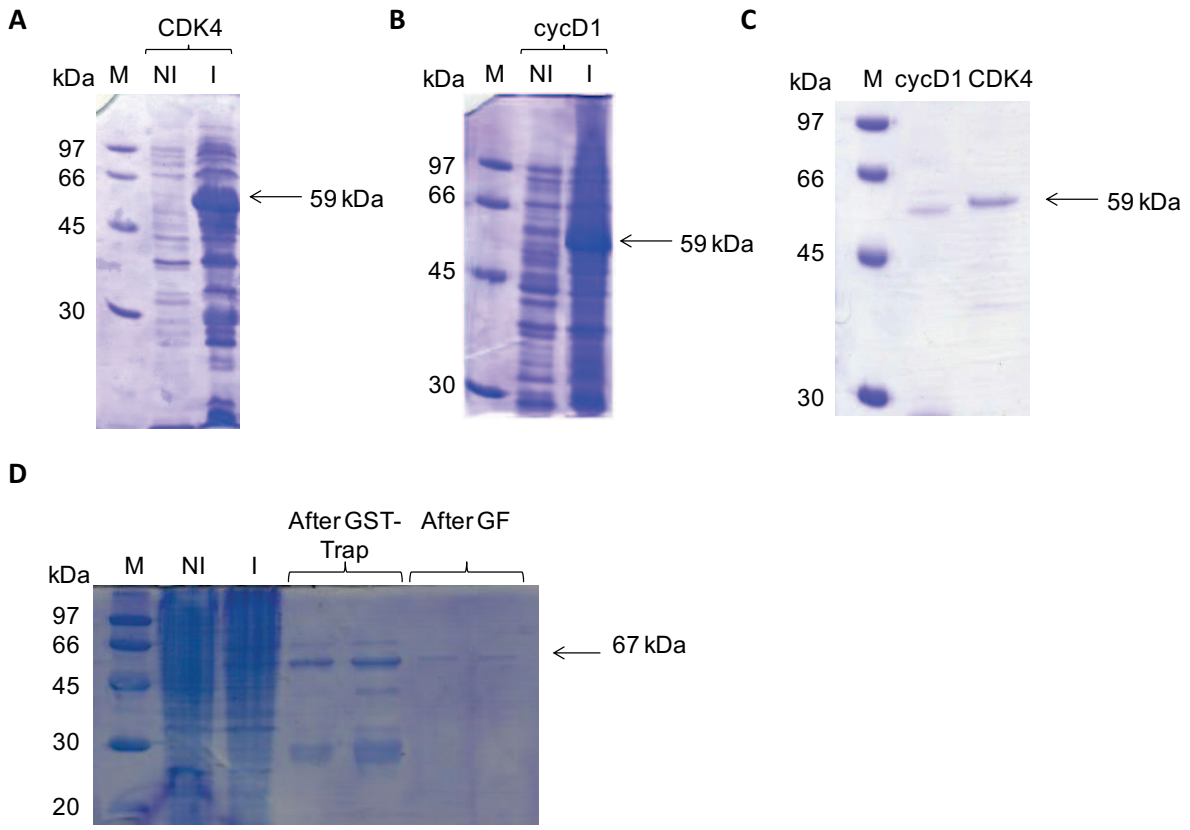

Figure 42: Expression and purification of GST-CDK4, GST-cyclin D1 and GST-CIV. (A) CDK4 - M: marker protein; NI: before induction; I: protein induction. (B) cyclin D1 - M: marker protein; NI: before induction; I: protein induction. (C) Protein fractions from gel filtration FPLC purification M: Marker protein. (D) CIV - M: marker protein; NI: before induction; I: protein induction; protein fractions after GST-Trap; After Gel Filtration (GF) : protein fractions from gel filtration FPLC purification.

1.2.4. *In vitro* characterization with recombinant CDK4/cyclin D

In order to validate the ability of CDKACTRb to report on CDK4/cyclin D phosphorylation *in vitro* and further characterize this protein biosensor, spectrofluorimetric experiments were performed in 96-well plates in standard kinase assay conditions for 50 min at 30°C in the presence of 0.5 mM ATP and 5 mM $MgCl_2$. CDKACTRb was labeled with the fluorescent probe Cy3. Fluorescence emission of Cy3-labelled CDKACTRb was measured at 570 nm following excitation at 544 nm on a Polarstar™ fluorimeter. Since the fluorescently-labeled biosensor has a basal fluorescence, responses of the biosensor resulting from incubation with recombinant proteins and inhibitors are always obtained following subtraction of background fluorescence of Cy3-CDKACTRb alone.

The first experiment was performed using 50 nM CDKACTRb-Cy3, 50 nM CDK4/cyclin D1 and 50 nM CIV. A specific CDK4/6 inhibitor, PD-0332991 (also called Palbociclib) was used at 20 µM to inhibit CDK4 activity. The results showed that the addition of active CDK4/cyclin D1 led to a 15% enhancement of the fluorescence intensity of the biosensor, after 50 min (3000s) of reaction (Figure 43B). Upon addition of 20 µM of PD-0332991, the fluorescent signal of the biosensor was decreased by 5%. This experiment indicates that CDKACTRb biosensor reports on CDK4/cyclin D1 kinase activity *in vitro*. The weak increase in fluorescence of Cy3-CDKACTRb could be explained by the presence of the GST-tag in CDK4, cyclin D and CDKACTRb. As GST-tag has a tendency to dimerize, it could induce the formation of homo/heterodimers between the biosensor itself, CDK4 itself, cyclin D itself or between the biosensor and the kinase, consequently preventing a robust fluorescent signal.

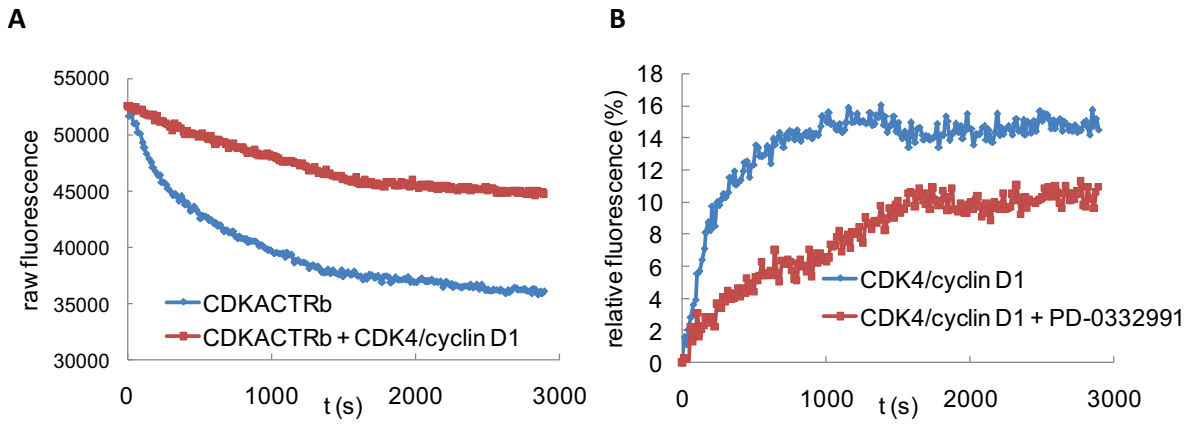

Figure 43: CDKACTRb-Cy3 (50 nM) fluorescence was monitored over time upon incubation with 50 nM active recombinant CDK4/cyclin D1 and 50 nM CIV +/- 20 µM PD-0332991. (A) Fluorescence emission of Cy3-CDKACTRb alone or upon incubation with active CDK4/cyclin D1 was measured at 570 nm following excitation at 544 nm. (B) Relative increase in fluorescence of the biosensor incubated with kinase following subtraction of background fluorescence of Cy3-CDKACTRb alone.

1.2.5. *In extracto* characterization

To assess the ability of CDKACTRb to report on the activity of endogenous CDK4/cyclin D, a melanoma cell line A375, in which CDK4/cyclin D is hyperactivated, was used as a source of endogenous kinase. A375 cell extracts were prepared from subconfluent cell cultures and then dosed at 280 nm to calculate the total protein concentration.

Determination of the working concentration window

The working concentration window was determined by testing different concentrations of both the biosensor and A375 cell extracts. The first series was set up with a fixed concentration of 20 µg of proteins from A375 cell extracts and increasing concentrations of Cy3-labelled CDKACTRb (10, 25 and 50 nM). Figure 44A presents fluorescence emission at 570 nm of CDKACTRb-Cy3 overtime following excitation at 544 nm. In Figure 44B, maximal fluorescence of the biosensor at the end of the reaction (3000s) is represented in a linear plot as a function of its concentration. The results demonstrated that, in standard kinase assay conditions at 30°C, in the presence of 0.5 mM ATP and 5 mM $MgCl_2$, fluorescence emission increased in a dose-dependent fashion (30 - 90% enhancement) within a window of 10 - 50 nM CDKACTRb-Cy3. By enhancing biosensor concentration from 10 nM to 25 nM, the fluorescence intensity strongly increased from 30 to 70%. Upon enhancement of the biosensor concentration from 25 nM to 50 nM, the fluorescence intensity was slightly amplified, suggesting that saturation has been reached for this concentration of cell extracts.

The second series of experiments was set up with a fixed concentration of 25 nM of Cy3-labelled CDKACTRb and increasing concentrations of 5 - 100 µg proteins from A375 cell extracts (Figure 44C/D/E). The fluorescence emission of CDKACTRb increased in a dose-dependent fashion (30-100% enhancement) within a window of 5 - 20 µg proteins. Upon addition of higher concentrations of A375 cell extracts (40 - 100 µg), there was a drop in the fluorescent signal compared to that obtained with 20 µg (Figure 44E). This reduction in fluorescence could be explained by the presence of phosphatases whose concentrations are enhanced upon addition of increasing cell extracts concentrations. Indeed, as phosphatases remove phosphate groups, the substrate sequence is no longer phosphorylated, resulting in a shift of the biosensor from closed to open conformation which leads to a return to basal fluorescent signal. Another explanation could be that the excess of extracts shields the biosensor and leads to its aggregation.

Taken together, we observed that the greatest fluorescence enhancement was obtained with 25 - 50 nM CDKACTRb-Cy3 and 20 µg A375 cell extracts.

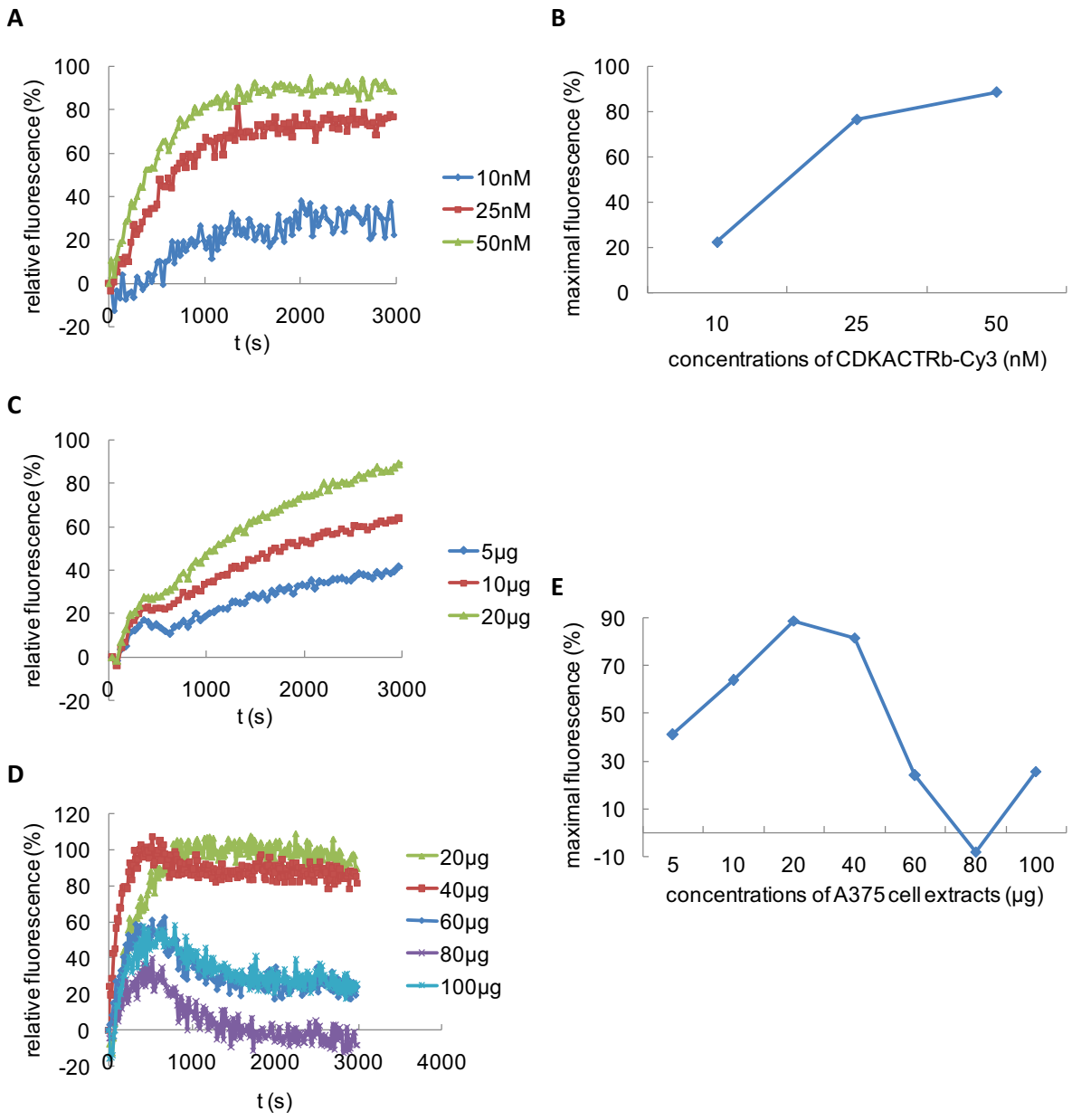

Figure 44: Determination of working concentrations of Cy3-CDKACTRb and A375 cell extracts in real-time fluorescent assays. The fluorescent signal after subtraction of the background fluorescence of Cy3-CDKACTRb alone is presented.

(A) 20 µg A375 cell extracts and increasing concentrations of CDKACTRb-Cy3 (10 - 50 nM)

(B) The linear plot represents the maximal fluorescence of the biosensor (at 3000s) as a function of its concentration upon addition of 20 µg A375 cell extracts.

(C) 25 nM CDKACTRb-Cy3 and increasing concentrations of A375 cell extracts (5 - 20 µg)

(D) 25 nM CDKACTRb-Cy3 and increasing concentrations of A375 cell extracts (20 - 100 µg).

(E) The linear plot represents the maximal fluorescence of the biosensor (25 nM) (at 3000s) as a function of A375 cell extract concentrations.

Response of CDKACTRb upon inhibition of CDK4/cyclin D activity with PD-0332991

The assays were performed in standard kinase assay conditions with 25 nM CDKACTRb-Cy3, 10 µg A375 cell extracts and different concentrations of PD-0332991 (from 0 to 100 µM). Figure 45A shows that addition of A375 cell extracts led to a 80% enhancement of the fluorescence intensity of the biosensor. The addition of increasing concentrations of PD-0332991 reduced the fluorescent signal of the biosensor in a dose-dependent fashion. The maxima of the curves at the end of the reaction are represented in a histogram (Figure 45B). Curve fitting of these points allowed the determination of an IC_{50} value of PD-0332991 in melanoma cell extracts, equal to 5.9 µM (Figure 45C) (see materials and methods for the IC_{50} equation used). Unlike standard IC_{50} values which are determined using the purified recombinant kinase alone (11 nM for PD-0332991 towards CDK4), this value reflects the inhibitory efficiency of PD-0332991 towards endogenous CDK4/cyclin D in a more physiological context.

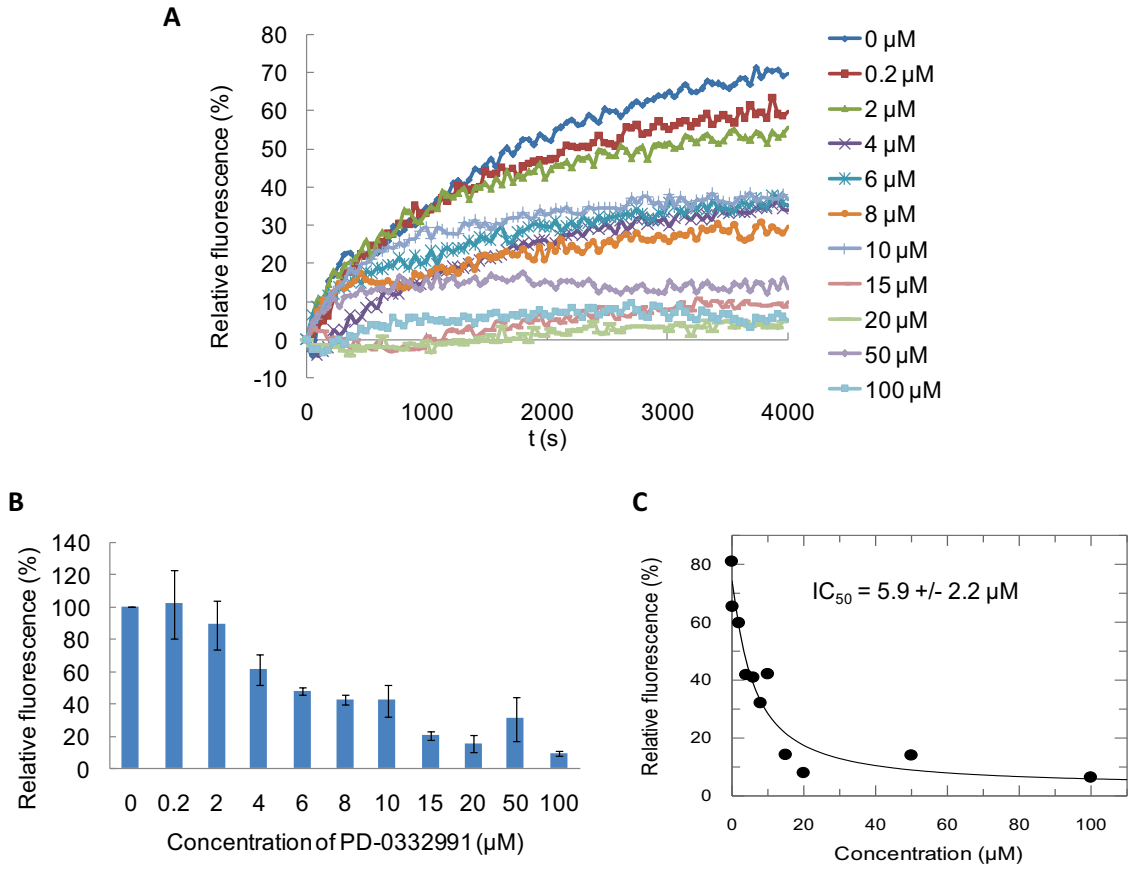

Figure 45: Real-time fluorescence assays with A375 melanoma cell extracts as source of endogenous CDK4/cyclin D and CDKACTRb-Cy3 in the presence of different concentrations of PD-

0332991. The fluorescent signal after subtraction of the background fluorescence of CDKACTRb alone is presented.

(A) Relative increase in the fluorescence of 25 nM CDKACTRb-Cy3 incubated with 10 µg A375 cell extracts +/- different concentrations of PD-0332991 (CDK4/6 inhibitor)

(B) Histogram representing the fluorescent signal at the endpoint of the assay (4000s). The fluorescent signal of CDKACTRb-Cy3 incubated with cell extracts without PD-0332991 was regarded as 100%.

(C) Curve fitting and IC_{50} determination of PD-0332991 on CDK4/cyclin D activity in melanoma cell extracts.

Selectivity and Specificity of CDKACTRb

To assess the selectivity and specificity of CDKACTRb for CDK4/cyclin D, different inhibitors were tested: some CDK/cyclin inhibitors including Roscovitine (CDK1/2/5/7/9), RO3306 (CDK1) and AT7519 (CDK2/4/5/9); and some inhibitors of kinases not related to CDK/cyclins such as Src (PP2), PKA (H89), MEK (U0126). The assays were performed as described above with 25 nM CDKACTRb-Cy3, 10 µg A375 cell extracts and different concentrations of inhibitors (from 0 to 20 µM).

These experiments demonstrated that there were no significant changes of the fluorescence intensity of CDKACTRb when adding these inhibitors at different concentrations, compared to PD-0332991 (Figure 46A and B).

Taken together, these data provide evidence that CDKACTRb reports specifically on endogenous CDK4/cyclin D activity.

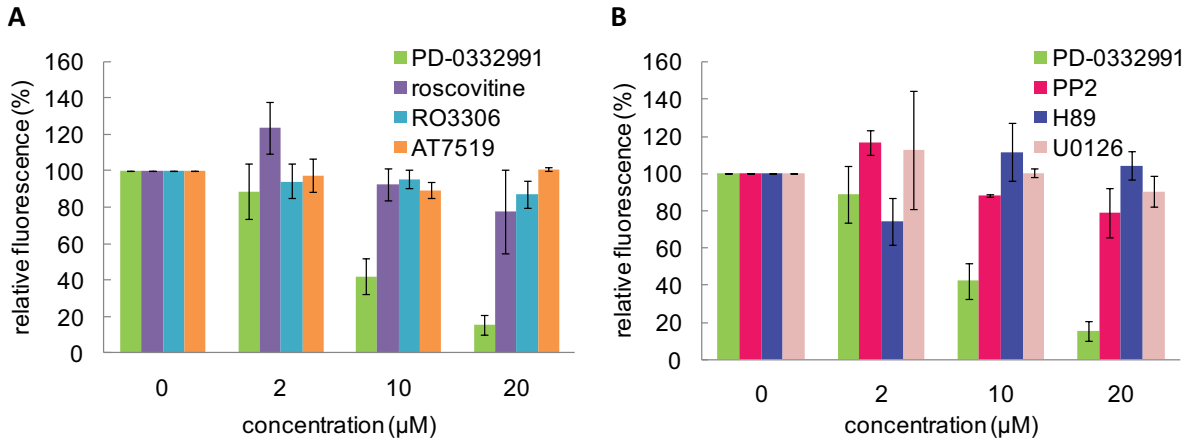

Figure 46: CDKACTRb-Cy3 (25 nM) fluorescence was monitored over time upon incubation with 10 µg A375 cell extracts +/- different inhibitor concentrations (0 - 20 µM). The fluorescent signal was

obtained following subtraction of background fluorescence of Cy3-CDKACTRb alone and the histogram represents the fluorescent signal at the endpoint of the assay (4000s).

(A) CDK/cyclin inhibitors: PD-0332991 (CDK4/6 inhibitor), Roscovitine (CDK1/2/5/7/9 inhibitor), RO3306 (CDK1 inhibitor) and AT7519 (CDK2/4/5/9 inhibitor)

(B) Inhibitors of other kinases: PP2 (Src inhibitor), U0126 (MAPK inhibitor) and H89 (PKA inhibitor).

Profiling CDK4/cyclin D activity in different cancer cell lines

CDKACTRb was used to compare differences in endogenous CDK4/cyclin D activity in cell extracts derived from different human cancer cell lines including cervical cancer HeLa, melanoma A375, lung carcinoma A549 and acute T cell leukemia Jurkat. Cell extracts were prepared and their concentration was normalized at 280 nm. Western blot analysis of these extracts allowed to compare the abundance of CDK4 and cyclin D1. The results in Figure 47A showed that cyclin D1 levels were comparable between the different cell types while CDK4 was significantly more abundant in HeLa than in A375, A549 and Jurkat cell extracts. Figure 47B represents CDK4 levels relative to cyclin D levels. Fluorescent kinase assays were performed to measure CDK4/cyclin D activity in 10 µg cell extracts from these four cell lines using 25 nM CDKACTRb-Cy3 (Figure 47C). Figure 47D represents the fluorescent signal of the biosensor at the endpoint of five independent assays. The results showed that CDKACTRb fluorescence intensity measured in cell extracts, in response to CDK4/cyclin D activity, was comparable in the four cell lines. These similar response profiles differ from the protein expression profiles revealed by Western blotting. This difference can be explained by analysing the genotypes of these strains. Indeed, unlike HeLa and Jurkat cell lines which bear wild-type CDK4, $p16^{INK4A}$ and pRb, A375 and A549 cell lines harbour a mutation of $p16^{INK4A}$, the endogenous inhibitor of CDK4 which leads to unrestricted activity of CDK4. Thus, even if CDK4 is less abundant in A375 and A549 than in HeLa, CDKACTRb highlights kinase hyperactivation in these two cell lines that harbour molecular alterations converging on CDK4/cyclin D activity.

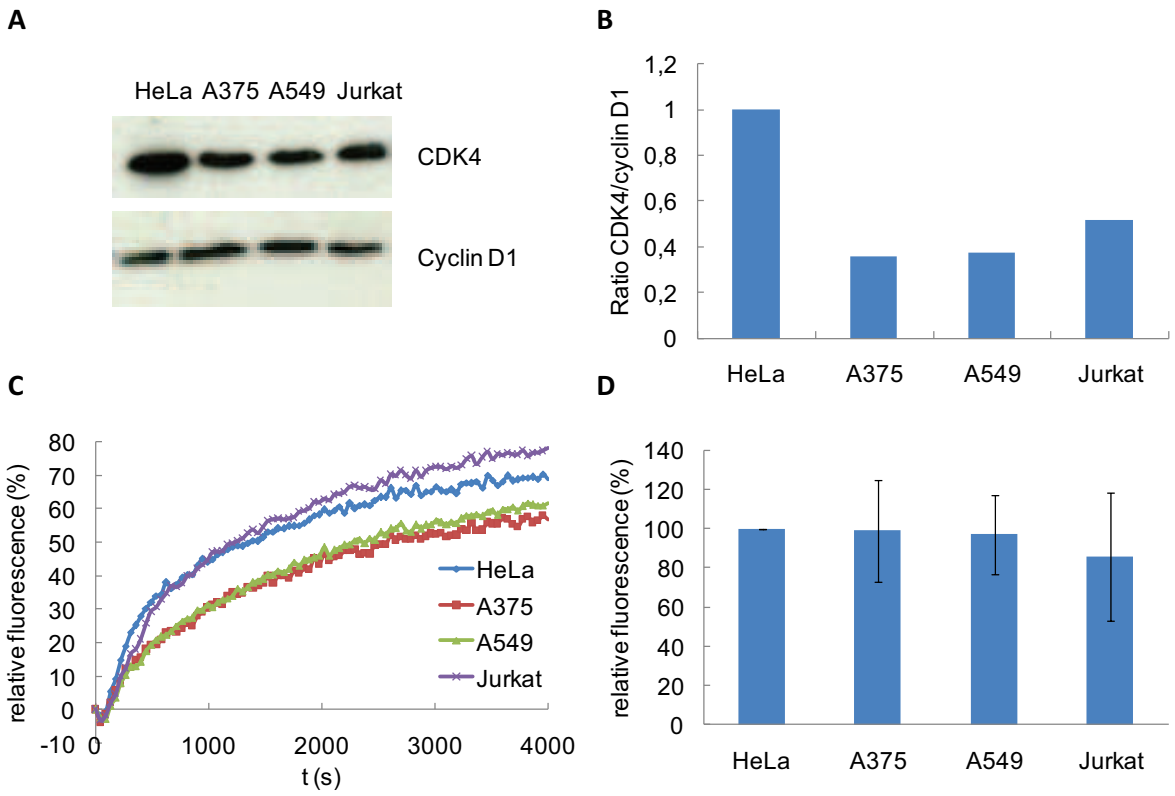

Figure 47: CDKACTRb-Cy3 reports on differences in CDK4/cyclin D activity of different cancer cell lines. Cell extracts from HeLa, A375, A549 and Jurkat cell lines were normalized at 280 nm and used for Western blotting and fluorescence kinase assays.

(A) Western blotting of CDK4 and cyclin D1 in HeLa, A375, A549 and Jurkat cancer cell lines.

(B) Quantification of CDK4/cyclin D1 levels. The ratio CDK4/cyclin D1 in HeLa cell extracts was regarded as 1.

(C) Example of response of 25 nM CDKACTRb-Cy3 upon incubation with 10 µg cell extracts from different cancer cell lines: Hela, A375, A549 and Jurkat. The fluorescent signal was obtained following subtraction of background fluorescence of Cy3-CDKACTRb alone.

(D) Histogram representing the fluorescent signal at the endpoint of 5 independent assays (4000s). The fluorescent signal of CDKACTRb-Cy3 incubated with HeLa cell extracts was regarded as 100%.

1.3. WWRb

In order to probe CDK4/cyclin D activity routinely in cell extracts derived from melanoma cells and biopsies and *in cellulo*, we decided to generate a peptide version of CDKACTRb, WWRb, which was smaller, easier to manipulate and which could be easily stored without suffering degradation.

WWRb is a 44 amino acid peptide, whose PAABD derived from the WW domain of Pin1, from residue 10 to 39 (30 amino acids) (Figure 48). This WW domain was previously used in a hybrid biosensor to probe CDK9 activity (Anai et al., 2007).

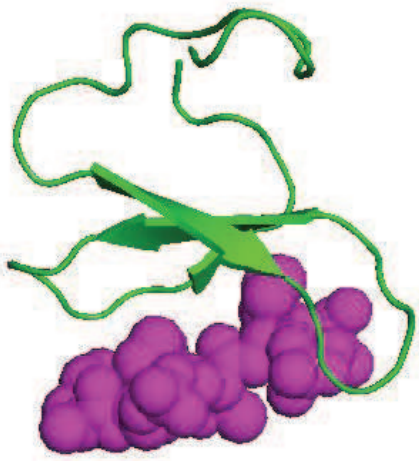

Figure 48: Crystal structure of the WW Domain of Pin1 (green) in complex with a phosphopeptide (magenta) (PDB 1F8A).

1.3.1. *In extracto* characterization

Determination of the working concentration window

WWRb was first tested upon incubation with melanoma cell extracts, in real time fluorescence assays using the same conditions as for CDKACTRb. Hence, WWRb was labeled with the fluorescent probe Cy3. Spectrofluorimetric experiments were performed in 96-well plates in standard kinase assay conditions for 1h at 30°C in the presence of 0.5 mM ATP and 5 mM $MgCl_2$. Given the predetermined optimal conditions for assays with CDKACTRb, the first experiment was performed using 25 - 50 nM WWRb-Cy3 and 20 - 40 µg A375 cell extracts. Fluorescence emission of Cy3-labelled WWRb was measured at 570 nm following excitation at 544 nm on a Clariostar™ fluorimeter. As for CDKACTRb, the response of Cy3-WWRb was obtained following subtraction of background fluorescence of Cy3-WWRb alone (Figure 49A). This experiment indicated that Cy3-labelled WWRb responded to the addition of cell extracts with 50% fluorescence enhancement, irrespective of the concentration of biosensor and cell extracts (Figure 49B). These data revealed that Cy3-labelled WWRb biosensor did not respond in a dose-dependent fashion to different concentrations of melanoma cell extracts.

Moreover, a second experiment, performed using 20 - 40 µg BSA instead of A375 cell extracts, demonstrated that the biosensor also responded to the addition of BSA (Figure 49C). These data indicated that Cy3-labelled WWRb biosensor did not respond specifically to CDK4 activity.

In the protein biosensor comprising a large PAABD derived from Plk1, the Cy3 dye responded to CDK4 activity. However, since Cy3 does not respond in WWRb, we hypothesized that this fluorophore was not suited for probing phosphosubstrate recognition by WW domain.

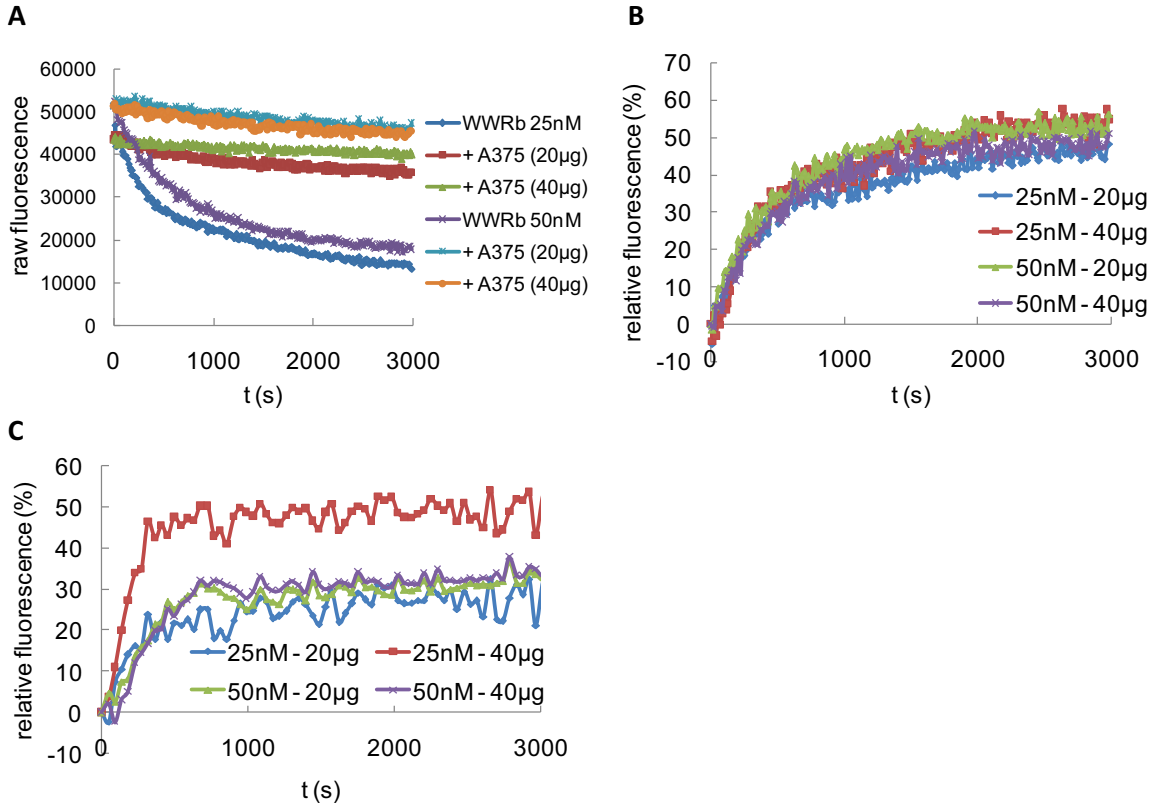

Figure 49: The response of 25 nM and 50 nM Cy3-WWRb upon incubation with different concentrations of A375 cell extracts or BSA (20 - 40 µg) was monitored in real time fluorescent assays. (A) Fluorescence emission of Cy3-WWRb alone or upon incubation with cell extracts was measured at 570 nm following excitation at 544 nm. (B) Fluorescent signals were obtained following subtraction of background fluorescence of WWRb-Cy3 alone. (C) Fluorescence emission of Cy3-WWRb alone or upon incubation with BSA was measured at 570 nm following excitation at 544 nm and fluorescent signals were obtained following subtraction of background fluorescence of WWRb-Cy3 alone.

Response of WWRb when labeled with different fluorescent probes

Given these unconclusive results, WWRb was labelled with TAMRA and compared with Cy3. A set of experiments in which 50 nM Cy3-WWRb and TAMRA-WWRb was incubated with 20 µg proteins from

A375 cell extracts was performed and PD-0332991 was used at 20 µM to inhibit CDK4 activity. The results from two independent experiments are presented in Figure 50. They demonstrated that, whether labeled with Cy3 or TAMRA, WWRb did not respond in a robust and reproducible fashion to the addition of A375 cell extracts, with or without addition of PD-0332991. This high variability renders the biosensor impossible to use with either of these probes.

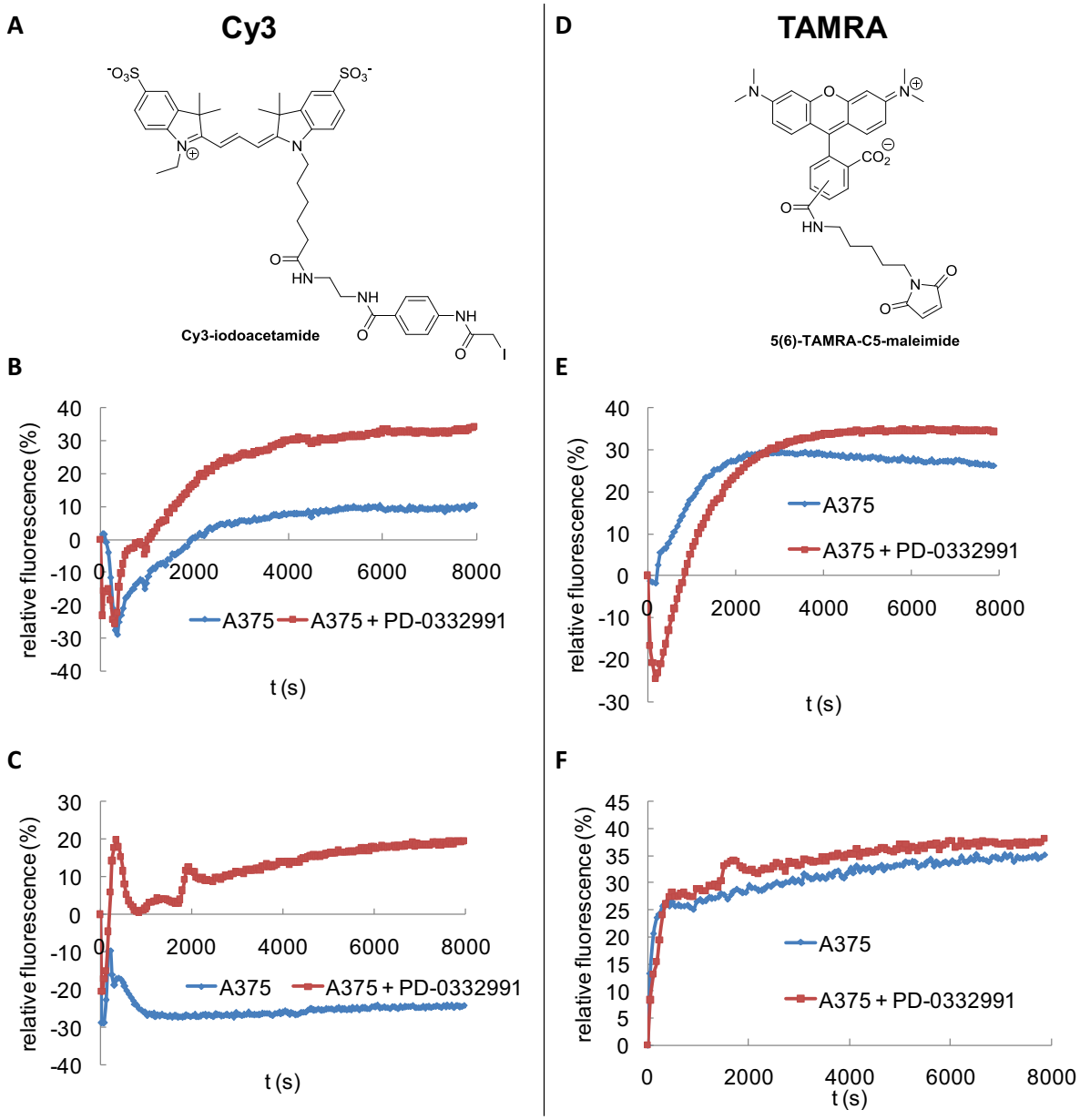

Figure 50: The response of 50 nM Cy3-WWRb (left panel) and TAMRA-WWRb (right panel) upon incubation with 20 µg A375 cell extracts and 20 µM PD-0332991 were monitored in real time fluorescence assays. Two independent experiments are shown (B&C for Cy3-WWRb and E&F for TAMRA-WWRb). The fluorescent signal was obtained following subtraction of background fluorescence of WWRb-Cy3 or WWRb-TAMRA alone. Chemical structures of Cy3 and TAMRA are presented in panels A and D.

Two other probes, Texas Red and FITC, were then tested for labeling WWRb. The same experiments as above were performed and results are shown in Figure 51. They revealed that, whether labeled with Texas Red or FITC, the biosensor responded in a robust and dose-dependent fashion to the addition of 20 - 40 µg A375 cell extracts (from 60 to 80% enhancement for Texas Red-WWRb and from 50 to 80% enhancement for FITC-WWRb). Moreover, they responded much less to the addition of 40 µg BSA (30% enhancement) compared to that of cell extracts. However, the inhibition of CDK4/cyclin D activity by PD-0332991 did not affect the fluorescence intensity of WWRb labeled with Texas Red or FITC, suggesting that they are again not responding specifically to CDK4.

A : Texas Red

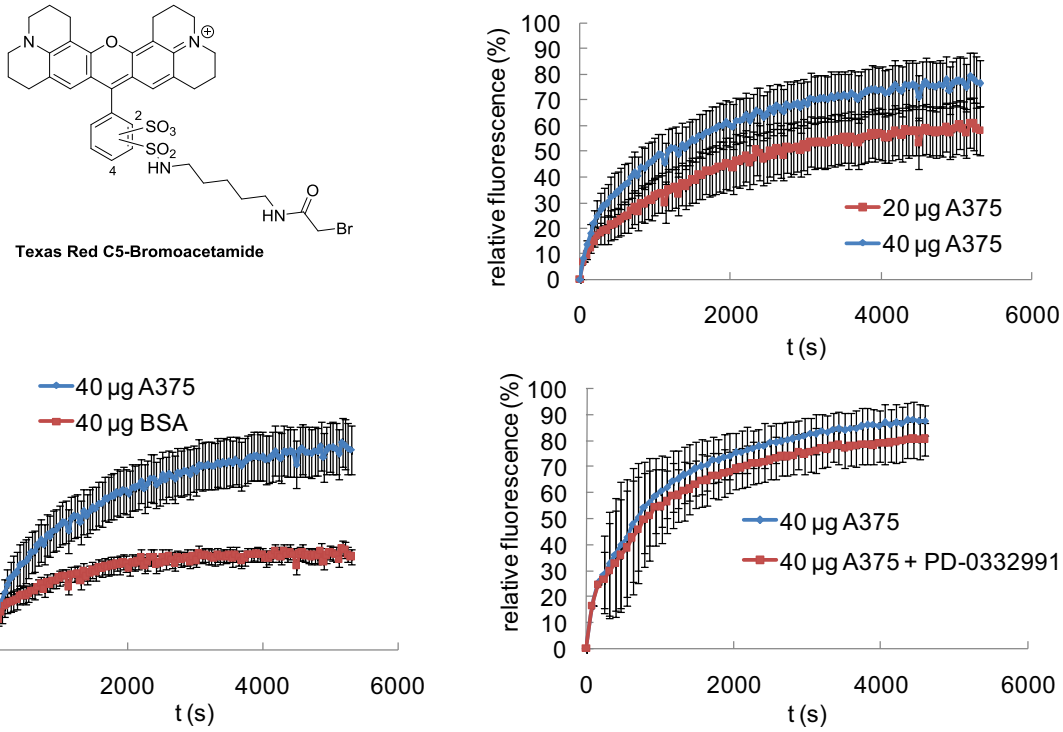

B : FITC

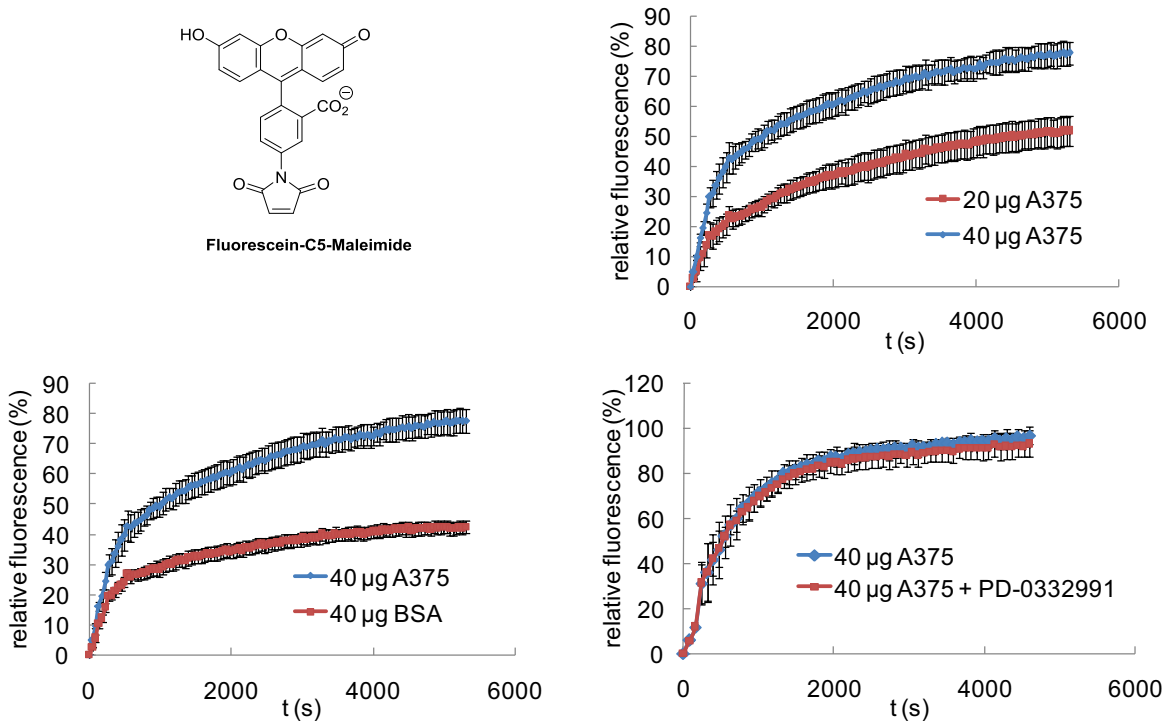

Figure 51: Responses of 50 nM Texas Red-WWRb (A) and FITC-WWRb (B) upon incubation with 20 - 40 µg A375 cell extracts or BSA and 20 µM PD-0332991 were monitored in real time fluorescent assays. The fluorescent signal was obtained following subtraction of background fluorescence of WWRb-Texas Red or WWRb-FITC alone. Chemical structures of Texas Red and FITC are shown together with corresponding curves.

Taken together, these data demonstrated that, irrespective of the fluorescent probe chosen for labeling WWRb, it did not respond specifically to CDK4/cyclin D activity when incubated with total proteins from cell extracts. This lack of specific response might be associated with a lack of conformation of WW domain in lysis buffer which is used for cell extract preparation and which contains detergents.

1.3.2. *In vitro* characterization

To validate this hypothesis, WWRb biosensor was tested *in vitro* with recombinant CDK4/cyclin D1. The experiment was performed with 150 nM TAMRA-WWRb, 75 nM CDK4/cyclin D1, 50 nM CIV and 10 µM PD-0332991 to inhibit CDK4 activity (Figure 52). Analysis of changes in fluorescence intensity showed that the biosensor responded to the addition of both monomeric CDK4 and dimeric CDK4/cyclin D1 through a net increase in relative fluorescence intensity (60 and 65%, respectively).

Relative increase in fluorescence further reached 75% when CDK4/cyclin D1 was pre-incubated with the CDK-activating kinase CIV (to phosphorylate the activation loop), but was reduced to 45% upon incubation with PD-0332991 (Figure 52). These data demonstrate that WWRb is capable of reporting on kinase activity of recombinant CDK4/cyclin D1, and that the signal observed can be uncoupled into a kinase binding step, which induces a first net increase in biosensor fluorescence (60% and 65% for the monomeric and the dimeric form, respectively), followed by a phosphotransfer step (10% additional contribution). The net decrease in fluorescence observed upon addition of PD-0332991 suggests that the inhibitor, when bound to the ATP pocket, prevents substrate phosphorylation but also modifies CDK4/cyclin D conformation, therefore reducing binding of the substrate to its kinase.

This experiment and the *in extracto* data suggest that WWRb responds to CDK4/cyclin D activity *in vitro* but is not sensitive and specific enough to be implemented for further experiments.

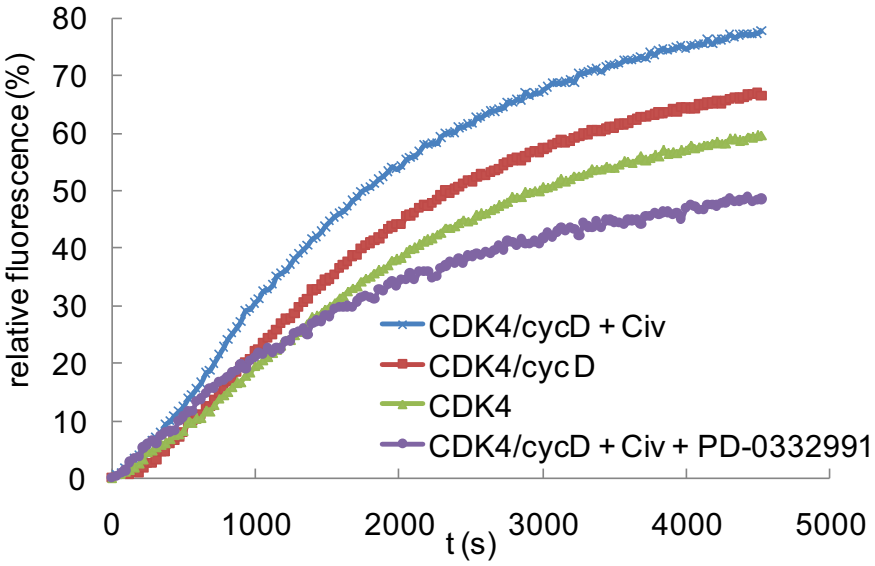

Figure 52: Fluorescence profile of 150 nM TAMRA-labelled WWRb peptide biosensor incubated with 75 nM recombinant GST-CDK4, GST-CDK4/GST-cyclin D1 or GST-CDK4/cyclin D1 pre-incubated with CIV to phosphorylate Thr172 +/- 10 µM PD-0332991. The fluorescent signal after subtraction of the background fluorescence of WWRb-TAMRA alone is presented.

1.4. WWshortRb

We therefore designed another peptide biosensor, **WWshortRb,** containing an artificial shorter PAABD sequence derived from the interface of the WW domain of Pin1 with a phosphopeptide substrate. This artificial domain was designed through analysis of the crystal structure of WW Pin1

complexed to a phosphopeptide substrate (PDB 1F8A) revealing that the residues which are critical for the interaction with the phosphosubstrate are Arg14, Arg17, Tyr23 and Phe25, as well as Trp34 (GWEKRMSRSSGRVYYFNHITNASQWERPSG) (Figure 53). A short peptide derivative of this WW domain (WWshort) was therefore synthesized which comprises these key residues in the linear order of appearance that mimicks the interface (Phe25, Arg14, Tyr23, Arg17) interspaced by small uncharged amino acids, and which ends with Trp34 followed by the same five amino acids as in the native WW domain of Pin1 (GFARVYMSRSSGWERPSG).

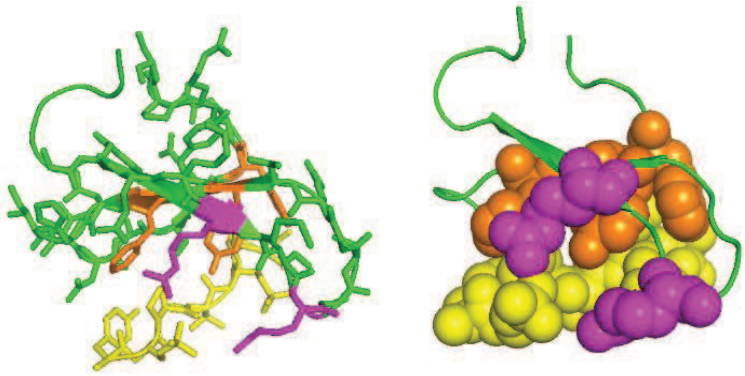

Figure 53: The Arg, Tyr, Phe and Trp residues at the interface between Pin1 WW domain (green) that recognize a phosphorylated peptide (yellow) are highlighted in pink (Arg14 and Arg 17) and orange (Tyr23, Phe25 and Trp34) (PDB 1F8A).

1.4.1. Titration experiments to validate the use of the WWshort PAABD

In order to validate the use of this novel shorter peptide sequence WWshort as PAABD, titration experiments were performed between the CDK4-specific Rb substrate peptide in its phosphorylated and unphosphorylated form labeled with FITC. 200 nM FITC-labelled peptides were titrated with increasing concentrations of WWlong (PAABD of WWRb) or WWshort (PAABD of WWshortRb) (from 0 to 3 µM). The results revealed that the WWshort peptide interacts with the phosphorylated form of Rb substrate peptide with a dissociation constant value of 80 +/- 37 nM, similar to the WWlong peptide (118 +/- 37 nM) (Figure 54A). In comparison the WWshort and WWlong peptides bound the unphosphorylated substrate peptide with significantly lower dissociation values 628 +/- 109 nM and 675 +/- 260 nM, indicating that they preferentially bind the phosphorylated substrate, as expected from a PAABD (Figure 54B). Moreover, in both cases, the WWshort peptide promoted greater

fluorescence enhancement of the fluorescently-labelled Rb substrate than its native counterpart, suggesting it was better suited as a PAABD for a biosensing application.

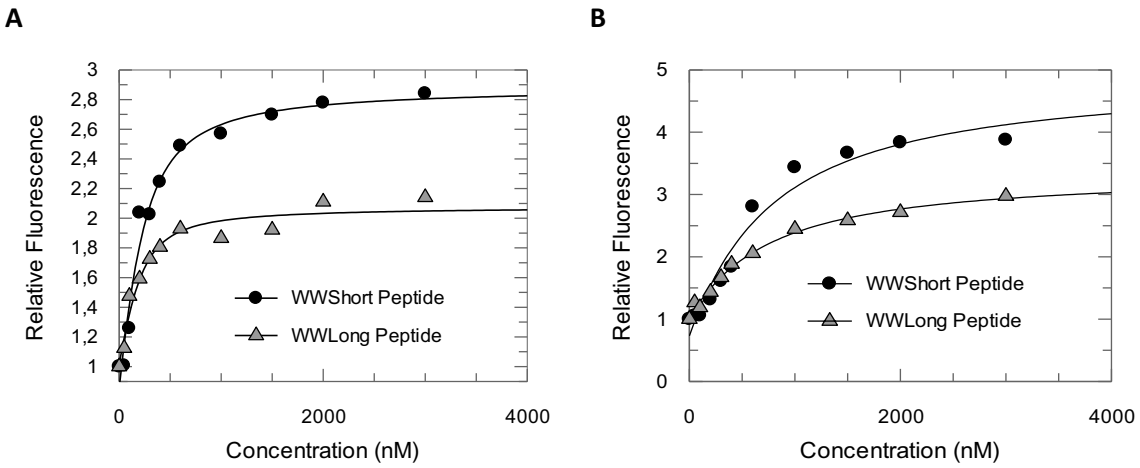

Figure 54: Fluorescence titration of 200 nM FITC-labelled phospho-Rb (A) and Rb (B) peptides. Both the WWlong peptide and the WWshort peptide interacted preferentially with the phospho-Rb substrate peptide. In both cases, the WWshort peptide promoted greater fluorescence enhancement of the fluorescently-labelled Rb substrate than the WWlong peptide.

The WWshortRb biosensor was synthesized, with the WWshort peptide followed by the CDK4-specific Rb substrate sequence. To verify that the Rb substrate peptide could bind the recombinant form of CDK4, fluorescence titration assays were performed with 200 nM FITC-labelled Rb substrate peptide and increasing concentrations of GST-CDK4 or GST-CDK4/GST-cyclin D1 (from 0 to 200 nM). The experiments revealed that it bound monomeric GST-CDK4 with a dissociation constant of 30 +/- 5 nM and its affinity increased to 7 +/- 3 nM when the kinase was complexed to cyclin D1 (Figure 55). This result is in line with studies showing that the substrate preferentially binds the catalytic cleft of heterodimeric CDK2/cyclin A, which is conformationally more favourable than that of monomeric CDK2.

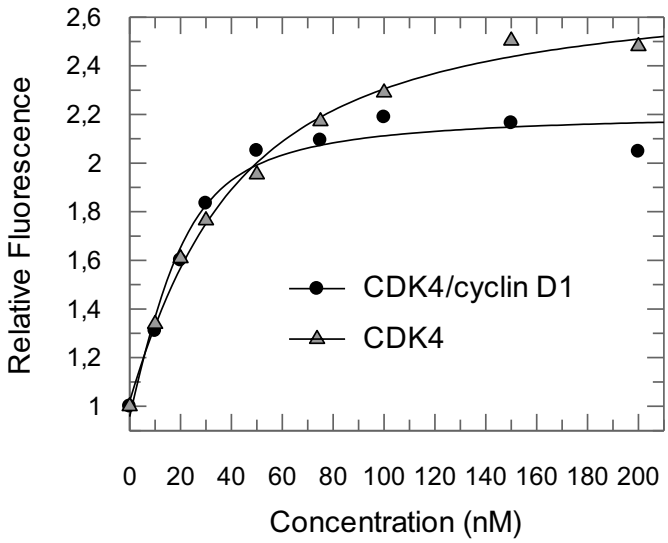

Figure 55: Fluorescence titration of FITC-labeled Rb substrate peptide (200 nM) with monomeric GST-CDK4 and GST-CDK4/cyclin D1 complex. The Rb peptide interacts preferentially with the heterodimeric complex than with the monomeric GST-CDK4.

1.4.2. *In extracto* characterization

Choice of the probe

WWshortRb was first tested in real time fluorescence assays using the same conditions as CDKACTRb. Hence, WWshortRb was labeled with the environmentally-sensitive fluorescent probe Cy3. Spectrofluorimetric experiments were performed in 96-well plates in standard kinase assay conditions for 1h at 30°C in the presence of 0.5 mM ATP and 5 mM $MgCl_2$. The first experiment was performed using 50 nM WWshortRb-Cy3 and 20 µg A375 cell extracts. Fluorescence emission of Cy3-labelled WWshortRb was measured at 570 nm following excitation at 544 nm on a Clariostar™ fluorimeter. This experiment revealed that Cy3-labelled WWshortRb did not respond in a robust and reproducible fashion to the addition of cell extracts and the fluorescent signal of the biosensor was only amplified by 5% (Figure 56).

Instead of Cy3, TAMRA was then tested for labeling WWshortRb. The same experiment as above was performed and results demonstrated that TAMRA-labelled WWshortRb responds robustly to the addition of A375 cell extracts (Figure 56). The fluorescent signal of the biosensor is amplified by 20% alter 1h of reaction. Based on these results, TAMRA was further used for labeling WWshortRb.

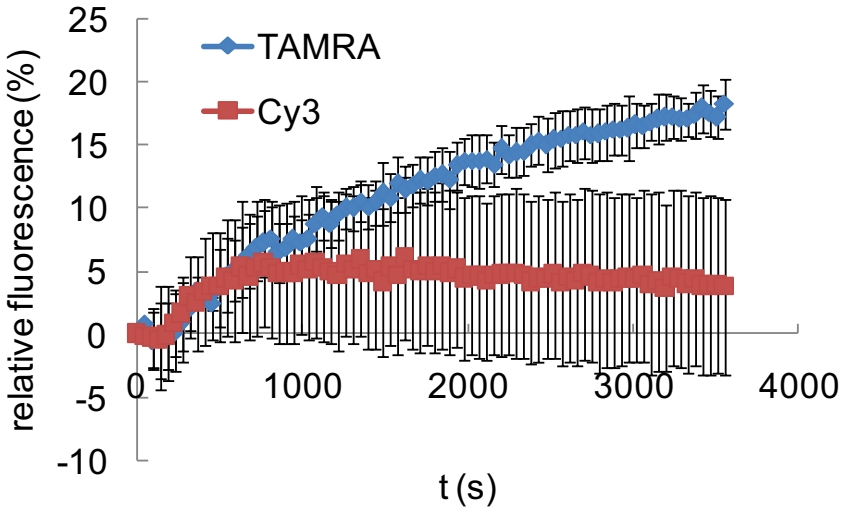

Figure 56: Real-time fluorescence assays with 20 µg A375 melanoma cell extracts as source of endogenous CDK4/cyclin D and 50 nM WWshortRb labeled either with TAMRA (blue) or Cy3 (red). The fluorescent signal after subtraction of the background fluorescence of WWshortRb alone is presented.

In order to determine the appropriate working window for TAMRA-labelled WWshortRb, different concentrations of both the biosensor and A375 cell extracts were tested. The first experiment was set up with a fixed concentration of 40 µg of proteins from A375 cell extracts and increasing concentrations of TAMRA-labelled WWshortRb, between 50 and 200 nM. The results showed that fluorescence emission increased in a dose-dependent fashion (10 - 40% enhancement) within a window of 50 - 150 nM WWshortRb-TAMRA (Figure 57A). At 50 nM, the biosensor started to display fluorescence enhancement, whilst at 200 nM, there was a drop in the fluorescent signal compared to that of 150 nM. It was hypothesized that this reduction in fluorescence was due to homoquenching between probes at this concentration of biosensor.

The second experiment was set up with a fixed concentration of 150 nM TAMRA-labelled WWshortRb and increasing concentrations of proteins from A375 cell extracts (from 10 to 100 µg) (Figure 57B). The results indicated that the biosensor displayed the greatest fluorescence increase within a window of 40 – 100 µg cell extracts (40% enhancement). The fact that any additional fluorescence increase was observed upon incubation with more than 40 µg cell extracts suggested that, a 1:1 stoichiometry is reached between the biosensor and the kinase at this threshold

concentration. The same experiment was performed using increasing concentrations of BSA instead of A375 cell extracts (Figure 57C). No fluorescence enhancement was observed with BSA, revealing that the biosensor did not respond to the addition of irrelevant proteins.

In conclusion, the greatest fluorescence enhancement was obtained with 150 nM TAMRA-labelled WWshortRb and 40 µg proteins from A375 cell extracts.

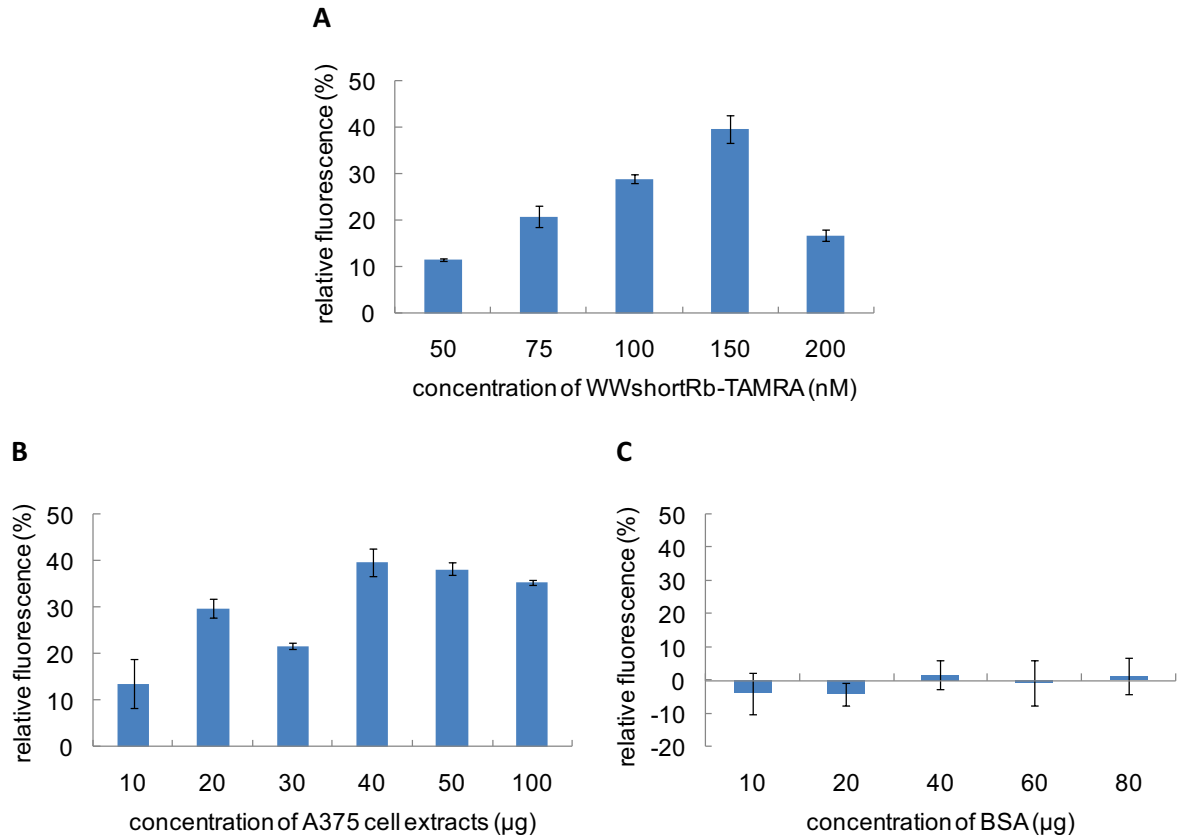

Figure 57: Determination of working concentrations of WWshortRb and A375 cell extracts in real time fluorescent assays. Fluorescence emission of TAMRA-WWshortRb was measured at 570 nm following excitation at 544 nm. The fluorescent signal was obtained following subtraction of background fluorescence of TAMRA-WWshortRb alone and the histograms represent the fluorescent signal at the endpoint of the assay (5000s).

(A) Assays with 40 µg A375 cell extracts and increasing concentrations of TAMRA-WWshortRb

(B) Assays with 150 nM of TAMRA-WWshortRb and increasing concentrations of proteins from A375 cell extracts.

(C) Assays with 150 nM of TAMRA-WWshortRb and increasing concentrations of BSA.

Additional controls

The response of 150 nM TAMRA-WWshortRb was then compared to other peptides labeled with TAMRA upon incubation with 40 µg melanoma cell extracts. The incubation with A375 cell extracts resulted in a robust increase in fluorescence of TAMRA-WWshortRb (30%) whereas TAMRA-labelled Rb substrate peptide and TAMRA-labelled MP26 peptide (an irrelevant peptide that does not bind CDKs or cyclins) did not exhibit any change in fluorescence (Figure 58A and B). These experiments showed that the increase in fluorescence of TAMRA-WWshortRb was not a response of the probe itself. Moreover they demonstrated the requirement of the PAABD for robust response to CDK4 kinase activity in cell extracts.

The response of TAMRA-WWshortRb was then compared to Dylight650-WWshortRb. While the incubation with A375 cell extracts resulted in a robust increase in fluorescence of TAMRA-WWshortRb (30%), the Dylight650-labelled WWshortRb peptide barely responded to CDK4 activity in cell extracts (10% enhancement) (Figure 58C). This result indicated that the response of WWshortRb was associated with the sensitivity of the dye conjugated to the peptide, as previously shown with Cy3-labelled WWshortRb. Moreover, as Dylight650 (λexc = 652 nm; λem = 672 nm) and TAMRA (λexc = 540 nm; λem = 565 nm) have different spectral properties, the Dylight650-labelled WWshortRb peptide constitutes a useful negative control.

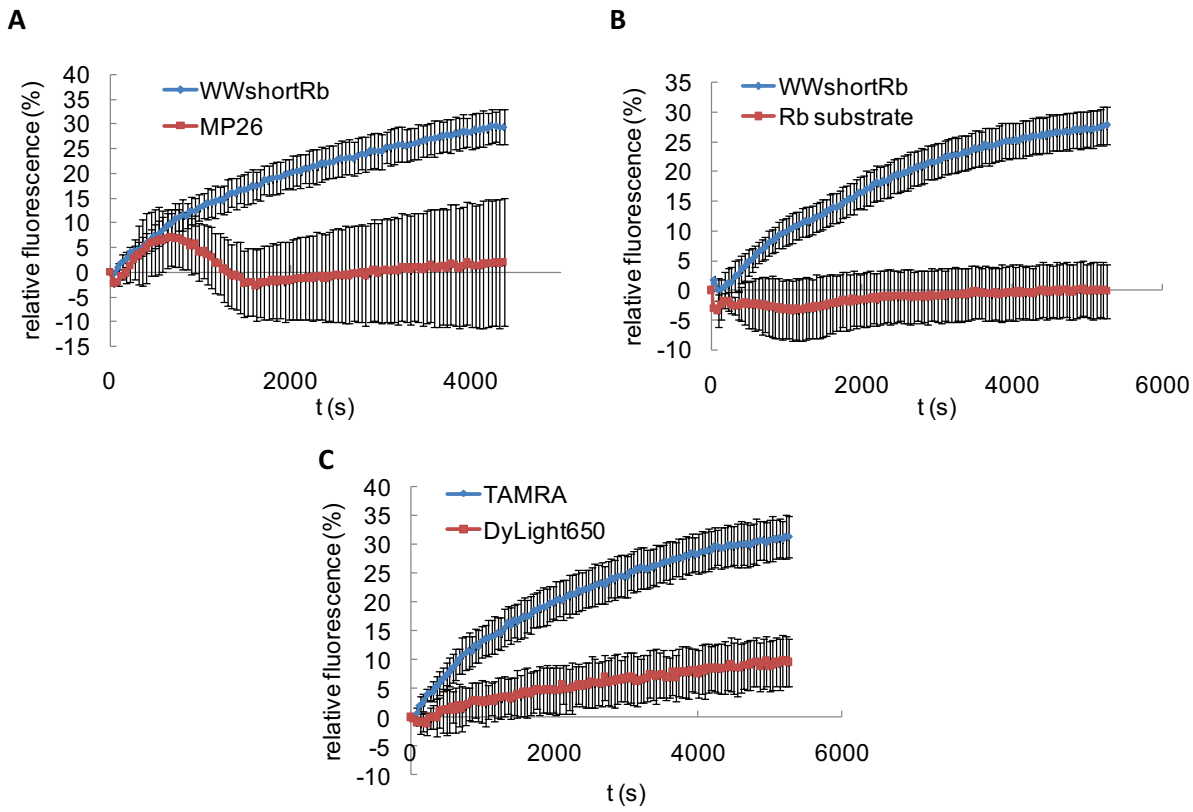

Figure 58: Fluorescence of 150 nM TAMRA-labelled WWshortRb peptide biosensor was monitored over time upon incubation with 40 µg A375 cell extracts and compared to (A) 150 nM TAMRA-labelled MP26 peptide; (B) 150 nM TAMRA-labelled Rb substrate peptide; (C) 150 nM Dylight650-labelled WWshortRb. The fluorescent signal was obtained following subtraction of background fluorescence of TAMRA-labelled or DyLight650-labelled WWshortRb alone.

Response of WWshortRb upon incubation with A375 cell extracts +/- siRNA targeting CDK4

To verify whether the biosensor was sensitive to CDK4 expression in cells, an experiment was performed, in standard kinase assay conditions, with 150 nM WWshortRb-TAMRA and 40 µg cell extracts from A375 cells that had been treated or not with siRNA targeting CDK4. Western blotting was performed in parallel to assess the efficacy of the siRNA. After 48h of treatment, CDK4 levels were decreased by 45% compared with that of the control sample (Figure 59A & B). The activity assay showed that the fluorescence response of WWshortRb was reduced (25%) upon incubation with extracts from A375 cells that had been treated with siRNA compared with extracts from untreated A375 (30% enhancement) (Figure 59C & D). The correlation between Western blot and the activity fluorescent curves demonstrates the sensitivity of the sensor for CDK4.

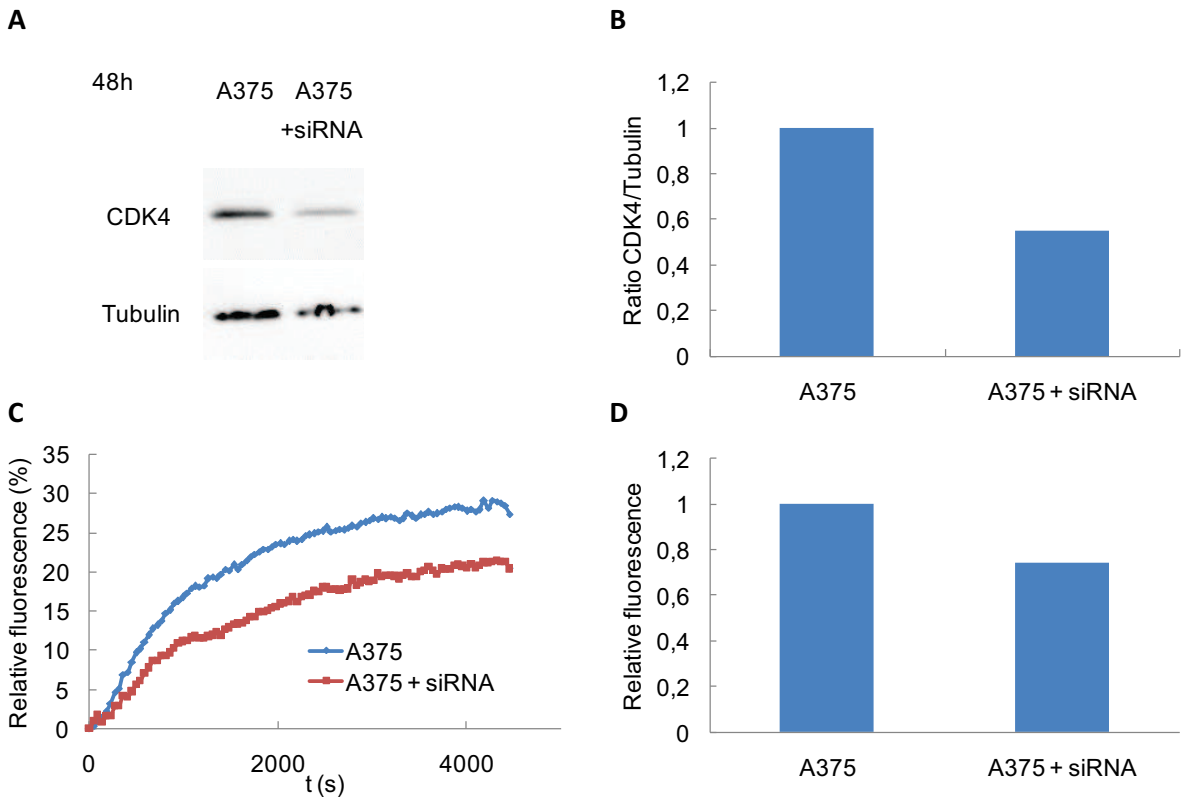

Figure 59: Real time fluorescence of TAMRA-labelled WWshortRb upon incubation with A375 cell extracts +/- siRNA targeting CDK4.

(A) Western blotting of CDK4 in A375 cells treated or not with siRNA targeting CDK4; (B) Quantification of CDK4/Tubulin levels.

(C) Fluorescent kinase assays with 150 nM WWshortRb-TAMRA and 40 µg cell extracts from A375 cells treated or not with siRNA targeting CDK4. The fluorescent signal was obtained following subtraction of background fluorescence of WWshortRb-TAMRA alone; (D) The histogram represents the fluorescent signal at the endpoint of the assay (5000s)

Identification of fractions containing CDK4 activity from A375 cell extracts fractionated by gel filtration chromatography

To assess whether the biosensor could be exploited to discriminate between fractions which contained CDK4 or not, real time fluorescence assays were performed with 150 nM WWshortRb-TAMRA and A375 cell extracts fractionated by gel filtration chromatography (Superose 6). Results presented in Figure 60 demonstrate that only fractions containing CDK4 (as detected by Western blotting) promoted a significant increase in WWshortRb biosensor fluorescence. Calibration of the Superose 6 column with Dextran, Conalbumin, Ovalbumin and Carboxic anhydrase allowed to determine the molecular weight of proteins contained in the different fractions. This experiment

provides further evidence of the utility of WWshortRb to distinguish all fractions in which CDK4 is active or not.

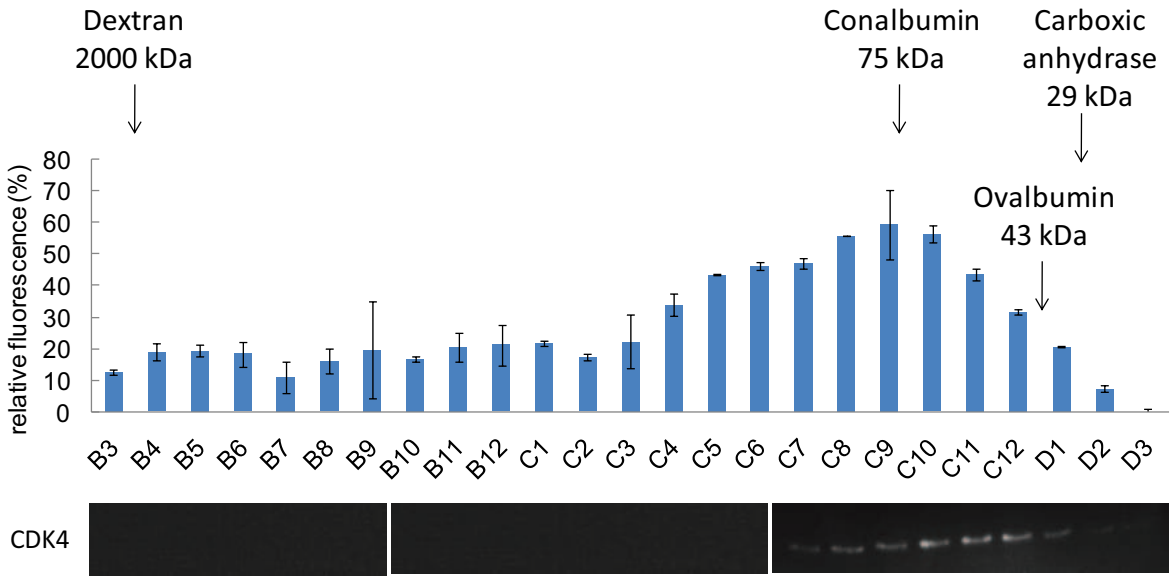

Figure 60: Fluorescence of 150 nM TAMRA-labelled WWshortRb biosensor upon incubation with fractions of A375 cell extracts purified by gel filtration chromatography (Superose 6). The fluorescent signal was obtained following subtraction of background fluorescence of TAMRA-WWshortRb alone and the histogram represents the fluorescent signal at the endpoint of the assay (5000s). At the bottom, Western blotting of CDK4 in the different fractions is presented.

Response of WWshortRb upon incubation with A375 cell extracts +/- ATP/$MgCl_2$

To further validate that observed fluorescence enhancement was associated with kinase activity, a set of assays was performed in which 150 nM WWshortRb-TAMRA was incubated with 40 µg A375 cell extracts in the presence or absence of 0.5 mM ATP and 5 mM $MgCl_2$. Figure 61A shows the fluorescent signal of the biosensor in both conditions, revealing that the maximal fluorescence of WWshortRb-TAMRA was reduced in the absence of ATP/$MgCl_2$ (10% fluorescence decrease). The difference in WWshortRb response in the presence or absence of ATP/$MgCl_2$ corresponds to the phospho-transfer contribution (10% delta) (Figure 61B).

These data demonstrate that, when the phosphotransfer reaction is prevented, binding of CDK4 kinase to the Rb substrate sequence is responsible for a first increase in fluorescence, which is then further enhanced by phosphorylation. This experiment therefore demonstrates that WWshortRb is capable of reporting on kinase activity of CDK4/cyclin D in melanoma cell extracts, and that the signal

observed can be uncoupled into a kinase binding step which induces a first partial increase in biosensor fluorescence, followed by a phosphotransfer step.

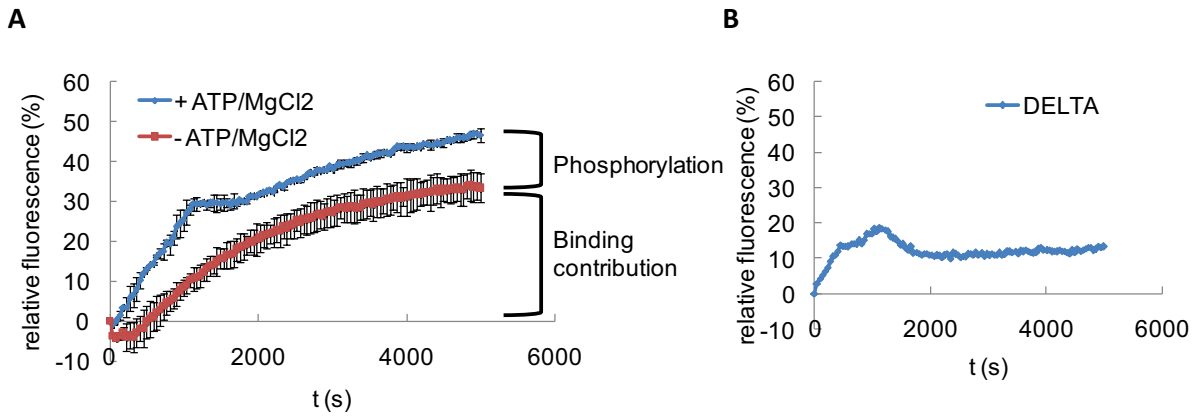

Figure 61: Response of 150 nM WWshortRb upon incubation with 40 µg A375 cell extracts +/- ATP/$MgCl_2$. Fluorescence emission of TAMRA-WWshortRb was measured at 570 nm following excitation at 544 nm on Clariostar™ fluorimeter.

(A) The fluorescent signal after substraction of the background fluorescence of WWshortRb alone is presented.

(B) The curve displays the contribution of the phosphotransfer step in the fluorescence response of WWshortRb. The kinetic curve in the absence of ATP/$MgCl_2$ was subtracted from the curve in the presence of ATP/$MgCl_2$.

Response of WWshortRb upon addition of different kinase inhibitors

Experiments were performed in standard kinase assay conditions with 150 nM WWshortRb-TAMRA and 40 µg cell extracts from A375 cells treated with different concentrations of PD-0332991, LY2835219 or Roscovitine (from 0 to 20 µM).

Figure 62 shows that the addition of increasing concentrations of CDK4/6 inhibitors PD-0332991 and LY2835219 decreased the fluorescent signal of the biosensor in a dose-dependent fashion whereas no significant fluorescence decrease was detected upon the addition of Roscovitine, inhibitor of CDK1/2/5/7/9. Taken together, these results and those obtained with the protein biosensor suggest that the CDK4-specific Rb substrate sequence enables both biosensors to be selective and specific for CDK4/cyclin D.

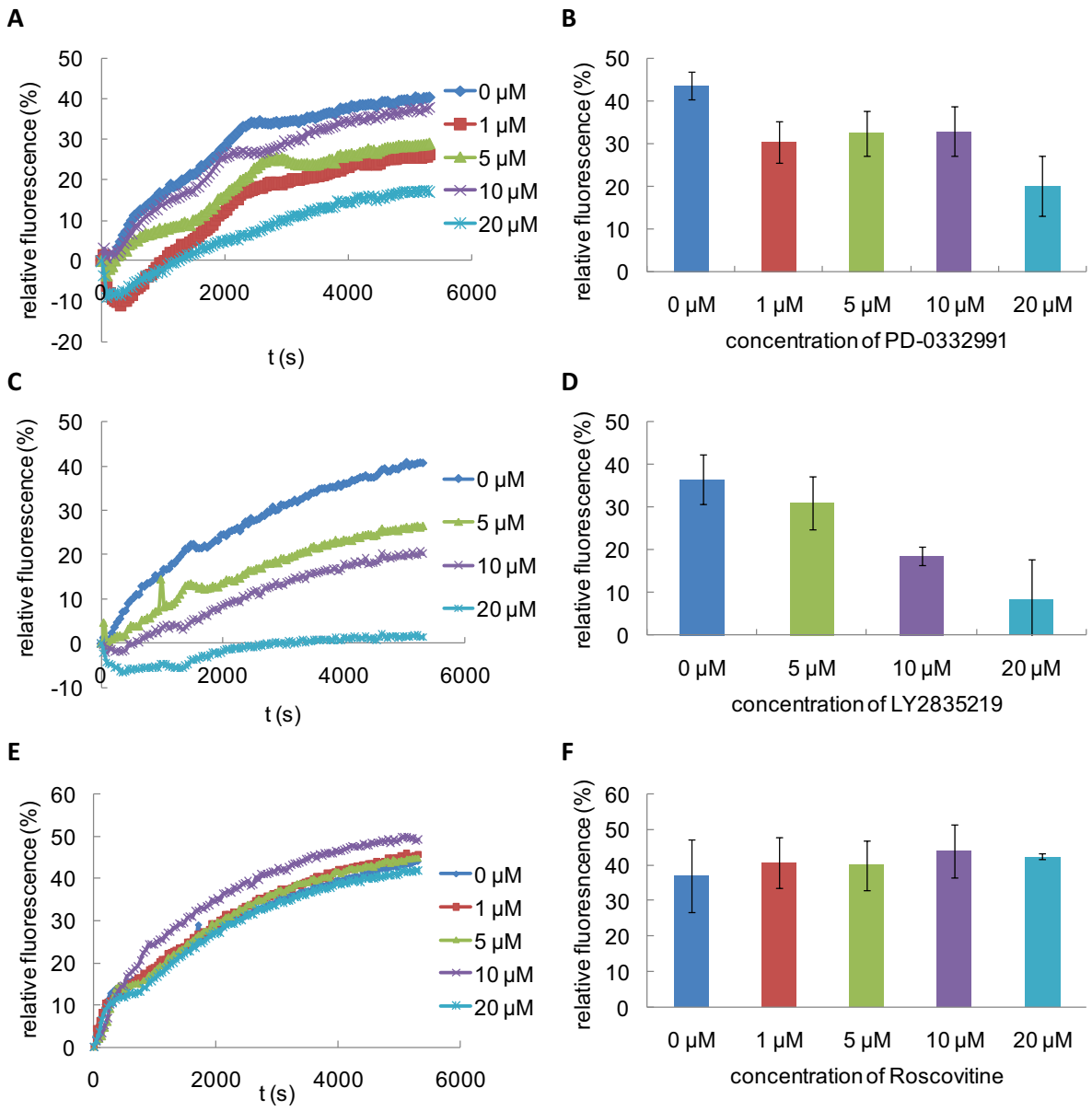

Figure 62: Fluorescence of 150 nM TAMRA-labelled WWshortRb biosensor was monitored over time upon incubation with 40 µg cell extracts from A375 cells treated with different concentrations PD-0332991 (A & B), LY2835219 (C & D) or Roscovitine (E & F) (from 0 to 20 µM). The fluorescent signal was obtained following subtraction of background fluorescence of TAMRA-WWshortRb alone and the histograms represent the fluorescent signal at the endpoint of the assay (5000s).

Since DMSO, in which all stock solutions of inhibitors were made, could affect the fluorescence of the biosensor alone, emission fluorescence of WWshortRb-TAMRA at 570 nm following excitation at 544 nm was measured in presence of different concentrations of DMSO. A range from 0 to 0.2% was tested, which corresponds to the residual concentrations of DMSO found after dilution of the inhibitors in a standard kinase assay. PD-0332991, LY2835219 and Roscovitine were also tested at

concentrations that were used to inhibit CDK4/cyclin D (from 0 to 20 µM). Histograms in Figure 63 correspond to the average emission fluorescence at 570 nm of duplicate experiments with standard deviation bars. The fluorescent signal of WWshortRb-TAMRA alone was arbitrarily considered as 1. These experiments provided evidence that neither PD-0332991, LY2835219, Roscovitine nor DMSO had any significant effect on the fluorescence of WWshortRb-TAMRA.

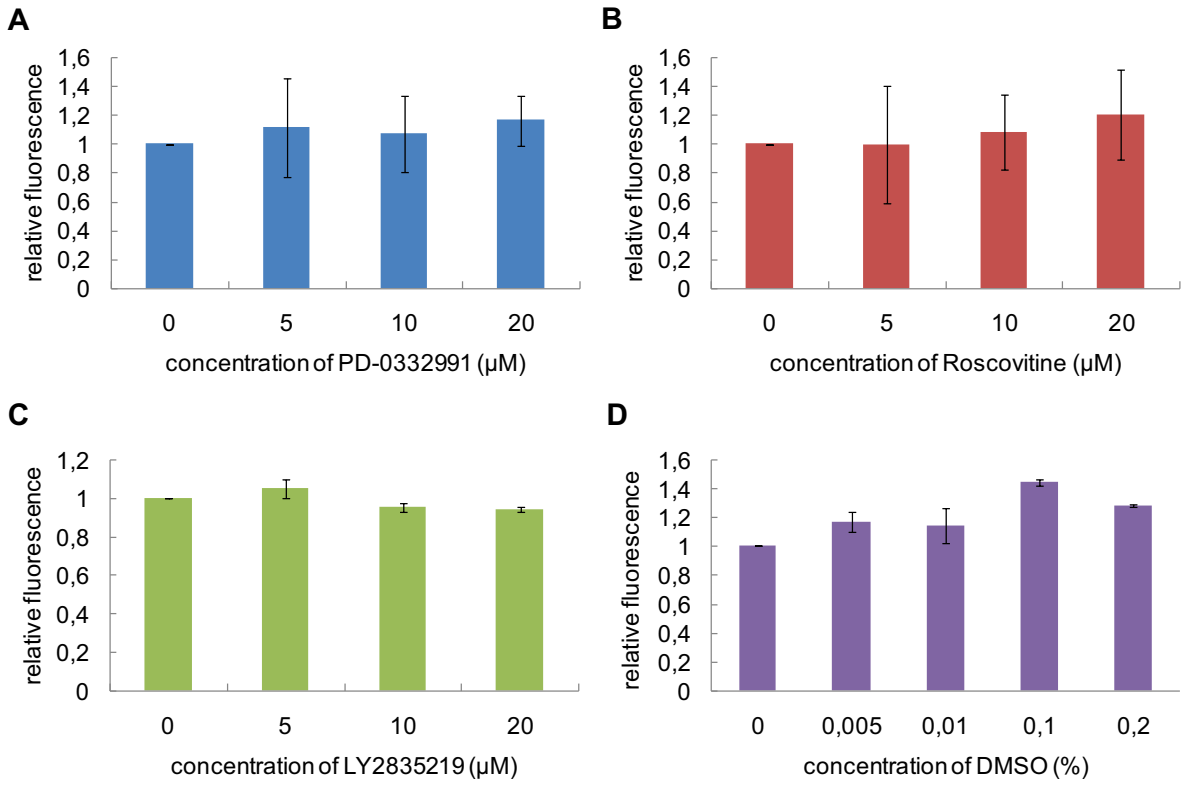

Figure 63: Effects of PD-0332991 (A), LY2835219 (B), Roscovitine (C) and DMSO (D) on the fluorescence of WWshortRb-TAMRA.

1.4.3. Characterization of recombinant CDK4 kinase activity

WWshortRb was then implemented to monitor response to recombinant CDK4 kinase *in vitro* in the presence of ATP and $MgCl_2$, following labelling with TAMRA. The experiment was performed with 150 nM TAMRA-WWshortRb, 75 nM CDK4/cyclin D1 and 50 nM CIV. PD-0332991 was used at 10 µM to inhibit CDK4 activity. Analysis of changes in fluorescence intensity showed that the biosensor responded to the addition of CDK4/cyclin D1 through a net increase in relative fluorescence intensity (65%) over time, whereas incubation with monomeric CDK4 had much less incidence on fluorescence increase (only 40%) (Figure 64). Relative increase in fluorescence further reached 75% when

CDK4/cyclin D1 was pre-incubated with the CDK-activating kinase CIV (to phosphorylate the activation loop), but was reduced to a similar level as inactive (unphosphorylated) CDK4/cyclin D1 (55%) upon incubation with PD-0332991 (Figure 64).

These data demonstrate that WWshortRb is capable of reporting on kinase activity of recombinant CDK4/cyclin D1, and that the signal observed can be uncoupled into a kinase binding step which induces a first increase in biosensor fluorescence, followed by a phosphotransfer step. The difference in WWshortRb response when incubated with inactive or active CDK4/cyclin D1 corresponds to the phospho-transfer contribution (10% delta). This result is in line with that obtained upon incubation of the biosensor with 40 µg A375 cell extracts in the presence or absence of ATP/$MgCl_2$ (Figure 61). The same phospho-transfer contribution (10% delta) is found in this experiment.

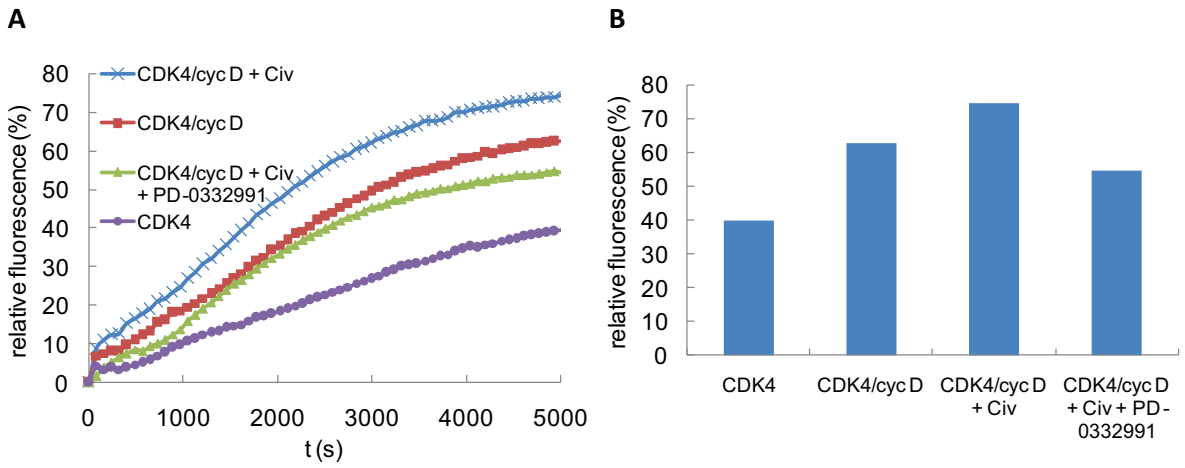

Figure 64: Typical fluorescence profile of 150 nM TAMRA-labelled WWshortRb peptide biosensor incubated with 75 nM recombinant GST-CDK4, GST-CDK4/GST-cyclin D1 or GST-CDK4/cyclin D1 pre-incubated with CIV to phosphorylate Thr172 +/- 10 µM PD-0332991. (A) The fluorescent signal was obtained following subtraction of background fluorescence of TAMRA-WWshortRb alone (B) The histogram represents the fluorescent signal at the endpoint of the assay (5000s).

1.4.4. Profiling CDK4/cyclin D activity in healthy and cancer cell lines

To ask whether WWshortRb could be implemented to compare CDK4 activity between different cell lines, real time fluorescence assays were performed with 150 nM WWshortRb-TAMRA and 40 µg proteins from different cell extracts. The human melanoma A375 cell line was first compared with a healthy human fibroblast cell line. Figure 65A and B present the fluorescence emission of TAMRA-WWshortRb at 570 nm following excitation at 544 nm. The addition of A375 cell extracts promoted a

significant 45% increase in WWshortRb fluorescence whereas only a 30% fluorescence increase was detected upon the addition of fibroblast cell extracts. The reaction rate was calculated over the first 15 min of the reaction and revealed that the kinetics of phosphorylation of the biosensor are much faster upon incubation with A375 than fibroblast cell extracts (Figure 65C). Then, A375 melanoma cell line was compared with different melanoma cell lines harbouring different combinations of wild-type or loss-of function $p16^{INK4A}$ (the endogenous inhibitor of CDK4), wild-type or mutated CDK4 (R24C mutation which prevents the binding of $p16^{INK4A}$), BRaf and NRas (Figure 65E/F). Fluorescent profiles of the WWshortRb revealed the highest CDK4 activity in A375 (CDKN2A loss of function, BRaf V600E), Mewo (CDKN2A loss of function, Wt CDK4) and SK-MEL28 (R24C CDK4, BRaf V600E) cell lines (about 40% enhancement), followed by SK-MEL2 (NRas mutation (Q61R)) (25%) and MV3 (20%). The reaction rate was calculated over the first 15 min of the reaction and revealed that the kinetics of phosphorylation of the biosensor are similar in A375, Mewo, SKMEL28 and SKMEL2 cell extracts and much slower upon incubation with MV3 cell extracts (Figure 65G). These response profiles are consistent with the genotypes of these strains in which loss of function of CDKN2A or mutation of the R24C CDK4 mutant both lead to unrestricted, constitutive activity of CDK4. However, they do not coincide with Western blot profiles, which only provide limited information on CDK4 protein levels (Figure 65D/H). Indeed, overall CDK4 activity is associated with expression levels but also with CDK4 regulation in the $p16^{INK4A}$ / CDK4/6-cyclin D / pRb pathway.

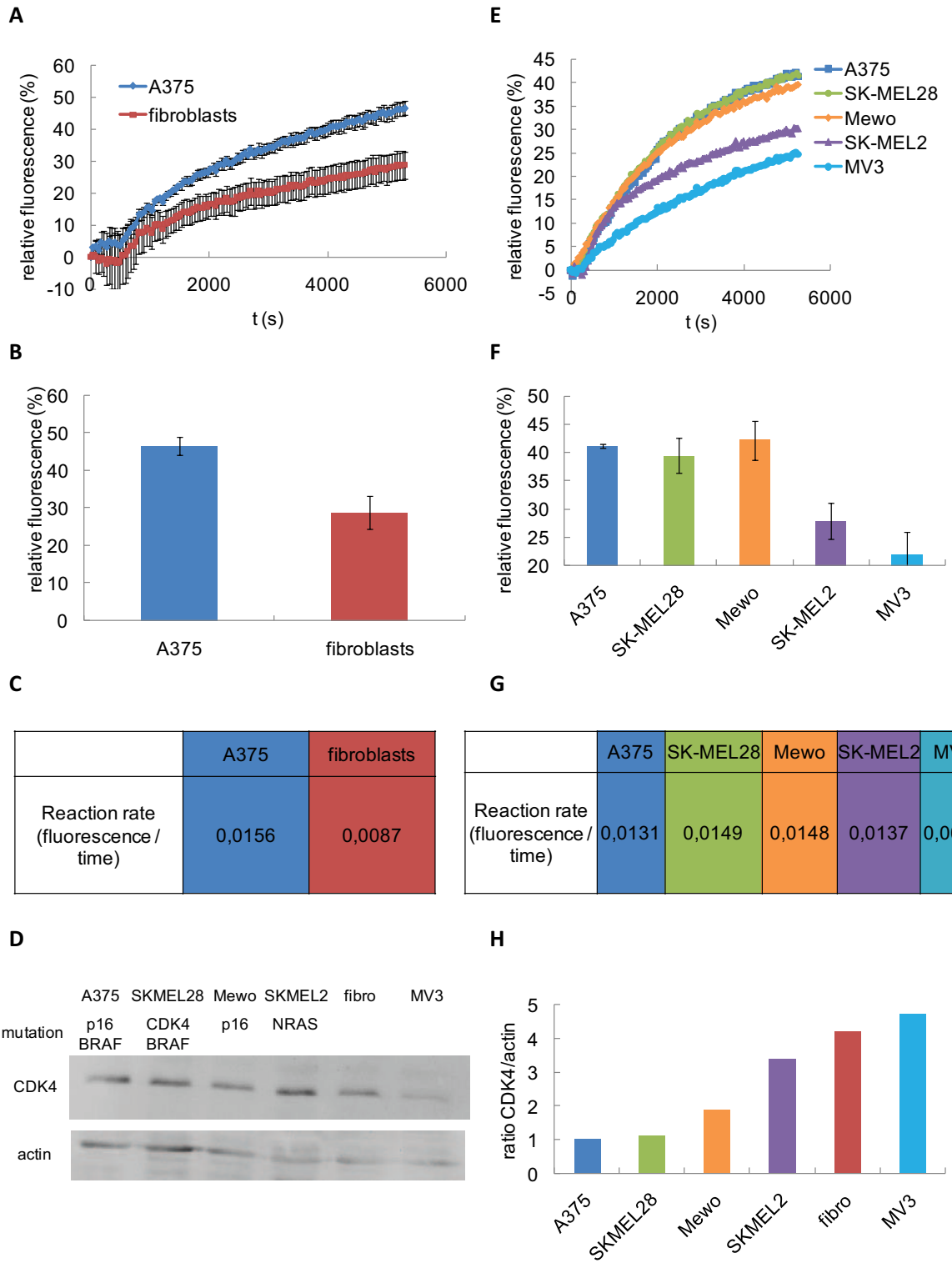

	A375	fibroblasts
Reaction rate (fluorescence / time)	0,0156	0,0087

	A375	SK-MEL28	Mewo	SK-MEL2	MV3
Reaction rate (fluorescence / time)	0,0131	0,0149	0,0148	0,0137	0,0067

Figure 65: Real time fluorescence of 150 nM TAMRA-labelled WWshortRb peptide biosensor upon incubation with 40 µg cell extracts from different cell lines. The fluorescent signal was obtained following subtraction of background fluorescence of TAMRA-WWshortRb alone and the histogram represents the fluorescent signal at the endpoint of the assay (5000s). The reaction rate was calculated from the linear slope of the reaction during the first 15 min (900s).

(A, B & C) A375 or fibroblast cell lines

(E, F & G) A375, Mewo, SK-MEL2, SK-MEL28, MV3 melanoma cell lines

(D) Western blotting profiles of CDK4 and actin in A375, SKMEL28, Mewo, SK-MEL2, MV3 and fibroblasts

(H) Quantification of CDK4/actin levels

1.4.5. Implementation of WWshortRb biosensor to probe CDK4 activity in skin biopsies

Since WWshortRb peptide biosensor responded to CDK4 activity in melanoma cell extracts and reported on differences between cell lines with different $p16^{INK4A}$ and CDK4 genotypes, its application to quantify CDK4 activity in skin biopsies was further investigated (materials and methods). Skin biopsies for kindly provided by Dr. Laurent Meunier (CHU, Nîmes). First, the response of 150 nM WWshortRb-TAMRA was calibrated using different concentrations of total healthy skin samples, relative to A375 cell extracts (Figure 66A and B). Fluorescence emission of TAMRA-WWshortRb increased in a dose-dependent fashion (5 - 30% enhancement) within a window of 10 - 100 µg skin samples. However, with 150 µg proteins from skin samples, the fluorescence intensity of the biosensor started to decrease (20%). This reduction in fluorescence at this high concentration of cell extracts may be explained by the presence of many phosphatases which dephosphorylate the biosensor. It could also be due to the presence of many proteins extracted from skin cells such as hair follicles, nerves, sweat glands and small blood capillaries but also by the presence of extracellular matrix proteins such as collagen, which can together alter the fluorescent signal of the biosensor.

As with melanoma cell extracts, WWshortRb fluorescence was decreased by addition of 20 µM PD-0332991, especially upon incubation with 100 µg skin samples (Figure 66C). It suggests that 100 µg of cell extracts provide the optimal concentration of CDK4 kinase to be phosphorylated by 20 µM PD-0332991.

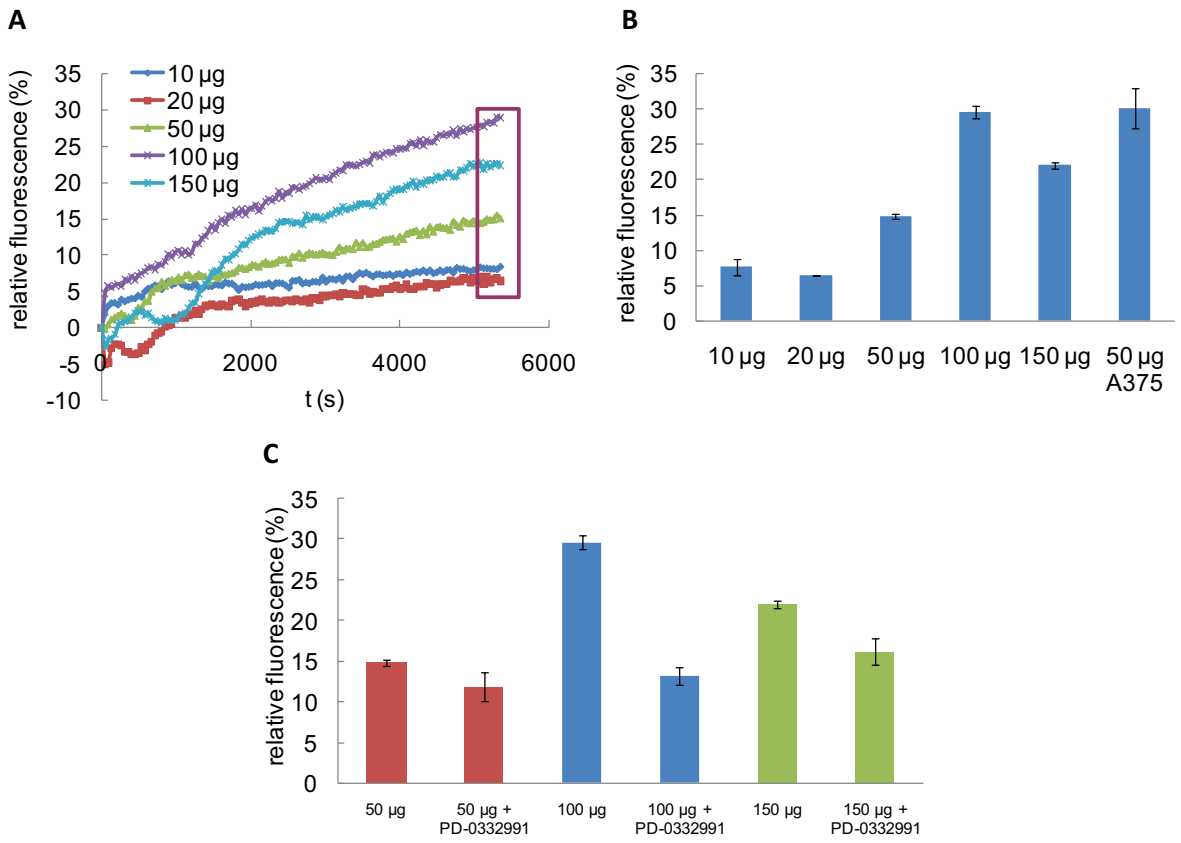

Figure 66: Real time fluorescence of 150 nM TAMRA-labelled WWshortRb upon incubation with healthy skin biopsies. The fluorescent signal was obtained following subtraction of background fluorescence of TAMRA-WWshortRb alone.

(A) Concentration-dependent response of healthy skin samples (from 10 to 150 µg).

(B) Results at the endpoint of the assay (5000 s) are presented as histograms corresponding to the average of duplicate experiments with standard deviation bars. Healthy skin samples are compared to 50 µg A375 cell extracts.

(C) Fluorescence response of TAMRA-WWshortRb peptide to 50, 100 and 150 µg healthy skin samples treated with PD-0332991. The histogram represents the fluorescent signal at the endpoint of the assay (5000s).

The biosensor was then applied to detect differences in CDK4 activity in the dermis and epidermis, and found that it was essentially present in the latter (Figure 67A). A 25% fluorescence enhancement occurred with the epidermis lysate whereas only a 5% increase was observed with the dermis lysate, consistent with the fact that rapidly dividing cells are found in the epidermis. As the protein concentration was very low after epidermis lysis, the experiment was only performed with 50 µg proteins. WWshortRb was further implemented to compare pathological skin biopsies, first eczema,

a skin inflammation, in which no hyperactivity of CDK4 was monitored, then psoriasis, a proliferative skin pathology in which CDK4 activity was found to be significantly downregulated (Figure 67B).

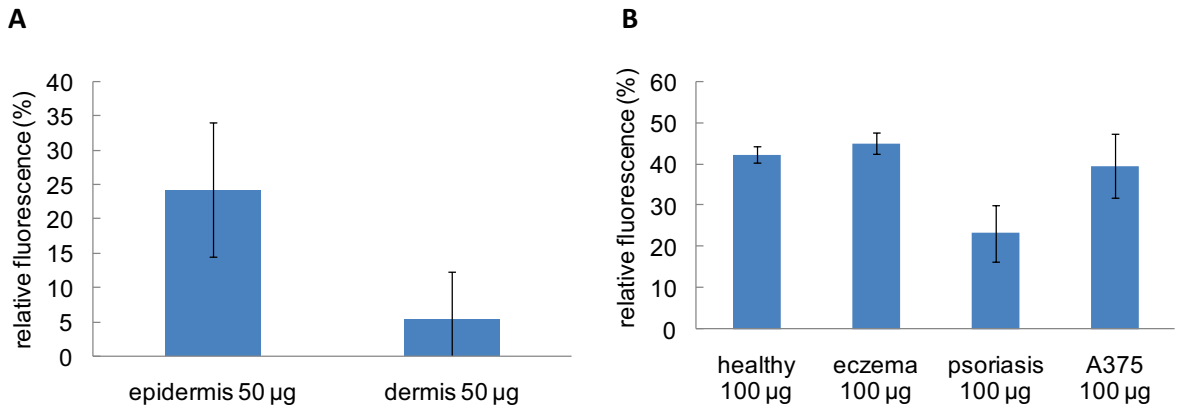

Figure 67: Real time fluorescence of 150 nM TAMRA-labelled WWshortRb upon incubation with healthy and pathological skin biopsies. The fluorescent signal was obtained following subtraction of background fluorescence of TAMRA-WWshortRb alone and the histogram represents the fluorescent signal at the endpoint of the assay (5000 s).

(A) Differential response of the biosensor upon incubation with 50 µg dermis and epidermis cell extracts

(B) Comparative response between 100 µg lysate prepared from healthy, eczema and psoriasis biopsies (100 µg A375 cell extracts was used as a control).

1.4.6. Implementation of WWshortRb biosensor to probe CDK4 activity in tumour xenograft lysates

The biosensor was then applied to detect CDK4 activity in melanoma xenograft extracts. The melanoma cell line A375 was implanted subcutaneously into the flank of nude mice by Véronique Josserand and Julien Vollaire (Institut Albert Bonniot, Grenoble). After 24 days, mice were then treated daily orally either with the CDK4 inhibitor PD-0332991 at 150 mg/kg for 3 or 7 days, or 75 mg/kg for 7 days (as described in (Fry et al., 2004)), or with the CDK2/5/7/9 inhibitor Roscovitine at 50 mg/kg for 5 or 11 days. Biopsies of the xenografted tumours were lysed and total proteins were normalized by spectrophotometric dosage at 280 nm and incubated with TAMRA-labelled WWshortRb peptide biosensor. These experiments revealed a slight reduction in CDK4 activity in the xenografts after a 3-days treatment with 150 mg/kg PD-0332991 which is more significant after 7 days of treatment in two of the three experiments (Figure 68A, blue and green histogrammes).

Importantly, no specific decrease in CDK4 protein levels was observed, nor any growth inhibition of the tumour xenografts (Figure 68B and Annex A).

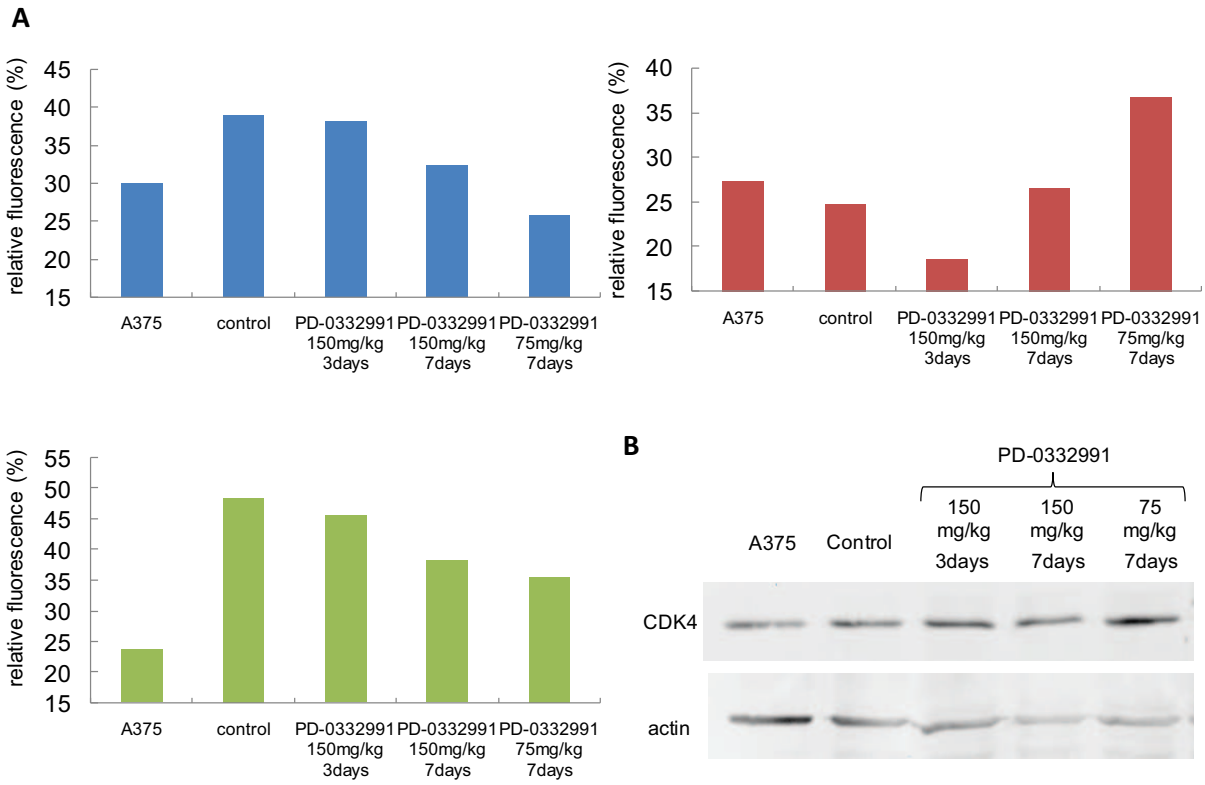

Figure 68: Response of WWshortRb peptide biosensor to A375 xenografts treated with PD-0332991.

(A) Fluorescence of 150 nM TAMRA-labelled WWshortRb peptide biosensor following incubation with 50 µg total proteins extracted from A375 xenografted tumour biopsies from mice treated with PD-0332991 at 150 mg/kg for 3 or 7 days, or with 75 mg/kg for 7 days in three independent experiments. Control: mock treated xenografts. The histogram represents the fluorescent signal at the endpoint of the assay (5000s).

(B) Western blot of CDK4 levels in biopsies of the first experiment.

To minimize any differences that might be associated with tumoral heterogeneity, the experiment was repeated by normalizing the response of WWshortRb in lysates prepared from different melanoma xenografts to the proportion of cancer cells (A375 luciferase) (Figure 69). Indeed, as proteins from stromal cells are also present in cell extracts and since each tumor behaves and grows differently, the ratio between hyperactive CDK4 kinase in cancer cells and its activity in non-cancer cells was likely to vary in the different melanoma xenografts. These experiments revealed a

systematic reduction of CDK4 activity after seven days treatment 150 mg/kg and 75 mg/kg PD-0332991 than after three days with 150 mg/kg, although no growth inhibition of the tumour xenografts was observed (Figure 69A and Annex A). In contrast, treatment of A375 xenografted tumours with 50 mg/kg Roscovitine, whether for 5 or 11 days, had no significant effect on WWshortRb fluorescence, although the latter treatment clearly affected tumour growth, consistent with the inhibitory action of this compound towards CDKs other than CDK4/6 (Figure 69B and Annex A).

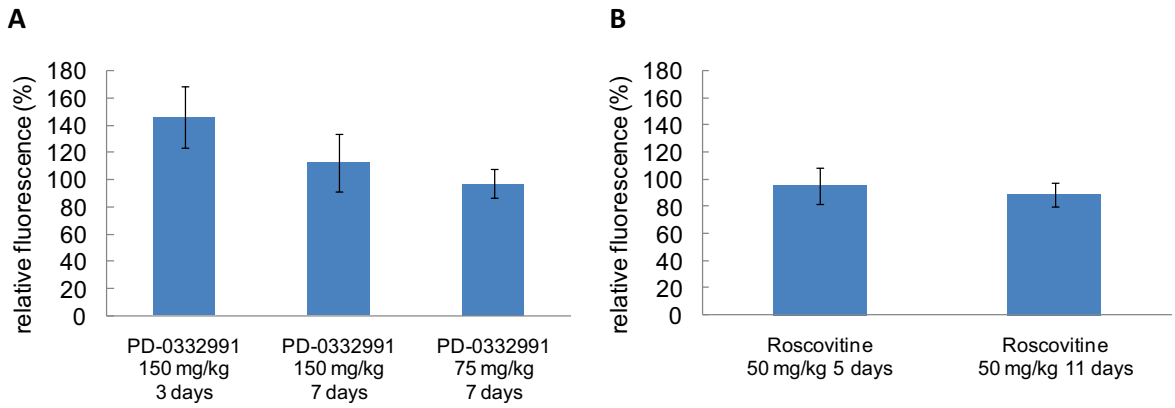

Figure 69: Fluorescence of 150nM TAMRA-labelled WWshortRb peptide biosensor following incubation with cell extracts from A375 xenografted tumour biopsies from mice treated either (A) with PD-0332991 at 150 mg/kg for 3 or 7 days or at 75mg/kg for 7days; or (B) with Roscovitine at 50 mg/kg for 5 or 11 days. Histogrammes represent the fluorescent signal at the endpoint of the assays (5000s), performed in duplicate from each of the three mouse xenografts, normalized to luciferase activity of A375 cells, and relative to control (untreated) tumour samples.

Taken together the results show that WWshortRb peptide biosensor can be implemented to quantify CDK4/Cyclin D kinase activity in skin biopsies and melanoma xenografts.

1.4.7. Application of WWshortRb to probe CDK4/cyclin D activity in living cells

Fixed cell imaging – Upright acquisitions

In order to monitor CDK4/cyclin D activity in living cells, TAMRA-labelled WWshortRb was internalized into A375 melanoma cells. TAMRA-WWshortRb was overlaid onto asynchronized A375 cells for 30min followed by 1h recovery at 37°C (addition of DMEM supplemented with 10% FCS), cell fixation and Hoechst staining. Figure 70A presents images of fluorescent acquisitions of Hoechst, TAMRA and overlay Hoechst-TAMRA. Surprisingly, unlike most peptides, the fluorescently-labelled

peptide was able to penetrate into living cells alone and thus did not require facilitated delivery for efficient internalization into living cells. In order to understand this result, we attempted to internalize TAMRA-MP26, TAMRA-Rb substrate and DyLight650-WWshortRb into cells. Neither MP26 nor Rb substrate could cross cell membranes alone (Figure 70A). However, DyLight650-WWshortRb entered living cells alone (Figure 70B). These results reveal that WWshortRb bears an inherent ability to cross cell membranes.

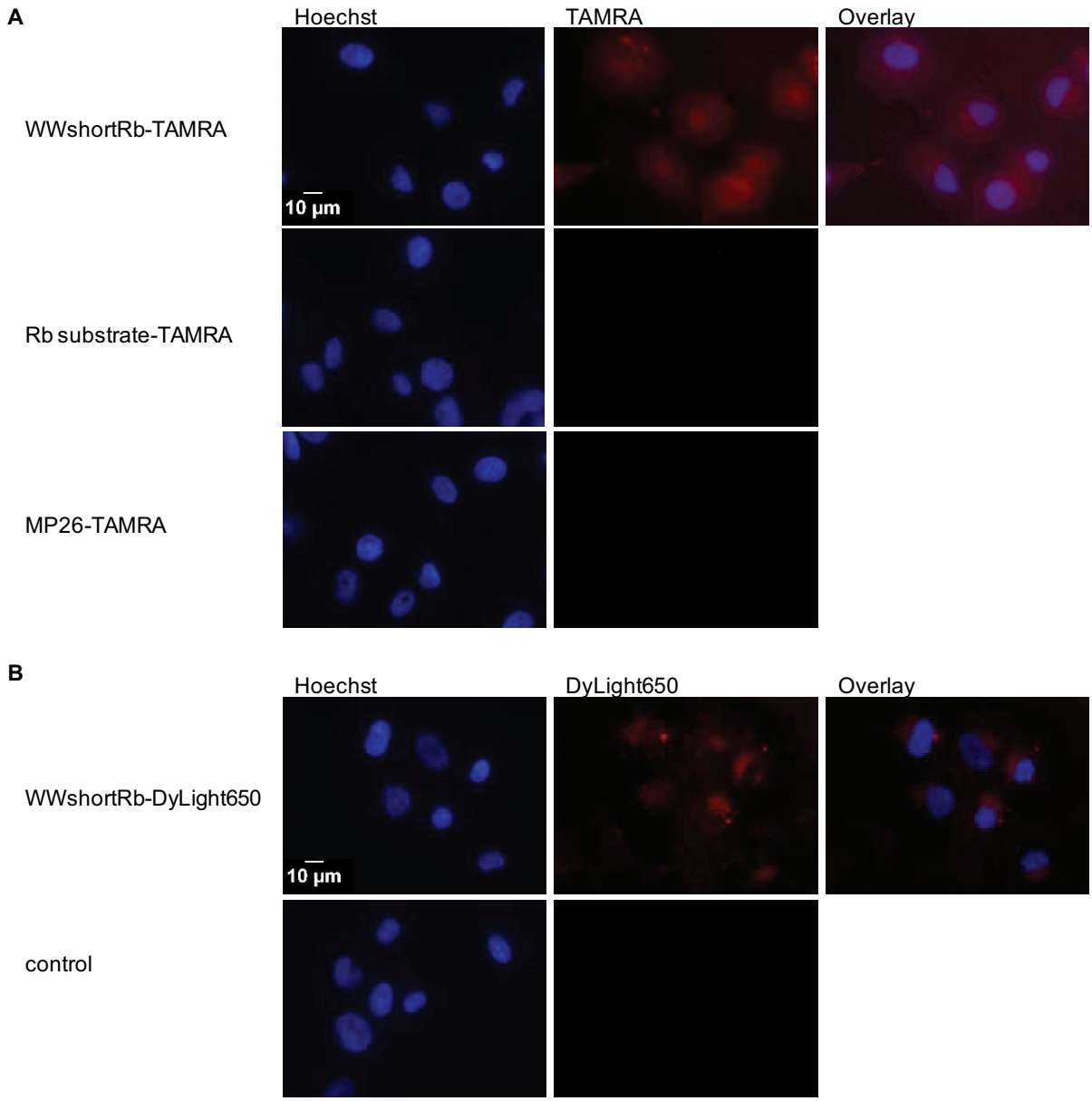

Figure 70: Internalization of TAMRA-WWshortRb, TAMRA-Rb substrate, TAMRA-MP26 (A) and DyLight650-WWshortRb (B) into A375 melanoma cells. Fluorescently-labelled peptides (2 µM) were overlaid onto asynchronized A375 cells followed by 30min incubation at 37°C, 1h recovery at

37°C, cell fixation and Hoechst staining. Fluorescent micrographs were acquired with a 63X objective.

(A) Fluorescent acquisitions of Hoechst, TAMRA with a 63X objective and overlay Hoechst-TAMRA.

(B) Fluorescent acquisitions of Hoechst, DyLight650 with a 63X objective and overlay Hoechst-DyLight650.

To verify that the internalization of WWshortRb did not affect the localization of CDK4, indirect immunofluorescence was performed in A375 melanoma cells using anti-CDK4 and Alexa488-conjugated anti-rabbit antibody (materials and methods). TAMRA-WWshortRb and Dylight650-WWshortRb were co-internalized into asynchronized A375 cells followed by cell fixation, immunofluorescence and Hoechst staining. Figure 71 presents images of fluorescent acquisitions of Hoechst, Alexa488, TAMRA and Dylight650. This experiment showed that TAMRA-WWshortRb and Dylight650-WWshortRb were efficiently co-internalized into cells and did not affect the localization of CDK4.

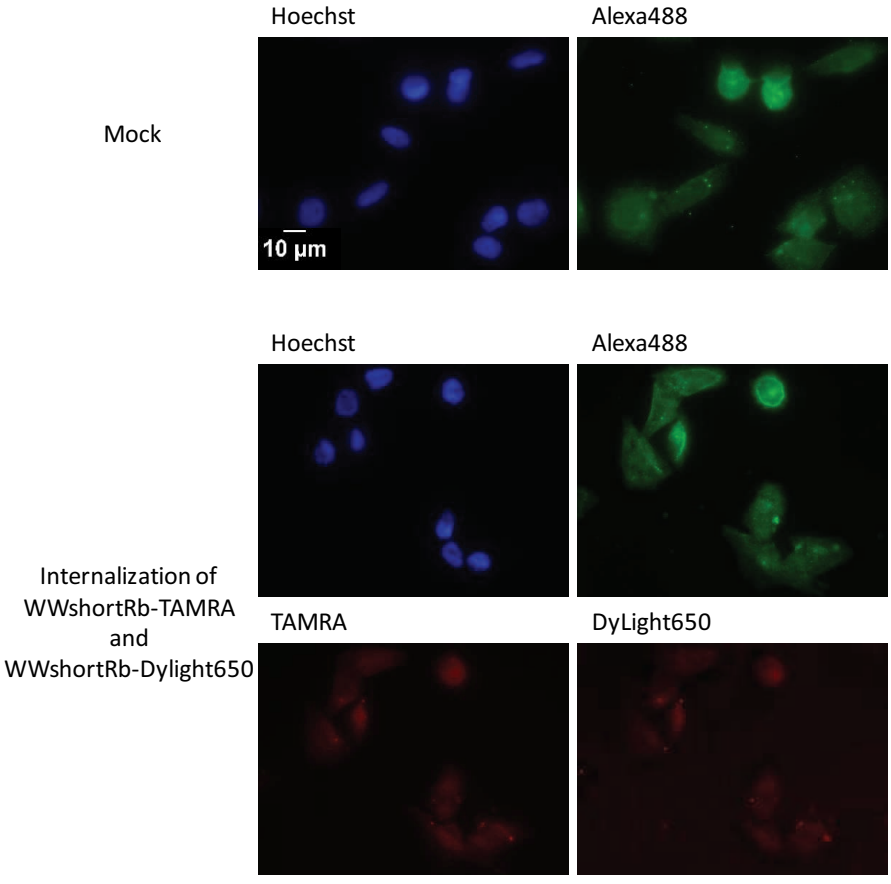

Figure 71: Indirect immunofluorescence of CDK4 protein and co-internalization of TAMRA-WWshortRb and DyLight650-WWshortRb into A375 melanoma cells. Fluorescently-labelled

WWshortRb (2 µM) was overlaid onto asynchronized A375 cells followed by 30min incubation at 37°C, 1h recovery at 37°C, cell fixation, immunofluorescence and Hoechst staining. Fluorescent micrographs were acquired with a 63X objective.

In order to investigate the ability of the biosensor to detect inhibition of CDK4/cyclin D, melanoma cells (A375) were treated 24h with different concentrations of PD-0332991 (0.5, 1, 10 and 20 µM). WWshortRb-TAMRA (2 µM) was then overlaid onto A375 cells for 30min followed by 1h recovery at 37°C, cell fixation and Hoechst staining. Figure 72A presents images of fluorescent acquisitions of Hoechst, TAMRA and overlay Hoechst-TAMRA. The histogram that is presented in Figure 72B corresponds to the average fluorescence ratio of the TAMRA-labelled biosensor over the Hoechst staining of three different fields of one experiment with standard deviation bars. These results showed that the addition of increasing concentrations of PD-0332991 enhanced the fluorescent signal of the biosensor in a dose-dependent fashion (fluorescence enhancement from 1 to 47). Thus, these experiments suggest that WWshortRb reports on CDK4/cyclin D activity in living cultured cells. Unlike *in extracto* experiments that demonstrated a decrease in fluorescence intensity of WWshortRb upon addition of PD-0332991, an increase of fluorescence upon addition of this inhibitor was observed in *in cellulo* experiments. These seemingly contradictory results could be explained by a difference in the environment of the probe in intact cells vs in cell extracts. As the probe is sensitive to the environment, we hypothesized it might behave differently in a living cells than in lysis buffer. Moreover, Western blot analysis of cell extracts from these cells demonstrated that the addition of increasing concentrations of PD-0332991 led to degradation of CDK4 (Figure 72C).

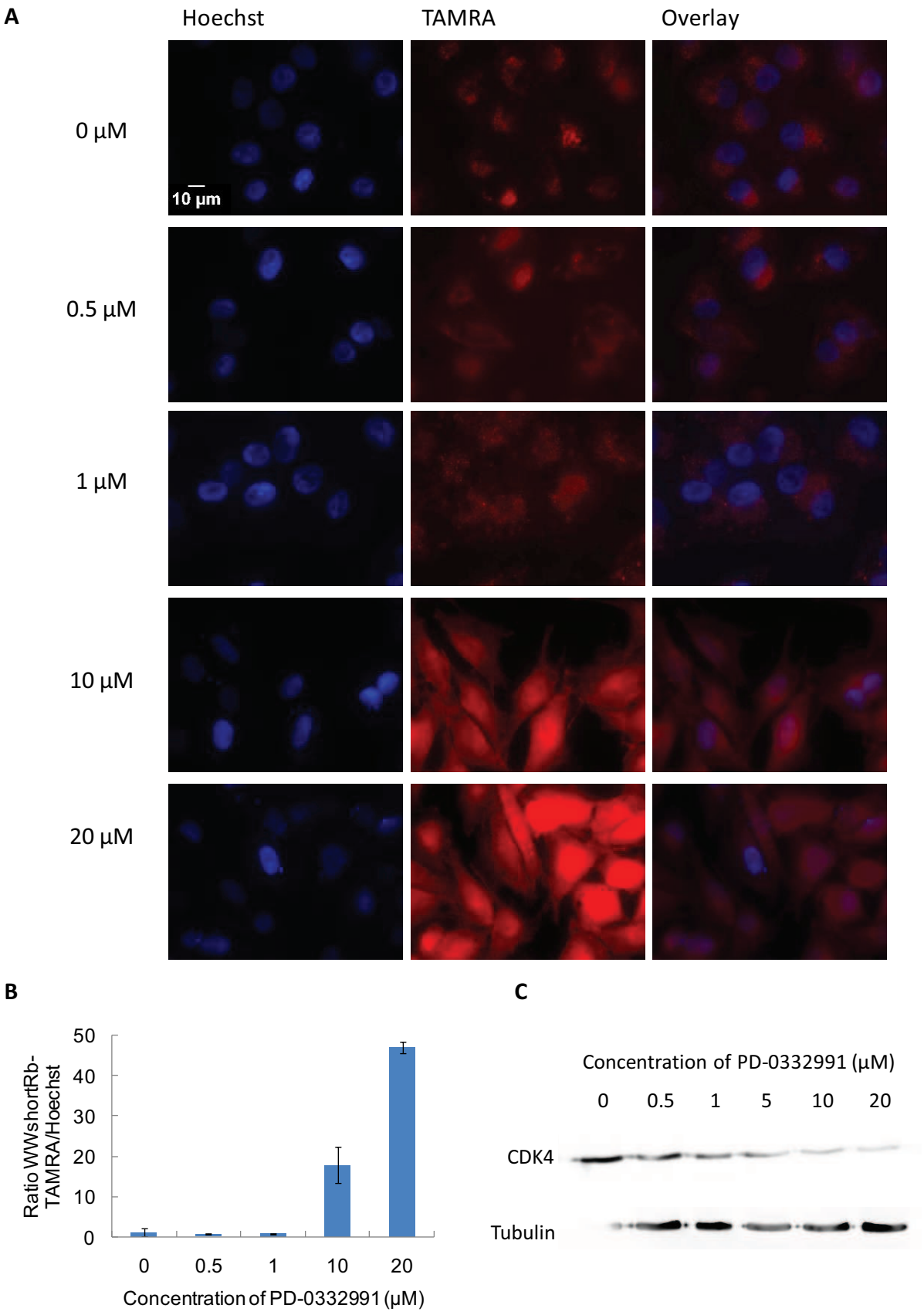

Figure 72: Internalization of TAMRA-WWshortRb into A375 melanoma cells treated with PD-0332991. Cells were treated with different concentrations of PD-0332991 (0.5, 1, 10, 20 µM) for 24h. WWshortRb-TAMRA (2 µM) was then overlaid onto asynchronized A375 cells followed by

30min incubation at 37°C, 1h recovery at 37°C, cell fixation and Hoechst staining. Fluorescent micrographs were acquired with a 63X objective.

(A) Fluorescent acquisitions of Hoechst, TAMRA with a 63X objective and overlay Hoechst-TAMRA.

(B) Histogram representing the fluorescence average ratio TAMRA/Hoechst of triplicate experiments with standard deviations as a function of PD-0332991 concentration. The ratio TAMRA/Hoechst in untreated A375 cells was regarded as 1.

(C) Western blotting profiles of CDK4 and tubulin in A375 cells with different concentrations of PD-0332991

In order to confirm this result, the same experiment was repeated. However, no fluorescence enhancement of the biosensor was observed upon addition of increasing concentrations of PD-0332991 (Figure 73). Moreover, indirect immunofluorescence, performed in these cells using anti-CDK4 and Alexa488-conjugated anti-rabbit antibody, revealed neither a reduction in CDK4 protein levels nor mislocalization of CDK4 (Figure 73A). This suggests that the fluorescence enhancement of the biosensor obtained in the first experiment was maybe due to the presence of a contaminant which led to CDK4 degradation and stimulated fluorescence.

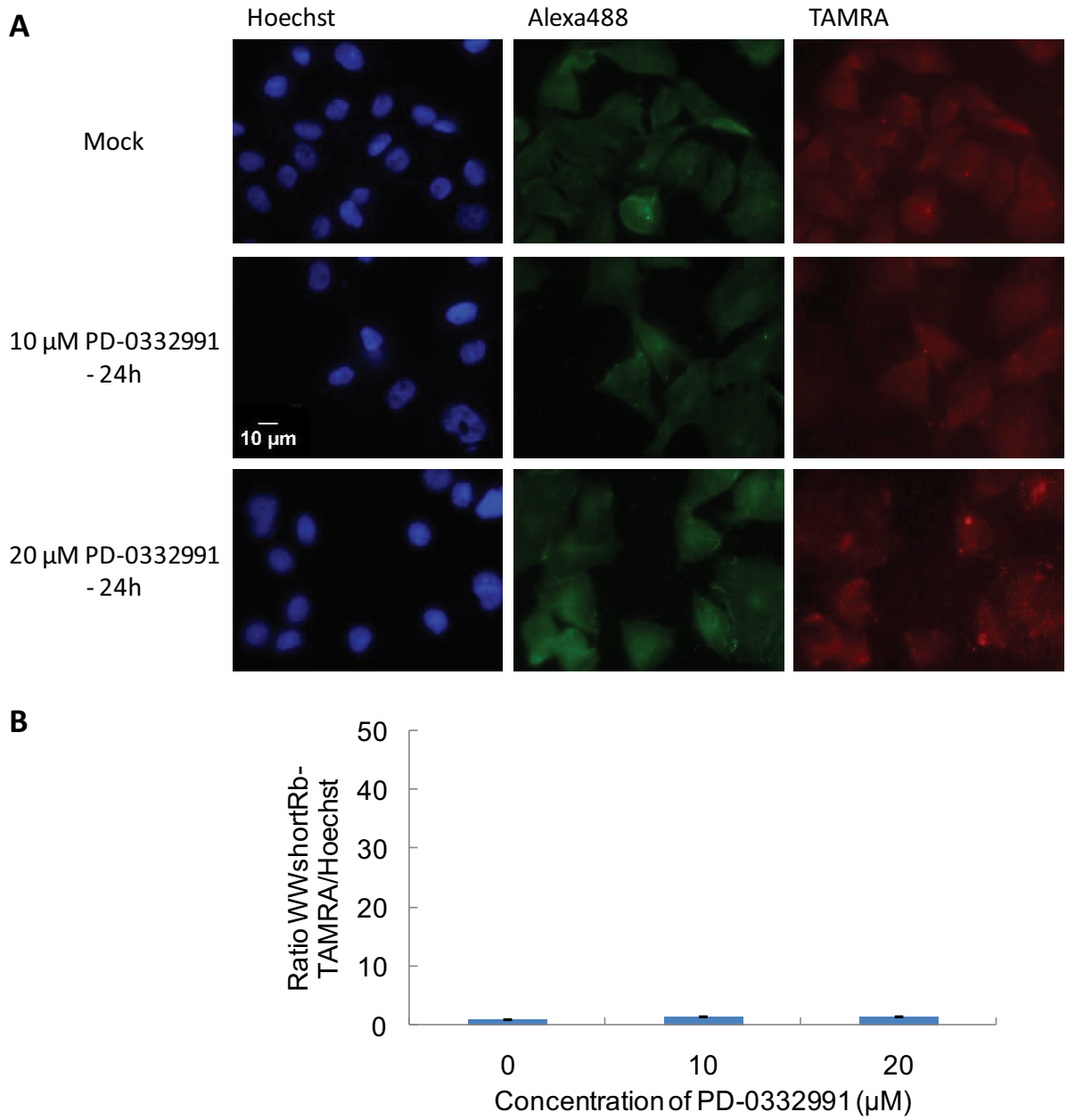

Figure 73: Indirect immunofluorescence of CDK4 protein and internalization of TAMRA-WWshortRb into A375 melanoma cells treated with 10 µM and 20 µM PD-0332991 for 24h. TAMRA-labelled WWshortRb (2 µM) was overlaid onto asynchronized A375 cells followed by 30min incubation at 37°C, 1h recovery at 37°C, cell fixation, immunofluorescence and Hoechst staining. Fluorescent micrographs were acquired with a 63X objective.

(A) Fluorescent acquisitions of Hoechst, TAMRA and Alexa488 with a 63X objective.

(B) Histogram representing the fluorescence average ratio TAMRA/Hoechst of three different fields of one experiment with standard deviation bars as a function of PD-0332991 concentration. The ratio TAMRA/Hoechst in untreated A375 cells was regarded as 1.

Live cell imaging – Time-lapse acquisition

TAMRA-WWshortRb and DyLight650-WWshortRb were internalized into A375 living cells for time-lapse acquisitions. DyLight650-WWshortRb served as a negative control since the probe was unresponsive in activity assays when coupled with the biosensor. Time-lapse imaging was performed over a window of 10-15h. Video stacks for each parameter were built from these acquisitions for signal analysis using Metamorph software. Images in Figure 74 show that both TAMRA-WWshortRb and DyLight650-WWshortRb were well internalized into A375 cells.

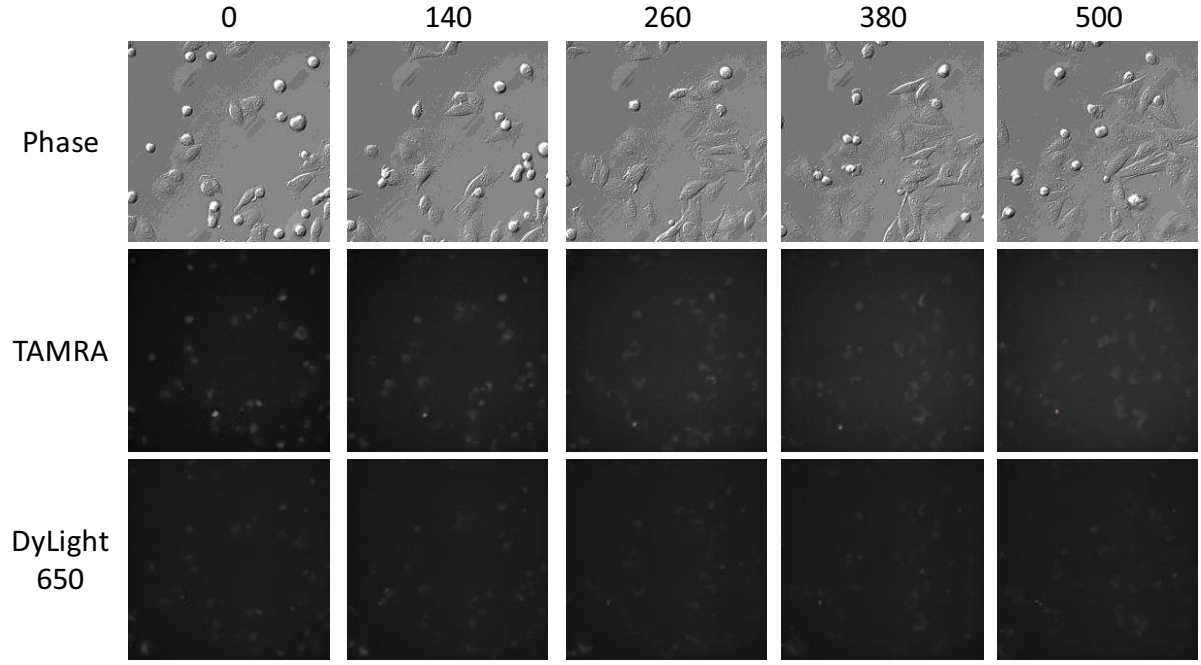

Figure 74: Co-internalization of WWshortRb-TAMRA and WWshortRb-DyLight650 into asynchronous A375 cells. Live cell imaging acquisitions were set up automatically for 10h with an inverted microscope equipped with 40X objectives for cell morphology (Phase), TAMRA and DyLight650 signals. Images of representative time points are presented (0, 140, 260, 380 and 500 min).

Ratiometric quantification of fluorescence in living cells

In order to determine the response of WWshortRb to CDK4/cyclin D activity in living cells, fluorescent signals of TAMRA and DyLight650 were acquired over time and used to determine the response of the biosensor. Single cells (dividing and non-dividing) were chosen in the regions of interest (ROI) in the images of TAMRA to ensure absence of aggregates and transferred to the two other stacks of the same time point for fluorescence intensity measurement.

The ratio of TAMRA/DyLight650 fluorescent signals was determined from individual cells in which changes in fluorescence of TAMRA correspond to CDK4/cyclin D activity and those of DyLight650 serve as an intracellular fluorescent control. After background subtraction, average fluorescent intensity of each ROI was measured for both TAMRA and DyLight650 using Metamorph software (annex B).

Figure 75 shows representative average fluorescent intensity of TAMRA and DyLight650 and the representative ratiometric quantification of TAMRA/DyLight650 signal obtained from three dividing and non-dividing cells. First, we observed that no fluorescence enhancement of DyLight650-WWshortRb was observed. It therefore constitutes an appropriate negative control in living cells. However, we then observed that the fluorescence of TAMRA-WWshortRb kept increasing over time, irrespective from cell division, suggesting that after initial response (> 300 min) the biosensor might be trapped, degraded, or somehow not responding appropriately to CDK4 activity.

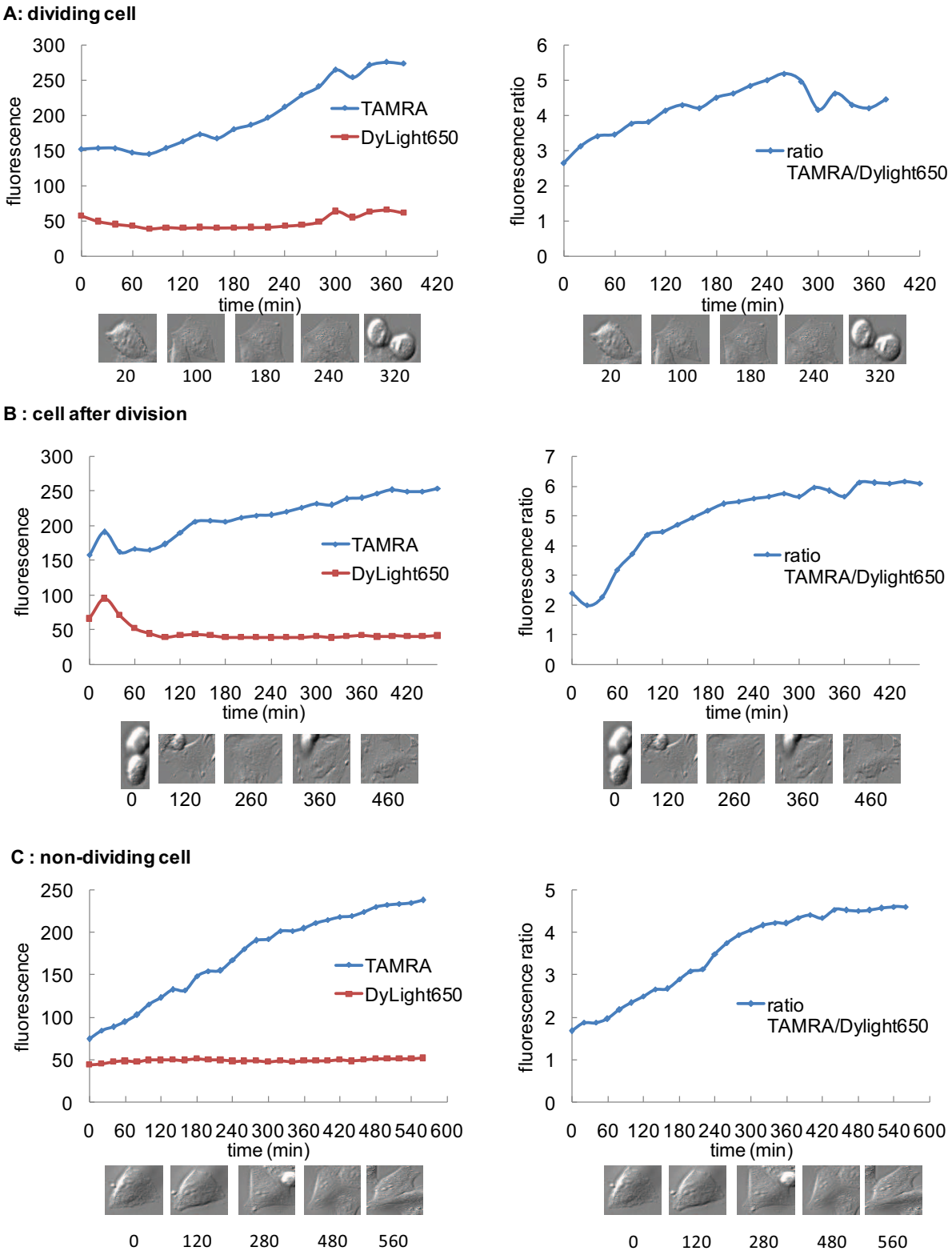

Figure 75: Representative ratiometric quantification of TAMRA/DyLight650 signal in A375 living cells internalized with WWshortRb-TAMRA and WWshortRb-DyLight650 followed by time-lapse acquisition in which phase, TAMRA and DyLight650 were imaged. Average fluorescent intensity of TAMRA and DyLight650 was measured from ROIs of individual cells.

The experiment was repeated to compare the response of WWshortRb in asynchronized and synchronized A375 cells. Cells were synchronized in S phase by addition of hydroxyurea for 24h and then released for 10h (materials and methods). In parallel, an experiment was performed with A375 cells treated with 10 µM PD-0332991 or Roscovitine for 24h. Ratiometric quantification of TAMRA/DyLight650 signal in A375 non-dividing cells is presented in Figure 76. A reduction of TAMRA/DyLight650 ratio was observed in cells treated with PD-0332991 and Roscovitine, indicating that TAMRA-WWshortRb reports a decrease of CDK4 activity. These results are in line with the fact that PD-0332991 inhibits CDK4 activity and that Roscovitine induces a cell cycle arrest which indirectly leads to an inactive CDK4. Synchronized cells displayed a lower TAMRA/DyLight650 ratio than asynchronized cells. This result suggests that CDK4 is more active in asynchronized than in synchronized cells which, after a 10h S phase release, should be in G1 phase.

Analysis of the curves indicates that the reaction can be divided in two phases: before and after three hours of reaction. Indeed, we first observe a significant increase in the fluorescence of the biosensor and then a linear response after three hours of reaction. Given this linearity and since the biosensor fluorescence never decreases or reaches a plateau could suggest that the biosensor is not reliable after several hours of internalization. It is possible that, once internalized into cells, the peptide is rapidly sequestered or metabolized, leading to a release of free probe and thus an inappropriate response of the biosensor.

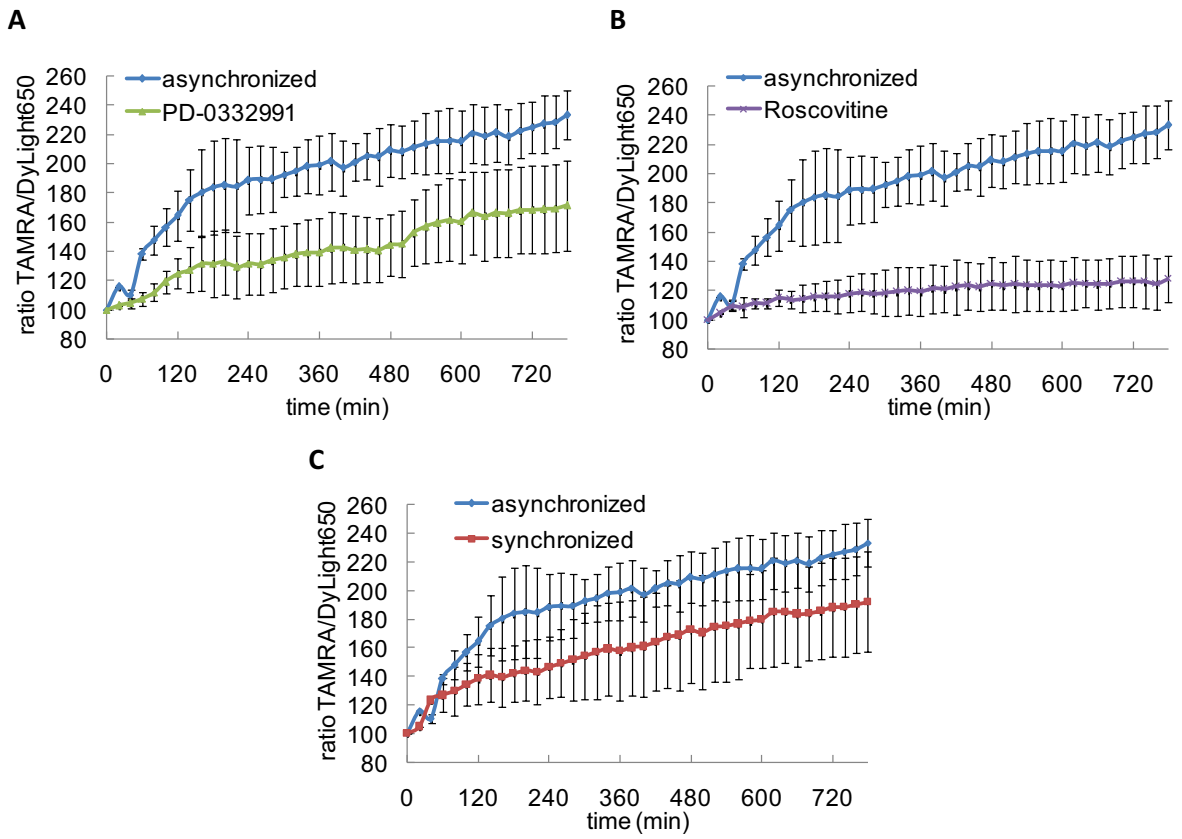

Figure 76: Ratiometric quantification of TAMRA/DyLight650 signal in A375 non-dividing cells internalized with WWshortRb-TAMRA and WWshortRb-DyLight650 followed by time-lapse acquisition in which phase, TAMRA and DyLight650 were imaged. The ratio at the beginning of the acquisition was regarded as 100%. The data presented correspond to the average ratiometric quantification of TAMRA/DyLight650 signal of three different cells with standard deviation bars.

2. Identification of non-ATP competitive compounds targeting CDK4/cyclin D

Alternative approaches that do not target the ATP pocket have been investigated to inhibit CDK4/cyclin D activity, by targeting either protein/protein interfaces or allosteric sites (Figure 77). As such, two strategies were developed, either by rational design of peptides or by high throughput screening of small molecules libraries thanks to fluorescent biosensors, based on CDK4 kinase scaffold.

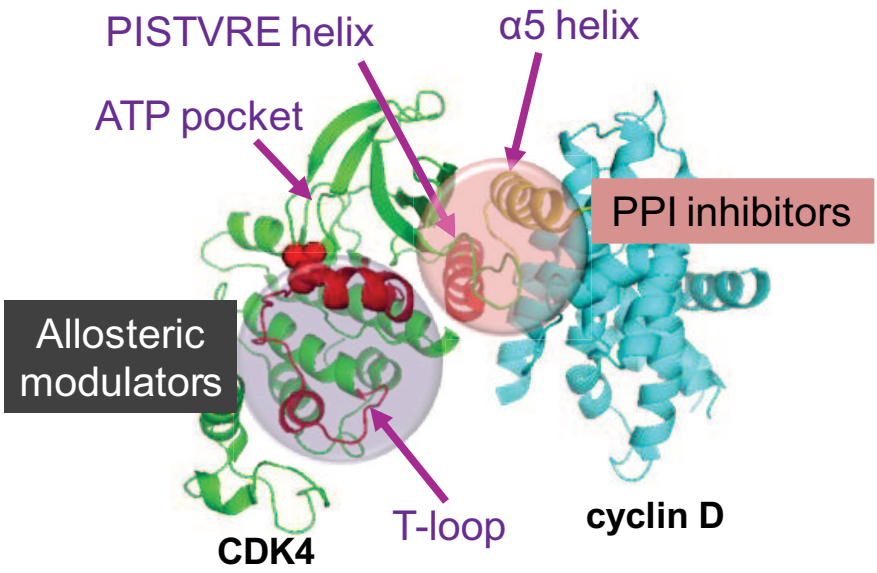

Figure 77: Two strategies to inhibit CDK4/cyclin D: with protein/protein interface (PPI) compounds or with allosteric T-loop modulators (crystal structure of CDK4/cyclin D3 (PDB 3G33))

A. Identification by screening of non-ATP competitive compounds

To this end, two fluorescent biosensors were designed:

- **CDKCONF4A**, for identifying compounds that can target the interface between the PISTVRE helix in the N-terminal lobe of CDK4 and the complementary α5 helix of cyclin D (Figure 77 and Figure 78A). Indeed, this interaction is critical for assembly of the functional heterodimeric kinase (Day et al., 2009; Takaki et al., 2009).

- **CDKCONF4B**, sensitive to conformational changes of CDK4, for identification of allosteric modulators of the CDK4 activation loop (or T-loop) (Figure 77 and Figure 78B).

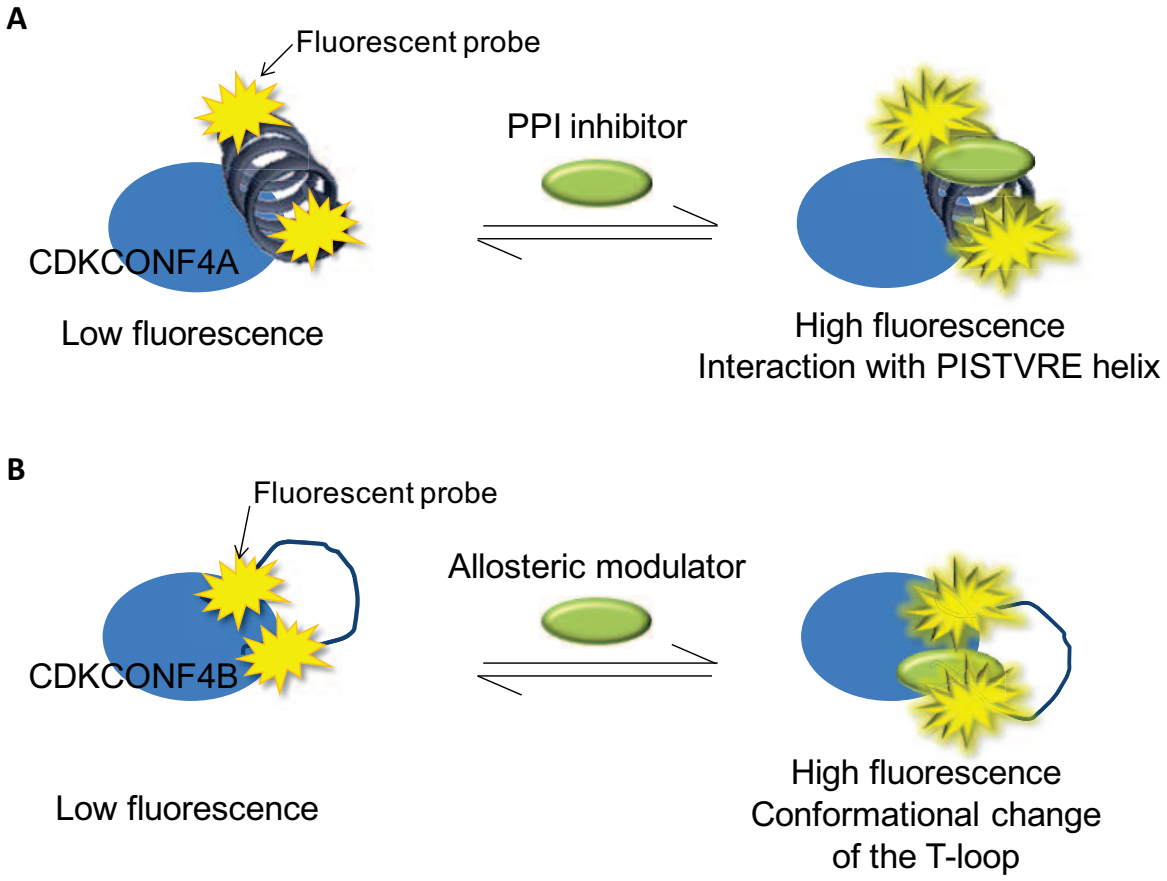

Figure 78: Development of two fluorescent biosensors for identifying CDK4/cyclin D inhibitors by screening. (A) CDKCONF4A to identify compounds that might interfere with the PISTVRE helix/α5 helix interface; (B) CDKCONF4B to identify allosteric modulators of CDK4/cyclin D

2.1. Design and engineering of CDKCONF4A and CDKCONF4B

The CDK4 sequence comprises 4 cysteines whose thiol groups are available for specific conjugation to fluorescent probes. CDKCONF4A and CDKCONF4B were engineered by site-directed mutagenesis of cysteine codons in mouse CDK4 cDNA so as to obtain a CDK4 sequence bearing only two cysteines, close to the targeted zone of interest (materials and methods and annex C) (Figure 79).

For CDKCONF4A, cysteine residues 202 and 215 were mutagenized to serine, so as to yield a mutant bearing only two cysteine residues, 78 and 135, spanning the PISTVRE helix of CDK4 (Figure 79A).

For CDKCONF4B, cysteine residues 78, 135 and 215 were mutagenized to serine and serine residue 189 was mutagenized to cysteine so as to obtain a mutant that contained only two cysteine residues, 189 and 202, spanning the T-loop of CDK4 (Figure 79B).

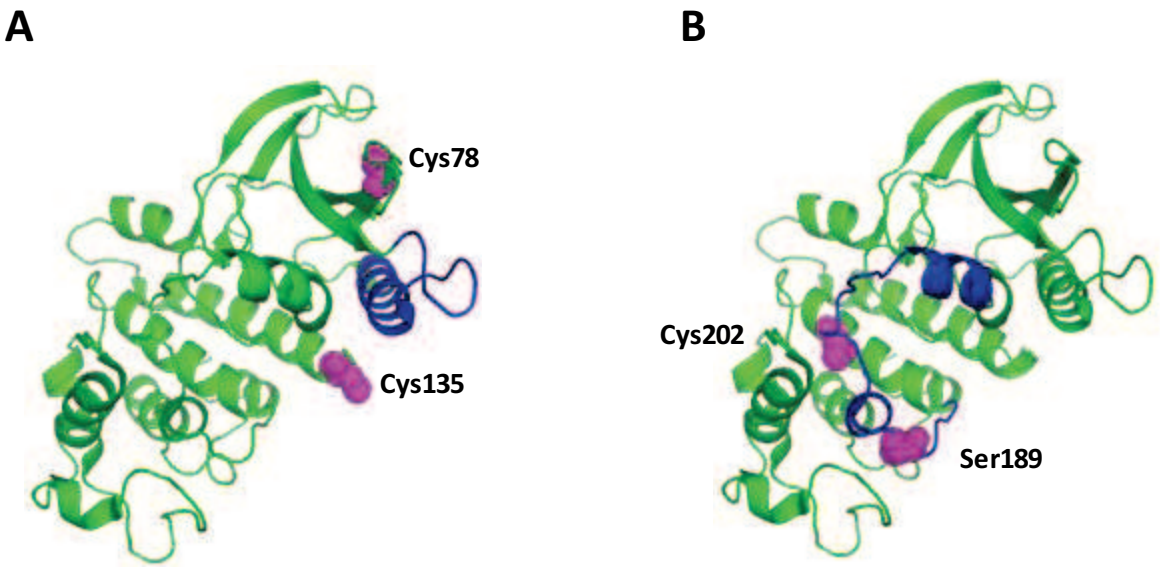

Figure 79: Design of CDKCONF4A (A) and CDKCONF4B (B): position of the cysteines on which fluorescent probes were coupled.

The two biosensors were expressed in fusion with a GST tag in *E.coli* and expression was verified by SDS-PAGE (59 kDa) (materials and methods) (Figure 80A/B). They were purified by affinity and gel filtration chromatography which yielded 80 µg pure CDKCONF4A and 240 µg pure CDKCONF4B from 1L of bacterial induction (average of 3 purifications) (materials and methods) (Figure 80C/D).

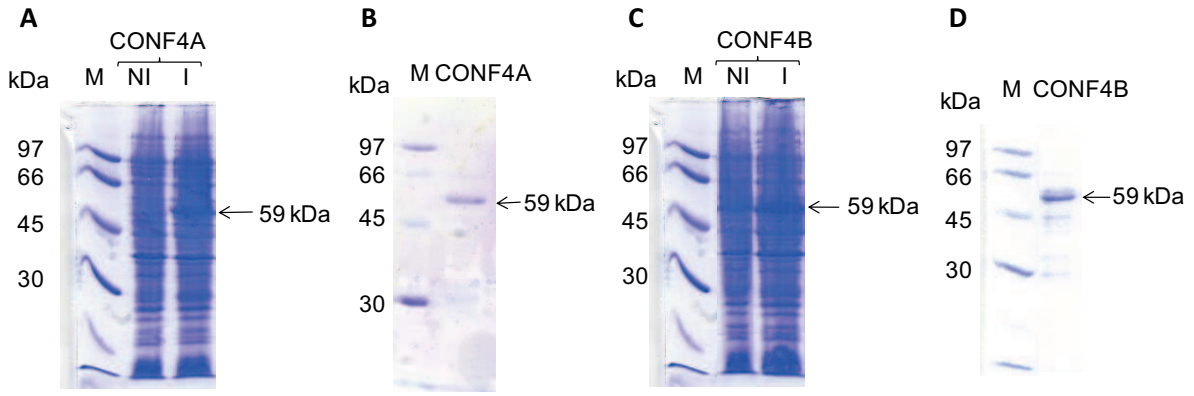

Figure 80: Expression and purification of GST-CDKCONF4A and GST-CDKCONF4B (A) Expression of CDKCONF4A M: Marker protein; NI: Before induction; I: Protein induction (B) Purification of CDKCONF4A: protein fraction from gel filtration chromatography M: Marker protein (C) Expression of CDKCONF4B M: Marker protein; NI: Before induction; I: Protein induction (D) Purification of CDKCONF4B: protein fraction from gel filtration chromatography M: Marker protein

CDKCONF4A and CDKCONF4B were then coupled, on cysteine residues, with the fluorescent probe Cy3, which yielded 50 µg Cy3-CDKCONF4A and 160 µg Cy3-CDKCONF4B (average of 3 experiments).

2.2. Characterization of CDKCONF4A and CDKCONF4B

To validate the use of Cy3-labelled CDKCONF4A, cyclin D1 protein and an irrelevant peptide derived from the T-loop of CDK4 (sequence: SYQMALEPGC) were used as positive and negative control respectively. Titration assays demonstrated that cyclin D1 promoted 80% fluorescence enhancement whereas the peptide did not affect the fluorescent signal of the biosensor (Figure 81A).

The retinoblastoma protein Rb, main substrate of CDK4/cyclin D, and an irrelevant peptide derived from the PISTVRE helix (PISTVRE peptide) (sequence: GGGCPISTVREVALLRRL) were used as positive and negative control respectively for CDKCONF4B biosensor. While Rb promoted a significant enhancement of Cy3-labelled CDKCONF4B biosensor fluorescence, the peptide barely affected the biosensor fluorescence (Figure 81B).

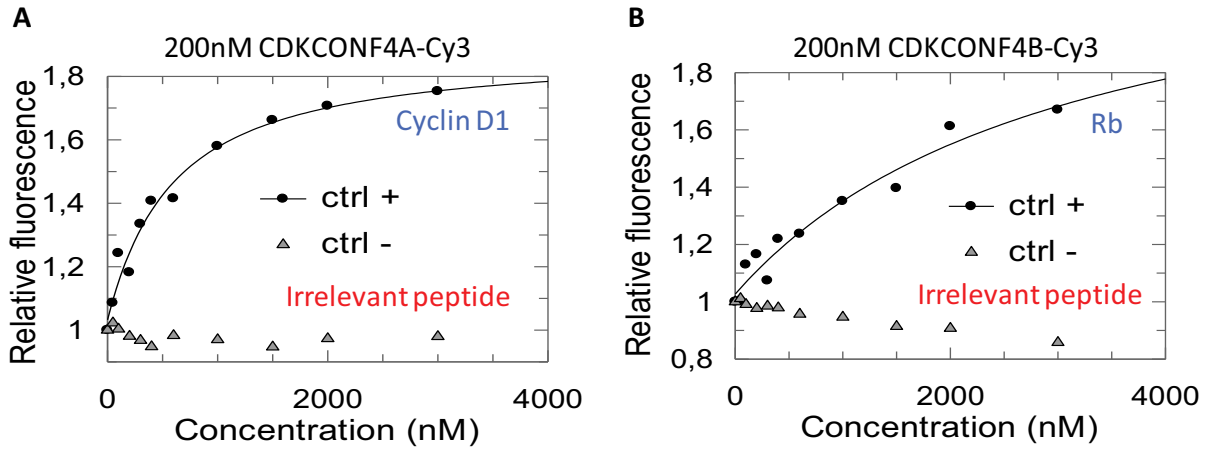

Figure 81: Characterization of Cy3-labelled CDKCONF4A (A) and 4B (B): titration assays using positive and negative controls.

2.3. Implementation, miniaturization and optimization of the assay

Prior to the screen, stability assays and downscaling experiments were performed to establish the best conditions for a miniaturized assay in 96-well plates and optimized so as to obtain a robust and reproducible signal (materials and methods). For both biosensors, optimal screening conditions were established as follows: **25 nM CDKCONF biosensor in 50 mM KH_2PO_4/K_2HPO_4, pH 6.4, 500 mM NaCl; 1% DMSO; controls at 2 µM; for 5 hours at room temperature in the dark** (Figure 82). In these conditions, the addition of cyclin D1 led to a 1.3 fold fluorescence enhancement of CDKCONF4A with

a Z factor equal to 0.89. For CDKCONF4B, the biosensor fluorescence was amplified to 1.8 fold by positive control (retinoblastoma protein) with a Z factor equal to 0.68. Calculation of Z-factor values allows us to assess the validity of the assays. Indeed, it takes into account the difference between positive and negative controls, the signal-to-noise (S/N) ratio and the variability of the assay Z-factor is equal to $1 - \frac{3(A^+ + A^-)}{B^+ - B^-}$, where A^+ and A^- correspond to the standard deviations of positive and negative controls, whilst B^+ and B^- are the average responses for positive and negative controls. For both biosensors, the Z factor value, which was greater than 0.5, allows to consider the assays suitable for screening.

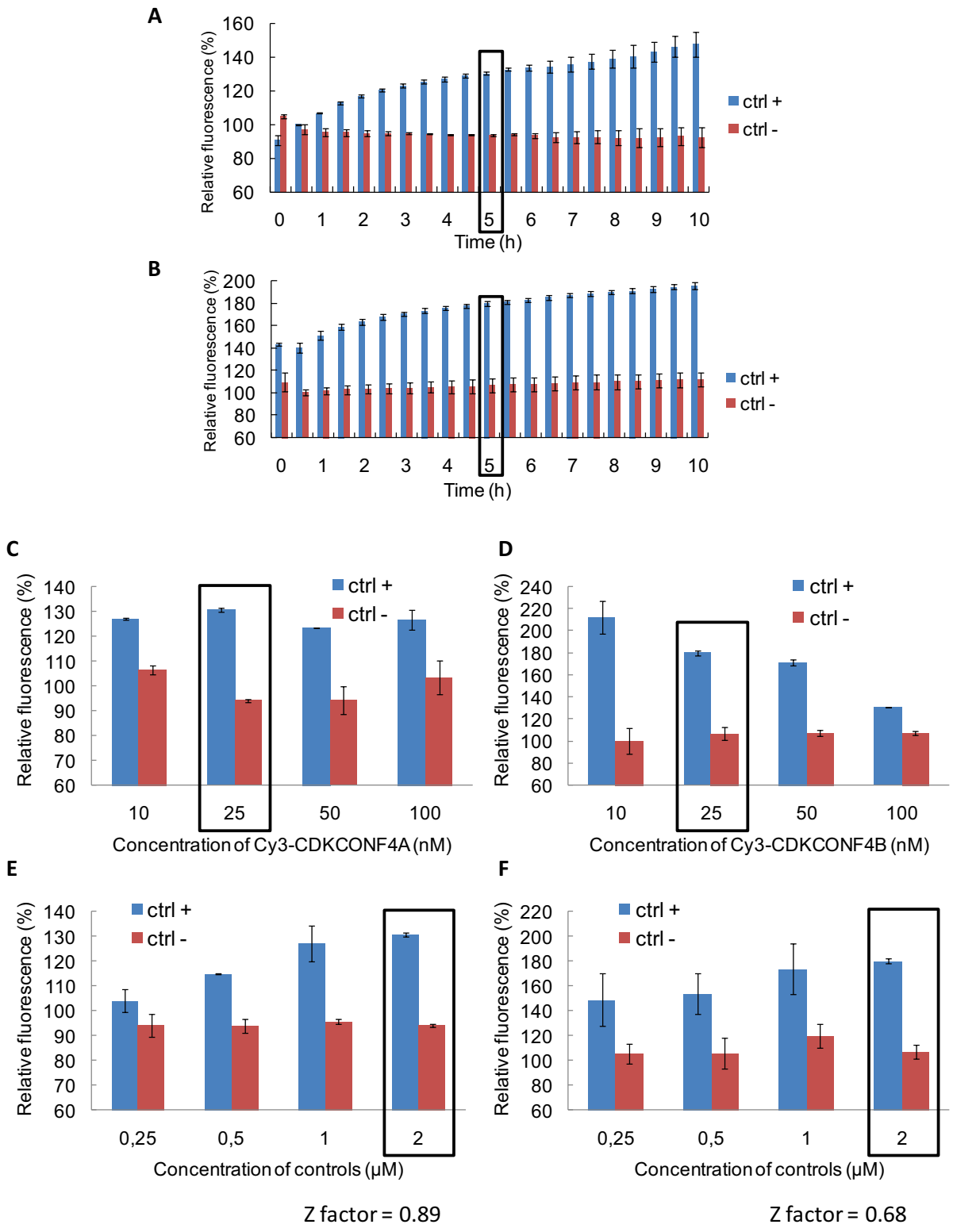

Figure 82: Miniaturization of the assay. Fluorescence of 25 nM Cy3-labelled CDKCONF4A (A) and CDKCONF4B (B) with 2 µM positive and negative control over time; Fluorescence of 25 - 100 nM Cy3-labelled CDKCONF4A (C) and CDKCONF4B (D) with 2 µM positive and negative control after 5h; Fluorescence of 25 nM Cy3-labelled CDKCONF4A (E) and CDKCONF4B (F) with positive and negative control (0.25 - 2 µM) after 5h. The fluorescent signal of CDKCONF4A/B-Cy3 alone at t=0h was regarded as 100%.

2.4. Screening of two small molecule libraries

Both biosensors were then implemented to screen two libraries of small chemical compounds: the National Chemical Essential (CNE) Library (480 compounds at 10 µM) and a library from Strasbourg (640 molecules at 10 µM) (collaboration with Dr Frédéric Bihel, Faculty of Strasbourg) (materials and methods). The screen was performed on a TECAN Freedom Evo^{TM} Robot at the MRI platform in Montpellier with the help of Dr. Julien Bellis. Figure 83 and Table 6 summarize the results of the screening assays (see annex D for details). Screens were performed with positive and negative controls as well as PD-0332991 since the biosensors CDKCONF4A and CDKCONF4B were designed to discriminate against ATP competitors. Importantly, screens confirmed that both biosensors were insensitive to PD-0332991.

The increase in fluorescence of each compound was calculated with reference to the basal fluorescence of Cy3-labelled CDKCONF4A or CDKCONF4B biosensor alone and was expressed as the relative percentage of increase. A molecule was considered a hit when induced amplification of Cy3-labelled CDKCONF4A/B biosensor fluorescence to a similar extent as positive control (annex D).

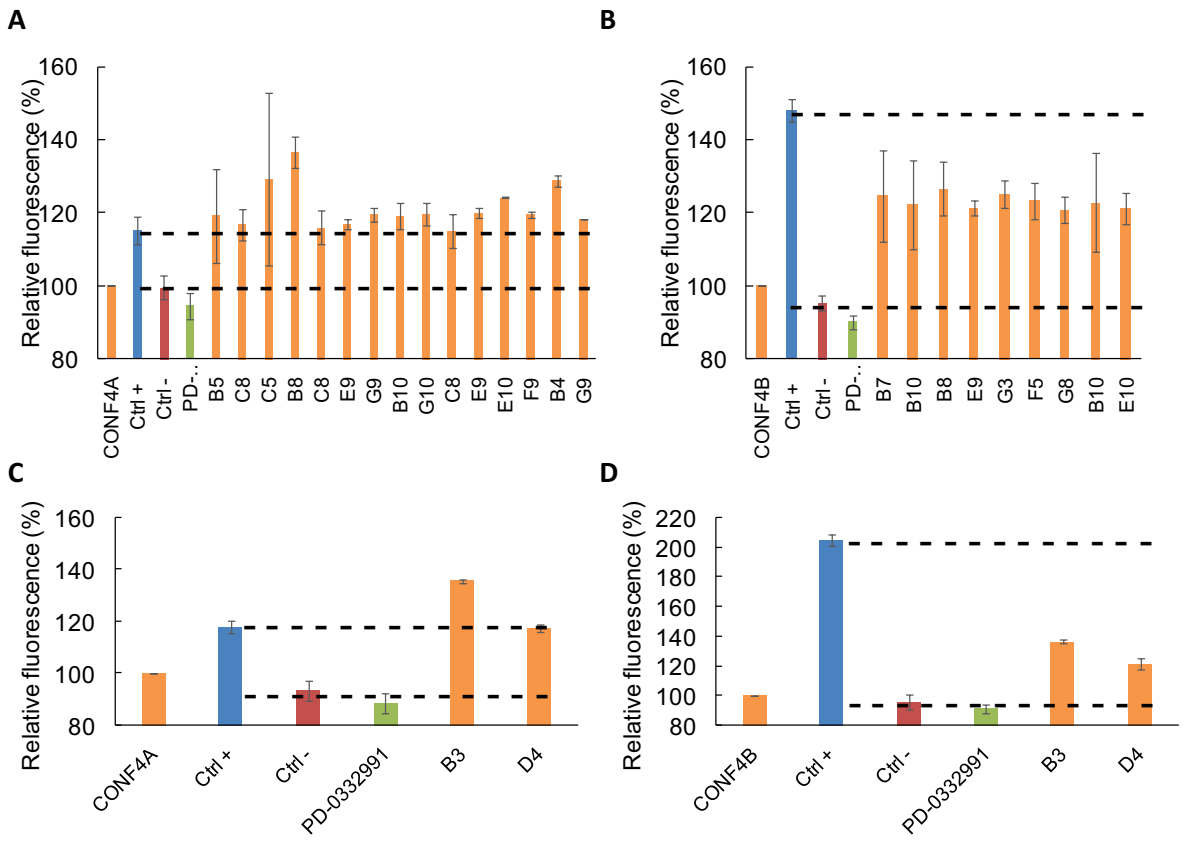

Figure 83: Results of the hits retained in the screens performed with 25 nM Cy3-labelled CDKCONF4A and CDKCONF4B and compounds from the libraries at 10 µM: (A) hits identified in the CNE with CDKCONF4A; (B) hits identified in the CNE with CDKCONF4B; (C) hits identified in the library from Strasbourg with CDKCONF4A; (D) hits identified in the library from Strasbourg with CDKCONF4B. The fluorescent signal of CDKCONF4A/B-Cy3 alone was regarded as 100%.

	CDKCONF4A	CDKCONF4B
Pre-screen	Z factor = 0.89	Z factor = 0.68
CNE	15 hits Z factor = -0.36	9 hits Z factor = 0.71
Strasbourg	2 hits Z factor = 0.23	2 hits Z factor = 0.76

Table 6: Results of the screening assays

In parallel, the intrinsic fluorescence of the library compounds at 570 nm following excitation at 544 nm was determined. In both libraries, no compounds exhibited autofluorescence at these wavelengths (Figure 84).

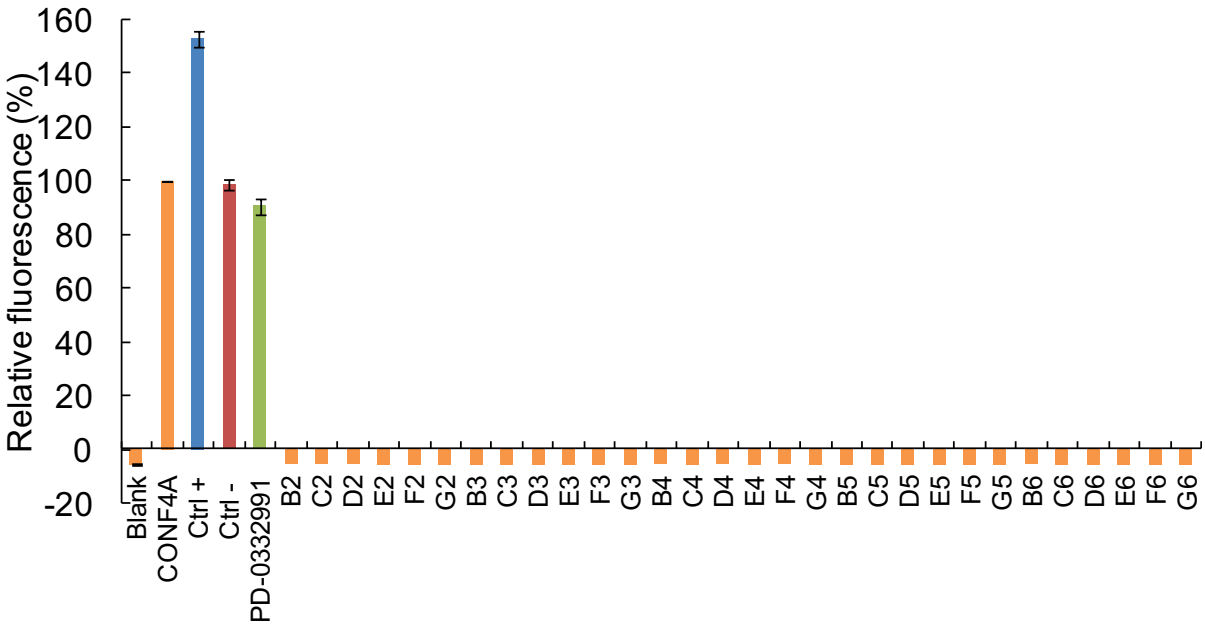

Figure 84: Determination of the intrinsic fluorescence of the library compounds at 570 nm following excitation at 544 nm, to eliminate autofluorescent compounds. Here is given an example of results obtained from one plate of compounds. The fluorescence of each compound was calculated with reference to the basal fluorescence of Cy3-labelled CDKCONF4A biosensor alone.

2.5. Characterization of hits

2.5.1. *In vitro* characterization

Confirmation of hits identified in the screens from powder stocks

Hits identified in both screens were obtained from source laboratories (annex D) and powder stocks were resuspended in DMSO. They were retested manually in duplicate to confirm they were positive hits with a fresh batch of Cy3-labelled CDKCONF4A and CDKCONF4B biosensor (Figure 85). 4 hits from the CNE promoted a fluorescence enhancement of Cy3-CDKCONF4A, AB-00016193, LPS401, LPS853 and ICMR-04-E10, whilst 2 compounds slightly amplified the fluorescent signal of Cy3-CDKCONF4B, CEsr-1409000 and LPS401.

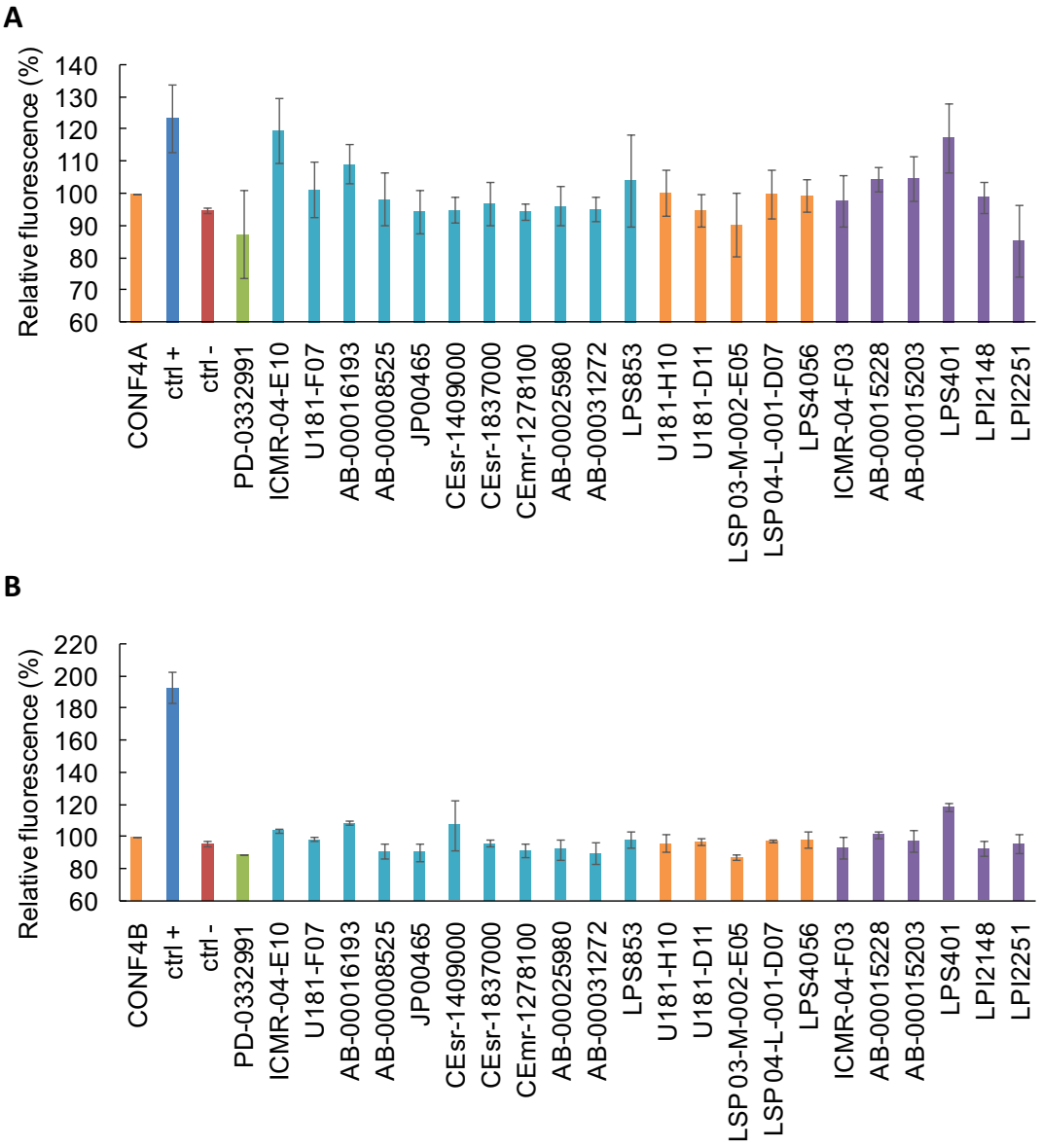

Figure 85: Confirmation of hits identified in the screens at 10 µM with a fresh batch of Cy3-labelled CDKCONF4A (A) and CDKCONF4B (B) biosensors. Compounds identified with both biosensors are in purple, compounds identified only with CDKCONF4A are in blue and compounds identified only with CDKCONF4B are in orange. The fluorescent signal of CDKCONF4A/B-Cy3 alone was regarded as 100%.

Dose response of CDKCONF4A/B-Cy3 to hits identified in the two libraries

Since few hits promoted a fluorescence increase of the biosensors at 10 µM, the response of Cy3-labelled CDKCONF4A and CDKCONF4B was therefore investigated using different concentrations of compounds (examples are given in Figure 86). While a response of CDKCONF4A/B-Cy3 was obtained with AB-00015228, AB-00015203, AB-00016193, LPI2148 and LPI2251 at 10^{-5}M in the original screen,

the biosensors only responded to these compounds when diluted at 10^{-4}M in this experiment. This difference can be explained by the use of fresh powder stocks of compounds. However, Cy3-CDKCONF4A responded to ICMR-04-E10 and LPS853 in a dose-dependent fashion (Figure 86A/B), and LPS401 promoted a dose-dependent response of both Cy3-CDKCONF4A and Cy3-CDKCONF4B (Figure 86E/F).

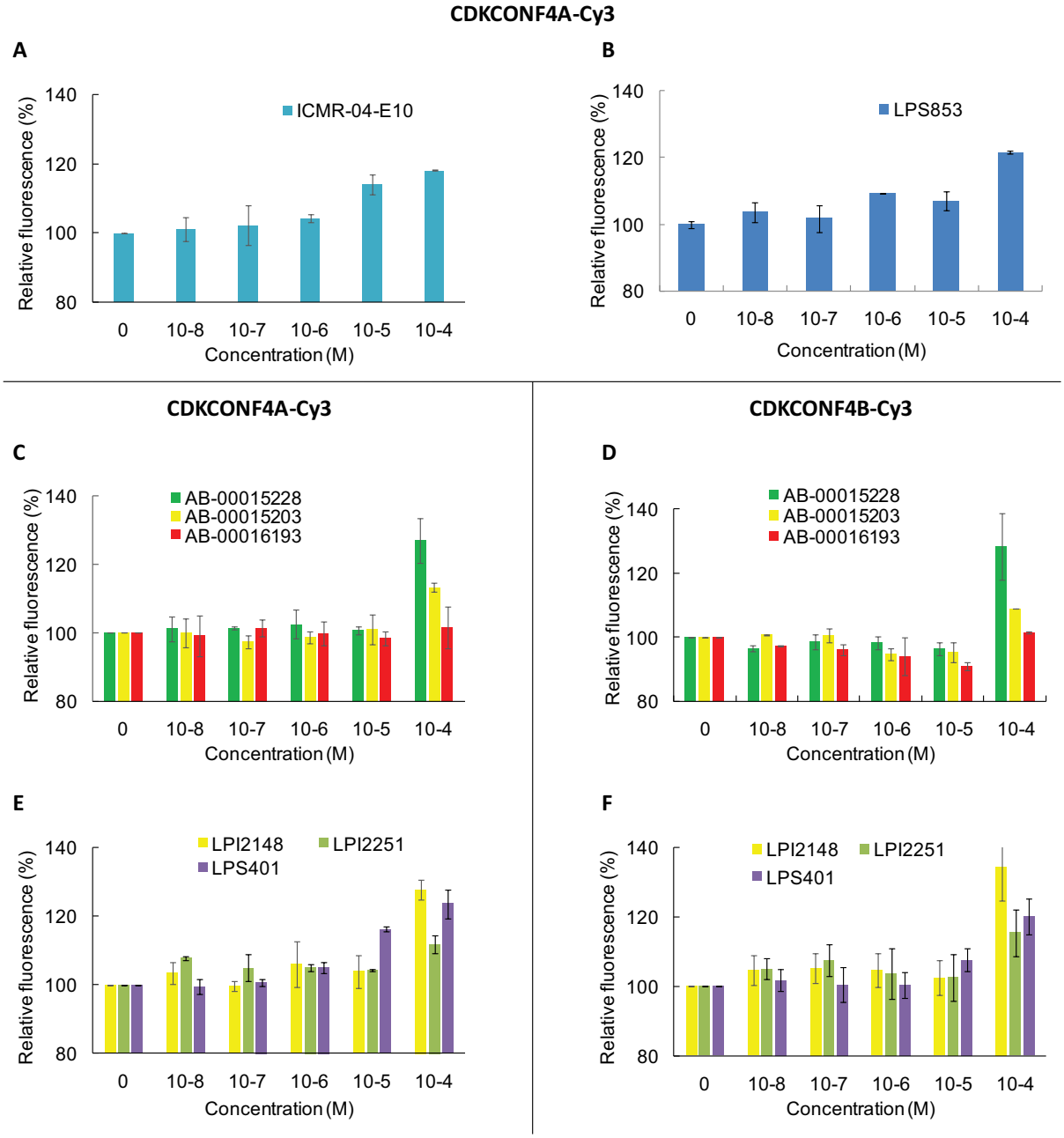

Figure 86: Dose response of Cy3-labelled CDKCONF4A to (A) ICMR-04-E10 and (B) LPS853. Dose response of Cy3-labelled CDKCONF4A (left panel) and CDKCONF4B (right panel) to (C & D) AB-00015228, AB-00015203, AB-00016193 and (E & F) LPI2148 and LPI2251, from the library of

Strasbourg, and LPS401, which respond to both biosensors. Compounds were tested at 10^{-4}, 10^{-5}, 10^{-6}, 10^{-7} and 10^{-8}M. The fluorescent signal of CDKCONF4A/B-Cy3 alone was regarded as 100%.

Given the robust response of Cy3-CDKCONF4A/B to LPI2148 and LPI2251 at 10^{-4}M and since we started a close collaboration with Dr. Frédéric Bihel, the chemist who synthesized these compounds, we decided to focus only on these two hits to further *in vitro* characterization, with respect to their identification by CDKCONF4A as PPI inhibitors.

Identification of PISTVRE helix binders

To verify whether these hits might bind the PISTVRE helix of CDK4 directly, a peptide derived from this helix, named PISTVRE peptide, was labelled and a fluorescence titration assay was performed using, as a positive control, a peptide named D1 which derived from the complementary interface, the α5 helix of cyclin D1 (Figure 87). TP2Rho was used as fluorescent probe because of its important fluorescence enhancement upon interaction with targets (Dr Florence Mahuteau-Betzer, Institut Curie) (Dumat et al., 2012, 2013). One of these compounds, LPI2251 indeed enhanced the fluorescence of TP2Rho-labelled PISTVRE significantly and in a dose-dependent fashion, whereas the other, LPI2148 (which will not be described any further) did not.

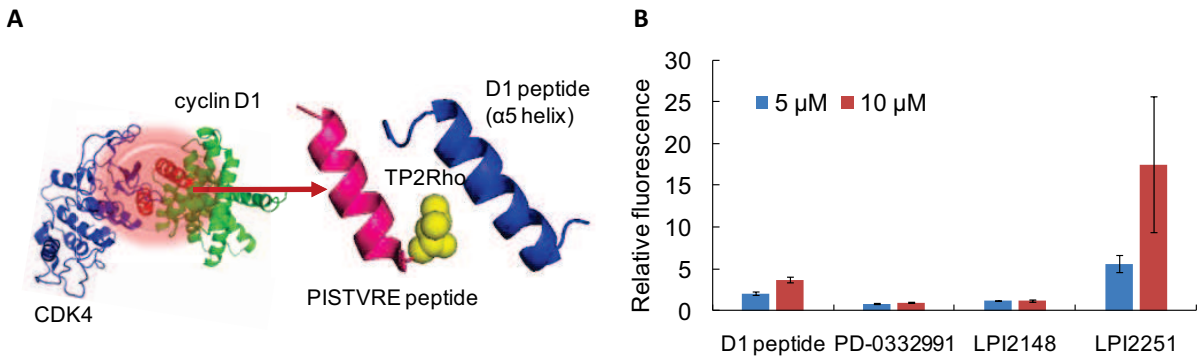

Figure 87: (A) Design of two peptides derived from the CDK4/cyclin D1 interface (B) Fluorescence binding assay of LPI2148 and LPI2251 (at 5 and 10 µM), compared to D1 peptide, with 200 nM TP2Rho-PISTVRE peptide. The increase in fluorescence of each compound was calculated with reference to the basal fluorescence of TP2Rho-labelled PISTVRE peptide (regarded as 1).

LPI2251 derivatives

To further explore the chemical and structural determinants of LPI2251 involved in the interaction with the PISTVRE helix, a family of derivatives was synthesized in the team of Dr. Frédéric Bihel. Their general structure is shown in Figure 88.

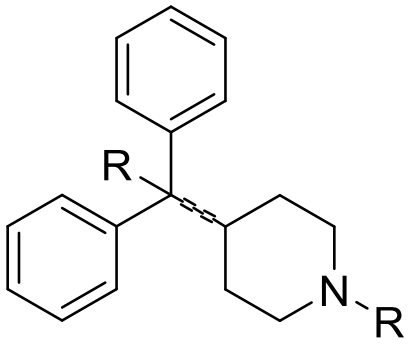

Figure 88: The general structure of LPI2251 derivatives

Dose response of CDKCONF4A-Cy3 to LPI2251 derivatives

The ability of LPI derivatives to enhance fluorescence of Cy3-labelled CDKCONF4A was examined (Figure 89). All the compounds, except for LPI2183, promoted a similar fluorescence enhancement of Cy3-labelled CDKCONF4A at 5 µM and 10 µM as the positive control (D1 peptide). Only MED0128 induced a greater fluorescence enhancement at 5 µM and 10 µM than that of D1 peptide.

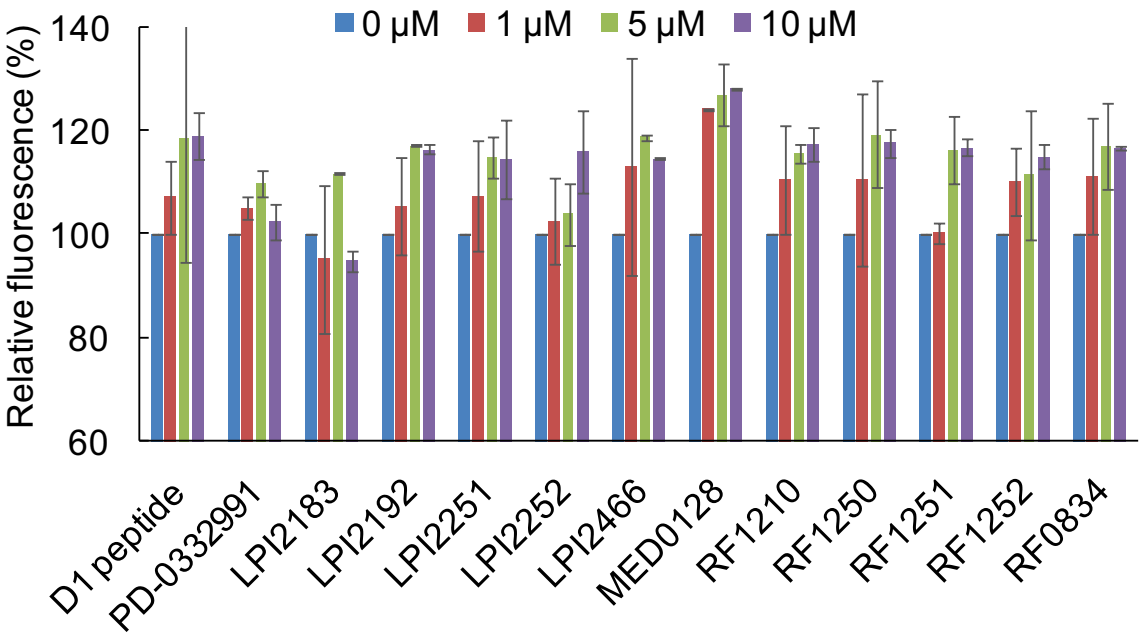

Figure 89: Fluorescence binding assay of LPI2251 derivatives (at 1, 5 and 10 µM) with 200 nM Cy3-CDKCONF4A. The increase in fluorescence of each compound was calculated with reference to the basal fluorescence of Cy3-CDKCONF4A, regarded as 100%.

Dose response of TP2Rho-PISTVRE peptide to LPI2251 derivatives

Then, their ability to enhance fluorescence of TP2Rho-PISTVRE peptide was investigated. Three compounds LPI2252, LPI2466 and RF1210 induced a similar response of the CDK4-derived PISTVRE peptide compared to the original hit LPI2251 (Figure 90).

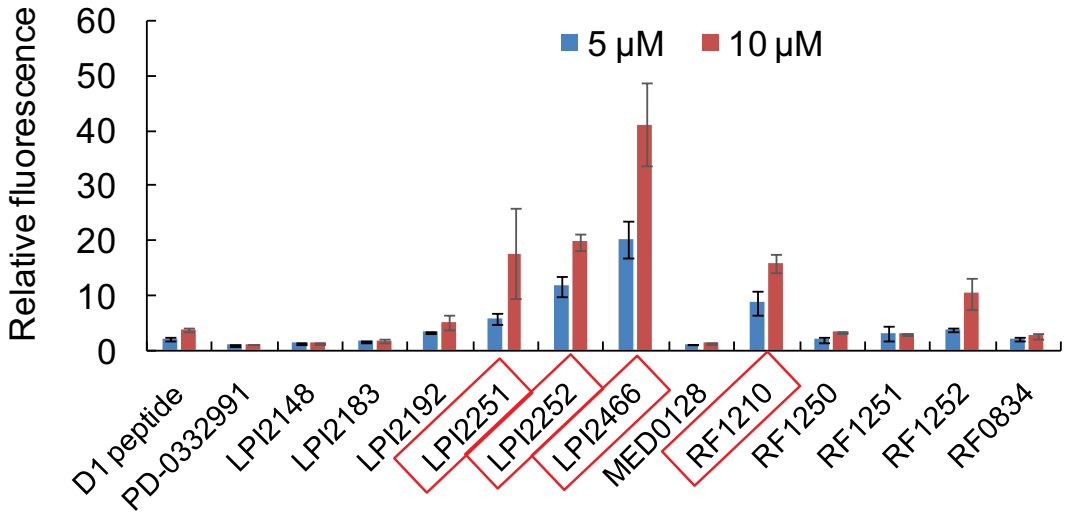

Figure 90: Fluorescence binding assay of LPI2251 derivatives (at 5 and 10 µM) with 200 nM TP2Rho-PISTVRE peptide. The increase in fluorescence of each compound was calculated with reference to the basal fluorescence of TP2Rho-labelled PISTVRE peptide, regarded as 1.

In order to assess that the increase in fluorescence was indeed due to interaction between the PISTVRE peptide and LPI derivatives and not a response of the fluorescent probe TP2Rho itself, a control experiment was performed with an irrelevant peptide, MP26, labeled with TP2-Rho (Figure 91). Unfortunately, upon incubation with LPI derivatives, a similar fluorescence enhancement was observed with TP2Rho-MP26 compared to TP2Rho-PISTVRE, indicating that TP2Rho binds LPI compounds.

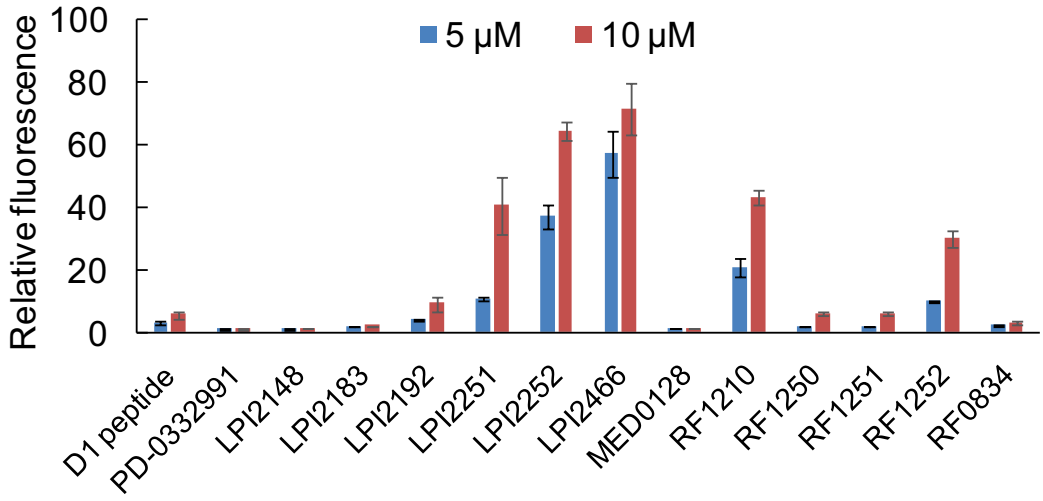

Figure 91: Fluorescence control assay with 200 nM TP2Rho-MP26 peptide and LPI2251 derivatives (at 5 and 10 µM). The increase in fluorescence of each compound was calculated with reference to the basal fluorescence of TP2Rho-labelled MP26 peptide, regarded as 1.

The fluorescent probe Cy5 was then tested in fluorescence binding assay of LPI2251, LPI2252, LPI2466 and RF1210 (at 5 and 10 µM) with 200 nM PISTVRE peptide. Cy5-labelled PISTVRE peptide responded to these compounds in a dose-dependent fashion, whilst a much lower increase in fluorescence of Cy5-MP26 was observed (Figure 92). This experiment suggested that Cy5 could be used for fluorescence binding assays since this fluorescent probe did not bind LPI compounds.

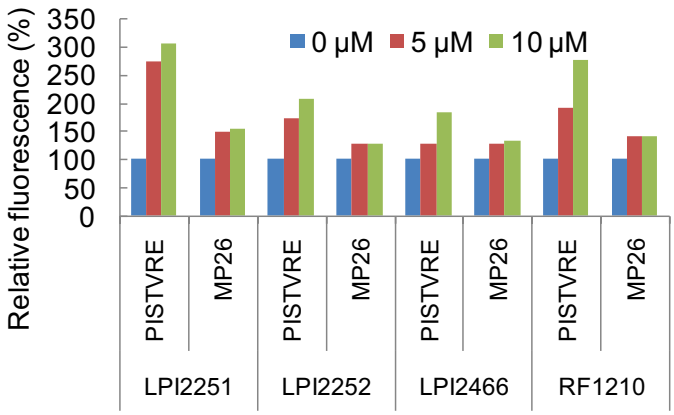

Figure 92: Fluorescence binding assay of LPI2251 derivatives (at 5 and 10 µM) with 200 nM Cy5-PISTVRE peptide and Cy5-MP26. The increase in fluorescence of each compound was calculated with reference to the basal fluorescence of Cy5-labelled PISTVRE or MP26, regarded as 100%.

Fluorescence titration of PISTVRE and D1 peptides with LPI derivatives

Fluorescence titration assays of PISTVRE peptide with LPI derivatives were performed to determine the dissociation constant values of the compounds (Figure 93A). LPI2252, LPI2466 and RF1210 interacted with TP2Rho-PISTVRE peptide with affinities in the micromolar range, similar to that of the complementary peptide derived from the interface of cyclin D1 (D1 peptide) (dissociation constant values of 17 µM for D1 peptide, 3.35 µM for LPI2466, 17 µM for RF1210 and 34 µM for LPI2252).

Then, to verify that these compounds could bind the α5 helix peptide of cyclin D1, fluorescence titration assays of D1 peptide with LPI derivatives were performed (Figure 93B). Compared to the PISTVRE peptide, LPI2466, RF1210 and LPI2252 indeed bound the interface of cyclin D1, yet with much lower affinity (dissociation constant values of 180 nM for PISTVRE, 6.88 µM for LPI2466, 21 µM for RF1210 and 47 µM for LPI2252).

A.

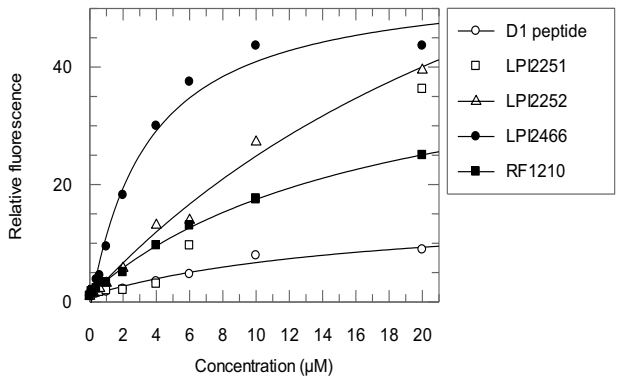

	Kd (µM)
PISTVRE vs D1	17 ± 7
PISTVRE vs LPI2251	ND
PISTVRE vs LPI2252	34 ± 12
PISTVRE vs LPI2466	3,35 ± 0,71
PISTVRE vs RF1210	17 ± 2

B.

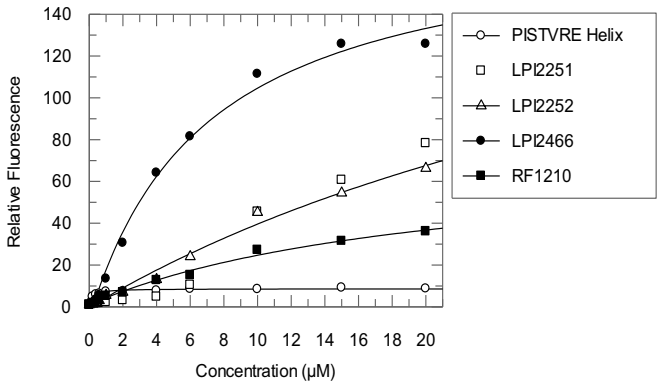

	Kd (µM)
D1 vs PISTVRE	0,18 ± 0,04
D1 vs LPI2251	> 100
D1 vs LPI2252	47 ± 23
D1 vs LPI2466	6,88 ± 1,28
D1 vs RF1210	21 ± 5

Figure 93: (A) Fluorescence titration of 200 nM PISTVRE peptide-TP2Rho with D1 peptide, LPI2251, LPI2252, LPI2466 and RF1210. ND: Not Determined - No Kd value could be calculated for LPI2251 (B) Fluorescence titration of 200 nM D1 peptide-TP2Rho with the PISTVRE peptide, LPI2251, LPI2252, LPI2466 and RF1210.

Determination of the intrinsic fluorescence of the library compounds at 614 nm following excitation at 510 nm

Importantly, autofluorescence of the LPI derivatives was examined and none of these compounds emitted any fluorescence at 614 nm when excited at 510 nm compared to TP2Rho-PISTVRE peptide (Figure 94).

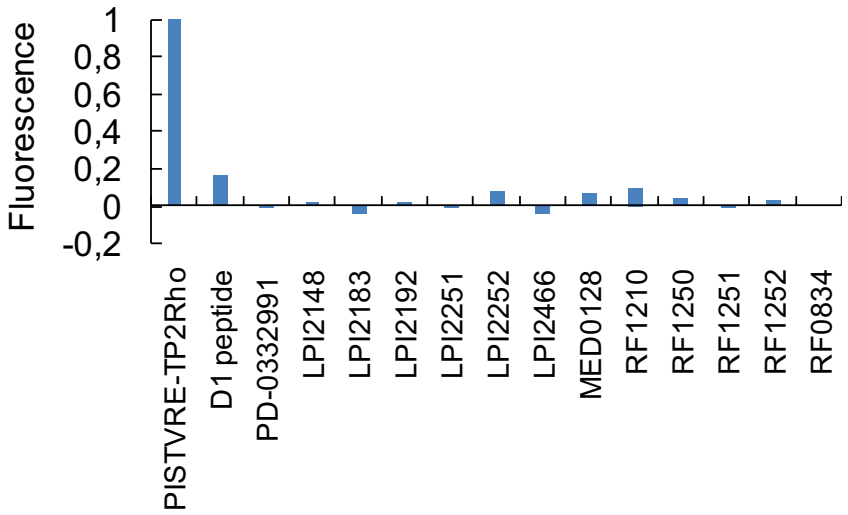

Figure 94: Determination of the intrinsic fluorescence of the library compounds at 614 nm following excitation at 510 nm, to eliminate autofluorescent compounds.

2.5.2. *In cellulo* characterization

CNE compounds

The ability of the different CNE compounds (AB-00015228 / AB-00015203 / AB-00016193 / ICMR-04-E10 / LPS 401 / LPS853 / Cesr-1409000) to inhibit cell growth was examined on the A375 melanoma cell line which harbours a wild-type CDK4 but a loss of function of CDKN2A ($p16^{INK4A}$) and the V600E BRaf mutation. Compounds were tested at 10^{-6}, 10^{-7}, 10^{-8} and 10^{-9} M and relative cell growth was measured at 6, 12, 24h (Figure 95) (materials and methods). This experiment showed that any compound promoted a significant decrease in the number of cells under these conditions.

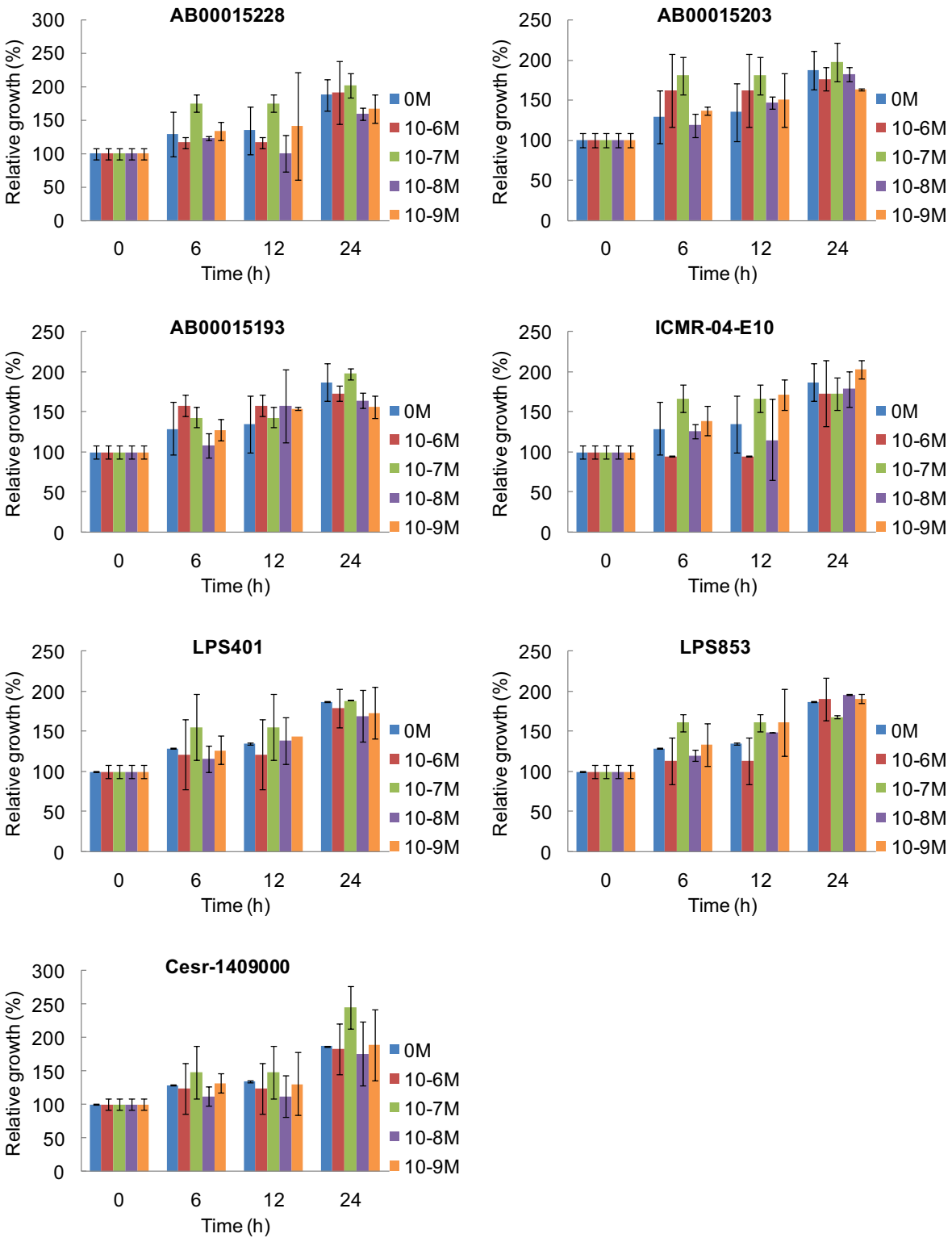

Figure 95: Proliferation inhibition studies of the CNE compounds in melanoma A375 cell line at 6, 12, 24 and 48h.

LPI derivatives

Since the LPI derivatives provided promising results *in vitro*, their ability to inhibit proliferation of melanoma cells was investigated. To this aim, the efficiency of the different compounds at 1 µM and

10 µM was first examined on the A375 melanoma cell line (Figure 96). While no compound inhibited A375 cell proliferation at 1 µM, one compound, LPI2192, promoted efficient cell growth inhibition at 10 µM at 24 and 48h (Figure 96A).

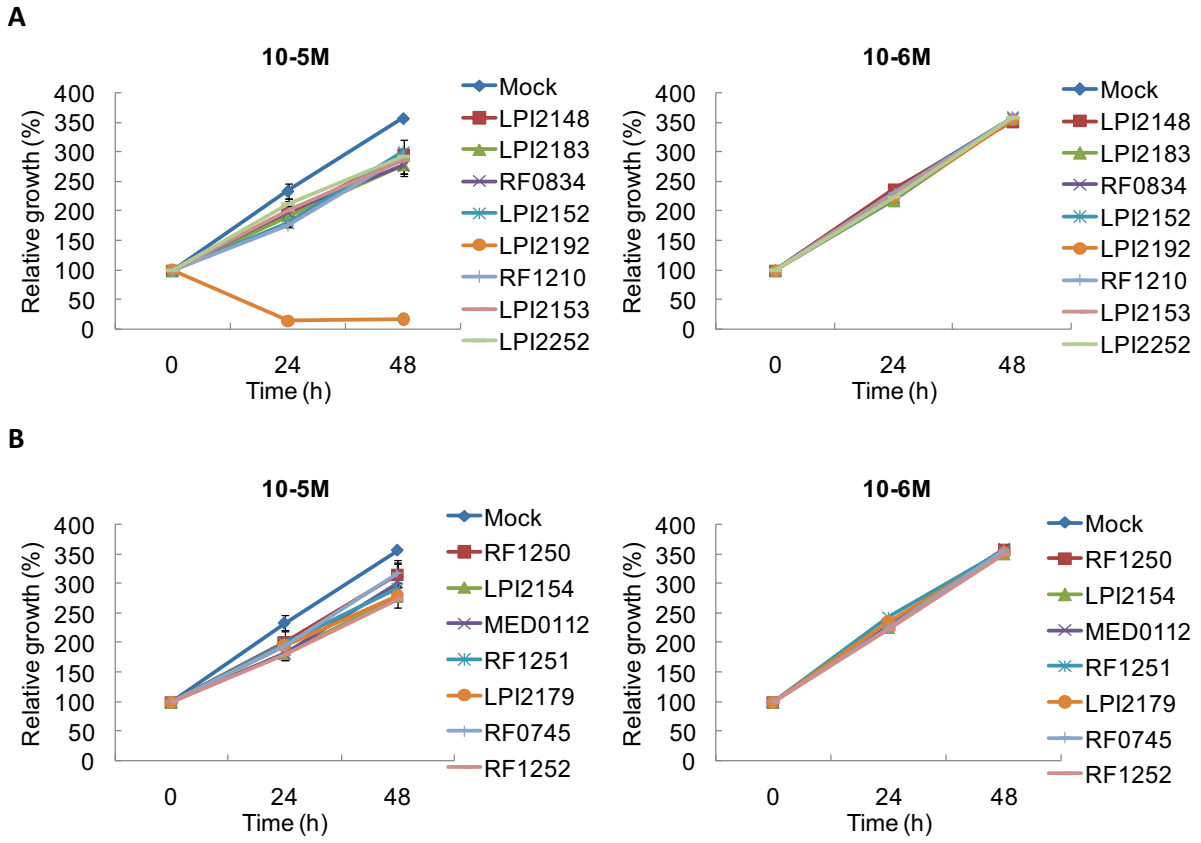

Figure 96: Proliferation inhibition studies of the LPI derivatives in melanoma A375 cell line at 1 µM (left panel) and 10 µM (right panel) at 24 and 48h.

The dose-dependent inhibitory potency of the most efficient compounds *in vitro* in binding and titration assays and/or *in cellulo* (LPI2192 / RF1210 / LPI2251 / LPI2252 / MED0128) was then investigated on the melanoma (A375) and fibroblast cell lines and compared to PD-0332991 (Figure 97). Table 7 provides the IG_{50} values of the compounds determined for A375 at 48h (materials and methods and annex E). IG_{50} were all in the micromolar range and comparable with that of PD-0332991. One compound, LPI2192, had a significant inhibitory potency on fibroblasts, suggesting that it could alter the proliferation of healthy cells. It is therefore more relevant to focus on compounds which only alter cancer cells such as RF1210, LPI2251, LPI2252 and MED0128.

A

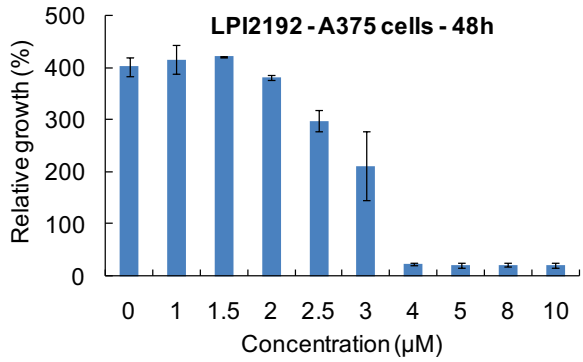
LPI2192 - A375 cells - 48h
Relative growth (%)
500
400
300
200
100
0
0 1 1.5 2 2.5 3 4 5 8 10
Concentration (µM)

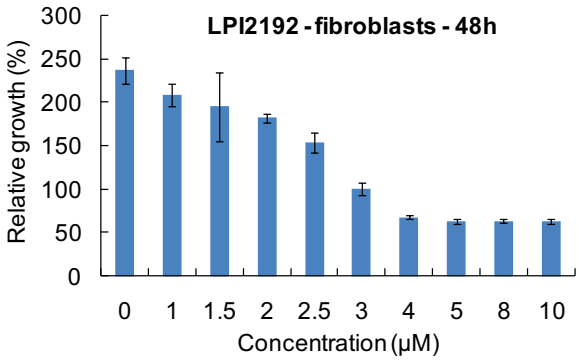
LPI2192 - fibroblasts - 48h
Relative growth (%)
300
250
200
150
100
50
0
0 1 1.5 2 2.5 3 4 5 8 10
Concentration (µM)

B

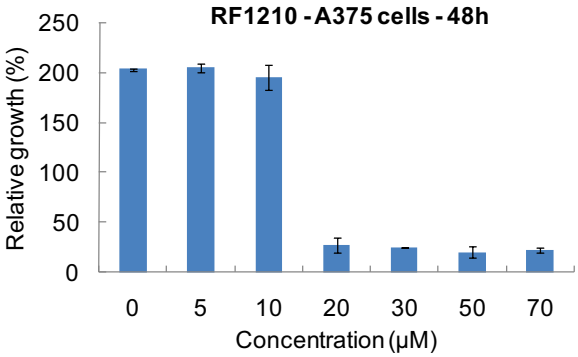
RF1210 - A375 cells - 48h
Relative growth (%)
250
200
150
100
50
0
0 5 10 20 30 50 70
Concentration (µM)

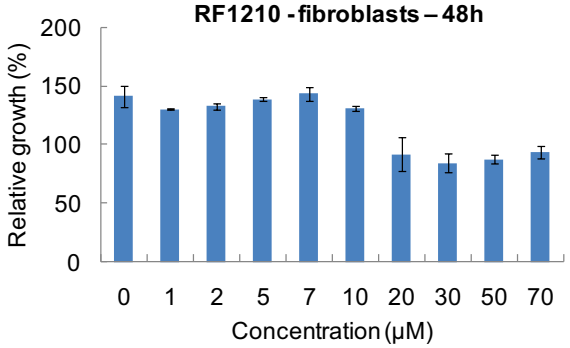
RF1210 - fibroblasts – 48h
Relative growth (%)
200
150
100
50
0
0 1 2 5 7 10 20 30 50 70
Concentration (µM)

C

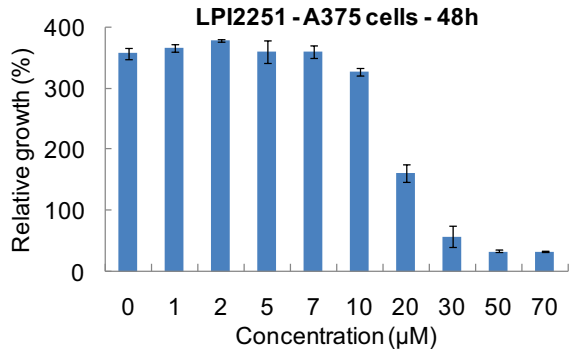
LPI2251 - A375 cells - 48h
Relative growth (%)
400
300
200
100
0
0 1 2 5 7 10 20 30 50 70
Concentration (µM)

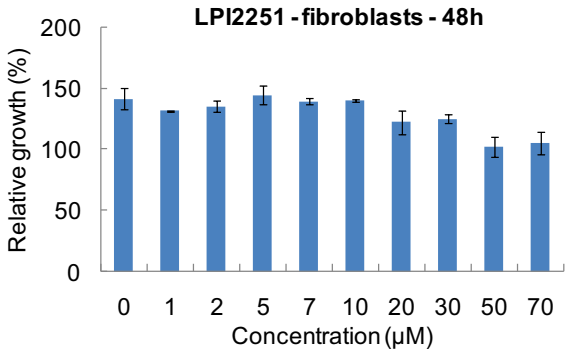
LPI2251 - fibroblasts - 48h
Relative growth (%)
200
150
100
50
0
0 1 2 5 7 10 20 30 50 70
Concentration (µM)

D

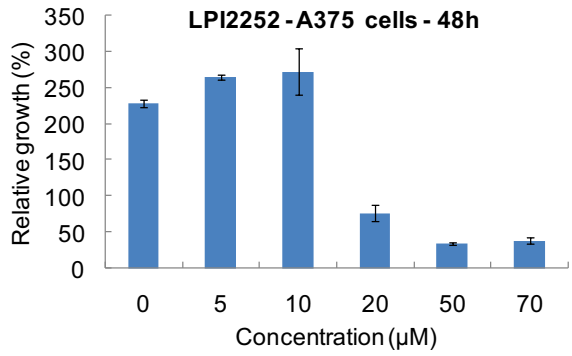
LPI2252 - A375 cells - 48h
Relative growth (%)
350
300
250
200
150
100
50
0
0 5 10 20 50 70
Concentration (µM)

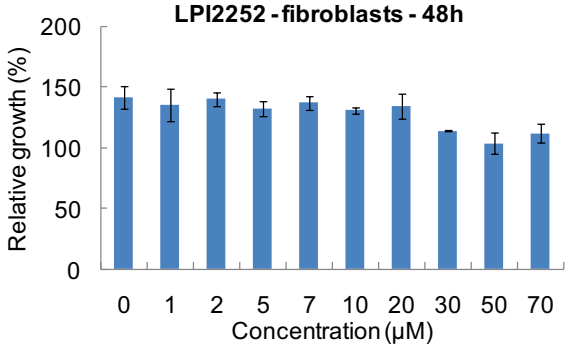
LPI2252 - fibroblasts - 48h
Relative growth (%)
200
150
100
50
0
0 1 2 5 7 10 20 30 50 70
Concentration (µM)

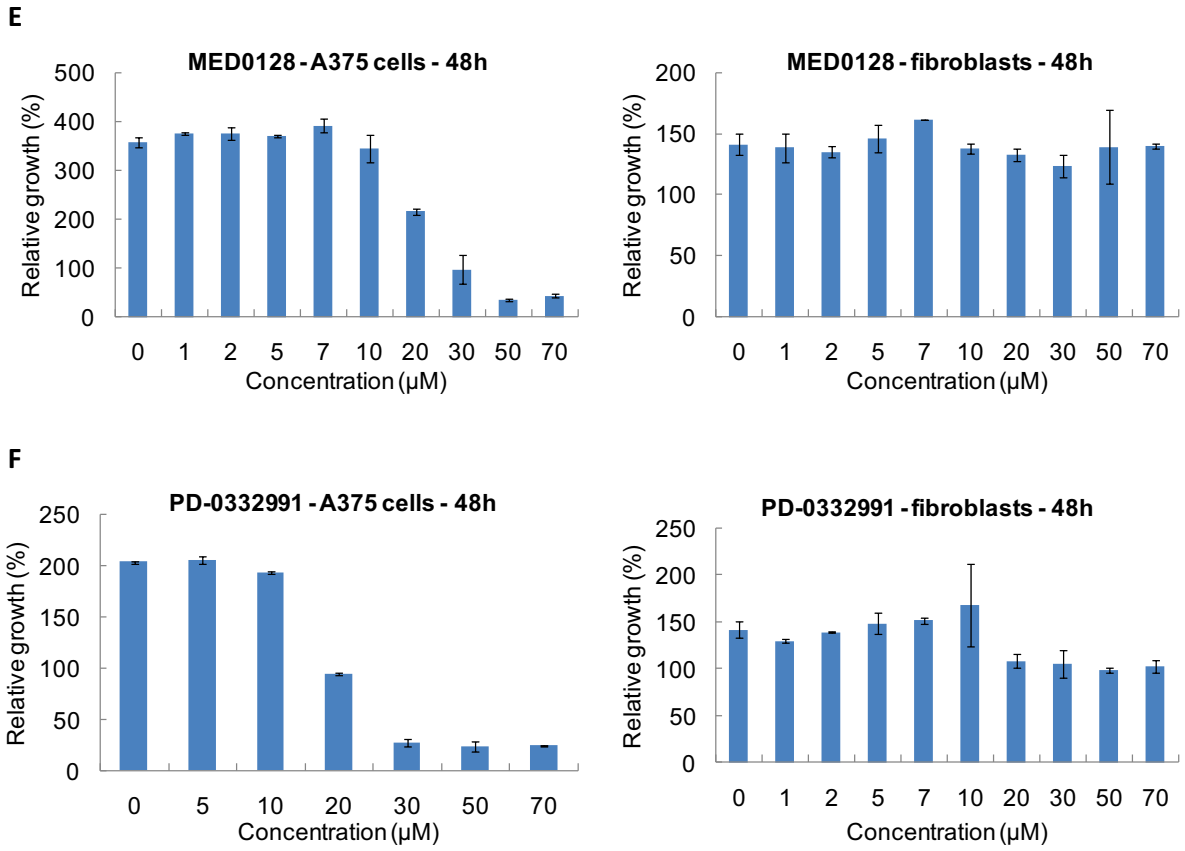

Figure 97: Proliferation inhibition studies in A375 melanoma (left panel) and fibroblast (right panel) cell lines at 48h of the most promising LPI derivatives: (A) LPI2192, (B) RF1210, (C) LPI2251, (D) LPI2252, (E) MED0128 and (F) PD-0332991 as control.

A375	IG_{50} (µM)
LPI2192	2.9 +/- 0.1
RF1210	13.6 +/- 0.4
LPI2251	17.6 +/- 0.5
LPI2252	17.9 +/- 2.2
MED0128	20.7 +/- 0.8
PD-0332991	18.7 +/- 0.4

Table 7: Inhibition constants (IG_{50}) of LPI compounds in A375 cell line.

Proliferation assays were then performed in different melanoma cell lines bearing wild-type $p16^{INK4A}$, BRAF and CDK4 (Mewo cells), the NRAS Q61R mutation (SK-MEL2 cell line) or the R24C CDK4 and BRAF V600E mutation (SK-MEL28 cell line). Table 2 lists the genetic alterations identified for the

different components of the $p16^{INK4A}$ / CDK4/6-cyclin D / pRb pathway and for BRAF and NRAS in A375, Mewo, MV3, SK-MEL2 and SK-MEL28 cell lines.

	CDKN2A	CDK4	Rb	BRAF	NRAS
A375	mutated (E61Stop, Loss of function)	WT	WT	V600E	WT
Mewo	mutated (R80Stop, Loss of function)	WT	WT	WT	WT
MV3	ND	ND	ND	WT	WT
SK-MEL2	WT	WT	WT	WT	mutated (Q61R)
SK-MEL28	WT	R24C	WT	V600E	WT

Table 8: Genetic alterations identified in A375, Mewo, MV3, SK-MEL2 and SK-MEL28 cell lines (ND: data not found).

We decided to focus on RF1210 because it proved to be one of the most potent compounds *in vitro* in binding and titration assays. The IG_{50} values of RF1210 are similar between the different melanoma cell lines, from 10 µM to 13.6 µM (Table 9 and annex E). They are similar to the IG_{50} values obtained with PD-0332991 (from 10.7 µM to 18.7 µM).

	IG_{50} (PD-0332991) (µM)	IG_{50} (RF1210) (µM)
A375	18.7 +/- 0.4	13.6 +/- 0.4
MV3	11.0 +/- 0.8	10.8 +/- 4.4
SKMEL2	10.7 +/- 1.6	10.1 +/- 1.0
SKMEL28	11.5 +/- 3.2	12.0 +/- 0.2

Table 9: Inhibition Constants (IG_{50}) of PD-0332991 and RF1210 in different melanoma cell lines.

Combined administration of RF1210 with other drugs

Finally, proliferation assays were performed to investigate whether RF1210 and LPI2252 could cooperate with other drugs in promoting efficient inhibition of A375 melanoma cell proliferation. Indeed, at suboptimal concentrations of 10 µM RF1210 and LPI2252, the combination of these compounds with CDK4 inhibitors such as PD-0332991 and LY2835219 proved to inhibit proliferation of A375 cells more efficiently than either compound alone (Figure 98 and Table 10). Cooperation was

also observed with LEE011, another CDK4 inhibitor, but also with drugs not related to CDK4 such as Paclitaxel and Methotrexate which are commonly used for treatment of cancer.

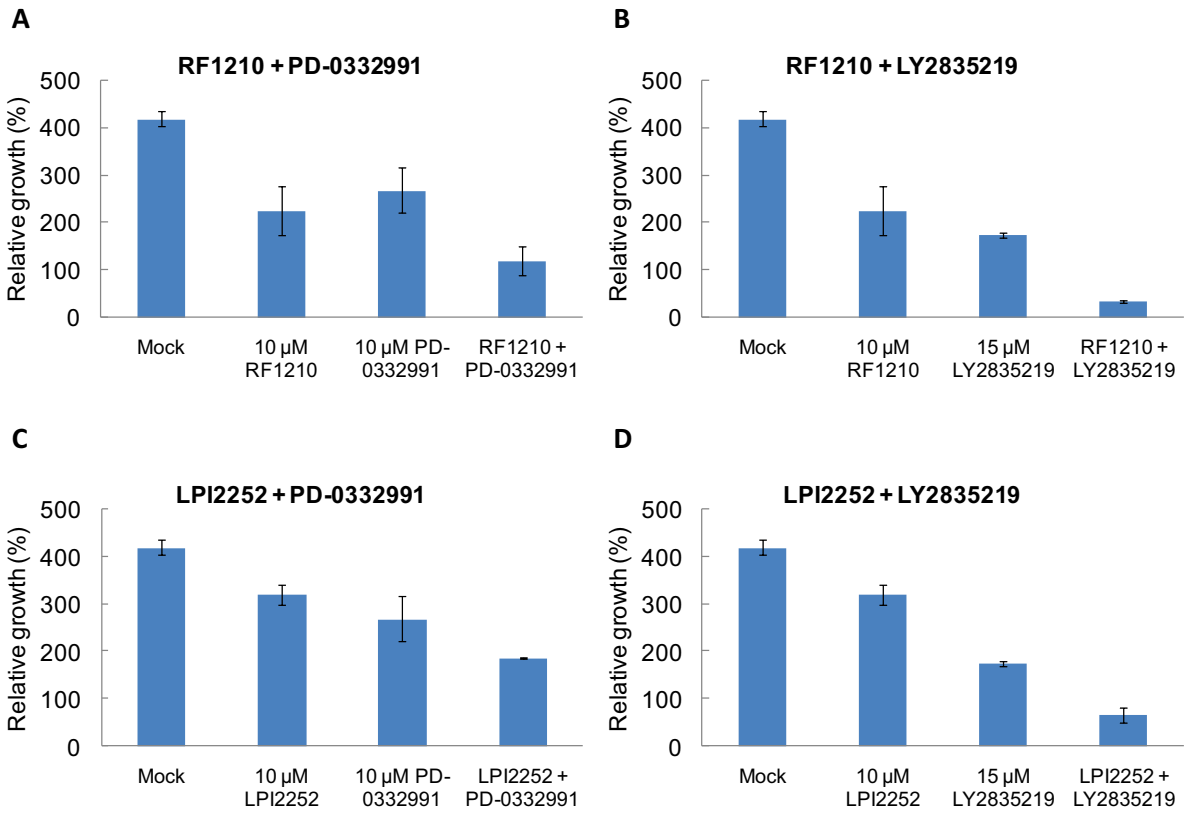

Figure 98: Cooperation between (A) RF1210 (10 µM) and PD-0332991 (10 µM); (B) RF1210 (10 µM) and LY2835219 (15 µM); LPI2252 (10 µM) and PD-0332991 (10 µM); LPI2252 (10 µM) and LY2835219 (15 µM) at 48h in A375 cell line.

A

Cooperation – RF1210	Degree of inhibition (%)
10 µM RF1210	46.2
15 µM LEE011	20.5
15 µM LY2835219	58.6
15 µM Paclitaxel	48.4
15 µM Methotrexate	31.4
10 µM PD-0332991	36.0
RF1210 + LEE011	73.4
RF1210 + LY2835219	92.0
RF1210 + Paclitaxel	72.4
RF1210 + Methotrexate	58.0
RF1210 + PD-0332991	71.7

B

Cooperation – LPI2252	Degree of inhibition (%)
10 µM LPI2252	23.7
15 µM LEE011	20.5
15 µM LY2835219	58.6
15 µM Paclitaxel	48.4
15 µM Methotrexate	31.4
10 µM PD-0332991	36.0
LPI2252 + LEE011	37.7
LPI2252 + LY2835219	84.5
LPI2252 + Paclitaxel	73.2
LPI2252 + Methotrexate	48.8
LPI2252 + PD-0332991	55.6

Table 10: Proliferation inhibition studies in melanoma A375 of (A) RF1210 (10 µM) and (B) LPI2252 (10 µM) in combination with other drugs at 48h.

B. Development of peptide inhibitors that target the CDK4/cyclin D interface

2.6. Concept and design

Peptides were designed to target the interface between CDK4 and cyclin D through structural analysis of the helices involved in the protein-protein interaction (PPI) (Figure 99).

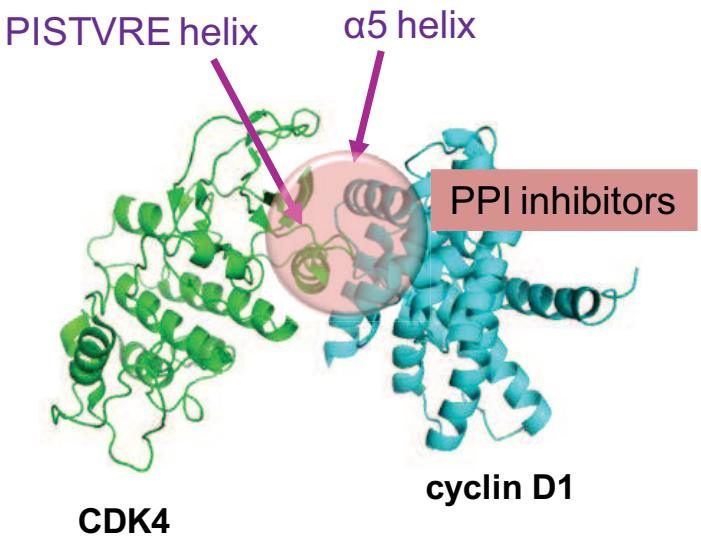

Figure 99: Design of peptides that can target the interface between the PISTVRE helix of CDK4 and the α5 helix of cyclin D (crystal structure of CDK4/cyclin D1 (PDB 2W99)).

In the team, this strategy was already implemented for targeting the interface between CDK2 and cyclin A (Gondeau et al., 2005). Given the success of this work, two peptides were designed to target the interface between the PISTVRE helix of CDK4 and the α5 helix of cyclin D1: one peptide, named D1, derived from the α5 helix sequence; and the other, PISTVRE, derived from the PISTVRE helix sequence (Table 11). A cysteine residue was introduced in both peptide sequences for labeling with fluorescent probes.

Peptide	Derived from	Sequence
PISTVRE	PISTVRE helix of CDK4	H-GGGCPISTVREVALLRRL
D1	α5 helix of cyclin D1	SIRPEELLQMELLLVNKLKWNLC

Table 11: Amino acid sequence of the two peptides that have been designed to target the CDK4/cyclin D interface

2.7. *In cellulo* characterization

Proliferation assays were performed in A375 melanoma cells to determine the ability of the two peptides to inhibit cell proliferation. These peptides were delivered into cells using the cell penetrating peptide CADY2 (Figure 99) (Kurzawa et al., 2010). CADY2 is an amphipathic peptide that can interact with proteins and peptides and deliver them efficiently into living cells. This strategy has

already been implemented to deliver peptide inhibitors targeting a PPI (eg MP51) (Kurzawa et al., 2010).

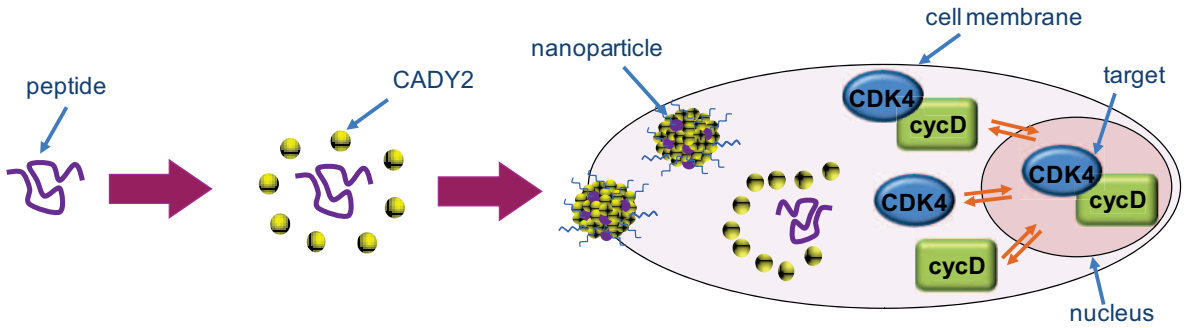

Figure 100: Delivering into cells of PISTVRE and D1 peptides thanks to the cell-penetrating peptide CADY2.

The PISTVRE peptide inhibited A375 cell proliferation similarly than PD-0332991 with a 22% and 27% decrease in melanoma cell growth at 10^{-6}M and 10^{-7}M, respectively (Figure 101 A&B). The D1 peptide was more efficient at 10^{-6}M with a 56% decrease in melanoma cell growth and was comparable to PISTVRE at 10^{-7}M (22% decrease) (Figure 101 C&D). At 10^{-6}M and 10^{-7}M, neither PISTVRE nor D1 inhibit melanoma cell growth when administrated alone, without facilitated delivery (Figure 101 E&F).

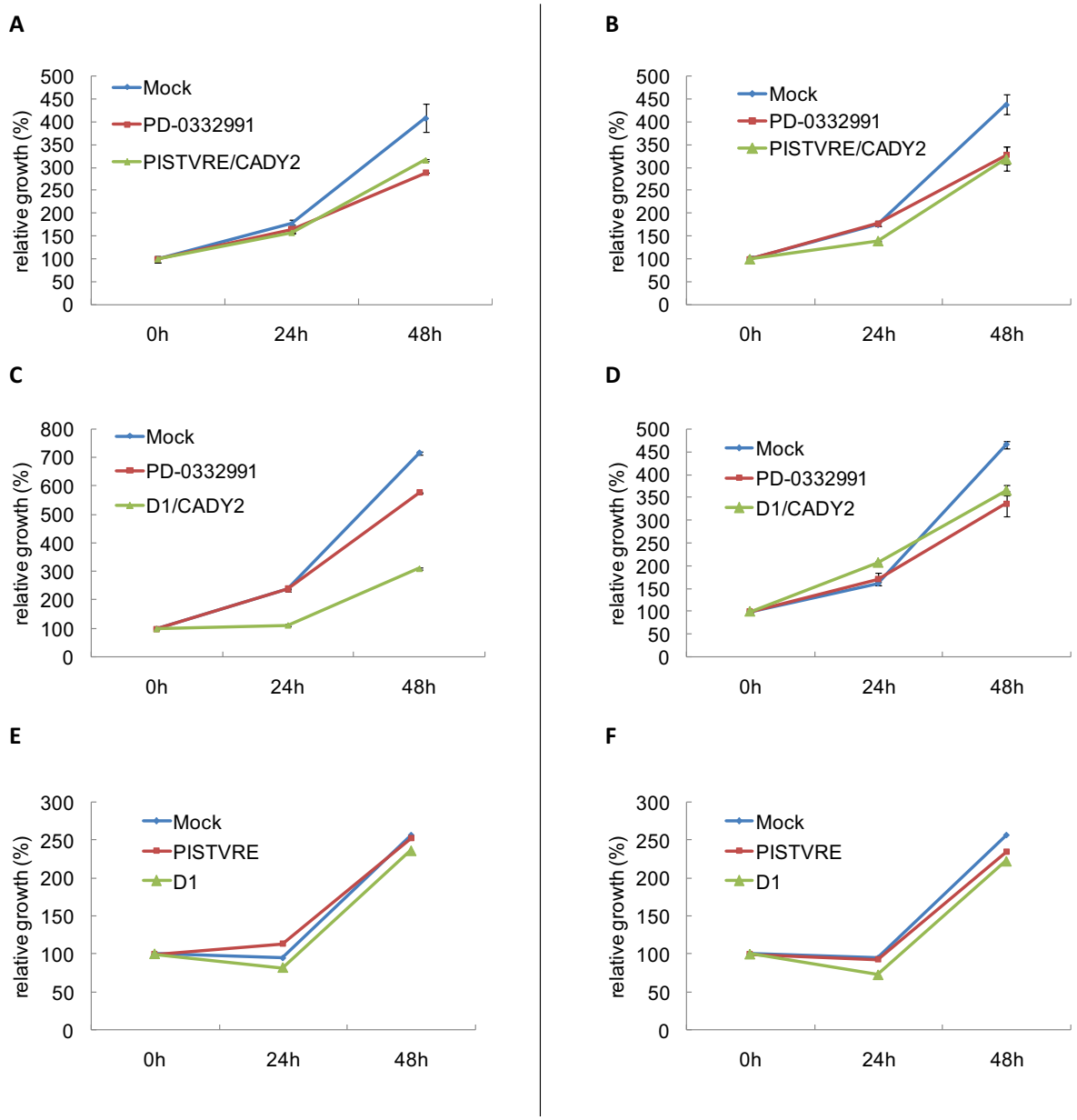

Figure 101: Proliferation inhibition studies of PISTVRE and D1 peptides at 10^{-6}M (left panel) and 10^{-7}M (right panel) in A375 melanoma cell lines at 24 and 48h. (A & B) PISTVRE/CADY2 (ratio 1/20) compared to PD-0332991; (C & D) D1/CADY2 (ratio 1/20) compared to PD-0332991; (E & F) PISTVRE and D1 peptides administrated without CADY2.

2.8. *In vitro* characterization

Some variants of PISTVRE were generated in order to determine the minimal sequence that can efficiently target the interface. Shorter and longer sequences derived from the CDK4/cyclin D interface were synthesized to investigate whether N- and C-terminal extensions could favour

interactions (Figure 102 and Table 12). For each variant, an N-terminal acetylated derivative was also synthesized so as to cap the N-terminus and prevent its recognition by the proteolytic machinery.

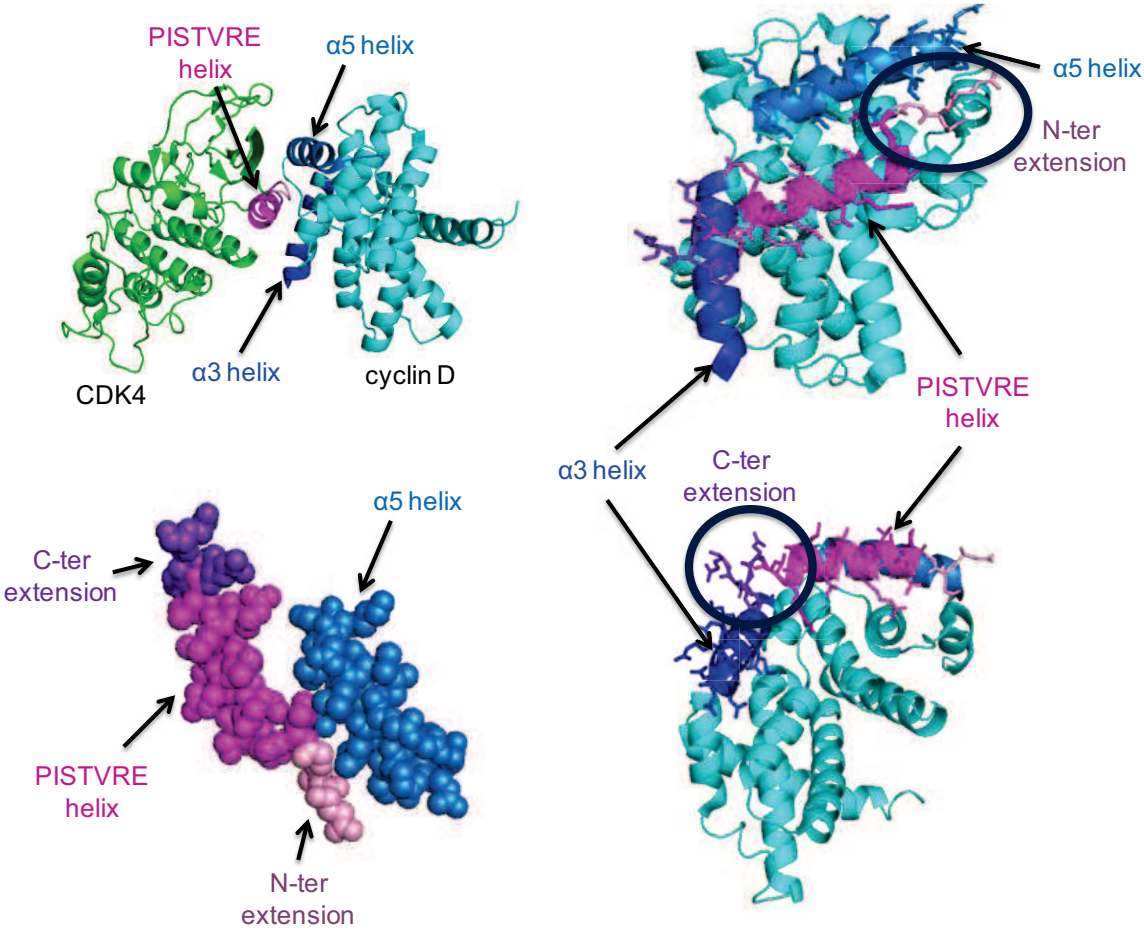

Figure 102: Design of PISTVRE variants. They all contain the sequence corresponding strictly to helical region and additional amino acids that are thought to be involved in the main interactions between CDK4 and cyclin D (crystal structure of CDK4/cyclin D1 (PDB 2W99)). These amino acids are highlighted with circles.

	sequence
D1	SIRPEELLQMELLLVNKLKWNLC
PISTVRE	H-GGGCPISTVREVALLRRL
Ac-PISTVRE	Ac-GGGCPISTVREVALLRRL
PISTVRE-A	H-CPISTVREVALLRRL
Ac-PISTVRE-A	Ac-CPISTVREVALLRRL
PISTVRE-B	H-CPISTVREVALLRRLEAFE
Ac-PISTVRE-B	Ac-CPISTVREVALLRRLEAFE
PISTVRE-C	H-GGGCPISTVREVALLRRLEAFE
Ac-PISTVRE-C	Ac-GGGCPISTVREVALLRRLEAFE

Table 12: Sequence of the PISTVRE variants. They contain the original PISTVRE sequence and N-terminal and/or C-terminal extensions.

In order to determine the best derivative, binding assays of the variants (from 0 to 3000 nM) with 500 nM TAMRA-labelled D1 peptide were performed (Figure 103). Dissociation constant (Kd) values demonstrated that the shorter PISTVRE variant, PISTVRE-A, bound with the greatest affinity (Kd = 172 +/- 113 nM).

A

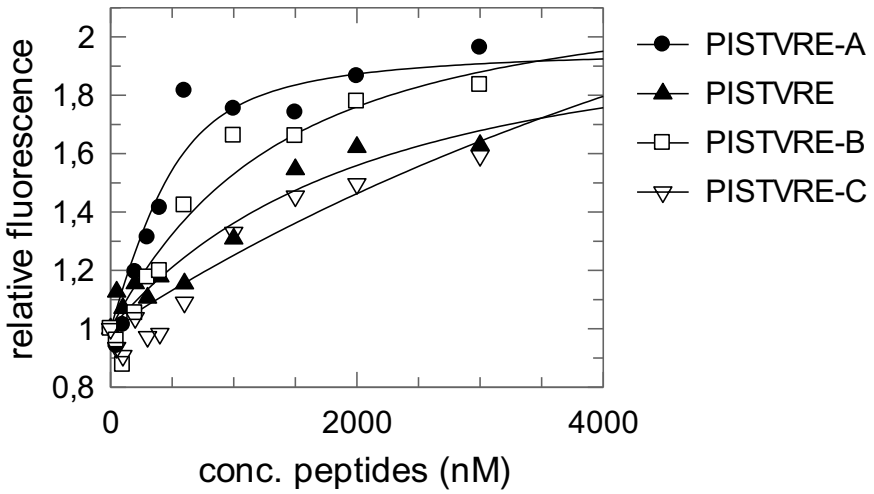

B

	sequence	Kd (nM)
PISTVRE	H-GGGCPISTVREVALLRRL	1757 +/- 1007
PISTVRE-A	H-CPISTVREVALLRRL	172 +/- 113
PISTVRE-B	H-CPISTVREVALLRRLEAFE	1016 +/- 581
PISTVRE-C	H-GGGCPISTVREVALLRRLEAFE	9498 +/- 16655

Figure 103: Binding assays of the PISTVRE variants (from 0 to 3000 nM) with 500 nM TAMRA-labelled D1 peptide. (A) Binding curves; (B) Constant dissociation (Kd) values calculated for the different variants.

Further experiments will include studies of the interaction with cyclin D1 protein to characterize the affinity and the specificity of interaction between the PISTVRE peptide and the α5 helix of cyclin D1, taking into account the whole environment surrounding this interface and all the secondary interactions existing at this interface.

Discussion & Perspectives

1. Development of a fluorescent biosensor for probing CDK4/cyclin D activity

1.1. Assessment

We have developed a CDK4-specific fluorescent peptide biosensor, WWshortRb, which comprises a substrate sequence derived from Rb and a newly designed phosphorecognition domain. This biosensor binds CDK4 and reports on the enzymatic activity of recombinant CDK4/cyclin D kinase *in vitro* through changes in fluorescence intensity. It is also well suited to probe CDK4 activity in cell extracts, skin biopsies, melanoma xenograft lysates and living cells, thereby providing a scaled and predictive readout of this cancer biomarker for diagnostic purposes.

Moreover, WWshortRb biosensor provides sensitive means of comparing CDK4 activity between different melanoma cell lines that harbour molecular alterations converging on CDK4/cyclin D activity, and of quantifying differences which cannot be identified by simple analysis of protein kinase expression levels.

WWshortRb has also proved to be efficient *in extracto* to quantify alterations in CDK4 activity following treatment with selective inhibitors or siRNA in a more physiologically-relevant environment than in buffer containing purified recombinant kinase. It therefore offers promising perspectives for drug discovery programs since it could enable to monitor the progression of melanoma and to monitor response to CDK4 inhibitors over time.

1.2. Biosensor design and importance of PAABD

We first generated a CDK4-specific fluorescent protein biosensor, CDKACTRb, which contains a CDK4-specific substrate sequence and a PAABD derived from the PBD of Plk1.

Despite the very promising results obtained *in vitro* and *in extracto*, we investigated an alternative strategy, the development of a peptide biosensor, WWRb, which offers a more practical handling and cellular delivery. WWRb contains the same substrate sequence as CDKACTRb but a different PAABD, derived from the WW domain of Pin1. This switch between protein and peptide allowed to highlight the importance of the phospho-recognition domain for the proper functioning of the biosensor.

Indeed, while the Pin1 WW domain had been successfully used in a hybrid biosensor to probe CDK9 activity (Anai et al., 2007), it did not seem to be functional in WWRb upon incubation of cell extracts. Since the lack of response of WWRb was observed with different probes *in extracto* and as the biosensor responded to recombinant CDK4/cyclin D *in vitro*, we hypothesized that the presence of lysis buffer, which contains detergents, prevented a proper folding of the WW domain.

This lack of functionality led to the design of a new shorter phosphorecognition domain, WWshort, derived from the interface of the WW domain of Pin1 with a phosphopeptide substrate. We found that the WWshort interacted better than the WWlong with Rb substrate and phospho-Rb substrate. Moreover, WWshortRb responded to CDK4/cyclin D *in vitro* and *in extracto*, validating the use of this artificial PAABD.

Thanks to WWshortRb biosensor, we are able to dissect the two steps involved in protein kinase phosphorylation. First, the kinase binds independently of the presence of ATP/$MgCl_2$, followed by the phosphotransfer reaction itself which is dependent on ATP/$MgCl_2$.

1.3. Sensitivity of the biosensors - Importance of the probe

First of all, it has to be noted that, compared to radioactive assays in which micromolar concentration of reagents are needed, only nanomolar concentrations are required in fluorescence-based assays. For instance, WWshortRb biosensor displayed a high sensitivity to recombinant CDK4/cyclin D activity in fluorescent assays, which were performed with 150 nM of biosensor and 75 nM recombinant protein. CDKACTRb was used at lower concentrations (50 nM) and exhibited greater fluorescence compared to peptide variants *in extracto* (see *in extracto* experiments). However, as the fluorescent probe was not the same, it is difficult to provide a quantitative comparison.

In extracto studies performed with WWRb and WWshortRb have demonstrated that the choice of the probe was essential to monitor response of the biosensor. The size and structure of the probe was crucial in these dynamic systems. For WWshortRb, TAMRA was the only probe suited to report on a conformational change. This result was an advantage for *in cellulo* experiments and ratiometric quantification since WWshortRb could be labelled with either a responsive or unresponsive probe

and co-internalized in living cells. Compared to TAMRA, Cy3 and DyLight650 display a higher extinction coefficient which allows better detection at low concentrations. However, WWshortRb only responds to CDK4 activity when labeled with TAMRA. Our hypothesis is that the size of the fluorophores plays a crucial role in the response of the biosensor. Indeed, DyLight650, a stable sulfonate derivative of Cy5, and Cy3 are much larger than the tetramethylrhodamine TAMRA. As the fluorophore is close to the phosphorylation site, it can be hypothesized that a large fluorophore sterically prevents the complete conformational change upon phosphorecognition.

The maximal fluorescence enhancement of TAMRA-WWshortRb biosensor observed was 40% upon phosphorylation by CDK4/cyclin D. This limitation in fluorescence enhancement may be due to the fact that TAMRA is not extremely sensitive in comparison with other dyes. It could therefore be interesting to test fluorophores such as merocyanine or DMN4 which could allow to get a more robust increase in fluorescence (Gulyani et al., 2011; Loving and Imperiali, 2008). However, it is not certain that changing the probe will improve the fluorescence enhancement. Indeed, it is possible that the interaction between the PAABD and the phosphorylated residue does not lead to enough changes in the surrounding environment in terms of pH or solvent polarity to increase the fluorescent signal more than 40%.

Moreover, additionally to fluorescence enhancement, it is important to analyze the kinetics of the curves obtained under different treatments or conditions. Indeed, WWshortRb response overtime provides precious information on the phosphorylation rate and allows to assess the efficacy of an inhibitor for example.

Even though TAMRA is not highly sensitive, TAMRA-labelled WWshortRb biosensor allows to compare CDK4 activity between different melanoma cell lines, and to quantify differences which cannot be identified by simple analysis of protein kinase expression levels. TAMRA-WWshortRb is therefore sensitive enough to highlight kinase hyperactivation in cell lines that harbour molecular alterations converging on CDK4/cyclin D activity.

Finally, cellular internalization and live cell imaging were performed with WWshortRb biosensor which exhibited alterations in fluorescent intensity at 2 µM in response to CDK4/cyclin D activity. It is a much lower concentration compared to that of other peptide biosensors such as NBD-based PKC biosensor or mero53-based Src biosensor, microinjected into cells at 200 µM and 40 µM, respectively (Gulyani et al., 2011; Yeh et al., 2002). The fact that WWshortRb crosses cell membranes alone allows to treat much more cells compared to microinjection and to prevent them from stress due to this technique.

1.4. Specificity of the biosensors

In extracto studies demonstrated that CDKACTRb reported on endogenous CDK4 activity from melanoma cell extracts in a dose-dependent fashion, since addition of increasing concentrations of PD-0332991 reduced the fluorescent signal of CDKACTRb accordingly. In contrast other CDK inhibitors and other protein kinase inhibitors had no significant effect on CDKACTRb fluorescence. The full spectrum of protein kinase inhibitors have not been screened but, as CDKACTRb did not respond to those tested and given the CDK4-specific substrate sequence contained in the biosensor, we can infer it responds specifically to CDK4 activity in cell extracts. However, its specificity has not been investigated *in cellulo* and could differ from that obtained *in extracto*.

Regarding WWshortRb, its fluorescence was decreased upon incubation or treatment of cells with the CDK4 inhibitors PD-0332991 and LY2835219, but not upon addition of Roscovitine, which preferentially inhibits CDK1, CDK2, CDK5, CDK7 and CDK9. We observed a residual fluorescence response of WWshortRb upon addition of high concentrations of PD-0332991 whereas no residual fluorescence was observed following addition of 20 µM LY2835219. This suggests that PD-0332991 is not as potent as LY2835219 to inhibit CDK4/cyclin D activity in melanoma cell extracts. This result highlights the utility of the biosensor to compare, in a cellular context, the efficacy of CDK4 inhibitors which display a similar IC_{50} value *in vitro* (2 and 11 nM for LY2835219 and PD-0332991, respectively). Likewise, the biosensor reported on a reduced CDK4 activity in A375 cells in which CDK4 protein levels were reduced following treatment with siRNA targeting CDK4. Finally, WWshortRb peptide

biosensor was implemented to identify fractions bearing CDK4 activity following fractionation of A375 cell extracts by gel filtration chromatography. Taken together, these experiments reveal that WWshortRb constitutes a specific tool to quantify CDK4 activity in melanoma cell extracts following treatment with selective inhibitors or downregulation of kinase levels by RNA silencing.

1.5. Application of WWshortRb to probe CDK4 activity in skin biopsies and in tumour xenograft lysates

We have shown that WWshortRb reports on CDK4/cyclin D in skin biopsies and that CDK4 was essentially active in the epidermis, compared to the dermis, consistent with the fact that rapidly dividing cells are found in the epidermis. The biosensor further reported a similar CDK4 activity in eczema skin biopsies compared to healthy samples, whereas a significant downregulation of CDK4 activity was found in psoriasis, skin pathology in which cells are renewed excessively. WWshortRb allows to demonstrate for the first time a deregulation of CDK4 in psoriasis. This discovery could further help to treat this pathology and understand why ultraviolet B (UVB) phototherapy is an effective treatment for psoriasis. Indeed, it has been demonstrated that $p16^{INK4a}$ accumulation, in response to UV radiation, leads to inhibition of CDK4 activity which appears to be involved in the G_2 phase cell cycle arrest (Gabrielli et al., 1999; Pavey et al., 2001).

Finally, WWshortRb was applied to quantify CDK4/cyclin D kinase activity in melanoma xenograft lysates from mice treated with PD-0332991. However, we realized that it was essential to normalize lysates prepared from different melanoma xenografts to the proportion of cancer cells (A375 luciferase). Indeed, as stromal cells are also present in the tumour, the lysate contains normal and hyperactive proteins, such as CDK4/cyclin D. Since each tumor behaves and grows differently, the ratio between hyperactive and normal protein expression level changes, resulting in an inaccurate normalization.

1.6. Application of WWshortRb to probe CDK4/cyclin D activity in living cells

Internalization of WWshortRb

One of the major drawbacks of peptide/protein-based biosensors is the requirement of effective delivery strategies for *in cellulo* and *in vivo* studies and applications, as cellular membranes constitute barriers. However, although we did not identify any obvious sequence that could confer a cell-penetrating ability to WWshortRb, we found that it could cross cell membranes alone. This result renders imaging experiments more straightforward since the labeled peptide biosensor does not require any additional preparation. However, the stability of the peptide biosensor for *in vivo* applications has to be investigated. Indeed, peptides are subject to degradation by proteases and WWshortRb is completely unprotected since it does not require cell-penetrating peptides to facilitate its delivery. Some strategies to improve its stability should be considered (see future developments).

Ratiometric quantification of fluorescence in living cells

Time-lapse acquisitions were performed following co-internalization of TAMRA-WWshortRb and DyLight650-WWshortRb into A375 melanoma cells. DyLight650-WWshortRb was confirmed to be unresponsive in living cells and therefore constituted an appropriate negative control. Ratiometric quantification of TAMRA/DyLight650 signal demonstrated that TAMRA-WWshortRb fluorescence was significantly decreased upon addition of PD-0332991, which inhibits CDK4 activity, and Roscovitine, which arrests the cell cycle in a phase where CDK4 is not active. However, the linearity of the signal after three hours of reaction suggests that the biosensor is not responding properly after 200 min. This data show that WWshortRb is not really well suited for *in cellulo* applications and should rather be applied *in vitro* in which it proved to be highly efficient.

1.7. Future developments

WWshortRb biosensor constitutes a first-of-a kind tool for detection of a relevant enzymatic biomarker, whose predictive value complements immunological approaches for identification of serological and histological markers. We can therefore anticipate it will enable to establish a diagnostic assay for early-stage detection of melanoma onset, providing information on CDK4 activity which complement data on biomarker expression levels, obtained from immunological approaches. Moreover, as the biosensor exhibits a sensitive response to CDK4 inhibition by specific CDK4

inhibitors, it represents a powerful technology for drug discovery programmes, to monitor the response to treatment and to assess the efficacy of new generations of CDK4 inhibitors. WWshortRb could also be applied to probe CDK4 activity in other cancers such as Non Small Cell Lung Cancer NSCLC) and lymphoma in which the $p16^{INK4A}$/CDK4/cyclin D/Rb pathway is also deregulated.

WWshortRb constitutes a potent alternative tool to radioactivity or antibody-based approaches to probe CDK4 activity *in vitro*. Moreover, it reports on enzymatic activities in complex biological samples such as the cellular cytoplasm or the tumoral environment. To our knowledge, WWshortRb constitutes the first chemical tool applied to quantify kinase activities in skin or tumour biopsies.

As previously mentioned, the technology might be further improved through incorporation of more sensitive or solvatochromic dyes, such as merocyanine or DMN4, to obtain greater enhancement in fluorescence (Gulyani et al., 2011; Loving and Imperiali, 2008). Moreover, the contribution of CDK4 binding to the biosensor contributes to a large increase in fluorescence compared to phosphorylation itself. It might therefore be relevant to investigate the use of a probe which would only respond to phosphorylation, such as the solvatochromic Sox (sulfonamide-oxine) dye, which binds Mg^{2+} and undergoes chelation-enhanced fluorescence (CHEF) upon phosphorylation (Shults et al., 2003). However, despite this large contribution of binding in WWshortRb fluorescence, the biosensor responds to inhibitors such as PD-0332991. We hypothesize that the inhibitor, when bound to the ATP pocket, prevents the substrate phosphorylation but also modifies CDK4/cyclin D conformation, therefore reducing the binding of the substrate to its kinase.

With the aim of optimizing the signal-to-noise (S/N) ratio, controlling the timing observation of the reaction and increasing the intensity of the biosensor response, photoactivation strategies could be implemented by “caging” the phosphorylatable residue with a photo-labile group which can be released upon UV irradiation. This strategy has previously been proposed in the development of other biosensors (Dai et al., 2007; Veldhuyzen et al., 2003; Wang et al., 2006b).

Furthermore, efforts have to be made to improve the stability of WWshortRb, especially for *in vivo* applications. For instance, chemical modifications of the peptide sequence could be made to prevent proteolysis such as incorporation of non-natural amino acids or incorporation of pseudo-peptide bonds (Gentilucci et al., 2010). Moreover, formulations with carriers such as microparticles, nanoparticles, liposomes or carbon nanotubes, which are used for facilitated delivery could also be tested with WWshortRb (Patel et al., 2014).

2. Identification of non-ATP competitive compounds targeting CDK4/cyclin D

A. Identification by screening of non-ATP competitive compounds

2.1. Assessment

Several ATP-competitive inhibitors of CDK4 tested in clinical trials, such as Palbociclib (PD-0332991), Ribociclib (LEE011) and Abemaciclib (LY2835219), exhibit promising perspectives for Rb-positive melanomas. However, response to these inhibitors is associated with loss, or functional downregulation of $p16^{INK4A}$, most likely because this endogenous inhibitor of CDK4/cyclin D prevents their binding within the ATP pocket of CDK4. As such, and since the classical mechanism of action of ATP-competitive inhibitors is notorious for its lack of selectivity, alternative strategies to target CDK4 kinase function should provide new avenues to develop therapeutics for melanoma.

We have engineered two fluorescent biosensors, CDKCONF4A and CDKCONF4B, to identify competitors of essential protein/protein interfaces between CDK4 and cyclin D, and allosteric inhibitors that perturb the conformational dynamics of CDK4, respectively. These tools enabled to establish assays for screening of chemical compound libraries, thereby leading to identification of hits with promising potential for selective chemotherapeutic application for melanoma based on postscreen characterization *in vitro* and *in cellulo*.

2.2. Implementation of an HTS assay

CDKCONF4A and CDKCONF4B biosensors were applied to screen the National Chemical Essential Library and a library from the Faculty of Pharmacy of Strasbourg (Laboratoire d'innovation

thérapeutique; collaboration Dr. F. Bihel) in a high throughput format. Prior to HTS, I spent a lot of time performing stability assays and downscaling experiments in order to establish the best conditions for a miniaturized assay in 96-well plates. Positive and negative controls were validated in fluorescent binding assays. Conditions of the assay were then optimized in a time and concentration dependent fashion so as to obtain a robust and reproducible signal at lower cost and with a manageable quantity of proteins. The assay was assessed by calculating the Z-factor whose value must be above 0.5 to lead HTS assays.

For the screening of the CNE with CDKCONF4A, the positive control (cyclin D1) did not respond as well as expected, leading to a negative Z-factor value. This result can be explained by the fact that different batches of both biosensor and positive control were prepared and used for prescreening assays and the screen itself. Although protein expression and purification was verified by SDS-PAGE, recombinant proteins are not always expressed in the same way, for example because of a temperature change that leads to a misfolded protein which will be less soluble. Since some CNE compounds promoted a significant increase in fluorescence of Cy3-CDKCONF4A, we decided to retain 15 hits, despite the lack of positive control. Importantly, the two biosensors did not respond to PD-0332991, proving that they could discriminate against ATP analogues. Finally, 4% CNE compounds and 0.3% molecules from Strasbourg were retained with both biosensors.

2.3. Post-screen characterization

Hits identified in the screen were retested manually from fresh powder stocks resuspended in DMSO to confirm they were positive with a fresh batch of Cy3-labelled CDKCONF4A/B biosensor. This validation did not allow to reconfirm all the hits. It is probably due to the fact that fresh powders were used instead of stock solutions used in the screens. Indeed, unlike fresh powders which normally contain only pure product, solutions from the 96-well plates might contain secondary products resulting from molecule degradation since they were frozen and thawed several times. Thus, a response of the biosensor obtained from the screen could potentially be promoted by a secondary product instead of the compound itself.

In vitro characterization

Since a close collaboration started with Frédéric Bihel, the post-screen characterization mainly focused on the two hits identified in the library from Strasbourg and on their mechanism of action at the CDK4/cyclin D interface. This work is in part summarized in a manuscript (see section "Articles in preparation").

Fluorescence titration assays were performed in order to verify whether these two hits might interact with a peptide derived from the PISTVRE helix of CDK4. The evidence that only one hit could bind this peptide led to the characterization of a family of compounds derived from LPI2251. Unfortunately, the first set of experiments performed to validate binding involved the use of a fluorescent probe TP2Rho, which yielded misinterpreting results. However, docking and mutagenesis experiments revealed that LPI2251 derivatives bound a new pocket below the PISTVRE helix of CDK4 and not far from the T-loop (cf manuscript in section "Articles in preparation"). The position of this new pocket could explain why the two original hits were retained in the screen with both CDKCONF4A and CDKCONF4B. We have therefore identified allosteric small molecule inhibitors which can potentially target the CDK4/cyclin D interface, perturb the association between CDK4 and cyclin D and indirectly modulate the T-loop and prevent the binding of the substrate. We can also hypothesize that the binding site of LPIs is close enough to the T-loop to directly modulate this latter.

In cellulo characterization

LPI derivatives were found to inhibit melanoma cell proliferation (A375 cells) with an efficacy in the same range as PD-0332991. Moreover, RF1210 promoted efficient inhibition of different melanoma cell lines harbouring different combinations of wild-type or loss-of function $p16^{INK4A}$ (the endogenous inhibitor of CDK4), wild-type or mutated CDK4 (R24C mutation which prevents the binding of $p16^{INK4A}$), BRaf and NRas, with IG_{50} values from 10 µM to 13.6 µM.

RF1210 and LPI2252 further cooperated with CDK4 inhibitors and also with traditional anticancer inhibitors at sub-IC50 concentrations, suggesting that it could provide real benefit for the treatment of melanoma. Moreover, this finding suggests that dual targeting of CDK4 kinase with an ATP-

competitive and a non-ATP-competitive inhibitor may provide a more effective means of targeting its function in melanoma, thereby offering new therapeutic perspectives to target the $p16^{INK4A}$/CDK4/cyclin D/Rb pathway in this deadly disease.

2.4. Future developments

Some LPI derivatives, such as RF1210 and LPI2252, constitute promising small molecules to target CDK4/cyclin D and inhibit its activity. Additional *in vitro* experiments have to be performed to fully understand their mechanism of action at the CDK4/cyclin D interface.

The CNE hit compounds remain to be characterized with respect to their inhibitory potential and mechanism of action towards CDK4. Some of them, such as LPS401 and ICMR-04-E10, displayed promising preliminary results in binding assays with CDKCONF4A. It would also be interesting to test other cell lines to characterize the inhibitory potential of the hits in different cancer cells such as Non Small Cell Lung Cancer (NSCLC) cells in which the CDK4 pathway is also deregulated.

The CDKCONF technology, which was previously successfully implemented to identify allosteric inhibitors of CDK2, was demonstrated to be a powerful tool to identify non-ATP competitive inhibitors of CDK4. This strategy could therefore be applied to other CDK kinases and also be extended to other kinases. Rauh and co-workers have previously developed biosensors based on FLiK (fluorescent labels in kinases) to identify non-ATP inhibitors of Akt (Fang et al., 2015). All these examples illustrate the potency of FLiK (fluorescent labels in kinases)-based approaches for drug discovery programmes.

B. Development of peptide inhibitors that target the CDK4/cyclin D interface

2.5. Assessment

To target the CDK4/cyclin D interface, we have developed an approach based on rational design of peptides. Following analysis of the interaction between the PISTVRE helix of CDK4 and the α5 helix of cyclin D, we designed two peptides, PISTVRE and D1. We found that they efficiently inhibit melanoma cell growth when administrated with the cell-penetrating peptide CADY2. Moreover, fluorescent

binding assays of the PISTVRE variants with the D1 peptide suggested that the shorter PISTVRE variant, PISTVRE-A, bound with the greatest affinity.

2.6. Future developments

The mechanism of action of the PISTVRE variants, with an emphasis on PISTVRE-A, remains to be determined *in vitro* in competition and dissociation assays, using recombinant CDK4 and cyclin D1, and their inhibitory potential towards CDK4 kinase activity will be characterized in activity and proliferation assays. The most potent derivatives could further be optimized in terms of stability and cellular uptake with the aim of undertaking *in vivo* experiments.

2.7. Comparison of the two strategies

During my thesis, I have developed two different strategies to inhibit CDK4/cyclin D activity. The screening approach is in a much more advanced stage than the rational approach. Nevertheless, some features can already be compared. In terms of time and costs, the rational strategy is much less time consuming and expensive. Indeed, miniaturization and optimization of a HTS assay take time and require small molecule libraries which can be expensive. However, the screening strategy allows the identification of several hits, with different chemical structures, and offers the possibility to optimize the hits by synthesizing derivatives. Moreover, no facilitated delivery is required to internalize small molecules. However, peptides can also be optimized in size and the generation of mutants allows identification of essential amino acids. They can also be improved in terms of cellular uptake. Compared to peptides, small hydrophobic molecules can be difficult to characterize *in vitro,* in binding assays, as they easily stick to fluorescent probes.

Finally, our screening approach, coupled with docking experiments, led to an unexpected discovery, the identification of a novel allosteric pocket, which is not to be expected with a rational approach.

Materials and methods

1. Design of protein biosensors

1.1. CDKACTRb biosensor

CDKACTRb is a derivative of CDKACT, a biosensor previously developed by the team for probing CDK/cyclin activity *in vitro* and in living cells (Van et al., 2014).

CDKACTRb was engineered by replacing the substrate sequence of CDKACT derived from histone H1 by a substrate sequence derived from the retinoblastoma protein (Rb), which is specifically phosphorylated by CDK4/cyclin D (S795 residue) (Grafstrom et al., 1999). The proline at position -2 relative to the SP phosphorylation site was replaced by a cysteine group (YKFCSSPLRIPG).

CDKACTRb contains the same PAABD as CDKACT which derived from the Polo Box Domain of Plk1 (García-Alvarez et al., 2007), from residue 367 to 603 (237 amino acids) in which all cysteine residues were mutated to serines (GEVVD**S**HLSDMLQQLHSVNASKPSERGLVRQEEAEDPA**S**IPIFWVSKWVDYSDK YGLGYQL**S**DNSVGVLFNDSTRLILYNDGDSLQYIERDGTESYLTVSSHPNSLMKKITLLKYFRNYMSEHLLKAGANITP REGDELARLPYLRTWFRTRSAIILHLSNGSVQINFFQDHTKLIL**S**PLMAAVTYIDEKRDFRTYRLSLLEEYG**SS**KELASRL RYARTMVDKLLSSRSASNRLKAS).

It also contains a short glycine-rich **linker** to ensure flexibility between the two domains (EFPGAGGTGGLPGG).

The complete sequence of CDKACTRb is as follows:

GEVVDSHLSDMLQQLHSVNASKPSERGLVRQEEAEDPASIPIFWVSKWVDYSDKYGLGYQLSDNSVGVLFNDSTRL ILYNDGDSLQYIERDGTESYLTVSSHPNSLMKKITLLKYFRNYMSEHLLKAGANITPREGDELARLPYLRTWFRTRSAII LHLSNGSVQINFFQDHTKLILSPLMAAVTYIDEKRDFRTYRLSLLEEYGSSKELASRLRYARTMVDKLLSSRSASNRLKA S EFPGAGGTGGLPGG YKFCSSPLRIPG

1.2. CDKCONF4A biosensor

The cDNA sequence of mouse CDK4 was cloned into the pGex6P1 vector (GE Healthcare) 5'BamHI 3' EcoRI. Cysteine residues 202 and 215 were mutagenized to serine, so as to yield a mutant bearing only two cysteine residues, 78 and 135, spanning the PISTVRE helix of CDK4 (annex C).

1.3. CDKCONF4B biosensor

The cDNA sequence of mouse CDK4 was cloned into the pGex6P1 vector (GE Healthcare) 5'BamHI 3' EcoRI. Cysteine residues 78, 135 and 215 were mutagenized to serine and serine residue 189 was mutagenized to cysteine so as to yield a mutant bearing only two cysteine residues, 189 and 202, spanning the T-loop of CDK4 (annex C).

2. Design and synthesis of peptides

2.1. Peptide biosensors for probing CDK4/cyclin D activity

Peptides were synthesized by GLS Biochem and purified to 95%.

The long WW peptide, WWRb, was derived from the native WW domain of Pin1 previously described by Anai et al. to generate a phosphopeptide hybrid biosensor (residues 6-39) (Anai et al., 2007). The shorter version, WWshortRb, was derived from the residues that line the interface with the phosphopeptide in the crystal structure of WW Pin1 complexed to a phosphopeptide substrate (PDB 1F8A). The residues that are critical for the interaction with the phosphosubstrate are Arg14, Arg17, Tyr23 and Phe25, as well as Trp34 (GWEKRMSRSSGRVYYFNHITNASQWERPSG). WWshortRb therefore comprised these key residues in the linear order of appearance that mimicks the interface (Phe25, Arg14, Tyr23, Arg17) interspaced by small uncharged amino acids, and which ends with Trp34 followed by the same five amino acids as in the native WW domain of Pin1 (GFARVYMSRSSGWERPSG).

The Rb substrate peptide was derived from the retinoblastoma protein (Rb) sequence, which is specifically phosphorylated by CDK4/cyclin D (S795 residue) (Grafstrom et al., 1999). A unique cysteine was introduced at position -2 relative to the phosphoserine for labelling with a synthetic environmentally-sensitive fluorescent probe. A phosphorylated form of this peptide was also synthesized.

MP26 peptide is a non-binder of CDK/cyclins and was used as an irrelevant peptide (Kurzawa et al., 2011).

Peptide name	Sequence	Number of Amino Acids	Molecular weight (g/mol)
WW long	GWEKRMSRSSGRVYYFNHITNASQWERPSG	30	3587.9
WW short	GFARVYMSRSSGWERPSGG	19	2087.3
Rb substrate	GGYKFCSSPLRIPG	14	1481.7
PhosphoRb substrate	YKFCSpSPLRIPG	12	1446.6
WWRb	GWEKRMSRSSGRVYYFNHITNASQWERPSGGGYKFCSSPLRIPG	44	5051.6
WWshortRb	GFARVYMSRSSGWERPSGGYKFCSSPLRIPG	31	3436.9
MP26	VESSDTIDNVKSKIQDKEGC	20	2195.3

Table 13: Sequence, number of amino acids and molecular weight of the peptides that have been used in activity assays

2.2. Peptides that target the interface between CDK4 and cyclin D

The PISTVRE peptide was derived from the PISTVRE helix domain of CDK4 whilst the D1 peptide was derived from the α5 helix domain of cyclin D1. They were synthesized by GLS Biochem and purified to 95%. A peptide derived from the T-loop of CDK4 and used as negative control for CDKCONF4A was also synthesized by GLS Biochem and purified to 95%. PISTVRE variants were synthesized at the IBMM facility. Solid-phase peptide synthesis (SPPS) on a Rink amide resin using Fmoc- protected amino acid was performed for synthesizing them (purity > 98%).

Peptide name	Sequence	Number of Amino Acids	Molecular weight (g/mol)
PISTVRE	H-GGGCPISTVREVALLRRL	18	1897.2
D1	SIRPEELLQMELLLVNKLKWNLC	23	2783.3
irrelevant peptide derived from the T-loop of CDK4	SYQMALEPGC	10	1098.2
Ac-PISTVRE	Ac-GGGCPISTVREVALLRRL	18	1939.2
PISTVRE-A	H-CPISTVREVALLRRL	15	1726.1
Ac-PISTVRE-A	Ac-CPISTVREVALLRRL	15	1768.1
PISTVRE-B	H-CPISTVREVALLRRLEAFE	19	2202.6
Ac-PISTVRE-B	Ac-CPISTVREVALLRRLEAFE	19	2244.6

PISTVRE-C	H-GGGCPISTVREVALLRRLEAFE	22	2373.7
Ac-PISTVRE-C	Ac-GGGCPISTVREVALLRRLEAFE	22	2415.7

Table 14: Sequence, number of amino acids and molecular weight of the peptides developed to target CDK4/cyclin D interface.

3. Molecular biology : site-directed mutagenesis

3.1. PCR

Site-directed mutagenesis was performed according to the QuickChange™ protocol (Stratagene). Primers were designed so as to introduce the desired mutation sites in the middle of the primer of about 45 bp.

50 µL PCR reaction was prepared as follows: 36 µL distilled H_2O; 5 µL Buffer PFU 10X; 2 µL forward primer (100 ng/µL); 2 µL reverse primer (100 ng/µL); 2 µL dNTP (5 mM); 2 µL DNA template (5 ng/µL); 1 µL *Pfu* DNA Polymerase (3 units/µL; Promega).

PCR reactions were performed on a thermocycler (T-personal Combi™; Biometra) starting with denaturation of DNA template at 95°C for 3 min followed by 15 cycles: 95°C for 30s (Denaturation); 55°C for 1 min (Annealing); 72°C for 2 min/kb (Extension/Elongation). Reactions were terminated by the addition of an extension step at 72°C for 10 min. PCR products were then stored at 4°C.

Dpn I restriction enzyme (20 units/µL; BioLabs) was added at 37°C for 1h to digest the parental DNA template.

3.2. DNA plasmid transformation

Library competent *E.coli* DH5α were purchased from Invitrogen for transformation of mutagenesis products. Competent cells were removed from -80°C and thawed on ice. 2 µL of plasmid containing at least 100ng DNA was mixed with 50 µL competent bacteria. The mixture was incubated on ice for 20min before heat shock at 42°C for 45s. 300 µL LB Broth was then added and the culture was incubated at 37°C for 1h before spreading onto LB plates (50 µg/mL ampicilline) (annex F). The plates were incubated at 37°C overnight for colony growth.

Single colonies picked, grown in 3 mL LB + Ampicilline (50 µg/mL), then DNA was extracted by miniprep (QIAGEN kits) and sequenced by Eurofins MWG.

3.3. Preparation of competent *E.coli* BL21 for protein induction

E.coli BL21 pLysS codon + cells were grown in 100ml LB broth (annex F) until 0D600 reached 0,6. Cells were harvested by centrifugation at 4500 rpm, at 4°C for 15min. The cell pellet was re-suspended in 5ml ice cold TSS buffer (10 mL LB; 10% PEG 3000-8000; 50 mM MgCl2; 5% DMSO; filter through 0.2 µm), aliquoted into 200 µL aliquots, and flash frozen in liquid nitrogen. Competent cells were then stored at –80°C until needed.

4. Protein Engineering

4.1. Induction of CDKACTRb

A single colony of *E. coli* BL21 transformed with pGex6P1-CDKACTRb was picked and grown into 50 mL LB + Amp (50 µg/mL) at 37^{o}C, under agitation, overnight. The overnight culture was diluted into 1 L LB/Amp broth and incubated in the same conditions until OD(600) reached 0.6 (for 2-3h), at which point 0.5 mM IPTG was added. The temperature was then reduced to 20^{o}C and the culture was incubated overnight for expression of soluble recombinant GST-CDKACTRb. Cells were then harvested by centrifugation at 4000 rpm for 20 min (TX-1000 rotor, Thermo Scientific). The cell pellet was resuspended in 30 mL TBS lysis buffer (annex F) and stored at -80^{o}C until the next manipulation. CDKACTRb expression was verified by comparing a fraction of non-induced and induced cultures by SDS-PAGE prior to purification.

4.2. Purification of CDKACTRb

Bacterial lysate

Bacterial cell pellets were thawed and lysed by sonication. Supernatant was recovered by centrifugation at 13000 rpm for 30min (F15-8x50cy rotor, Thermo Scientific) and then filtered through 0,45 µm and 0,2 µm membranes (Millipore) prior to chromatography purification.

Glutathione sepharose resin equilibration

1 mL glutathione sepharose HP (High Performance) was prepared for each 30 mL bacterial lysate as follows: the slurry was washed in 30 mL H_2O; centrifuged 3000 rpm for 5 min (F15-8x50cy rotor, Thermo Scientific); and resin was washed and equilibrated 15 min in 30 mL TBS buffer (twice) then centrifuged 3000 rpm for 5min.

GST Batch purification

The supernatant containing GST-CDKACTRb was incubated with 1 mL equilibrated resin at 4°C for 3h, then centrifuged at 3000 rpm for 5min and washed with 30mL cold TBS buffer followed by centrifugation at 3000 rpm for 5min (F15-8x50cy rotor, Thermo Scientific) (twice). The supernatant was then removed and GST-CDKACTRb was eluted on Econocolumns using 3-4 mL freshly prepared 50 mM glutathione in TBS buffer. 1 mL fractions were recovered in eppendorf tubes. Eluted fragments were checked on SDS-PAGE to select those containing GST-CDKACTRb.

FPLC purification

Selected samples were centrifuged for 5 min at 13000 rpm in microcentrifuge to remove any precipitate. Remaining supernatant was injected onto a Gel Filtration column Superdex 75 (GE Healthcare) connected to an FPLC system (FPLC ÄKTA, GE Healthcare). Peak fractions were eluted in TBS buffer (flow rate 1 mL/min) and verified on SDS-PAGE to identify those containing GST-CDKACTRb.

4.3. Induction of CDK4, CDKCONF4A and B, cyclin D1 and CIV

Recombinant GST-CDK4, GST-CDKCONF4A/B, GST-cyclin D1 and GST-CIV, the CDK-activating kinase of *Saccharomyces cerevisiae*, were expressed in *E. coli* by IPTG induction as described above except for the buffer (PBS) (annex F).

4.4. Purification of CDK4, CDKCONF4A and B, cyclin D and CIV

Bacterial lysate

Bacterial cell pellets were retrieved from -80^{o}C, thawed and lysed by sonication. Supernatant was recovered by centrifugation at 13000 rpm for 30 min and then filtered through 0,45 µm and 0,2 µm membranes (Millipore).

FPLC purification

The supernatant was purified on High Performance Glutathione Sepharose (GE Healthcare) in PBS buffer and eluted with 50 mM glutathione in the same buffer, followed by gel filtration chromatography on Superdex75 (FPLC ÄKTA, GE Healthcare).

GST-CDK4 / GST-cyclin D1 complex was formed following individual purification of each subunit and incubation of stoichiometric concentrations, then further incubated with CIV to ensure its activation.

5. Biochemistry

5.1. SDS-PAGE (SDS-polyacrylamide Gel Electrophoresis)

Sample preparation

To verify the induction of GST-CDK4, GST-cyclin D1, GST-CIV and GST-CDKACTRb, 1 mL of bacterial culture were taken before and after IPTG induction. After centrifugation for 5 min at 10000 rpm in microcentrifuge, the bacterial pellet was resuspended in 50 µL H_2O + 50 µL Laemmli buffer (annex F) and then sonicated for 20 s. Samples were then heated at 95°C for 5 min and loaded on SDS-PAGE.

SDS-PAGE

4% acryl/bisacryl stacking gels and 15% acryl/bisacryl running gels were prepared (annex F) and run using Biorad equipments (Mini-PROTEAN Tetra Cell). Denatured protein samples and Protein Marker (Low Molecular Weight Calibration Kit, Amersham) were loaded onto gel and run at 250V for 1 h. Gels were stained with Coomassie Brilliant Blue (annex F) for 2 min and then destained in water before observing the protein bands.

5.2. Western-Blotting

Sample preparation

See paragraph 9.2 for cell extract preparation. Protein concentration was determined by measure of OD(280) using a spectrophometer Nanodrop™ (Thermo Scientific) with BSA standard curve. Normalization to obtain 25 µg proteins was made by dilution in PBS lysis. After addition of Laemmli buffer, samples were heated at 95°C for 5 min and loaded on SDS-PAGE.

SDS-PAGE

4% acryl/bisacryl stacking gels and 15% acryl/bisacryl running gels running gels and were prepared (annex F) and run using Biorad equipments (Mini-PROTEAN Tetra Cell). Denatured protein samples and pre-stained protein marker (PageRuler^{TM} Plus Prestained Protein Ladder; Life Technologies) were loaded onto gel and run at 90 V for 15 min and 140 V for 1h15.

Protein transfer

Proteins were then transferred to a PVDF membrane (Membrane Immobilon-P, PVDF; Merck Millipore) for 2h at 100 V using a cold transfer buffer (annex F) and a liquid blotting system (Biorad).

Blocking step

5% skimmed milk (Régilait) was prepared in PBS with 0,1% Tween and membranes were blocked by incubation for 1h.

Incubation with the primary antibody

Antibodies against CDK4 (C22, sc-260; Santa Cruz), cyclin D1 (C20, sc-717; Santa Cruz) and anti-tubulin (Amersham, N356) were diluted 1/500 in PBS tween. The membrane was incubated with the corresponding primary antibody overnight followed by 3 washes for 10 min in PBS tween.

Incubation with the secondary antibody

Horseradish peroxidase (HRP)-conjugated anti-mouse (Amersham, NXA931) or anti-rabbit (Amersham, NA934) antibodies were diluted 1/10000 in blocking solution. The membrane was incubated for 60 min followed by 3 washes for 5 min in PBS tween.

Detection

ECL (Amersham; GE Healthcare) was added onto the membrane and incubated for 2 min. Chemiluminescence was detected using a chemiluminescence imaging camera (Chemi-Smart 5000; Vilber Lourmat).

6. Thiol labeling of peptide/protein with fluorescent probe

Proteins and peptides were fluorescently labelled using maleimide or isothyocyanate probes on the thiol group of cysteine residues at pH 7,0 as described by Molecular Probes^{TM}.

Fluorophores stocks were prepared at a concentration of $2*10^{-3}$ M in DMSO and stored at -20°C. Peptides were prepared at a concentration of 10^{-3}M (in H_2O, 1% DMSO) and then diluted at 10^{-4}M in PBS before labeling.

Fluorophores were added at 2-10 fold greater excess concentration and labelling was performed overnight at 4°C or by microwave radiation for 10-20 s. Peptides and proteins were further purified on NAP5 columns (GE Healthcare) in PBS to remove excess label. Absorbance of labelled protein/peptide were measured on Nanodrop™ (Thermo Scientific) at appropriate wavelengths (see table) followed by calculation of the molar concentration using the Beer-Lambert law defined as A= ε*l*C where A corresponds to the Absorbance, ε is the molar extinction coefficient, l corresponds to the path length of the beam of light through the material sample, whilst C is the concentration.

	Molar extinction coefficient Ɛ ($M^{-1}.cm^{-1}$)	λabs (nm)	λem (nm)	supplier
TAMRA	61000	540	565	FluoProbes
Cy3	150000	544	570	GE Healthcare
Cy5	250000	649	670	GE Healthcare
FITC	70000	495	520	FluoProbes
Texas Red	85000	592	614	Life technologies
DyLight650	250000	652	672	Life technologies
TP2Rho	58900	510	614	Florence Mahuteau, Curie Institute, Paris

Table 15: Spectral properties of the fluorescent probes that were used

7. Real-time fluorescence kinase assays

Fluorescence kinase assays were performed in 96-well plates in a thermostated chamber (Polarstar™ or Clariostar™, BMG) at 30°C in 200µL PBS buffer supplemented with 5 mM $MgCl_2$, 0.5 mM ATP,

except when stated otherwise. In all experiments, relative fluorescence was calculated following subtraction of fluorescently-labelled CDKACTRb, WWRb or WWshortRb fluorescence from fluorescence values obtained in the presence of protein kinases, inhibitors or cell extracts.

Inhibition assays were performed in the same conditions as above except the addition of 0 - 20 µM CDK inhibitor: PD-0332991 (Palbociclib; SelleckChem), LY2835219 (Abemaciclib; Euromedex), LEE011 (Ribociclib; Euromedex), Roscovitine (SelleckChem), RO3306 (Calbiochem) and AT7519 (Euromedex); or inhibitors of kinases not related to CDK/cyclins: PP2 (Sigma), H89 (Euromedex) and U0126 (Euromedex).

All stock inhibitor solutions were made in DMSO and diluted in PBS to the desired concentration freshly prior to use.

8. Fluorescence titration experiments

Fluorescence titration assays were performed in 96-well plates using a Clariostar™ spectrofluorimeter (BMG) at room temperature for 40 min in 200 µL PBS (Sigma). The fluorescence of 200 nM FITC-labelled Rb substrate peptide with WWlong and WWshort was acquired at 495 nm following excitation at 520 nm. The fluorescence of 200 nM Cy3-labelled CDKCONF4A/B biosensor with positive and negative controls, PD-0332991 or small molecules was acquired at 570 nm following excitation at 544 nm. The fluorescence of 200 nM TP2-Rho-labelled PISTVRE peptide with D1 peptide, PD-0332991 or small molecules was acquired at 614 nm following excitation at 510 nm. The fluorescence of 200 nM TP2-Rho-labelled D1 peptide with PISTVRE peptide, PD-0332991 or small molecules was acquired at 614 nm following excitation at 510 nm. The fluorescence of 500 nM TAMRA-labelled D1 peptide with PISTVRE variants was acquired at 570 nm following excitation at 544 nm. Data analysis was performed using the GraFit Software (Erathicus Ltd) and curve fitting was performed using a quadratic equation, as described in (Gondeau et al., 2005). The quadratic equation is defined as $F = Fmax - (Fmax - Fmin) * (((Kd + l + p) - \frac{\sqrt{(\sqrt{Kd+l+p)^2} - 4*l*p))}}{2*p})$ where F

corresponds to the fluorescence, whilst K_d is the dissociation constant, p is the fluorescent peptide concentration and l is the ligand/substrate or partner.

9. Cell biology

9.1. Cell lines and cell culture

Cell culture media, serum and antibiotics were purchased from Invitrogen. A375, HeLa, A549 and Jurkat cell lines were purchased from ATCC. Human fibroblast, SK-MEL2, MV3 and Mewo cell lines were kindly provided by Dr. Pauline Henri (IBMM, Montpellier). SK-MEL28 cell line was kindly provided by Dr. Céline Gongora (IRCM, Montpellier). All cell lines were cultured in DMEM/RPMI + Glutamax supplemented with 10% FCS, 100 units/mL penicillin (G sodium salt) and 100 µg/mL streptomycin at 37°C in an atmosphere containing 5% CO_2. For microscopy experiments, DMEM without phenol red was used.

Melanoma cell lines used:

	CDKN2A	CDK4	Rb	BRAF	NRAS
A375	mutated (E61Stop, Loss of function)	WT	WT	V600E	WT
Mewo	mutated (R80Stop, Loss of function)	WT	WT	WT	WT
MV3	ND	ND	ND	WT	WT
SK-MEL2	WT	WT	WT	WT	mutated (Q61R)
SK-MEL28	WT	R24C	WT	V600E	WT

Table 16: Genetic alterations identified for the different components of the $p16^{INK4a}$ / CDK4/6-cyclin D / pRb pathway and for BRAF and NRAS in A375, Mewo, MV3, SK-MEL2 and SK-MEL28 cell lines (ND: data not found).

9.2. Cell extract preparation

Cells were grown to 90% confluence, washed with PBS then harvested by scraping in PBS followed by centrifugation for 10 min at 10000 rpm in microcentrifuge at 4°C. Cell pellets were then lysed in PBS lysis buffer (annex F) through 21G and 26G gauge needle (Terumo) syringing, respectively. Supernatant was collected following centrifugation of cell extracts for 10 min at 13000 rpm at 4°C.

Protein concentration was determined by measuring OD(280) using a spectrophotometer Nanodrop™ (Thermo Scientific) with BSA standard curve, followed by normalization through dilution on PBS lysis buffer to the same concentration before further use.

9.3. Fractionation of A375 cell extracts

Fractionation of A375 cell extracts prepared from 5 million cells in 500µL PBS lysis buffer was performed by gel filtration chromatography on a Superose 6 10/300 GL column (GE Healthcare). 500 µL fractions were eluted in PBS buffer (50 mM KH_2PO_4/K_2HPO_4, pH 7.4, 150 mM NaCl) (flow rate 0.3 mL/min) and 50 µL were used for kinase activity assays.

9.4. Drug treatment for activity assays

Unsynchronized cells were cultured to subconfluency (60-70%). 0-20 µM inhibitor (PD-0332991, LY2835219, Roscovitine, RO3306, AT7519, H89, U0126 and PP2) were added and the cells were further incubated for 24 hours followed by washing with PBS. Cell extracts were then prepared as described in paragraph 9.2.

9.5. Cell synchronization experiments

Unsynchronized cells were cultured to subconfluency (60-70%). For S phase synchrony, cell medium was replaced by medium containing 2 mM hydroxyurea (Sigma) for 24h. Cells were then washed twice with fresh medium and either directly harvested or incubated with fresh medium for 10h.

9.6. CDK4 knock-down by addition of siRNA

Internalization of siRNA in cells was performed using CADY peptide (amino acid sequence: Ac-GLWRALWRLLRSLWRLLWRA-Cy) (Crombez et al., 2009). CADY is an amphipathic cell penetrating peptide which forms non covalent complexes with siRNAs. Ratios used of CADY/siRNA were 20/1 and 40/1. The siRNA targeting CDK4 is a pool of 4 siRNA and was purchased from Santa Cruz (sc-29261). Unsynchronized cells were cultured until 60% of confluence. Stock solutions of CADY (1 mM) were prepared in H2O and homogeneised by vortexing and then sonicated in a small bath sonicator for 10 min. CADY solution was then diluted in Volvic water to obtain a concentration of 2 µM (for 20/1

ratio) and 4 µM (for 40/1 ratio). The CDK4 siRNA was diluted in PBS (Sigma) to obtain a concentration of 100 nM. The solution of CADY was gently added to an equivalent volume of siRNA and mixed by gently tapping the tube. The mixture was incubated at 37°C for 30 min. Cells were then washed with PBS (Sigma) twice before addition of the CADY/siRNA solution. After incubation of 5 min, DMEM without serum was added for 2h followed by addition of DMEM and serum to obtain a medium containing 10% FBS. Cells were then incubated 24 and 48h.

9.7. Proliferation assays

Proliferation assays were performed in 96-well plates. The day before addition of inhibitors, cells were seeded at a density of 10000-15000 cells/well.

Then, either 0 - 75 µM small molecules in DMEM or peptides (targeting the CDK4/cyclin D interface) complexed to CADY2 peptide (amino acid sequence: Ac-GLWWRLWWRLRSWFRLWFRA-Cy) (Kurzawa et al., 2010) were added onto cells. CADY2 is an amphipathic cell penetrating peptide which forms non covalent complexes with proteins and peptides. CADY2 solutions were prepared as described for CADY. Peptides were added at 1 µM and CADY2/peptide ratio used was 20/1.

Cells were further incubated for 6-48 hours and then washed twice with PBS. Fixation was performed by incubation in 4% PFA (diluted in PBS) for 10 min at room temperature followed by addition of crystal violet (Sigma) for 30 min (Gillies et al., 1986). Cells were then washed three times with H_2O before addition of 10% acetic acid. Relative cell growth is obtained for each well by measurement of OD(595) using a Clariostar™ spectrofluorimeter (BMG).

Data analysis was performed using the GraFit Software (Erathicus Ltd) and IG_{50} values were determined using the equation $y = \frac{Range}{1+\left(\frac{x}{IC50}\right)^{s}} + Background$ where ***Range*** is the fitted uninhibited value minus the background, and *s* is a slope factor (annex E). This equation assumes that *y* falls with increasing *x.*

9.8. Peptide internalization

Labeled WWshortRb peptide was prepared in PBS at a concentration of 2 µM. A375 cells were grown on coverslips or 6 well plates to 80% confluence. Cells were then washed twice with PBS. 200 µL of peptides were gently overlaid onto cells and incubated for 30 min at 37°C in an atmosphere containing 5% CO_2. DMEM was then added followed by an additional incubation in the same conditions for 1h. Cells were washed extensively before fixing (coverslips) or performing time lapse acquisition (6 well plates).

Co-internalization of WWshortRb-TAMRA and WWshortRb-DyLight650 into A375 cells were performed as follows: WWshortRb-DyLight650 was first internalized into A375 cells by overlaying the biosensor onto cells followed by 30 min of incubation at 37°C in an atmosphere containing 5% CO_2. DMEM was then added followed by an additional incubation in the same conditions for 30 min. Cells were washed extensively 3 times with PBS followed by application of WWshortRb-TAMRA and additional incubation of 30 min in the same conditions. DMEM was then added followed by additional incubation in the same conditions for 30 min. Cells were again washed extensively 3 times with PBS, then replaced in DMEM for 1h at the same conditions before performing time lapse acquisition.

9.9. Cell fixation and Hoechst staining

Fixation was performed by incubation in 4% PFA (diluted in PBS) for 5 min at room temperature followed by 3 washes in PBS. Hoechst 33342 (Sigma) diluted in H_2O (1 µg/mL) was added to stain nuclei at room temperature for 5 min and then washed twice in PBS. Coverslips were then fixed on microscope slides (Superfrost™; Thermo Scientific) with Mowiol for fluorescent microscopy acquisitions.

9.10. Indirect immunofluorescence

Fixation was performed by incubation in 4% PFA (diluted in PBS) for 5 min at room temperature followed by 3 washes in PBS. Blocking buffer was added at room temperature for 1 h and then cells were incubated overnight at 4°C with anti-CDK4 (C22, sc-260; Santa Cruz) diluted 1/500 in blocking solution. Cells were washed three times with PBS for 15 min and then incubated for 1h at room

temperature with Alexa488-conjugated anti-rabbit antibody followed by 3 washes in PBS for 15 min. Hoechst 33342 (Sigma) diluted in H_2O (1 µg/mL) was added to stain nuclei at room temperature for 5 min and then washed twice in PBS. Coverslips were then fixed on microscope slides (Superfrost™; Thermo Scientific) with Mowiol for fluorescent microscopy acquisitions.

10. Preparation of cell extracts from skin biopsies

Skin biopsies were kindly provided by Dr. Laurent Meunier (CHU, Nîmes).

Epidermis and dermis were separated by addition of thermolysine (0.5 mg/mL diluted in PBS (Sigma)) for 3h at 37°C. Total proteins were extracted from frozen skin biopsies by addition of a total extraction buffer (annex F) through Ultra Turrax^{TM} grinding and normalized following spectrophotometric dosage at 280 nm.

11. A375 xenografts in mice

In vivo experiments were performed by Véronique Josserand and Julien Vollaire at the Albert Bonniot institute in Grenoble. All animal experiments were conducted in agreement with the Principles of Laboratory Animal Care (National Institutes of Health publication no. 86-23, revised 1985) and approved by the regional ethics committee. Female 6 weeks old NMRI nude mice (Janvier, Le Genest-Isle, France) were anesthetized (isoflurane/oxygen 3.5 % for induction and 1.5 % thereafter) and 3.10^6 A375 cells in 200 µL phosphate-buffered saline were implanted subcutaneously into the flank. After 24 days, tumors had reached 257 ± 64 mm^3, mice were then treated daily orally with 150 mg/kg or 75 mg/kg PD-0332991 (diluted in sodium lactate buffer 50 mM) for 7 days, or 150 mg/kg for 3 days, or through intraperitoneal injection with Roscovitine (also diluted in sodium lactate buffer 50 mM) at 50 mg/kg for 5 or 11 days. Mice were then sacrificed and tumors were collected and frozen.

In the first set of experiments, tumors samples were lysed and total proteins were extracted by addition of a total extraction buffer (annex F) and grinding with an Ultra TurraxTM, then normalized following spectrophotometric dosage at 280 nm. In the second set of experiments, total proteins were extracted by addition of a luciferase cell culture lysis reagent (annex F) and normalized to the proportion of cancer cells (A375 luciferase) (Victor^3 V luminescence microplate reader, Perkin Elmer).

12. Fluorescence Microscopy

12.1. Upright acquisitions – fixed cell imaging

Internalization experiments of WWshortRb were performed in fixed A375 cells. The images were acquired with a Leica DM6000 microscope equipped with a Coolsnap HQ2 camera and 63X objectives and piloted by Metamorph software.

12.2. Time-lapse acquisition – live cell imaging

A375 melanoma cells internalized with WWshortRb were subjected to time-lapse acquisition for live cell imaging. The plates of cells was placed in an incubation chamber containing 5% CO_2 and thermostated at 37°C. Video microscopy acquisitions were set up automatically with an Olympus IX83 inverted microscope equipped with a sCMOS Andor Zyla 5.5 camera and 40X objectives for 5-10h.

The biosensor WWshortRb was labeled either with TAMRA or DyLight650 and the two solutions were co-internalized sequentially into A375 cells. WWShortRb-DyLight650 served as negative control since the probe was unresponsive in activity assays when coupled with the biosensor. Multiple positions and parameters, including phase for cell morphology and DyLight650 or TAMRA fluorescence, for either the responsive or unresponsive WWshortRb biosensor, were acquired every 20 min.

Fluorescence intensity of both fluorophores was analyzed for ratiometric quantification of TAMRA/DyLight650 signals.

12.3. Image analysis and ratiometric quantification

Upright acquisitions – fixed cell imaging

Images analysis was performed using the ImageJ software. The fluorescent signal of the TAMRA-labelled biosensor was quantified and compared by determination of the ratio TAMRA-Hoechst. Region of interest (ROI) comprising three or four cells was created for each image (Hoechst and TAMRA) to determine the fluorescence intensity. Then, background fluorescence was subtracted in all images. The ratio “TAMRA” / “Hoechst” was then calculated. Final histograms that are presented

correspond to the average fluorescence ratio of the TAMRA-labelled biosensor over the Hoechst staining of nuclei in three different fields.

Time-lapse acquisitions – live cell imaging

Ratiometric fluorescence intensity quantification was performed for live cell imaging. Using MetaMorph software, stacks of images (Phase, DyLight650 and TAMRA) were built up to quantify fluorescent signals over time. Background signal of DyLight650 and TAMRA stacks was subtracted by elimination of the signal of a blank region that did not contain any cells. A region of interest (ROI) delimiting single cells on the phase stacks at each time point was transferred to DyLight650 and TAMRA stacks of the same time point (after background subtraction). Average fluorescence intensity was determined at each time point (annex B). The ratio of the fluorescent signal of TAMRA-WWshortRb biosensor over that of the control DyLight650-WWshortRb was calculated representing relative responses of the biosensor to CDK4 activity in living cells over time.

13. Automated High Throughput Screen conditions and hit validation

CDKCONF4A and CDKCONF4B biosensors were applied to screen two libraries: the National Chemical Essential Library (480 compounds) and a library from Strasbourg (640 compounds, Dr. F. Bihel, Fac. Pharma, Strasbourg) in a high throughput format. Prior to HTS, stability assays and downscaling experiments were performed to establish the best conditions for a miniaturized assay in 96-well plates on Polarstar^{TM} (BMG Labtech) and optimized so as to obtain a robust and reproducible signal. Performance criteria for reproducibility, sensitivity (in the presence of DMSO), tolerance, robustness and best response over time were established with:

- 10 µM PD-0332991, the ATP-competitive inhibitor of CDK4
- 2 µM cyclin D1 and 2 µM retinoblastoma protein, as positive control of CDKCONF4A and CDKCONF4B respectively, that promotes significant enhancement of Cy3-labelled biosensor fluorescence

Optimal screening conditions were established as follows: 25 nM freshly purified Cy3-labelled CDKCONF4A/B biosensor in 50 mM KH_2PO_4/K_2HPO_4, pH 6.4, 500 mM NaCl, 1% DMSO, for 5 hours at room temperature in the dark.

For CDKCONF4A, these conditions led to a 1.3 fold fluorescence enhancement by positive control (cyclin D1) with a Z factor equal to 0.89. For CDKCONF4B, these conditions led to a 1.8 fold fluorescence enhancement by positive control (retinoblastoma protein) with a Z factor equal to 0.68.

Z-factor is equal to $1 - \frac{3(A^+ + A^-)}{B^+ - B^-}$, where A^+ and A^- correspond to the standard deviations of positive and negative controls, whilst B^+ and B^- are the average responses for positive and negative controls.

The screen itself was performed in 96-well black Greiner Bio One plates. Compounds from the library were used at 10^{-5} M final concentration against 25 nM Cy3-labelled CDKCONF4A/B biosensor in 50 mM KH2PO4/K2PO4, pH 6.4, 500 mM NaCl and fluorescence emission of Cy3 was measured at 570 nm following excitation at 550 nm after 5 hours. The screen was performed on a TECAN Freedom Evo™ Robot. In parallel, the intrinsic fluorescence of the library compounds at 570 nm following excitation at 550 nm was determined, to eliminate autofluorescent compounds. The increase in fluorescence of each compound was determined relative to the basal fluorescence of Cy3-labelled CDKCONF4A/B biosensor alone. A molecule was considered a hit when it was not autofluorescent, yet induced amplification of Cy3-labelled CDKCONF4A/B biosensor fluorescence to a similar extent as positive control (annex D). Hits identified in the screen were retested manually from fresh powder stocks resuspended in DMSO in duplicate to confirm they were positive hits with a fresh batch of Cy3-labelled CDKCONF4A/B biosensor.

Annex A

Growth curves of A375 xenografts treated with PD-0332991 or Roscovitine

Growth curves of A375 xenografts implanted in mice and treated with PD-0332991 at 150 mg/kg for 3 or 7 days, or with 75 mg/kg for 7 days, or Roscovitine at 50 mg/kg for 5 or 11 days. Control : mock treated mice. Arrows indicate time of treatment.

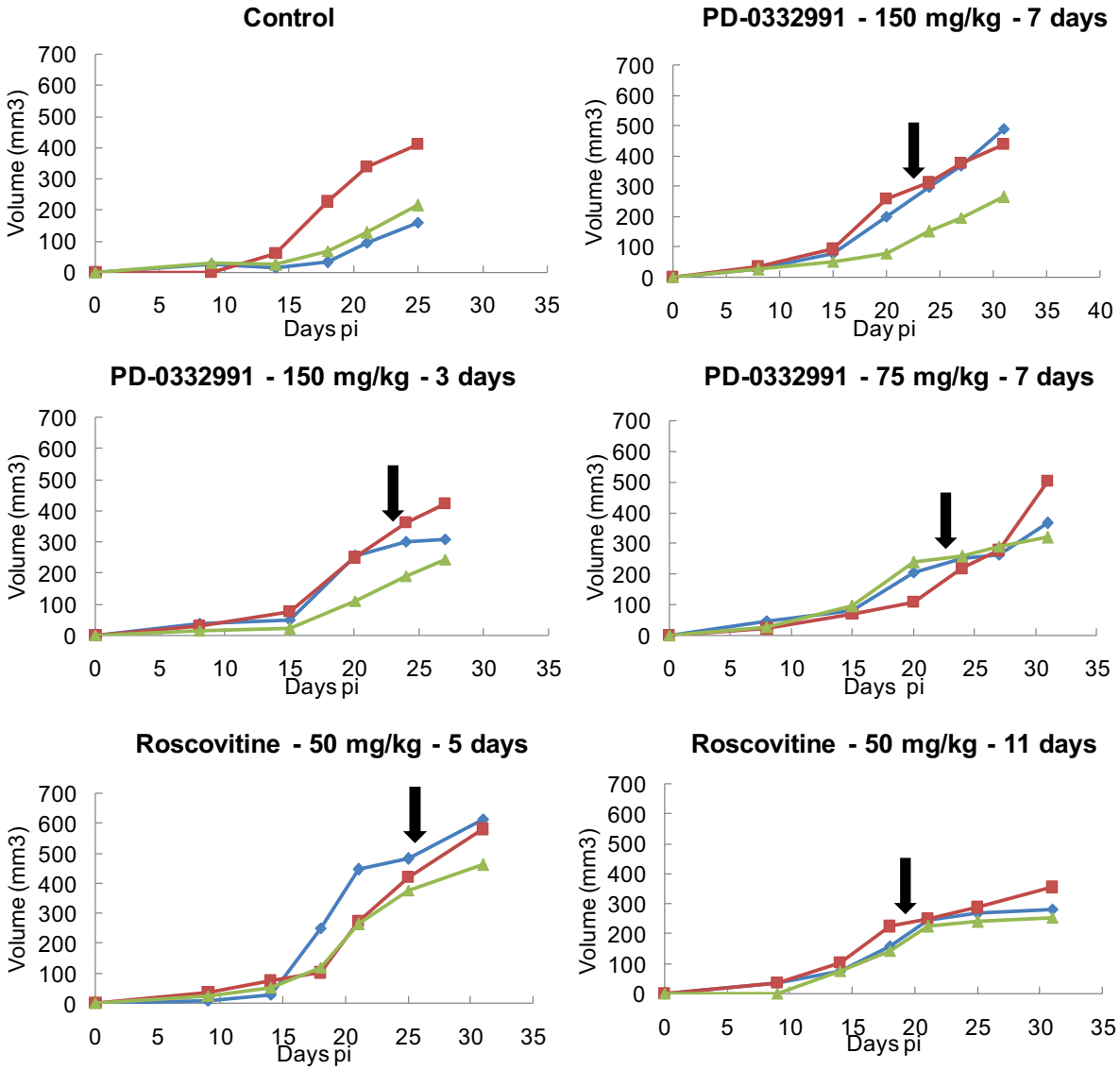

Annex B

	dividing cell		
time (min)	TAMRA	DyLight650	ratio TAMRA/Dylight650
0	151.83	57.32	2.65
20	153.30	49.09	3.12
40	153.16	44.95	3.41
60	147.04	42.53	3.46
80	145.01	38.53	3.76
100	153.61	40.27	3.81
120	162.93	39.42	4.13
140	172.91	40.31	4.29
160	167.20	39.78	4.20
180	180.19	40.05	4.50
200	186.55	40.38	4.62
220	196.70	40.69	4.83
240	212.12	42.46	5.00
260	228.77	44.20	5.18
280	241.03	48.63	4.96
300	264.63	63.69	4.16
320	253.89	54.98	4.62
340	271.49	63.22	4.29
360	275.62	65.59	4.20
380	273.33	61.37	4.45

	cell after division		
time (min)	TAMRA	DyLight650	Ratio TAMRA/Dylight650
0	158.68	66.15	2.40
20	190.62	95.40	2.00
40	162.25	71.71	2.26
60	166.69	52.16	3.20
80	165.32	44.33	3.73
100	173.47	39.71	4.37
120	189.73	42.46	4.47
140	206.02	43.74	4.71
160	207.49	42.00	4.94
180	206.03	39.79	5.18
200	211.71	39.18	5.40
220	214.78	39.10	5.49
240	215.42	38.56	5.59
260	220.65	39.08	5.65
280	226.70	39.36	5.76
300	231.93	41.01	5.66
320	229.83	38.59	5.96

340	238.53	40.88	5.84
360	239.92	42.39	5.66
380	246.57	40.25	6.13
400	251.69	41.22	6.11
420	249.72	40.99	6.09
440	249.58	40.50	6.16
460	253.79	41.66	6.09

	cell after division		
time (min)	TAMRA	DyLight650	ratio TAMRA/Dylight650
0	74.24	44.36	1.67
20	84.44	45.17	1.87
40	88.61	47.36	1.87
60	94.28	48.23	1.95
80	102.56	47.30	2.17
100	115.46	49.41	2.34
120	122.69	49.37	2.49
140	132.18	49.85	2.65
160	131.32	49.17	2.67
180	148.08	51.06	2.90
200	153.86	49.98	3.08
220	154.93	49.40	3.14
240	167.28	48.03	3.48
260	180.57	48.25	3.74
280	190.18	48.37	3.93
300	192.34	47.44	4.05
320	201.27	48.39	4.16
340	201.69	47.77	4.22
360	204.61	48.62	4.21
380	210.72	48.57	4.34
400	214.27	48.63	4.41
420	218.02	50.29	4.34
440	219.13	48.34	4.53
460	224.42	49.70	4.52
480	230.26	51.04	4.51
500	232.32	51.40	4.52
520	233.54	51.15	4.57
540	234.74	51.00	4.60
560	237.73	51.69	4.60

Annex C

Nucleotide sequence of mouse CDK4 (Source : UniProtKB - P30285)

ATGGCTGCCACTCGATATGAACCCGTGGCTGAAATTGGTGTCGGTGCCTATGGGACGGTGTACAAAGCCCGAGAT
CCCCACAGTGGCCACTTTGTGGCCCTCAAGAGTGTGAGAGTTCCTAATGGAGGAGCAGCTGGAGGGGGCCTTCCC
GTCAGCACAGTTCGTGAGGTGGCCTTGTTAAGGAGGCTGGAGGCCTTTGAACATCCCAATGTTGTACGGCTGATG
GATGTCTGTGCTACTTCCCGAACTGATCGGGACATCAAGGTCACCCTAGTGTTTGAGCATATAGACCAGGACCTG
AGGACATACCTGGACAAAGCACCTCCACCGGGCCTGCCGGTTGAGACCATTAAGGATCTAATGCGTCAGTTTCTA
AGCGGCCTGGATTTTCTTCATGCAAACTGCATTGTTCACCGGGACCTGAAGCCAGAGAACATTCTAGTGACAAGT
AATGGGACCGTCAAGCTGGCTGACTTTGGCCTAGCTAGAATCTACAGCTACCAGATGGCCCTCACGCCTGTGGTG
GTTACGCTCTGGTACCGAGCTCCTGAAGTTCTTCTGCAGTCTACATACGCAACACCCGTGGACATGTGGAGCGTT
GGCTGTATCTTTGCAGAGATGTTCCGTCGGAAGCCTCTCTTCTGTGGAAACTCTGAAGCCGACCAGTTGGGGAAA
ATCTTTGATCTCATTGGATTGCCTCCAGAAGACGACTGGCCTCGAGAGGTATCTCTACCTCGAGGAGCCTTTGCC
CCCAGAGGGCCTCGGCCAGTGCAGTCAGTGGTGCCAGAGATGGAGGAGTCTGGAGCGCAGCTGCTACTGGAAATG
CTGACCTTTAACCCACATAAGCGAATCTCTGCCTTCCGAGCCCTGCAGCACTCCTACCTGCACAAGGAGGAAAGC
GACGCAGAGTGA

Amino acid sequence of mouse CDK4 (Source : UniProtKB - P30285)

MAATRYEPVAEIGVGAYGTVYKARDPHSGHFVALKSVRVPNGGAAGGGLPVSTVREVALLRRLEAFEHPNVVRLM
DVCATSRTDRDIKVTLVFEHIDQDLRTYLDKAPPPGLPVETIKDLMRQFLSGLDFLHANCIVHRDLKPENILVTS
NGTVKLADFGLARIYSYQMALTPVVVTLWYRAPEVLLQSTYATPVDMWSVGCIFAEMFRRKPLFCGNSEADQLGK
IFDLIGLPPEDDWPREVSLPRGAFAPRGPRPVQSVVPEMEESGAQLLLEMLTFNPHKRISAFRALQHSYLHKEES
DAE

Design of primers for CDKCONF4A and CDKCONF4B

CDKCONF4A		
C202S	forward	GACATGTGGAGTGTTGGCTCTATCTTTGCAGAGATGTTTCGT
	reverse	ACGAAACATCTCTGCAAAGATAGAGCCAACACTCCACATGTC
C215S	forward	CGTCGAAAGCCTCTCTTCTCTGGAAACTCTGAAGCCGAC
	reverse	GTCGGCTTCAGAGTTTCCAGAGAAGAGAGGCTTTCGACG
CDKCONF4B		
C78S	forward	GTCCGGCTGATGGACGTCTCTGCCACATCCCGAACTGAC
	reverse	GTCAGTTCGGGATGTGGCAGAGACGTCCATCAGCCGGAC
C135S	forward	GATTTCCTTCATGCCAATTCCATCGTTCACCGAGATCTG
	reverse	CAGATCTCGGTGAACGATGGAATTGGCATGAAGGAAATC
S189C	forward	CCTGAAGTTCTTCTGCAGTGTACATACGCAACACCCGTG
	reverse	CACGGGTGTTGCGTATGTACACTGCAGAAGAACTTCAGG

Annex D

Compounds identified in the screens: names, origin and response to CDKCONF4A and/or CDKCONF4B

Compound Name	Molecular weight (g/mol)	Lab Source	Identified with
ICMR-04-E10	516	ICMR-Reims	CDKCONF4A
ICMR-04-F03	300	ICMR-Reims	CDKCONF4A and B
U181-10-12-L-F07	476.44	Université Claude Bernard -Lyon	CDKCONF4A
U181-03-13-L-H10	290.29	Université Claude Bernard -Lyon	CDKCONF4B
U181-10-08-L-D11	252.27	Université Claude Bernard -Lyon	CDKCONF4B
AB-00015228	427.56	ICSN	CDKCONF4A and B
AB-00016193	549.06	ICSN	CDKCONF4A
AB-00015203	412.54	ICSN	CDKCONF4A and B
LSP 03-M-002-E05	214.35	Paris, Saint-Pères	CDKCONF4B
LSP 04-L-001-D07	331.22	Paris, Saint-Pères	CDKCONF4B
AB-00008525	389.26	Lille	CDKCONF4A
JP00465	400.48	Université Joseph Fourier, Grenoble	CDKCONF4A
CEsr-1409000	339.4	Université de Caen	CDKCONF4A
CEsr-1837000	258.3	Université de Caen	CDKCONF4A
CEmr-1278100	362.3	Université de Caen	CDKCONF4A
AB-00025980	294.27	Institut Curie	CDKCONF4A

AB-00031272	235.24	Institut Curie	CDKCONF4A
LPS401	285.39	LPS Strasbourg	CDKCONF4A and B
LPS853	361.37	LPS Strasbourg	CDKCONF4A
LPS4056	297.32	LPS Strasbourg	CDKCONF4B
LPI2148	418.92	Strasbourg (F. Bihel)	CDKCONF4A and B
LPI2251	565	Strasbourg (F. Bihel)	CDKCONF4A and B

Results of the screen performed with Cy3-CDKCONF4A and compounds from the CNE

CDKCONF4A	plate	position	value	standard deviation
Above 115%	1	B5	119.147	12.894
	1	C8	116.755	4.211
	2	C5	129.098	23.633
	4	B8	136.483	4.254
	4	C8	116.027	4.629
	4	E9	116.890	1.470
	4	G9	119.556	1.949
	5	B10	119.116	3.697
	5	G10	119.653	3.129
	6	C8	115.004	4.629
	6	E9	119.962	1.470
	6	E10	124.227	0.168
	7	F9	119.488	0.771
	8	B4	128.714	1.419
	8	G9	118.357	
Between 105 and 115%	1	C5	108.361	2.370
	1	D8	105.429	2.329
	1	E4	106.601	6.904
	1	F9	105.114	1.034
	1	F11	109.144	4.308
	2	C7	110.115	6.435
	2	C8	109.685	7.035
	2	C11	108.951	9.438
	2	D3	107.033	0.922
	2	D5	105.411	4.546
	2	D7	106.274	3.893
	2	D8	105.790	5.520
	2	E4	108.033	1.540

	2	E5	109.683	1.404
	2	E6	105.409	2.649
	2	F5	107.736	0.052
	2	F8	111.740	2.816
	2	F9	111.932	13.825
	3	B9	109.933	6.221
	3	B10	112.803	3.587
	3	B11	113.148	3.243
	3	C6	107.984	3.244
	3	C7	114.375	2.839
	3	D5	110.085	5.116
	3	D9	107.202	3.706
	3	E4	110.297	5.328
	3	F7	105.097	1.071
	3	F8	105.285	0.488
	4	B4	108.380	2.035
	4	B10	106.747	3.697
	4	B11	108.313	3.540
	4	C5	105.649	4.133
	4	C7	108.819	3.092
	4	C9	106.740	0.395
	4	C10	105.205	2.678
	4	D8	106.293	5.891
	4	D9	107.319	5.915
	4	E5	105.337	6.573
	4	E8	105.440	1.004
	4	E10	106.737	0.168
	4	F9	106.933	4.575
	4	G4	109.271	0.568
	4	G5	106.353	8.319
	5	C7	107.131	3.092
	5	C8	109.907	4.629
	5	C9	107.548	0.395
	5	D3	105.751	1.255
	5	D5	110.713	2.661
	5	D8	106.797	5.891
	5	E8	105.636	1.004
	5	F4	113.824	0.888
	5	F5	112.540	3.874
	5	F7	106.159	2.977
	5	F8	105.517	1.535
	5	G3	112.411	2.063
	6	C2	114.962	1.267
	6	C7	105.436	3.092
	6	E4	105.223	0.454
	6	E8	112.349	1.004
	6	G9	106.207	1.949
	7	B3	112.741	19.944

	7	B8	105.316	1.095
	7	C10	106.387	6.893
	7	D4	108.091	3.701
	7	E7	112.045	8.275
	7	F8	107.216	5.671
	7	F10	108.850	0.435
	7	G11	105.429	11.113
	8	B8	111.655	
	8	B9	105.737	
	8	B10	105.616	
	8	C5	109.481	0.030
	8	C8	106.220	
	8	C9	108.696	
	8	D5	105.344	1.329
	8	D8	112.560	
	8	D9	105.435	
	8	D10	106.159	
	8	E4	106.250	1.117
	8	E7	107.065	
	8	E8	106.159	
	8	E9	108.152	
	8	F6	106.944	0.181
	8	F7	108.696	
	8	G7	107.548	
	8	G8	109.481	
Between 80 and 90%	1	B9	89.512	2.711
	1	D2	87.591	3.108
	1	D3	80.268	3.442
	1	D6	80.531	1.287
	1	E6	89.039	2.238
	1	E9	89.106	0.667
	1	G3	87.865	3.885
	1	G10	81.215	2.022
	2	B2	84.825	2.628
	2	B4	89.831	4.596
	2	B5	85.882	4.216
	2	B7	88.775	2.567
	2	B9	87.124	1.356
	2	C3	89.883	1.247
	2	F2	83.418	3.007
	3	C10	80.247	1.592
	3	C11	84.991	3.529
	3	F3	86.846	3.408
	4	F7	80.855	2.977
	4	G10	83.983	3.129
	5	B2	89.063	0.654
	5	D2	88.202	1.707
	5	G2	88.816	3.971

	5	G5	86.981	8.319
	5	G6	81.903	0.993
	6	B11	83.123	3.540
	6	E2	82.214	1.446
	6	G4	89.401	0.568
	7	F3	89.061	5.043
	7	F6	87.303	1.822
	7	G2	88.342	0.610
	7	G6	89.807	0.626
	8	B2	89.553	2.536
	8	B3	80.767	0.030
	8	D4	89.825	0.513
	8	D7	87.923	
	8	E11	89.493	
Between 70 and 80%	1	C9	75.871	2.269
	1	E11	76.603	6.477
	1	F6	76.698	4.910
	1	F8	76.414	1.269
	1	G5	72.569	5.466
	1	G6	75.282	3.594
	2	E8	72.518	0.224
	2	F10	71.085	1.263
	3	E2	73.588	0.829
	3	E5	77.791	2.791
	5	G9	72.468	1.949
	5	G11	75.159	5.154
	6	B7	73.763	1.104
	6	D5	74.400	2.661
Below 70%	1	B6	59.971	6.923
	1	B7	66.032	1.598
	2	E11	64.484	1.389
	2	G5	54.585	0.148
	3	C4	65.264	0.044
	3	E3	69.692	1.525
	4	F8	67.453	1.535
	7	G3	68.750	5.835

Table 17 : The increase in fluorescence of each compound was calculated with reference to the basal fluorescence of Cy3-labelled CDKCONF4A biosensor alone and was expressed as the percentage of increase. Only compounds that promoted an increase in fluorescence greater than 115% were considered as hits.

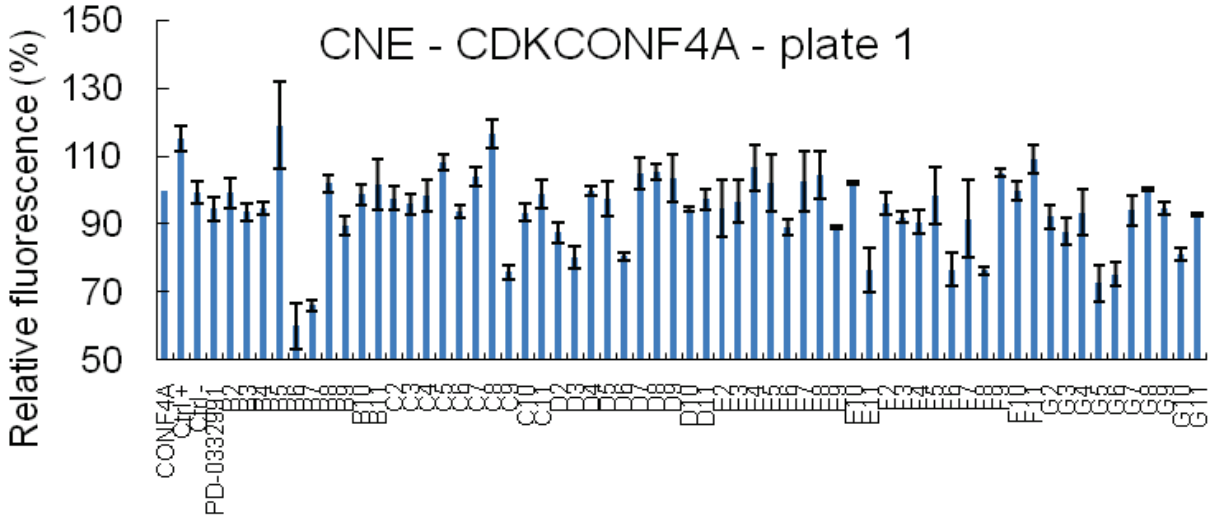
CNE - CDKCONF4A - plate 1
Relative fluorescence (%)
150
130
110
90
70
50
CONF4A
Ctrl+
Ctrl-
PD-0332991

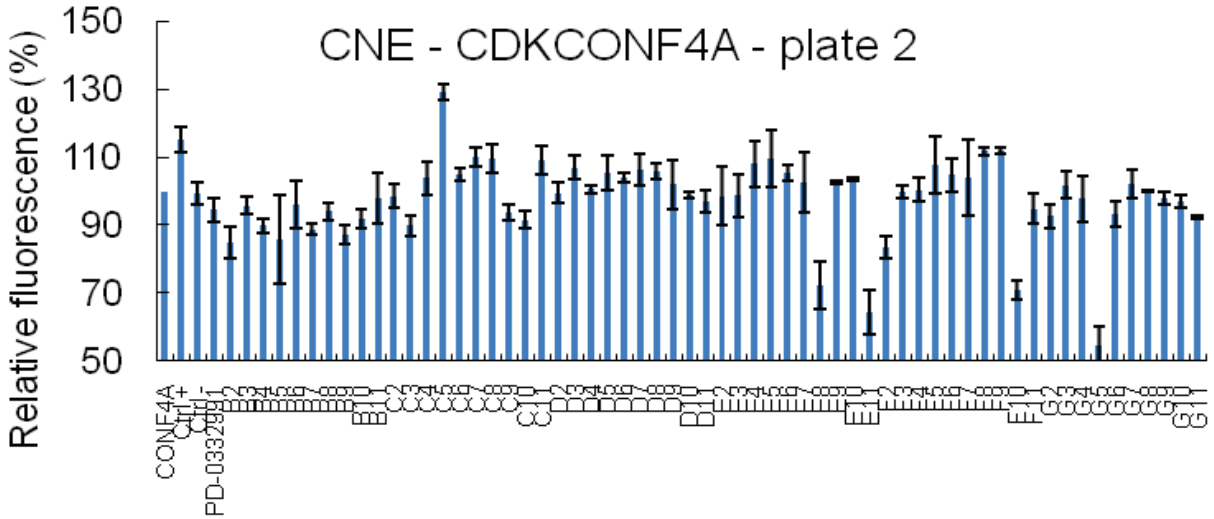
CNE - CDKCONF4A - plate 2
Relative fluorescence (%)
150
130
110
90
70
50
CONF4A
Ctrl+
Ctrl-
PD-0332991

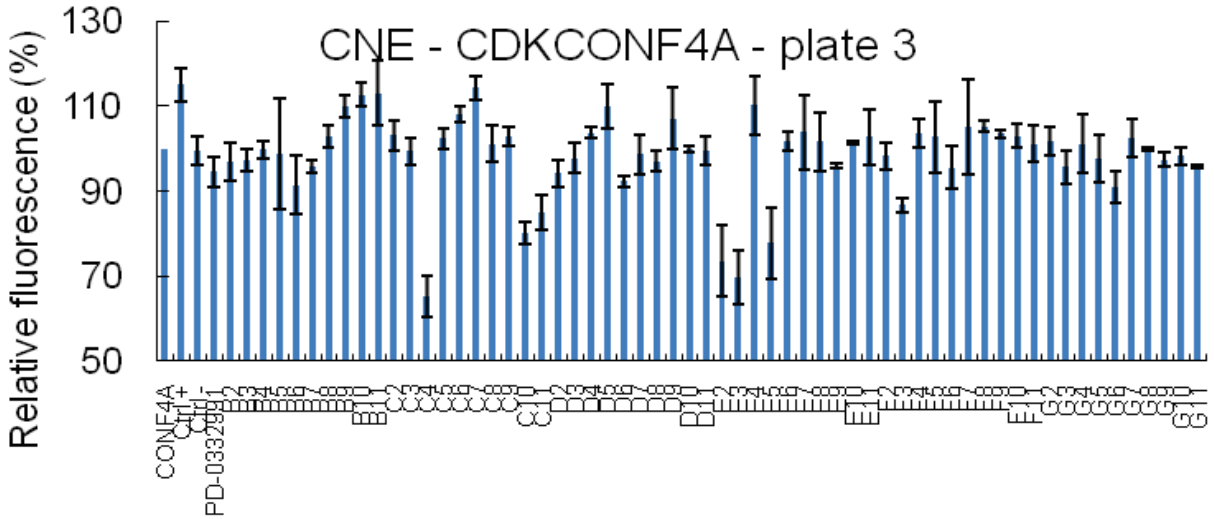
CNE - CDKCONF4A - plate 3
Relative fluorescence (%)
130
110
90
70
50
CONF4A
Ctrl+
Ctrl-
PD-0332991

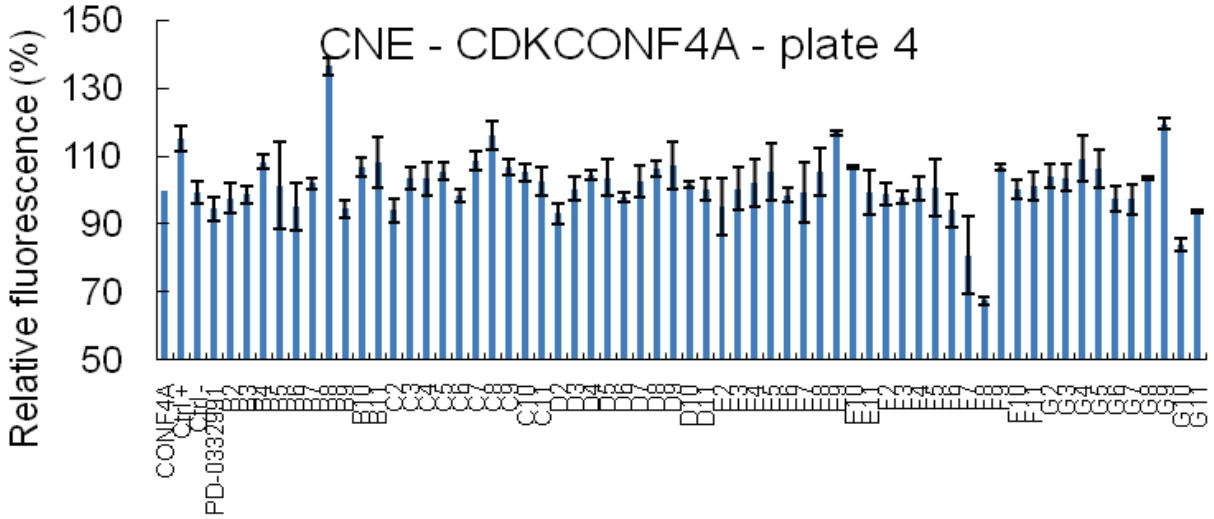
CNE - CDKCONF4A - plate 4
Relative fluorescence (%)
150
130
110
90
70
50
CONF4A
Ctl+
PD-0332991

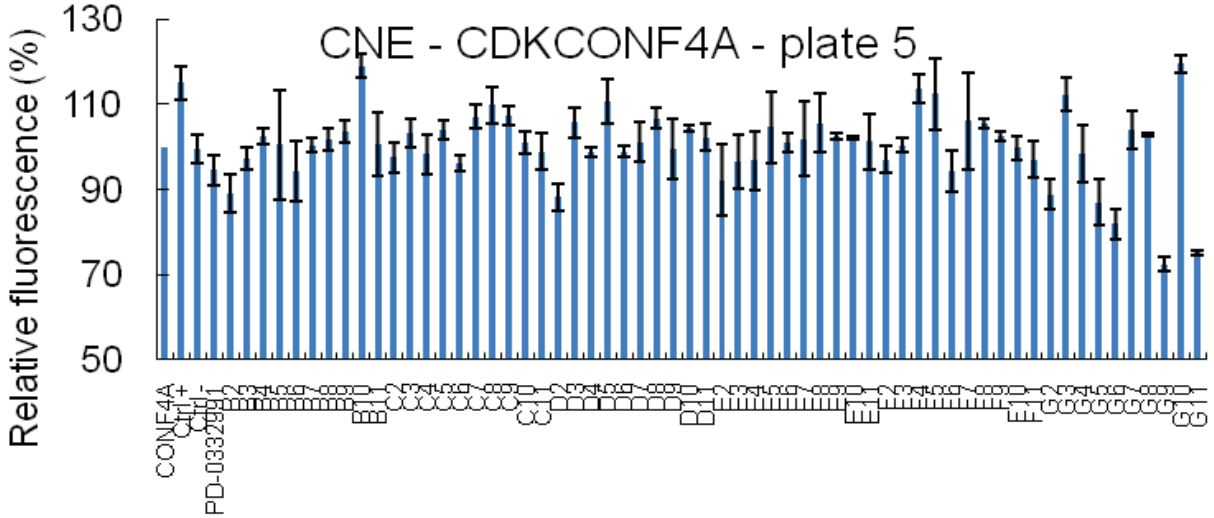
CNE - CDKCONF4A - plate 5
Relative fluorescence (%)
130
110
90
70
50
CONF4A
Ctl+
PD-0332991

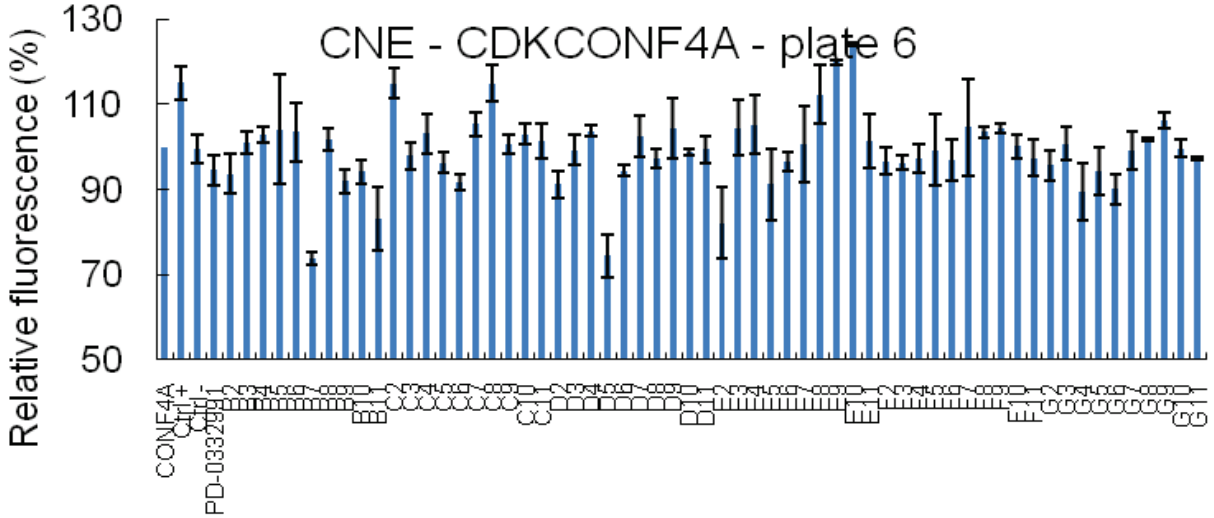
CNE - CDKCONF4A - plate 6
Relative fluorescence (%)
130
110
90
70
50
CONF4A
Ctl+
PD-0332991

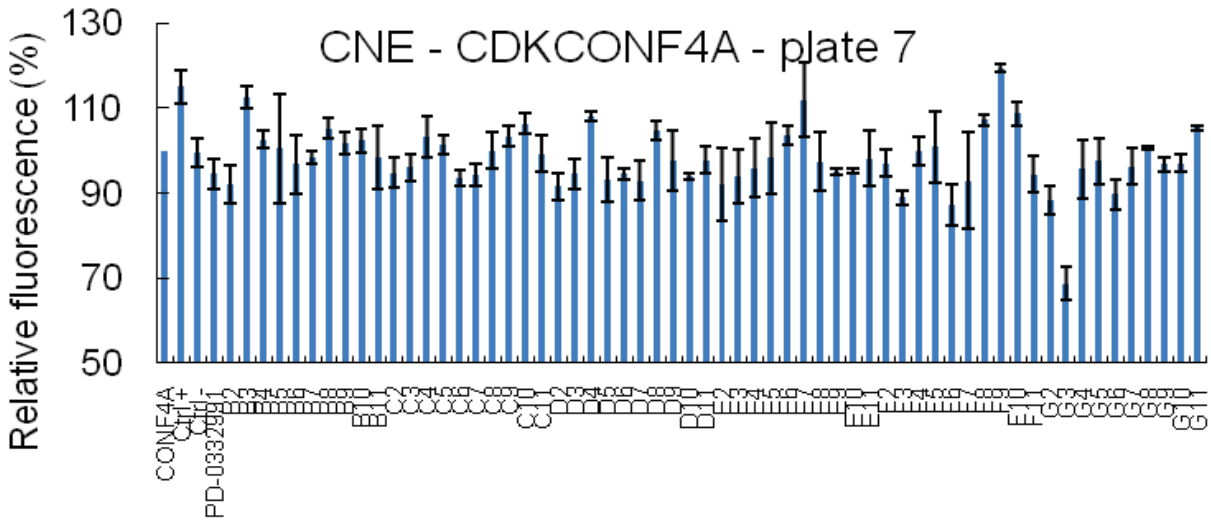

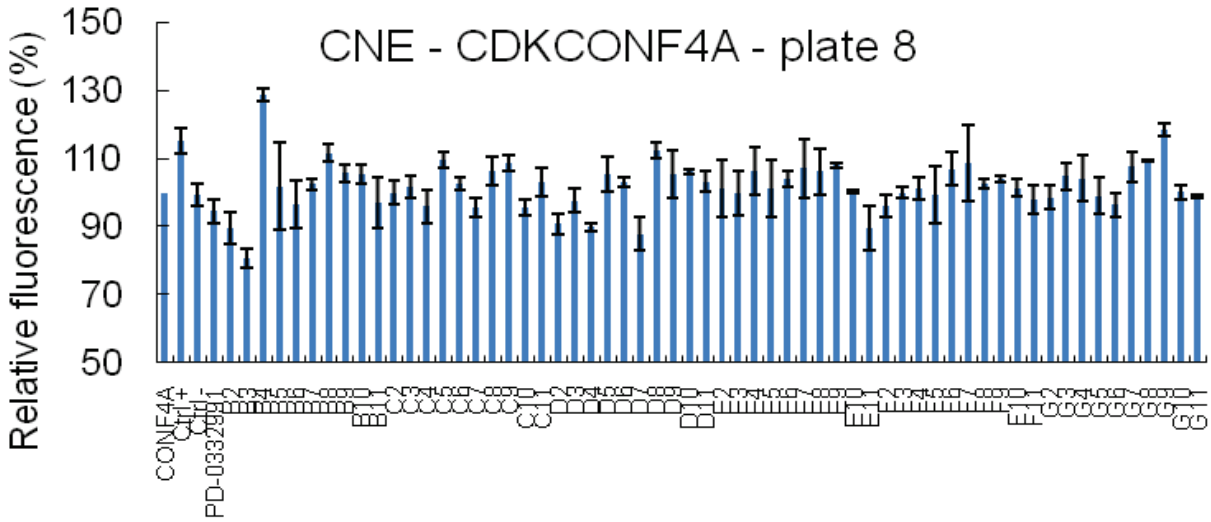

Results of the screen performed with Cy3-CDKCONF4B and compounds from the CNE

CDKCONF4B	plate	position	value	standard deviation
Above 120%	3	B7	124.620	12.603
	3	B10	122.257	12.233
	4	B8	126.571	7.432
	4	E9	121.455	2.008
	5	G3	125.194	3.682
	5	F5	123.288	4.845
	5	G8	120.769	3.585
	5	B10	122.854	13.516
	6	E10	121.249	4.308
Between 110 and 120%	1	B2	113.488	9.958
	1	B4	112.593	8.109
	1	B8	119.913	10.031
	1	B10	114.559	9.382

	1	E10	111.059	4.308
	1	B11	113.111	7.228
	2	E7	111.765	4.635
	2	D8	110.368	1.575
	3	B2	111.132	10.951
	3	B5	110.010	9.137
	3	D7	113.496	2.023
	3	B8	116.525	12.057
	3	B9	114.725	8.687
	3	B11	119.670	13.934
	4	C7	116.813	3.513
	4	D7	111.982	1.317
	4	C9	110.790	2.635
	4	F9	111.481	0.941
	4	C10	110.194	4.308
	4	C11	111.418	1.129
	5	F4	119.832	0.194
	5	E5	110.788	4.877
	5	D6	115.310	20.478
	5	B7	118.005	3.083
	5	C7	114.696	2.487
	5	D7	119.574	2.132
	5	E7	117.216	4.942
	5	F7	117.797	2.552
	5	C8	114.632	1.260
	5	E8	111.079	1.195
	5	F8	115.924	0.484
	5	C9	116.925	1.873
	5	E9	110.982	0.904
	5	D10	116.990	4.308
	5	E10	112.468	4.308
	5	F10	114.115	4.308
	6	C2	111.543	0.582
	6	C4	110.165	4.108
	6	C7	113.595	3.001
	6	D7	110.716	0.674
	6	F7	110.808	2.113
	6	C8	115.248	0.000
	6	E9	111.911	0.827
	6	D10	119.290	4.308
	6	D11	112.278	4.133
	7	D7	110.066	1.748
	7	E7	112.086	3.888
	7	C10	112.447	4.308
Between 80 and 90%	1	F2	87.853	6.088
	1	C6	85.941	2.000
	1	D6	83.382	0.559
	1	E6	87.029	3.206

	1	F8	82.118	2.176
	1	C9	81.529	0.588
	1	E9	83.971	0.147
	1	G10	86.029	4.308
	2	B2	81.543	0.097
	2	B3	89.975	1.146
	2	B4	88.760	0.395
	2	F4	82.828	3.238
	2	B5	88.823	0.066
	2	G6	86.809	0.891
	2	E8	83.541	1.664
	2	C9	87.611	2.882
	3	E2	82.126	1.510
	3	F5	87.017	1.329
	3	D6	82.760	0.030
	3	E6	87.077	1.872
	3	F6	86.141	1.419
	3	G6	87.953	0.936
	3	C10	80.707	4.308
	3	C11	85.145	2.778
	4	C2	88.739	0.784
	4	B6	87.935	6.419
	4	G6	86.857	0.031
	4	F7	88.959	0.376
	4	B9	88.547	4.741
	4	G10	86.575	4.308
	5	G6	83.204	0.452
	5	G9	83.721	0.517
	5	G11	83.818	1.195
	6	E2	88.151	1.745
	6	E5	83.435	1.255
	6	B7	86.088	0.478
	6	B9	85.360	0.739
	6	B11	81.804	2.519
	7	F3	87.161	2.110
	7	F6	87.191	2.140
	7	E10	86.618	4.308
	8	B2	88.969	3.525
	8	D3	89.971	0.860
	8	F3	89.341	0.344
	8	D4	88.195	1.261
	8	F4	88.166	1.347
	8	D6	89.370	1.003
	8	G6	85.587	3.410
	8	G10	88.682	4.308
Between 70 and 80%	1	D3	70.824	2.941
	1	G5	77.382	2.676
	1	B6	77.124	1.830

	1	F6	70.088	2.088
	1	G6	75.529	2.118
	1	E11	78.412	0.647
	2	C3	75.936	1.426
	2	F10	74.242	4.308
	2	E11	71.955	1.664
	3	F3	71.679	0.181
	3	C4	77.264	10.094
	3	E5	78.321	0.634
	6	D5	75.964	3.368
	8	B9	75.160	0.490
	8	E11	72.894	1.834
Below 70%	2	F2	59.358	2.139
	2	G5	69.370	0.000
	3	E3	35.085	4.710
	4	F8	65.339	0.345
	7	G3	64.286	0.995
	8	B3	52.440	0.692

Table 18 : The increase in fluorescence of each compound was calculated with reference to the basal fluorescence of Cy3-labelled CDKCONF4B biosensor alone and was expressed as the percentage of increase. Only compounds that promoted an increase in fluorescence greater than 120% were considered as hits

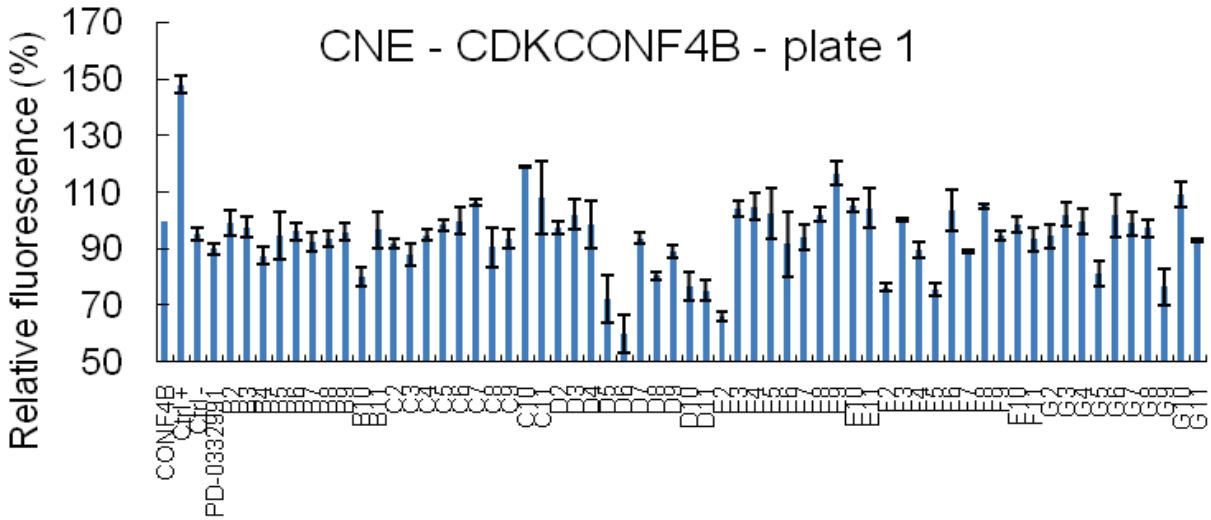

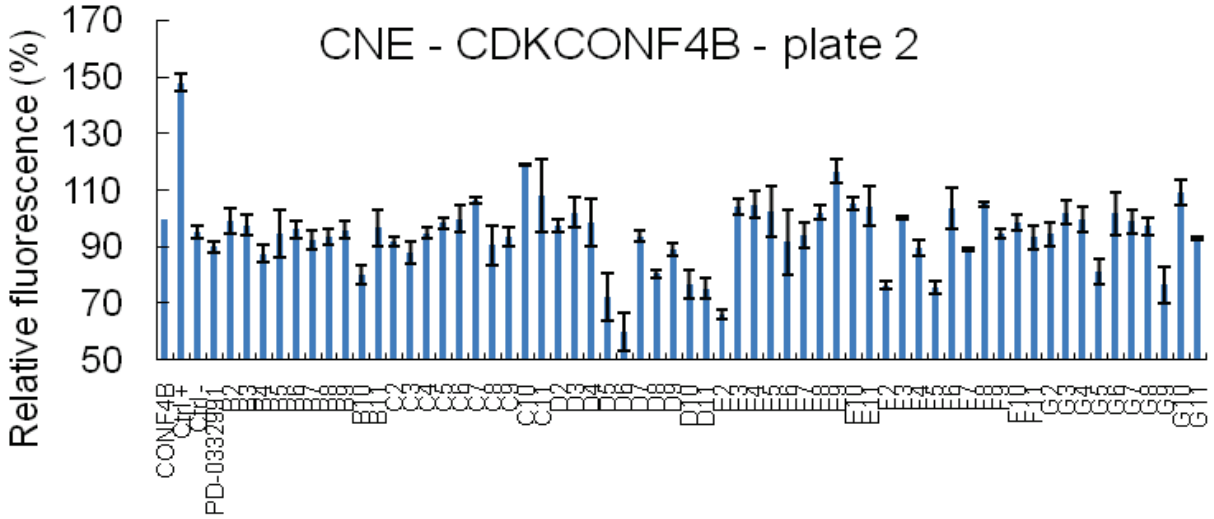
CNE - CDKCONF4B - plate 2
Relative fluorescence (%)
170
150
130
110
90
70
50
CONF4B
Ctrl+
Ctrl-
PD-0332991

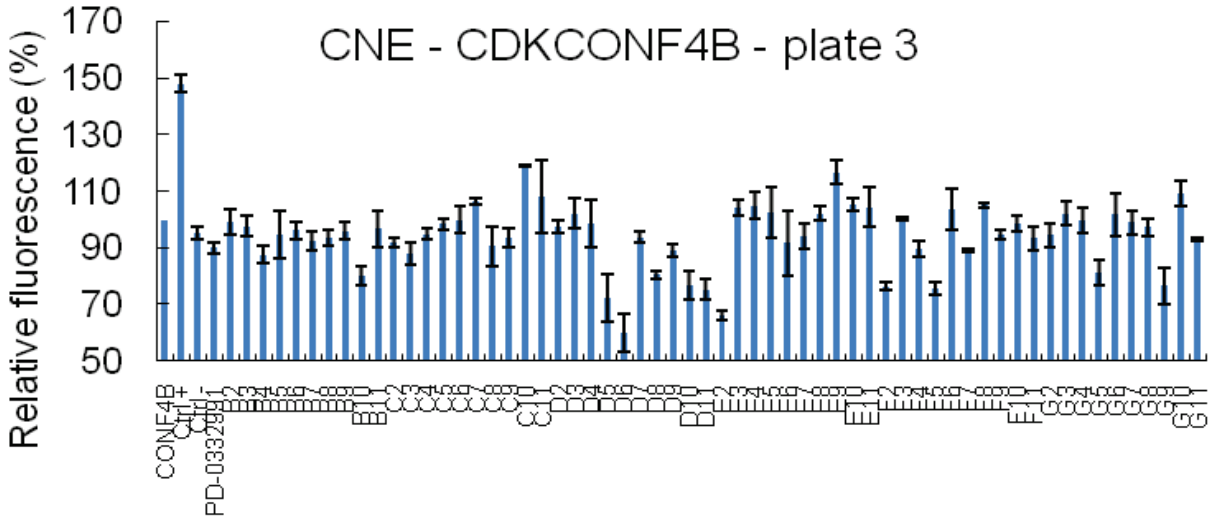
CNE - CDKCONF4B - plate 3
Relative fluorescence (%)
170
150
130
110
90
70
50
CONF4B
Ctrl+
Ctrl-
PD-0332991

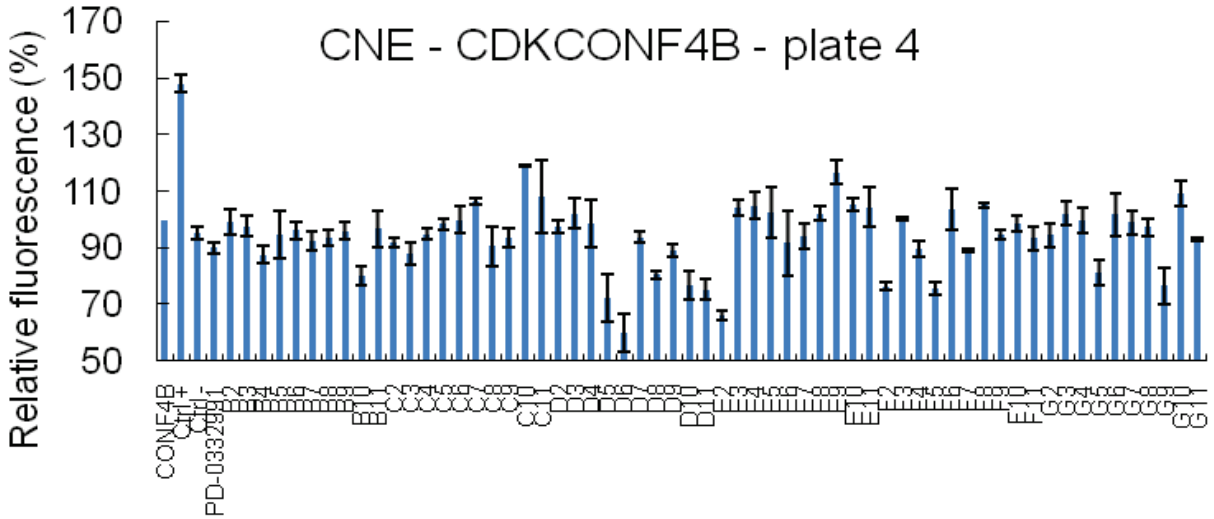
CNE - CDKCONF4B - plate 4
Relative fluorescence (%)
170
150
130
110
90
70
50
CONF4B
Ctrl+
Ctrl-
PD-0332991

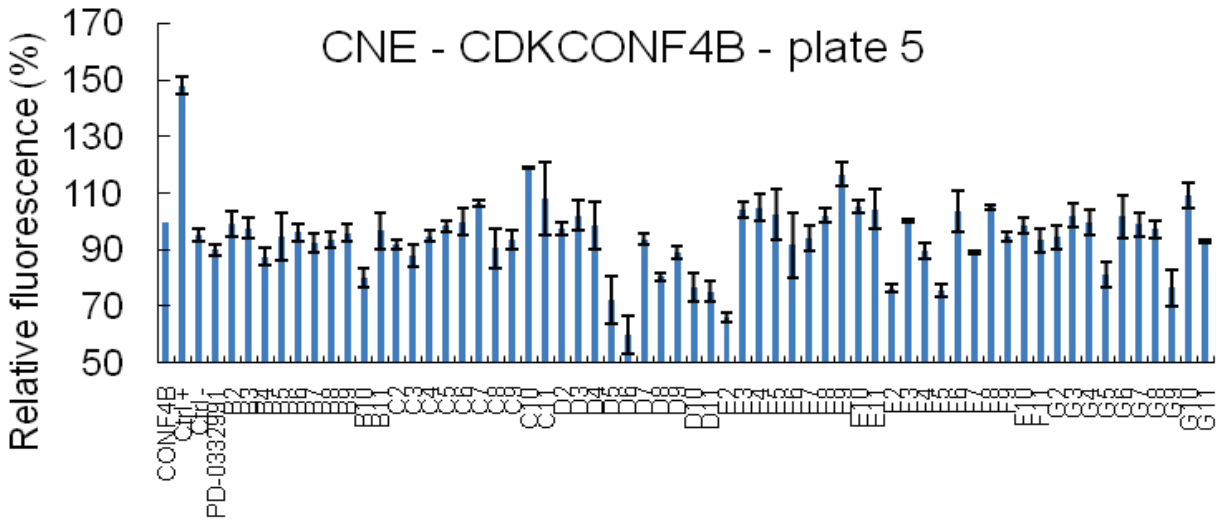
CNE - CDKCONF4B - plate 5
Relative fluorescence (%)
170
150
130
110
90
70
50
CONF4B
Ctrl+
PD-0332991

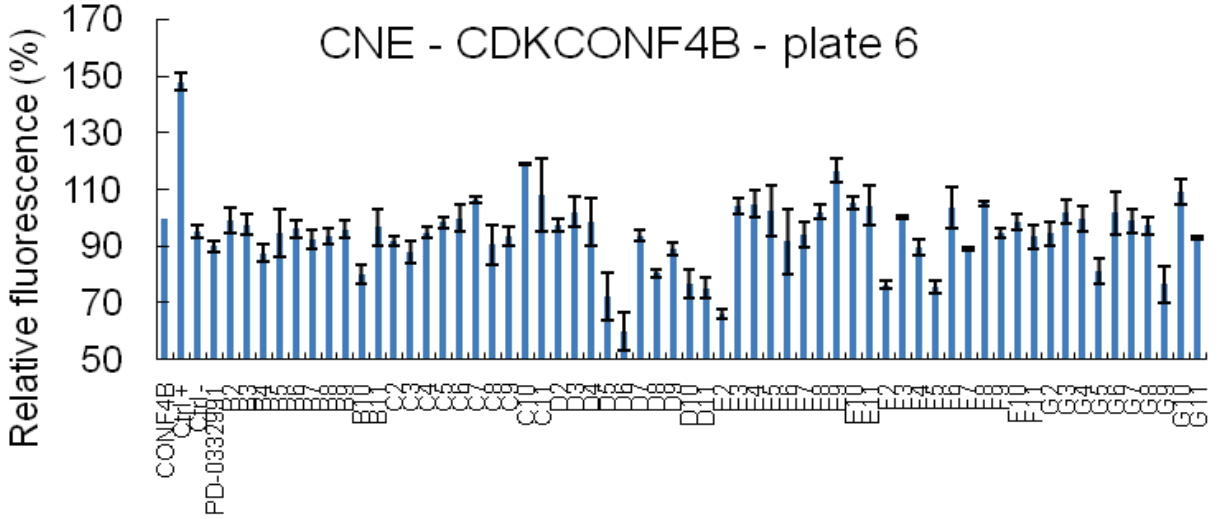
CNE - CDKCONF4B - plate 6
Relative fluorescence (%)
170
150
130
110
90
70
50
CONF4B
Ctrl+
PD-0332991

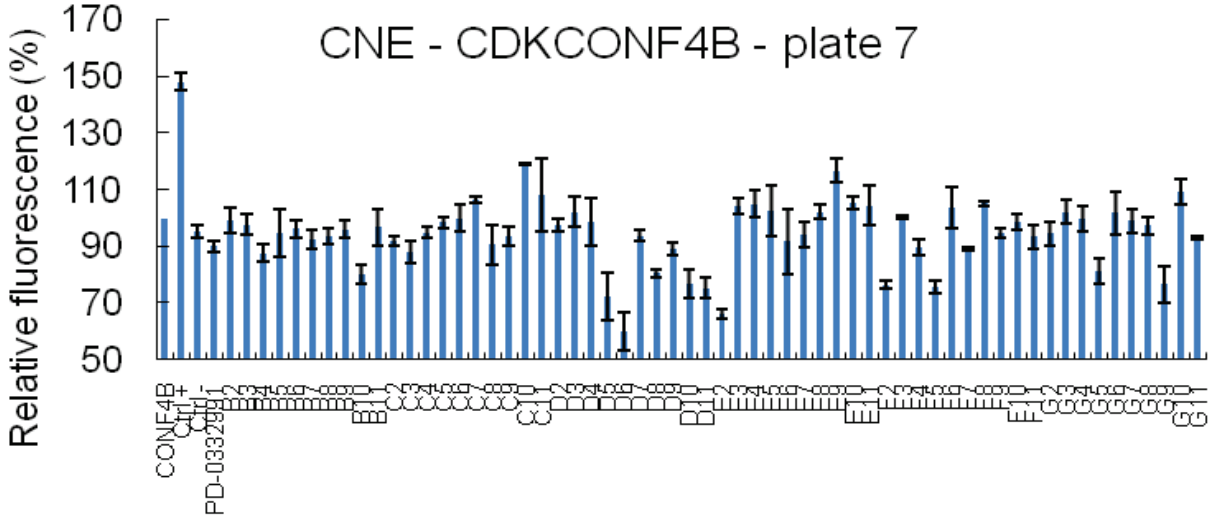
CNE - CDKCONF4B - plate 7
Relative fluorescence (%)
170
150
130
110
90
70
50
CONF4B
Ctrl+
PD-0332991

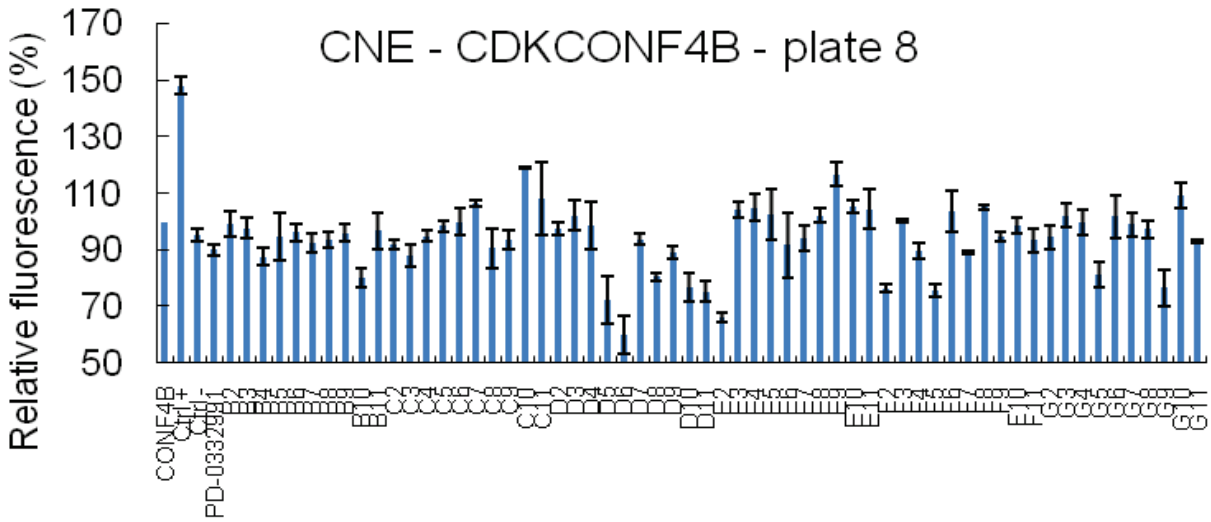

Results of the screen performed with Cy3-CDKCONF4A and compounds from Strasbourg

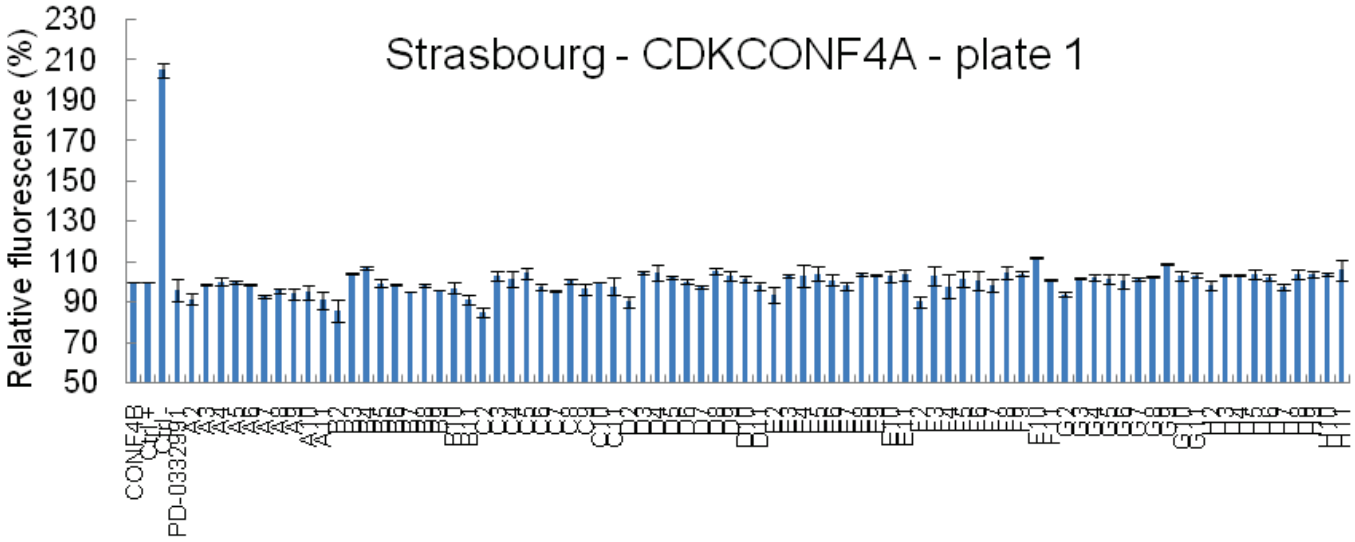

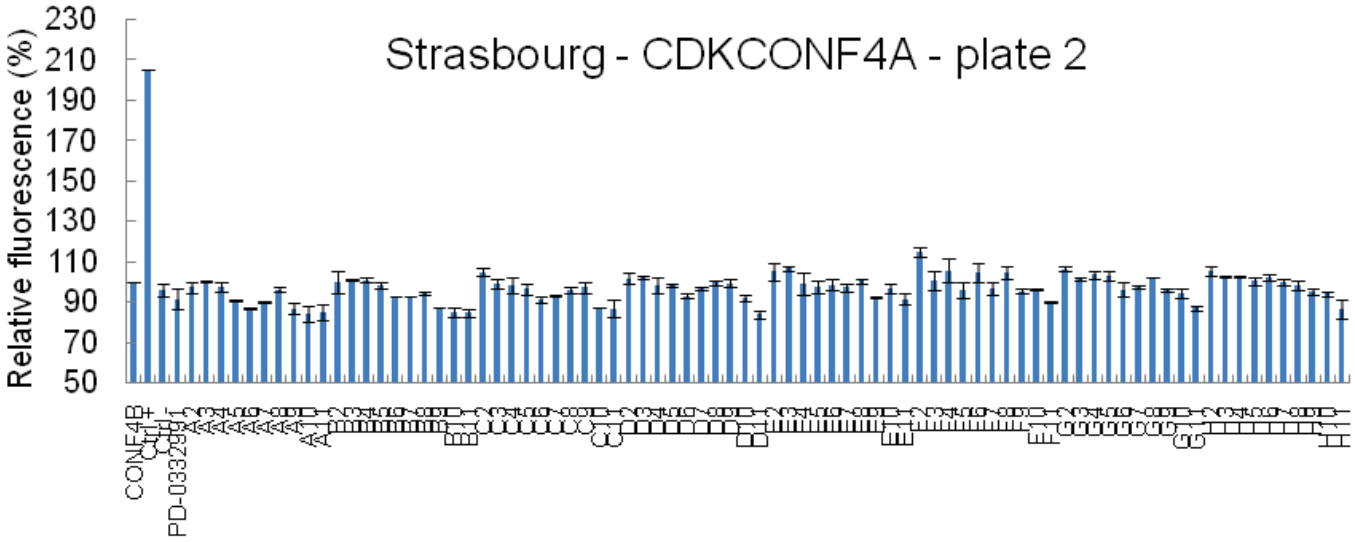

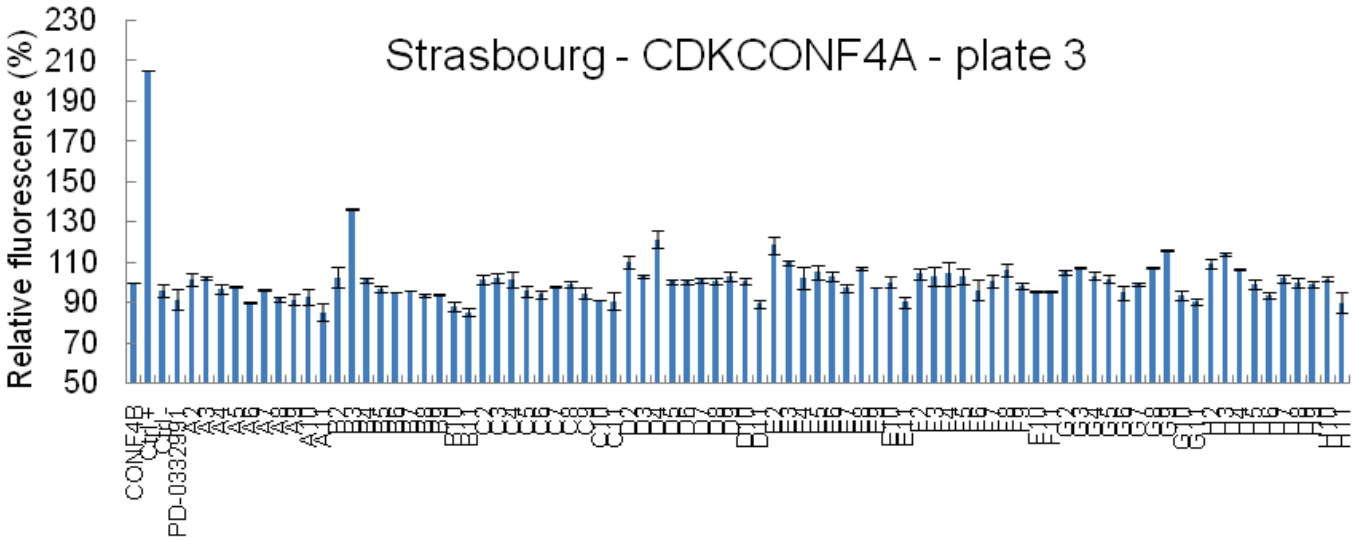
Strasbourg - CDKCONF4A - plate 3
Relative fluorescence (%)
230
210
190
170
150
130
110
90
70
50
CONF4B
Ctrl+
PD-0332991

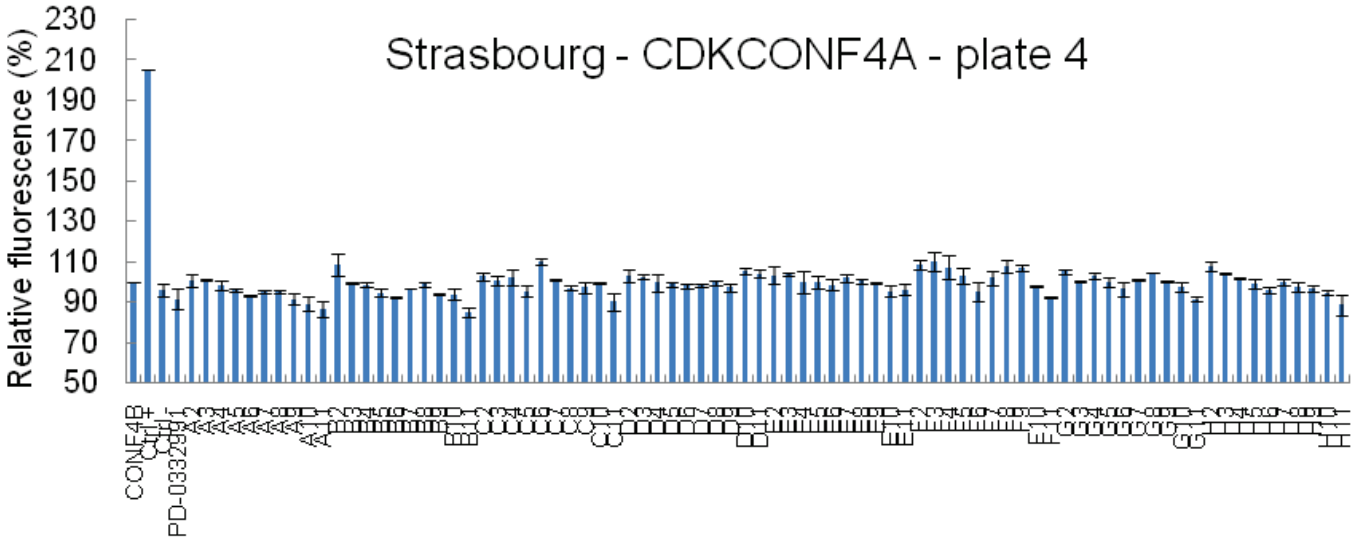
Strasbourg - CDKCONF4A - plate 4
Relative fluorescence (%)
230
210
190
170
150
130
110
90
70
50
CONF4B
Ctrl+
PD-0332991

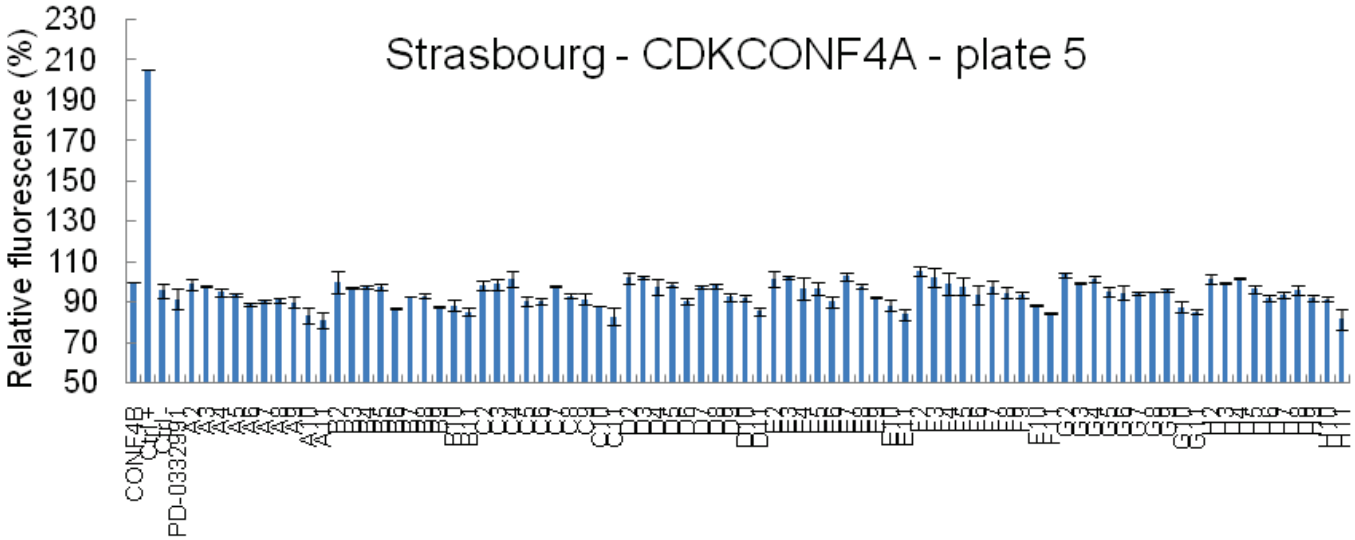
Strasbourg - CDKCONF4A - plate 5
Relative fluorescence (%)
230
210
190
170
150
130
110
90
70
50
CONF4B
Ctrl+
PD-0332991

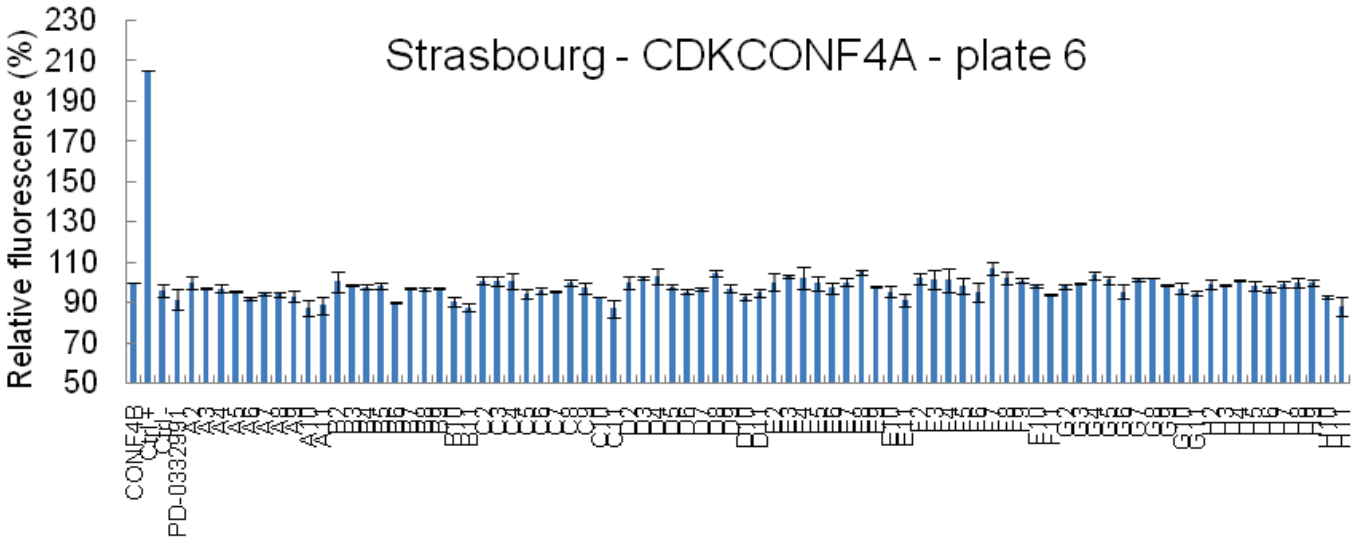
Strasbourg - CDKCONF4A - plate 6
Relative fluorescence (%)
230
210
190
170
150
130
110
90
70
50
CONF4B
Ctrl+
Ctrl-
PD-0332991

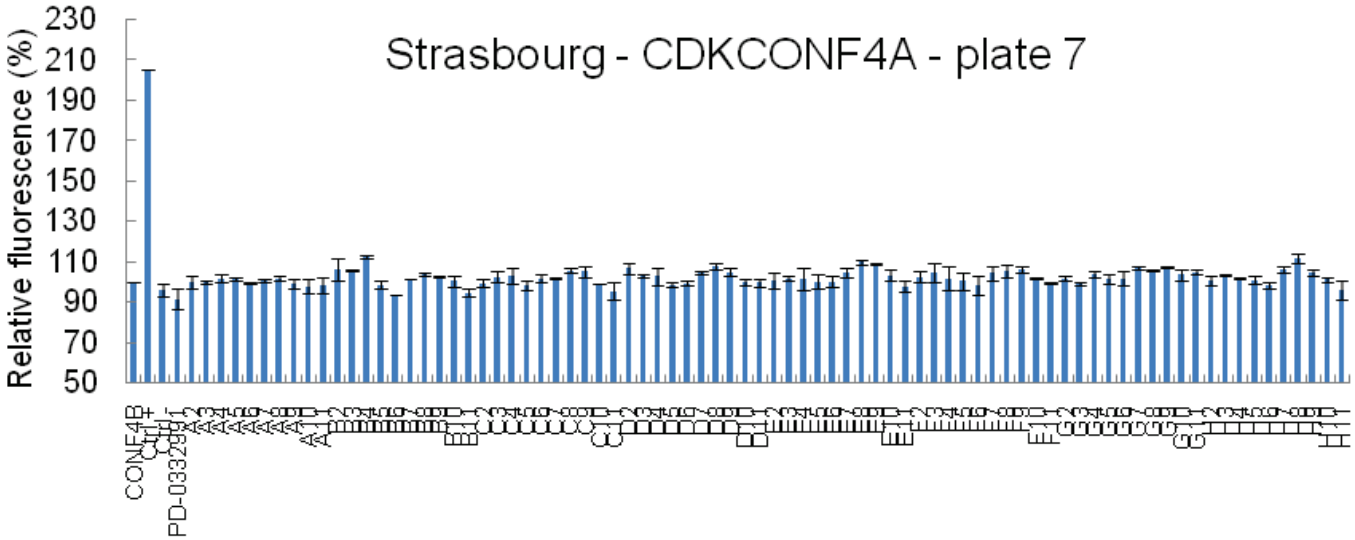
Strasbourg - CDKCONF4A - plate 7
Relative fluorescence (%)
230
210
190
170
150
130
110
90
70
50
CONF4B
Ctrl+
Ctrl-
PD-0332991

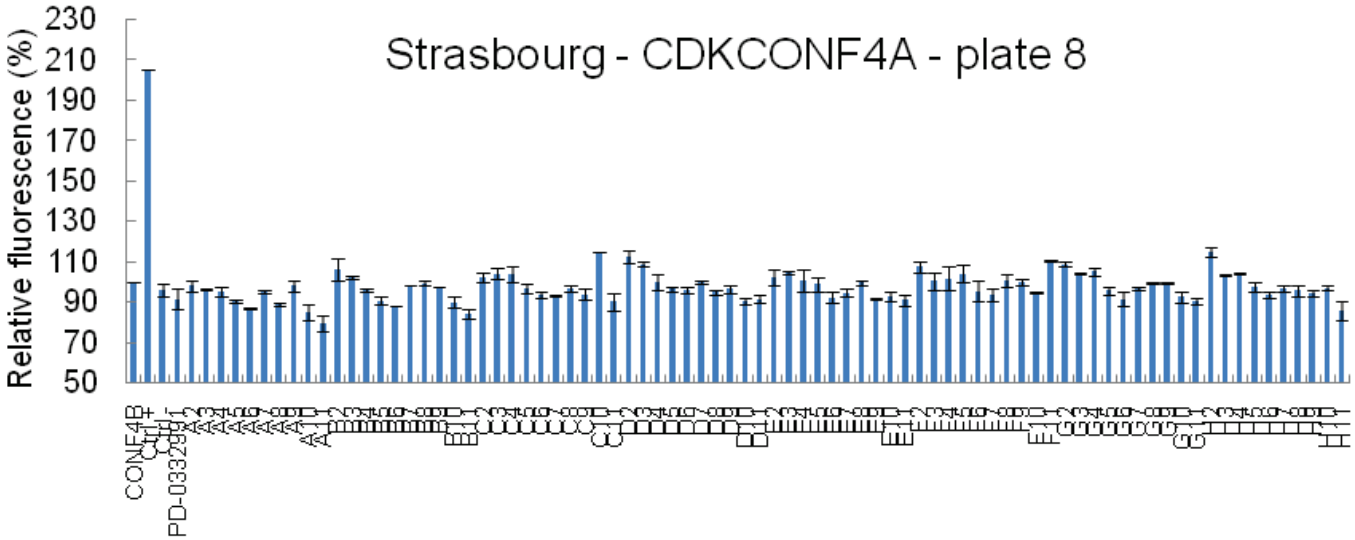
Strasbourg - CDKCONF4A - plate 8
Relative fluorescence (%)
230
210
190
170
150
130
110
90
70
50
CONF4B
Ctrl+
Ctrl-
PD-0332991

Results of the screen performed with Cy3-CDKCONF4B and compounds from Strasbourg

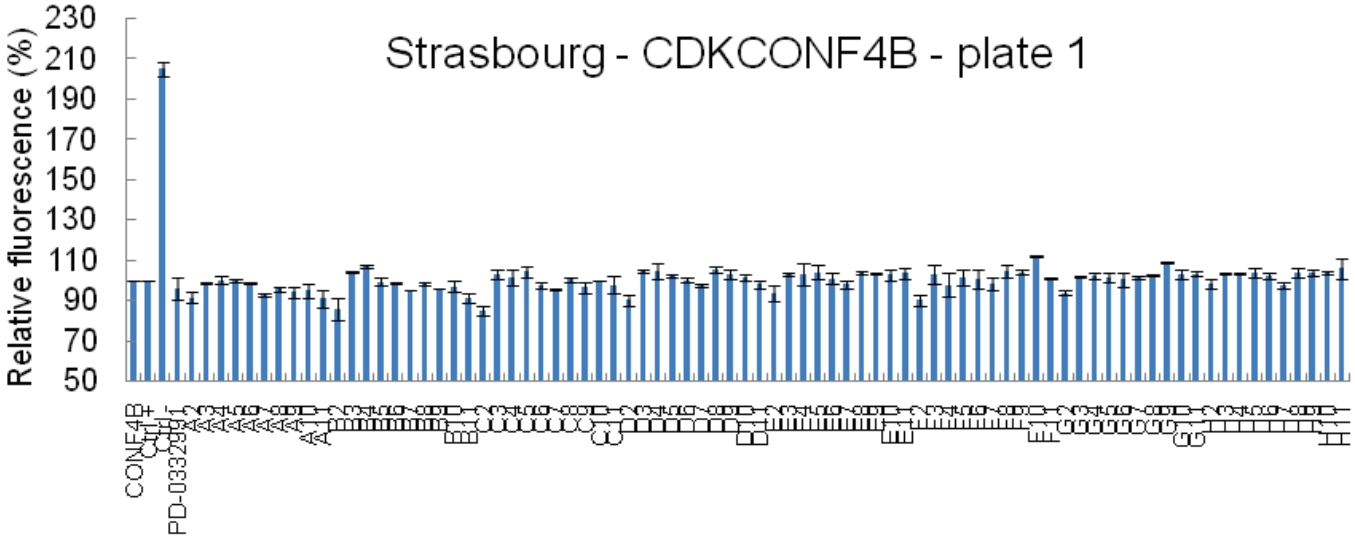

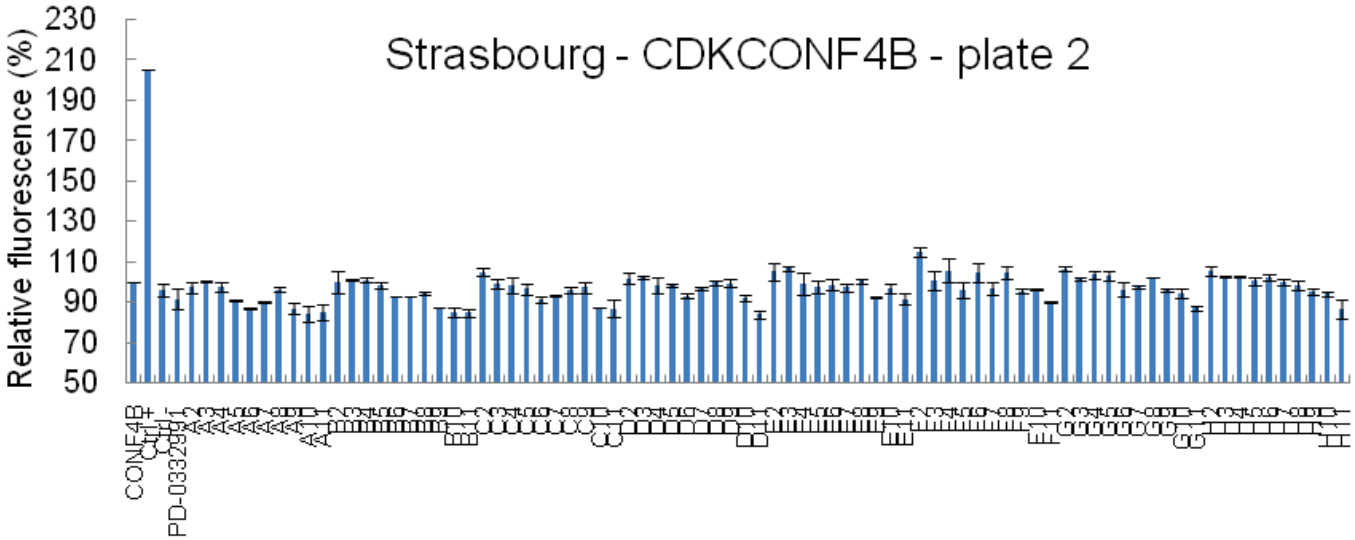

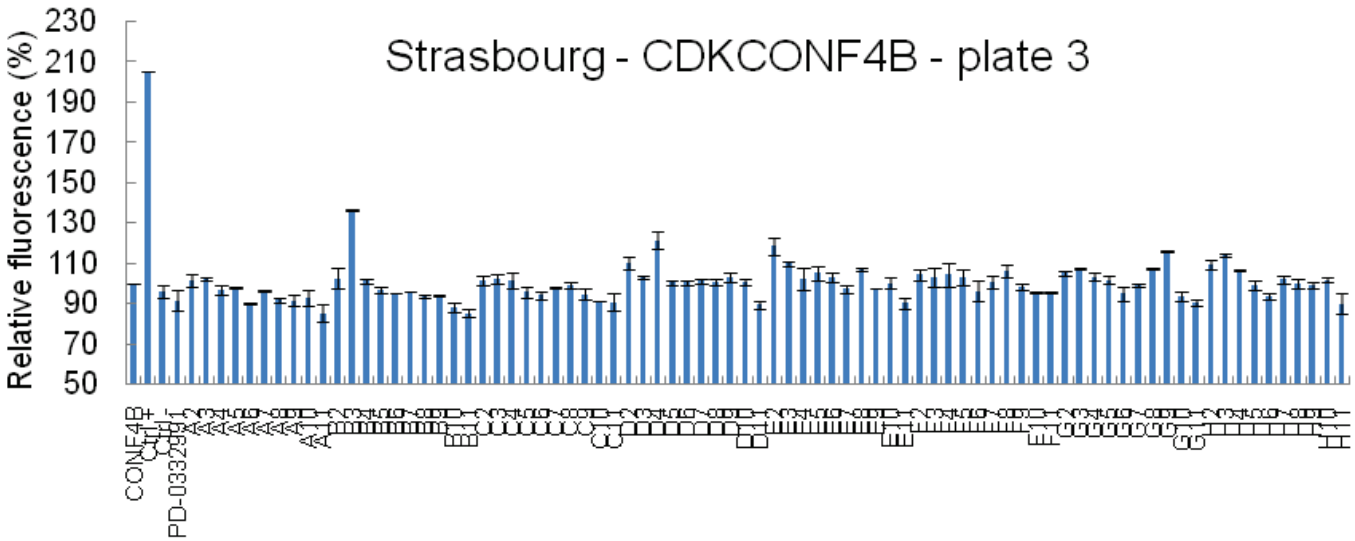

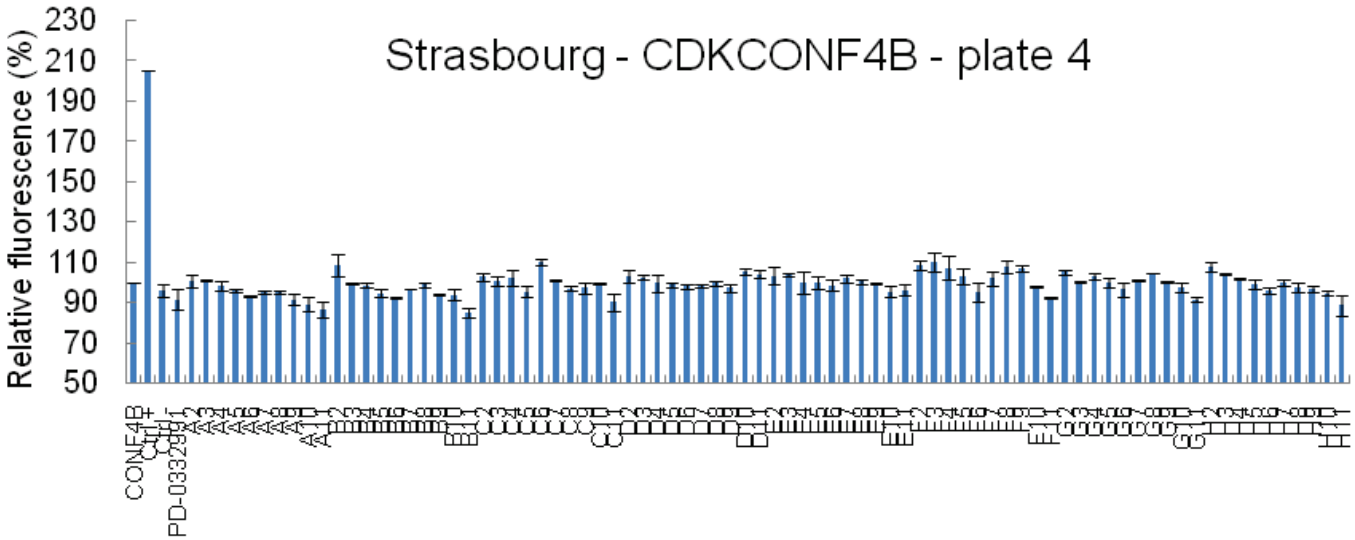
Strasbourg - CDKCONF4B - plate 4
Relative fluorescence (%)
230
210
190
170
150
130
110
90
70
50
CONF4B
Ctrl+
Ctrl-
PD-0332991

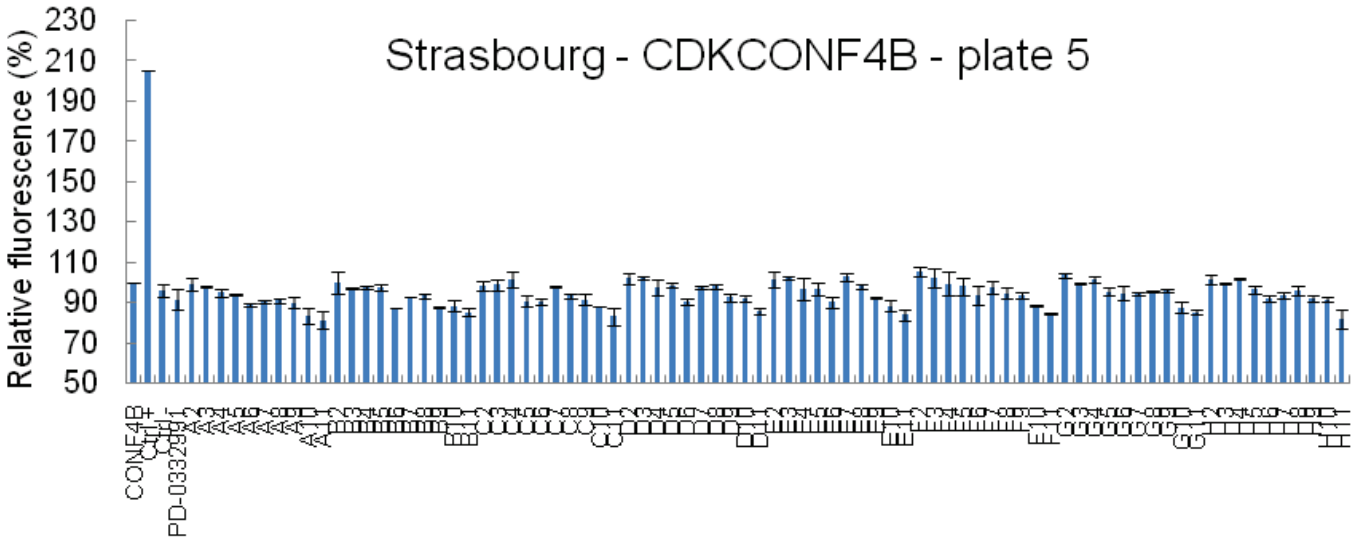
Strasbourg - CDKCONF4B - plate 5
Relative fluorescence (%)
230
210
190
170
150
130
110
90
70
50
CONF4B
Ctrl+
Ctrl-
PD-0332991

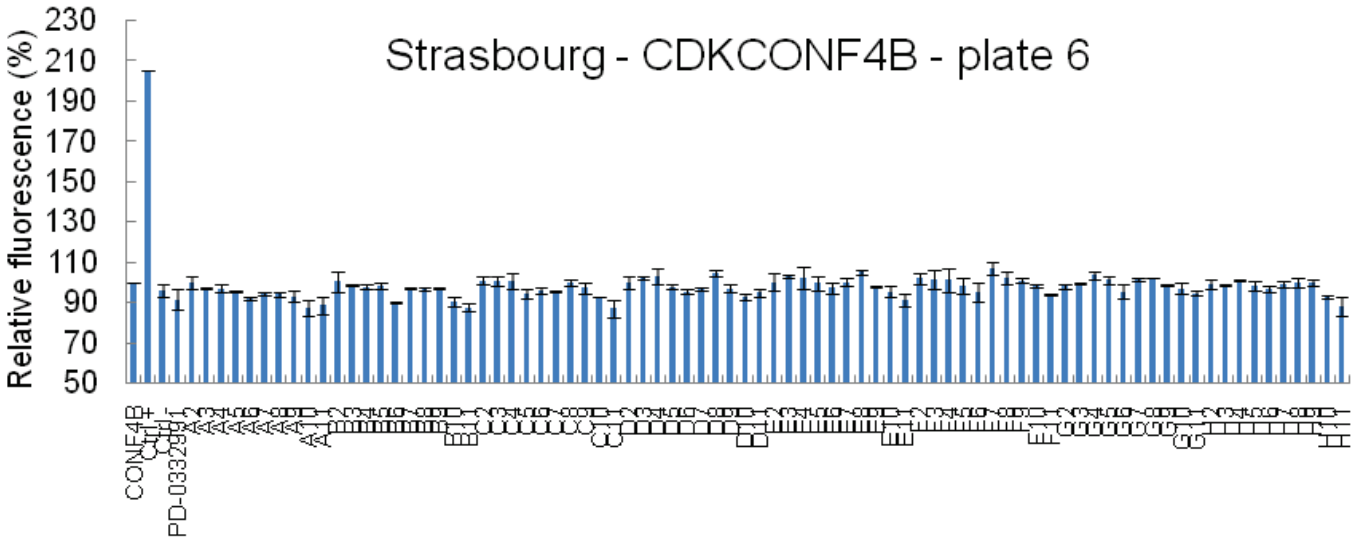
Strasbourg - CDKCONF4B - plate 6
Relative fluorescence (%)
230
210
190
170
150
130
110
90
70
50
CONF4B
Ctrl+
Ctrl-
PD-0332991

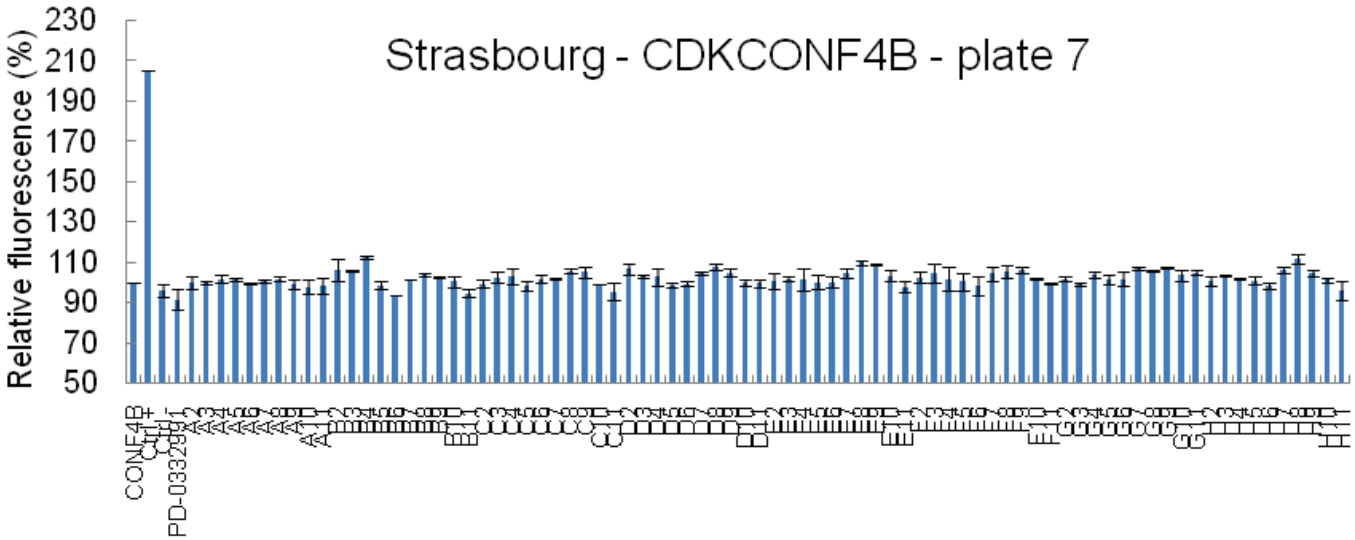
Strasbourg - CDKCONF4B - plate 7
Relative fluorescence (%)
230
210
190
170
150
130
110
90
70
50
CONF4B
Ctrl+
Ctrl-
PD-0332991

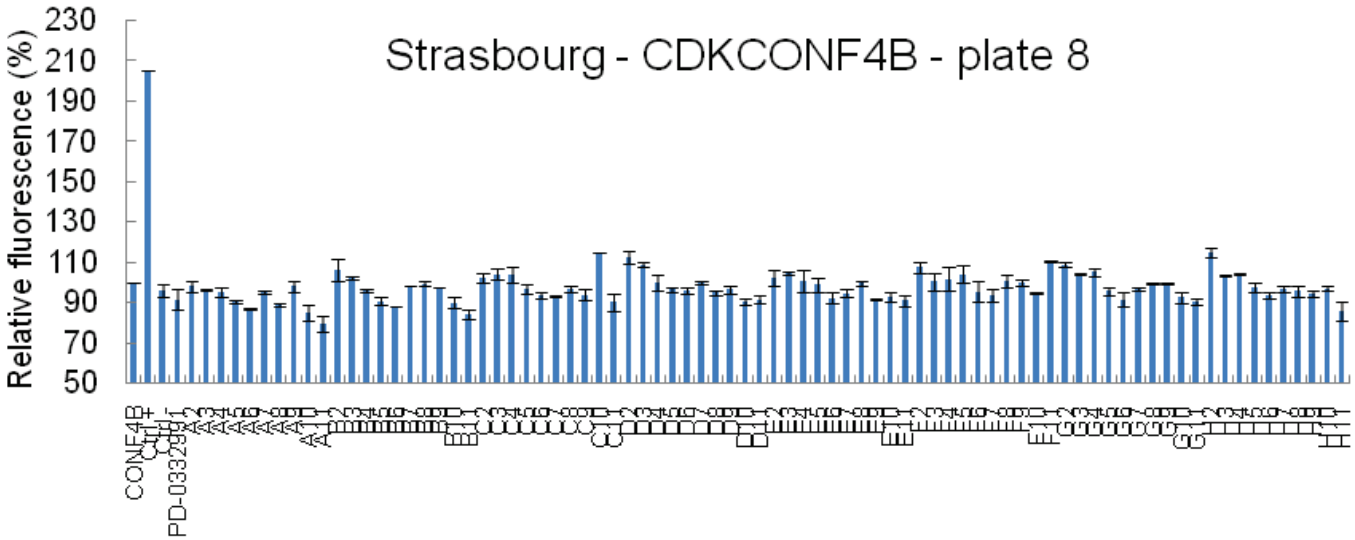
Strasbourg - CDKCONF4B - plate 8
Relative fluorescence (%)
230
210
190
170
150
130
110
90
70
50
CONF4B
Ctrl+
Ctrl-
PD-0332991

Annex E

Proliferation inhibition studies of LPI2192, LPI2550, RF1210, LPI2251, LPI2252, MED0128 and PD-0332991 in A375 cell line

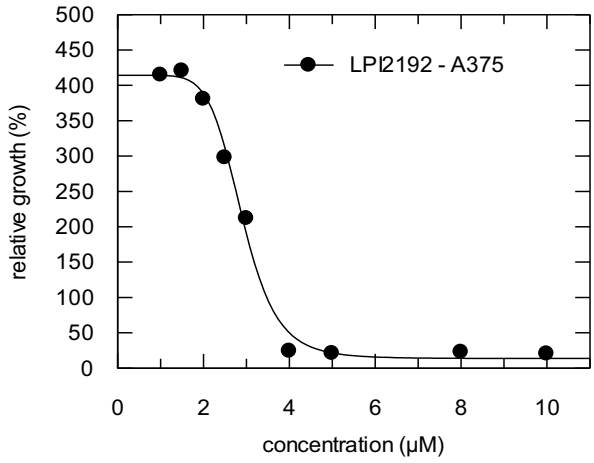

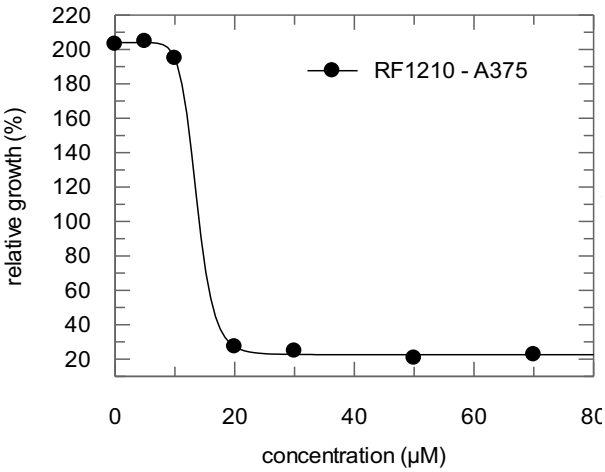

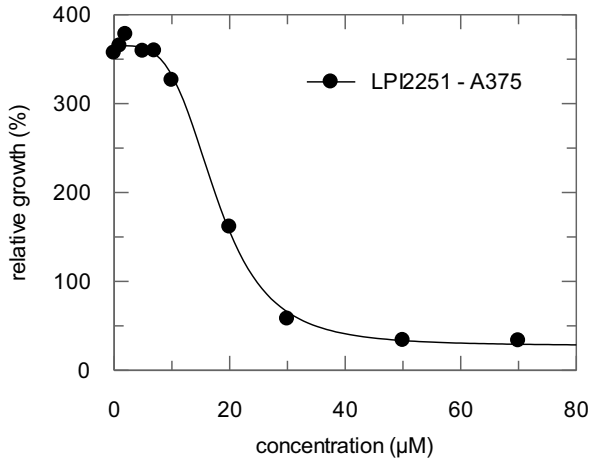

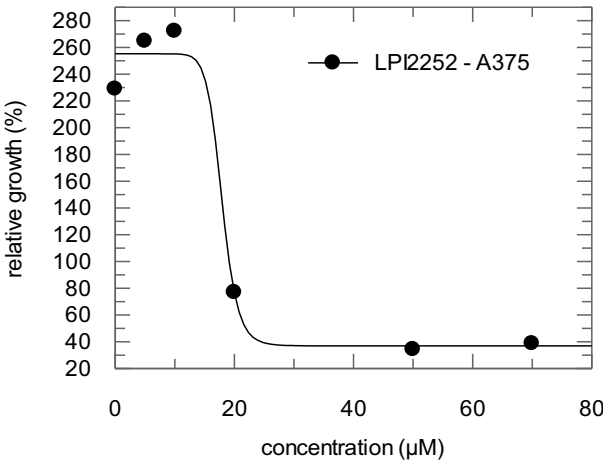

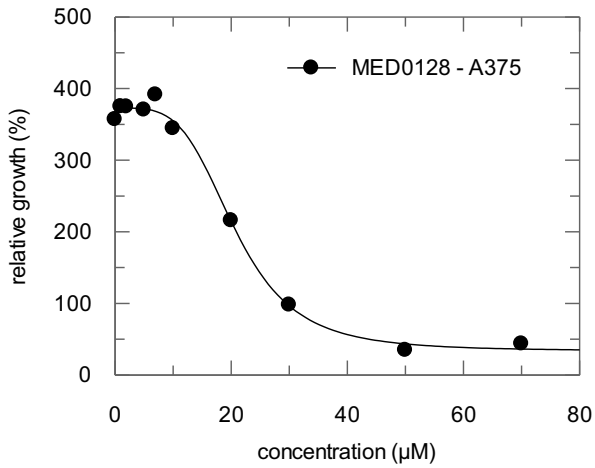

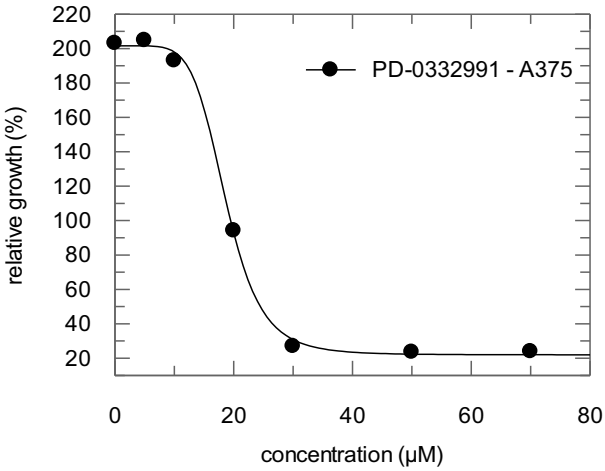

Proliferation inhibition studies of PD-0332991 and RF1210 in melanoma cell lines (A375, MV3, SKMEL2 and SKMEL28)

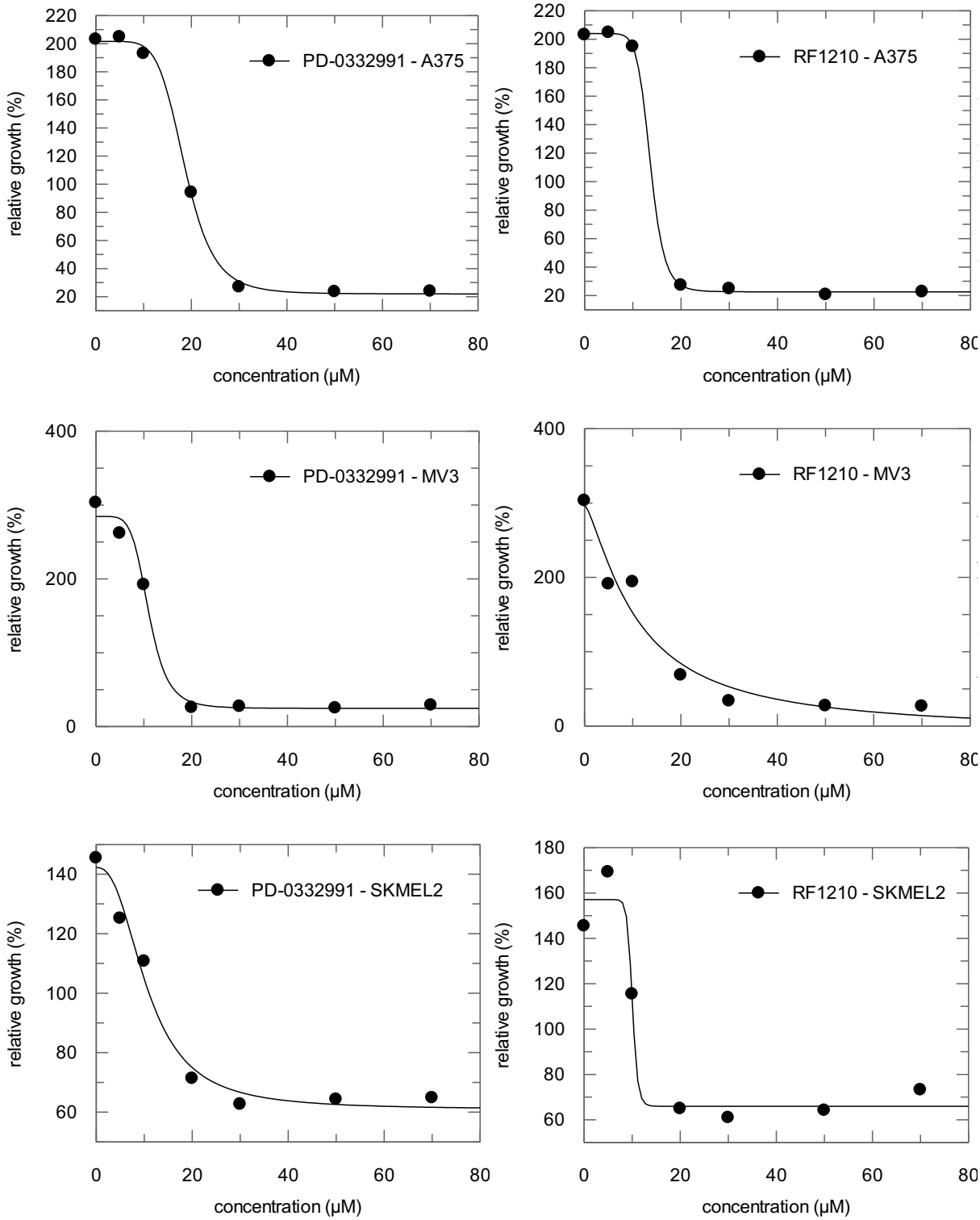

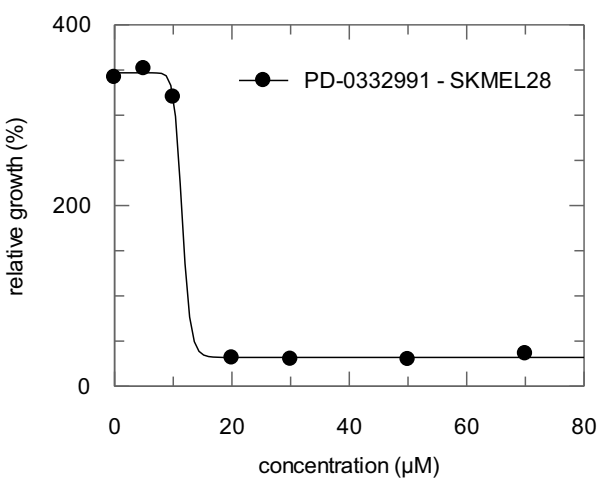
400
200
0
relative growth (%)
PD-0332991 - SKMEL28
0
20
40
60
80
concentration (μM)

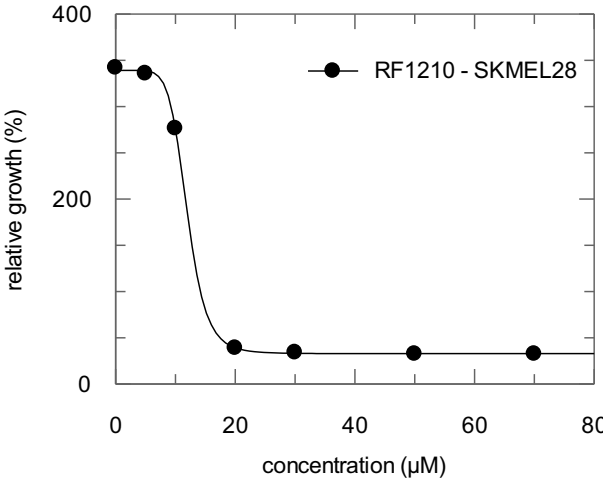
400
200
0
relative growth (%)
RF1210 - SKMEL28
0
20
40
60
80
concentration (μM)

Annex F

PBS buffer

50 mM KH_2PO_4/K_2HPO_4, pH 6.4

500 mM NaCl

TBS buffer

50 mM Tris-HCl, pH 7.4

150 mM NaCl

PBS/TBS lysis buffer

PBS/TBS buffer

+ 0.1 % NP40

+ 3.3 mM PMSF

+ 0.33 mg/mL lysozyme

LB broth

10 g/L Tryptone

10 g/L NaCl

5 g/L yeast extract

TSS buffer (filter through 0.2 µm)

10 mL LB

10 % Polyethylene glycol 3000 - 8000

50 mM $MgCl_2$

5 % DMSO

LB/amp broth

LB broth

+ 50 mg/L ampicillin

LB/amp plates

LB broth

+ 15 g/L Agar

Autoclave for 20min

Let the solution cool to 50°C

In a sterile atmosphere, add 100 mg/L ampicillin and pour ~25 mL of LB agar per 10 cm Petri dish

When LB agar is solidified, invert the plates, seal with parafilm and store at 4°C

Laemmli buffer 2.5X

1 mL Bromophenol Blue 2 % (diluted in ethanol 96%)

15 mL glycerol 100 %

1.54 g DTT

10 mL SDS 20 %

8 mL Tris 1M pH=6.8

46 mL H_2O

SDS-PAGE mix 15% (200mL)

75 mL Acrylamide/Bis-Acrylamide (37,5/1) mix

50 mL Tris 1.5 M pH=8.8

73 mL H_2O

2 mL SDS 10 %

SDS-PAGE stack 4% (200mL)

22 mL Acrylamide

13 mL Bis-Acrylamide

25 mL Tris 1 M pH=6.8

2 mL SDS 10 %

138 mL H_2O

Coomassie Brilliant Blue

6 g Brilliant Blue R (Sigma Aldrich)

Add 100 mL acetic acid to solubilize the powder

Add 300 mL ethanol 96%

Add 600 mL H_2O

Transfer buffer

144 g glycine

30.2 g Tris-Base

900mL H_2O

Blocking buffer

PBS buffer

4 % BSA

4 % goat serum

0.1 % triton X-100

Filter through 0.2 µm

PBS lysis buffer

PBS pH 7.4 (Sigma)

0.2 % NP40

2 mM PMSF

1 mM EDTA

Complete^{TM} protease inhibitors (Roche)

PBS lysis buffer + phosphatase inhibitors

PBS lysis buffer

+ 500 mM NaF

+ 10 mM Na_3VO_4

Total extraction buffer

50 mM Trizma Base

0.5 M NaCl

5 mM EDTA

0.6 % NP40

Luciferase cell culture lysis reagent

25 mM Tris-phosphate (pH 7.8)

2 mM DTT

2 mM EDTA

10 % glycerol

1 % Triton X-100

References

Abate, A.A., Pentimalli, F., Esposito, L., and Giordano, A. (2013). ATP-noncompetitive CDK inhibitors for cancer therapy: an overview. Expert Opin. Investig. Drugs *22*, 895–906.

Abella, A., Dubus, P., Malumbres, M., Rane, S.G., Kiyokawa, H., Sicard, A., Vignon, F., Langin, D., Barbacid, M., and Fajas, L. (2005). Cdk4 promotes adipogenesis through PPARgamma activation. Cell Metab. *2*, 239–249.

Abramson, V.G., Troxel, A.B., Feldman, M., Mies, C., Wang, Y., Sherman, L., McNally, S., Diehl, A., and Demichele, A. (2010). Cyclin D1b in human breast carcinoma and coexpression with cyclin D1a is associated with poor outcome. Anticancer Res. *30*, 1279–1285.

Agami, R., and Bernards, R. (2000). Distinct initiation and maintenance mechanisms cooperate to induce G1 cell cycle arrest in response to DNA damage. Cell *102*, 55–66.

Aggarwal, P., Vaites, L.P., Kim, J.K., Mellert, H., Gurung, B., Nakagawa, H., Herlyn, M., Hua, X., Rustgi, A.K., McMahon, S.B., et al. (2010). Nuclear cyclin D1/CDK4 kinase regulates CUL4 expression and triggers neoplastic growth via activation of the PRMT5 methyltransferase. Cancer Cell *18*, 329–340.

Agnes, R.S., Jernigan, F., Shell, J.R., Sharma, V., and Lawrence, D.S. (2010). Suborganelle sensing of mitochondrial cAMP-dependent protein kinase activity. J. Am. Chem. Soc. *132*, 6075–6080.

Ahsen, O. von, and Bömer, U. (2005). High-Throughput Screening for Kinase Inhibitors. ChemBioChem *6*, 481–490.

Akervall, J.A., Michalides, R.J., Mineta, H., Balm, A., Borg, A., Dictor, M.R., Jin, Y., Loftus, B., Mertens, F., and Wennerberg, J.P. (1997). Amplification of cyclin D1 in squamous cell carcinoma of the head and neck and the prognostic value of chromosomal abnormalities and cyclin D1 overexpression. Cancer *79*, 380–389.

Alao, J.P. (2007). The regulation of cyclin D1 degradation: roles in cancer development and the potential for therapeutic invention. Mol. Cancer *6*, 24.

Allen, M.D., DiPilato, L.M., Rahdar, M., Ren, Y.R., Chong, C., Liu, J.O., and Zhang, J. (2006). Reading dynamic kinase activity in living cells for high-throughput screening. ACS Chem. Biol. *1*, 371–376.

Alt, J.R., Cleveland, J.L., Hannink, M., and Diehl, J.A. (2000). Phosphorylation-dependent regulation of cyclin D1 nuclear export and cyclin D1-dependent cellular transformation. Genes Dev. *14*, 3102–3114.

An, H.-X., Beckmann, M.W., Reifenberger, G., Bender, H.G., and Niederacher, D. (1999). Gene Amplification and Overexpression of CDK4 in Sporadic Breast Carcinomas Is Associated with High Tumor Cell Proliferation. Am. J. Pathol. *154*, 113–118.

Anai, T., Nakata, E., Koshi, Y., Ojida, A., and Hamachi, I. (2007). Design of a hybrid biosensor for enhanced phosphopeptide recognition based on a phosphoprotein binding domain coupled with a fluorescent chemosensor. J. Am. Chem. Soc. *129*, 6232–6239.

Anand, P., Kunnumakara, A.B., Sundaram, C., Harikumar, K.B., Tharakan, S.T., Lai, O.S., Sung, B., and Aggarwal, B.B. (2008). Cancer is a Preventable Disease that Requires Major Lifestyle Changes. Pharm. Res. *25*, 2097–2116.

Anderson, A.A., Child, E.S., Prasad, A., Elphick, L.M., and Mann, D.J. (2010). Cyclin D1 and cyclin D3 show divergent responses to distinct mitogenic stimulation. J. Cell. Physiol. *225*, 638–645.

Antczak, C., Mahida, J.P., Bhinder, B., Calder, P.A., and Djaballah, H. (2012). A high-content biosensor-based screen identifies cell-permeable activators and inhibitors of EGFR function: implications in drug discovery. J. Biomol. Screen. *17*, 885–899.

Arkin, M.R., and Wells, J.A. (2004). Small-molecule inhibitors of protein-protein interactions: progressing towards the dream. Nat. Rev. Drug Discov. *3*, 301–317.

Asghar, U., Witkiewicz, A.K., Turner, N.C., and Knudsen, E.S. (2015). The history and future of targeting cyclin-dependent kinases in cancer therapy. Nat. Rev. Drug Discov. *14*, 130–146.

Aye-Han, N.-N., Ni, Q., and Zhang, J. (2009). Fluorescent biosensors for real-time tracking of post-translational modification dynamics. Curr. Opin. Chem. Biol. *13*, 392–397.

De Azevedo, W.F., Leclerc, S., Meijer, L., Havlicek, L., Strnad, M., and Kim, S.H. (1997). Inhibition of cyclin-dependent kinases by purine analogues: crystal structure of human cdk2 complexed with roscovitine. Eur. J. Biochem. FEBS *243*, 518–526.

Bach, S., Knockaert, M., Reinhardt, J., Lozach, O., Schmitt, S., Baratte, B., Koken, M., Coburn, S.P., Tang, L., Jiang, T., et al. (2005). Roscovitine targets, protein kinases and pyridoxal kinase. J. Biol. Chem. *280*, 31208–31219.

Bagella, L., Sun, A., Tonini, T., Abbadessa, G., Cottone, G., Paggi, M.G., De Luca, A., Claudio, P.P., and Giordano, A. (2007). A small molecule based on the pRb2/p130 spacer domain leads to inhibition of cdk2 activity, cell cycle arrest and tumor growth reduction in vivo. Oncogene *26*, 1829–1839.

Banaszynski, M., and Kolesar, J.M. (2013). Vemurafenib and ipilimumab: new agents for metastatic melanoma. Am. J. Health-Syst. Pharm. AJHP Off. J. Am. Soc. Health-Syst. Pharm. *70*, 1205–1210.

Bandarchi, B., Ma, L., Navab, R., Seth, A., and Rasty, G. (2010). From Melanocyte to Metastatic Malignant Melanoma. Dermatol. Res. Pract. *2010*.

Barvian, M., Boschelli, D.H., Cossrow, J., Dobrusin, E., Fattaey, A., Fritsch, A., Fry, D., Harvey, P., Keller, P., Garrett, M., et al. (2000). Pyrido[2,3-d]pyrimidin-7-one inhibitors of cyclin-dependent kinases. J. Med. Chem. *43*, 4606–4616.

Bastiaens, P.I., and Pepperkok, R. (2000). Observing proteins in their natural habitat: the living cell. Trends Biochem. Sci. *25*, 631–637.

Bathini, Y., Singh, I., Harvey, P.J., Keller, P.R., Singh, R., Micetich, R.G., Fry, D.W., Dobrusin, E.M., and Toogood, P.L. (2005). 2-Aminoquinazoline inhibitors of cyclin-dependent kinases. Bioorg. Med. Chem. Lett. *15*, 3881–3885.

Bellail, A.C., Olson, J.J., and Hao, C. (2014). SUMO1 modification stabilizes CDK6 protein and drives the cell cycle and glioblastoma progression. Nat. Commun. *5*, 4234.

Belpomme, D., Irigaray, P., Hardell, L., Clapp, R., Montagnier, L., Epstein, S., and Sasco, A.J. (2007). The multitude and diversity of environmental carcinogens. Environ. Res. *105*, 414–429.

Benzeno, S., and Diehl, J.A. (2004). C-terminal sequences direct cyclin D1-CRM1 binding. J. Biol. Chem. *279*, 56061–56066.

Benzeno, S., Lu, F., Guo, M., Barbash, O., Zhang, F., Herman, J.G., Klein, P.S., Rustgi, A., and Diehl, J.A. (2006). Identification of mutations that disrupt phosphorylation-dependent nuclear export of cyclin D1. Oncogene *25*, 6291–6303.

Berezin, M.Y., and Achilefu, S. (2010). Fluorescence Lifetime Measurements and Biological Imaging. Chem. Rev. *110*, 2641–2684.

Bergsagel, P.L., and Kuehl, W.M. (2005). Molecular Pathogenesis and a Consequent Classification of Multiple Myeloma. J. Clin. Oncol. *23*, 6333–6338.

Bertoni, F., Rinaldi, A., Zucca, E., and Cavalli, F. (2006). Update on the molecular biology of mantle cell lymphoma. Hematol. Oncol. *24*, 22–27.

Bettayeb, K., Oumata, N., Echalier, A., Ferandin, Y., Endicott, J.A., Galons, H., and Meijer, L. (2008). CR8, a potent and selective, roscovitine-derived inhibitor of cyclin-dependent kinases. Oncogene *27*, 5797–5807.

Betticher, D.C., Thatcher, N., Altermatt, H.J., Hoban, P., Ryder, W.D., and Heighway, J. (1995). Alternate splicing produces a novel cyclin D1 transcript. Oncogene *11*, 1005–1011.

Bienvenu, F., Jirawatnotai, S., Elias, J.E., Meyer, C.A., Mizeracka, K., Marson, A., Frampton, G.M., Cole, M.F., Odom, D.T., Odajima, J., et al. (2010). Transcriptional role of cyclin D1 in development revealed by a genetic–proteomic screen. Nature *463*, 374–378.

Blagosklonny, M.V., and Pardee, A.B. (2002). The Restriction Point of the Cell Cycle. Cell Cycle *1*, 102–109.

Bockstaele, L., Coulonval, K., Kooken, H., Paternot, S., and Roger, P.P. (2006). Regulation of CDK4. Cell Div. *1*, 25.

Boonstra, J. (2003). Progression through the G1-phase of the on-going cell cycle. J. Cell. Biochem. *90*, 244–252.

Boutros, R., Dozier, C., and Ducommun, B. (2006). The when and wheres of CDC25 phosphatases. Curr. Opin. Cell Biol. *18*, 185–191.

Brooker, L.G.S., Keyes, G.H., and Heseltine, D.W. (1951). Color and Constitution. XI.1 Anhydronium Bases of p-Hydroxystyryl Dyes as Solvent Polarity Indicators. J. Am. Chem. Soc. *73*, 5350–5356.

Brown, N.R., Noble, M.E., Lawrie, A.M., Morris, M.C., Tunnah, P., Divita, G., Johnson, L.N., and Endicott, J.A. (1999). Effects of phosphorylation of threonine 160 on cyclin-dependent kinase 2 structure and activity. J. Biol. Chem. *274*, 8746–8756.

Brown, V.L., Harwood, C.A., Crook, T., Cronin, J.G., Kelsell, D.P., and Proby, C.M. (2004). p16INK4a and p14ARF tumor suppressor genes are commonly inactivated in cutaneous squamous cell carcinoma. J. Invest. Dermatol. *122*, 1284–1292.

Brune, M., Hunter, J.L., Corrie, J.E., and Webb, M.R. (1994). Direct, real-time measurement of rapid inorganic phosphate release using a novel fluorescent probe and its application to actomyosin subfragment 1 ATPase. Biochemistry (Mosc.) *33*, 8262–8271.

Burd, C.J., Petre, C.E., Morey, L.M., Wang, Y., Revelo, M.P., Haiman, C.A., Lu, S., Fenoglio-Preiser, C.M., Li, J., Knudsen, E.S., et al. (2006). Cyclin D1b variant influences prostate cancer growth through aberrant androgen receptor regulation. Proc. Natl. Acad. Sci. U. S. A. *103*, 2190–2195.

Cancer Genome Atlas Network (2015). Genomic Classification of Cutaneous Melanoma. Cell *161*, 1681–1696.

Canela, N., Orzáez, M., Fucho, R., Mateo, F., Gutierrez, R., Pineda-Lucena, A., Bachs, O., and Pérez-Payá, E. (2006). Identification of an hexapeptide that binds to a surface pocket in cyclin A and inhibits the catalytic activity of the complex cyclin-dependent kinase 2-cyclin A. J. Biol. Chem. *281*, 35942–35953.

Carlson, H.J., and Campbell, R.E. (2009). Genetically encoded FRET-based biosensors for multiparameter fluorescence imaging. Curr. Opin. Biotechnol. *20*, 19–27.

Carpenter, A.E. (2007). Image-based chemical screening. Nat. Chem. Biol. *3*, 461–465.

Cen, L., Carlson, B.L., Schroeder, M.A., Ostrem, J.L., Kitange, G.J., Mladek, A.C., Fink, S.R., Decker, P.A., Wu, W., Kim, J.-S., et al. (2012). p16-Cdk4-Rb axis controls sensitivity to a cyclin-dependent kinase inhibitor PD0332991 in glioblastoma xenograft cells. Neuro-Oncol. *14*, 870–881.

Chalfie, M., Tu, Y., Euskirchen, G., Ward, W.W., and Prasher, D.C. (1994). Green fluorescent protein as a marker for gene expression. Science *263*, 802–805.

Chang, Y.T., Gray, N.S., Rosania, G.R., Sutherlin, D.P., Kwon, S., Norman, T.C., Sarohia, R., Leost, M., Meijer, L., and Schultz, P.G. (1999). Synthesis and application of functionally diverse 2,6,9-trisubstituted purine libraries as CDK inhibitors. Chem. Biol. *6*, 361–375.

Chapman, P.B., Hauschild, A., Robert, C., Haanen, J.B., Ascierto, P., Larkin, J., Dummer, R., Garbe, C., Testori, A., Maio, M., et al. (2011). Improved Survival with Vemurafenib in Melanoma with BRAF V600E Mutation. N. Engl. J. Med. *364*, 2507–2516.

Chawla, R., Procknow, J.A., Tantravahi, R.V., Khurana, J.S., Litvin, J., and Reddy, E.P. (2010). Cooperativity of Cdk4R24C and Ras in melanoma development. Cell Cycle Georget. Tex *9*, 3305–3314.

Chen, C.-A., Yeh, R.-H., and Lawrence, D.S. (2002). Design and synthesis of a fluorescent reporter of protein kinase activity. J. Am. Chem. Soc. *124*, 3840–3841.

Chen, C.-A., Yeh, R.-H., Yan, X., and Lawrence, D.S. (2004). Biosensors of protein kinase action: from in vitro assays to living cells. Biochim. Biophys. Acta *1697*, 39–51.

Chène, P. (2004). Inhibition of the p53-MDM2 interaction: targeting a protein-protein interface. Mol. Cancer Res. MCR *2*, 20–28.

Chesi, M., Bergsagel, P.L., Brents, L.A., Smith, C.M., Gerhard, D.S., and Kuehl, W.M. (1996). Dysregulation of cyclin D1 by translocation into an IgH gamma switch region in two multiple myeloma cell lines [see comments]. Blood *88*, 674–681.

Cheung, T.H., Yu, M.M., Lo, K.W., Yim, S.F., Chung, T.K., and Wong, Y.F. (2001). Alteration of cyclin D1 and CDK4 gene in carcinoma of uterine cervix. Cancer Lett. *166*, 199–206.

Chilosi, M., Doglioni, C., Yan, Z., Lestani, M., Menestrina, F., Sorio, C., Benedetti, A., Vinante, F., Pizzolo, G., and Inghirami, G. (1998). Differential expression of cyclin-dependent kinase 6 in cortical thymocytes and T-cell lymphoblastic lymphoma/leukemia. Am. J. Pathol. *152*, 209–217.

Chin, K.T., Ohki, S.Y., Tang, D., Cheng, H.C., Wang, J.H., and Zhang, M. (1999). Identification and structure characterization of a Cdk inhibitory peptide derived from neuronal-specific Cdk5 activator. J. Biol. Chem. *274*, 7120–7127.

Chin, L., Garraway, L.A., and Fisher, D.E. (2006). Malignant melanoma: genetics and therapeutics in the genomic era. Genes Dev. *20*, 2149–2182.

Christian, B.A., Grever, M.R., Byrd, J.C., and Lin, T.S. (2007). Flavopiridol in the treatment of chronic lymphocytic leukemia. Curr. Opin. Oncol. *19*, 573–578.

Chudakov, D.M., Matz, M.V., Lukyanov, S., and Lukyanov, K.A. (2010). Fluorescent proteins and their applications in imaging living cells and tissues. Physiol. Rev. *90*, 1103–1163.

Ciemerych, M.A., Kenney, A.M., Sicinska, E., Kalaszczynska, I., Bronson, R.T., Rowitch, D.H., Gardner, H., and Sicinski, P. (2002). Development of mice expressing a single D-type cyclin. Genes Dev. *16*, 3277–3289.

Cirillo, D., Pentimalli, F., and Giordano, A. (2011). Peptides or small molecules? Different approaches to develop more effective CDK inhibitors. Curr. Med. Chem. *18*, 2854–2866.

Ciruela, F. (2008). Fluorescence-based methods in the study of protein-protein interactions in living cells. Curr. Opin. Biotechnol. *19*, 338–343.

Clark, L.C., and Lyons, C. (1962). Electrode systems for continuous monitoring in cardiovascular surgery. Ann. N. Y. Acad. Sci. *102*, 29–45.

Cohen, P. (2002). The origins of protein phosphorylation. Nat. Cell Biol. *4*, E127–E130.

Cohen, P., and Alessi, D.R. (2013). Kinase drug discovery--what's next in the field? ACS Chem. Biol. *8*, 96–104.

Coleman, T.R., and Dunphy, W.G. (1994). Cdc2 regulatory factors. Curr. Opin. Cell Biol. *6*, 877–882.

Comstock, C.E.S., Augello, M.A., Benito, R.P., Karch, J., Tran, T.H., Utama, F.E., Tindall, E.A., Wang, Y., Burd, C.J., Groh, E.M., et al. (2009). Cyclin D1 splice variants: polymorphism, risk, and isoform-specific regulation in prostate cancer. Clin. Cancer Res. Off. J. Am. Assoc. Cancer Res. *15*, 5338–5349.

Cooper, M.A. (2002). Optical biosensors in drug discovery. Nat. Rev. Drug Discov. *1*, 515–528.

Corbel, C., Wang, Q., Bousserouel, H., Hamdi, A., Zhang, B., Lozach, O., Ferandin, Y., Tan, V.B.C., Guéritte, F., Colas, P., et al. (2011). First BRET-based screening assay performed in budding yeast leads to the discovery of CDK5/p25 interaction inhibitors. Biotechnol. J. *6*, 860–870.

Corcoran et al. (1999). Dysregulation of cyclin dependent kinase 6 expression in splenic marginal zone lymphoma through chromosome 7q translocations. Publ. Online 17 Novemb. 1999 Doi101038sjonc1203033 *18*.

Corsino, P., Horenstein, N., Ostrov, D., Rowe, T., Law, M., Barrett, A., Aslanidi, G., Cress, W.D., and Law, B. (2009). A novel class of cyclin-dependent kinase inhibitors identified by molecular docking act through a unique mechanism. J. Biol. Chem. *284*, 29945–29955.

Costello, J.F., Plass, C., Arap, W., Chapman, V.M., Held, W.A., Berger, M.S., Huang, H.-J.S., and Cavenee, W.K. (1997). Cyclin-dependent Kinase 6 (CDK6) Amplification in Human Gliomas Identified Using Two-dimensional Separation of Genomic DNA. Cancer Res. *57*, 1250–1254.

Courbet, A., Endy, D., Renard, E., Molina, F., and Bonnet, J. (2015). Detection of pathological biomarkers in human clinical samples via amplifying genetic switches and logic gates. Sci. Transl. Med. *7*, 289ra83.

Croce, C.M. (2008). Oncogenes and Cancer. N. Engl. J. Med. *358*, 502–511.

Crombez, L., Aldrian-Herrada, G., Konate, K., Nguyen, Q.N., McMaster, G.K., Brasseur, R., Heitz, F., and Divita, G. (2009). A new potent secondary amphipathic cell-penetrating peptide for siRNA delivery into mammalian cells. Mol. Ther. J. Am. Soc. Gene Ther. *17*, 95–103.

Dai, Z., Dulyaninova, N.G., Kumar, S., Bresnick, A.R., and Lawrence, D.S. (2007). Visual snapshots of intracellular kinase activity at the onset of mitosis. Chem. Biol. *14*, 1254–1260.

Damayanti, N.P., Parker, L.L., and Irudayaraj, J.M.K. (2013). Fluorescence Lifetime Imaging of Biosensor Peptide Phosphorylation in Single Live Cells. Angew. Chem. Int. Ed. *52*, 3931–3934.

Day, P.J., Cleasby, A., Tickle, I.J., O'Reilly, M., Coyle, J.E., Holding, F.P., McMenamin, R.L., Yon, J., Chopra, R., Lengauer, C., et al. (2009). Crystal structure of human CDK4 in complex with a D-type cyclin. Proc. Natl. Acad. Sci. U. S. A. *106*, 4166–4170.

Deisseroth, K. (2011). Optogenetics. Nat. Methods *8*, 26–29.

Demange, L., Abdellah, F.N., Lozach, O., Ferandin, Y., Gresh, N., Meijer, L., and Galons, H. (2013). Potent inhibitors of CDK5 derived from roscovitine: synthesis, biological evaluation and molecular modelling. Bioorg. Med. Chem. Lett. *23*, 125–131.

Dey, D., and Goswami, T. (2011). Optical Biosensors: A Revolution Towards Quantum Nanoscale Electronics Device Fabrication. BioMed Res. Int. *2011*, e348218.

Dickson, M.A. (2014). Molecular pathways: CDK4 inhibitors for cancer therapy. Clin. Cancer Res. Off. J. Am. Assoc. Cancer Res. *20*, 3379–3383.

Diehl, J.A., Cheng, M., Roussel, M.F., and Sherr, C.J. (1998). Glycogen synthase kinase-3beta regulates cyclin D1 proteolysis and subcellular localization. Genes Dev. *12*, 3499–3511.

Dobashi, Y., Goto, A., Fukayama, M., Abe, A., and Ooi, A. (2004). Overexpression of cdk4/cyclin D1, a possible mediator of apoptosis and an indicator of prognosis in human primary lung carcinoma. Int. J. Cancer J. Int. Cancer *110*, 532–541.

Dudgeon, D.D., Shinde, S., Hua, Y., Shun, T.Y., Lazo, J.S., Strock, C.J., Giuliano, K.A., Taylor, D.L., Johnston, P.A., and Johnston, P.A. (2010). Implementation of a 220,000-compound HCS campaign to identify disruptors of the interaction between p53 and hDM2 and characterization of the confirmed hits. J. Biomol. Screen. *15*, 766–782.

Dumat, B., Bordeau, G., Aranda, A.I., Mahuteau-Betzer, F., Harfouch, Y. El, Metgé, G., Charra, F., Fiorini-Debuisschert, C., and Teulade-Fichou, M.-P. (2012). Vinyl-triphenylamine dyes, a new family of switchable fluorescent probes for targeted two-photon cellular imaging: from DNA to protein labeling. Org. Biomol. Chem. *10*, 6054–6061.

Dumat, B., Bordeau, G., Faurel-Paul, E., Mahuteau-Betzer, F., Saettel, N., Metge, G., Fiorini-Debuisschert, C., Charra, F., and Teulade-Fichou, M.-P. (2013). DNA switches on the two-photon efficiency of an ultrabright triphenylamine fluorescent probe specific of AT regions. J. Am. Chem. Soc. *135*, 12697–12706.

Easton, J., Wei, T., Lahti, J.M., and Kidd, V.J. (1998). Disruption of the cyclin D/cyclin-dependent kinase/INK4/retinoblastoma protein regulatory pathway in human neuroblastoma. Cancer Res. *58*, 2624–2632.

Eglen, R.M., and Reisine, T. (2010). Human kinome drug discovery and the emerging importance of atypical allosteric inhibitors. Expert Opin. Drug Discov. *5*, 277–290.

Esposito, L., Indovina, P., Magnotti, F., Conti, D., and Giordano, A. (2013). Anticancer therapeutic strategies based on CDK inhibitors. Curr. Pharm. Des. *19*, 5327–5332.

Fajas, L. (2013). Re-thinking cell cycle regulators: the cross-talk with metabolism. Front. Oncol. *3*, 4.

Fajas, L., Blanchet, E., and Annicotte, J.-S. (2010). CDK4, pRB and E2F1: connected to insulin. Cell Div. *5*, 6.

Fang, Z., Grütter, C., and Rauh, D. (2013). Strategies for the selective regulation of kinases with allosteric modulators: exploiting exclusive structural features. ACS Chem. Biol. *8*, 58–70.

Fang, Z., Simard, J.R., Plenker, D., Nguyen, H.D., Phan, T., Wolle, P., Baumeister, S., and Rauh, D. (2015). Discovery of Inter-Domain Stabilizers—A Novel Assay System for Allosteric Akt Inhibitors. ACS Chem. Biol. *10*, 279–288.

Fantl, V., Stamp, G., Andrews, A., Rosewell, I., and Dickson, C. (1995). Mice lacking cyclin D1 are small and show defects in eye and mammary gland development. Genes Dev. *9*, 2364–2372.

Feldmann, G., Mishra, A., Bisht, S., Karikari, C., Garrido-Laguna, I., Rasheed, Z., Ottenhof, N.A., Dadon, T., Alvarez, H., Fendrich, V., et al. (2011). Cyclin-dependent kinase inhibitor Dinaciclib (SCH727965) inhibits pancreatic cancer growth and progression in murine xenograft models. Cancer Biol. Ther. *12*, 598–609.

Fiancette, R., Rouaud, P., Vincent-Fabert, C., Laffleur, B., Magnone, V., Cogné, M., and Denizot, Y. (2011). A p53 defect sensitizes various stages of B cell development to lymphomagenesis in mice carrying an IgH 3' regulatory region-driven c-myc transgene. J. Immunol. Baltim. Md 1950 *187*, 5772–5782.

Fischer, P.M., Endicott, J., and Meijer, L. (2003). Cyclin-dependent kinase inhibitors. Prog. Cell Cycle Res. *5*, 235–248.

Fisher, R.P. (2005). Secrets of a double agent: CDK7 in cell-cycle control and transcription. J. Cell Sci. *118*, 5171–5180.

Floquet, N., Costa, M.G.S., Batista, P.R., Renault, P., Bisch, P.M., Raussin, F., Martinez, J., Morris, M.C., and Perahia, D. (2015). Conformational Equilibrium of CDK/Cyclin Complexes by Molecular Dynamics with Excited Normal Modes. Biophys. J.

Förster, T. (1948). Zwischenmolekulare Energiewanderung und Fluoreszenz. Ann. Phys. *437*, 55–75.

Fosbrink, M., Aye-Han, N.-N., Cheong, R., Levchenko, A., and Zhang, J. (2010). Visualization of JNK activity dynamics with a genetically encoded fluorescent biosensor. Proc. Natl. Acad. Sci. U. S. A. *107*, 5459–5464.

Fox, I.J., and Wood, E.H. (1960). Indocyanine green: physical and physiologic properties. Proc. Staff Meet. Mayo Clin. *35*, 732–744.

Fox, I.J., Brooker, L.G., Heseltine, D.W., Essex, H.E., and Wood, E.H. (1957). A tricarbocyanine dye for continuous recording of dilution curves in whole blood independent of variations in blood oxygen saturation. Proc. Staff Meet. Mayo Clin. *32*, 478–484.

Frangioni, J.V. (2003). In vivo near-infrared fluorescence imaging. Curr. Opin. Chem. Biol. *7*, 626–634.

Frangioni, J.V. (2008). New technologies for human cancer imaging. J. Clin. Oncol. Off. J. Am. Soc. Clin. Oncol. *26*, 4012–4021.

Frommer, W.B., Davidson, M.W., and Campbell, R.E. (2009). Genetically encoded biosensors based on engineered fluorescent proteins. Chem. Soc. Rev. *38*, 2833–2841.

Fry, D.W., Bedford, D.C., Harvey, P.H., Fritsch, A., Keller, P.R., Wu, Z., Dobrusin, E., Leopold, W.R., Fattaey, A., and Garrett, M.D. (2001). Cell cycle and biochemical effects of PD 0183812. A potent inhibitor of the cyclin D-dependent kinases CDK4 and CDK6. J. Biol. Chem. *276*, 16617–16623.

Fry, D.W., Harvey, P.J., Keller, P.R., Elliott, W.L., Meade, M., Trachet, E., Albassam, M., Zheng, X., Leopold, W.R., Pryer, N.K., et al. (2004). Specific inhibition of cyclin-dependent kinase 4/6 by PD 0332991 and associated antitumor activity in human tumor xenografts. Mol. Cancer Ther. *3*, 1427–1438.

Gabrielli, B.G., Sarcevic, B., Sinnamon, J., Walker, G., Castellano, M., Wang, X.Q., and Ellem, K.A. (1999). A cyclin D-Cdk4 activity required for G2 phase cell cycle progression is inhibited in ultraviolet radiation-induced G2 phase delay. J. Biol. Chem. *274*, 13961–13969.

Gadbois, D.M., Hamaguchi, J.R., Swank, R.A., and Bradbury, E.M. (1992). Staurosporine is a potent inhibitor of p34cdc2 and p34cdc2-like kinases. Biochem. Biophys. Res. Commun. *184*, 80–85.

Gansauge, S., Gansauge, F., Ramadani, M., Stobbe, H., Rau, B., Harada, N., and Beger, H.G. (1997). Overexpression of Cyclin D1 in Human Pancreatic Carcinoma Is Associated with Poor Prognosis. Cancer Res. *57*, 1634–1637.

García-Alvarez, B., de Cárcer, G., Ibañez, S., Bragado-Nilsson, E., and Montoya, G. (2007). Molecular and structural basis of polo-like kinase 1 substrate recognition: Implications in centrosomal localization. Proc. Natl. Acad. Sci. U. S. A. *104*, 3107–3112.

Garibyan, L., and Fisher, D.E. (2010). How sunlight causes melanoma. Curr. Oncol. Rep. *12*, 319–326.

Garrett, M.D., and Fattaey, A. (1999). CDK inhibition and cancer therapy. Curr. Opin. Genet. Dev. *9*, 104–111.

Gautschi, O., Ratschiller, D., Gugger, M., Betticher, D.C., and Heighway, J. (2007). Cyclin D1 in non-small cell lung cancer: a key driver of malignant transformation. Lung Cancer Amst. Neth. *55*, 1–14.

Gavet, O., and Pines, J. (2010). Progressive activation of CyclinB1-Cdk1 coordinates entry to mitosis. Dev. Cell *18*, 533–543.

Gelbert, L.M., Cai, S., Lin, X., Sanchez-Martinez, C., Del Prado, M., Lallena, M.J., Torres, R., Ajamie, R.T., Wishart, G.N., Flack, R.S., et al. (2014). Preclinical characterization of the CDK4/6 inhibitor LY2835219: in-vivo cell cycle-dependent/independent anti-tumor activities alone/in combination with gemcitabine. Invest. New Drugs.

Gentilucci, L., De Marco, R., and Cerisoli, L. (2010). Chemical modifications designed to improve peptide stability: incorporation of non-natural amino acids, pseudo-peptide bonds, and cyclization. Curr. Pharm. Des. *16*, 3185–3203.

Getlik, M., Simard, J.R., Termathe, M., Grütter, C., Rabiller, M., van Otterlo, W.A.L., and Rauh, D. (2012). Fluorophore Labeled Kinase Detects Ligands That Bind within the MAPK Insert of p38α Kinase. PLoS ONE *7*, e39713.

Giacinti, C., and Giordano, A. (2006). RB and cell cycle progression. Oncogene *25*, 5220–5227.

Giepmans, B.N.G., Adams, S.R., Ellisman, M.H., and Tsien, R.Y. (2006). The fluorescent toolbox for assessing protein location and function. Science *312*, 217–224.

Gilardi, G., Zhou, L.Q., Hibbert, L., and Cass, A.E. (1994). Engineering the maltose binding protein for reagentless fluorescence sensing. Anal. Chem. *66*, 3840–3847.

Gillett, C., Fantl, V., Smith, R., Fisher, C., Bartek, J., Dickson, C., Barnes, D., and Peters, G. (1994). Amplification and Overexpression of Cyclin D1 in Breast Cancer Detected by Immunohistochemical Staining. Cancer Res. *54*, 1812–1817.

Gillies, R.J., Didier, N., and Denton, M. (1986). Determination of cell number in monolayer cultures. Anal. Biochem. *159*, 109–113.

Giordano, A., Bellacchio, E., Bagella, L., and Paggi, M.G. (2007). Interaction between the Cdk2/cyclin A complex and a small molecule derived from the pRb2/p130 spacer domain: a theoretical model. Cell Cycle Georget. Tex *6*, 2591–2593.

Glab, N., Labidi, B., Qin, L.X., Trehin, C., Bergounioux, C., and Meijer, L. (1994). Olomoucine, an inhibitor of the cdc2/cdk2 kinases activity, blocks plant cells at the G1 to S and G2 to M cell cycle transitions. FEBS Lett. *353*, 207–211.

Gondeau, C., Gerbal-Chaloin, S., Bello, P., Aldrian-Herrada, G., Morris, M.C., and Divita, G. (2005). Design of a novel class of peptide inhibitors of cyclin-dependent kinase/cyclin activation. J. Biol. Chem. *280*, 13793–13800.

González-Vera, J.A. (2012). Probing the kinome in real time with fluorescent peptides. Chem. Soc. Rev. *41*, 1652–1664.

Grafstrom, R.H., Pan, W., and Hoess, R.H. (1999). Defining the substrate specificity of cdk4 kinase–cyclin D1 complex. Carcinogenesis *20*, 193–198.

Gray, N.S., Wodicka, L., Thunnissen, A.M., Norman, T.C., Kwon, S., Espinoza, F.H., Morgan, D.O., Barnes, G., LeClerc, S., Meijer, L., et al. (1998). Exploiting chemical libraries, structure, and genomics in the search for kinase inhibitors. Science *281*, 533–538.

Griss, R., Schena, A., Reymond, L., Patiny, L., Werner, D., Tinberg, C.E., Baker, D., and Johnsson, K. (2014). Bioluminescent sensor proteins for point-of-care therapeutic drug monitoring. Nat. Chem. Biol. *10*, 598–603.

Guha, M. (2013). Blockbuster dreams for Pfizer's CDK inhibitor. Nat. Biotechnol. *31*, 187–187.

Gulyani, A., Vitriol, E., Allen, R., Wu, J., Gremyachinskiy, D., Lewis, S., Dewar, B., Graves, L.M., Kay, B.K., Kuhlman, B., et al. (2011). A biosensor generated via high-throughput screening quantifies cell edge Src dynamics. Nat. Chem. Biol. *7*, 437–444.

Haas, K.L., and Franz, K.J. (2009). Application of metal coordination chemistry to explore and manipulate cell biology. Chem. Rev. *109*, 4921–4960.

Hagopian, J.C., Kirtley, M.P., Stevenson, L.M., Gergis, R.M., Russo, A.A., Pavletich, N.P., Parsons, S.M., and Lew, J. (2001). Kinetic basis for activation of CDK2/cyclin A by phosphorylation. J. Biol. Chem. *276*, 275–280.

Hanahan, D., and Weinberg, R.A. (2000). The hallmarks of cancer. Cell *100*, 57–70.

Hanks, S.K. (1987). Homology probing: identification of cDNA clones encoding members of the protein-serine kinase family. Proc. Natl. Acad. Sci. U. S. A. *84*, 388–392.

Hanson, G.T., and Hanson, B.J. (2008). Fluorescent probes for cellular assays. Comb. Chem. High Throughput Screen. *11*, 505–513.

Harper, J.V., and Brooks, G. (2005). The mammalian cell cycle: an overview. Methods Mol. Biol. Clifton NJ *296*, 113–153.

Hartwell, L.H., Culotti, J., Pringle, J.R., and Reid, B.J. (1974). Genetic control of the cell division cycle in yeast. Science *183*, 46–51.

Hayward, N.K. (2003). Genetics of melanoma predisposition. Oncogene *22*, 3053–3062.

He, J., Olson, J.J., and James, C.D. (1995). Lack of p16INK4 or retinoblastoma protein (pRb), or amplification-associated overexpression of cdk4 is observed in distinct subsets of malignant glial tumors and cell lines. Cancer Res. *55*, 4833–4836.

Heim, R., Cubitt, A.B., and Tsien, R.Y. (1995). Improved green fluorescence. Nature *373*, 663–664.

Hermeking, H., Rago, C., Schuhmacher, M., Li, Q., Barrett, J.F., Obaya, A.J., O'Connell, B.C., Mateyak, M.K., Tam, W., Kohlhuber, F., et al. (2000). Identification of CDK4 as a target of c-MYC. Proc. Natl. Acad. Sci. U. S. A. *97*, 2229–2234.

Herschel, J.F.W. (1845a). No. I. On a Case of Superficial Colour Presented by a Homogeneous Liquid Internally Colourless. Philos. Trans. R. Soc. Lond. *135*, 143–145.

Herschel, J.F.W. (1845b). No. II. On the Epipolic Dispersion of Light, Being a Supplement to a Paper Entitled, "On a Case of Superficial Colour Presented by a Homogeneous Liquid Internally Colourless." Philos. Trans. R. Soc. Lond. *135*, 147–153.

Hertzman Johansson, C., and Egyhazi Brage, S. (2014). BRAF inhibitors in cancer therapy. Pharmacol. Ther. *142*, 176–182.

Ho, A., and Dowdy, S.F. (2002). Regulation of G(1) cell-cycle progression by oncogenes and tumor suppressor genes. Curr. Opin. Genet. Dev. *12*, 47–52.

Ho, N., Weissleder, R., and Tung, C.-H. (2006). Development of water-soluble far-red fluorogenic dyes for enzyme sensing. Tetrahedron *62*, 578–585.

Hodgson, J.T., and Darnton, A. (2000). The quantitative risks of mesothelioma and lung cancer in relation to asbestos exposure. Ann. Occup. Hyg. *44*, 565–601.

Hodis, E., Watson, I.R., Kryukov, G.V., Arold, S.T., Imielinski, M., Theurillat, J.-P., Nickerson, E., Auclair, D., Li, L., Place, C., et al. (2012). A landscape of driver mutations in melanoma. Cell *150*, 251–263.

Hoebe, R.A., Van Oven, C.H., Gadella, T.W.J., Dhonukshe, P.B., Van Noorden, C.J.F., and Manders, E.M.M. (2007). Controlled light-exposure microscopy reduces photobleaching and phototoxicity in fluorescence live-cell imaging. Nat. Biotechnol. *25*, 249–253.

Hoessel, R., Leclerc, S., Endicott, J.A., Nobel, M.E., Lawrie, A., Tunnah, P., Leost, M., Damiens, E., Marie, D., Marko, D., et al. (1999). Indirubin, the active constituent of a Chinese antileukaemia medicine, inhibits cyclin-dependent kinases. Nat. Cell Biol. *1*, 60–67.

Horowitz, J.M., Park, S.H., Bogenmann, E., Cheng, J.C., Yandell, D.W., Kaye, F.J., Minna, J.D., Dryja, T.P., and Weinberg, R.A. (1990). Frequent inactivation of the retinoblastoma anti-oncogene is restricted to a subset of human tumor cells. Proc. Natl. Acad. Sci. U. S. A. *87*, 2775–2779.

Hu, F., Wang, K., Zhang, Y., Gou, L., Luo, M., Zhang, X., and Yang, S. (2014). δEF1 upregulates CDK4 transcription via the E2-box element on the CDK4 promoter. Exp. Ther. Med. *7*, 161–164.

Huard, J.M., Forster, C.C., Carter, M.L., Sicinski, P., and Ross, M.E. (1999). Cerebellar histogenesis is disturbed in mice lacking cyclin D2. Dev. Camb. Engl. *126*, 1927–1935.

Iavarone, A., and Massagué, J. (1997). Repression of the CDK activator Cdc25A and cell-cycle arrest by cytokine TGF-beta in cells lacking the CDK inhibitor p15. Nature *387*, 417–422.

Ibraheem, A., and Campbell, R.E. (2010). Designs and applications of fluorescent protein-based biosensors. Curr. Opin. Chem. Biol. *14*, 30–36.

Infante, J.R., Shapiro, G.I., Witteveen, P.O., Gerecitano, J.F., Ribrag, V., Chugh, R., Chakraborty, A., Matano, A., Zhao, X., Parasuraman, S., et al. (2013). Abstract A276: Phase 1 multicenter, open label, dose-escalation study of LEE011, an oral inhibitor of cyclin-dependent kinase 4/6, in patients with advanced solid tumors or lymphomas. Mol. Cancer Ther. *12*, A276–A276.

Inglese, J., Shamu, C.E., and Guy, R.K. (2007). Reporting data from high-throughput screening of small-molecule libraries. Nat. Chem. Biol. *3*, 438–441.

Jabłoński, A. (1933). Efficiency of Anti-Stokes Fluorescence in Dyes.

Jahnke, W., Blommers, M.J.J., Fernández, C., Zwingelstein, C., and Amstutz, R. (2005). Strategies for the NMR-based identification and optimization of allosteric protein kinase inhibitors. Chembiochem Eur. J. Chem. Biol. *6*, 1607–1610.

Jeffrey, P.D., Russo, A.A., Polyak, K., Gibbs, E., Hurwitz, J., Massagué, J., and Pavletich, N.P. (1995). Mechanism of CDK activation revealed by the structure of a cyclinA-CDK2 complex. Nature *376*, 313–320.

Jeffrey, P.D., Tong, L., and Pavletich, N.P. (2000). Structural basis of inhibition of CDK-cyclin complexes by INK4 inhibitors. Genes Dev. *14*, 3115–3125.

Jen, J., Harper, J.W., Bigner, S.H., Bigner, D.D., Papadopoulos, N., Markowitz, S., Willson, J.K., Kinzler, K.W., and Vogelstein, B. (1994). Deletion of p16 and p15 genes in brain tumors. Cancer Res. *54*, 6353–6358.

Jia, Y., Quinn, C.M., Kwak, S., and Talanian, R.V. (2008). Current in vitro kinase assay technologies: the quest for a universal format. Curr. Drug Discov. Technol. *5*, 59–69.

Jirawatnotai, S., Hu, Y., Michowski, W., Elias, J.E., Becks, L., Bienvenu, F., Zagozdzon, A., Goswami, T., Wang, Y.E., Clark, A.B., et al. (2011). A function for cyclin D1 in DNA repair uncovered by protein interactome analyses in human cancers. Nature *474*, 230–234.

Kaldis, P. (1999). The cdk-activating kinase (CAK): from yeast to mammals. Cell. Mol. Life Sci. CMLS *55*, 284–296.

Kawaguchi, K., Oda, Y., Saito, T., Yamamoto, H., Tamiya, S., Takahira, T., Miyajima, K., Iwamoto, Y., and Tsuneyoshi, M. (2003). Mechanisms of inactivation of the p16INK4a gene in leiomyosarcoma of soft tissue: decreased p16 expression correlates with promoter methylation and poor prognosis. J. Pathol. *201*, 487–495.

Kim, J.K., and Diehl, J.A. (2009). Nuclear cyclin D1: an oncogenic driver in human cancer. J. Cell. Physiol. *220*, 292–296.

Kim, S., Loo, A., Chopra, R., Caponigro, G., Huang, A., Vora, S., Parasuraman, S., Howard, S., Keen, N., Sellers, W., et al. (2013). Abstract PR02: LEE011: An orally bioavailable, selective small molecule inhibitor of CDK4/6– Reactivating Rb in cancer. Mol. Cancer Ther. *12*, PR02–PR02.

Kitagawa, M., Okabe, T., Ogino, H., Matsumoto, H., Suzuki-Takahashi, I., Kokubo, T., Higashi, H., Saitoh, S., Taya, Y., and Yasuda, H. (1993). Butyrolactone I, a selective inhibitor of cdk2 and cdc2 kinase. Oncogene *8*, 2425–2432.

Knudsen, K.E., Diehl, J.A., Haiman, C.A., and Knudsen, E.S. (2006). Cyclin D1: polymorphism, aberrant splicing and cancer risk. Oncogene *25*, 1620–1628.

Koide, Y., Urano, Y., Hanaoka, K., Piao, W., Kusakabe, M., Saito, N., Terai, T., Okabe, T., and Nagano, T. (2012). Development of NIR fluorescent dyes based on Si-rhodamine for in vivo imaging. J. Am. Chem. Soc. *134*, 5029–5031.

Kollmann, K., Heller, G., Schneckenleithner, C., Warsch, W., Scheicher, R., Ott, R.G., Schäfer, M., Fajmann, S., Schlederer, M., Schiefer, A.-I., et al. (2013). A Kinase-Independent Function of CDK6 Links the Cell Cycle to Tumor Angiogenesis. Cancer Cell *24*, 167–181.

König, A., Schwartz, G.K., Mohammad, R.M., Katib, A. Al-, and Gabrilove, J.L. (1997). The novel cyclin-dependent kinase inhibitor flavopiridol downregulates Bcl-2 and induces growth arrest and apoptosis in chronic B-cell leukemia lines. Blood *90*, 4307–4312.

Kozar, K., Ciemerych, M.A., Rebel, V.I., Shigematsu, H., Zagozdzon, A., Sicinska, E., Geng, Y., Yu, Q., Bhattacharya, S., Bronson, R.T., et al. (2004). Mouse development and cell proliferation in the absence of D-cyclins. Cell *118*, 477–491.

Kupcho, K., Somberg, R., Bulleit, B., and Goueli, S.A. (2003). A homogeneous, nonradioactive high-throughput fluorogenic protein kinase assay. Anal. Biochem. *317*, 210–217.

Kurzawa, L., Pellerano, M., and Morris, M.C. (2010). PEP and CADY-mediated delivery of fluorescent peptides and proteins into living cells. Biochim. Biophys. Acta *1798*, 2274–2285.

Kurzawa, L., Pellerano, M., Coppolani, J.B., and Morris, M.C. (2011). Fluorescent peptide biosensor for probing the relative abundance of cyclin-dependent kinases in living cells. PloS One *6*, e26555.

LaBaer, J., Garrett, M.D., Stevenson, L.F., Slingerland, J.M., Sandhu, C., Chou, H.S., Fattaey, A., and Harlow, E. (1997). New functional activities for the p21 family of CDK inhibitors. Genes Dev. *11*, 847–862.

Labbe, J.C., Lee, M.G., Nurse, P., Picard, A., and Doree, M. (1988). Activation at M-phase of a protein kinase encoded by a starfish homologue of the cell cycle control gene cdc2+. Nature *335*, 251–254.

Labbe, J.C., Picard, A., Peaucellier, G., Cavadore, J.C., Nurse, P., and Doree, M. (1989). Purification of MPF from starfish: identification as the H1 histone kinase p34cdc2 and a possible mechanism for its periodic activation. Cell *57*, 253–263.

Lakowicz, J.R. (1999). Principles of fluorescence spectroscopy (New York: Kluwer Academic/Plenum).

Lam, E.W., Glassford, J., Banerji, L., Thomas, N.S., Sicinski, P., and Klaus, G.G. (2000). Cyclin D3 compensates for loss of cyclin D2 in mouse B-lymphocytes activated via the antigen receptor and CD40. J. Biol. Chem. *275*, 3479–3484.

Lang, P., Yeow, K., Nichols, A., and Scheer, A. (2006). Cellular imaging in drug discovery. Nat. Rev. Drug Discov. *5*, 343–356.

Lapenna, S., and Giordano, A. (2009). Cell cycle kinases as therapeutic targets for cancer. Nat. Rev. Drug Discov. *8*, 547–566.

Lavis, L.D., and Raines, R.T. (2008). Bright ideas for chemical biology. ACS Chem. Biol. *3*, 142–155.

Lawrence, D.S., and Wang, Q. (2007). Seeing is believing: peptide-based fluorescent sensors of protein tyrosine kinase activity. Chembiochem Eur. J. Chem. Biol. *8*, 373–378.

Lazzaro, F., Giannattasio, M., Puddu, F., Granata, M., Pellicioli, A., Plevani, P., and Muzi-Falconi, M. (2009). Checkpoint mechanisms at the intersection between DNA damage and repair. DNA Repair *8*, 1055–1067.

Lebakken, C.S., Reichling, L.J., Ellefson, J.M., and Riddle, S.M. (2012). Detection of allosteric kinase inhibitors by displacement of active site probes. J. Biomol. Screen. *17*, 813–821.

Lee, T.M.-H. (2008). Over-the-Counter Biosensors: Past, Present, and Future. Sensors *8*, 5535–5559.

Lee, M.G., and Nurse, P. (1987). Complementation used to clone a human homologue of the fission yeast cell cycle control gene cdc2. Nature *327*, 31–35.

Lee, H.-M., Larson, D.R., and Lawrence, D.S. (2009). Illuminating the chemistry of life: design, synthesis, and applications of “caged” and related photoresponsive compounds. ACS Chem. Biol. *4*, 409–427.

Lee, J.O., Russo, A.A., and Pavletich, N.P. (1998). Structure of the retinoblastoma tumour-suppressor pocket domain bound to a peptide from HPV E7. Nature *391*, 859–865.

Lemke, E.A., and Schultz, C. (2011). Principles for designing fluorescent sensors and reporters. Nat. Chem. Biol. *7*, 480–483.

Li, J.-Y., Gaillard, F., Moreau, A., Harousseau, J.-L., Laboisse, C., Milpied, N., Bataille, R., and Avet-Loiseau, H. (1999). Detection of Translocation t(11;14)(q13;q32) in Mantle Cell Lymphoma by Fluorescence in Situ Hybridization. Am. J. Pathol. *154*, 1449–1452.

Li, R., An, S.-J., Chen, Z.-H., Zhang, G.-C., Zhu, J.-Q., Nie, Q., Xie, Z., Guo, A.-L., Mok, T.S., and Wu, Y.-L. (2008). Expression of cyclin D1 splice variants is differentially associated with outcome in non-small cell lung cancer patients. Hum. Pathol. *39*, 1792–1801.

Li, Z., Jiao, X., Wang, C., Shirley, L.A., Elsaleh, H., Dahl, O., Wang, M., Soutoglou, E., Knudsen, E.S., and Pestell, R.G. (2010). Alternative cyclin D1 splice forms differentially regulate the DNA damage response. Cancer Res. *70*, 8802–8811.

Lim, S., and Kaldis, P. (2013). Cdks, cyclins and CKIs: roles beyond cell cycle regulation. Dev. Camb. Engl. *140*, 3079–3093.

Lin, M.Z., McKeown, M.R., Ng, H.-L., Aguilera, T.A., Shaner, N.C., Campbell, R.E., Adams, S.R., Gross, L.A., Ma, W., Alber, T., et al. (2009a). Autofluorescent proteins with excitation in the optical window for intravital imaging in mammals. Chem. Biol. *16*, 1169–1179.

Lin, T.S., Ruppert, A.S., Johnson, A.J., Fischer, B., Heerema, N.A., Andritsos, L.A., Blum, K.A., Flynn, J.M., Jones, J.A., Hu, W., et al. (2009b). Phase II study of flavopiridol in relapsed chronic lymphocytic leukemia demonstrating high response rates in genetically high-risk disease. J. Clin. Oncol. Off. J. Am. Soc. Clin. Oncol. *27*, 6012–6018.

Lippincott-Schwartz, J., and Patterson, G.H. (2003). Development and use of fluorescent protein markers in living cells. Science *300*, 87–91.

Lippincott-Schwartz, J., Snapp, E., and Kenworthy, A. (2001). Studying protein dynamics in living cells. Nat. Rev. Mol. Cell Biol. *2*, 444–456.

Liu, Y., and Gray, N.S. (2006). Rational design of inhibitors that bind to inactive kinase conformations. Nat. Chem. Biol. *2*, 358–364.

Liu, E., Li, X., Yan, F., Zhao, Q., and Wu, X. (2004). Cyclin-dependent kinases phosphorylate human Cdt1 and induce its degradation. J. Biol. Chem. *279*, 17283–17288.

Liu, H., Liu, K., Huang, Z., Park, C.-M., Thimmegowda, N.R., Jang, J.-H., Ryoo, I.-J., He, L., Kim, S.-O., Oi, N., et al. (2013). A chrysin derivative suppresses skin cancer growth by inhibiting cyclin-dependent kinases. J. Biol. Chem. *288*, 25924–25937.

Lodish, H. (2008). Molecular Cell Biology (W. H. Freeman).

Lohka, M.J., Hayes, M.K., and Maller, J.L. (1988). Purification of maturation-promoting factor, an intracellular regulator of early mitotic events. Proc. Natl. Acad. Sci. U. S. A. *85*, 3009–3013.

Lolli, G. (2010). Structural dissection of cyclin dependent kinases regulation and protein recognition properties. Cell Cycle Georget. Tex *9*, 1551–1561.

Long, G.V., Trefzer, U., Davies, M.A., Kefford, R.F., Ascierto, P.A., Chapman, P.B., Puzanov, I., Hauschild, A., Robert, C., Algazi, A., et al. (2012). Dabrafenib in patients with Val600Glu or Val600Lys BRAF-mutant melanoma metastatic to the brain (BREAK-MB): a multicentre, open-label, phase 2 trial. Lancet Oncol. *13*, 1087–1095.

Losiewicz, M.D., Carlson, B.A., Kaur, G., Sausville, E.A., and Worland, P.J. (1994). Potent inhibition of CDC2 kinase activity by the flavonoid L86-8275. Biochem. Biophys. Res. Commun. *201*, 589–595.

Loving, G., and Imperiali, B. (2008). A versatile amino acid analogue of the solvatochromic fluorophore 4-N,N-dimethylamino-1,8-naphthalimide: a powerful tool for the study of dynamic protein interactions. J. Am. Chem. Soc. *130*, 13630–13638.

Loving, G.S., Sainlos, M., and Imperiali, B. (2010). Monitoring protein interactions and dynamics with solvatochromic fluorophores. Trends Biotechnol. *28*, 73–83.

Lu, S., and Wang, Y. (2010). Fluorescence resonance energy transfer biosensors for cancer detection and evaluation of drug efficacy. Clin. Cancer Res. Off. J. Am. Assoc. Cancer Res. *16*, 3822–3824.

Lu, P.J., Zhou, X.Z., Shen, M., and Lu, K.P. (1999). Function of WW domains as phosphoserine- or phosphothreonine-binding modules. Science *283*, 1325–1328.

Lukinavičius, G., Umezawa, K., Olivier, N., Honigmann, A., Yang, G., Plass, T., Mueller, V., Reymond, L., Corrêa, I.R., Luo, Z.-G., et al. (2013). A near-infrared fluorophore for live-cell super-resolution microscopy of cellular proteins. Nat. Chem. *5*, 132–139.

Luković, E., González-Vera, J.A., and Imperiali, B. (2008). Recognition-domain focused chemosensors: versatile and efficient reporters of protein kinase activity. J. Am. Chem. Soc. *130*, 12821–12827.

Luković, E., Vogel Taylor, E., and Imperiali, B. (2009). Monitoring protein kinases in cellular media with highly selective chimeric reporters. Angew. Chem. Int. Ed Engl. *48*, 6828–6831.

Ma, H., Deacon, S., and Horiuchi, K. (2008). The challenge of selecting protein kinase assays for lead discovery optimization. Expert Opin. Drug Discov. *3*, 607–621.

Mahadevan, D., Plummer, R., Squires, M.S., Rensvold, D., Kurtin, S., Pretzinger, C., Dragovich, T., Adams, J., Lock, V., Smith, D.M., et al. (2011). A phase I pharmacokinetic and pharmacodynamic study of AT7519, a cyclin-dependent kinase inhibitor in patients with refractory solid tumors. Ann. Oncol. Off. J. Eur. Soc. Med. Oncol. ESMO *22*, 2137–2143.

Mahony, D., Parry, D.A., and Lees, E. (1998). Active cdk6 complexes are predominantly nuclear and represent only a minority of the cdk6 in T cells. Oncogene *16*, 603–611.

Malumbres, M. (2011). Physiological relevance of cell cycle kinases. Physiol. Rev. *91*, 973–1007.

Malumbres, M., and Barbacid, M. (2001). To cycle or not to cycle: a critical decision in cancer. Nat. Rev. Cancer *1*, 222–231.

Malumbres, M., and Barbacid, M. (2005). Mammalian cyclin-dependent kinases. Trends Biochem. Sci. *30*, 630–641.

Malumbres, M., and Barbacid, M. (2007). Cell cycle kinases in cancer. Curr. Opin. Genet. Dev. *17*, 60–65.

Malumbres, M., Pevarello, P., Barbacid, M., and Bischoff, J.R. (2008). CDK inhibitors in cancer therapy: what is next? Trends Pharmacol. Sci. *29*, 16–21.

Mann, J. (2002). Natural products in cancer chemotherapy: past, present and future. Nat. Rev. Cancer *2*, 143–148.

Marmé, N., Knemeyer, J.-P., Sauer, M., and Wolfrum, J. (2003). Inter- and intramolecular fluorescence quenching of organic dyes by tryptophan. Bioconjug. Chem. *14*, 1133–1139.

Martín, J., Hunt, S.L., Dubus, P., Sotillo, R., Néhmé-Pélluard, F., Magnuson, M.A., Parlow, A.F., Malumbres, M., Ortega, S., and Barbacid, M. (2003). Genetic rescue of Cdk4 null mice restores pancreatic beta-cell proliferation but not homeostatic cell number. Oncogene *22*, 5261–5269.

Martin, N.G., McAndrew, P.C., Eve, P.D., and Garrett, M.D. (2008). Phosphorylation of cyclin dependent kinase 4 on tyrosine 17 is mediated by Src family kinases. FEBS J. *275*, 3099–3109.

Marx, V. (2015). Probes: paths to photostability. Nat. Methods *12*, 187–190.

Matsushime, H., Ewen, M.E., Strom, D.K., Kato, J.Y., Hanks, S.K., Roussel, M.F., and Sherr, C.J. (1992). Identification and properties of an atypical catalytic subunit (p34PSK-J3/cdk4) for mammalian D type G1 cyclins. Cell *71*, 323–334.

Matsuura, I., Denissova, N.G., Wang, G., He, D., Long, J., and Liu, F. (2004). Cyclin-dependent kinases regulate the antiproliferative function of Smads. Nature *430*, 226–231.

Matz, M.V., Fradkov, A.F., Labas, Y.A., Savitsky, A.P., Zaraisky, A.G., Markelov, M.L., and Lukyanov, S.A. (1999). Fluorescent proteins from nonbioluminescent Anthozoa species. Nat. Biotechnol. *17*, 969–973.

MayC Morris (2012). Fluorescent Biosensors for Cancer Cell Imaging and Diagnostics. In Biosensors and Cancer, (Science Publishers), pp. 101–124.

McCann, T.E., Kosaka, N., Koide, Y., Mitsunaga, M., Choyke, P.L., Nagano, T., Urano, Y., and Kobayashi, H. (2011). Activatable optical imaging with a silica-rhodamine based near infrared (SiR700) fluorophore: a comparison with cyanine based dyes. Bioconjug. Chem. *22*, 2531–2538.

McMahon, C., Suthiphongchai, T., DiRenzo, J., and Ewen, M.E. (1999). P/CAF associates with cyclin D1 and potentiates its activation of the estrogen receptor. Proc. Natl. Acad. Sci. U. S. A. *96*, 5382–5387.

McNeil, P.L. (2001). Direct introduction of molecules into cells. Curr. Protoc. Cell Biol. Editor. Board Juan Bonifacino Al *Chapter 20*, Unit 20.1.

Mendoza, N., Fong, S., Marsters, J., Koeppen, H., Schwall, R., and Wickramasinghe, D. (2003). Selective cyclin-dependent kinase 2/cyclin A antagonists that differ from ATP site inhibitors block tumor growth. Cancer Res. *63*, 1020–1024.

Meredith, S.D., Levine, P.A., Burns, J.A., Gaffey, M.J., Boyd, J.C., Weiss, L.M., Erickson, N.L., and Williams, M.E. (1995). Chromosome 11q13 amplification in head and neck squamous cell carcinoma. Association with poor prognosis. Arch. Otolaryngol. Head Neck Surg. *121*, 790–794.

Michalides, R.J., van Veelen, N.M., Kristel, P.M., Hart, A.A., Loftus, B.M., Hilgers, F.J., and Balm, A.J. (1997). Overexpression of cyclin D1 indicates a poor prognosis in squamous cell carcinoma of the head and neck. Arch. Otolaryngol. Head Neck Surg. *123*, 497–502.

Millar, E.K.A., Dean, J.L., McNeil, C.M., O'Toole, S.A., Henshall, S.M., Tran, T., Lin, J., Quong, A., Comstock, C.E.S., Witkiewicz, A., et al. (2009). Cyclin D1b protein expression in breast cancer is independent of cyclin D1a and associated with poor disease outcome. Oncogene *28*, 1812–1820.

Minta, A., Kao, J.P., and Tsien, R.Y. (1989). Fluorescent indicators for cytosolic calcium based on rhodamine and fluorescein chromophores. J. Biol. Chem. *264*, 8171–8178.

Mishra, A., Behera, R.K., Behera, P.K., Mishra, B.K., and Behera, G.B. (2000). Cyanines during the 1990s: A Review. Chem. Rev. *100*, 1973–2012.

Mitchison, T.J. (1989). Polewards microtubule flux in the mitotic spindle: evidence from photoactivation of fluorescence. J. Cell Biol. *109*, 637–652.

Miyawaki, A., Llopis, J., Heim, R., McCaffery, J.M., Adams, J.A., Ikura, M., and Tsien, R.Y. (1997). Fluorescent indicators for Ca2+based on green fluorescent proteins and calmodulin. Nature *388*, 882–887.

Mizutani, T., Kondo, T., Darmanin, S., Tsuda, M., Tanaka, S., Tobiume, M., Asaka, M., and Ohba, Y. (2010). A novel FRET-based biosensor for the measurement of BCR-ABL activity and its response to drugs in living cells. Clin. Cancer Res. Off. J. Am. Assoc. Cancer Res. *16*, 3964–3975.

Molenaar, J.J., Koster, J., Ebus, M.E., van Sluis, P., Westerhout, E.M., de Preter, K., Gisselsson, D., Øra, I., Speleman, F., Caron, H.N., et al. (2012). Copy number defects of G1-cell cycle genes in neuroblastoma are frequent and correlate with high expression of E2F target genes and a poor prognosis. Genes. Chromosomes Cancer *51*, 10–19.

Moons, D.S., Jirawatnotai, S., Parlow, A.F., Gibori, G., Kineman, R.D., and Kiyokawa, H. (2002). Pituitary hypoplasia and lactotroph dysfunction in mice deficient for cyclin-dependent kinase-4. Endocrinology *143*, 3001–3008.

Moore, J.D. (2013). In the wrong place at the wrong time: does cyclin mislocalization drive oncogenic transformation? Nat. Rev. Cancer *13*, 201–208.

Moreno-Bueno, G., Rodríguez-Perales, S., Sánchez-Estévez, C., Marcos, R., Hardisson, D., Cigudosa, J.C., and Palacios, J. (2004). Molecular alterations associated with cyclin d1 overexpression in endometrial cancer. Int. J. Cancer *110*, 194–200.

Morgan, D.O. (1995). Principles of CDK regulation. Nature *374*, 131–134.

Morgan, D.O. (1997). Cyclin-dependent kinases: engines, clocks, and microprocessors. Annu. Rev. Cell Dev. Biol. *13*, 261–291.

Morris, M.C. (2010). Fluorescent biosensors of intracellular targets from genetically encoded reporters to modular polypeptide probes. Cell Biochem. Biophys. *56*, 19–37.

Morris, M.C. (2013). Fluorescent biosensors - probing protein kinase function in cancer and drug discovery. Biochim. Biophys. Acta *1834*, 1387–1395.

Morris, M.C., Gondeau, C., Tainer, J.A., and Divita, G. (2002). Kinetic mechanism of activation of the Cdk2/cyclin A complex. Key role of the C-lobe of the Cdk. J. Biol. Chem. *277*, 23847–23853.

Mueller, P.R., Coleman, T.R., Kumagai, A., and Dunphy, W.G. (1995). Myt1: A Membrane-Associated Inhibitory Kinase That Phosphorylates Cdc2 on Both Threonine-14 and Tyrosine-15. Science *270*, 86–90.

Musgrove, E.A., Caldon, C.E., Barraclough, J., Stone, A., and Sutherland, R.L. (2011). Cyclin D as a therapeutic target in cancer. Nat. Rev. Cancer *11*, 558–572.

Nagasawa, M., Melamed, I., Kupfer, A., Gelfand, E.W., and Lucas, J.J. (1997). Rapid nuclear translocation and increased activity of cyclin-dependent kinase 6 after T cell activation. J. Immunol. *158*, 5146–5154.

Nagasawa, M., Gelfand, E.W., and Lucas, J.J. (2001). Accumulation of high levels of the p53 and p130 growth-suppressing proteins in cell lines stably over-expressing cyclin-dependent kinase 6 (cdk6). Oncogene *20*, 2889–2899.

Nalbant, P., Hodgson, L., Kraynov, V., Toutchkine, A., and Hahn, K.M. (2004). Activation of endogenous Cdc42 visualized in living cells. Science *305*, 1615–1619.

Narasimha, A.M., Kaulich, M., Shapiro, G.S., Choi, Y.J., Sicinski, P., and Dowdy, S.F. (2014). Cyclin D activates the Rb tumor suppressor by mono-phosphorylation. eLife e02872.

Nhu Ngoc Van, T., and Morris, M.C. (2013). Fluorescent sensors of protein kinases: from basics to biomedical applications. Prog. Mol. Biol. Transl. Sci. *113*, 217–274.

Noble, M., Barrett, P., Endicott, J., Johnson, L., McDonnell, J., Robertson, G., and Zawaira, A. (2005). Exploiting structural principles to design cyclin-dependent kinase inhibitors. Biochim. Biophys. Acta *1754*, 58–64.

Nurse, P. (1975). Genetic control of cell size at cell division in yeast. Nature *256*, 547–551.

O'Dowd, B.F., Alijaniaram, M., Ji, X., Nguyen, T., Eglen, R.M., and George, S.R. (2007). Using ligand-induced conformational change to screen for compounds targeting G-protein-coupled receptors. J. Biomol. Screen. *12*, 175–185.

Orlando, S., Gallastegui, E., Besson, A., Abril, G., Aligué, R., Pujol, M.J., and Bachs, O. (2015). p27Kip1 and p21Cip1 collaborate in the regulation of transcription by recruiting cyclin-Cdk complexes on the promoters of target genes. Nucleic Acids Res. *43*, 6860–6873.

Ormö, M., Cubitt, A.B., Kallio, K., Gross, L.A., Tsien, R.Y., and Remington, S.J. (1996). Crystal structure of the Aequorea victoria green fluorescent protein. Science *273*, 1392–1395.

Orzáez, M., Gortat, A., Mondragón, L., Bachs, O., and Pérez-Payá, E. (2009). ATP-noncompetitive inhibitors of CDK-cyclin complexes. ChemMedChem *4*, 19–24.

Pakhomov, A.A., and Martynov, V.I. (2008). GFP family: structural insights into spectral tuning. Chem. Biol. *15*, 755–764.

Pardee, A.B. (1974). A Restriction Point for Control of Normal Animal Cell Proliferation. Proc. Natl. Acad. Sci. U. S. A. *71*, 1286–1290.

Park, S., Lee, J., Do, I.-G., Jang, J., Rho, K., Ahn, S., Maruja, L., Kim, S.J., Kim, K.-M., Mao, M., et al. (2014). Aberrant CDK4 Amplification in Refractory Rhabdomyosarcoma as Identified by Genomic Profiling. Sci. Rep. *4*.

Parker, L.L., and Piwnica-Worms, H. (1992). Inactivation of the p34cdc2-cyclin B complex by the human WEE1 tyrosine kinase. Science *257*, 1955–1957.

Parry, D., Guzi, T., Shanahan, F., Davis, N., Prabhavalkar, D., Wiswell, D., Seghezzi, W., Paruch, K., Dwyer, M.P., Doll, R., et al. (2010). Dinaciclib (SCH 727965), a novel and potent cyclin-dependent kinase inhibitor. Mol. Cancer Ther. *9*, 2344–2353.

Paruch, K., Dwyer, M.P., Alvarez, C., Brown, C., Chan, T.-Y., Doll, R.J., Keertikar, K., Knutson, C., McKittrick, B., Rivera, J., et al. (2010). Discovery of Dinaciclib (SCH 727965): A Potent and Selective Inhibitor of Cyclin-Dependent Kinases. ACS Med. Chem. Lett. *1*, 204–208.

Patel, A., Cholkar, K., and Mitra, A.K. (2014). Recent developments in protein and peptide parenteral delivery approaches. Ther. Deliv. *5*, 337–365.

Patel, V., Senderowicz, A.M., Pinto, D., Igishi, T., Raffeld, M., Quintanilla-Martinez, L., Ensley, J.F., Sausville, E.A., and Gutkind, J.S. (1998). Flavopiridol, a novel cyclin-dependent kinase inhibitor, suppresses the growth of head and neck squamous cell carcinomas by inducing apoptosis. J. Clin. Invest. *102*, 1674–1681.

Pavey, S., Russell, T., and Gabrielli, B. (2001). G2 phase cell cycle arrest in human skin following UV irradiation. Oncogene *20*, 6103–6110.

Peng, X., Yang, Z., Wang, J., Fan, J., He, Y., Song, F., Wang, B., Sun, S., Qu, J., Qi, J., et al. (2011). Fluorescence ratiometry and fluorescence lifetime imaging: using a single molecular sensor for dual mode imaging of cellular viscosity. J. Am. Chem. Soc. *133*, 6626–6635.

Peyressatre, M., Prével, C., Pellerano, M., and Morris, M.C. (2015). Targeting cyclin-dependent kinases in human cancers: from small molecules to Peptide inhibitors. Cancers *7*, 179–237.

Piljic, A., and Schultz, C. (2008). Simultaneous recording of multiple cellular events by FRET. ACS Chem. Biol. *3*, 156–160.

Pinyol, M., Cobo, F., Bea, S., Jares, P., Nayach, I., Fernandez, P.L., Montserrat, E., Cardesa, A., and Campo, E. (1998). p16(INK4a) gene inactivation by deletions, mutations, and hypermethylation is associated with transformed and aggressive variants of non-Hodgkin's lymphomas. Blood *91*, 2977–2984.

Pommier, Y., and Cherfils, J. (2005). Interfacial inhibition of macromolecular interactions: nature's paradigm for drug discovery. Trends Pharmacol. Sci. *26*, 138–145.

Prével, C., Kurzawa, L., Van, T.N.N., and Morris, M.C. (2014a). Fluorescent biosensors for drug discovery new tools for old targets - Screening for inhibitors of cyclin-dependent kinases. Eur. J. Med. Chem. *88*, 74–88.

Prével, C., Pellerano, M., Van, T.N.N., and Morris, M.C. (2014b). Fluorescent biosensors for high throughput screening of protein kinase inhibitors. Biotechnol. J. *9*, 253–265.

Puyol, M., Martín, A., Dubus, P., Mulero, F., Pizcueta, P., Khan, G., Guerra, C., Santamaría, D., and Barbacid, M. (2010). A synthetic lethal interaction between K-Ras oncogenes and Cdk4 unveils a therapeutic strategy for non-small cell lung carcinoma. Cancer Cell *18*, 63–73.

Rader, J., Russell, M.R., Hart, L.S., Nakazawa, M.S., Belcastro, L.T., Martinez, D., Li, Y., Carpenter, E.L., Attiyeh, E.F., Diskin, S.J., et al. (2013). Dual CDK4/CDK6 inhibition induces cell-cycle arrest and senescence in neuroblastoma. Clin. Cancer Res. Off. J. Am. Assoc. Cancer Res. *19*, 6173–6182.

Rane, S.G., Dubus, P., Mettus, R.V., Galbreath, E.J., Boden, G., Reddy, E.P., and Barbacid, M. (1999). Loss of Cdk4 expression causes insulin-deficient diabetes and Cdk4 activation results in beta-islet cell hyperplasia. Nat. Genet. *22*, 44–52.

Reddy, M.V.R., Akula, B., Cosenza, S.C., Athuluridivakar, S., Mallireddigari, M.R., Pallela, V.R., Billa, V.K., Subbaiah, D.R.C.V., Bharathi, E.V., Vasquez-Del Carpio, R., et al. (2014). Discovery of 8-cyclopentyl-2-[4-(4-methyl-piperazin-1-yl)-phenylamino]-7-oxo-7,8-dihydro-pyrido[2,3-d]pyrimidine-6-carbonitrile (7x) as a potent inhibitor of cyclin-dependent kinase 4 (CDK4) and AMPK-related kinase 5 (ARK5). J. Med. Chem. *57*, 578–599.

Reichardt, C. (1994). Solvatochromic Dyes as Solvent Polarity Indicators. Chem. Rev. *94*, 2319–2358.

Roberts, P.J., Bisi, J.E., Strum, J.C., Combest, A.J., Darr, D.B., Usary, J.E., Zamboni, W.C., Wong, K.-K., Perou, C.M., and Sharpless, N.E. (2012). Multiple roles of cyclin-dependent kinase 4/6 inhibitors in cancer therapy. J. Natl. Cancer Inst. *104*, 476–487.

Rocco, J.W., and Sidransky, D. (2001). p16(MTS-1/CDKN2/INK4a) in Cancer Progression. Exp. Cell Res. *264*, 42–55.

Romoser, V.A., Hinkle, P.M., and Persechini, A. (1997). Detection in living cells of Ca2+-dependent changes in the fluorescence emission of an indicator composed of two green fluorescent protein variants linked by a calmodulin-binding sequence. A new class of fluorescent indicators. J. Biol. Chem. *272*, 13270–13274.

Rubin, C.S., and Rosen, O.M. (1975). Protein phosphorylation. Annu. Rev. Biochem. *44*, 831–887.

Russo, A.A., Jeffrey, P.D., and Pavletich, N.P. (1996). Structural basis of cyclin-dependent kinase activation by phosphorylation. Nat. Struct. Biol. *3*, 696–700.

Sagona, A.P., and Stenmark, H. (2010). Cytokinesis and cancer. FEBS Lett. *584*, 2652–2661.

Sanchez-Martinez, C., Gelbert, L.M., Shannon, H., Dios, A.D., Staton, B.A., Ajamie, R.T., Sawada, G., Wishart, G.N., and Raub, T.J. (2011). Abstract B234: LY2835219, a potent oral inhibitor of the cyclin-dependent kinases 4 and 6 (CDK4/6) that crosses the blood-brain barrier and demonstrates in vivo activity against intracranial human brain tumor xenografts. Mol. Cancer Ther. *10*, B234–B234.

Santamaría, D., Barrière, C., Cerqueira, A., Hunt, S., Tardy, C., Newton, K., Cáceres, J.F., Dubus, P., Malumbres, M., and Barbacid, M. (2007). Cdk1 is sufficient to drive the mammalian cell cycle. Nature *448*, 811–815.

Santo, L., Vallet, S., Hideshima, T., Cirstea, D., Ikeda, H., Pozzi, S., Patel, K., Okawa, Y., Gorgun, G., Perrone, G., et al. (2010). AT7519, A novel small molecule multi-cyclin-dependent kinase inhibitor, induces apoptosis in multiple myeloma via GSK-3beta activation and RNA polymerase II inhibition. Oncogene *29*, 2325–2336.

Sarruf, D.A., Iankova, I., Abella, A., Assou, S., Miard, S., and Fajas, L. (2005). Cyclin D3 promotes adipogenesis through activation of peroxisome proliferator-activated receptor gamma. Mol. Cell. Biol. *25*, 9985–9995.

Satyanarayana, A., and Kaldis, P. (2009). Mammalian cell-cycle regulation: several Cdks, numerous cyclins and diverse compensatory mechanisms. Oncogene *28*, 2925–2939.

Sausville, E.A. (2002). Complexities in the development of cyclin-dependent kinase inhibitor drugs. Trends Mol. Med. *8*, S32–S37.

Schachter, M.M., Merrick, K.A., Larochelle, S., Hirschi, A., Zhang, C., Shokat, K.M., Rubin, S.M., and Fisher, R.P. (2013). A Cdk7-Cdk4 T-loop phosphorylation cascade promotes G1 progression. Mol. Cell *50*, 250–260.

Schmidt, E.E., Ichimura, K., Reifenberger, G., and Collins, V.P. (1994). CDKN2 (p16/MTS1) Gene Deletion or CDK4 Amplification Occurs in the Majority of Glioblastomas. Cancer Res. *54*, 6321–6324.

Schneider, R., Becker, C., Simard, J.R., Getlik, M., Bohlke, N., Janning, P., and Rauh, D. (2012). Direct binding assay for the detection of type IV allosteric inhibitors of Abl. J. Am. Chem. Soc. *134*, 9138–9141.

Seong, J., Chung, E.J., Kim, H., Kim, G.E., Kim, N.K., Sohn, S.K., Min, J.S., and Suh, C.O. (1999). Assessment of biomarkers in paired primary and recurrent colorectal adenocarcinomas. Int. J. Radiat. Oncol. *45*, 1167–1173.

Shang, Y. (2007). Hormones and cancer. Cell Res. *17*, 277–279.

Sharma, V., Agnes, R.S., and Lawrence, D.S. (2007). Deep quench: an expanded dynamic range for protein kinase sensors. J. Am. Chem. Soc. *129*, 2742–2743.

Sharma, V., Wang, Q., and Lawrence, D.S. (2008). Peptide-based fluorescent sensors of protein kinase activity: design and applications. Biochim. Biophys. Acta *1784*, 94–99.

Shcherbakova, D.M., Subach, O.M., and Verkhusha, V.V. (2012). Red fluorescent proteins: advanced imaging applications and future design. Angew. Chem. Int. Ed Engl. *51*, 10724–10738.

Shcherbo, D., Shemiakina, I.I., Ryabova, A.V., Luker, K.E., Schmidt, B.T., Souslova, E.A., Gorodnicheva, T.V., Strukova, L., Shidlovskiy, K.M., Britanova, O.V., et al. (2010). Near-infrared fluorescent proteins. Nat. Methods *7*, 827–829.

Shen, R., Wang, X., Drissi, H., Liu, F., O'Keefe, R.J., and Chen, D. (2006). Cyclin D1-cdk4 induce runx2 ubiquitination and degradation. J. Biol. Chem. *281*, 16347–16353.

Sheppard, K.E., and McArthur, G.A. (2013). The cell-cycle regulator CDK4: an emerging therapeutic target in melanoma. Clin. Cancer Res. Off. J. Am. Assoc. Cancer Res. *19*, 5320–5328.

Sherr, C.J. (1996). Cancer cell cycles. Science *274*, 1672–1677.

Sherr, C.J., and Roberts, J.M. (1999). CDK inhibitors: positive and negative regulators of G1-phase progression. Genes Dev. *13*, 1501–1512.

Sherr, C.J., and Roberts, J.M. (2004). Living with or without cyclins and cyclin-dependent kinases. Genes Dev. *18*, 2699–2711.

Shimomura, O., Johnson, F.H., and Saiga, Y. (1962). Extraction, Purification and Properties of Aequorin, a Bioluminescent Protein from the Luminous Hydromedusan, Aequorea. J. Cell. Comp. Physiol. *59*, 223–239.

Shukla, V., Zheng, Y.-L., Mishra, S.K., Amin, N.D., Steiner, J., Grant, P., Kesavapany, S., and Pant, H.C. (2013). A truncated peptide from p35, a Cdk5 activator, prevents Alzheimer's disease phenotypes in model mice. FASEB J. Off. Publ. Fed. Am. Soc. Exp. Biol. *27*, 174–186.

Shults, M.D., Pearce, D.A., and Imperiali, B. (2003). Modular and tunable chemosensor scaffold for divalent zinc. J. Am. Chem. Soc. *125*, 10591–10597.

Shults, M.D., Janes, K.A., Lauffenburger, D.A., and Imperiali, B. (2005). A multiplexed homogeneous fluorescence-based assay for protein kinase activity in cell lysates. Nat. Methods *2*, 277–283.

Shults, M.D., Carrico-Moniz, D., and Imperiali, B. (2006). Optimal Sox-based fluorescent chemosensor design for serine/threonine protein kinases. Anal. Biochem. *352*, 198–207.

Sicinska, E., Aifantis, I., Le Cam, L., Swat, W., Borowski, C., Yu, Q., Ferrando, A.A., Levin, S.D., Geng, Y., Boehmer, H. von, et al. (2003). Requirement for cyclin D3 in lymphocyte development and T cell leukemias. Cancer Cell *4*, 451–461.

Sicinski, P., Donaher, J.L., Parker, S.B., Li, T., Fazeli, A., Gardner, H., Haslam, S.Z., Bronson, R.T., Elledge, S.J., and Weinberg, R.A. (1995). Cyclin D1 provides a link between development and oncogenesis in the retina and breast. Cell *82*, 621–630.

Sicinski, P., Donaher, J.L., Geng, Y., Parker, S.B., Gardner, H., Park, M.Y., Robker, R.L., Richards, J.S., McGinnis, L.K., Biggers, J.D., et al. (1996). Cyclin D2 is an FSH-responsive gene involved in gonadal cell proliferation and oncogenesis. Nature *384*, 470–474.

Simard, J.R., Grütter, C., Pawar, V., Aust, B., Wolf, A., Rabiller, M., Wulfert, S., Robubi, A., Klüter, S., Ottmann, C., et al. (2009a). High-throughput screening to identify inhibitors which stabilize inactive kinase conformations in p38alpha. J. Am. Chem. Soc. *131*, 18478–18488.

Simard, J.R., Getlik, M., Grütter, C., Pawar, V., Wulfert, S., Rabiller, M., and Rauh, D. (2009b). Development of a fluorescent-tagged kinase assay system for the detection and characterization of allosteric kinase inhibitors. J. Am. Chem. Soc. *131*, 13286–13296.

Simard, J.R., Klüter, S., Grütter, C., Getlik, M., Rabiller, M., Rode, H.B., and Rauh, D. (2009c). A new screening assay for allosteric inhibitors of cSrc. Nat. Chem. Biol. *5*, 394–396.

Simard, J.R., Getlik, M., Grütter, C., Schneider, R., Wulfert, S., and Rauh, D. (2010). Fluorophore labeling of the glycine-rich loop as a method of identifying inhibitors that bind to active and inactive kinase conformations. J. Am. Chem. Soc. *132*, 4152–4160.

Sittampalam, G.S., Kahl, S.D., and Janzen, W.P. (1997). High-throughput screening: advances in assay technologies. Curr. Opin. Chem. Biol. *1*, 384–391.

Smalley, K.S.M., Contractor, R., Nguyen, T.K., Xiao, M., Edwards, R., Muthusamy, V., King, A.J., Flaherty, K.T., Bosenberg, M., Herlyn, M., et al. (2008). Identification of a novel subgroup of melanomas with KIT/cyclin-dependent kinase-4 overexpression. Cancer Res. *68*, 5743–5752.

Sokolov, A.N., Roberts, M.E., and Bao, Z. (2009). Fabrication of low-cost electronic biosensors. Mater. Today *12*, 12–20.

Solvason, N., Wu, W.W., Parry, D., Mahony, D., Lam, E.W., Glassford, J., Klaus, G.G., Sicinski, P., Weinberg, R., Liu, Y.J., et al. (2000). Cyclin D2 is essential for BCR-mediated proliferation and CD5 B cell development. Int. Immunol. *12*, 631–638.

Sotillo, R., Dubus, P., Martín, J., la Cueva, E. de, Ortega, S., Malumbres, M., and Barbacid, M. (2001a). Wide spectrum of tumors in knock-in mice carrying a Cdk4 protein insensitive to INK4 inhibitors. EMBO J. *20*, 6637–6647.

Sotillo, R., García, J.F., Ortega, S., Martin, J., Dubus, P., Barbacid, M., and Malumbres, M. (2001b). Invasive melanoma in Cdk4-targeted mice. Proc. Natl. Acad. Sci. U. S. A. *98*, 13312–13317.

Sotillo, R., Renner, O., Dubus, P., Ruiz-Cabello, J., Martín-Caballero, J., Barbacid, M., Carnero, A., and Malumbres, M. (2005). Cooperation between Cdk4 and p27kip1 in tumor development: a preclinical model to evaluate cell cycle inhibitors with therapeutic activity. Cancer Res. *65*, 3846–3852.

Squires, M.S., Feltell, R.E., Wallis, N.G., Lewis, E.J., Smith, D.-M., Cross, D.M., Lyons, J.F., and Thompson, N.T. (2009). Biological characterization of AT7519, a small-molecule inhibitor of cyclin-dependent kinases, in human tumor cell lines. Mol. Cancer Ther. *8*, 324–332.

Squires, M.S., Cooke, L., Lock, V., Qi, W., Lewis, E.J., Thompson, N.T., Lyons, J.F., and Mahadevan, D. (2010). AT7519, a cyclin-dependent kinase inhibitor, exerts its effects by transcriptional inhibition in leukemia cell lines and patient samples. Mol. Cancer Ther. *9*, 920–928.

Stains, C.I., Luković, E., and Imperiali, B. (2011). A p38α-selective chemosensor for use in unfractionated cell lysates. ACS Chem. Biol. *6*, 101–105.

Stokes, G.G. (1852). On the Change of Refrangibility of Light. Philos. Trans. R. Soc. Lond. *142*, 463–562.

Stryer, L., and Haugland, R.P. (1967). Energy transfer: a spectroscopic ruler. Proc. Natl. Acad. Sci. U. S. A. *58*, 719–726.

Su, L., Jia, W., Hou, C., and Lei, Y. (2011). Microbial biosensors: A review. Biosens. Bioelectron. *26*, 1788–1799.

Subach, F.V., Piatkevich, K.D., and Verkhusha, V.V. (2011). Directed molecular evolution to design advanced red fluorescent proteins. Nat. Methods *8*, 1019–1026.

Sui, Y., and Wu, Z. (2007). Alternative statistical parameter for high-throughput screening assay quality assessment. J. Biomol. Screen. *12*, 229–234.

Sun, W., and Yang, J. (2010). Functional mechanisms for human tumor suppressors. J. Cancer *1*, 136–140.

Sundaram, J.R., Poore, C.P., Sulaimee, N.H.B., Pareek, T., Asad, A.B.M.A., Rajkumar, R., Cheong, W.F., Wenk, M.R., Dawe, G.S., Chuang, K.-H., et al. (2013). Specific inhibition of p25/Cdk5 activity by the Cdk5 inhibitory peptide reduces neurodegeneration in vivo. J. Neurosci. Off. J. Soc. Neurosci. *33*, 334–343.

Takaki, T., Echalier, A., Brown, N.R., Hunt, T., Endicott, J.A., and Noble, M.E.M. (2009). The structure of CDK4/cyclin D3 has implications for models of CDK activation. Proc. Natl. Acad. Sci. U. S. A. *106*, 4171–4176.

Tamaoki, T., Nomoto, H., Takahashi, I., Kato, Y., Morimoto, M., and Tomita, F. (1986). Staurosporine, a potent inhibitor of phospholipidCa++dependent protein kinase. Biochem. Biophys. Res. Commun. *135*, 397–402.

Tarrant, M.K., and Cole, P.A. (2009). The chemical biology of protein phosphorylation. Annu. Rev. Biochem. *78*, 797–825.

Taylor, D.L. (2010). A personal perspective on high-content screening (HCS): from the beginning. J. Biomol. Screen. *15*, 720–725.

Teale, F.W.J., and Weber, G. (1957). Ultraviolet fluorescence of the aromatic amino acids. Biochem. J. *65*, 476–482.

Terada, Y., Tatsuka, M., Jinno, S., and Okayama, H. (1995). Requirement for tyrosine phosphorylation of Cdk4 in G1 arrest induced by ultraviolet irradiation. Nature *376*, 358–362.

Tian, H., Ip, L., Luo, H., Chang, D.C., and Luo, K.Q. (2007). A high throughput drug screen based on fluorescence resonance energy transfer (FRET) for anticancer activity of compounds from herbal medicine. Br. J. Pharmacol. *150*, 321–334.

Tiemann, K., Alluin, J.V., Honegger, A., Chomchan, P., Gaur, S., Yun, Y., Forman, S.J., Rossi, J.J., and Chen, R.W. (2011). siRNAs targeting cyclin D1 and cyclin D2 enhance the cytotoxicity of chemotherapeutic agents in mantle cell lymphoma cell lines. Leuk. Lymphoma *52*, 2148–2154.

Ting, A.Y., Kain, K.H., Klemke, R.L., and Tsien, R.Y. (2001). Genetically encoded fluorescent reporters of protein tyrosine kinase activities in living cells. Proc. Natl. Acad. Sci. U. S. A. *98*, 15003–15008.

Toogood, P.L., Harvey, P.J., Repine, J.T., Sheehan, D.J., VanderWel, S.N., Zhou, H., Keller, P.R., McNamara, D.J., Sherry, D., Zhu, T., et al. (2005). Discovery of a potent and selective inhibitor of cyclin-dependent kinase 4/6. J. Med. Chem. *48*, 2388–2406.

Tos, A.P. Dei, Doglioni, C., Piccinin, S., Sciot, R., Furlanetto, A., Boiocchi, M., Dal Cin, P., Maestro, R., Fletcher, C.D., and Tallini, G. (2000). Coordinated expression and amplification of the MDM2, CDK4, and HMGI-C genes in atypical lipomatous tumours. J. Pathol. *190*, 531–536.

Tsao, H., Chin, L., Garraway, L.A., and Fisher, D.E. (2012). Melanoma: from mutations to medicine. Genes Dev. *26*, 1131–1155.

Tsutsui, T., Hesabi, B., Moons, D.S., Pandolfi, P.P., Hansel, K.S., Koff, A., and Kiyokawa, H. (1999). Targeted disruption of CDK4 delays cell cycle entry with enhanced p27(Kip1) activity. Mol. Cell. Biol. *19*, 7011–7019.

Tunceroglu, A., Matsuda, M., and Birge, R.B. (2010). Real-time fluorescent resonance energy transfer analysis to monitor drug resistance in chronic myelogenous leukemia. Mol. Cancer Ther. *9*, 3065–3073.

Turner, A.P.F. (2013). Biosensors: sense and sensibility. Chem. Soc. Rev. *42*, 3184–3196.

Ueki, K., Ono, Y., Henson, J.W., Efird, J.T., Deimling, A. von, and Louis, D.N. (1996). CDKN2/p16 or RB alterations occur in the majority of glioblastomas and are inversely correlated. Cancer Res. *56*, 150–153.

Utikal, J., Schadendorf, D., and Ugurel, S. (2007). Serologic and immunohistochemical prognostic biomarkers of cutaneous malignancies. Arch. Dermatol. Res. *298*, 469–477.

Van, T.N.N., Pellerano, M., Lykaso, S., and Morris, M.C. (2014). Fluorescent Protein Biosensor for Probing CDK/Cyclin Activity in vitro and in Living Cells. Chembiochem Eur. J. Chem. Biol.

VanArsdale, T., Boshoff, C., Arndt, K.T., and Abraham, R.T. (2015). Molecular Pathways: Targeting the Cyclin D–CDK4/6 Axis for Cancer Treatment. Clin. Cancer Res.

VanEngelenburg, S.B., and Palmer, A.E. (2008). Fluorescent biosensors of protein function. Curr. Opin. Chem. Biol. *12*, 60–65.

Veldhuyzen, W.F., Nguyen, Q., McMaster, G., and Lawrence, D.S. (2003). A light-activated probe of intracellular protein kinase activity. J. Am. Chem. Soc. *125*, 13358–13359.

Versteeg, H.H., Nijhuis, E., van den Brink, G.R., Evertzen, M., Pynaert, G.N., van Deventer, S.J., Coffer, P.J., and Peppelenbosch, M.P. (2000). A new phosphospecific cell-based ELISA for p42/p44 mitogen-activated protein kinase (MAPK), p38 MAPK, protein kinase B and cAMP-response-element-binding protein. Biochem. J. *350 Pt 3*, 717–722.

Vidwans, S.J., Flaherty, K.T., Fisher, D.E., Tenenbaum, J.M., Travers, M.D., and Shrager, J. (2011). A melanoma molecular disease model. PloS One *6*, e18257.

Vincent-Fabert, C., Fiancette, R., Rouaud, P., Baudet, C., Truffinet, V., Magnone, V., Guillaudeau, A., Cogné, M., Dubus, P., and Denizot, Y. (2012). A defect of the INK4-Cdk4 checkpoint and Myc collaborate in blastoid mantle cell lymphoma-like lymphoma formation in mice. Am. J. Pathol. *180*, 1688–1701.

Violin, J.D., Zhang, J., Tsien, R.Y., and Newton, A.C. (2003). A genetically encoded fluorescent reporter reveals oscillatory phosphorylation by protein kinase C. J. Cell Biol. *161*, 899–909.

Vogelstein, B., Papadopoulos, N., Velculescu, V.E., Zhou, S., Diaz, L.A., and Kinzler, K.W. (2013). Cancer Genome Landscapes. Science *339*, 1546–1558.

Voit, R., Hoffmann, M., and Grummt, I. (1999). Phosphorylation by G1-specific cdk-cyclin complexes activates the nucleolar transcription factor UBF. EMBO J. *18*, 1891–1899.

Wallace, M., and Ball, K.L. (2004). Docking-dependent regulation of the Rb tumor suppressor protein by Cdk4. Mol. Cell. Biol. *24*, 5606–5619.

Wallrabe, H., and Periasamy, A. (2005). Imaging protein molecules using FRET and FLIM microscopy. Curr. Opin. Biotechnol. *16*, 19–27.

Wang, Q., and Lawrence, D.S. (2005). Phosphorylation-driven protein-protein interactions: a protein kinase sensing system. J. Am. Chem. Soc. *127*, 7684–7685.

Wang, H., Nakata, E., and Hamachi, I. (2009). Recent progress in strategies for the creation of protein-based fluorescent biosensors. Chembiochem Eur. J. Chem. Biol. *10*, 2560–2577.

Wang, Q., Cahill, S.M., Blumenstein, M., and Lawrence, D.S. (2006a). Self-reporting fluorescent substrates of protein tyrosine kinases. J. Am. Chem. Soc. *128*, 1808–1809.

Wang, Q., Dai, Z., Cahill, S.M., Blumenstein, M., and Lawrence, D.S. (2006b). Light-regulated sampling of protein tyrosine kinase activity. J. Am. Chem. Soc. *128*, 14016–14017.

Wang, Q., Zimmerman, E.I., Toutchkine, A., Martin, T.D., Graves, L.M., and Lawrence, D.S. (2010). Multicolor monitoring of dysregulated protein kinases in chronic myelogenous leukemia. ACS Chem. Biol. *5*, 887–895.

Warenius, H.M., Kilburn, J.D., Essex, J.W., Maurer, R.I., Blaydes, J.P., Agarwala, U., and Seabra, L.A. (2011). Selective anticancer activity of a hexapeptide with sequence homology to a non-kinase domain of Cyclin Dependent Kinase 4. Mol. Cancer *10*, 72.

Waters, J.C. (2007). Live-cell fluorescence imaging. Methods Cell Biol. *81*, 115–140.

Waters, J.C. (2009). Accuracy and precision in quantitative fluorescence microscopy. J. Cell Biol. *185*, 1135–1148.

Wei, G., Lonardo, F., Ueda, T., Kim, T., Huvos, A.G., Healey, J.H., and Ladanyi, M. (1999). CDK4 gene amplification in osteosarcoma: Reciprocal relationship with INK4A gene alterations and mapping of 12q13 amplicons. Int. J. Cancer *80*, 199–204.

Weissleder, R., and Ntziachristos, V. (2003). Shedding light onto live molecular targets. Nat. Med. *9*, 123–128.

Welch, C.M., Elliott, H., Danuser, G., and Hahn, K.M. (2011). Imaging the coordination of multiple signalling activities in living cells. Nat. Rev. Mol. Cell Biol. *12*, 749–756.

Whitney, M.A., Crisp, J.L., Nguyen, L.T., Friedman, B., Gross, L.A., Steinbach, P., Tsien, R.Y., and Nguyen, Q.T. (2011). Fluorescent peptides highlight peripheral nerves during surgery in mice. Nat. Biotechnol. *29*, 352–356.

Wiestner, A., Tehrani, M., Chiorazzi, M., Wright, G., Gibellini, F., Nakayama, K., Liu, H., Rosenwald, A., Muller-Hermelink, H.K., Ott, G., et al. (2007). Point mutations and genomic deletions in CCND1 create stable truncated cyclin D1 mRNAs that are associated with increased proliferation rate and shorter survival. Blood *109*, 4599–4606.

Wölfel, T., Hauer, M., Schneider, J., Serrano, M., Wölfel, C., Klehmann-Hieb, E., De Plaen, E., Hankeln, T., Meyer zum Büschenfelde, K.H., and Beach, D. (1995). A p16INK4a-insensitive CDK4 mutant targeted by cytolytic T lymphocytes in a human melanoma. Science *269*, 1281–1284.

Wolff, M., Wiedenmann, J., Nienhaus, G.U., Valler, M., and Heilker, R. (2006). Novel fluorescent proteins for high-content screening. Drug Discov. Today *11*, 1054–1060.

Wouters, F.S., Verveer, P.J., and Bastiaens, P.I. (2001). Imaging biochemistry inside cells. Trends Cell Biol. *11*, 203–211.

Wunder, J.S., Eppert, K., Burrow, S.R., Gokgoz, N., Bell, R.S., Andrulis, I.L., and Gogkoz, N. (1999). Co-amplification and overexpression of CDK4, SAS and MDM2 occurs frequently in human parosteal osteosarcomas. Oncogene *18*, 783–788.

Wyatt, P.G., Woodhead, A.J., Berdini, V., Boulstridge, J.A., Carr, M.G., Cross, D.M., Davis, D.J., Devine, L.A., Early, T.R., Feltell, R.E., et al. (2008). Identification of N-(4-piperidinyl)-4-(2,6-dichlorobenzoylamino)-1H-pyrazole-3-carboxamide (AT7519), a novel cyclin dependent kinase

inhibitor using fragment-based X-ray crystallography and structure based drug design. J. Med. Chem. *51*, 4986–4999.

Xing, E.P., Nie, Y., Song, Y., Yang, G.-Y., Cai, Y.C., Wang, L.-D., and Yang, C.S. (1999). Mechanisms of Inactivation of p14ARF, p15INK4b, and p16INK4a Genes in Human Esophageal Squamous Cell Carcinoma. Clin. Cancer Res. *5*, 2704–2713.

Xiong, Y., Connolly, T., Futcher, B., and Beach, D. (1991). Human D-type cyclin. Cell *65*, 691–699.

Yaffe, M.B. (2002). Phosphotyrosine-binding domains in signal transduction. Nat. Rev. Mol. Cell Biol. *3*, 177–186.

Yaffe, M.B., and Elia, A.E. (2001). Phosphoserine/threonine-binding domains. Curr. Opin. Cell Biol. *13*, 131–138.

Yaffe, M.B., and Smerdon, S.J. (2001). PhosphoSerine/Threonine Binding Domains: You Can't pSERious? Structure *9*, R33–R38.

Yeh, R.-H., Yan, X., Cammer, M., Bresnick, A.R., and Lawrence, D.S. (2002). Real time visualization of protein kinase activity in living cells. J. Biol. Chem. *277*, 11527–11532.

Zacharek, S.J., Xiong, Y., and Shumway, S.D. (2005). Negative regulation of TSC1-TSC2 by mammalian D-type cyclins. Cancer Res. *65*, 11354–11360.

Zaman, G.J.R., Garritsen, A., de Boer, T., and van Boeckel, C. a. A. (2003). Fluorescence assays for high-throughput screening of protein kinases. Comb. Chem. High Throughput Screen. *6*, 313–320.

Zanella, F., Lorens, J.B., and Link, W. (2010). High content screening: seeing is believing. Trends Biotechnol. *28*, 237–245.

Zemelman, B.V., Lee, G.A., Ng, M., and Miesenböck, G. (2002). Selective photostimulation of genetically chARGed neurons. Neuron *33*, 15–22.

Zhang, J., and Allen, M.D. (2007). FRET-based biosensors for protein kinases: illuminating the kinome. Mol. Biosyst. *3*, 759–765.

Zhang, B., Corbel, C., Guéritte, F., Couturier, C., Bach, S., and Tan, V.B.C. (2011). An in silico approach for the discovery of CDK5/p25 interaction inhibitors. Biotechnol. J. *6*, 871–881.

Zhang, J., Ma, Y., Taylor, S.S., and Tsien, R.Y. (2001). Genetically encoded reporters of protein kinase A activity reveal impact of substrate tethering. Proc. Natl. Acad. Sci. U. S. A. *98*, 14997–15002.

Zhang, J., Yang, P.L., and Gray, N.S. (2009). Targeting cancer with small molecule kinase inhibitors. Nat. Rev. Cancer *9*, 28–39.

Zhang, J., Adrián, F.J., Jahnke, W., Cowan-Jacob, S.W., Li, A.G., Iacob, R.E., Sim, T., Powers, J., Dierks, C., Sun, F., et al. (2010). Targeting Bcr-Abl by combining allosteric with ATP-binding-site inhibitors. Nature *463*, 501–506.

Zhang, J.H., Chung, T.D.Y., and Oldenburg, K.R. (1999). A Simple Statistical Parameter for Use in Evaluation and Validation of High Throughput Screening Assays. J. Biomol. Screen. *4*, 67–73.

Zheng, Y.-L., Li, B.-S., Amin, N.D., Albers, W., and Pant, H.C. (2002). A peptide derived from cyclin-dependent kinase activator (p35) specifically inhibits Cdk5 activity and phosphorylation of tau protein in transfected cells. Eur. J. Biochem. FEBS *269*, 4427–4434.

Zheng, Y.-L., Kesavapany, S., Gravell, M., Hamilton, R.S., Schubert, M., Amin, N., Albers, W., Grant, P., and Pant, H.C. (2005). A Cdk5 inhibitory peptide reduces tau hyperphosphorylation and apoptosis in neurons. EMBO J. *24*, 209–220.

Zheng, Y.-L., Amin, N.D., Hu, Y.-F., Rudrabhatla, P., Shukla, V., Kanungo, J., Kesavapany, S., Grant, P., Albers, W., and Pant, H.C. (2010). A 24-residue peptide (p5), derived from p35, the Cdk5 neuronal activator, specifically inhibits Cdk5-p25 hyperactivity and tau hyperphosphorylation. J. Biol. Chem. *285*, 34202–34212.

Zhu, K., Liu, Q., Zhou, Y., Tao, C., Zhao, Z., Sun, J., and Xu, H. (2015). Oncogenes and tumor suppressor genes: comparative genomics and network perspectives. BMC Genomics *16*, S8.

Zou, X., Ray, D., Aziyu, A., Christov, K., Boiko, A.D., Gudkov, A.V., and Kiyokawa, H. (2002). Cdk4 disruption renders primary mouse cells resistant to oncogenic transformation, leading to Arf/p53-independent senescence. Genes Dev. *16*, 2923–2934.

Zuo, L., Weger, J., Yang, Q., Goldstein, A.M., Tucker, M.A., Walker, G.J., Hayward, N., and Dracopoli, N.C. (1996). Germline mutations in the p16INK4a binding domain of CDK4 in familial melanoma. Nat. Genet. *12*, 97–99.

Zwijsen, R.M., Buckle, R.S., Hijmans, E.M., Loomans, C.J., and Bernards, R. (1998). Ligand-independent recruitment of steroid receptor coactivators to estrogen receptor by cyclin D1. Genes Dev. *12*, 3488–3498.

Résumé en français

1. Introduction

1.1. CDK4/cycline D

1.1.1. CDK4/cycline D dans le cycle cellulaire

Les CDK/cyclines forment une famille de protéines kinases hétérodimériques constituées d'une sous-unité catalytique, la CDK (Cyclin-Dependent Kinase) et d'une sous-unité régulatrice, la cycline. Leur rôle majeur est d'assurer la régulation des différentes transitions du cycle cellulaire (Malumbres, 2011; Morgan, 1997). La phase G1, phase de croissance cellulaire et de réponse aux stimuli extracellulaires (facteurs de croissance), et la transition G1/S sont régulées par le complexe CDK4/cycline D. En effet, une fois actif, ce complexe phosphoryle les membres de la famille des protéines du rétinoblastome (pRb, p107 et p130), induisant une dérépression des facteurs de transcription E2F et permettant ainsi la transcription de la cycline E, nécessaire pour la transition entre la phase G1 et la phase S (Ho and Dowdy, 2002) (Figure 1). Une phosphorylation supplémentaire de pRb par le complexe CDK2/cycline E permet la libération complète des facteurs E2F, et donc leur action maximale comme activateurs transcriptionnels (Boonstra, 2003).

L'activité de CDK4/cycline D est régulée à plusieurs niveaux, via l'expression et la dégradation de cycline D mais aussi par interaction avec les inhibiteurs de CDK (CKI) (les protéines INK4 et les protéines Cip/Kip). CDK4/cycline D subit également une succession de phosphorylations et déphosphorylations qui conduit au final à l'activation complète du complexe (Boutros et al., 2006; Iavarone and Massagué, 1997; Jeffrey et al., 2000; Martin et al., 2008; Schachter et al., 2013; Sherr and Roberts, 1999; Terada et al., 1995).

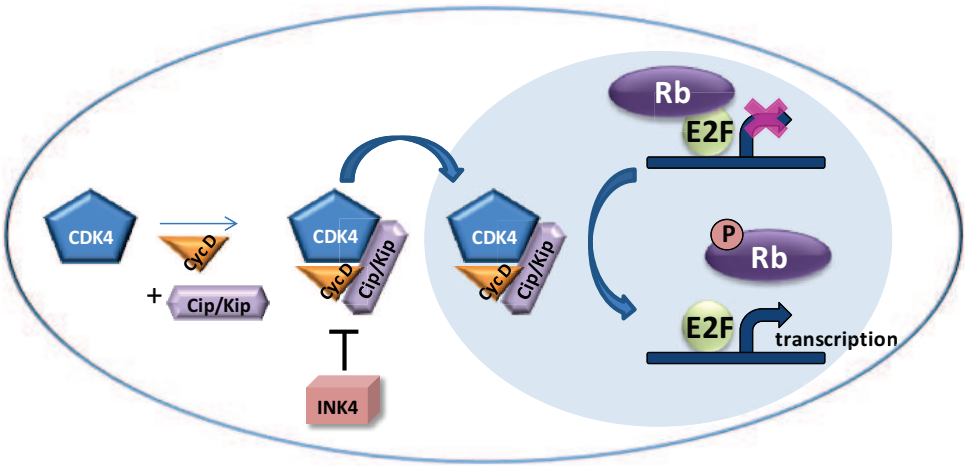

Figure 1: Fonction et régulation de CDK4/cycline D (source (Peyressatre et al., 2015)). L'expression de cycline D (orange) via des signaux mitogènes conduit à son association avec CDK4 (bleu) et à la formation du complexe dimérique. L'interaction avec les protéines Cip/Kip (violet clair) favorise l'assemblage du complexe et sa localisation nucléaire. L'activité de CDK4/cycline D est négativement régulée par interaction avec la famille de protéines INK4 (rose). Une fois actif, le complexe CDK4/cycline D régule la progression de la phase G1 et la transition G1/S. CDK4/cycline D phosphoryle la protéine du rétinoblastome (Rb) (violet foncé), ce qui induit la dérépression des facteurs de transcription E2F (vert), permettant ainsi la transcription de gènes essentiels à la transition G1/S.

1.1.2. Aspects structuraux et mécanistiques

Le mécanisme d'assemblage des CDK/cyclines a été décrit pour CDK2/cycline A (Brown et al., 1999; Hagopian et al., 2001; Jeffrey et al., 1995; Morris et al., 2002; Russo et al., 1996). On estime que ce mécanisme est commun pour toutes les CDK/cyclines même s'il existe des déterminants de spécificité qui font que chaque CDK s'associe de manière préférentielle avec un partenaire cycline et que chaque complexe possède des substrats différents des autres, une fonction biologique et physiologique différentes. La première étape du mécanisme consiste en l'association rapide entre l'hélice PSTAIRE de CDK2 et l'hélice α5 de cycline A. Cette association conduit à la réorientation de la poche ATP de CDK2 et à son alignement avec le site catalytique dans une position favorable au transfert du phosphate au substrat. La deuxième étape correspond à l'isomérisation lente du lobe C-terminal de CDK2 qui conduit à un changement conformationnel de la boucle d'activation (ou boucle T). Cette dernière est ainsi stabilisée dans une position qui permet sa phosphorylation par la CAK (Cyclin-Activating Kinase). Cette phosphorylation induit le déplacement de la boucle T dans une

position stabilisée par des interactions entre le groupe phosphate et plusieurs résidus du lobe C-terminal de CDK2, générant ainsi un site complètement accessible pour le substrat.

Les structures cristallographiques de CDK2/cycline A et CDK4/cycline D montrent que l'interaction entre l'hélice PISTVRE de CDK4 et l'hélice α5 de cycline D est conservée alors que les interactions entre le lobe C-ter de CDK4 et cycline D ne le sont pas (Figure 2) (Day et al., 2009; Lolli, 2010; Takaki et al., 2009). CDK2/cycline A est dans une conformation fermée contrairement à celle ouverte de CDK4/cycline D. De plus, la structure cristallographique du complexe CDK4/cycline D1 montre que CDK4, même liée à cycline D1 et phosphorylée sur la tyrosine 172 de la boucle T, est dans une conformation dite inactive (Day et al., 2009). La fixation du substrat et l'association avec les protéines Cip/Kip seraient donc nécessaires pour favoriser son activation complète (Day et al., 2009; Takaki et al., 2009). Cependant, une étude récente de dynamique moléculaire suggère qu'une conformation fermée, similaire à celle de CDK2/cycline A, peut exister pour CDK4/cycline D1 (Floquet et al., 2015).

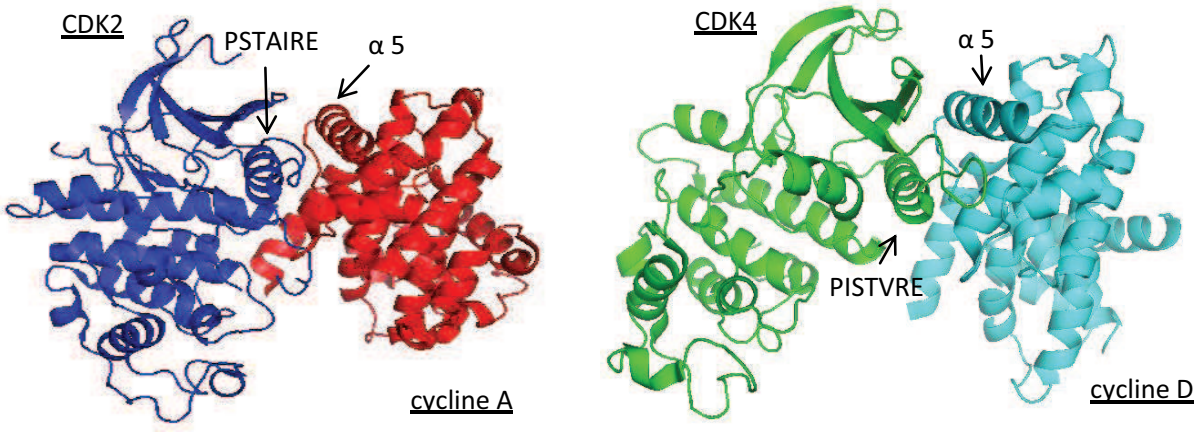

Figure 2: Représentation des structures cristallographiques de CDK2/cycline A (PDB 1QMZ) et CDK4/cycline D (PDB 3G33)

1.1.3. Dérégulation de CDK4/cycline D dans les cancers

Parmi les CDK/cyclines, CDK4/cycline D est le complexe qui présente le plus d'aberrations dans les cancers humains (Lapenna and Giordano, 2009; Malumbres and Barbacid, 2001). La dérégulation de la voie $p16^{INK4A}$ / CDK4-6 / cycline D / Rb est l'un des évènements les plus fréquents dans les cancers et suggère que l'inhibition de l'activité kinase dépendante de cycline D constitue une cible thérapeutique en tant que traitement anticancéreux (Musgrove et al., 2011; Sherr, 1996).

Cas particulier du mélanome

Le mélanome, qui se développe aux dépens des mélanocytes, est l'un des cancers humains les plus agressifs et est responsable de 60 à 80% des décès par cancers de la peau (Bandarchi et al., 2010). CDK4/cycline D est un biomarqueur avéré pour le mélanome. En effet, la voie $p16^{INK4A}$ / CDK4-6 / cycline D / Rb est dérégulée dans 90% des mélanomes. Dans les modèles de mélanomes humains et murins, l'activation de cette voie est étroitement liée à la mutation de BRAF et NRAS dans la transformation des mélanocytes. La voie RAS/RAF/MEK/ERK est dérégulée dans 65% à 90% des mélanomes métastatiques, augmentant davantage la voie $p16^{INK4A}$ / CDK4-6 / cycline D / Rb qui elle-même accroît l'expression de cycline D1 (Chawla et al., 2010; Chin et al., 2006). L'importance de la protéine CDK4 dans les cancers a particulièrement été décrite suite à l'identification de la mutation R24C dans le locus de CDK4 qui empêche la fixation de l'inhibiteur endogène $p16^{INK4A}$ et prédispose au mélanome (Wölfel et al., 1995; Zuo et al., 1996). Cependant, une très faible incidence de mélanomes spontanés a été constatée chez des souris $CDK4^{R24C/R24C}$. Une incidence accrue de mélanomes spontanés survient chez les souris exprimant l'oncogène HRAS (G12V) dans les mélanocytes, dans un contexte R24C (Chawla et al., 2010).

Le risque de développer un mélanome est aussi augmenté par l'hyperactivation de CDK4/cycline D due à l'amplification de cycline D (18% des mélanomes) ou à la perte de l'inhibiteur $p16^{INK4A}$ (délétion de *CDKN2A* dans 50-60 % des tumeurs métastatiques) (Tsao et al., 2012).

Cette kinase constitue donc un biomarqueur clé pour le diagnostic du mélanome et une cible thérapeutique pertinente (Sheppard and McArthur, 2013).

1.1.4. Inhibiteurs de CDK4/cycline D

À ce jour, la plupart des inhibiteurs des CDK/cyclines développés inhibent l'activité kinase en interférant avec le site de liaison de l'ATP des CDK (Bruyère and Meijer, 2013; Lapenna and Giordano, 2009). Trois inhibiteurs spécifiques de CDK4-6/cycline D ciblant le site de liaison de l'ATP sont actuellement en essais cliniques : le composé LEE011 (Ribociclib), le composé LY2835219 (Abemaciclib) et surtout le PD-0332991 (Palbociclib) (Asghar et al., 2015; Dickson, 2014; VanArsdale

et al., 2015). Ce dernier cible spécifiquement CDK4/cycline D1 et CDK6/cycline D2 avec un IC_{50} de 11 et 16nM respectivement. En 2015, PD-0332991 est devenu le premier inhibiteur de CDK/cyclines à être approuvé par la FDA (Food and Drug Administration) pour son utilisation en association avec le létrozole dans le traitement de première intention de femmes ménopausées atteintes d'un cancer du sein RE+ et HER2- de stade avancé (http://www.fda.gov/Drugs/InformationOnDrugs/ApprovedDrugs/ucm432886.htm).

Des stratégies alternatives ne ciblant pas la poche ATP ont été explorées pour inhiber la fonction des CDK/cyclines, en interférant par exemple avec la reconnaissance du substrat ou en ciblant les interfaces protéine/protéine essentielles (PPI) qui sont essentielles dans l'assemblage des complexes. Le criblage haut débit de banques de petites molécules ou le design rationnel de peptides mimant les interfaces rendent possible l'identification de tels composés (Arkin and Wells, 2004). Cette approche a été utilisée avec succès pour cibler différents complexes multimériques ou multiprotéiques, dont le complexe p53/MDM2 (Chène, 2004).

Des approches permettant l'identification d'inhibiteurs allostériques de kinases ont également été développées (Eglen and Reisine, 2010). Ces composés sont souvent plus spécifiques que les inhibiteurs ATP compétitifs puisqu'ils se lient sur des sites qui ne sont pas conservés chez toutes les kinases et qui sont accessibles seulement dans certaines conformations. Les inhibiteurs allostériques lient et stabilisent des kinases en conformation inactive et empêchent les transitions vers une conformation active. Cette classe de composés reste très difficile à concevoir d'un point de vue rationnel et requiert l'identification de poches allostériques ou de sites accessibles seulement dans des intermédiaires inactifs. L'identification de ces composés se fait donc le plus souvent par criblage haut débit (Jahnke et al., 2005; Lebakken et al., 2012; Liu and Gray, 2006; Prével et al., 2014b).

1.2. Développement de biosenseurs fluorescents pour étudier l'activité kinase

1.2.1. Concept de biosenseurs fluorescents

Compte tenu de l'importance des CDK/cyclines comme biomarqueurs en cancérologie, des approches efficaces et sensibles permettant de suivre l'activité de ces kinases sont requises. Actuellement, les seules méthodes permettant de mesurer l'activité des CDK/cyclines sont la radioactivité et les approches antigéniques (Jia et al., 2008). Ces tests biochimiques utilisent des enzymes recombinantes purifiées et/ou des substrats artificiels et sont basés sur la mesure de l'incorporation de phosphate radioactif dans des substrats de kinases ou sur l'utilisation d'anticorps qui reconnaissent des résidus phosphorylés spécifiques. Or ces méthodes requièrent de fortes concentrations en substrat et en enzyme et ne permettent pas de mesure en temps réel. Elles nécessitent également la fixation ou l'extraction de protéines cellulaires. C'est pourquoi le développement de nouvelles approches suffisamment sensibles et non-invasives est nécessaire pour évaluer qualitativement et quantitativement l'activité kinase des complexes CDK/cyclines dans leur environnement natif.

Les biosenseurs fluorescents permettent de répondre à ces nouveaux challenges. Ils sont capables de mesurer de façon sensible les changements de fluorescence associés à la phosphorylation du substrat par la kinase. Ils fournissent des informations cinétiques sur l'activité kinase *in vitro* et *in cellulo* et permettent d'évaluer l'effet d'un inhibiteur sur la kinase (Nhu Ngoc Van and Morris, 2013). Ils permettent de visualiser des processus dynamiques dans les cellules vivantes en continu et en temps réel, fournissant ainsi des informations précieuses sur la localisation subcellulaire, le comportement intracellulaire de cibles ou encore les interactions protéine/protéine (Chudakov et al., 2010; Morris, 2010; Weissleder and Ntziachristos, 2003). Ils constituent également des outils puissants pour détecter les changements conformationnels des kinases (Tarrant and Cole, 2009). Les biosenseurs fluorescents offrent de nombreux avantages tels qu'une grande sensibilité et sélectivité intrinsèque, une grande résolution spatiale et temporelle, une imagerie non-invasive et un large spectre de longueurs d'ondes.

Deux familles de biosenseurs fluorescents ont été développées : les biosenseurs génétiques, conçus à partir de protéines auto-fluorescentes (AFP) et les biosenseurs non génétiques, basés sur le couplage de petites sondes fluorescentes synthétiques sur des protéines ou des peptides.

1.2.2. Biosenseurs fluorescents génétiquement codés

Les biosenseurs génétiquement codés les plus connus sont ceux basés sur le FRET (Förster Resonance Energy Transfer) entre un couple d'AFP. Ils sont constitués d'un PAABD (Phospho Amino Acid Binding Domain) fusionné avec une AFP, qui reconnaît les résidus phosphorylés, et d'un domaine substrat spécifique d'une protéine kinase fusionné avec une autre AFP. Lorsque la kinase phosphoryle son substrat, le résidu phosphorylé est reconnu par le PAABD, ce qui induit un changement de conformation qui altère la distance et l'orientation des deux AFP. Ces biosenseurs ont été appliqués avec succès à l'étude de l'activité de nombreuses kinases. Un biosenseur a été développé pour étudier l'activité de CDK1/cycline B1 (Gavet and Pines, 2010). Pour l'heure, c'est le seul biosenseur génétique à avoir été conçu pour étudier l'activité d'un complexe CDK/cycline. Les biosenseurs génétiques sont considérés comme faciles à manipuler et à transfecter dans les cellules. Cependant, ils présentent certains inconvénients tels qu'une utilisation limitée aux applications *in cellulo*, une expression difficile à contrôler et hétérogène au sein d'une population de cellules, une taille importante et parfois une mauvaise localisation cellulaire (Giepmans et al., 2006; Morris, 2010).

1.2.3. Biosenseurs fluorescents non génétiques

Les biosenseurs non génétiques sont généralement constitués d'un scaffold peptidique ou protéique sur lequel est couplé une petite sonde fluorescente synthétique. Dans le cas des protéines kinases, les séquences peptidiques ou protéiques dérivent souvent de domaines qui reconnaissent spécifiquement une kinase, comme par exemple des séquences substrats contenant un site de phosphorylation. Suite à la phosphorylation de la séquence substrat par la kinase, les propriétés spectrales sont altérées directement ou indirectement par des changements de conformation intramoléculaires et/ou la reconnaissance du PAABD.

Les biosenseurs non-génétiques présentent certains avantages tels qu'une versatilité dans le design et une production aisée par synthèse chimique ou par purification de protéine recombinante. De plus, ils peuvent être utilisés *in vitro*, *in cellulo* and *in vivo*. Cependant, l'inconvénient majeur de ces outils est leur inaptitude à franchir les membranes cellulaires. La microinjection ou l'internalisation grâce à des peptides auto-pénétrants tels que PEP and CADY2 peuvent permettre de résoudre ce problème (Kurzawa et al., 2010; McNeil, 2001).

1.2.4. Biosenseurs fluorescents utilisés pour le criblage HTS/HCS

Les biosenseurs décrits précédemment, ainsi que les biosenseurs basés sur la technologie FLiK (Fluorescent Labels in Kinases) et les biosenseurs positionnels, ont été appliqués au criblage de banques de petites molécules dans le but d'identifier de nouveaux inhibiteurs de protéines kinases (Ahsen and Bömer, 2005; Allen et al., 2006; Hanson and Hanson, 2008; Prével et al., 2014b; Taylor, 2010; Wolff et al., 2006; Zaman et al., 2003). Les biosenseurs positionnels sont composés d'une AFP qui contient une séquence de localisation nucléaire (NLS) ou d'exclusion nucléaire (NES). L'exposition de cette séquence est modulée en réponse à l'activation/inhibition de la kinase cible. Ainsi, ils donnent des informations sur les changements subcellulaires de la cible.

La plupart des stratégies décrites précédemment contiennent un PAABD et conduisent souvent à l'identification de molécules compétant avec l'ATP. Dans le but d'identifier des inhibiteurs allostériques qui lient et stabilisent les kinases dans une conformation inactive, les biosenseurs FLiK ont été développés. Ils contiennent un scaffold kinase dans lequel des sondes fluorescentes sont introduites à des positions stratégiques et permettent de « senser » les ligands qui lient un état conformationnel spécifique. Ces biosenseurs ont été appliqués avec succès pour l'identification par criblage HTS/HCS (High Throughput Screening/High Content Screening) d'inhibiteurs de p38αMAPK, Src and Abl (Getlik et al., 2012; Schneider et al., 2012; Simard et al., 2009a, 2009b, 2009c, 2010; Zhang et al., 2010).

1.2.5. Biosenseurs fluorescents non génétiques développés au laboratoire pour étudier les CDK/cyclines

CDKSENS

L'équipe a développé une famille de biosenseurs peptidiques fluorescents permettant d'étudier l'abondance des CDK/cyclines (Kurzawa et al., 2011). Ces peptides biligands sont constitués d'une séquence substrat spécifique d'une CDK et d'une séquence de liaison à une cycline. Ils contiennent une unique cystéine qui, une fois couplée à une sonde fluorescente sensible à l'environnement, permet d'assurer la reconnaissance spécifique et affine des CDK/cyclines en complexe. L'abondance des CDK/cyclines a pu être déterminée *in vitro* mais également *in cellulo* en associant le biosenseur avec le peptide vecteur CADY2.

CDKACT

Une famille de biosenseurs fluorescents peptidiques et protéiques a été développée dans notre laboratoire de façon à étudier l'activité des CDK/cyclines. Ils contiennent un domaine de liaison aux acides aminés phosphorylés (PAABD) et un domaine substrat. Ils sont capables, lorsqu'ils sont couplés à des sondes fluorescentes sensibles à l'environnement, de détecter des altérations dans l'activité de ces kinases *in vitro*, mais également *in cellulo* lorsqu'ils sont associés à des stratégies de vectorisation basées sur des peptides vecteurs (Van et al., 2014).

CDKCONF

Dans le but d'identifier des inhibiteurs allostériques de CDK2, l'équipe a développé un biosenseur protéique basé sur la technologie FLiK (Fluorescent Labels in Kinases). Ce biosenseur contient un scaffold de CDK2 dans lequel des sondes fluorescentes sont introduites à des positions spécifiques et servent à détecter des ligands se liant à une conformation spécifique de CDK2. CDKCONF a été appliqué au criblage de la chimiothèque nationale (18480 composés) et a permis d'identifier des composés capables d'inhiber l'activité de CDK2 en interférant avec la boucle T.

2. Objectifs

Le premier objectif de ma thèse a porté sur le développement et l'application d'un biosenseur fluorescent permettant d'étudier l'activité de CDK4/cycline D. Ce biosenseur a été caractérisé *in vitro* et *in extracto* puis appliqué à la détection d'altérations de CDK4/cycline D dans des biopsies de peau

humaine et de xénogreffes de mélanome dans des essais fluorescents d'activité kinase, ainsi que dans des cellules cancéreuses vivantes par microscopie de fluorescence et vidéo-microscopie.

Le deuxième objectif de ma thèse a consisté à identifier des inhibiteurs non compétitifs de l'ATP, soit par élaboration rationnelle de peptides, soit par criblage de petites molécules. A cette fin, deux biosenseurs fluorescents ont été développés qui permettent d'identifier respectivement des composés ciblant l'interface entre CDK4 et cycline D ou des inhibiteurs allostériques capables de perturber la dynamique conformationnelle de CDK4. Des essais de criblage par fluorescence réalisés avec ces biosenseurs ont conduit à l'identification de touches qui ont été validées et caractérisées *in vitro* et dans des essais de prolifération cellulaire, et qui constituent des candidats prometteurs pour une chimiothérapie sélective du mélanome.

3. Résultats

3.1. Développement d'un biosenseur fluorescent pour étudier l'activité de CDK4/cycline D

Une famille de biosenseurs fluorescents a été développée pour suivre spécifiquement l'activité de CDK4/cycline D *in vitro* et *in cellulo*. Ils sont constitués de trois domaines:

- un domaine de liaison aux acides aminés phosphorylés (**Phospho Amino Acid Binding Domain** PAABD) qui est capable de reconnaître pSer et pThr.

- une **séquence substrat** qui dérive de la protéine du rétinoblastome (Rb) (résidus 790 à 801) et qui est spécifiquement phosphorylé par CDK4 (résidu Ser795) (Grafstrom et al., 1999). Une cystéine unique proche du site de phosphorylation permet de coupler une sonde fluorescente fonctionnalisée (maléimide ou iodoacétamide ou isothiocyanate) (YKFCSSPLRIPG).

- un **linker** peptidique court qui lie les deux domaines précédents et confère une certaine flexibilité.

Trois variants ont été conçus: une forme protéique (57 kDa) et deux formes peptidiques (44 et 31 acides aminés). Ils diffèrent selon l'origine et la taille du PAABD mais contiennent la même séquence substrat.

Les biosenseurs sont couplés à une sonde fluorescente sensible à l'environnement et permettent de suivre l'activité de CDK4/cycline D par mesure de changements de fluorescence. Leur mode d'action est le suivant : la phosphorylation d'un résidu sérine dans le domaine substrat (Rb) du biosenseur par CDK4/cycline D entraîne un changement conformationnel dû à l'interaction préférentielle du PAABD avec le substrat phosphorylé. Ce repliement du PAABD sur le substrat phosphorylé modifie l'environnement de la sonde fluorescente à proximité du site de phosphorylation, ce qui induit une variation de fluorescence.

3.1.1. CDKACTRb

Un biosenseur protéique de 57 kDa, GST-CDKACTRb, a d'abord été développé. Il contient un PAABD dérivé du domaine Polo Box de Plk1 (García-Alvarez et al., 2007), comprenant les résidus 367 à 603 (237 acides aminés) et dans lequel toutes les cystéines ont été mutées en sérines. CDKACTRb ne possède qu'une seule cystéine, proche du site de phosphorylation, pouvant être couplée avec des sondes fluorescentes telles que la cyanine 3.

Le biosenseur a été exprimé chez *E.coli* sous forme de fusion GST, purifié par chromatographie FPLC, puis marqué avec Cy3. Des expériences de spectrofluorimétrie ont été réalisées en incubant le biosenseur avec le complexe recombinant CDK4/cycline D ou des extraits cellulaires issus de lignées cellulaires de mélanome (A375) en présence d'ATP/$MgCl_2$. Afin de vérifier que les changements de fluorescence observés étaient bien associés à une activité kinase, l'inhibiteur compétiteur de l'ATP PD-0332991, spécifique de CDK4 et CDK6, était également ajouté à la kinase recombinante ou aux extraits cellulaires. Afin de déterminer sa sélectivité et sa spécificité vis-à-vis d'autres kinases et d'autres complexes CDK/cyclines, le biosenseur a également été caractérisé *in vitro* en utilisant différents inhibiteurs de kinases. Toutes ces expériences ont montré que CDKACTRb-Cy3 rapporte

spécifiquement l'activité du complexe recombinant *in vitro* et l'activité de CDK4/cycline D endogène dans des extraits cellulaires de mélanome.

3.1.2. WWRb

Afin d'étudier l'activité de CDK4/cycline D dans des biopsies de peau et *in cellulo*, un biosenseur peptidique plus court et plus facile à manipuler et à stocker a été généré. WWRb est un peptide de 44 acides aminés dont le PAABD dérive du domaine WW de Pin1 (résidus 10 à 39) (Lu et al., 1999; Macias et al., 2000).

Des expériences de spectrofluorimétrie ont été réalisées en incubant le biosenseur avec des extraits cellulaires issus de lignées cellulaires de mélanome (A375) en présence d'ATP/$MgCl_2$ et en ajoutant l'inhibiteur PD-0332991. Des expériences contrôles dans lesquelles le biosenseur était incubé avec de la BSA à la place des extraits cellulaires ont également été menées. Bien que WWRb ait été testé avec différentes sondes fluorescentes (Cy3, TAMRA, FITC, Texas Red), il n'a jamais répondu spécifiquement à l'activité de CDK4/cycline D *in extracto*. En effet, le biosenseur était soit insensible à l'ajout de PD-0332991, soit répondait à la présence de BSA, soit répondait de manière aléatoire. Nous avons alors émis l'hypothèse que le tampon de lyse utilisé pour faire les lysats cellulaires empêchait le repliement du PAABD, certainement à cause de la présence des détergents.

Pour valider cette hypothèse, WWRb, marqué avec la sonde fluorescente TAMRA, a ensuite été testé en présence de la protéine recombinante CDK4/cycline D et de l'inhibiteur PD-0332991. Cette expérience a démontré que le biosenseur était capable de rapporter l'activité de CDK4/cycline D *in vitro*.

Au vu des résultats obtenus *in extracto*, nous avons considéré que le biosenseur WWRb n'était pas assez sensible et spécifique pour être utilisé par la suite.

3.1.3. WWshortRb

Nous avons donc développé un second biosenseur peptidique, plus court (31 acides aminés), **WWshortRb**, dont le PAABD a été conçu après analyse de la structure cristallographique du domaine WW de Pin1 avec un phosphopeptide (PDB 1F8A). Cette étude a révélé que certains résidus étaient

essentiels à l'interaction : Arg14, Arg17, Tyr23, Phe25 et Trp34. Le PAABD qui a été développé, appelé WWshort, comprend donc ces résidus clés (Phe25, Arg14, Tyr23, Arg17), inter-espacés par des petits acides aminés non chargés, et termine par le résidu Trp34 suivi des cinq acides aminés contenus dans la séquence native du domaine WW de Pin1 (GFARVYMSRSSGWERPSG).

Des titrations de fluorescence réalisées avec WW ou avec WWshort ont démontré que WWshort interagissait mieux avec le peptide substrat Rb que WW et qu'il interagissait encore plus préférentiellement avec le substrat phosphorylé.

WWshortRb a ensuite été caractérisé *in extracto* et *in vitro*. Nous avons démontré que WWshortRb, marqué avec la sonde fluorescente TAMRA, était capable de rapporter l'activité du complexe CDK4/cycline D recombinant ou endogène. Nous avons également montré que WWshortRb répondait spécifiquement à CDK4/cycline D *in extracto* puisque seul l'ajout d'inhibiteurs spécifiques de CDK4 tels que PD-0332991 ou LY2835219 entraînait une diminution de la fluorescence du biosenseur.

Alors que WWshortRb répond à l'activité de CDK4 lorsqu'il est marqué avec TAMRA, il ne répond pas s'il est couplé avec DyLight650. Ainsi, comme Dylight650 (λexc = 652 nm; λem = 672 nm) et TAMRA (λexc = 540 nm; λem = 565 nm) possèdent des propriétés spectrales différentes, WWshortRb-DyLight650 peut être utilisé comme contrôle négatif.

WWshortRb a ensuite été utilisé pour comparer l'activité de CDK4/cycline D dans différentes lignées de mélanome. L'analyse du profil fluorescent de WWshortRb a montré que l'activité kinase de CDK4 était plus importante dans les lignées cellulaires A375 (perte de fonction *CDKN2A*, BRaf V600E), Mewo (perte de fonction *CDKN2A*, Wt CDK4) et SK-MEL28 (R24C CDK4, BRaf V600E) (augmentation d'environ 40%) comparée à la lignée SK-MEL2 (mutation NRas (Q61R)) (25% d'augmentation) et MV3 (20% d'augmentation). Ces réponses corrèlent avec les génotypes des lignées cellulaires dans lesquelles la perte de fonction de *CDKN2A* ou la mutation R24C de CDK4 conduit à une hyperactivité de CDK4. Pour autant ces résultats ne coïncident pas avec les profils de Western blot qui fournissent seulement une information sur l'abondance de CDK4. En effet, l'activité de CDK4 est associée au

niveau d'expression de CDK4 mais également à sa régulation au sein de la voie $p16^{INK4A}$ / CDK4-6 / cycline D / Rb.

WWshortRb a aussi été appliqué à la détection d'altérations de CDK4/cycline D dans des biopsies de peau humaine. Il a permis de mettre en évidence une activité plus forte de CDK4 dans l'épiderme que dans le derme, ce qui s'explique par le fait que de nombreuses cellules en division se trouvent dans l'épiderme. La réponse de WWshortRb a également été étudiée en l'incubant avec des extraits cellulaires provenant de biopsies de peau saine et de peau présentant une pathologie telle que l'eczéma et le psoriasis. Alors qu'une activité similaire de CDK4 a été observée dans les biopsies de peau saine et à eczéma, une activité beaucoup plus faible a été trouvée dans les biopsies de peau présentant un psoriasis.

WWshortRb a également été appliqué à la détection d'altérations de CDK4/cycline D dans des xénogreffes de mélanome provenant de souris traitées quotidiennement ou non avec l'inhibiteur PD-0332991. Les biopsies de xénogreffes ont été lysées et les extraits ont été incubés avec WWshortRb-TAMRA. Ces expériences ont montré une réduction plus forte de l'activité de CDK4 dans les xénogreffes traitées avec 150 mg/kg PD-0332991 pendant 7 jours plutôt que 3 jours.

Enfin, la capacité de WWshortRb à rapporter l'activité de CDK4 *in cellulo* a été examinée. Nous avons démontré que le biosenseur, marqué avec TAMRA ou DyLight650, franchissait les membranes cellulaires tout seul et n'avait donc pas besoin d'être associé à une stratégie de délivrance telle que les peptides vecteurs. Des expériences de vidéo-microscopie ont confirmé que le fait que WWshortRb-DyLight650 constituait un bon contrôle négatif *in cellulo* et qu'il permettait une quantification ratiométrique de la réponse du biosenseur. Dans des cellules vivantes de mélanome traitées avec PD-0332991 et Roscovitine, WWshortRb-TAMRA a montré qu'il était capable de détecter une inhibition de l'activité de CDK4/cycline D. Cependant, après plusieurs heures d'acquisition, la linéarité de réponse du biosenseur suggère qu'il ne répond plus de manière fiable à sa phosphorylation par CDK4/cycline D.

3.2. Identification d'inhibiteurs non compétitifs de l'ATP ciblant CDK4/cycline D

Dans le but de développer des inhibiteurs de CDK4/cycline D non compétitifs de l'ATP, des approches alternatives ciblant des interfaces protéine/protéine ou des sites allostériques ont été envisagées. Ces stratégies reposent soit sur la conception rationnelle de peptides, soit sur l'élaboration de biosenseurs fluorescents permettant de cribler des banques de petites molécules.

A. Identification par criblage

3.2.1. Développement de biosenseurs fluorescents - Criblage de chimiothèques

Deux biosenseurs fluorescents permettant une approche aléatoire par criblage ont été conçus:

-un biosenseur permettant d'identifier des inhibiteurs d'interface entre l'hélice PISTVRE de CDK4 et l'hélice α5 de cycline D (**CDKCONF4A**)

-un biosenseur sensible aux changements conformationnels de CDK4 permettant d'identifier des modulateurs allostériques de la boucle T de cette kinase (**CDKCONF4B**).

La séquence de CDK4 contient 4 cystéines dont les groupes thiol sont disponibles pour le couplage avec des sondes fluorescentes. CDKCONF4A et CDKCONF4B ont été générés à partir d'une construction plasmidique codant pour GST-CDK4 de souris. Pour CDKCONF4A, deux cystéines proches de l'hélice PISTVRE ont été conservées (Cys 78 et 135). Dans le cas de CDKCONF4B, deux cystéines proches de la boucle T ont été utilisées (Cys 202 et 189, la deuxième étant introduite par mutagenèse dirigée).

La cycline D et le substrat Rb ont été utilisés comme contrôle positif de l'interaction pour CDKCONF4A et CDKCONF4B respectivement, afin de valider le biosenseur puis d'optimiser les conditions d'essai pour le criblage. Tout le processus d'optimisation et de criblage a été effectué sur un robot (TECAN™ Freedom EVO) de la plateforme MRI au CRBM à Montpellier (collaboration J. Bellis et V. Georget).

Deux banques ont été criblées : la Chimiothèque Nationale Essentielle (CNE) (480 composés) et une banque de molécules provenant de la faculté de pharmacie de Strasbourg (collaboration avec le Dr. Frédéric Bihel) (640 molécules). Le criblage de la CNE a permis d'identifier 15 hits pour CDKCONF4A et 9 hits pour CDKCONF4B (pourcentage de retenus < 4%). Le criblage de la banque de Strasbourg a permis d'identifier deux hits, les mêmes pour CDKCONF4A et CDKCONF4B (pourcentage de retenus < 1%).

3.2.2. Caractérisation *in vitro* des hits identifiés

Des poudres fraîches des molécules identifiées à la suite du criblage ont été envoyées par les laboratoires d'origine et resuspendues dans du DMSO. Les hits ont ensuite été retestés manuellement pour confirmer les résultats du criblage. Seulement quelques composés de la CNE ont pu être validés et gardés pour la suite de l'étude (ICMR-04-E10, LPS401, LPS853). Les deux composés de Strasbourg ont été caractérisés au regard de leur identification par CDKCONF4A comme inhibiteurs d'interface. Pour vérifier s'ils étaient capables d'interagir avec l'hélice PISTVRE de CDK4, des tests d'interaction ont été menés avec le peptide PISTVRE, qui dérive de cette hélice, marqué avec une sonde fluorescente, et le peptide D1, qui dérive de l'hélice α5 de cycline D, comme contrôle positif. Un seul des composés, LPI2251, a montré une réelle interaction avec PISTVRE. Une collaboration avec Dr. Frédéric Bihel a alors débuté afin de tester différents dérivés de ce composé et d'identifier les variants permettant de cibler le plus efficacement possible CDK4/cycline D. Le même test d'interaction a été effectué entre ces 15 molécules et le peptide PISTVRE. Trois de ces composés ont induit un changement de fluorescence significatif qui indique qu'ils interagissent avec l'hélice PISTVRE de CDK4.

3.2.3. Caractérisation *in cellulo* des hits identifiés

Des tests de prolifération sur cellules de mélanome (A375) et sur cellules saines (fibroblastes) ont été réalisés afin d'évaluer la capacité des 15 molécules de Strasbourg à réduire la croissance cellulaire.

Les IG_{50} des six composés les plus prometteurs sont tous compris entre 2.9 et 20,7µM et sont comparables à la valeur obtenue pour PD-0332991 (18,7µM). Un seul des composés, LPI2192, a

également eu un effet sur la prolifération des fibroblastes sains. Il a donc été écarté de la suite de l'étude.

Des tests de prolifération ont également été menés avec un des composés, RF1210, sur d'autres lignées de mélanome (SK-MEL2, SK-MEL28, Mewo, MV3) présentant différentes altérations de la voie $p16^{INK4A}$ / CDK4-6 / cycline D / Rb. Les valeurs des IG_{50} sont similaires entre les différentes lignées, de 10µM à 13,6µM, et sont comparables à celles obtenues avec PD-0332991 (de 10,7µM à 18,7µM).

Enfin des tests de synergie ont été réalisés afin de déterminer si RF1210 and LPI2252 pouvaient coopérer avec d'autres drogues et inhiber plus efficacement la prolifération des cellules de mélanome A375. Ces expériences ont montré qu'à des concentrations sous-optimales de RF1210 et LPI2252 (10µM), l'ajout d'un inhibiteur de CDK4 tel que PD-0332991 réduisait le nombre de cellules plus significativement que le composé seul. Cette coopération a été observée avec d'autres inhibiteurs de CDK4 (LEE011 et LY2835219), mais aussi avec d'autres drogues fréquemment utilisées dans le traitement du cancer telles que le Paclitaxel et le Methotrexate.

B. Conception rationnelle de peptides ciblant l'interface entre CDK4 et cycline D

3.2.4. Concept et design

Des peptides ont été conçus pour cibler l'interface entre les deux sous-unités du complexe CDK4/cycline D. Dans notre laboratoire, cette stratégie a déjà été développée pour cibler l'interaction première entre CDK2 et cycline A (Gondeau et al., 2005). Au vu du succès de cette approche, deux autres peptides ont été élaborés pour cibler l'interface entre CDK4 et cycline D1 : un peptide nommé D1, qui dérive de l'hélice α5 de cycline D1 et un peptide nommé PISTVRE dérivant de l'hélice PISTVRE de CDK4.

3.2.5. Caractérisation *in cellulo*

Des tests de prolifération sur cellules de mélanome A375 ont été mis en place afin de déterminer l'effet de ces peptides sur la croissance cellulaire. Ces peptides ont été internalisés dans les cellules grâce au peptide vecteur CADY2 (Kurzawa et al., 2010). CADY2 est un peptide amphipathique qui

interagit avec les protéines et les peptides en formant des nanoparticules capables de traverser les membranes cellulaires. Après 48h de traitement, le peptide D1 s'est révélé être plus efficace que le peptide PISTVRE à 1µM pour inhiber la prolifération des cellules A375 (56 et 22% de réduction du nombre de cellules respectivement).

3.2.6. Caractérisation *in vitro*

Des variants courts et longs du peptide PISTVRE ont été conçus de façon à déterminer la séquence minimale permettant de cibler efficacement l'interface.

Afin de déterminer le meilleur variant dérivant de l'hélice PISTVRE, des tests d'interaction ont été réalisés entre ces peptides et le peptide D1 marqué avec la sonde fluorescente TAMRA. Au vu des constantes de dissociation (Kd) obtenues, le variant le plus court semble être celui qui interagit le mieux avec le peptide D1. Ces expériences devront également être réalisées avec la cycline D1, afin de caractériser l'affinité et la spécificité de l'interaction entre le peptide PISTVRE et l'hélice α5 de son partenaire, en tenant compte de tout l'environnement autour de cette interface et toutes les interactions secondaires présentes à cette interface.

4. Discussion et perspectives

4.1. Développement d'un biosenseur fluorescent pour étudier l'activité de CDK4/cycline D

Importance du PAABD

Nous avons d'abord développé un biosenseur protéique, CDKACTRb, contenant un PAABD dérivé du PBD de Plk1 et une séquence substrat spécifique de CDK4. Même si les résultats obtenus *in vitro* et *in extracto* étaient prometteurs, nous avons envisagé une autre stratégie, le développement d'un biosenseur peptidique, WWRb, plus facile à synthétiser, à internaliser dans les cellules et à stocker. Cependant, le manque de réponse du biosenseur *in extracto* montre que le PAABD qu'il contient et qui dérive du domaine WW de Pin1 n'est pas fonctionnel dans ce système en présence de tampon de lyse.

Ce manque de fonctionnalité nous a conduits à concevoir un nouveau biosenseur peptidique, WWshortRb, contenant un domaine de phospho-reconnaissance plus court, WWshort. Nous avons montré qu'il interagissait mieux avec le peptide substrat Rb et phospho-Rb que WWlong. De plus, WWshortRb a montré qu'il répondait à l'activité de CDK4/cycline D *in vitro* et *in extracto*.

Sensibilité des biosenseurs – importance de la sonde fluorescente

Les expériences menées *in vitro* ont montré que le choix de la sonde fluorescente était primordial pour obtenir une réponse du biosenseur WWshortRb. La taille et la structure de la sonde semble cruciale dans ces systèmes dynamiques. TAMRA, plus petite que DyLight650 et Cy3, est la seule sonde permettant de rapporter le changement conformationnel du biosenseur. On peut supposer qu'une grosse sonde fluorescente empêche stériquement le repliement du PAABD.

Lors de la phosphorylation du biosenseur par CDK4/cycline D, on observe une augmentation maximale de fluorescence de 40%. Cette limitation de l'intensité de fluorescence vient potentiellement du fait que TAMRA n'est pas extrêmement sensible par rapport à d'autres sondes. Il pourrait être intéressant de tester d'autres fluorophores comme DMN4 ou la merocyanine qui pourraient conduire à une augmentation plus forte de la fluorescence (Gulyani et al., 2011; Loving and Imperiali, 2008). Cependant, cette augmentation de fluorescence limitée ne provient peut-être pas de la sonde elle-même mais de l'environnement autour de l'interaction entre le PAABD et le susbtrat phosphorylé qui n'entraîne pas assez de changements de pH ou de polarité du solvant.

Bien que TAMRA ne soit pas reconnu comme étant un fluorophore très sensible, le biosenseur WWshortRb-TAMRA permet néanmoins de comparer l'activité de CDK4 dans différentes lignées de mélanome et de quantifier des différences qui ne peuvent pas être mises en évidence par simple analyse des profils d'expression.

Spécificité des biosenseurs

Les études menées *in extracto* ont permis de démontrer que CDKACTRb rapporte spécifiquement l'activité de CDK4/cycline D contenu dans des extraits de mélanome. Parmi les différents inhibiteurs

de kinases testés, seul PD-0332991 réduit le signal fluorescent de CDKACTRb de façon dose-dépendante.

La fluorescence de WWshortRb est réduite lorsqu'il est incubé avec PD-0332991 et LY2835219 mais pas avec la Roscovitine qui inhibe CDK1, CDK2, CDK5, CDK7 et CDK9. De la même façon, on observe une diminution du signal fluorescent WWshortRb lorsqu'il est incubé avec des extraits de cellules de mélanome préalablement traités avec un siRNA ciblant CDK4. De plus, après fractionation d'un extrait cellulaire A375 par gel filtration, WWshortRb est capable d'identifier les fractions contenant la protéine CDK4.

Application de WWshortRb pour détecter l'activité de CDK4 dans des lysats de biopsies de peau et de xénogreffes de mélanome

Nous avons montré que WWshortRb rapporte l'activité de CDK4/cycline D dans des extraits cellulaires provenant de biopsies de peau. WWshortRb a montré une activité plus faible de CDK4 dans des biopsies de peau présentant un psoriasis que dans des biopsies de peau saine.

WWshortRb a été appliqué à la quantification de l'activité de CDK4/cycline D dans des lysats de xénogreffes de mélanome implantées chez des souris ayant été traitées ou non avec PD-0332991. Ces expériences nous ont permis de réaliser l'importance de normaliser les extraits cellulaires par rapport à la proportion de cellules cancéreuses (A375 luciférase). En effet, comme les cellules stromales sont aussi présentes dans la tumeur, le lysat cellulaire contient des protéines normales et hyperactives, telles que CDK4/cycline D. Comme chaque tumeur grossit et se comporte différemment, le ratio faisant état du niveau d'expression entre les protéines normales et hyperactives change, entraînant ainsi une normalisation erronée.

Application de WWshortRb *in cellulo*

Nous avons démontré que WWshortRb était capable de franchir seul les membranes cellulaires, bien que nous n'ayons identifié aucune séquence particulière qui pourrait lui conférer un caractère auto-pénétrant. Ce résultat rend les expériences d'imagerie beaucoup plus simples puisque le biosenseur peptidique ne requiert, comme seule préparation, que son marquage fluorescent. Cependant la

stabilité *in vivo* du biosenseur doit être étudiée, car, n'ayant pas besoin d'une stratégie de vectorisation, il est complètement déprotégé vis à vis protéases.

Les expériences de vidéo-microscopie suggèrent qu'après plusieurs heures d'acquisition, le biosenseur ne répond plus de manière fiable. Il semblerait donc que WWshortRb soit plus adapté à des applications *in vitro* dans lesquelles il a prouvé être très fiable.

Conclusions et perspectives

Nous avons démontré que le biosenseur peptidique WWshortRb était un outil efficace *in vitro* pour détecter l'activité de CDK4/cycline D, biomarqueur établi dans le mélanome. Les informations fournies par WWshortRb complémentent celles obtenues par sérologie et histologie et pourraient permettre à terme d'établir un test diagnostic pour la détection précoce du mélanome.

De plus, étant donné que WWshortRb répond de manière sensible à l'inhibition de CDK4 par des inhibiteurs spécifiques de cette kinase, il représente une technologie puissante pour les programmes de drug discovery. Il permettrait d'évaluer la réponse au traitement et de s'assurer de l'efficacité de nouvelles générations d'inhibiteurs de CDK4.

WWshortRb pourrait être appliqué à la détection de l'hyperactivité de CDK4/cycline D dans d'autres cancers présentant une dérégulation de la voie the $p16^{INK4A}$ / CDK4-6 / cycline D / Rb tels que le cancer du poumon non à petites cellules (NSCLC).

WWshortRb constitue une alternative intéressante à la radioactivité ou aux approches antigéniques pour étudier l'activité de CDK4/cycline D *in vitro*. Il permet en plus de rapporter cette activité dans des échantillons biologiques complexes tels que le cytoplasme cellulaire ou l'environnement tumoral. A notre connaissance, WWshortRb est le premier outil permettant de quantifier l'activité kinase de CDK4 dans des biopsies de peau et dans des xénogreffes de mélanome.

Cette technologie peut être améliorée sur plusieurs points, notamment au niveau de la sonde fluorescente et sur la stabilité du biosenseur pour les applications *in vivo*. Des stratégies de photoactivation peuvent être envisagées afin de contrôler la période d'observation de la réaction et

d'améliorer le ratio signal/bruit. Pour empêcher la dégradation du biosenseur par les protéases, des modifications chimiques de la séquence peptidique peuvent être réalisées comme l'incorporation d'acides aminés non-naturels ou l'incorporation de liaison pseudo-peptidiques (Gentilucci et al., 2010). De plus, des formulations avec des vecteurs tels que les microparticules, nanoparticules, liposomes ou nanotubes de carbones pourraient également être testées (Patel et al., 2014).

4.2. Identification d'inhibiteurs non compétitifs de l'ATP ciblant CDK4/cycline D

A. Identification par criblage

Mise en place d'un criblage haut débit

Nous avons développé deux biosenseurs CDKCONF4A et CDKCONF4B qui ont été appliqués au criblage de deux chimiothèques. Mon travail a d'abord consisté à miniaturiser le test pour l'adapter à un format multi-plaques. Les conditions ont été optimisées de façon à réduire la concentration en réactifs et le temps de l'expérience. Ayant obtenu un Z-facteur supérieur à 0,5, nous avons procédé au criblage. 4% des composés de la CNE et 0,3% de ceux de la banque de Strasbourg ont été retenus avec les deux biosenseurs.

Caractérisation post-criblage

Les composés retenus ont été revalidés manuellement, à partir de poudres fraîches envoyées par les laboratoires d'origine. Des différences de réponse ont été observées entre le crible et la validation manuelle, probablement dues au fait que les poudres fraîches, à la différence des solutions contenues dans les plaques utilisées lors du criblage, ne contiennent que le composé pur, sans produits de dégradation.

Les deux hits de Strasbourg ont été caractérisés *in vitro* suite à leur identification par CDKCONF4A en tant qu'inhibiteurs protéine-protéine. Des expériences de binding ont été menées en utilisant le peptide PISTVRE fluorescent, qui dérive de l'hélice PISTVRE de CDK4. Nous avons montré qu'un seul hit interagissait avec ce peptide. Une famille de composés dérivant de ce hit a ensuite été

caractérisée. Cette étude a révélé que le choix de la sonde était crucial. En effet, la première sonde utilisée, TP2Rho, se liait aux composés et donnait donc des résultats erronés.

Les expériences *in cellulo* ont permis de démontrer que certains des dérivés, tels que RF1210 et LPI2252, étaient très efficaces pour réduire la prolifération de cellules cancéreuses A375. De plus, nous avons montré que ces deux composés étaient capables de coopérer avec d'autres inhibiteurs de CDK4 mais également avec des drogues utilisées fréquemment dans le traitement du cancer telles que le Paclitaxel et le methotrexate. Ces résultats offrent des perspectives très prometteuses dans le traitement du mélanome.

Conclusions et perspectives

Suite au criblage, nous avons identifié une famille de dérivés ayant un potentiel inhibiteur prometteur sur CDK4. Des simulations de dynamique moléculaire ont permis de montrer que, lorsque CDK4/cycline D est dans une conformation ouverte spécifique, ces composés se lient à une nouvelle poche, proche de l'hélice PISTVRE de CDK4. Des expériences de binding avec des mutants de CDK4 vont permettre de confirmer ce résultat.

Les composés de la CNE vont également être prochainement caractérisés *in vitro* et *in cellulo*.

Tous ces résultats permettent de mettre en évidence la puissance de la stratégie CDKCONF, basée sur la technologie FLiK (Fluorescent Labels in Kinases), pour identifier de nouveaux inhibiteurs non compétitifs de l'ATP.

B. Conception rationnelle de peptides ciblant l'interface entre CDK4 et cycline D

Conception de peptides

Pour cibler l'interface entre CDK4 et cycline D, nous avons développé une approche basée sur la conception rationnelle de peptides. Nous avons conçu deux peptides, PISTVRE et D1, qui dérivent de l'hélice PISTVRE de CDK4 et de l'hélice α5 de cycline D respectivement. Nous avons démontré que ces peptides inhibent efficacement la croissance des cellules de mélanome lorsqu'ils sont administrés

que CADY2. De plus, des expériences de titrations de fluorescence entre des variants de PISTVRE et le peptide D1 suggèrent que le variant le plus court, se lie avec la meilleure affinité.

Conclusions et perspectives

Le mécanisme d'action des variants de PISTVRE va être déterminé par des expériences *in vitro* en utilisant le complexe CDK4/cycline D recombinant. Leur potentiel inhibiteur vis-à-vis de l'activité de CDK4/cycline D sera caractérisé dans des tests d'activité et de prolifération.

Comparaison des deux stratégies

Pendant ma thèse, j'ai développé deux stratégies différentes pour inhiber l'activité de CDK4/cycline D. En termes de temps et de coûts, la stratégie rationnelle est beaucoup plus intéressante. En effet, la miniaturisation et l'optimisation du test HTS prennent du temps et requièrent l'utilisation de chimiothèques qui peuvent être coûteuses. De plus, les petites molécules, comparées aux peptides, nécessitent des stratégies de vectorisation afin d'être internalisées dans les cellules. Cependant, la stratégie de screening permet l'identification de hits ayant des structures chimiques très différentes, offrant ainsi une grande possibilité d'optimisation. Les peptides peuvent aussi être optimisés en taille et la génération de mutants permet l'identification d'acides aminés essentiels.

Enfin, notre approche de screening, couplée à de la modélisation moléculaire, a conduit à une découverte inattendue, l'identification d'une nouvelle poche allostérique, ce qui n'est pas possible avec une approche rationnelle.

5. Références

Ahsen, O. von, and Bömer, U. (2005). High-Throughput Screening for Kinase Inhibitors. ChemBioChem *6*, 481–490.

Allen, M.D., DiPilato, L.M., Rahdar, M., Ren, Y.R., Chong, C., Liu, J.O., and Zhang, J. (2006). Reading dynamic kinase activity in living cells for high-throughput screening. ACS Chem. Biol. *1*, 371–376.

Anai, T., Nakata, E., Koshi, Y., Ojida, A., and Hamachi, I. (2007). Design of a hybrid biosensor for enhanced phosphopeptide recognition based on a phosphoprotein binding domain coupled with a fluorescent chemosensor. J. Am. Chem. Soc. *129*, 6232–6239.

Arkin, M.R., and Wells, J.A. (2004). Small-molecule inhibitors of protein-protein interactions: progressing towards the dream. Nat. Rev. Drug Discov. *3*, 301–317.

Asghar, U., Witkiewicz, A.K., Turner, N.C., and Knudsen, E.S. (2015). The history and future of targeting cyclin-dependent kinases in cancer therapy. Nat. Rev. Drug Discov. *14*, 130–146.

Bandarchi, B., Ma, L., Navab, R., Seth, A., and Rasty, G. (2010). From Melanocyte to Metastatic Malignant Melanoma. Dermatol. Res. Pract. *2010*.

Boonstra, J. (2003). Progression through the G1-phase of the on-going cell cycle. J. Cell. Biochem. *90*, 244–252.

Boutros, R., Dozier, C., and Ducommun, B. (2006). The when and wheres of CDC25 phosphatases. Curr. Opin. Cell Biol. *18*, 185–191.

Brown, N.R., Noble, M.E., Lawrie, A.M., Morris, M.C., Tunnah, P., Divita, G., Johnson, L.N., and Endicott, J.A. (1999). Effects of phosphorylation of threonine 160 on cyclin-dependent kinase 2 structure and activity. J. Biol. Chem. *274*, 8746–8756.

Bruyère, C., and Meijer, L. (2013). Targeting cyclin-dependent kinases in anti-neoplastic therapy. Curr. Opin. Cell Biol. *25*, 772–779.

Chawla, R., Procknow, J.A., Tantravahi, R.V., Khurana, J.S., Litvin, J., and Reddy, E.P. (2010). Cooperativity of Cdk4R24C and Ras in melanoma development. Cell Cycle Georget. Tex *9*, 3305–3314.

Chène, P. (2004). Inhibition of the p53-MDM2 interaction: targeting a protein-protein interface. Mol. Cancer Res. MCR *2*, 20–28.

Chin, L., Garraway, L.A., and Fisher, D.E. (2006). Malignant melanoma: genetics and therapeutics in the genomic era. Genes Dev. *20*, 2149–2182.

Chudakov, D.M., Matz, M.V., Lukyanov, S., and Lukyanov, K.A. (2010). Fluorescent proteins and their applications in imaging living cells and tissues. Physiol. Rev. *90*, 1103–1163.

Day, P.J., Cleasby, A., Tickle, I.J., O'Reilly, M., Coyle, J.E., Holding, F.P., McMenamin, R.L., Yon, J., Chopra, R., Lengauer, C., et al. (2009). Crystal structure of human CDK4 in complex with a D-type cyclin. Proc. Natl. Acad. Sci. U. S. A. *106*, 4166–4170.

Dickson, M.A. (2014). Molecular pathways: CDK4 inhibitors for cancer therapy. Clin. Cancer Res. Off. J. Am. Assoc. Cancer Res. *20*, 3379–3383.

Eglen, R.M., and Reisine, T. (2010). Human kinome drug discovery and the emerging importance of atypical allosteric inhibitors. Expert Opin. Drug Discov. *5*, 277–290.

Floquet, N., Costa, M.G.S., Batista, P.R., Renault, P., Bisch, P.M., Raussin, F., Martinez, J., Morris, M.C., and Perahia, D. (2015). Conformational Equilibrium of CDK/Cyclin Complexes by Molecular Dynamics with Excited Normal Modes. Biophys. J.

García-Alvarez, B., de Cárcer, G., Ibañez, S., Bragado-Nilsson, E., and Montoya, G. (2007). Molecular and structural basis of polo-like kinase 1 substrate recognition: Implications in centrosomal localization. Proc. Natl. Acad. Sci. U. S. A. *104*, 3107–3112.

Gavet, O., and Pines, J. (2010). Progressive activation of CyclinB1-Cdk1 coordinates entry to mitosis. Dev. Cell *18*, 533–543.

Getlik, M., Simard, J.R., Termathe, M., Grütter, C., Rabiller, M., van Otterlo, W.A.L., and Rauh, D. (2012). Fluorophore Labeled Kinase Detects Ligands That Bind within the MAPK Insert of p38α Kinase. PLoS ONE *7*, e39713.

Giepmans, B.N.G., Adams, S.R., Ellisman, M.H., and Tsien, R.Y. (2006). The fluorescent toolbox for assessing protein location and function. Science *312*, 217–224.

Gondeau, C., Gerbal-Chaloin, S., Bello, P., Aldrian-Herrada, G., Morris, M.C., and Divita, G. (2005). Design of a novel class of peptide inhibitors of cyclin-dependent kinase/cyclin activation. J. Biol. Chem. *280*, 13793–13800.

Grafstrom, R.H., Pan, W., and Hoess, R.H. (1999). Defining the substrate specificity of cdk4 kinase–cyclin D1 complex. Carcinogenesis *20*, 193–198.

Hagopian, J.C., Kirtley, M.P., Stevenson, L.M., Gergis, R.M., Russo, A.A., Pavletich, N.P., Parsons, S.M., and Lew, J. (2001). Kinetic basis for activation of CDK2/cyclin A by phosphorylation. J. Biol. Chem. *276*, 275–280.

Hanson, G.T., and Hanson, B.J. (2008). Fluorescent probes for cellular assays. Comb. Chem. High Throughput Screen. *11*, 505–513.

Ho, A., and Dowdy, S.F. (2002). Regulation of G(1) cell-cycle progression by oncogenes and tumor suppressor genes. Curr. Opin. Genet. Dev. *12*, 47–52.

Iavarone, A., and Massagué, J. (1997). Repression of the CDK activator Cdc25A and cell-cycle arrest by cytokine TGF-beta in cells lacking the CDK inhibitor p15. Nature *387*, 417–422.

Jahnke, W., Blommers, M.J.J., Fernández, C., Zwingelstein, C., and Amstutz, R. (2005). Strategies for the NMR-based identification and optimization of allosteric protein kinase inhibitors. Chembiochem Eur. J. Chem. Biol. *6*, 1607–1610.

Jeffrey, P.D., Russo, A.A., Polyak, K., Gibbs, E., Hurwitz, J., Massagué, J., and Pavletich, N.P. (1995). Mechanism of CDK activation revealed by the structure of a cyclinA-CDK2 complex. Nature *376*, 313–320.

Jeffrey, P.D., Tong, L., and Pavletich, N.P. (2000). Structural basis of inhibition of CDK-cyclin complexes by INK4 inhibitors. Genes Dev. *14*, 3115–3125.

Jia, Y., Quinn, C.M., Kwak, S., and Talanian, R.V. (2008). Current in vitro kinase assay technologies: the quest for a universal format. Curr. Drug Discov. Technol. *5*, 59–69.

Kurzawa, L., Pellerano, M., and Morris, M.C. (2010). PEP and CADY-mediated delivery of fluorescent peptides and proteins into living cells. Biochim. Biophys. Acta *1798*, 2274–2285.

Kurzawa, L., Pellerano, M., Coppolani, J.B., and Morris, M.C. (2011). Fluorescent peptide biosensor for probing the relative abundance of cyclin-dependent kinases in living cells. PloS One *6*, e26555.

Lapenna, S., and Giordano, A. (2009). Cell cycle kinases as therapeutic targets for cancer. Nat. Rev. Drug Discov. *8*, 547–566.

Lebakken, C.S., Reichling, L.J., Ellefson, J.M., and Riddle, S.M. (2012). Detection of allosteric kinase inhibitors by displacement of active site probes. J. Biomol. Screen. *17*, 813–821.

Liu, Y., and Gray, N.S. (2006). Rational design of inhibitors that bind to inactive kinase conformations. Nat. Chem. Biol. *2*, 358–364.

Lolli, G. (2010). Structural dissection of cyclin dependent kinases regulation and protein recognition properties. Cell Cycle Georget. Tex *9*, 1551–1561.

Lu, P.J., Zhou, X.Z., Shen, M., and Lu, K.P. (1999). Function of WW domains as phosphoserine- or phosphothreonine-binding modules. Science *283*, 1325–1328.

Macias, M.J., Gervais, V., Civera, C., and Oschkinat, H. (2000). Structural analysis of WW domains and design of a WW prototype. Nat. Struct. Biol. *7*, 375–379.

Malumbres, M. (2011). Physiological relevance of cell cycle kinases. Physiol. Rev. *91*, 973–1007.

Malumbres, M., and Barbacid, M. (2001). To cycle or not to cycle: a critical decision in cancer. Nat. Rev. Cancer *1*, 222–231.

Martin, N.G., McAndrew, P.C., Eve, P.D., and Garrett, M.D. (2008). Phosphorylation of cyclin dependent kinase 4 on tyrosine 17 is mediated by Src family kinases. FEBS J. *275*, 3099–3109.

McNeil, P.L. (2001). Direct introduction of molecules into cells. Curr. Protoc. Cell Biol. Editor. Board Juan Bonifacino Al *Chapter 20*, Unit 20.1.

Morgan, D.O. (1997). Cyclin-dependent kinases: engines, clocks, and microprocessors. Annu. Rev. Cell Dev. Biol. *13*, 261–291.

Morris, M.C. (2010). Fluorescent biosensors of intracellular targets from genetically encoded reporters to modular polypeptide probes. Cell Biochem. Biophys. *56*, 19–37.

Morris, M.C., Gondeau, C., Tainer, J.A., and Divita, G. (2002). Kinetic mechanism of activation of the Cdk2/cyclin A complex. Key role of the C-lobe of the Cdk. J. Biol. Chem. *277*, 23847–23853.

Musgrove, E.A., Caldon, C.E., Barraclough, J., Stone, A., and Sutherland, R.L. (2011). Cyclin D as a therapeutic target in cancer. Nat. Rev. Cancer *11*, 558–572.

Nhu Ngoc Van, T., and Morris, M.C. (2013). Fluorescent sensors of protein kinases: from basics to biomedical applications. Prog. Mol. Biol. Transl. Sci. *113*, 217–274.

Peyressatre, M., Prével, C., Pellerano, M., and Morris, M.C. (2015). Targeting cyclin-dependent kinases in human cancers: from small molecules to Peptide inhibitors. Cancers *7*, 179–237.

Prével, C., Pellerano, M., Van, T.N.N., and Morris, M.C. (2014). Fluorescent biosensors for high throughput screening of protein kinase inhibitors. Biotechnol. J. *9*, 253–265.

Russo, A.A., Jeffrey, P.D., and Pavletich, N.P. (1996). Structural basis of cyclin-dependent kinase activation by phosphorylation. Nat. Struct. Biol. *3*, 696–700.

Schachter, M.M., Merrick, K.A., Larochelle, S., Hirschi, A., Zhang, C., Shokat, K.M., Rubin, S.M., and Fisher, R.P. (2013). A Cdk7-Cdk4 T-loop phosphorylation cascade promotes G1 progression. Mol. Cell *50*, 250–260.

Schneider, R., Becker, C., Simard, J.R., Getlik, M., Bohlke, N., Janning, P., and Rauh, D. (2012). Direct binding assay for the detection of type IV allosteric inhibitors of Abl. J. Am. Chem. Soc. *134*, 9138–9141.

Sheppard, K.E., and McArthur, G.A. (2013). The cell-cycle regulator CDK4: an emerging therapeutic target in melanoma. Clin. Cancer Res. Off. J. Am. Assoc. Cancer Res. *19*, 5320–5328.

Sherr, C.J. (1996). Cancer cell cycles. Science *274*, 1672–1677.

Sherr, C.J., and Roberts, J.M. (1999). CDK inhibitors: positive and negative regulators of G1-phase progression. Genes Dev. *13*, 1501–1512.

Simard, J.R., Grütter, C., Pawar, V., Aust, B., Wolf, A., Rabiller, M., Wulfert, S., Robubi, A., Klüter, S., Ottmann, C., et al. (2009a). High-throughput screening to identify inhibitors which stabilize inactive kinase conformations in p38alpha. J. Am. Chem. Soc. *131*, 18478–18488.

Simard, J.R., Getlik, M., Grütter, C., Pawar, V., Wulfert, S., Rabiller, M., and Rauh, D. (2009b). Development of a fluorescent-tagged kinase assay system for the detection and characterization of allosteric kinase inhibitors. J. Am. Chem. Soc. *131*, 13286–13296.

Simard, J.R., Klüter, S., Grütter, C., Getlik, M., Rabiller, M., Rode, H.B., and Rauh, D. (2009c). A new screening assay for allosteric inhibitors of cSrc. Nat. Chem. Biol. *5*, 394–396.

Simard, J.R., Getlik, M., Grütter, C., Schneider, R., Wulfert, S., and Rauh, D. (2010). Fluorophore labeling of the glycine-rich loop as a method of identifying inhibitors that bind to active and inactive kinase conformations. J. Am. Chem. Soc. *132*, 4152–4160.

Takaki, T., Echalier, A., Brown, N.R., Hunt, T., Endicott, J.A., and Noble, M.E.M. (2009). The structure of CDK4/cyclin D3 has implications for models of CDK activation. Proc. Natl. Acad. Sci. U. S. A. *106*, 4171–4176.

Tarrant, M.K., and Cole, P.A. (2009). The chemical biology of protein phosphorylation. Annu. Rev. Biochem. *78*, 797–825.

Taylor, D.L. (2010). A personal perspective on high-content screening (HCS): from the beginning. J. Biomol. Screen. *15*, 720–725.

Terada, Y., Tatsuka, M., Jinno, S., and Okayama, H. (1995). Requirement for tyrosine phosphorylation of Cdk4 in G1 arrest induced by ultraviolet irradiation. Nature *376*, 358–362.

Tsao, H., Chin, L., Garraway, L.A., and Fisher, D.E. (2012). Melanoma: from mutations to medicine. Genes Dev. *26*, 1131–1155.

Van, T.N.N., Pellerano, M., Lykaso, S., and Morris, M.C. (2014). Fluorescent Protein Biosensor for Probing CDK/Cyclin Activity in vitro and in Living Cells. Chembiochem Eur. J. Chem. Biol.

VanArsdale, T., Boshoff, C., Arndt, K.T., and Abraham, R.T. (2015). Molecular Pathways: Targeting the Cyclin D–CDK4/6 Axis for Cancer Treatment. Clin. Cancer Res.

Weissleder, R., and Ntziachristos, V. (2003). Shedding light onto live molecular targets. Nat. Med. *9*, 123–128.

Wölfel, T., Hauer, M., Schneider, J., Serrano, M., Wölfel, C., Klehmann-Hieb, E., De Plaen, E., Hankeln, T., Meyer zum Büschenfelde, K.H., and Beach, D. (1995). A p16INK4a-insensitive CDK4 mutant targeted by cytolytic T lymphocytes in a human melanoma. Science *269*, 1281–1284.

Wolff, M., Wiedenmann, J., Nienhaus, G.U., Valler, M., and Heilker, R. (2006). Novel fluorescent proteins for high-content screening. Drug Discov. Today *11*, 1054–1060.

Zaman, G.J.R., Garritsen, A., de Boer, T., and van Boeckel, C. a. A. (2003). Fluorescence assays for high-throughput screening of protein kinases. Comb. Chem. High Throughput Screen. *6*, 313–320.

Zhang, J., Adrián, F.J., Jahnke, W., Cowan-Jacob, S.W., Li, A.G., Iacob, R.E., Sim, T., Powers, J., Dierks, C., Sun, F., et al. (2010). Targeting Bcr-Abl by combining allosteric with ATP-binding-site inhibitors. Nature *463*, 501–506.

Zuo, L., Weger, J., Yang, Q., Goldstein, A.M., Tucker, M.A., Walker, G.J., Hayward, N., and Dracopoli, N.C. (1996). Germline mutations in the p16INK4a binding domain of CDK4 in familial melanoma. Nat. Genet. *12*, 97–99.

Articles in preparation

Monitoring CDK4 activity in cell extracts, melanoma xenografts and skin biopsies with a fluorescent peptide biosensor

Camille Prével[1], Morgan Pellerano[1], Juan A.González-Vera[1], Pauline Henri[1], Laurent Meunier[1], Julien Vollaire[2,3], Véronique Josserand[2,3]and May C. Morris[1]*

[1]Institut des Biomolécules Max Mousseron – IBMM -CNRS-UMR 5247,
Faculté de Pharmacie, 15, Av. Charles Flahault, 34093 Montpellier, France
[2]INSERM U823, Institut Albert Bonniot, F-38000 Grenoble, France
[3]Univ. Grenoble Alpes, Institut Albert Bonniot, F-38000 Grenoble, France

*To whom correspondance should be addressed.

Email: may.morris@univ-montp1.fr

#Corresponding author: M.C. Morris: may.morris@univ-montp1.fr

Tel : + 33 (0) 4 11 75 96 24 ; Fax : + 33 (0) 4 11 7596 41

Classification : biological sciences, biochemistry

ABSTRACT

Uncontrolled proliferation of melanocytes results in melanoma, the most aggressive form of skin cancer, which further metastasizes into a deadly form of cancer. The $p16^{INK4a}$-Cyclin D-CDK4/6-pRb pathway is dysregulated in 90% of melanomas and activation of this pathway potently cooperates with mutant BRAF or NRAS in transformation of melanocytes. CDK4/Cyclin D kinase hyperactivation, associated with mutation of CDK4, amplification of Cyclin D or loss of $p16^{INK4a}$ leads to increased risk of developing melanoma. This kinase therefore constitutes a key biomarker and an emerging pharmacological target in melanoma. Here we describe the design and characterization of a fluorescent peptide biosensor which reports on CDK4 activity *in vitro* and in melanoma cell extracts. CDKACT4 biosensor provides sensitive means of comparing CDK4 activity between different melanoma cell lines, and of quantifying differences which cannot be identified by simple analysis of protein kinase expression levels, associated with multiple molecular alterations that converge on CDK4 kinase activity. This biosensor further allows to quantify response to CDK4 inhibitors in cell extracts, providing a direct readout of their efficacy in a fluorescence-based assay. Finally CDKACT4 was applied to quantify this enzymatic biomarker in skin biopsies and in melanoma xenograft lysates, thereby demonstrating its utility to monitor CDK4 inhibition at an early stage following treatment with targeted kinase inhibitors. This first-of-a kind diagnostic tool offers an alternative to immunological identification of serological and histological markers, for early-stage detection of melanoma onset, progression of the disease and response to therapeutics.

Keywords:

Fluorescent Biosensor / CDK4/Cyclin D / Kinase activity / Melanoma

SIGNIFICANCE STATEMENT

Skin cancers, in particular melanoma, constitute an important cause of death worldwide. Although antibody-based approaches are currently implemented for detection of several histological and serological melanoma-specific biomarkers, new tools are required to monitor enzymatic biomarkers whose hyperactivity is associated with the onset and progression of this disease. The $p16^{INK4a}$-Cyclin D-CDK4/6-pRb pathway is dysregulated in 90% of melanomas, resulting in hyperactivity of CDK4 kinase, which promotes and sustains uncontrolled cell proliferation. Here we report on the design and development of a fluorescent peptide biosensor for quantification of CDK4 activity in melanoma cell extracts, skin biopsies and melanoma xenografts. This biosensor constitutes a promising tool for diagnostic and prognostic purposes, which affords means of monitoring cancer-associated alterations in kinase activity which are complementary to immunological identification of melanoma-specific biomarkers.

INTRODUCTION

Skin cancers constitute an important cause of death worldwide, with an estimated 80 000 deaths a year as of 2010, 49 000 of which are due to melanoma. This aggressive and invasive form of skin cancer arises from deregulated proliferation of melanocytes, and can metastasize into a deadly form of cancer (1). Several morphological, histological and serological biomarkers currently serve to diagnose malignant melanoma and establish a prognostic profile, including melanocyte lineage and differentiation antigens such as S100-beta, melanoma inhibitory activity (MIA) and tyrosinase, proangiogenic factors such as VEGF (Vascular Endothelial Growth Factor), molecules involved in cell adhesion and motility such as matrix metalloproteinases MMP-1 and 9, cytokines and cytokine receptors IL-6, IL-10 and sIL-2R, HLA molecules and other more general cancer biomarkers including C-reactive protein, albumin and lactate dehydrogenase (2–4). Histological analysis of skin biopsies constitutes the standard procedure for melanoma diagnostics, but remains poorly standardized, and is not implemented to monitor the onset and early-stage progression of this disease (5). Moreover, immunohistochemistry and ELISA convey information concerning the presence and relative abundance of biomarkers, but do not translate mutations in pathways that alter enzymatic activities associated with deregulated cell growth and proliferation. Hence, new tools are required to provide complementary information concerning enzymatic biomarkers of interest for diagnostic and prognostic purposes.

More recent genetic, transcriptomic and proteomic profiling studies have led to characterization of the landscape of genomic mutations in cutaneous melanoma, to identification of driver mutations and establishment of a framework for genomic classification of melanoma into four subtypes based on the most prevalent significantly mutated genes (6, 7). These studies highlight molecular pathways and targets which offer new perspectives for the development of complementary diagnostic and therapeutic tools. In particular, the cyclin-dependent kinase CDK4 has been identified as an emerging pharmacological target in human melanoma (8–10). This serine/threonine kinase associates with D-type cyclins and integrates stimuli that promote exit from quiescence, entry into and progression through G1, through phosphorylation of its substrate, the Retinoblastoma tumour suppressor protein (pRb) (11). The $p16^{INK4a}$-Cyclin D-CDK4/6-pRb pathway is dysregulated in 90% of melanomas and CDK4 hyperactivation may occur through various fashions, including mutation of CDK4 (R24C) which prevents binding of the endogenous inhibitor $p16^{INK4a}$, amplification of Cyclin D (18% melanomas), genetic deletion or loss-of-function of its endogenous inhibitor $p16^{INK4a}$ (deletion of CDK2NA in 50-60% metastatic tumours) (12, 13). Moreover in both human and mouse models of melanoma, activation of the CDK4 pathway potently cooperates with mutant BRAF or NRAS in transformation of melanocytes (14) inferring that combination strategies utilizing inhibition of complementary oncogenic pathways may offer a very promising approach (9). Furthermore, recent data suggest that cell cycle inhibition by CDK4 inhibitors sensitizes melanoma cells to compounds that induce apoptosis (15). Taken together, these studies identify CDK4/Cyclin D activity as a relevant biomarker of

melanoma, and suggest that tools reporting on CDK4 kinase activity and assays enabling quantification of its hyperactivity directly from skin biopsies would offer promising means of identifying the onset of melanoma and monitoring progression of this disease.

In this study we describe a fluorescent peptide biosensor that reports on CDK4/Cyclin D kinase activity through sensitive changes in fluorescence intensity. We show that this biosensor responds to recombinant CDK4/Cyclin D1 and can report on CDK4 activity in melanoma cell extracts, thereby enabling quantification of differences in kinase activity which cannot be identified by simple analysis of protein kinase expression levels, associated with molecular alterations in individual components of the $p16^{INK4a}$-Cyclin D-CDK4/6-pRb pathway. This biosensor further reports on CDK4 kinase inhibition following treatment with small molecule inhibitors or siRNA, thereby allowing to assess their overall efficacy in a physiologically-relevant environment. Finally we show that this technology can be readily be implemented to probe CDK4 activity in skin biopsies and in melanoma xenograft lysates, thereby constituting an attractive tool for diagnostics, prediction of pathological progression and response to therapeutics targeting the CDK4 biomarker.

RESULTS

Design and characterization of a CDK4-specific protein biosensor

Although CDK4/Cyclin D kinase constitutes an established biomarker and pharmacological target in melanoma, there are no means of probing its hyperactivity in a sensitive and quantitative fashion. Indeed, the larger part of technologies to probe this kinase activity currently rely on radioactivity or antibody-based approaches. Therefore, in order to probe CDK4/Cyclin D activity, we engineered a CDK4-specific protein biosensor derived from a previously-developed biosensor that responds to overall CDK/Cyclin activity through sensitive changes in fluorescence intensity (16). CDKACTRb was designed by incorporating a substrate sequence derived from the phosphorylation site of Retinoblastoma protein (Rb) which is specifically phosphorylated by CDK4/Cyclin D (S795) (17) with the phosphoamino acid binding domain (PAABD) derived from Polo-box domain of Plk1, devoid of cysteine residues (16) (**Fig.1*A***). When CDKACTRb was labelled with a Cy3 dye on the unique cysteine proximal to the phosphorylation site of the Rb substrate sequence, this protein biosensor responded to recombinant CDK4/Cyclin D1 through enhancement of fluorescence emission (20-25%), inferring an intramolecular interaction between the PAABD and the phosphorylated substrate moiety that alters the local environment of the probe, as reported for the generic CDKACT biosensor. Moreover this fluorescence enhancement was significantly reduced upon addition of the CDK4-specific inhibitor PD-0332991 (**Fig.1*B***). CDKACTRb further reported on endogenous CDK4 activity from A375 melanoma cell extracts in a dose-dependent fashion, since addition of increasing concentrations of PD-0332991 reduced the fluorescent signal of CDKACTRb accordingly (**Fig.1*C*** and **1*D***). These results further allowed to determine an IC_{50} value of 5.9 µM for PD-0332991 using A375 melanoma cell extracts (**Fig.1*D*** and **Fig.S1**), a value which reflects the inhibitory efficiency of this compound in a more

physiological context than with the purified recombinant kinase alone. In contrast, other CDK kinase inhibitors (Roscovitine, RO3306, AT7519) and other protein kinase inhibitors (PP2, H89, U0126) had no significant effect on CDKACTRb fluorescence, inferring it responds specifically to CDK4 activity (**Fig.1*E*** and **1*F***).

Development of a CDK4-specific peptide biosensor

Preparation of the CDKACTRb protein biosensor requires expression and purification of a recombinant protein scaffold with limited yield and long-term storage, since it suffers from degradation over time. To circumvent this issue, we designed a bipartite modular peptide derivative of CDKACTRb, which can be readily synthesized at a large-scale and stored in a lyophilized form. This peptide derivative (WWRb) bears the same Rb substrate and a short PAABD derived from the WW domain of the prolyl-isomerase Pin1, which was previously used as a phosphorecognition domain in a hybrid biosensor (18) (**Fig.2*A***). However, following labelling of this peptide biosensor on the unique cysteine at position -2 relative to the serine group phosphorylated by CDK4/Cyclin D, we found that it failed to respond in a robust and reproducible fashion (**Fig.S2**). We hypothesized that this might be due to a lack of proper conformation of the WW domain, and therefore designed a shorter artificial PAABD derived from the interface of the WW domain of Pin1 with a phosphopeptide substrate. Analysis of the crystal structure of this domain complexed to a phosphopeptide substrate (PDB 1F8A) led us to identify Arg14, Arg17, Tyr23 and Phe25, as well as Trp34 as critical residues for the interaction with the phosphosubstrate (GWEKRMSRSSGRVYYFNHITNASQWERPSG) (**Fig.2*B***). We therefore synthesized a short peptide derivative of this WW domain (WWshort) which comprises these key residues in the linear order of appearance that mimicks the interface (Phe25, Arg14, Tyr23, Arg17) interspaced by small uncharged amino acids, and which ends with Trp34 followed by the same five amino acids as in the native WW domain of Pin1 (GFARVYMSRSSGWERPSG). Titration experiments performed with an FITC-labelled Rb substrate peptide revealed that the WWshort peptide indeed interacted with the phosphorylated form of Rb substrate peptide with a dissociation constant value of 80 +/- 37 nM, similar to the long WW peptide (118 +/- 37 nM) (**Fig.2*C***). In comparison the WWshort and WWlong peptides bound the unphosphorylated substrate peptide with significantly lower dissociation values 628 +/- 109 nM and 675 +/- 260 nM, indicating that they preferentially bind the phosphorylated substrate, as expected from a PAABD (**Fig.S3**). Moreover, in both cases, the WWshort peptide promoted greater fluorescence enhancement of the fluorescently-labelled Rb substrate than its native counterpart, suggesting it was better suited as a PAABD for a biosensing application. We further asked whether the Rb substrate peptide could bind the recombinant form of CDK4. Indeed the FITC-labelled Rb substrate peptide bound monomeric GST-CDK4 with a dissociation constant value of 30 +/- 5 nM and its affinity increased to a Kd value of 7+/- 3 nM when the kinase was complexed to Cyclin D1 (**Fig.2*D***), as expected from studies showing that the substrate preferentially binds the catalytic cleft of heterodimeric CDK2/Cyclin A, which is conformationally more favourable than that of monomeric CDK2 (19).We therefore synthesized a CDK4

peptide biosensor, CDKACT4, comprising the WWshort peptide followed by the Rb substrate sequence. This peptide biosensor was further implemented to monitor response to recombinant CDK4 kinase *in vitro* in the presence of ATP and $MgCl_2$, following labelling of the unique cysteine within the substrate sequence with TAMRA. Analysis of changes in fluorescence intensity over time revealed that monomeric CDK4 bound the biosensor, inducing fluorescence enhancement of 40%, but that the biosensor responded to CDK4/Cyclin D1 complex further, with a net increase in relative fluorescence intensity (60%). The relative increase in fluorescence reached 75% when CDK4/CyclinD1 was preincubated with the CDK-activating kinase (to phosphorylate the activation loop), inferring that the kinase is catalytically more active in these conditions; in contrast, activity was partially reduced (55%) upon incubation with the CDK4 inhibitor PD-0332991 (**Fig.2*E***).

We further implemented the TAMRA-labelled CDKACT4 peptide biosensor to probe CDK4/Cyclin D kinase activity in A375 melanoma cell extracts, which resulted in a robust increase in fluorescence (similar to the enhancement profile observed with recombinant CDK4/Cyclin D1), whereas TAMRA-labelled Rb substrate peptide did not exhibit any change in fluorescence (**Fig.3*A***). In contrast, a Cy3 or Dylight-650-labelled CDKACT4 peptide barely responded to CDK4 activity in cell extracts, indicating that the response is associated with the sensitivity of the dye conjugated to the peptide (**Fig.S4**). The fluorescence of the TAMRA-CDKACT4 peptide biosensor was decreased upon treatment of cells with the CDK4 inhibitors PD-0332991 and LY2835219 in a dose-dependent fashion, but not upon addition of Roscovitine, which preferentially inhibits CDK2,CDK1,CDK5, CDK7 and CDK9 (**Fig.3*B***). Neither PD-0332991, Roscovitine, LY2835219 nor DMSO had any significant effect on the fluorescence of TAMRA-CDKACT4 peptide biosensor (**Fig.S5**). Likewise, the biosensor reported on a reduced CDK4 activity in A375 cells in which CDK4 protein levels were reduced following treatment with siRNA targeting CDK4 (**Fig.3*C***). Finally, CDKACT4 peptide biosensor was implemented to identify fractions bearing CDK4 activity following fractionation of A375 cell extracts by gel filtration chromatography (**Fig.3*D***).

These results reveal that the CDKACT4 peptide biosensor, comprising a short artificial phosphorecognition domain derived from the WW domain of Pin1 and a substrate sequence derived from Rb, constitutes a specific and sensitive tool to quantify CDK4 activity in melanoma cell extracts following treatment with selective inhibitors or downregulation of kinase levels by RNA silencing.

We next addressed whether CDKACT4 peptide biosensor was suited to quantify differences in CDK4 hyperactivity in different cell lines. First, comparison of the biosensor response to cell extracts from healthy fibroblasts and the A375 melanoma cell line revealed a significantly greater activity in A375 cells, consistent with the lack of control of CDK4 in this cell line due to $p16^{INK4a}$ loss of function (**Fig.4*A*** and **4*B***). We next asked whether CDKACT4 could serve to measure sensitive differences in CDK4 activity between melanoma cell lines harbouring different molecular alterations that ultimately converge on CDK4/Cyclin D activity. Specifically, CDKACT4 was incubated with normalized extracts derived from cell lines harbouring different

combinations of wild-type or loss-of function $p16^{INK4a}$ (the endogenous inhibitor of CDK4), wild-type or mutated CDK4 (R24C mutation which prevents the binding of $p16^{INK4a}$), BRaf and NRas. Fluorescent profiles of the CDKACT4 peptide biosensor revealed the highest CDK4 activity in A375 (CDKN2A loss of function, BRaf V600E), Mewo (CDKN2A loss of function, Wt CDK4) and SK-MEL28 (R24C CDK4, BRaf V600E) cell lines, followed by SK-MEL2 (NRas mutation (Q61R)) (**Fig.4*C*** and **4*D***). Quantification of the relative fluorescence intensity values at the plateau of response in a histogram clearly reveals significant differences in CDK4 activity between these cell lines (**Fig.4*D***). These response profiles are consistent with the genotypes of these strains in which loss of function of CDKN2A or mutation of the R24C CDK4 mutant both lead to unrestricted, constitutive activity of CDK4 in A375, SK-MEL28 and Mewo cell lines, in comparison with SK-MEL2 cell line which bears wild-type CDK4, $p16^{INK4a}$ and pRb. Importantly, the information provided by the biosensor differs from the protein expression profiles revealed by Western blotting, which do not predict any major differences in CDK4 activity between the different melanoma cell lines (**Fig.4*E*** and **4*F***).

Taken together these experiments show that the CDKACT4 peptide biosensor is a useful tool to compare and quantify differences in CDK4/Cyclin D kinase activity between different melanoma cell lines, which cannot be identified by quantification of protein kinase expression levels alone, as they reflect mutations or molecular alterations in components of the $p16^{INK4a}$-Cyclin D-CDK4/6-pRb pathway which ultimately converge on CDK4 kinase activity.

Quantifying CDK4/Cyclin D activity in skin biopsies and melanoma xenograft lysates

Since the CDKACT4 peptide biosensor responded to CDK4 activity in melanoma cell extracts and reported differences between cell lines with different $p16^{INK4a}$ and CDK4 genotypes, we asked whether it could be applied to quantify CDK4 activity in skin biopsies. First, we assessed and calibrated its response to different concentrations of total healthy skin samples, relative to A375 cell extracts (**Fig.5*A***). As with melanoma cell extracts, CDKACT4 fluorescence was decreased by addition of PD-0332991 (**Fig.5*B***). We further sought to determine whether CDK4 activity could be detected in the dermis or epidermis, and found that it was essentially present in the latter (**Fig.5*C***), consistent with the fact that rapidly dividing cells are found in the epidermis.

Finally we asked whether CDKACT4 could be implemented to monitor subtle differences in CDK4 activity in tumour xenografts following short- and long-term administration of kinase inhibitors. To this aim, we implanted the melanoma cell line A375 subcutaneously into the flank of nude mice and after 24 days of tumour growth, mice were treated daily orally either with the CDK4 inhibitor PD-0332991 at 150 mg/kg for 3 or 7 days, or 75 mg/kg for 7 days, or with the CDK2/5/7/9 inhibitor Roscovitine at 50 mg/kg for 5 or 11 days. Following treatment with PD-0332991, we did not observe any growth inhibition of melanoma tumour xenografts (**Fig. S6**), nor any specific decrease in CDK4 protein levels (**Fig. S7**). Likewise treatment with Roscovitine had no major effect after 5 days, but significantly affected tumour growth after 11 days

(**Fig. S6**). Biopsies of the xenografted tumours from three mice for each of these conditions were lysed and cell extracts incubated with TAMRA-labelled CDKACT4 peptide biosensor. We further normalized the response of CDKACT4 to that of luciferase activity of the A375 xenograft lysates, to minimize any differences that might be associated with tumoral heterogeneity, and found that all samples responded in a consistent fashion (**Fig. 6** and **Fig. S8**). Indeed, these experiments revealed that 150 mg/kg PD-0332991 had no inhibitory effect on CDK4 activity after three days of treatment. However, CDK4 activity began to decrease slightly after 7 days of treatment with 150 mg/kg and 75 mg/kg PD-0332991. In contrast, treatment of A375 xenografted tumours with 50 mg/kg Roscovitine, whether for 5 or 11 days, had no significant effect on CDKACT4 fluorescence, although the latter treatment clearly affected tumour growth, consistent with the inhibitory action of this compound towards CDKs other than CDK4/6.

Taken together our results show that CDKACT4 peptide biosensor can be implemented to quantify CDK4/Cyclin D kinase activity in skin biopsies and melanoma xenografts, thereby reporting on CDK4 inhibition in a sensitive and specific fashion. Moreover our results demonstratethe utility of this technology to monitor inhibition of CDK4 by small molecule drugs targeting this kinase, at early stages when measurement of tumoral volumes does not yet reflect any detectable effect of these drugs.

DISCUSSION

The limited efficacy of current therapeutics for treatment of melanoma and the lack of diagnostic assays to detect the onset of this disease calls for new strategies to probe relevant melanoma-specific biomarkers at an early stage and monitor their response to targeted therapeutics. The development of novel technologies is indeed essential since melanoma can be readily treated if detected at an early stage, but is incurable once it metastasizes. In particular enzymatic activities associated with dysregulated molecular signaling pathways constitute attractive biomarkers that may reflect the molecular alterations of one or several upstream regulatory partners, thereby complementing existing immunological approaches.

Fluorescent biosensors constitute potent tools for reporting on enzymatic activities in complex biological samples such as the cellular cytoplasm or the tumoral environment. Over the past decade, a wide variety of fluorescent biosensors have been developed to monitorand image enzymatic activities in living cells and have more recently proven to constitute attractive tools for biomedical applications (20). Indeed, several genetically-encoded FRET-based fluorescent biosensors have been developed to monitor aberrant kinase activity associated with cancer, such as the Bcr-Abl biosensor implemented to measure hyperactivity in cells of CML patients (21) or the Src biosensor applied to study spatial control of Src in pancreatic cancer by intravital FLIM-FRET imaging (22)**.** However, these systems require transfection and time for ectopic expression in living cells and are therefore not adapted for diagnostic assays using cell extracts or biopsies. In contrast, non-genetic fluorescent reporters based on polymeric or polypeptide scaffolds are well suited for such applications, since they can directly be incubated with enzymes or lysates containing activities to

be probed, and can further be conjugated to a large choice of synthetic probes, providing a controlled platform which can be readily implemented to probe specific targets of interest (23). Several non-genetic biosensors have been engineered to monitor extracellular proteolytic activities, such as metalloproteases secreted at the tumour site (24, 25). Moreover a wide variety of peptide biosensors have been developed to probe protein kinase activities (26, 27). These include peptide biosensors conjugated to solvatochromic probes, which respond either directly to proximal phosphorylation within the substrate sequence of the biosensor by kinases such as PKA, PKC, ERK, Bcr-Abl, Lyn and Abl (28–32), or indirectly following interactions with phosphorecognition domains that alter biosensor fluorescence, or through quenching/unquenching strategies (33–35). The recent implementation of fluorescent peptide biosensors to monitor kinase activities in cell extracts offers promising perspectives. However, to date, none of these chemical tools has been applied to quantify kinase activities in skin or tumour biopsies.

CDK4/Cyclin D kinase constitutes an established biomarker and pharmacological target in melanoma, hyperactivity of which is associated with mutations in the $p16^{INK4a}$-Cyclin D-CDK4/6-pRb pathway. Here we report on a new fluorescent biosensor, which constitutes a potent tool for probing CDK4 activity in cell extracts, skin biopsies and melanoma xenograft lysates, thereby providing a scaled and predictive readout of this enzymatic cancer biomarker. Besides being the first CDK4-specific biosensor, this bipartite peptide offers a novel and original design comprising a substrate sequence derived from Rb and an artificial phosphorecognition motif derived from the interface of a WW domain. Since this biosensor responds to CDK4 activity through changes in fluorescence intensity, it offers a straightforward and sensitive means of monitoring kinase activity in a continuous fluorescence-based assay over time. We show here that CDKACT4 is well suited to quantify differences in CDK4 activity in lysates from different cell lines, thereby highlighting alterations that cannot be identified by Western blot analysis of protein kinase expression levels. Moreover this biosensor provides means of assessing the efficacy of CDK4 inhibitors in a more physiologically-relevant environment than in buffer containing purified recombinant kinase, thereby offering promising perspectives for drug discovery programs.

Our work highlights the potency of fluorescent biosensors to monitor cancer-associated alterations in kinase activity, thereby offering an alternative to antibody-based approaches for developing diagnostic assays, and providing essential information for tailored therapeutic intervention. CDKACT4 biosensor constitutes a first-of-a kind tool for detection of a relevant enzymatic biomarker in melanoma, CDK4 kinase activity, and we anticipate it will enable to establish a diagnostic assay for monitoring melanoma onset, early-stage progression of this disease and response to therapeutics.

MATERIALS AND METHODS

Design and engineering of CDKACTRb protein biosensor. CDKACTRb was engineered by replacing the substrate sequence of CDKACT derived from histone H1 (16) by a substrate sequence derived from Rb in which the proline at position -2 relative to the SP phosphorylation site 795 was replaced by a cysteine residue.

The complete sequence of CDKACTRb is as follows:

GEVVDSHLSDMLQQLHSVNASKPSERGLVRQEEAEDPASIPIFWVSKWVDYSDKYGLGYQLSDNSVGVLFNDSTRLILYND GDSLQYIERDGTESYLTVSSHPNSLMKKITLLKYFRNYMSEHLLKAGANITPREGDELARLPYLRTWFRTRSAIILHLSNGSVQI NFFQDHTKLILSPLMAAVTYIDEKRDFRTYRLSLLEEYGSSKELASRLRYARTMVDKLLSSRSASNRLKASEFPGAGGTGLPGG YKFCSSPLRIPG.

GST-CDKACTRb was expressed in *E. coli* BL21pLyS following induction with 0.5 mM IPTG, at 20°C overnight, then purified on High Performance Glutathione Sepharose (GE Healthcare) in 50 mM Tris HCl, pH 7.4, 150 mM NaCl, and eluted with 50 mM glutathione in the same buffer, followed by gel filtration chromatography on Superdex75 (GE Healthcare) in the same buffer. Following purification, CDKACTRb was labelled with a 10-fold molar excess of Cy3-maleimide, then further purified on NAP5 columns in 50 mM Tris HCl, pH 7.4, 150 mM NaCl, to remove excess label.

Design and synthesis of CDKACT4 peptide biosensors and derived peptides.

Peptides were synthesized by GLSBiochem and purified to 95%.

The long WW peptide was derived from the native WW domain of Pin1 previously described by *Anai et al.* to generate a phosphopeptide hybrid biosensor (residues 6-39) (18). The shorter version was derived from the residues that line the interface with the phosphopeptide in the crystal structure of WW Pin1 complexed to a phosphopeptide substrate (PDB 1F8A).

The Rb substrate peptide was derived from the sequence around S795.

WW long	GWEKRMSRSSGRVYYFNHITNASQWERPSG
WW short	GFARVYMSRSSGWERPSGG
Rb substrate	GGYKFCSSPLRIPG
PhosphoRb substrate	GGYKFCSpSPLRIPG
WWRb	GWEKRMSRSSGRVYYFNHITNASQWERPSG GG YKFCSSPLRIPG
CDKACT4	GFARVYMSRSSGWERPSGG YKFCSSPLRIPG

Protein expression and purification of cyclin-dependent kinases. Recombinant GST-CDK4, GST-Cyclin D1

and GST-CIV, the CDK-activating kinase of *Saccharomyces cerevisiae*, were expressed in *E. coli* by IPTG induction and purified by chromatography as described previously (36). GST-CDK4 / Cyclin D1 complex was formed following individual purification of each subunit and stoichiometric incubation, then further incubated with GST-CIV to ensure its complete activation.

Fluorescence titration assays. Fluorescence titration assays were performed in 96-well plates in a thermostated chamber (Polarstar, BMG) at 30°C in 200 μL phosphate buffer saline with 200 nM concentration of FITC-labelled species (Rb peptide or Rb phosphopeptide). Changes in fluorescence emission were recorded at 520 nm following excitation at 495 nm. Data analysis was performed using the GraFit Software (Erathicus Ltd) and curve fitting was performed using a quadratic equation, as described in (36).

Fluorescence kinase assays. Fluorescence kinase assays were performed in 96-well plates in a thermostated chamber (Polarstar, BMG) at 30°C in 200 μL phosphate buffer saline supplemented with 5 mM $MgCl_2$, 0.5 mM ATP, except when stated otherwise. Changes in TAMRA and Cy3 fluorescence emission were recorded at 570 nm following excitation at 544 nm. In all experiments, relative fluorescence was calculated following subtraction of CDKACTRb-Cy3 or CDKACT4-TAMRA fluorescence from fluorescence values obtained in the presence of protein kinases, inhibitors or cell extracts. Data analysis was performed using the GraFit Software (Erathicus Ltd). Experiments were performed in triplicate, and error bars indicate standard deviation from average. Histograms represent relative fluorescence intensity values after 5000s, unless specified otherwise.

Inhibitors. Roscovitine, PD-0332991, LY2835219, AT7519, H89 and U0126 were purchased from Euromedex. RO3306 was purchased from CalbioChem. PP2 was purchased from Sigma. All stock solutions were made in DMSO and diluted in PBS to the desired concentration freshly prior to use. For animal experiments, PD-0332991 and Roscovitine were diluted in sodium lactate buffer 50 mM.

Cell culture and extract preparation. Cell culture media, serum and antibiotics were purchased from Invitrogen. All cell lines were cultured in DMEM/RPMI + Glutamax supplemented with 10% FCS, 100 units/mL penicillin (G sodium salt) and 100 μg/mL streptomycin at 37°C in an atmosphere containing 5% CO_2.

Melanoma cell lines used in this study:

	CDKN2A	CDK4	Rb	BRAF	NRAS
A375	mutated (E61Stop, Loss of function)	WT	WT	V600E	WT
Mewo	mutated (R80Stop, Loss of function)	WT	WT	WT	WT
SK-MEL2	WT	WT	WT	WT	mutated (Q61R)
SK-MEL28	WT	R24C		V600E	WT

siRNA targeting CDK4 were purchased from Santa Cruz (sc-29261). Internalization of siRNA in cells was performed using CADY peptide (37). Unsynchronized A375 cells were cultured to 60% confluence. A375 cells were treated with complexes of siRNA (100 nM) / CADY (4 µM) (1/40 ratio) for 48h.
Cell extracts were prepared in PBS lysis buffer containing PBS (Sigma), pH 7.4, 150 mM NaCl, 0.2% NP40, 1 mM EDTA, 2 mM PMSF, CompleteTM protease inhibitors (Roche), and normalized following spectrophotometric dosage at 280 nm.
Fractionation of A375 cell extracts prepared from 5 million cells in 500 µL PBS lysis buffer was performed by gel filtration chromatography on a Superose 6 10/300 GL column (GE Healthcare). 500 µL fractions were collected and 50 µL were used for kinase activity assays.

Western blotting. Polyclonal rabbit anti-CDK4 antibody was purchased from Santa Cruz (sc-260). Monoclonal mouse α-tubulin antibody was purchased from Amersham (N356). Polyclonal rabbit anti-actin antibody was purchased from Cell Signaling (4967).

Preparation of extracts from skin biopsies. Epidermis and dermis were separated by addition of thermolysine (0.5 mg/mL diluted in PBS (Sigma)) for 3h at 37°C. Total proteins were extracted from frozen skin biopsies in 50 mM Trizma Base, 0.5 M NaCl, 5 mM EDTA, 0.6% NP40 and grinding with an Ultra TurraxTM, then normalized following spectrophotometric dosage at 280 nm.

A375 xenografts in mice. All animal experiments were conducted in agreement with the Principles of Laboratory Animal Care (National Institutes of Health publication no. 86-23, revised 1985) and approved by the regional ethics committee. Female 6 weeks old NMRI nude mice (Janvier, Le Genest- Isle, France) were anesthetized (isoflurane/oxygen 3.5% for induction and 1.5% thereafter) and 3.10^6 A375 (luciferase-transfected) cells in 200 µL phosphate-buffered saline were implanted subcutaneously into the flank of mice and after 24 days of tumour growth, when tumours had reached 257 +/- 64 mm^3, mice were treated daily orally with CDK4 inhibitor PD-0332991 at 150 mg/kg or 75 mg/kg for 7 days, or 150 mg/kg for 3 days, or through intraperitoneal injection with the CDK2/5/7/9 inhibitor Roscovitine at 50 mg/kg for 5 or 11 days.

Mice were then sacrificed and tumours were collected and frozen. Total proteins were extracted from tumour samples by addition of a luciferase cell culture lysis reagent (25 mM Tris-phosphate pH 7.8, 2 mM DTT, 2 mM EDTA, 10% glycerol, 1% Triton X-114) and grinding with an Ultra TurraxTM, then normalized to the proportion of cancer cells (A375 luciferase) (Victor^3 V luminescence microplate reader, Perkin Elmer).

ACKNOWLEDGEMENTS

This work was supported by the CNRS (Centre National de la RechercheScientifique) and grants from the Region Languedoc-Roussillon (Subvention "Chercheuse d'Avenir") and Institut de Recherche contre Cancer (INCA) to MCM. CP was supported by a fellowship from the CBS2 doctoral school of Montpellier University. JAGV was supported by a Marie-Curie fellowship EC-FP7 Framework. We thank Carmen-Mihaela Tîlmaciu for critical reading of the manuscript.

REFERENCES

1. Lozano R, et al. (2012) Global and regional mortality from 235 causes of death for 20 age groups in 1990 and 2010: a systematic analysis for the Global Burden of Disease Study 2010. *Lancet* 380(9859):2095–2128.

2. Utikal J, Schadendorf D, Ugurel S (2007) Serologic and immunohistochemical prognostic biomarkers of cutaneous malignancies. *Arch Dermatol Res* 298(10):469–477.

3. GuoHB, Stoffel-Wagner B, Bierwirth T, Mezger J, Klingmüller D (1995) Clinical significance of serum S100 in metastatic malignant melanoma. *Eur J Cancer*31A(6):924–928.

4. Bosserhoff AK, et al. (1997) Melanoma-inhibiting activity, a novel serum marker for progression of malignant melanoma. *Cancer Res* 57(15):3149–3153.

5. Taylor CR (2000) The total test approach to standardization of immunohistochemistry. *Arch Pathol Lab Med* 124(7):945–951.

6. Hodis E, et al. (2012) A landscape of driver mutations in melanoma. *Cell* 150(2):251–263.

7. Cancer Genome Atlas Network (2015) Genomic Classification of Cutaneous Melanoma. *Cell* 161(7):1681–1696.

8. Sheppard KE, McArthur GA (2013) The cell-cycle regulator CDK4: an emerging therapeutic target in melanoma. *Clin Cancer Res* 19(19):5320–5328.

9. Miller DM, Flaherty KT (2014) Cyclin-dependent kinases as therapeutic targets in melanoma. *Pigment Cell Melanoma Res* 27(3):351–365.

10. Mahgoub T, et al. (2015) Kinase inhibitor screening identifies CDK4 as a potential therapeutic target for melanoma. *Int J Oncol* 47(3):900–908.

11. Malumbres M, Barbacid M (2009) Cell cycle, CDKs and cancer: a changing paradigm. *Nat Rev Cancer* 9(3):153–166.

12. Tsao H, Chin L, Garraway LA, Fisher DE (2012) Melanoma: from mutations to medicine. *Genes Dev* 26(11):1131–1155.

13. Young RJ, et al. (2014) Loss of CDKN2A expression is a frequent event in primary invasive melanoma and correlates with sensitivity to the CDK4/6 inhibitor PD0332991 in melanoma cell lines. *Pigment Cell Melanoma Res* 27(4):590–600.

14. Chawla R, et al. (2010) Cooperativity of Cdk4R24C and Ras in melanoma development. *Cell Cycle* 9(16):3305–3314.

15. Quast S-A, Steinhorst K, Plötz M, Eberle J (2015) Sensitization of Melanoma Cells for Death Ligand Trail is Based on Cell Cycle Arrest, Ros Production and Activation of ProapoptoticBcl-2 Proteins. *J Invest Dermatol*. doi:10.1038/jid.2015.250.

16. Van TNN, Pellerano M, Lykaso S, Morris MC (2014) Fluorescent Protein Biosensor for Probing CDK/Cyclin Activity in vitro and in Living Cells. *Chembiochem*.doi:10.1002/cbic.201402318.

17. Grafstrom RH, Pan W, Hoess RH (1999) Defining the substrate specificity of cdk4 kinase–cyclinD1 complex. *Carcinogenesis* 20(2):193–198.

18. Anai T, Nakata E, Koshi Y, Ojida A, Hamachi I (2007) Design of a hybrid biosensor for enhanced phosphopeptide recognition based on a phosphoprotein binding domain coupled with a fluorescent chemosensor. *J Am ChemSoc* 129(19):6232–6239.

19. Brown NR, et al. (1999) Effects of phosphorylation of threonine 160 on cyclin-dependent kinase 2 structure and activity. *J BiolChem* 274(13):8746–8756.

20. Lemke EA, Schultz C (2011) Principles for designing fluorescent sensors and reporters. *Nat ChemBiol* 7(8):480–483.

21. Mizutani T, et al. (2010) A novel FRET-based biosensor for the measurement of BCR-ABL activity and its response to drugs in living cells. *Clin Cancer Res* 16(15):3964–3975.

22. Nobis M, et al. (2013) IntravitalFLIM-FRET Imaging Reveals Dasatinib-Induced Spatial Control of Src in Pancreatic Cancer. *Cancer Res* 73(15):4674–4686.

23. Pazos E, Vázquez O, MascareñasJL, Vázquez ME (2009) Peptide-based fluorescent biosensors. *ChemSoc Rev* 38(12):3348–3359.

24. Bogyo M (2006) Metalloproteases see the light. *Nat ChemBiol* 2(5):229–230.

25. Weissleder R, Pittet MJ (2008) Imaging in the era of molecular oncology. *Nature* 452(7187):580–589.

26. González-Vera JA (2012) Probing the kinome in real time with fluorescent peptides. *ChemSoc Rev* 41(5):1652–1664.

27. Nhu Ngoc Van T, Morris MC (2013) Fluorescent sensors of protein kinases: from basics to biomedical applications. *ProgMolBiolTranslSci* 113:217–274.

28. Chen C-A, Yeh R-H, Lawrence DS (2002) Design and synthesis of a fluorescent reporter of protein kinase activity. *J Am ChemSoc* 124(15):3840–3841.

29. Shults MD, Janes KA, Lauffenburger DA, Imperiali B (2005) A multiplexed homogeneous fluorescence-based assay for protein kinase activity in cell lysates. *Nat Methods* 2(4):277–283.

30. Luković E, Vogel Taylor E, Imperiali B (2009) Monitoring Protein Kinases in Cellular Media with Highly Selective Chimeric Reporters. *AngewandteChemie International Edition* 48(37):6828–6831.

31. Damayanti NP, Parker LL, IrudayarajJMK (2013) Fluorescence Lifetime Imaging of Biosensor Peptide Phosphorylation in Single Live Cells. *AngewChemInt Ed* 52(14):3931–3934.

32. Wang Q, et al. (2010) Multicolor monitoring of dysregulated protein kinases in chronic myelogenous leukemia. *ACS ChemBiol* 5(9):887–895.

33. Sharma V, Agnes RS, Lawrence DS (2007) Deep quench: an expanded dynamic range for protein kinase sensors. *J Am ChemSoc* 129(10):2742–2743.

34. Wang Q, Lawrence DS (2005) Phosphorylation-driven protein-protein interactions: a protein kinase sensing system. *J Am ChemSoc* 127(21):7684–7685.

35. Wang Q, Dai Z, Cahill SM, Blumenstein M, Lawrence DS (2006) Light-regulated sampling of protein tyrosine kinase activity. *J Am ChemSoc* 128(43):14016–14017.

36. Gondeau C, et al. (2005) Design of a novel class of peptide inhibitors of cyclin-dependent kinase/cyclin activation. *J BiolChem* 280(14):13793–13800.

37. Crombez L, et al. (2009) A new potent secondary amphipathic cell-penetrating peptide for siRNA delivery into mammalian cells. *Mol Ther* 17(1):95–103.

FIGURE LEGENDS

Figure 1. The CDKACTRb protein biosensor responds specifically to recombinant CDK4/Cyclin D1 and CDK4 activity from melanoma cell extracts. (A) CDKACTRb biosensor consists of a CDK4-specific substrate sequence derived from pRb in which a cysteine residue was introduced at position -2 relative to the SP phosphorylation site (795), and a phospho amino acid-binding domain derived from the PBD of Plk1 (16) which recognizes the substrate sequence phosphorylated by CDK4/Cyclin D kinase. (B) Fluorescence of 50 nM CDKACTRb-Cy3 was monitored over time upon incubation with 75 nM active recombinant CDK4/Cyclin D1 alone (open circles) and with 20 µM PD-0332991 (black circles). (C) Fluorescence of 25 nM CDKACTRb-Cy3 was monitored over time upon incubation with 10 µg A375 cell extracts +/- PD-0332991 alone (open circles) and with 20 µM PD-0332991 (black circles). (D) Fluorescence of 25 nM CDKACTRb-Cy3 was monitored upon incubation with 10 µg A375 cell extracts +/- different concentrations of PD-0332991 (CDK4/6 inhibitor), or (E) Roscovitine (CDK1/2/5/7/9 inhibitor), RO3306 (CDK1 inhibitor), AT7519 (CDK2/4/5/9 inhibitor), (F) PP2 (Src inhibitor), U0126 (MAPK inhibitor) or H89 (PKA inhibitor).

Figure 2. Design and characterization of the CDKACT4 peptide biosensor. (A) CDKACT4 peptide biosensor consists of a substrate sequence derived from pRb (as in CDKACTRb), and a phospho amino acid-binding peptide derived from the interface of Pin1 WW domain with a phosphorylated substrate peptide. (B) The Arg, Tyr, Phe and Trp residues at interface between Pin1 WW domain (green) that recognize a phosphorylated peptide (yellow) are highlighted in pink (Arg) and orange (Tyr, Phe and Trp) (PDB 1F8A). (C) Fluorescence titration of 200 nM FITC-labelled phospho-Rb peptide with full-length WW peptide (triangles) and WWshort peptide (circles). (D) Fluorescence titration of 200 nM FITC-labelled Rb substrate peptide with monomeric GST-CDK4 (triangles) and GST-CDK4/Cyclin D1 complex (circles). (E) Fluorescence profile of 150 nM TAMRA-labelled CDKACT4 peptide biosensor incubated with 75 nM recombinant GST-CDK4 (black triangles), GST-CDK4/Cyclin D1 (black circles) or GST-CDK4/Cyclin D1 preincubated with the CDK-activating kinase CIV to phosphorylate Thr172 (open circles) and with 10 µM PD-0332991 (open triangles).

Figure 3. Monitoring CDK4/Cyclin D activity in melanoma cell extracts. Fluorescence of 150 nM TAMRA-labelled CDKACT4 peptide biosensor was monitored over time upon incubation with (A) 40 µg A375 cell extracts (circles) and compared to the 150 nM TAMRA-labelled Rb substrate peptide alone (triangles). (B) 40 µg A375 cell extracts treated with 0 µM (open circles), 1 µM (black circles), 5 µM (open triangles), 10 µM (black triangles), 20 µM (open squares) PD-0332991, Roscovitine or LY2835219. (C) 40 µg A375 cell extracts untreated (open circles) or treated with siRNA targeting CDK4 (black circles) and Western blot of CDK4 and tubulin protein levels from these cell extracts.(D) Histogramme representation of CDK4 activity measured in fractions of A375 cell extracts purified by gel filtration chromatography (Superose 6) and Western blot of CDK4 levels in the same fractions.

Figure 4. Monitoring CDK4/Cyclin D activity in different melanoma cell lines. Fluorescence of 150 nM TAMRA-labelled CDKACT4 peptide biosensor was monitored over time upon incubation with (A and B) 40 µg A375 cell extracts (circles) or fibroblasts (triangles) (C and D) 40 µg from melanoma cell lines A375 (open circles), Mewo (open triangles), SK-MEL2 (black triangles), SK-MEL28 (black circles). Histogramme quantifications in B and D represent relative fluorescence values of the assay at 5000s. (E) Western Blot of CDK4 levels in these different melanoma cell lines. (F) Quantification of CDK4/Actin levels.

Figure 5. Quantifying CDK4/Cyclin D activity in skin biopsies. Fluorescence of 150 nM TAMRA-labelled CDKACT4 peptide biosensor was monitored over time upon incubation with skin biopsies. Results are presented as histograms corresponding to the average of fluorescent intensity measurements at 5000s in duplicate experiments with standard deviation bars. (A) Concentration-dependent response to healthy skin samples compared to 50 µg A375 cell extracts. (B) Inhibition of response to CDK4/Cyclin D activity upon addition of 20 µM PD-0332991 to 100 µg skin samples. (C) Differential response to 50 µg total proteins extracted from dermis versus epidermis.

Figure 6. Response of CDKACT4 peptide biosensor to CDK4 activity in A375 xenografts treated with PD-0332991.

Fluorescence of 150 nM TAMRA-labelled CDKACT4 peptide biosensor, following incubation with 100 µL total proteins extracted from A375 tumour xenografts, normalized to luciferase activity measured in the same samples, and normalized to control (untreated samples) (A) from mice treated orally and daily with PD-0332991 at 150 mg/kg for 3 or 7 days, or with 75 mg/kg for 7 days (B) with Roscovitine at 50 mg/kg for 5 or 11 days. Histogrammes represent experiments performed in duplicate from three mice for each condition and relative to control (untreated) tumour samples.

Supplementary Figure 1. Dose–dependent inhibition of CDK4/Cyclin D activity monitored thanks to the CDKACTRb protein biosensor. (A) Fluorescence response of 25 nM Cy3-CDKACTRb protein biosensor to 10 µg A375 cell extracts treated with PD-0332991. (B) IC_{50} Plot - representation of the relative fluorescence of CDKACT4 biosensor at 8000 s, incubated with 10 µg A375 cell extracts and increasing concentrations of PD-0332991.

Supplementary Figure 2. Fluorescence response of 50 nM Cy3- and TAMRA-labelled WWRb peptide biosensor comprising the full-length native WW motif upon incubation with 20 µg A375 cell extracts alone (triangles) and with 20 µM PD-0332991 (circles).

Supplementary Figure 3. Titration of FITC-labelled unphosphorylated Rb substrate peptide with WW short (circles) and WW long peptide (triangles).

Supplementary Figure 4. (A) Comparative response of 50 nM TAMRA-labelled (circles) and Cy3-labelled (triangles) CDKACT4 peptide biosensor incubated with 20 µg A375 cell extracts. (B) Comparative response of 150 nM TAMRA-labelled (circles) and Dylight-650-labelled (triangles) CDKACT4 peptide biosensor incubated with 40 µg A375 cell extracts.

Supplementary Figure 5. CDKACT4 peptide biosensor does not respond to PD-0332991, Roscovitine, LY2835219 or DMSO. Fluorescence of 150 nM TAMRA-labelled CDKACT4 measured in the presence of increasing concentrations of (A) PD-0332991, (B) Roscovitine, (C) LY2835219, and (D) DMSO (no kinase or cell extracts).

Supplementary Figure 6. Growth curves of A375 xenografts treated with PD-0332991 or Roscovitine. Growth curves of A375 xenografts implanted in mice and treated with PD-0332991 at 150 mg/kg for 3 or 7 days, or with 75 mg/kg for 7 days, or Roscovitine at 50 mg/kg for 5 or 11 days. Control : mock treated mice. Arrows indicate time of treatment.

Supplementary Figure 7. CDK4 protein levels remain constant in tumour xenografts treated with PD-0332991

Western blot of CDK4 levels in the A375 xenograft extracts used in the first set of tumour xenografts prepared for measuring CDK4 activity in Figure 6.

Supplementary Figure 8. Response of CDKACT4 peptide biosensor to CDK4 activity in A375 xenografts treated with PD-0332991 or Roscovitine.

Fluorescence of 150 nM TAMRA-labelled CDKACT4 peptide biosensor following incubation with 100 µL total proteins extracted from A375 xenografted tumour biopsies and normalized to luciferase activity measured in the same tumour sample, (A) from mice treated orally and daily with PD-0332991 at 150 mg/kg for 3 or 7 days, or with 75 mg/kg for 7 days, or (B) Roscovitine for 50 mg/kg for 5 or 11 days. Each mouse sample was treated in duplicate.

Figure 1.

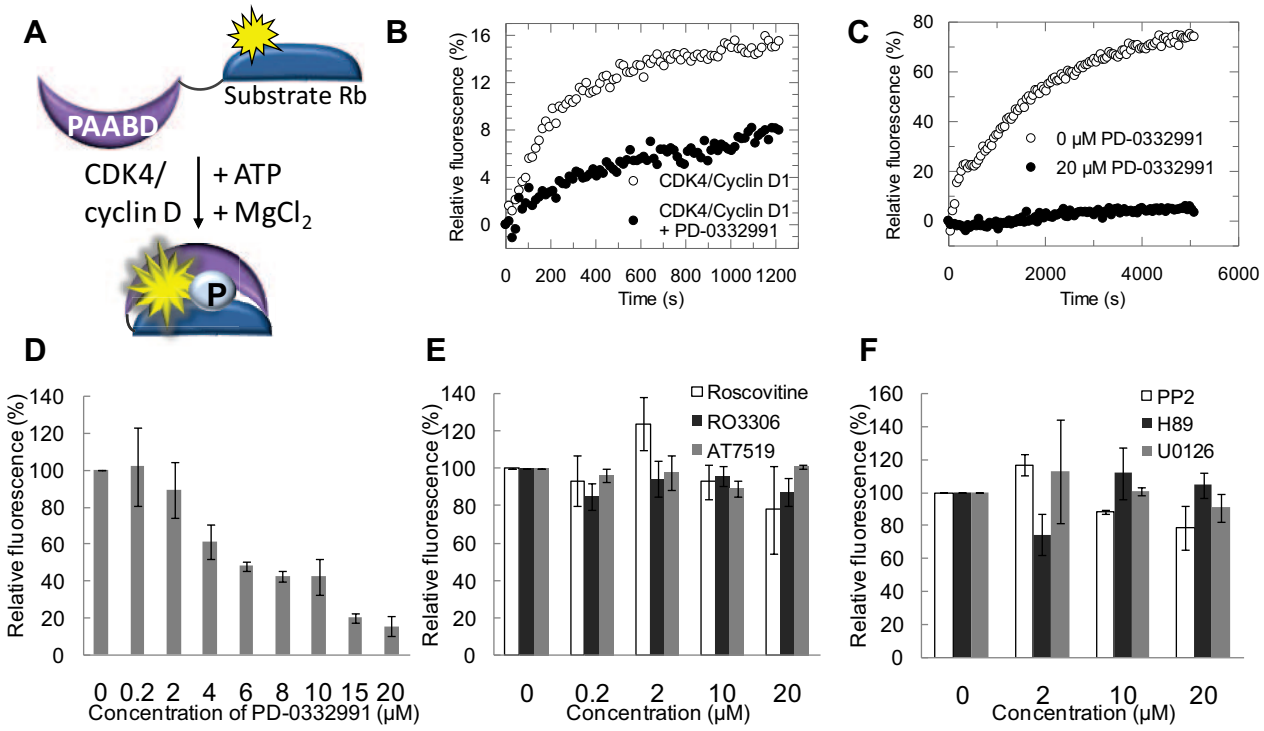

Figure 2.

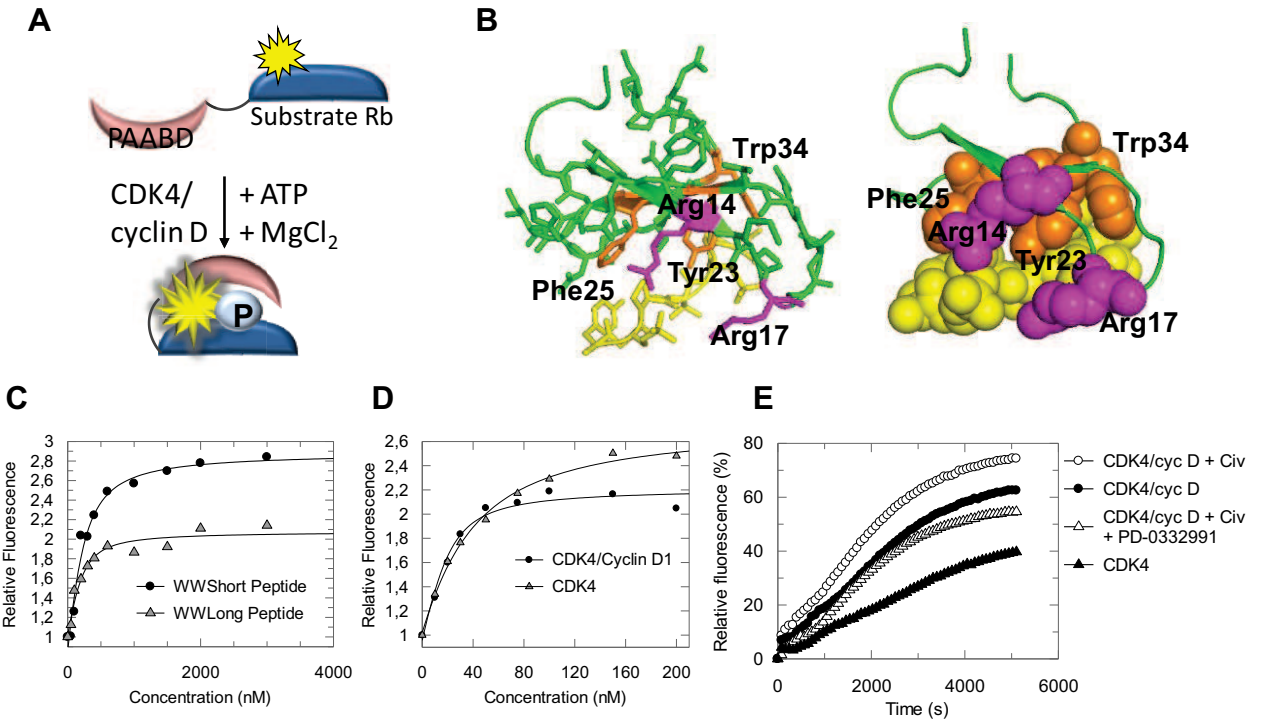

Figure 3.

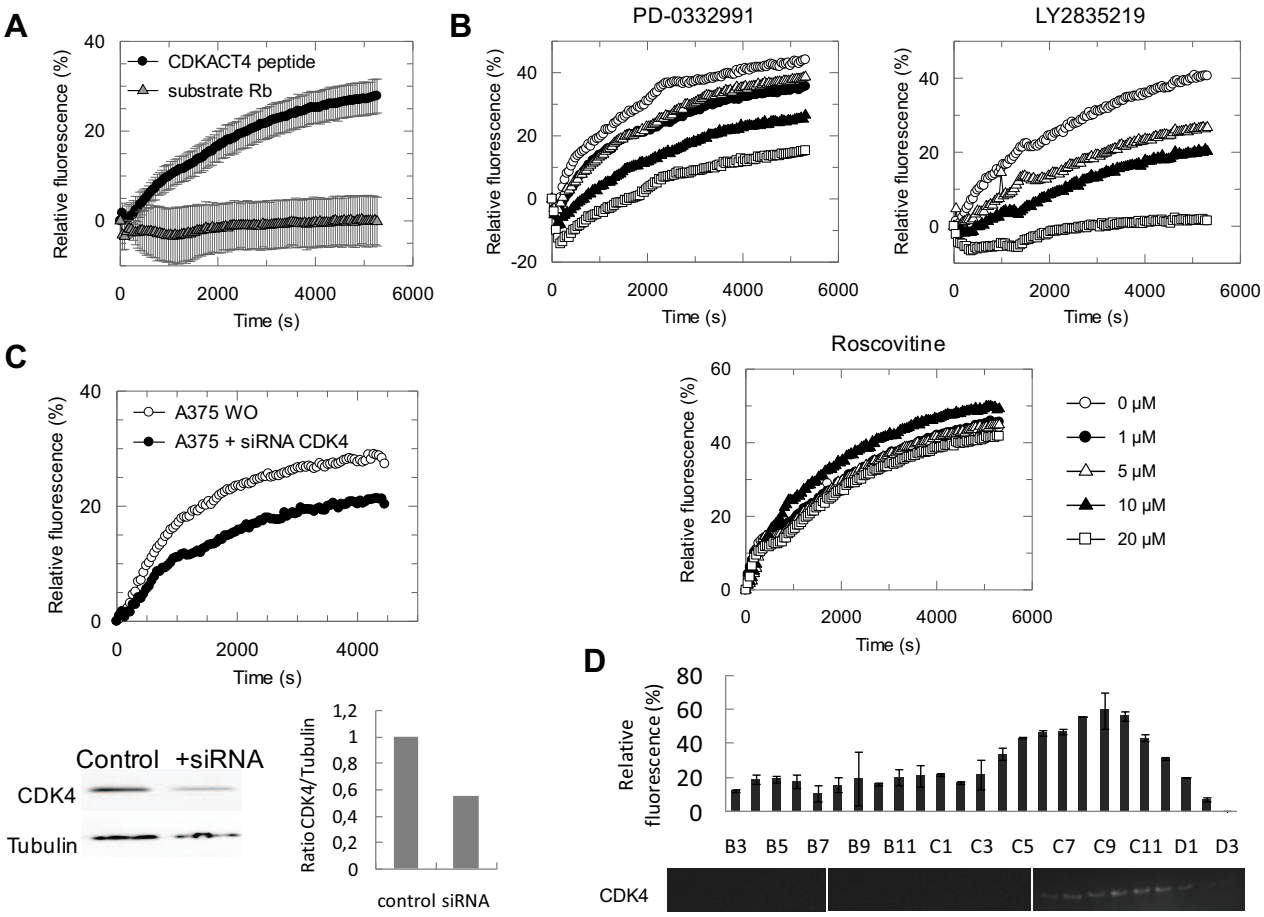
A
CDKACT4 peptide
substrate Rb
Relative fluorescence (%)
Time (s)
B
PD-0332991
LY2835219
Relative fluorescence (%)
Time (s)
C
A375 WO
A375 + siRNA CDK4
Relative fluorescence (%)
Time (s)
Control +siRNA
CDK4
Tubulin
Ratio CDK4/Tubulin
control siRNA
Roscovitine
0 µM
1 µM
5 µM
10 µM
20 µM
Relative fluorescence (%)
Time (s)
D
Relative fluorescence (%)
B3 B5 B7 B9 B11 C1 C3 C5 C7 C9 C11 D1 D3
CDK4

Figure 4.

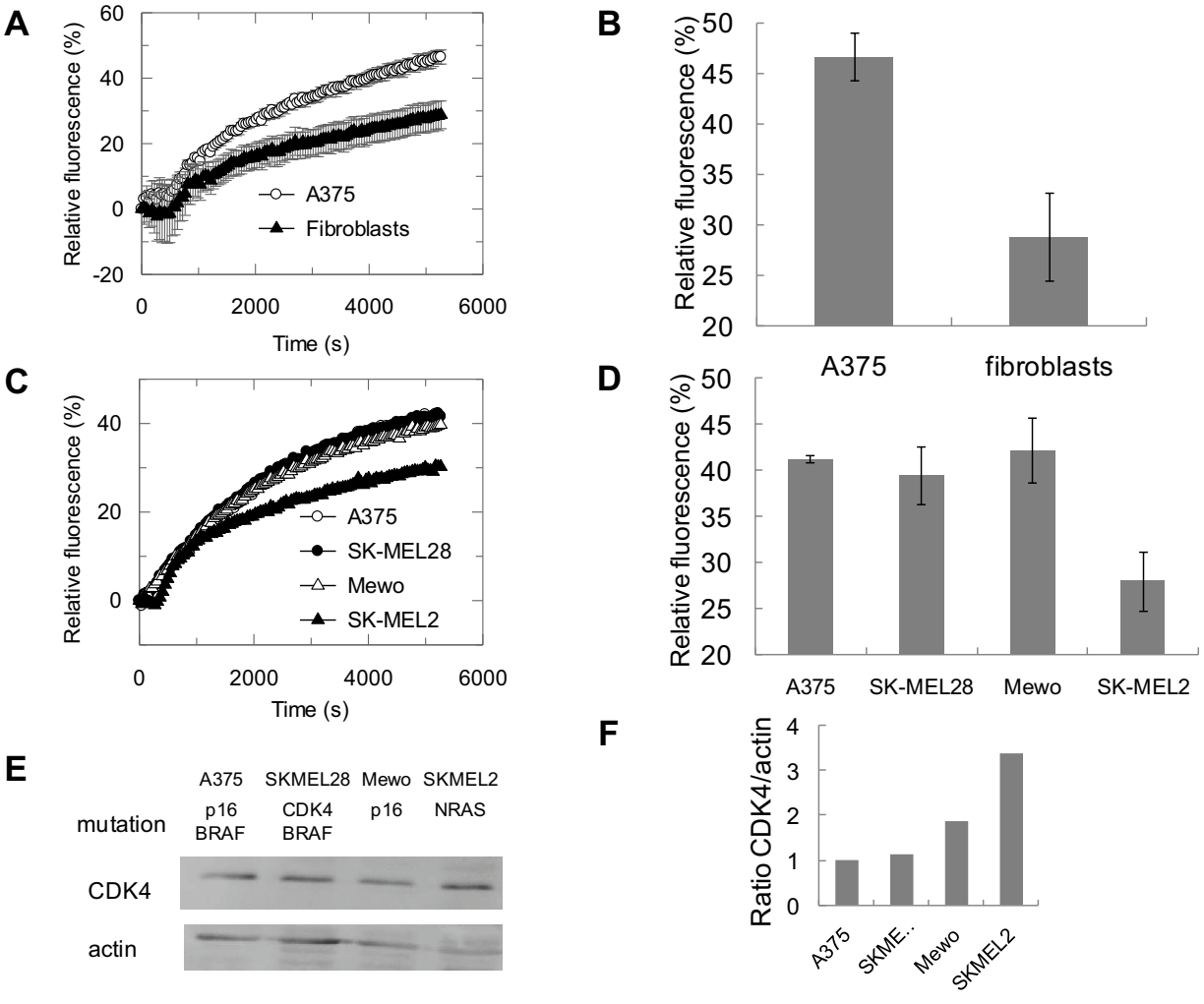

Figure 5.

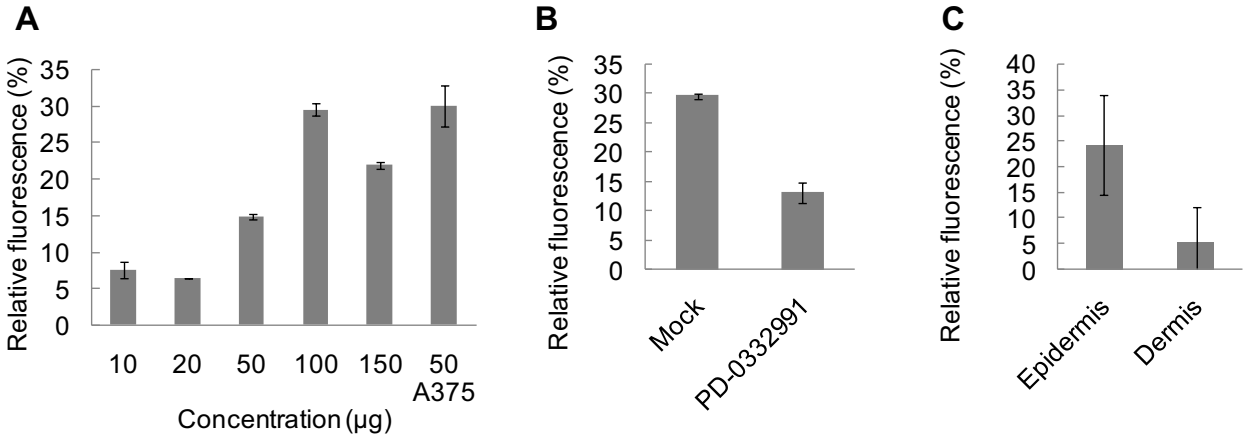

Figure 6.

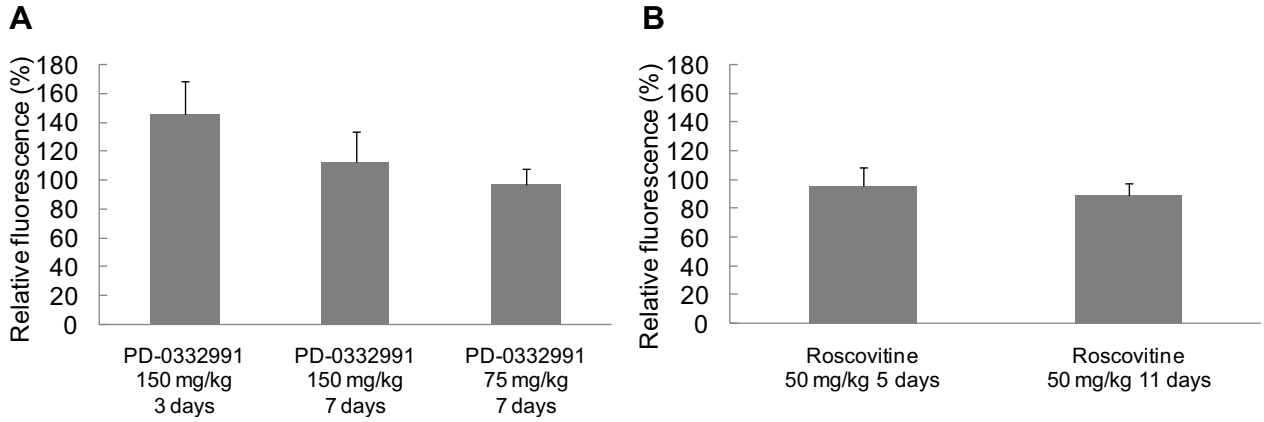

Supplementary Figure 1.

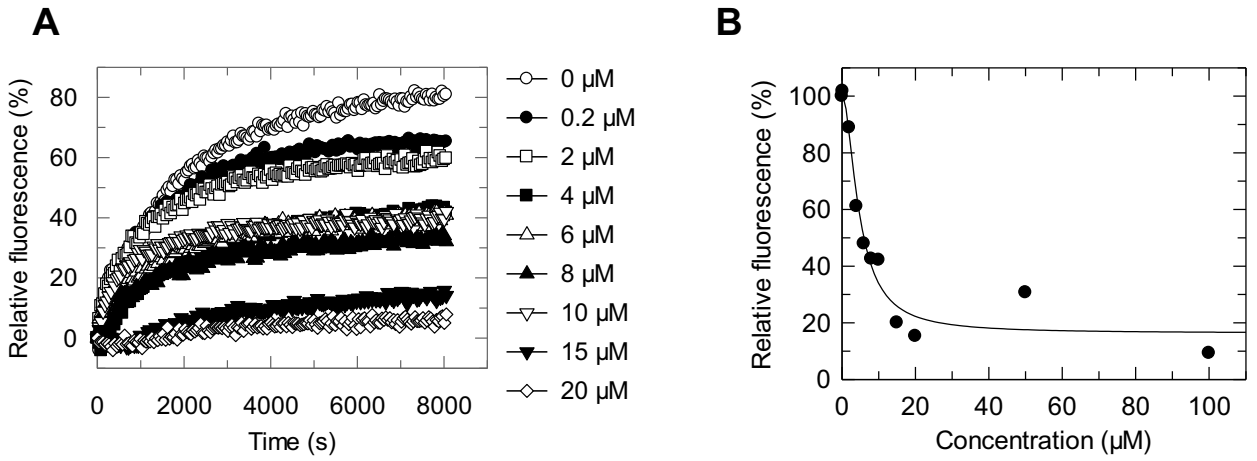

Supplementary Figure 2.

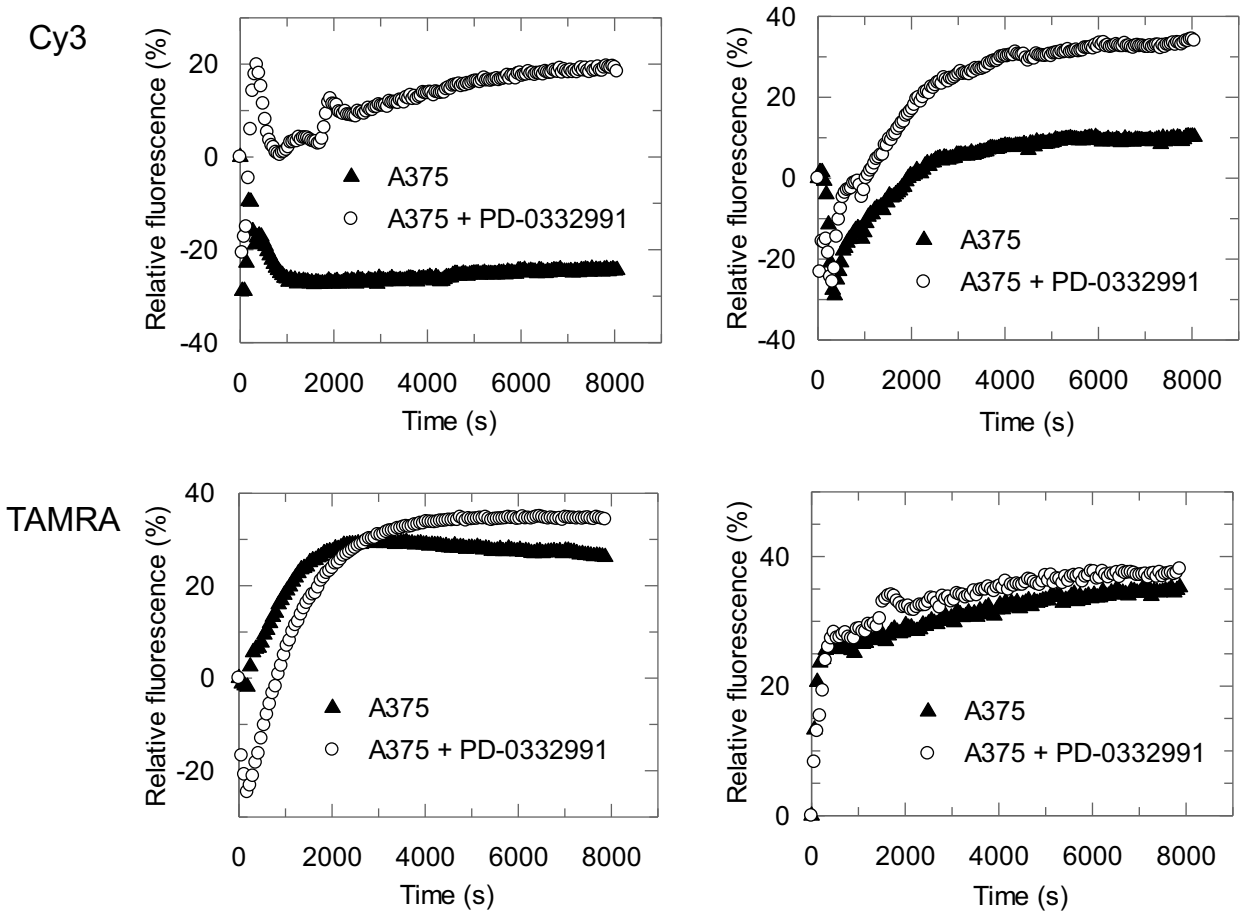

Supplementary Figure 3.

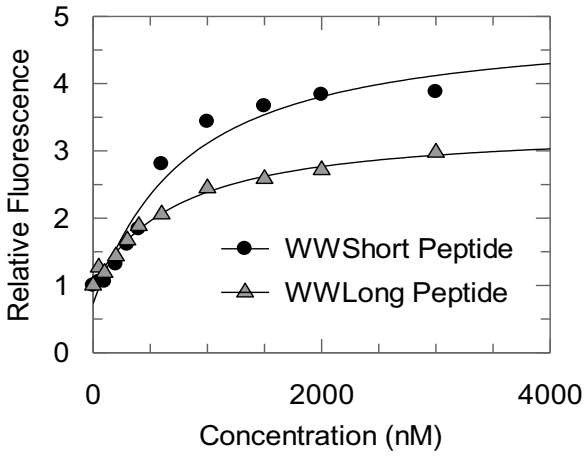

Supplementary Figure 4.

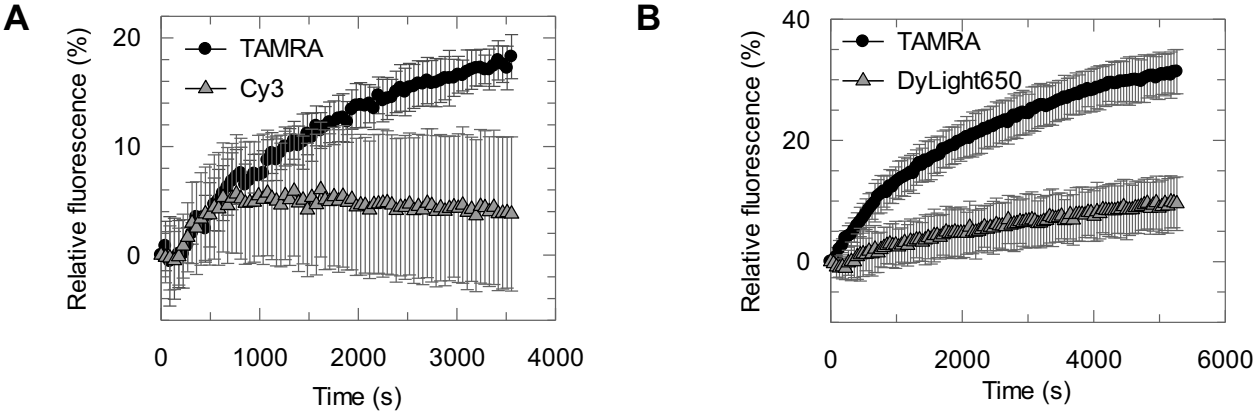

Supplementary Figure 5.

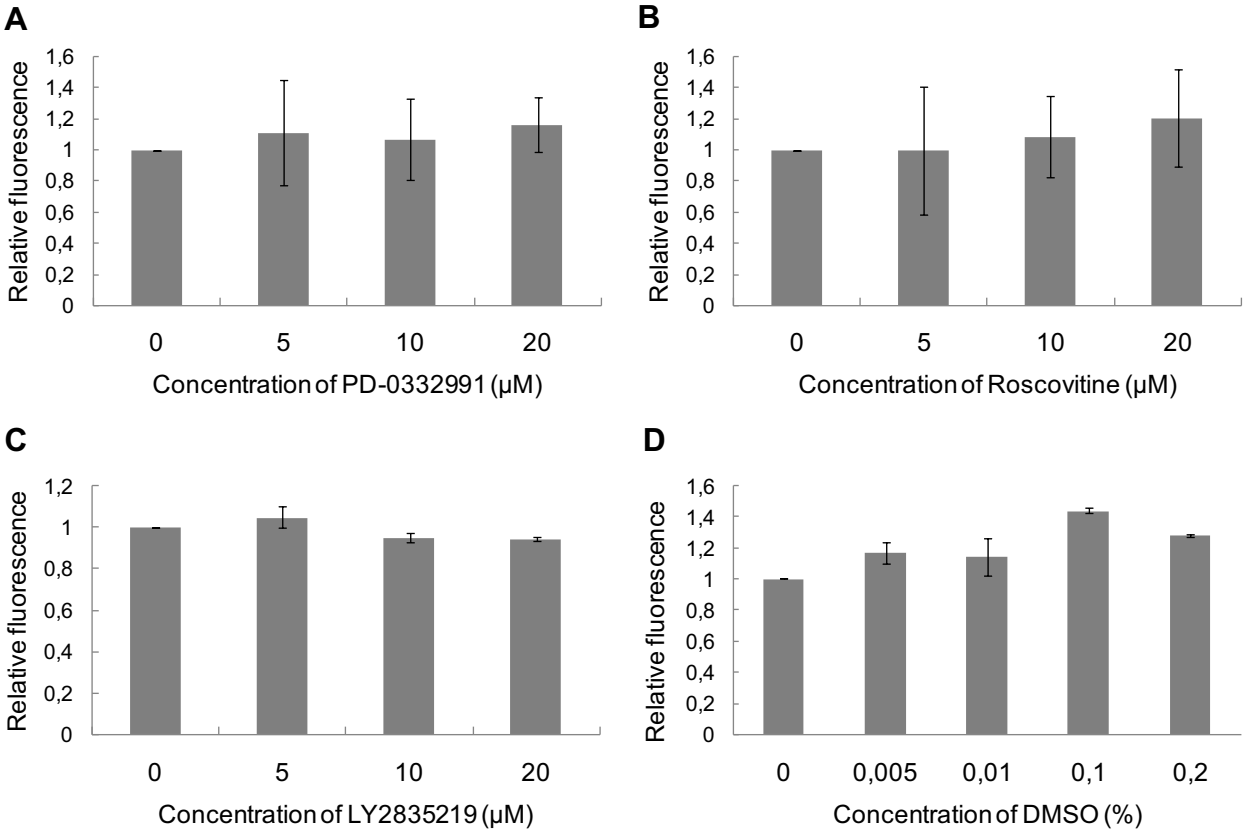

Supplementary Figure 6.

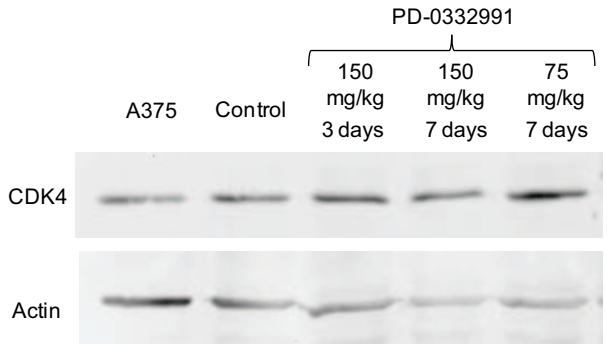

Supplementary Figure 7.

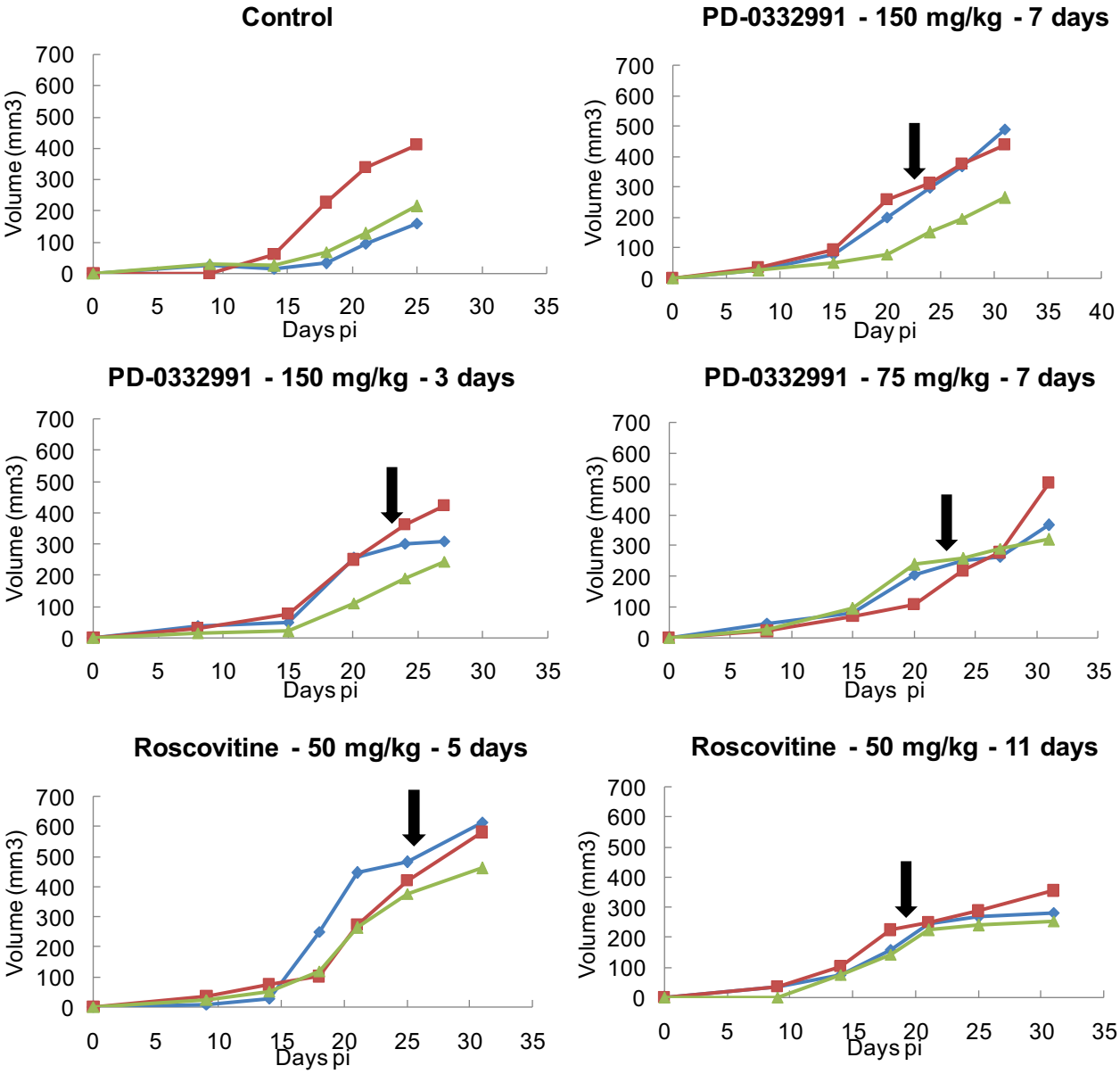

Supplementary Figure 8.

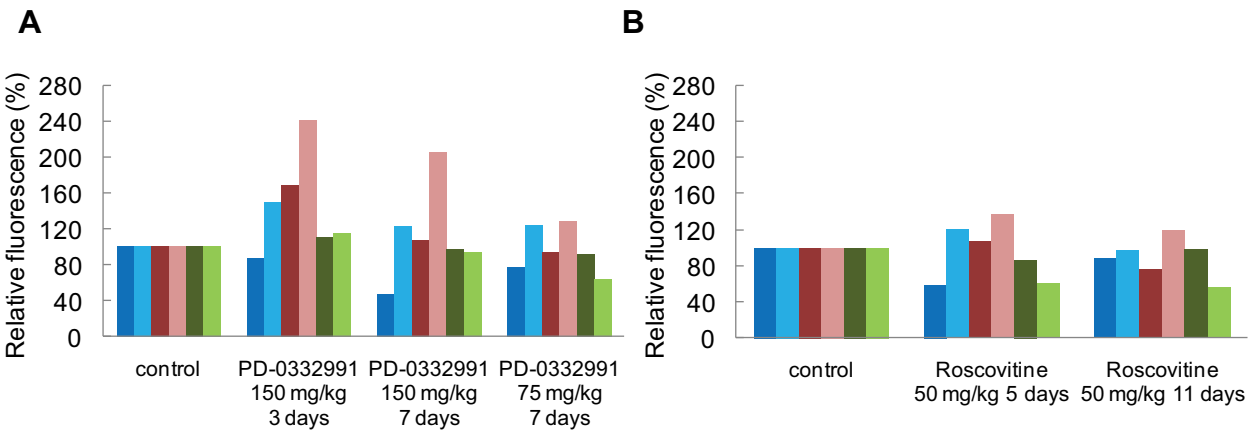

Targeting the interaction between CDK4 and Cyclin D in melanoma

-

Identification of a small molecule inhibitor targeting CDK4/Cyclin D

Camille Prével[1], Morgan Pellerano[1], Elvira Guegel[1], Nicolas Floquet[1], Julien Bellis[2], Cédric Hassen-Khodja[2], Frédéric Bihel[3] & May C. Morris[1]*

[1]Institut des Biomolécules Max Mousseron – IBMM -CNRS-UMR 5247,
Faculté de Pharmacie, 15, Av. Charles Flahault, 34093 Montpellier, France
[2] Centre de Recherches en Biochimie Macromoléculaire, 1919 Route de Mende, 34293 Montpellier
[3] Laboratoire d'Innovation Thérapeutique, Faculté de Pharmacie, Strasbourg

*To whom correspondance should be addressed.

Email: may.morris@univ-montp1.fr

#Corresponding author: M.C. Morris: may.morris@univ-montp1.fr

Tel : + 33 (0) 4 11 75 96 24 ; Fax : + 33 (0) 4 11 7596 41

Keywords:

CDK4/Cyclin D kinase / Non-ATP competitive inhibitor / PPI interface

Fluorescent biosensor / Melanoma

ABSTRACT

The p16/CDK4/Cyclin D/Rb pathway is frequently altered in human cancers, in particular melanoma. By designing a fluorescent biosensor of CDK4 that reports on compounds that bind the C helix of CDK4 and discriminates against ATP-pocket binders, we have identified a class of compounds that bind a novel allosteric pocket at the interface between CDK4 and Cyclin D1, thereby inhibiting kinase activity and inhibiting melanoma cell proliferation.

XXXX

The p16/CDK4/Cyclin D/Rb pathway is frequently altered in melanoma, resulting in a hyperactive form of CDK4, which therefore constitutes an attractive pharmacological target. Here we report on the identification of a family of small molecules that bind a novel allosteric pocket at the interface between CDK4 and Cyclin D, tamper with CDK4/Cyclin D kinase activity and inhibit melanoma cell proliferation.

INTRODUCTION

Melanoma is the most aggressive form of skin cancer which is lethal when it metastasizes. Current melanoma drugs include ipilimumab, a monoclonal antibody which targets CTLA4 (cytotoxic T lymphocyte-associated antigen 4) and vemurafenib which targets B-Raf mutations[1,2]. Nevertheless several cancers exhibit/develop resistance to these drugs. Therefore, novel targeted therapies are still actively sought for, in particular strategies involving cell cycle targets such as CDK4[3]. Indeed the p16 ^{INK4A}/CDK4/Cyclin D/Rb pathway is frequently altered in melanoma, resulting in a hyperactive form of CDK4, which therefore constitutes an attractive pharmacological target, and several inhibitors of this kinase have recently been proposed for trials in melanoma therapy[3–6]. Moreover, in primary invasive melanoma, an increase in gene copy number has been reported for CDK4 (37%) and Cyclin D – CCND1 (18%) and loss of CDKN2A expression is a frequent event (56%), whilst the combination of gene copy variability in CDK4, CCND1 or CDKN2A is associated with poor survival[7].

A wide variety of ATP competitive inhibitors of CDK/cyclins have already been developed for anticancer therapeutics[6]. Whilstfirst generation pan-CDK inhibitors such as flavopiridol or R-roscovitine have shown disappointingly low activity and high toxicity in clinical trials due to their notorious lack of selectivity, efforts to develop second-generation CDK inhibitors with improved potency and selectivity have yielded 16 ATP-competitive CDK inhibitors which are currently in clinical trials for anticancer therapy, including the CDK4 inhibitors PD-0332991, LEE011 and LY2835219, also known as Palbociclib, Ribociclib and Abemaciclib respectively[8,9]. These CDK4 inhibitors offer promising perspectives for Rb-positive melanomas[6], but are nonetheless poorly efficient in monotherapy, thereby calling for novel classes of drugs for combination therapy. Moreover, in primary invasive melanoma, response/sensitivity to PD-0332991 is associated with loss, methylation or mutation of p16^{INK4A} (CDKN2A gene product) and resistance to this drug has been described in Rb-deficient cancers/cells[7].

Several strategies have been deployed to identify compounds that target sites other than the ATP-binding pocket or the catalytic site of cyclin-dependent kinases, but so far no druggable inhibitors have been identified[10,11]. Compounds that targetprotein/protein interactions (PPIs) which are essential for enzyme function constitute an attractive alternative, as exemplified by drugs targeting p53/Mdm2 interface[12,13]. We have previously shown that targeting the CDK2/Cyclin A interface with a peptide derived from Cyclin A specifically inhibited CDK2 activity without disrupting the complex, and efficiently reduced cancer cell proliferation *in vitro*[14]. More recent studies further demonstrate that targeting the interface between a CDK and a partner protein constitutes a relevant alternative to ATP-competitive inhibitors[15,16]. Consequently, the identification of low-molecular-weight compounds that would tamper with the main interface between CDK4 and Cyclin D should constitute a selective means of targeting this kinase and offer novel therapeutic perspectives for melanoma.

The interaction between CDK4 and Cyclin D is essentially mediated by the PISTVRE helix in the N-terminal lobe of CDK4 and the complementary alpha 5 helix of Cyclin D, which is critical for assembly of the functional heterodimeric kinase[17,18] (**Figure 1A**). In order to identify compounds that would bind the PISTVRE helix, we engineered a fluorescent biosensor derived from the kinase scaffold of CDK4 in which cysteine residues 78 and 135 were specifically labelled with the fluorescent dye Cy3, thereby spanning the chemical space surrounding the PISTVRE helix (**Figure 1B**). The CDK4-PISTVRE biosensor is insensitive to ATP-competitive inhibitors such as PD-0332991 but responds robustly to Cyclin D1, promoting fluorescence enhancement of the Cy3 probes (**Figure 1C, Suppl. Fig. 1**). As such this biosensor constitutes a highly sensitive probe for discriminating against ATP competitive inhibitors and identifying compounds which selectively bind the region surrounding the PISTVRE interface. This biosensor was successfully applied to screen a library of small chemical compounds (FRED Describe) leading to identification of a compound, LPI2251, which enhanced fluorescence of the biosensor to a similar extent as Cyclin D1 (**Figure 1D)**.

Since the p16/CDK4/Cyclin D/Rb pathway is notoriously deregulated in melanoma, we asked whether this compound and two of its derivatives (LPI2252 and RF1210) could inhibit proliferation of the A375 melanoma cell line (**Figure 1E, Suppl. Fig. 4, 5)**. Both LPI2251 and LPI2252 inhibited melanoma cell proliferation to a similar extent as the gold star reference PD-0332991, but RF1210 was more efficient with an IG_{50} 13.6 µM compared to 17.6, 17.9 and 18.7 µM for LPI2251, LPI2252 and PD-0332991, respectively. In contrast, neither of these compounds displayed any significant inhibition of fibroblasts (**Suppl. Fig. 6**). We further characterized the inhibitory potential of RF1210 towards different cell lines, bearing either wild-type p16, BRAF and CDK4 (Mewo cells), the NRAS Q61R mutation (SK-MEL2 cell line), the R24C CDK4 and BRAF V600E mutation (SKMEL28 cell line) or a loss of function mutation of CDKN2A (p16) and the V600E BRaf mutation, but otherwise wild-type CDK4 (A375 cells)**.** This study revealed that RF1210 was most efficient against SKMEL2 cells, with IG_{50} 10.1 µM, followed by MV3 with an IG_{50} 10.8 µM, SKMEL28 with an IG_{50} 12 µM and A375 cells with IG_{50} 13.6 µM. (**Fig 1F, Suppl. Fig. 7 & 8**).

Finally we asked whether the RF1210 might cooperate with other CDK4 inhibitors in promoting efficient inhibition of melanoma cell proliferation (**Fig. 1G, Suppl. Fig. 9 & 10**). Indeed, at suboptimal concentrations of 10 µM RF1210 and 10 µM PD-0332991, the combination of these compounds proved to inhibit proliferation of A375 cells more efficiently (72% inhibition) than either compound alone (46% inhibition by 10 µM RF1210 and 36% inhibition by 10 µM PD-0332991). Likewise, combined administration of RF1210 with LY2835219 or LEE011 at suboptimal concentrations (15 µM) inhibited A375 proliferation more efficiently than either compound alone (73 and 92% inhibition compared to 46% by 10 µM RF1210, 20.5% by 15 µM LY2835219 and 59% inhibition by 15 µM LEE011). Finally to completely validate that RF1210 had such significant effect on melanoma cell proliferation through inhibition of CDK4/Cyclin D activity, we examined the status of Rb phosphorylation.

To verify whether these compounds affected CDK4 kinase activity, we asked whether treatment of cells with LPI2252 and RF1210 induced a reduction in phosphorylation of Retinoblastoma (Rb), the major substrate of CDK4, by Western blotting of treated cell extracts.

In an attempt to identify the binding site of these inhibitors and gain insight into their mechanism of action, molecular modelling docking experiments were performed. This study revealed binding of the compounds within a pocket that lies beneath the PISTVRE alpha helix of CDK4 (**Figure 2A**). We further mutagenized CDK4-PISTVRE biosensor at the bottom face of the helix and compared binding of RF1210, LPI2251 and LPI2252. This experiment revealed a significantly reduced binding affinity of the CDK4 inhibitors to these mutants (**Figure 2C**). Moreover, we synthesized a peptide derived from the PISTVRE helix of CDK4 and characterized its affinity for CDK4 inhibitors in fluorescence titration assays using a peptide derived from the complementary interface, the alpha 5 helix of Cyclin D1 as a positive control (**Figure 2D**). All three compounds, LPI2251, LPI2252 and RF1210 enhanced the fluorescence of fluorescently-labelled PISTVRE significantly. We repeated this experiment with mutant forms of the PISTVRE peptide, in which hydrophobic residues were replaced by charges, and found that mutant fluorescently-labelled PISTVRE peptide no longer bound the small molecule inhibitors of CDK4.

Finally we asked whether LPI2251, LPI2252 and RF1210 interfered either directly or indirectly with ATP, cyclin partner or substrate binding. To this aim CDK4 was preincubated with each of these compounds, then used to evaluate binding of the Rb substrate, ATP (mant-ATP) in fluorescence titration assays (**Figure 2E**).

Taken together these data highlight a new allosteric pocket in CDK4 as well as a novel class of CDK4 inhibitors which specifically bind this pocket (LPI2251, LPI2252 and RF1210).

Concluding remarks

Melanoma is an aggressive and lethal form of skin cancer when it metastasizes in which the $p16^{INK4A}$/CDK4/Cyclin D/Rb pathway is frequently altered, resulting in a hyperactive form of CDK4 kinase. Several ATP-competitive inhibitors of CDK4 tested in clinical trials exhibit promising perspectives for Rb-positive melanomas. However, response to these inhibitors is associated with loss, or functional downregulation of p16INK4A, most likely because this endogenous inhibitor of CDK4/Cyclin D prevents their binding within the ATP pocket of CDK4. As such, and since the classical mechanism of action of ATP-competitive inhibitors is notorious for its lack of selectivity, ATP being required for the ensemble of protein kinases as well as for several other enzymes and chaperones, alternative strategies to target CDK4 kinase function should provide new avenues to develop therapeutics for melanoma. Here we report on a novel class of CDK4 inhibitors which we identified thanks to a fluorescent biosensor that discriminates against ATP-competitive inhibitors, which preferentially retains compounds that bind the chemical space around

the alpha helix of CDK4. These compounds are the first small molecules reported to target the alpha helix of CDK4 through binding to a newly identified pocket beneath the PISTVRE helix. We show here that these compounds bind the PISTVRE helix of CDK4 and interfere with ATP, partner and substrate binding. Moreover, these compounds inhibit melanoma cell proliferation with an efficacy in the same range as PD-0332991, and further synergize with the latter at sub-IC50 concentrations. Our work clearly suggests that dual targeting of CDK4 kinase with an ATP-competitive and a non-ATP-competitive inhibitor may provide a more effective means of targeting its function in melanoma, thereby offering new therapeutic perspectives to target the p16/CDK4/Cyclin D/Rb pathway in this deadly disease.

FIGURE LEGENDS

FIGURE 1 – Identification of compounds that target the PISTVRE helix of CDK4 and inhibit melanoma cell proliferation. A. Structure of CDK4/Cyclin D highlighting the interface between the PISTVRE helix of CDK4 and the alpha 5 helix of Cyclin D1. B. Schematic representation of CDK4-PISTVRE biosensor and C. its response to Cyclin D1 and PD-0332991. D. Fluorescence response of CDK4-PISTVRE to positive (Cyclin D) and negative (peptide) controls, PD-0332991 and LPI2251 in the screen. E. Proliferation inhibition assays of LPI2251, LPI2252 and RF1210 in A375 cells. F. Proliferation inhibition assays of RF1210 in different melanoma cell lines: A375 cells (CDKN2A loss of function, BRaf V600E), SKMEL28 (wt CDKN2A, R24C CDK4, BRaf V600E), SKMEL2 (NRas mutation (Q61R)), Mewo (CDKN2A loss of function, Wt CDK4) and fibroblasts. G. Comparison of inhibition potential of RF1210, PD-0332991 and coadministrated compounds at sub IG_{50} concentrations. H. Comparison of inhibition potential of RF1210, Paclitaxel and coadministrated compounds atsub IG_{50} concentrations. I. Western blot of phosphoRb status in cell extracts treated with inhibitors as described in G and H.

FIGURE 2 – Identification of the binding site and mechanism of action of RF1210, LPI2251 and LPI2252.
A. Molecular Docking of RF1210, LPI2251 and LPI2252 onto CDK4/Cyclin D1. B. Structural representation of RF1210, LPI2251 and LPI2252. C. Fluorescence binding assay of inhibitors to TP2-Rho-PISTVRE peptide and mutants of the PISTVRE helix. D. Fluorescence binding assay of inhibitors to a CDK4-derived PISTVRE peptide and its mutants. E. Fluorescence titration of CDK4 and CDK4-inhibitor complexes with mant-ATP. F. Fluorescence titration of CDK4 and CDK4-inhibitor complexes with FITC-Rb substrate peptide. G. Fluorescence titration of CDK4-PISTVRE and CDK4-PISTVRE/inhibitor complexes with Cyclin D.

SUPPLEMENTAL INFORMATION

SUPPLEMENTAL FIGURES & TABLES

***Results from CDK4 PISTVRE Screen – Excell Table**

Supplementary Figure 1 – Optimization of concentrations and Kinetics for the Screen
A. 25 nM Cy3-labelled CDK4-PISTVRE biosensor was incubated with 2 µM positive control (recombinant Cyclin D1) or negative control (irrelevant peptide) and fluorescence emission intensity of Cy3 was monitored over time. B. Different concentrations of CDK4-PISTVRE-Cy3 labelled biosensor were incubated with 2 µM controls and fluorescence emission intensity of Cy3 was measured at 5h. C. 25 nM CDK4-PISTVRE-Cy3 labelled biosensor was incubated with different concentrations of controls and fluorescence emission intensity of Cy3 was measured at 5h. Experiments were performed in duplicate and error bars indicate the standard deviation of positive and negative controls.

Supplementary Figure 2 – Dose response of CDKCONF4A-Cy3 to LPI2251 variants

Supplementary Figure 3 – Fluorescence emission spectra of LPI2251 derivatives - do not fluoresce following excitation at 510 nm

Supplementary Figure 4 – A375 melanoma cell proliferation assays performed with LPI2251, LPI2252, RF1210 and PD-0332991

Supplementary Figure 5 – A375 melanoma cell proliferation assays performed with LEE011, LY2835219, Paclitaxel and Methotrexate

Supplementary Figure 6 – Fibroblast proliferation assays performed with LPI2251, LPI2252, RF1210 and PD-0332991

Supplementary Figure 7 – Comparative cell proliferation assays performed with RF1210 and PD-0332991 on A375 and MV3 melanoma cell lines

Supplementary Figure 8 – Comparative cell proliferation assays performed with RF1210 and PD-0332991 on SKMEL2 and SKMEL-28 melanoma cell lines

Supplementary Figure 9 – A375 cell proliferation assays performed with RF1210, PD-0332991 or LY2835219, either alone or combined at sub IG_{50} concentrations

Supplementary Figure 10 – A375 cell proliferation assays performed with LPI2252, PD-0332991 or LY2835219, either alone or combined at sub IG_{50} concentrations

Supplementary Figure 11 – A375 cell proliferation assays performed after 48h with 10 µM RF1210, 15 µM LEE011, 15 µM LY2835219, 15 µM Paclitaxel, 15 µM Methotrexate, 10 µM PD-0332991 either alone or combined at sub IG_{50} concentrations

Supplementary Figure 12 – A375 cell proliferation assays performed after 48h with 10 µM LPI2252, 15 µM LEE011, 15 µM LY2835219, 15 µM Paclitaxel, 15 µM Methotrexate, 10 µM PD-0332991 either alone or combined at sub IG_{50} concentrations

Online methods - Experimental section

Design and engineering of CDK4 PISTVRE biosensor and mutants. The cDNA sequence of mouse CDK4 was cloned into the pGex6P1 vector (GE Healthcare) 5'BamHI 3' EcoRI. Cysteine residues 202 and 215 were mutagenized to serine, so as to yield a mutant bearing only two cysteine residues, 78 and 135, spanning the PISTVRE helix of CDK4. The « bottom » V51E S52R L59R L60R L63R and « top » T53K V54E V57E A58E A65E of CDK4-PISTVRE biosensor were further generated by site directed mutagenesis. Site-directed mutagenesis was performed according to the QuickStart protocole (Strategene) and all mutants were completely sequenced to verify the presence of the desired mutation and absence of any other undesired mutations or stop codons.

Protein expression and purification of cyclin-dependent kinases. Recombinant GST-CDK4 and Cyclin D were expressed in E. coli by IPTG induction and purified by chromatography as described previously[14], first on a GST-Trap column, then by gel filtration chromatography.

Fluorescence titration experiments

Fluorescence titration assays were performed in 96-well plates using a Clariostar spectrofluorimeter (BMG) in 200 µL PBS (Sigma), 150 mM NaCl. The fluorescence of Cy3-labelled CDK4-PISTVRE biosensor with recombinant Cyclin D, PD-0332991 or small molecules was acquired at 570 nm following excitation at 550 nm. The fluorescence of TP2-Rho-labelled PISTVRE peptide with D1 peptide (derived from the complementary interface in Cyclin D1), with a control peptide, PD-0332991 or small molecules was acquired at 510 nm following excitation at 614 nm. Data analysis was performed using the GraFit Software (Erathicus Ltd). Experiments were performed in triplicate, and error bars indicate standard deviation from average.

Peptide synthesis and labelling

PISTVRE (GGGCPISTVRAVALLRRL), D1 (SIRPEELLQMELLLVNKLKWNLC) and control (VESSDTIDNVKSKIQDKEGC) peptides were purchased from GLS Biochem, (Shanghai, China), and were labelled on their unique cysteine with TP2-Rho-maleimide (F.Mahuteau) then further purified on NAP-5 columns (GE Healthcare) as described previously[19].

Small molecule inhibitors

PD-0332991 (Palbociclib), LEE011 (Ribociclib), LY2835219 (Abemaciclib), Vemurafenib, Cisplatin, Paclitaxel and Methotrexate were all purchased from Euromedex and resuspended in DMSO, according to the manufacturer's advice.

CDK4 kinase activity assays

CDK4 kinase activity assays were performed using GST-CDK4 kinase incubated with A375 cell extracts as a source of active CDK4/Cyclin D complexes which phosphorylate and increase the fluorescence of the CDKACT biosensor[20]. As a control, kinase activity assays were performed with PD-0332991. Fluorescence kinase assays were performed as described previously[20] in 96-well plates in a thermostated chamber using a Clariostar™ spectrofluorimeter (BMG) at 30°C in 200μL PBS (Sigma) supplemented with 5 mM $MgCl_2$, 0.5mM ATP. The fluorescence of Cy3-labelled CDKACT was monitored over time. In all experiments, relative fluorescence was calculated following subtraction of CDKACT-Cy3 fluorescence from fluorescence values obtained in the presence of CDK4/Cyclin D kinase incubated with or without inhibitors. Data analysis was performed using the GraFit Software (Erathicus Ltd). Experiments were performed in triplicate, and error bars indicate standard deviation from average.

Automated high throughput screen conditions and hit validation

Prior to the HTS, stability assays and downscaling experiments were performed to establish the best conditions for a miniaturized assay in 96-well plates and optimized so as to obtain a robust and reproducible signal. Performance criteria for reproducibility, sensitivity (in the presence of DMSO), tolerance and robustness were established with the ATP-competitive inhibitor of CDK4 PD-0332991, and a control peptide that barely affected Cy3-labelled CDK4-PISTVRE biosensor fluorescence and the 2 μM Cyclin D, as a positive control, that promotes significant enhancement of Cy3-labelled CDK4-PISTVRE biosensor fluorescence. Optimal screening conditions were established as follows: 25 nM freshly purified Cy3-labelled CDK4-PISTVRE biosensor in 50 mM KH_2PO_4/K_2HPO_4, pH 6.5, 500 mM NaCl, 1% DMSO, for 5 hours at room temperature in the dark. Prescreen Conditions: amplification by positive control (Cyclin D) 1.8 fold enhancement. Prescreen Zfactor = 0.89.

The screen itself was performed in 96-well black Greiner Bio One plates. Compounds from the library were used at 10^{-5} M final concentration against 25 nM Cy3-labelled CDK4-PISTVRE biosensorin 50 mM KH_2PO_4/K_2HPO_4, pH 6.5, 500 mM NaCl and fluorescence emission of Cy3 was measured at 570 nm following excitation at 550 nm after 3 hours. The screen was performed on a TECAN Freedom Evo Robot. In parallel, the intrinsic fluorescence of the library compounds at 570 nm following excitation at 550 nm was determined, to eliminate autofluorescent compounds. The increase in fluorescence was calculated with reference to the basal fluorescence of Cy3-labelled CDK4-PISTVRE biosensor alone and is expressed as the percentage of increase. A molecule was considered a hit when it was not autofluorescent, yet induced amplification of Cy3-labelled CDK4-PISTVRE biosensor fluorescence 3 times or greater the standard deviation of CDK4-PISTVRE biosensorfluorescence alone (or p=0.01).

Hits identified in the screen were retested manually in quadruplet to confirm they were positive hits with a fresh batch of Cy3-labelled CDK4-PISTVRE biosensor and stock solutions of the library compounds in DMSO.

Cell culture and extract preparation

Melanoma cell lines used in this study:

	CDKN2A	CDK4	Rb	BRAF	NRAS
A375	mutated (E61Stop, Loss of function)	WT	WT	V600E	WT
Mewo	mutated (R80Stop, Loss of function)	WT	WT	WT	WT
MV3					
SKMEL2	WT	WT	WT	WT	mutated (Q61R)
SKMEL28	WT	R24C		V600E	WT

Cell culture media, serum and antibiotics were purchased from Life Technologies. Cells were cultured in DMEM/RPMI + Glutamax supplemented with 10% FCS, 100 units/mL penicillin (G sodium salt) and 100 µg/mL streptomycin at 37°C in an atmosphere containing 5% CO2.

Cell extracts were prepared in PBS lysis buffer pH 7.4, 0.2% NP40, 1 mM EDTA, 2 mM PMSF, CompleteTM protease inhibitors (Roche), and normalized following spectrophotometric dosage at 280 nm.

Chemical Synthesis of Small Molecule Inhibitors - FRED

Small Molecules …

Library ….

DOCKING Experiments - Nicolas

Acknowledgements

This work was supported by the CNRS (Centre National de la Recherche Scientifique) and grants from the Association de Recherche contre le Cancer (ARC) and the Institut de Recherche contre le Cancer (INCA) to MCM.

Author Contributions

C.P. and M.P. generated, purified and characterized the CDK4-PISTVRE biosensor *in vitro* in fluorescence titration experiments, established the conditions for the HTS and performed the screen. J.B. provided technical assistance and advice on the TECAN Robot for the screen. C. H-K performed a biostatistical analysis of screening results. C.P., M.P. and M.C.M. analysed the results from the screen and determined hit compounds to be characterized further. M.P. characterized the mechanism of action of the hits and derivatives *in vitro*, C.P. performed the *in vitro* kinase assays. C.P. and E.G. performed the cell proliferation assays and time-lapse imaging experiments. F.B. provided the chemical compound library as well as hit derivatives. N.F. performed the docking experiments. M.C.M. designed CDK4-PISTVRE biosensor and its implementation for HTS, coordinated the study, and wrote the manuscript.

REFERENCES

1. Flaherty, K. T., Hodi, F. S. & Fisher, D. E. From genes to drugs: targeted strategies for melanoma. *Nat. Rev. Cancer* **12,** 349–361 (2012).

2. Flaherty, K. T. & Fisher, D. E. New strategies in metastatic melanoma: oncogene-defined taxonomy leads to therapeutic advances. *Clin. Cancer Res.* **17,** 4922–4928 (2011).

3. Lee, B., Sandhu, S. & McArthur, G. Cell cycle control as a promising target in melanoma. *Curr Opin Oncol* **27,** 141–150 (2015).

4. Sheppard, K. E. & McArthur, G. A. The cell-cycle regulator CDK4: an emerging therapeutic target in melanoma. *Clin. Cancer Res.* **19,** 5320–5328 (2013).

5. Roberts, P. J. *et al.* Multiple roles of cyclin-dependent kinase 4/6 inhibitors in cancer therapy. *J. Natl. Cancer Inst.* **104,** 476–487 (2012).

6. Asghar, U., Witkiewicz, A. K., Turner, N. C. & Knudsen, E. S. The history and future of targeting cyclin-dependent kinases in cancer therapy. *Nat Rev Drug Discov* **14,** 130–146 (2015).

7. Young, R. J. *et al.* Loss of CDKN2A expression is a frequent event in primary invasive melanoma and correlates with sensitivity to the CDK4/6 inhibitor PD0332991 in melanoma cell lines. *Pigment Cell Melanoma Res* **27,** 590–600 (2014).

8. Bruyère, C. & Meijer, L. Targeting cyclin-dependent kinases in anti-neoplastic therapy. *Curr. Opin. Cell Biol.* **25,** 772–779 (2013).

9. Dickson, M. A. Molecular Pathways: CDK4 Inhibitors for Cancer Therapy. *Clin Cancer Res* clincanres.1551.2014 (2014). doi:10.1158/1078-0432.CCR-13-1551

10. Cirillo, D., Pentimalli, F. & Giordano, A. Peptides or small molecules? Different approaches to develop more effective CDK inhibitors. *Curr. Med. Chem.* **18,** 2854–2866 (2011).

11. Abate, A. A., Pentimalli, F., Esposito, L. & Giordano, A. ATP-noncompetitive CDK inhibitors for cancer therapy: an overview. *Expert Opin Investig Drugs* **22,** 895–906 (2013).

12. Wilson, A. J. Inhibition of protein-protein interactions using designed molecules. *Chem Soc Rev* **38,** 3289–3300 (2009).

13. Ivanov, A. A., Khuri, F. R. & Fu, H. Targeting protein-protein interactions as an anticancer strategy. *Trends Pharmacol. Sci.* **34,** 393–400 (2013).

14. Gondeau, C. *et al.* Design of a novel class of peptide inhibitors of cyclin-dependent kinase/cyclin activation. *J. Biol. Chem.* **280,** 13793–13800 (2005).

15. Hamdi, A. *et al.* Tampering with cell division by using small-molecule inhibitors of CDK-CKS protein interactions. *Chembiochem* **16,** 432–439 (2015).

16. Corbel, C. *et al.* First BRET-based screening assay performed in budding yeast leads to the discovery of CDK5/p25 interaction inhibitors. *Biotechnol J* **6,** 860–870 (2011).

17. Day, P. J. *et al.* Crystal structure of human CDK4 in complex with a D-type cyclin. *Proc. Natl. Acad. Sci. U.S.A.* **106,** 4166–4170 (2009).

18. Takaki, T. *et al.* The structure of CDK4/cyclin D3 has implications for models of CDK activation. *Proc. Natl. Acad. Sci. U.S.A.* **106,** 4171–4176 (2009).

19. Kurzawa, L., Pellerano, M., Coppolani, J. B. & Morris, M. C. Fluorescent peptide biosensor for probing the relative abundance of cyclin-dependent kinases in living cells. *PLoS ONE* **6,** e26555 (2011).

20. Van, T. N. N., Pellerano, M., Lykaso, S. & Morris, M. C. Fluorescent Protein Biosensor for Probing CDK/Cyclin Activity in vitro and in Living Cells. *Chembiochem* (2014). doi:10.1002/cbic.201402318

Figure 1.

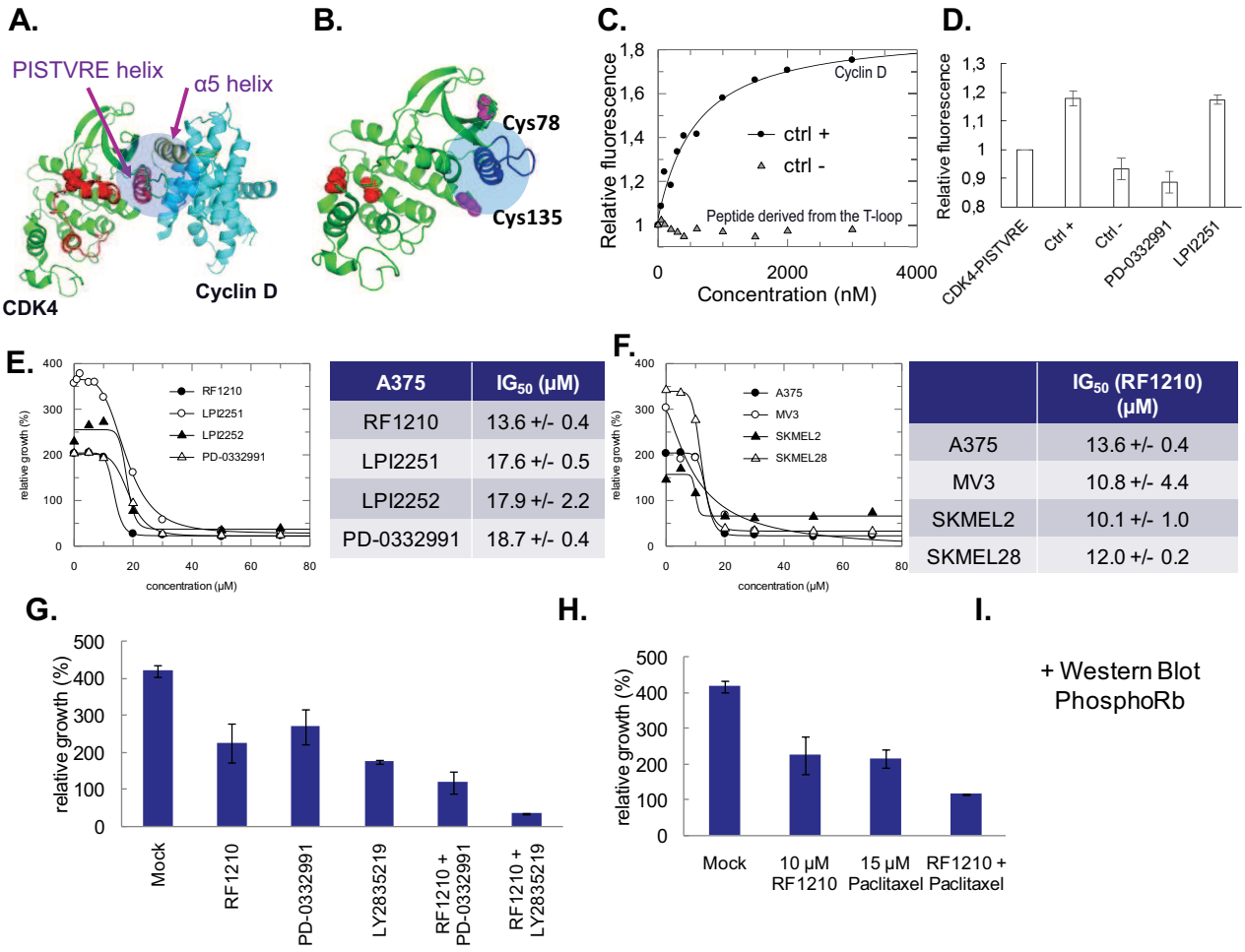

A375	IG_{50} (μM)
RF1210	13.6 +/- 0.4
LPI2251	17.6 +/- 0.5
LPI2252	17.9 +/- 2.2
PD-0332991	18.7 +/- 0.4

	IG_{50} (RF1210) (μM)
A375	13.6 +/- 0.4
MV3	10.8 +/- 4.4
SKMEL2	10.1 +/- 1.0
SKMEL28	12.0 +/- 0.2

Figure 2.

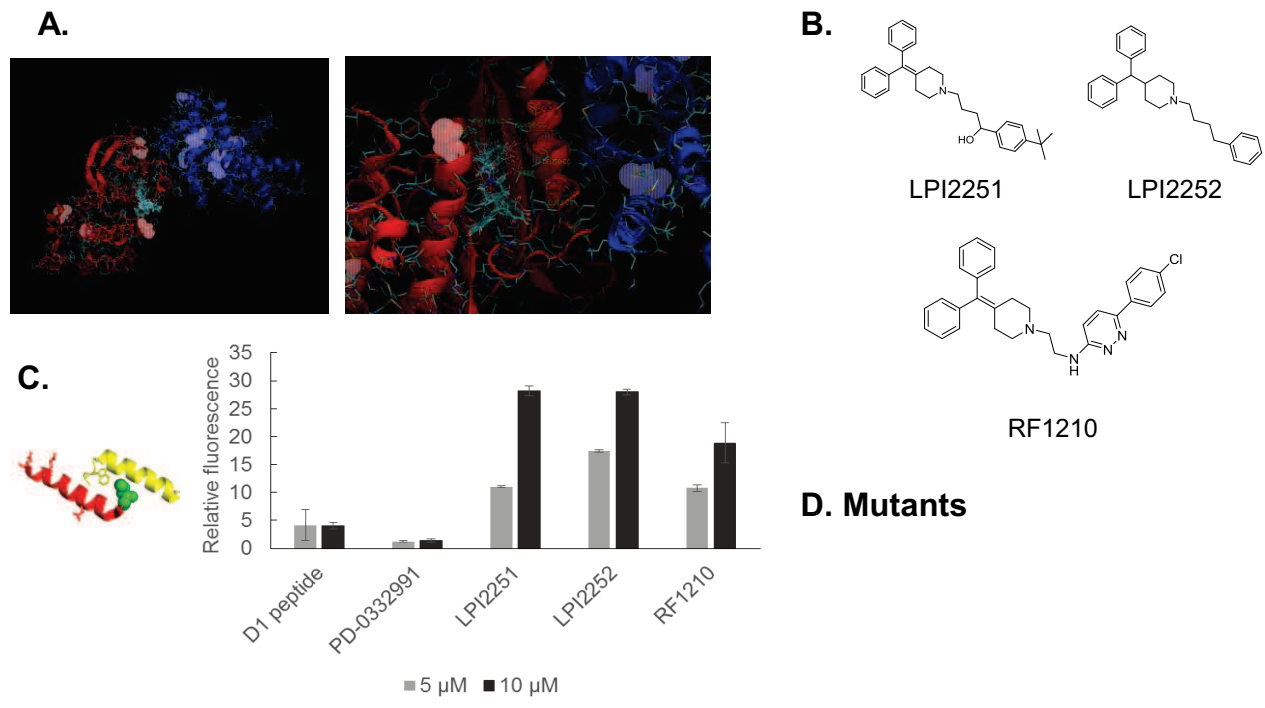

Supplementary Figure 1 – Optimization of concentrations and Kinetics for the Screen

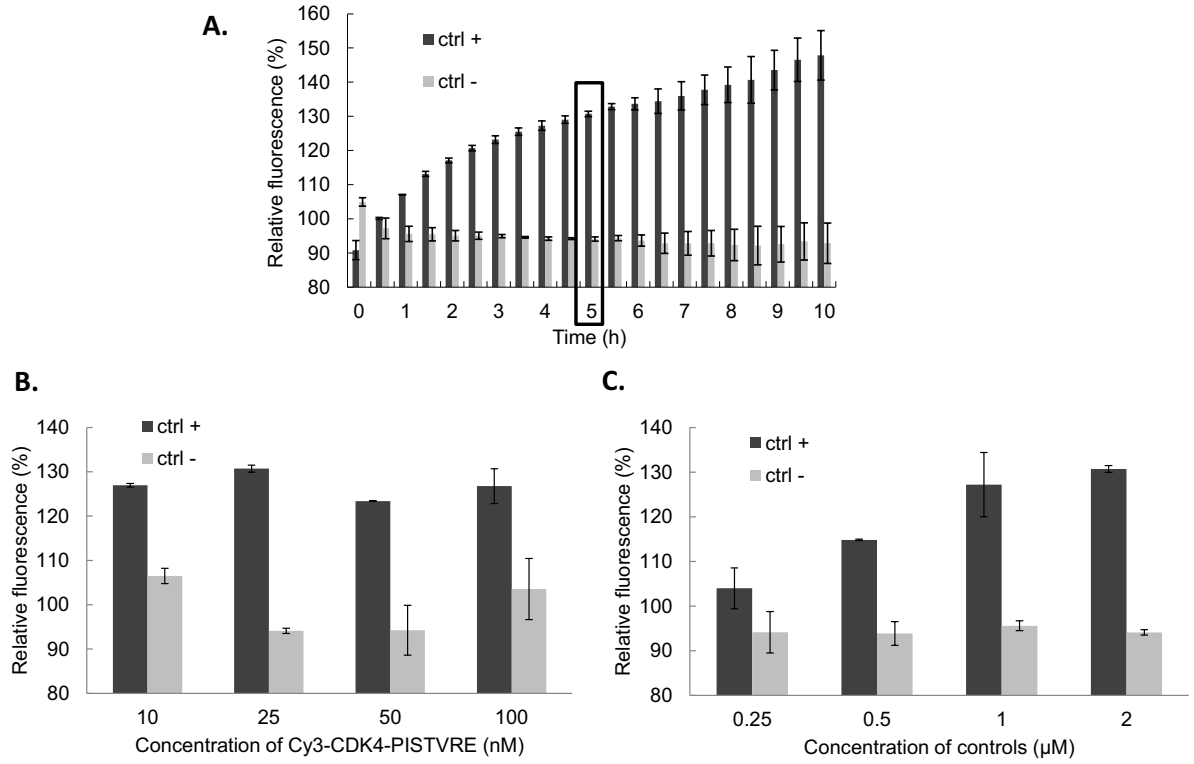

Supplementary Figure 2 – Dose response of CDK4-PISTVRE-Cy3 to LPI2251 variants

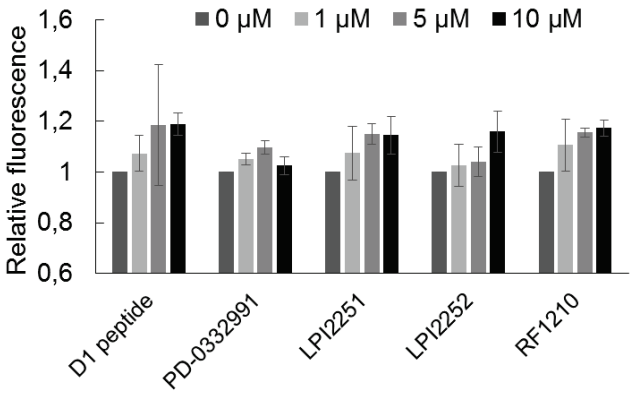

Supplementary Figure 3 – Fluorescence emission spectra of PISTVRE-TP2-Rho and LPI derivatives

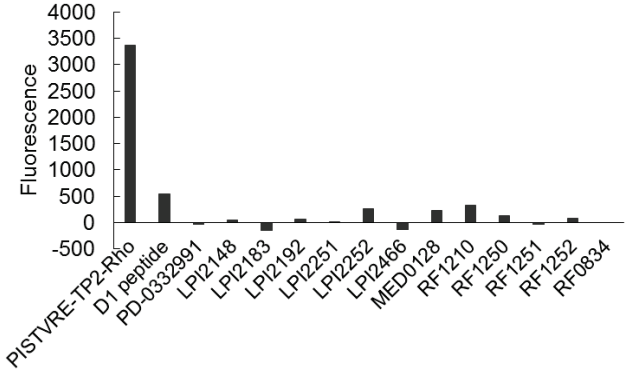

Supplementary Figure 4 – Proliferation assays in melanoma A375 cell line

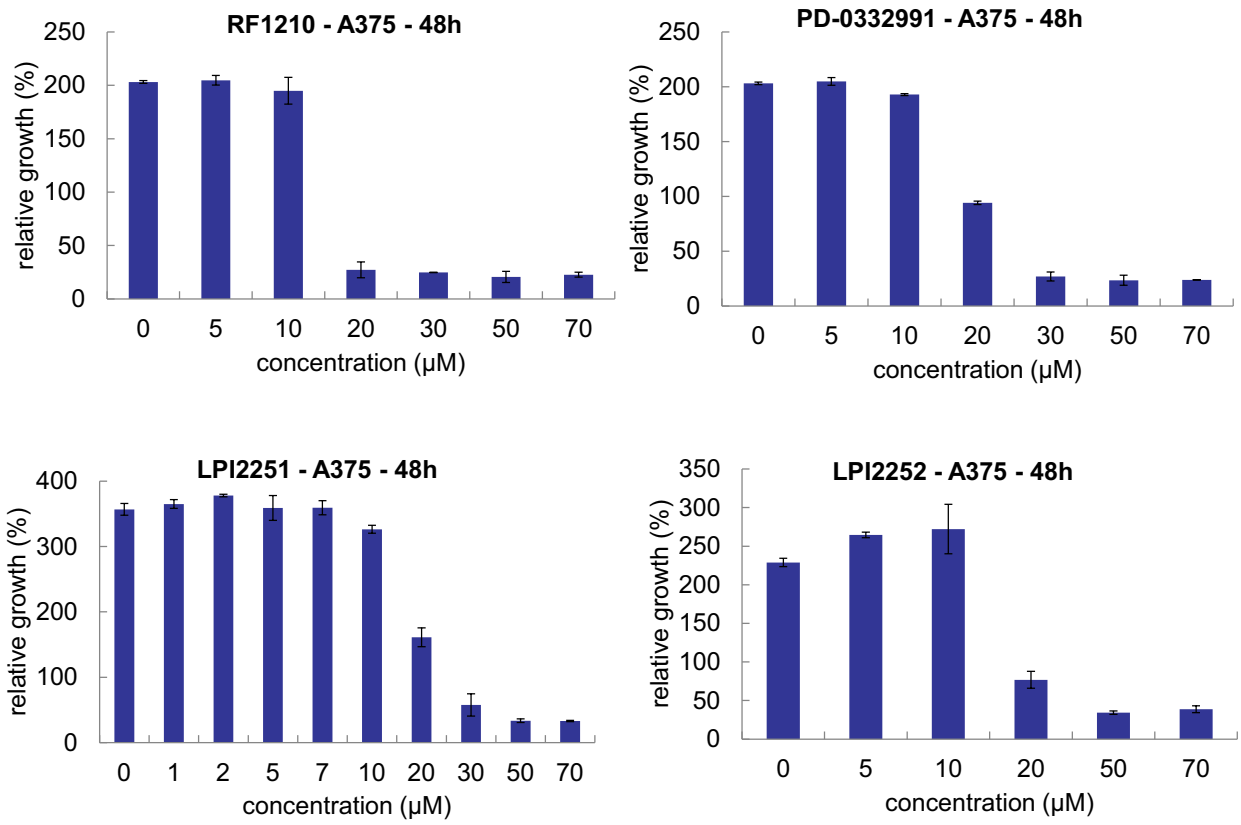

Supplementary Figure 5 – Proliferation assays in melanoma A375 cell line

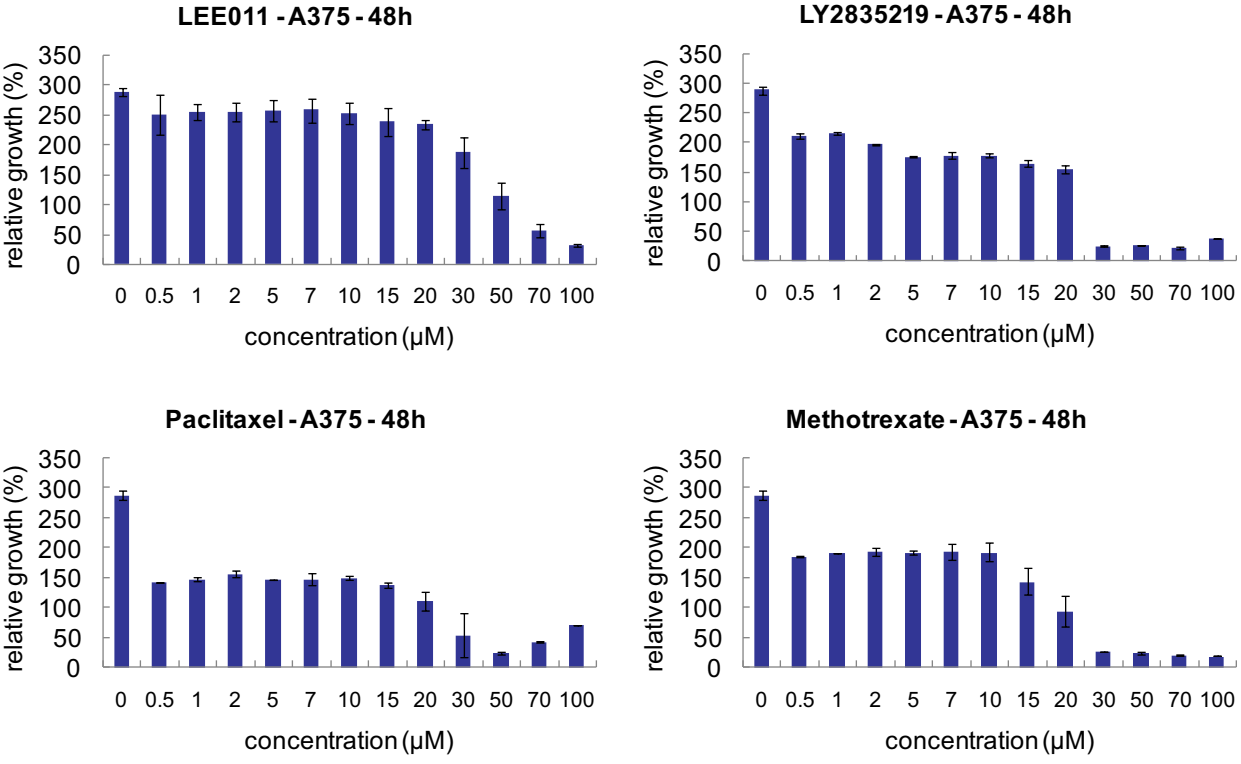

Supplementary Figure 6 – Proliferation assays in fibroblasts

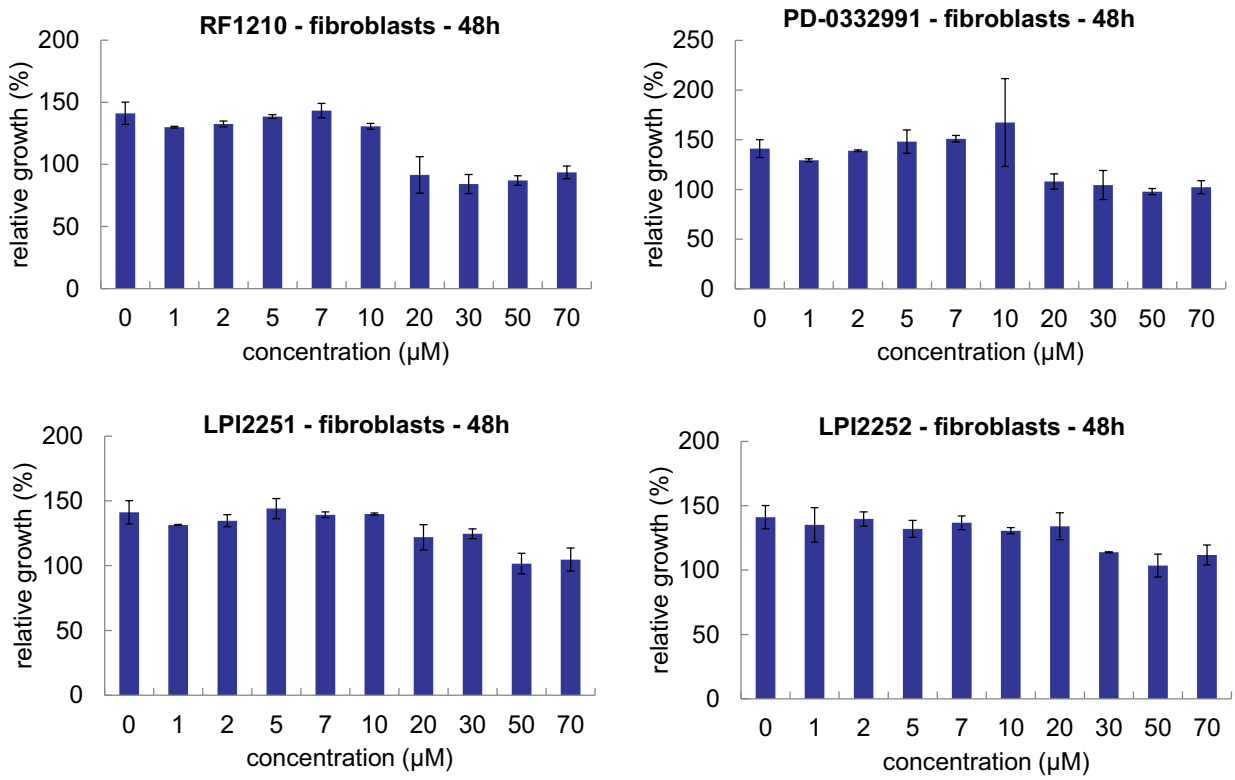

Supplementary Figure 7 – Proliferation assays – Comparison PD-0332991 & RF1210 in different melanoma cell lines

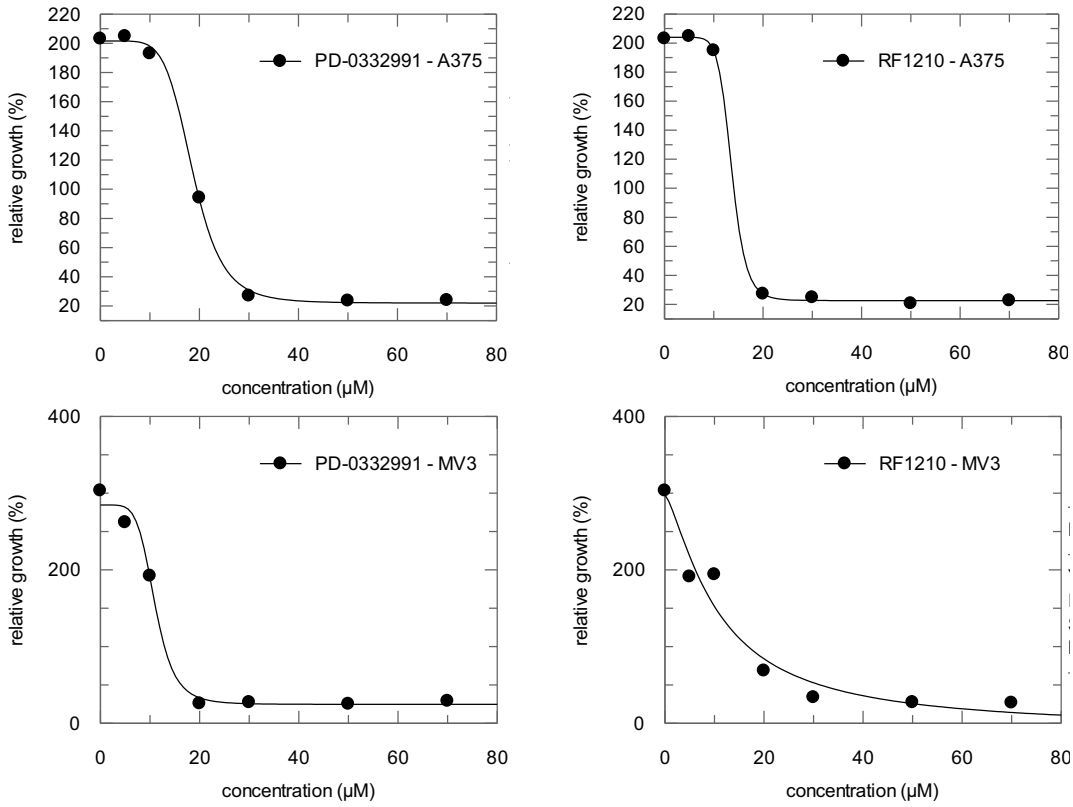

Supplementary Figure 8 – Proliferation assays – Comparison PD-0332991 & RF1210 in different melanoma cell lines

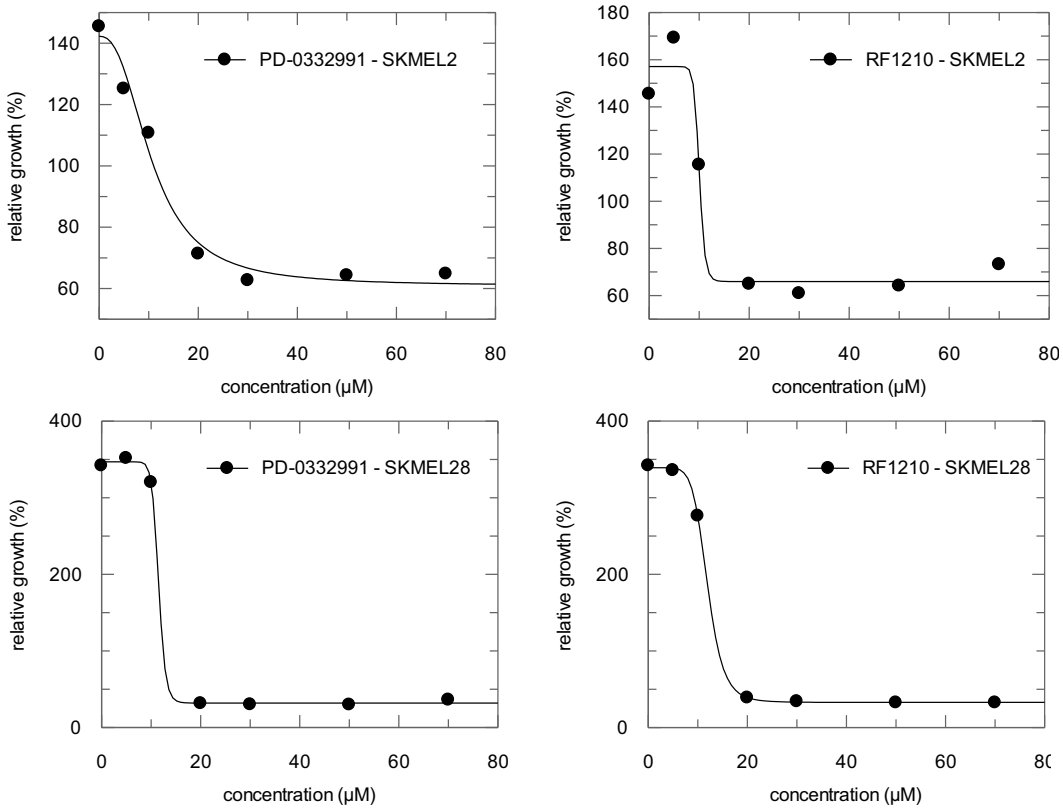

Supplementary Figure 9 – Synergy assays with RF1210 – A375 cells

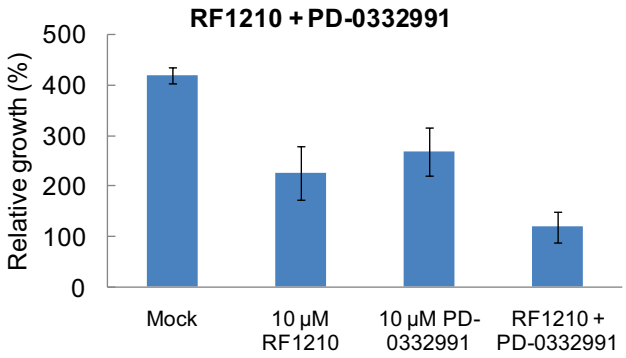

Cooperation – RF1210	Degree of inhibition (%)
10 µM RF1210	46.2
15 µM LY2835219	58.6
10 µM PD-0332991	36.0
RF1210 + LY2835219	92.0
RF1210 + PD-0332991	71.7

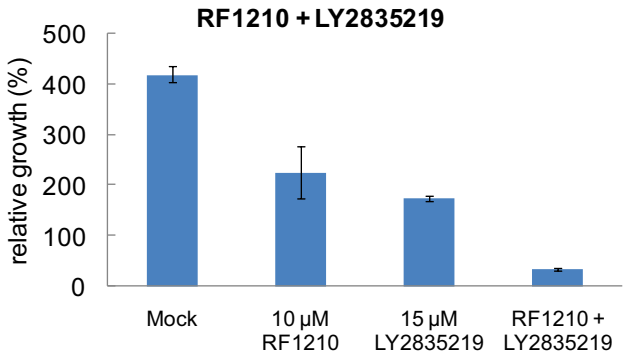

Supplementary Figure 10 – Synergy assays with LPI2252 – A375 cells

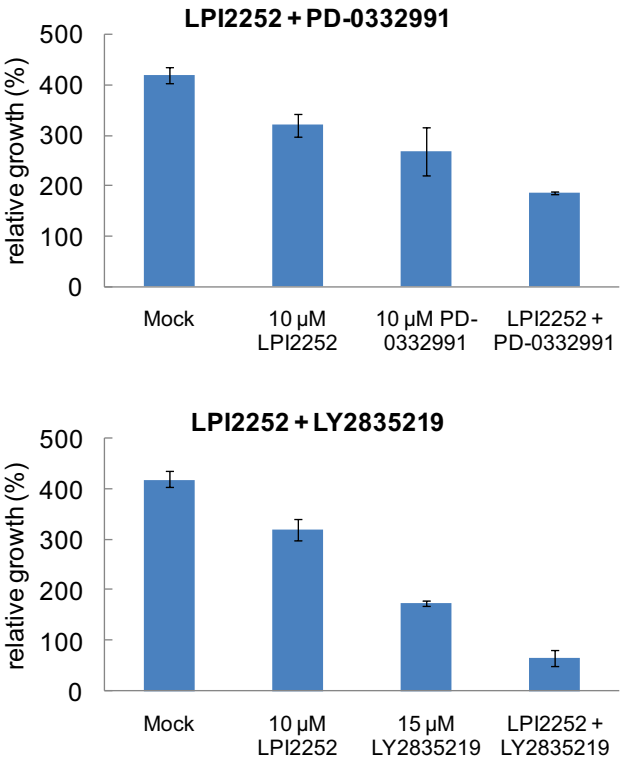

Cooperation – LPI2252	Degree of inhibition (%)
10 µM LPI2252	23.7
15 µM LY2835219	58.6
10 µM PD-0332991	36.0
LPI2252 + LY2835219	84.5
LPI2252 + PD-0332991	55.6

Supplementary Figure 11 – Synergy assays – A375 cells

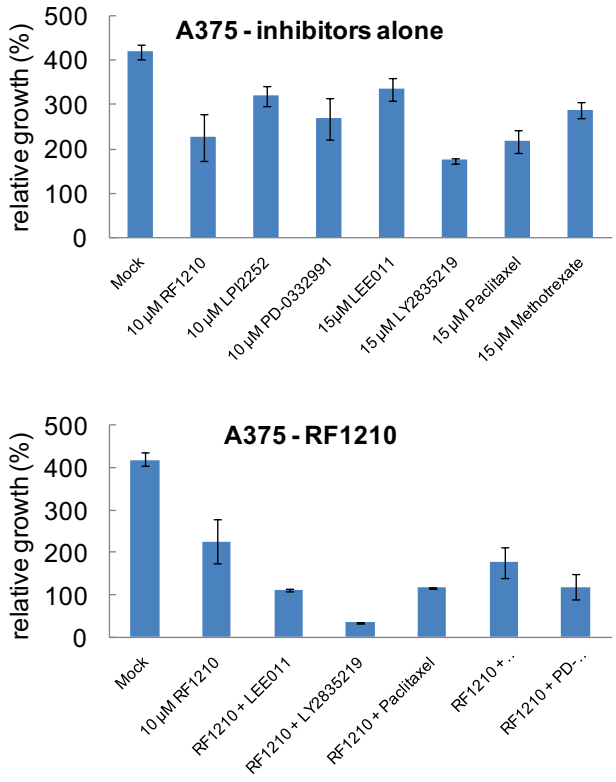

Cooperation – RF1210	Degree of inhibition (%)
10 µM RF1210	46.2
15 µM LEE011	20.5
15 µM LY2835219	58.6
15 µM Paclitaxel	48.4
15 µM Methotrexate	31.4
10 µM PD-0332991	36.0
RF1210 + LEE011	73.4
RF1210 + LY2835219	92.0
RF1210 + Paclitaxel	72.4
RF1210 + Methotrexate	58.0
RF1210 + PD-0332991	71.7

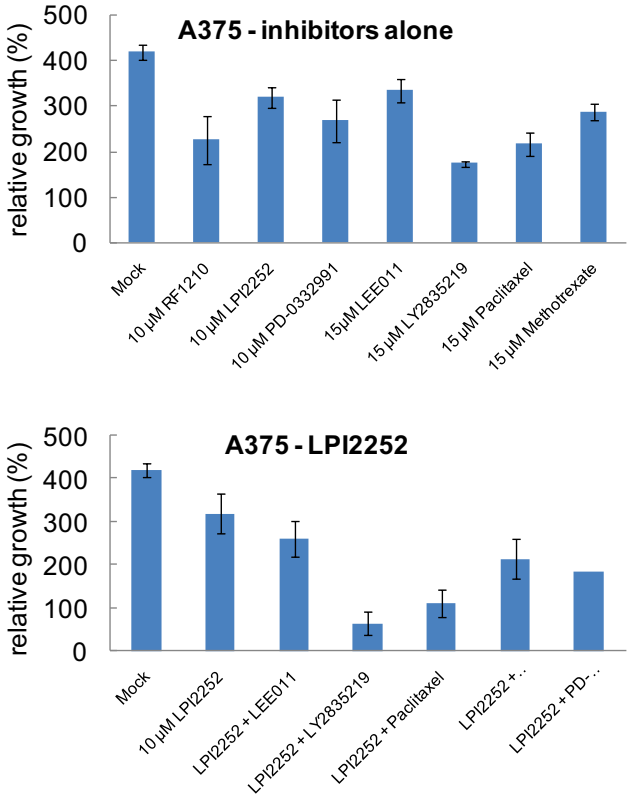

Cooperation – LPI2252	Degree of inhibition (%)
10 µM LPI2252	23.7
15 µM LEE011	20.5
15 µM LY2835219	58.6
15 µM Paclitaxel	48.4
15 µM Methotrexate	31.4
10 µM PD-0332991	36.0
LPI2252 + LEE011	37.7
LPI2252 + LY2835219	84.5
LPI2252 + Paclitaxel	73.2
LPI2252 + Methotrexate	48.8
LPI2252 + PD-0332991	55.6

Supplementary Tables – Summary of IG_{50} values determined for melanoma cell lines

A375	IG_{50} (µM)
RF1210	13.6 +/- 0.4
LPI2251	17.6 +/- 0.5
LPI2252	17.9 +/- 2.2
PD-0332991	18.7 +/- 0.4

	IG_{50} (PD-0332991) (µM)	IG_{50} (RF1210) (µM)
A375	18.7 +/- 0.4	13.6 +/- 0.4
MV3	11.0 +/- 0.8	10.8 +/- 4.4
SKMEL2	10.7 +/- 1.6	10.1 +/- 1.0
SKMEL28	11.5 +/- 3.2	12.0 +/- 0.2

	CDKN2A	CDK4	Rb	BRAF	NRAS
A375	mutated (E61Stop. Loss of function)	WT	WT	V600E	WT
Mewo	mutated (R80Stop. Loss of function)	WT	WT	WT	WT
MV3	ND	ND	ND	WT	WT
SK-MEL2	WT	WT	WT	WT	mutated (Q61R)
SK-MEL28	WT	R24C	WT	V600E	WT

Développement de biosenseurs fluorescents pour suivre et cibler CDK4/cycline D dans le mélanome

Les CDK/cyclines jouent un rôle majeur dans la progression du cycle cellulaire et dans le maintien de la prolifération des cellules cancéreuses, constituant ainsi des biomarqueurs clés et des cibles pharmacologiques attractives. Plus particulièrement, l'activité de CDK4/cycline D, kinase responsable de la progression de la phase G1 et de la transition G1/S, est dérégulée dans de nombreux cancers dont le mélanome. Cette hyperactivation est associée à des mutations, à l'amplification ou à la surexpression de CDK4, cycline D, $p16^{INK4a}$ ou encore pRb.

Comme aucune approche sensible et directe n'existe pour évaluer l'activité de CDK4/cycline D dans des conditions physiologiques et pathologiques, le premier objectif de ma thèse a consisté à développer un biosenseur fluorescent permettant d'étudier cette kinase *in vitro* et *in cellulo.* Une fois caractérisé et validé *in vitro,* le biosenseur a été appliqué à la détection d'altérations de CDK4/cycline D dans des biopsies de peau humaine et de xénogreffes de mélanome dans des essais fluorescents d'activité kinase, ainsi que dans des cellules cancéreuses vivantes par microscopie de fluorescence et vidéo microscopie.

Par ailleurs, peu d'inhibiteurs sont actuellement disponibles pour inhiber CDK4/cycline D et la plupart d'entre eux ciblent la poche de fixation de l'ATP. C'est pourquoi le second objectif de ma thèse a consisté à identifier des inhibiteurs non compétitifs de l'ATP, soit par élaboration rationnelle de peptides, soit par criblage de petites molécules. A cette fin, deux biosenseurs fluorescents ont été développés qui permettent d'identifier respectivement des composés ciblant l'interface entre CDK4 et cycline D ou des inhibiteurs allostériques capables de perturber la dynamique conformationnelle de CDK4. Des essais de criblage par fluorescence réalisés avec ces biosenseurs ont conduit à l'identification de touches qui ont été validées et caractérisées *in vitro* et dans des essais de prolifération cellulaire, et qui constituent des candidats prometteurs pour une chimiothérapie sélective du mélanome.

Mots clés : CDK4/cycline D, cancer, biosenseur fluorescent, diagnostic, inhibiteurs, HTS

Development of fluorescent biosensors to probe and target CDK4/cyclin D in melanoma

CDK/cyclins play a central role in coordinating cell cycle progression, and in sustaining proliferation of cancer cells, thereby constituting established cancer biomarkers and attractive pharmacological targets. In particular, CDK4/cyclin D, which is responsible for coordinating cell cycle progression through G1 into S phase, is a relevant target in several cancers including melanoma, associated with mutation of CDK4, cyclin D, $p16^{INK4a}$ and pRb.

As there are no sensitive and direct approaches to probe CDK4/cyclin D activity in physiological and pathological conditions, the first goal of my thesis has consisted in engineering a fluorescent biosensor to probe this kinase *in vitro* and *in cellulo.* Once characterized and validated *in vitro,* the biosensor was applied to detect CDK4/cyclin D alterations in biopsies from human skin and melanoma xenografts in fluorescence-based activity assays, and in living cancer cells by fluorescence microscopy and timelapse imaging.

Moreover, only few inhibitors are currently available to target CDK4/cyclin D and most of them bind the ATP pocket. As such, the second major goal of my thesis project has consisted in identifying non-ATP competitive inhibitors, either through rational design of peptides or by screening small molecule libraries. To this aim, two fluorescent biosensors were engineered which discriminate compounds that target the interface between CDK4 and cyclin D, or that perturb the conformational dynamics of CDK4, respectively, from ATP-pocket binding compounds. Fluorescence-based screening assays performed with these biosensors lead to identification of hits, which were validated and characterized *in vitro* and in cell proliferation assays, and which constitute promising candidates for selective chemotherapy in melanoma.

Key words : CDK4/cyclin D, melanoma, fluorescent biosensor, diagnostic assay, inhibitors, HTS